University of Stuttgart
Institute for Theoretical Physics III

Functional Rydberg Complexes in the VdW Model

Master's thesis by

Simon Fell

November 20, 2024

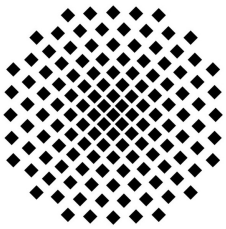

Primary Corrector and Supervisor
Prof. Dr. H. P. Büchler

Secondary Corrector
Prof. Dr. J. Main

Supervised by
Dr. Nicolai Lang

Statutory Declaration

I herewith formally declare that I have composed the submitted thesis myself and without use of any other than the cited sources and aids. The thesis in the same or similar form has not been submitted to any examination body and has not been published. This thesis was not yet, even in part, used in another examination. Furthermore I declare that the bound and the electronic copies of the thesis are consistent with each other in contents.

Stuttgart, November 20, 2024 Simon Fell

Abstract

In this thesis we consider the construction of *functional Hilbert spaces* as the low-energy sector of a microscopic system. The construction of such Hilbert spaces is of large interest as it provides a path towards the realization of quantum phases with long-range entanglement, stable quantum memories and fault-tolerant quantum computing.
To construct such a Hilbert space, a suitable platform must offer fine-grained control of its degrees of freedom and decouple the environment. Recent experimental advances promise the individual control of hundreds of atoms[11, 32] and allow for the construction of three-dimensional structures[4]. This motivates a promising ansatz for such a platform, given by individually trapped neutral atoms that can be excited into Rydberg states.

Such excited Rydberg atoms exhibit strong interactions. In previous studies[38, 42, 30, 23] this was often approximated via a blockade between nearby atoms in the *PXP model*, neglecting interactions between distant atoms. In this thesis we consider more realistic, algebraic decaying *van der Waals (VdW) interactions* $U \propto 1/r^6$ as a model for Rydberg interactions and we compare our results with previous studies from the PXP model.

As one part of this thesis we work towards the elusive goal of realizing the paradigmatic *surface code* with Abelian $\mathbb{Z}_2$ topological order. Additionally we consider the *Fibonacci model* as a string-net condensate with non-Abelian anyons which promises applications in fault-tolerant quantum computation. As such models are notoriously hard to realize we focus on a *reductionist approach* via engineering elementary building blocks of *synthetic quantum matter* on the Rydberg platform. This approach proposes carefully designed lattice structures which can give rise to long-range entangled ground states under *quantum fluctuations*[42]. As one part of this thesis, we derive the possible *local mappings* to the Rydberg platform and construct the elementary building blocks in the VdW model. We also formulate general statements on how string-nets with loops behave on tessellated Rydberg structures with algebraic decaying interactions and study local excitations.

Besides the design of synthetic quantum matter, a promising near term application of the Rydberg platform for the NISQ era is the *geometric programming* via encoding algorithmic problems in the geometry of the atomic structure. A reductionist approach considers the construction of the logic elementaries on the Rydberg platform which can be concatenated to construct larger *logic circuits*. This has been demonstrated for the PXP model within in the blockade approximation[38]. The study of logic circuits in the context of algebraic decaying VdW interactions makes the second part of this thesis.

The studies in this thesis are supported by an exhaustive list of provably minimal and optimal building blocks for two and three-dimensional structures within the VdW framework which we thoroughly compare with the building blocks from the PXP model.

Kurzzusammenfassung

In dieser Arbeit betrachten wir die Konstruktion von *funktionalen Hilberträumen* als Niedrigenergiesektor eines mikroskopischen Systems. Die Konstruktion solcher Hilbert-Räume ist von großem Interesse, da sie einen Weg zur Realisierung von Quantenphasen mit weitreichender Verschränkung, stabilen Quantenspeichern und fehlertoleranten Quantencomputern bietet.
Um einen solchen Hilbert-Raum zu konstruieren, muss eine geeignete Plattform eine feinkörnige Kontrolle ihrer Freiheitsgrade bieten und die Umgebung entkoppeln. Jüngste experimentelle Fortschritte versprechen die individuelle Kontrolle von Hunderten von Atomen[11, 32] und ermöglichen die Konstruktion dreidimensionaler Strukturen[4]. Dies motiviert einen vielversprechenden Ansatz für eine solche Plattform; durch einzeln gefangene, neutrale Atome, die in Rydberg-Zustände angeregt werden können.

Solche angeregten Rydberg-Atome weisen starke Wechselwirkungen auf. In früheren Studien wurde dies oft durch eine Blockade zwischen nahegelegenen Atomen im *PXP-Modell* approximiert, wobei Wechselwirkungen zwischen entfernten Atomen vernachlässigt wurden. In dieser Arbeit betrachten wir realistischere, algebraisch abklingende *van der Waals (VdW)-Wechselwirkungen* $U \propto 1/r^6$ als ein Modell für Rydberg-Wechselwirkungen und vergleichen unsere Ergebnisse mit früheren Studien aus dem PXP-Modell.

Als ein Teil dieser Arbeit arbeiten wir auf das schwer fassbare Ziel hin, den paradigmatischen '*Surface Code*' mit abelscher $\mathbb{Z}_2$ topologischer Ordnung zu realisieren. Zusätzlich betrachten wir das *Fibonacci-Modell* als 'String'-Netz-Kondensat mit nicht-abelschen Anyonen, das Anwendungen in der fehlertoleranten Quantenberechnung verspricht. Da solche Modelle bekanntermaßen schwer zu realisieren sind, konzentrieren wir uns auf einen *reduktionistischen Ansatz*, bei dem elementare Bausteine der *synthetischen Quantenmaterie* auf der Rydberg-Plattform entwickelt werden. Dieser Ansatz schlägt sorgfältig entworfene Gitterstrukturen vor, die unter *Quantenfluktuationen* verschränkte Grundzustände mit langer Reichweite hervorbringen können[42]. Im Rahmen dieser Arbeit leiten wir die möglichen *lokalen Projektionen* auf die Rydberg-Plattform ab und konstruieren die elementaren Bausteine im VdW-Modell. Wir formulieren auch allgemeine Aussagen darüber, wie sich 'String'-Netz-Kondensate mit Schleifen auf mosaikartigen Rydberg-Strukturen mit algebraischen abklingenden Wechselwirkungen verhalten und untersuchen lokale Anregungen.

Neben dem Entwurf synthetischer Quantenmaterie ist eine vielversprechende kurzfristige Anwendung der Rydberg-Plattform für die NISQ-Ära die *geometrische Programmierung* über die Kodierung algorithmischer Probleme in der Geometrie der atomaren Struktur. Ein reduktionistischer Ansatz sieht die Konstruktion von Logikelementen auf der Rydberg-Plattform vor, die zur Konstruktion größerer *logischer Schaltungen* verkettet werden können. Dies wurde für das PXP-Modell im Rahmen der Blockade-Näherung demonstriert[38]. Die Untersuchung logischer

Schaltungen im Zusammenhang mit algebraisch abklingenden VdW-Wechselwirkungen bildet den zweiten Teil dieser Arbeit.

Die Untersuchungen in dieser Arbeit werden durch eine erschöpfende Liste von bewiesen minimalen und optimalen Bausteinen für zwei- und dreidimensionale Strukturen im Rahmen des VdW-Modells unterstützt und gründlich mit den Bausteinen aus dem PXP-Modell verglichen.

Contents

Statutory Declaration **3**

Abstract **5**

Kurzzusammenfassung **7**

Contents **12**

Overview **14**

1 Summary **15**

2 Theoretical Foundation **19**
2.1 Introduction of the Model 20
2.2 Languages, L-Manifolds and L-Complexes 22
2.3 Setting the Objective 24
2.4 A reductionist Approach 25
2.5 Measures of Quality 27
2.6 Some general Remarks 30

Appendices **32**
2.A An upper bound for the Robustness 32

3 The Problem and Methods **35**
3.1 Rejection Sampling Algorithm 36
3.1.1 Construction of Samples 36
3.1.2 Application of the Algorithm 41
3.2 Minimization Algorithm 44
3.2.1 Numerical Optimization of Samples 44
3.2.2 Exponential Time Complexity 46
3.2.3 The Energy Structure in the VdW Model 47

3.2.4 Efficient Computation of LESs . . . 51
3.2.5 Efficient Computation of the MISs . . . 52
3.2.6 Optimization of the NOR-Gates . . . 56
3.3 Achieving Ground State Degeneracy . . . 59
3.4 Exploiting Symmetries . . . 67

Appendices **73**
3.A The Generalization of Corollary VI . . . 73

4 Logic Elementaries **75**
4.1 PXP-minimal logic Elementaries . . . 76
4.1.1 PXP-minimal Primitives . . . 76
4.1.2 The Crossing of Edges . . . 80
4.1.3 Family 1 of Elementary Logic Gates . . . 82
4.1.4 Family 2 of Elementary Logic Gates . . . 84
4.1.5 An additional PXP-minimal XOR-gate . . . 84
4.2 VdW-minimal logic Elementaries . . . 86
4.2.1 VdW-minimal Primitives . . . 87
4.2.2 VdW-minimal (inverted) Crossings . . . 87
4.2.3 Family 3 of Elementary Logic Gates . . . 90
4.3 Non-minimal VdW-Elementaries . . . 95
4.3.1 The XNOR4-Gate . . . 95

Appendices **97**
4.A The VdW-specific XNOR-Gates with two Ancillaries . . . 97

5 Elementaries of tessellated Languages **100**
5.1 Surface Code . . . 101
5.1.1 General Theory . . . 101
5.1.2 PXP-minimal Surface Code Elementaries . . . 105
5.1.3 VdW-specific SC Elementaries in Representation I . . . 107
5.1.4 VdW-specific SC Elementaries in Representation II . . . 110
5.2 Fibonacci Model . . . 112
5.2.1 General Theory . . . 112
5.2.2 PXP-derived Fibonacci Model Elementaries . . . 114
5.2.3 VdW-specific Fibonacci Model Elementaries . . . 118

Appendices **121**
5.A Surface Code Unit Cells . . . 121
5.A.1 Finite Energy Splitting of the SC-I Unit Cells . . . 122
5.A.2 Additional SC-I Unit Cells . . . 124
5.A.3 Impossibility of two-dimensional the SC Unit Cells with one Ancillary . . . 126
5.B Fibonacci Model Elementaries . . . 128
5.B.1 Minimality and Uniqueness for the FMSI-2 Site . . . 128
5.B.2 Finite Energy Splitting of the FMUI Unit Cells . . . 131
5.B.3 Additional FMUI Unit Cells . . . 133

6 Tessellated Theory **135**
6.1 Non-elementary loop Structures . . . 135
6.2 On Tessellated Loop Structures . . . 140
6.3 A lower bound on the Quality Factor . . . 145
6.3.1 A Chain of Atoms . . . 145
6.3.2 Appendage of atomic Chains . . . 146
6.3.3 Tessellated Languages on the Honeycomb Grid . . . 147
6.4 Local Languages on the Honeycomb Grid . . . 149
6.4.1 The local Energy Structure . . . 149
6.4.2 A lower Bound on the Honeycomb Grid . . . 150
6.4.3 A upper Bound on the Honeycomb Grid . . . 152
6.5 A Comparative Study on the Bounds . . . 153
6.5.1 Visualizing the Bounds . . . 153
6.5.2 The asymptotic behavior of the Bounds . . . 156

Appendices **159**
6.A Proofs for the lower bound on the Quality . . . 159
6.A.1 Proof for the N_E-Chain . . . 159
6.A.2 Proof for the Appendage of N_E-Chains . . . 165
6.A.3 Proof for Tessellated Languages on the HC-Grid . . . 168
6.B Proofs for Local Languages on the HC-Grid . . . 173
6.B.1 Proof for Lower Bounds to local Languages on the HC-Grid . . . 173
6.B.2 Proof for Upper Bounds to local Languages on the HC-Grid . . . 175

7 Boolean Theory **178**
7.1 Virtual Ancillaries . . . 179
7.2 Implementability of Boolean Functions . . . 182
7.3 Outlook: Sub-exponential Realizations . . . 185
7.3.1 A counting Argument against sub-exponential Realizations . . . 185
7.3.2 Examples in limiting cases . . . 186

Appendices **188**
7.A Proof of the Implementability of Boolean Functions . . . 188

8 Higher Dimensions **192**
8.1 Binary Logic Elementaries . . . 194
8.1.1 VdW-specific logic Elementaries . . . 194
8.1.2 PXP-derived logic Elementaries . . . 195
8.2 Ternary Logic Elementaries . . . 199
8.2.1 Unit effective Hamming Weight . . . 202
8.2.2 Effective Hamming Weight Three . . . 202
8.2.3 Effective Hamming Weight Two . . . 204
8.2.4 Interpretations of the Connectives . . . 206
8.2.5 Non-minimal Gates . . . 207
8.3 Asymmetric Ternary Logic Gates . . . 209
8.3.1 The Toffoli-Gate . . . 209
8.3.2 Inverted SWITCH-Gate . . . 211
8.3.3 Controlled SWAP-Gate . . . 212
8.4 Binary Multi Logic Gates . . . 215
8.4.1 Double Logic Gates . . . 215

8.4.2 Triple Logic Gates . . . 217
8.5 Surface Code Unit Cells . . . 219
8.5.1 Quasiplanar Surface Code . . . 219
8.5.2 Surface Code in higher Dimensions . . . 220
8.6 Fibonacci Model Sites . . . 223
8.6.1 Representation IV . . . 223
8.6.2 Representation II . . . 225
8.6.3 Representation III . . . 227
8.6.4 Summary and Conclusion . . . 228

Appendices **229**
8.A Completeness and Minimality of the Ternary Logic Elementaries . . . 229
8.A.1 Unit effective Hamming Weight . . . 230
8.A.2 Effective Hamming Weight Three . . . 232
8.A.3 Effective Hamming Weight Two . . . 234
8.B Completeness and Minimality of the Multi Gates . . . 236
8.B.1 Double Logic Gates . . . 236
8.B.2 Triple Logic Gates . . . 238

9 Outlook **239**

List Of Figures **245**

Bibliography **250**

Acknowledgments **253**

Overview

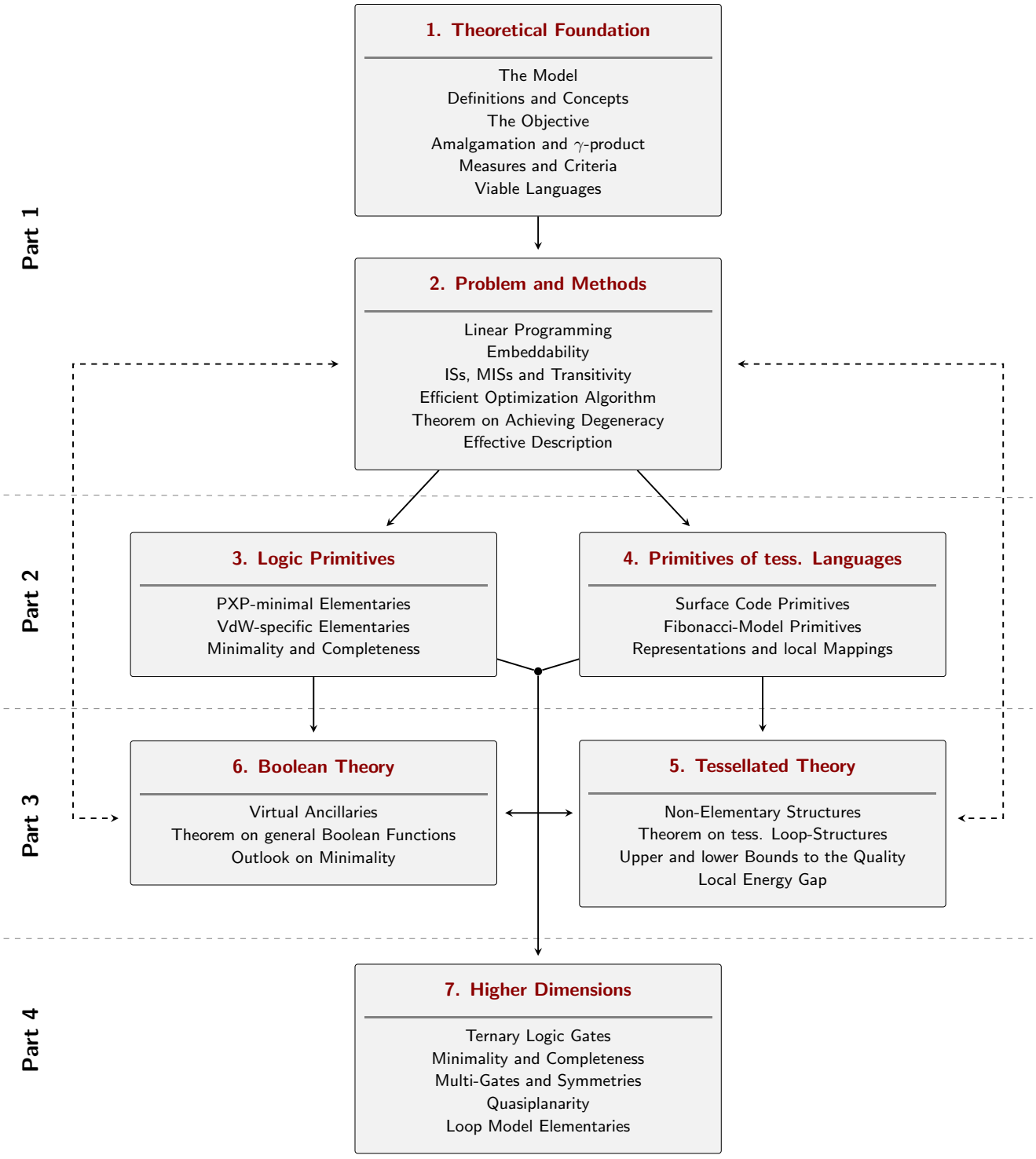
Part 1
1. Theoretical Foundation
The Model
Definitions and Concepts
The Objective
Amalgamation and γ-product
Measures and Criteria
Viable Languages
2. Problem and Methods
Linear Programming
Embeddability
ISs, MISs and Transitivity
Efficient Optimization Algorithm
Theorem on Achieving Degeneracy
Effective Description
Part 2
3. Logic Primitives
PXP-minimal Elementaries
VdW-specific Elementaries
Minimality and Completeness
4. Primitives of tess. Languages
Surface Code Primitives
Fibonacci-Model Primitives
Representations and local Mappings
Part 3
6. Boolean Theory
Virtual Ancillaries
Theorem on general Boolean Functions
Outlook on Minimality
5. Tessellated Theory
Non-Elementary Structures
Theorem on tess. Loop-Structures
Upper and lower Bounds to the Quality
Local Energy Gap
Part 4
7. Higher Dimensions
Ternary Logic Gates
Minimality and Completeness
Multi-Gates and Symmetries
Quasiplanarity
Loop Model Elementaries

1 | Summary

In this thesis we study functional structures of Rydberg atoms interacting via VdW interactions in two and three dimensions. The thesis can be thematically split in *four parts* which include one or two chapter each. We refer to previous overview for a visualization of the parts, the chapters and the main topics of this thesis. The first part introduces the theoretical framework, the formulation of the problem and the tools we developed to tackle this problem. The remaining parts can be thematically split between the two main topics of this thesis, namely *geometric programming* and the engineering of *synthetic quantum matter*. For latter topic we focus on two important string-net models with loop degrees of freedom: the paradigmatic *surface code* and the *Fibonacci model* which supports non-Abelian anyons. In the following we want to give a brief overview over the chapters and their main results:

- ➔ In chap. 2 (part 1) we introduce the physical model and the mathematical framework. We rigorously define the important concepts of languages, L-manifolds and L-complexes in sec. 2.2. With this new vocabulary in sec. 2.3 we rigorously formulate the objective of this thesis as to construct functional Rydberg structures. Such a construction is generally highly nontrivial for more complex targets which motivates us to introduce a reductionist approach called 'amalgamation' (sec. 2.4). To evaluate our results we introduce useful measures of quality in sec. 2.5.

- ➔ In chap. 3 (part 1) we discuss the *problems* which arise during the construction of functional Rydberg complexes and introduce *tools and methods* to tackle these problems. Finally, we exemplarily apply the tools to complexes to picture their advantages and disadvantages. In sec. 3.1 we start by introducing a *rejection sampling algorithm* which constructs sample structures implementing a given target. The problem arises that such samples are generally not quite optimal. Therefore in sec. 3.2 we introduce a minimization algorithm to optimize the sample structures in the measures of quality. Especially for large structures this is numerically intensive. This motivates us to formulate alg. 3.3 which allows for an efficient calculation of the relevant quantities based on lemma III. Still such a numerical algorithm has troubles achieving perfect quality. In sec. 3.3 we formulate theorem V and multiple corollaries which guarantee perfect quality. In sec. 3.4 we study the effect of symmetries. We introduce the formalism of effective languages which allow us to generalize theorem V

for symmetric targets. Theorem V and its derived corollaries are central to this thesis and are frequently used. This chapter concludes part 1 of the thesis.

➔ We consider elementary logic gates in chap. 4 (part 2). For all gates of this chapter we were able to achieve perfect quality. In sec. 4.1 we start by reconstructing and optimizing the known logic gates from the PXP model[38] in the VdW model. We add additional gates to complete the list of elementary logic gates for the PXP model. We continue with VdW specific elementary gates in sec. 4.2 and sec. 4.3. For every elementary logic gate we find a *more atom-efficient* implementation in the VdW model. We prove that these gates are the *most atom-efficient gates* and that the list of gates is *complete*. The VdW-specific gates are mainly based on the *intermediate and low-energy regime* which can not be accurately portrayed in the PXP model. This suggests that the simplification by the PXP 'blockade-approximation' removes important degrees of freedom which are useful for the construction of more atom-efficient Rydberg structures. As a trade-off the VdW-specific gates based on the low-energy regime possess a smaller energy gap to the excited states. Nevertheless the VdW-specific gates based on the intermediate energy regime possess similar or larger energy gaps than the PXP-inspired gates.

➔ In chap. 5 (part 2) we focus on the elementary building blocks of the tessellated string-net Hilbert spaces, namely the *surface code* and the FIBONACCI model, in two dimensions. We introduce and discuss the different *mappings* to the Rydberg platform in sec. 5.1.1 and 5.2.1. In the next sections 5.1.2 and 5.2.2 we reconstruct the elementaries of the PXP model. We find that they can not be implemented in the VdW model with perfect quality due to the additional long-range interactions. In the following subsections 5.1.3, 5.1.4 and 5.2.3 we derive more atom-efficient realizations in the VdW model, for some of which we are able to achieve perfect quality. For the surface code we find that the asymmetric mapping is more natural to implement on the Rydberg platform. This concludes part 2 of this thesis.

➔ We continue with a study on tessellated structures constructed from the elementary building blocks in chap. 6 (part 3). We start with a numerical analysis of tessellated structures in sec. 6.1 however this is only possible for small structures due to numerical limitations. Thus from sec. 6.2 onward we concentrate on an analytical approach: We formulate the central theorem XI which excludes the existence of systems with *independent loop (*BOOLEAN*) degrees of freedom* on tessellated structures in the VdW model. For the analogous case we formulate theorem XIV for tessellated languages on the honeycomb grid which quantifies the interplay between the quality, the size of the grid and the distance between vertices. In sec. 6.4 we consider the case of *local languages* on the honeycomb grid. We determine quantitative upper and lower bounds on the quality and study them in sec. 6.5.

➔ In chap. 7 (part 3) we consider general BOOLEAN functions for which we want to achieve perfect quality. This leads us to the concept of *virtual ancillaries* (sec. 7.1). We generalize this concept in sec. 7.2 with theorem XVII which guarantees that the implementation of any BOOLEAN or check function with exponentially many ancillaries in the number of variables. In the outlook 7.3 we offer an argument why for general cases we can not expect a realization of BOOLEAN functions with sub-exponentially many ancillaries.

➔ Lastly in part 4, in the most comprehensive chap. 8 we consider quasiplanar ('almost two-dimensional') and three-dimensional structures of atoms. We find that some elementary structures profit from an embedding in three dimensional space (subsec. 8.1.1). In sec. 8.2 we construct a complete list of atom-efficient ternary logic gates with perfect quality: some noteworthy examples ar the minority-gate, the TOFFOLI gate and the FREDKIN gate.

We consider gates which realize multiple logical connectives simultaneously in sec. 8.4 and subsec. 8.1.2. Especially latter gates are highly symmetric such that they promise an equal-weight superposition of the ground states when perturbatively introducing quantum fluctuations. In the final two sections 8.5 and 8.6 we focus on surface code and FIBONACCI model elementaries in three dimensions. Especially for the surface code we can more efficiently implement a unit cell by including the third dimension. For the FIBONACCI model we include a comparative study between all possible atom-efficient realizations in two and three dimensions.

In conclusion we find for each elementary building block a more atom-efficient implementation in the VdW model with *at most one ancillary*. It turns out useful to consider *different mappings* to the Rydberg platform or to include the third spatial dimension. The VdW model introduces *additional DOFs* in the long-range interactions. They can be useful for the construction of efficient gates but they also *perturb larger structures*. This can *prevent the construction* of tessellated Hilbert spaces. The perturbations can be balanced with *additional atoms*.

2 | Theoretical Foundation

"The great book of nature can be read only by those who know the language in which it was written. And this language is mathematics."

– Galileo Galilei

In this chapter we introduce the *physical* foundation for this thesis. As this is a work on theoretical physics it includes a considerable amount of mathematics. In this chapter we do not want to repeat the mathematical basics but instead refer to common literature. We start with a brief overview over this chapter:

In sec. 2.1 we describe the physical model we consider for this thesis. We introduce the important definitions and concepts in sec. 2.2. This allows us to precisely formulate the goal of this thesis in sec. 2.3 as to construct functional structures on the Rydberg platform. As this is generally hard to fulfill for larger systems we follow a reductionist approach which we introduce in sec. 2.4. Afterwards in sec. 2.5 we introduce some measures which allow us to evaluate the constructed structures. We conclude with some general preliminary remarks and assumptions on which this thesis is based in sec. 2.6.

In this thesis in chap. 5 and chap. 6 we exemplarily consider two tessellated systems characterized by local gauge constraints, namely the surface code and the Fibonacci model. We do not want to introduce their fundamentals in this chapter but instead refer to subsec. 5.1.1 for the surface code and subsec. 5.2.1 for the Fibonacci model.

2.1 | Introduction of the Model

We consider an arrangement of trapped neutral atoms in two- or three dimensional flat space interacting via isotropic Van der Waals interactions. The set of atoms is denoted by $\mathcal{N}$, the atoms are denoted by Fraktur letters $\mathfrak{i}, \mathfrak{j}, \mathfrak{k}, \mathfrak{l}, \ldots \in \mathcal{N}$ and the number of atoms is denoted by $N = |\mathcal{N}|$. The atoms are placed at positions $\boldsymbol{r}_\mathfrak{i} \in \mathbb{R}^d$ where $d \in \{2, 3\}$ is the dimension we are considering. Within *two-level approximation* the atoms are assumed to behave as a *spin-1/2 particle* with an electronic ground state $|n = 0\rangle$ and an excited Rydberg state $|n = 1\rangle$. The electronic ground state of each atom $\mathfrak{i} \in \mathcal{N}$ is coupled to the Rydberg state via an external laser fields of RABI frequency $\Omega_\mathfrak{i}$. The detuning of the driving lasers from the Rydberg state is denoted by $\Delta_\mathfrak{i}$ which is potentially different for every atom.

The VdW model. In the VAN DER WAALS (VdW) model we assume repulsive VdW interactions $U_{\mathrm{VdW}}(r_{\mathfrak{ij}}) = C/r_{\mathfrak{ij}}^6$ between excited Rydberg atoms at distance $r_{\mathfrak{ij}} = \|\boldsymbol{r}_\mathfrak{i} - \boldsymbol{r}_\mathfrak{j}\|$. C is denoted the *coupling strength* or *interaction strength*. Here we are only interested in the classical limit of low RABI frequencies $\Omega_\mathfrak{i} \to 0$. The quantum dynamics of this system is (within *rotating wave approximation*) governed by the Hamiltonian

$$H[\mathcal{C}] = -\sum_{\mathfrak{i}\in\mathcal{N}} \Delta_\mathfrak{i} n_\mathfrak{i} + \frac{1}{2}\sum_{\mathfrak{i}\neq\mathfrak{j}} U_{\mathrm{VdW}}(r_{\mathfrak{ij}}) n_\mathfrak{i} n_\mathfrak{j}. \tag{2.1}$$

The tuple $\mathcal{C} = (\boldsymbol{r}_\mathfrak{i}, \Delta_\mathfrak{i} \mid \mathfrak{i} \in \mathcal{N})$ is called the *(Rydberg) structure* of the system. It is determined by the geometry $G_\mathcal{C} = (\boldsymbol{r}_\mathfrak{i} \mid \mathfrak{i} \in \mathcal{N})$ and the detunings $\Delta_\mathcal{C} = (\Delta_\mathfrak{i} \mid \mathfrak{i} \in \mathcal{N})$. In the following we are only interested in *physical* geometries with some finite distance between atoms. The Hamiltonian acts on the Hilbert space $\mathcal{H} = (\mathbb{C}^2)^{\otimes N} \cong \mathbb{C}^{2^N}$ of states $|\boldsymbol{n}\rangle = |n_\mathfrak{i}, n_\mathfrak{j}, \ldots\rangle$ with representation $n_\mathfrak{i} = |1\rangle\langle 1|_\mathfrak{i}$. By ramping up the RABI frequencies $\Omega_\mathfrak{i}$ we can perturbatively introduce quantum fluctuations.

The PXP model. At this point we want to mention the general concept of γ-models with power-law interaction $U_\gamma(r_{\mathfrak{ij}}) = C/r_{\mathfrak{ij}}^\gamma$ with inverse exponent $\gamma > 0$[25]. In the case $\gamma = 6$ we recover the VdW model $U_6(r_{\mathfrak{ij}}) \equiv U_{\mathrm{VdW}}(r_{\mathfrak{ij}})$, in the case $\gamma = 3$ we recover a model for dipole-dipole interaction. In the limit $\gamma \to \infty$ we recover the *blockade model* or *PXP model*.

The PXP model is defined by unit *blockade radii* $r_{B,\mathfrak{i}} = 1$ where $U_\infty(r_{\mathfrak{ij}}) \equiv U_{\mathrm{PXP}}(r_{\mathfrak{ij}}) = U_\infty \Theta(1 - r_{\mathfrak{ij}})$. Here Θ is the HEAVISIDE (unit) step function. In the PXP model we consider the limit $U_\infty \to \infty$. Two atoms are said two be in blockade if they are of distance smaller than the blockade radius. Such eigenstates are energetically gapped out, i.e. it is energetically unfavorable to excite atoms which are in blockade in the PXP model. This motivates to the definition of the blockade graph $\mathcal{B} = (V, E)$. Its vertices $V = \mathcal{N}$ are the atoms and two atoms $\mathfrak{i}, \mathfrak{j} \in V$ are connected via an edge $\{\mathfrak{i}, \mathfrak{j}\} \in E$ if and only if the are in blockade. In the PXP model with unit blockade radii this corresponds to a unit-d-ball graph. The blockade graph fully incorporates the kinematic

constraints of the PXP model. Only the *independent sets (ISs)* of the blockade graph possess finite energies, i.e. sets of vertices such that no two vertices are connected via an edge in the blockade graph. It is always energetically favorable to construct a *maximal independent set (MIS)* which is an IS that is no subset of any other IS. The energetic ground states of a Rydberg structure in the PXP model are the *maximum weighted independent sets (MWIS)* of the blockade graph and the detunings, i.e. the MIS of atoms/ vertices which maximizes the sum its detunings $\Delta_{\mathcal{C}}$.

The PXP model has been studied as a reasonable approximation for the low-energy physics of Rydberg structures[38, 43]. However it can not accurately depict the intermediate energy regime and omits residual long-range interactions. Particularly for these cases the VdW model is physically more accurate. On the one hand its finite interaction energies offer new degrees of freedom (DOFs) which promise new possibilities and qualitatively new behavior in the regime of intermediate energies. On the other hand the long-range interaction energies between atom perturb structures constructed in the PXP model which introduces new difficulties. In this thesis we focus on the VdW model unless stated otherwise. Nevertheless many statements and findings are valid for different γ-models (for finite $\gamma < \infty$) as well or may be generalized straightforwardly.

Blockade Radii. In analogy to the PXP model we can also introduce the concept of blockade radii in other γ-models. For each atom $\mathfrak{i} \in \mathcal{N}$ we associate a blockade radius $r_{B,\mathfrak{i}} = (C/\Delta_{\mathfrak{i}})^{1/\gamma}$ which is defined as the radius of atom $\mathfrak{i}$ where the interaction energy with a test atom would equal the detuning $\Delta_{\mathfrak{i}}$. For finite $\gamma < \infty$ the blockade radii will be in general different for different atoms however the dependence on the detuning becomes quite weak for large $\gamma \gg 1$. Note that in the limit $\gamma \to \infty$ we recover the unit blockade radii $r_{B,\mathfrak{i}} = 1$ of the PXP model. Two atoms are then said to be *in blockade* with each other if at least one of the atoms lies in the blockade radius of the other atom. In this case the state where just one atom (the atom with the larger detuning) is excited is energetically favorable compared to the state where both atoms are excited simultaneously. This allows us to generalize the concept of a *blockade graph* $\mathcal{B} = (V, E)$ to different γ-models. The concept of blockade radii and the blockade graph is going to be used all over this thesis. The reader should be aware however that these concepts lose some physical relevance for finite $\gamma \ll \infty$. While the concepts encompass the VdW interaction between two atoms, the physics of more than two atoms is not fully portrayed by these concepts.

Example 1. (Blockade Radii in the VdW model)

> For instance consider the case of three atoms where no two atoms are in blockade with each other in the VdW model. The state where all three atoms are excited simultaneously might still be energetically disfavourable compared to the states where only two or one atoms are excited. This is the case if their distances are (barely) larger than the blockade radii however the sum of any two interactions is larger than the third detuning. One could interpret this as a 'collective blockade radius'.

Nevertheless the blockade radii are going to be useful for a clear visualization of the geometry and to obtain a notion of distance in plots especially in $d = 2$ dimensions. The blockade graph only contains edges between nearby atoms and offers a quick overview of vicinity of atoms.

2.2 | Languages, L-Manifolds and L-Complexes

The goal of this thesis is going to be to construct structures $\mathcal{C}$ such that the Hamiltonian $H[\mathcal{C}]$ possesses a gapped low-energy eigenspace $\mathcal{H}_0 = \mathcal{H}_0[H[\mathcal{C}]]$ 'equal' to some target Hilbert space $\mathcal{H}_t$. More precisely, we are interested in target Hilbert spaces defined by some (formal) language L on the binary alphabet $\mathbb{F}_2 = \{0,\ 1\}$ in the following way: A *word* $\boldsymbol{x} = (x_1, \dots\ x_N) \in \mathbb{F}_2^N$ on the binary alphabet is a string of *letters* (also called *bits*) $x_i \in \mathbb{F}_2$ of the alphabet. The set of all words is denoted by $\mathbb{F}_2^* = \bigcup_{N\in\mathbb{N}} \mathbb{F}_2^N$. A (formal) *language* is then defined as a set of words $L \subseteq \mathbb{F}_2^*$. in the following we are interested in uniform languages with words of equal length N, i.e. $L \subseteq \mathbb{F}_2^N$. Such a uniform language naturally defines a Hilbert space called *L-manifold* via the linear span

$$\mathcal{H}(L) = \mathrm{span}\left(\{|\boldsymbol{x}\rangle \mid \boldsymbol{x} \in L\}\right) \leq (\mathbb{C}^2)^{\otimes N}, \tag{2.2}$$

where we identified the words $\boldsymbol{x} \simeq |\boldsymbol{x}\rangle$ with vectors and L as the spanning set of vectors. The language realizing a target Hilbert space $\mathcal{H}_t = \mathcal{H}(L)$ is also denoted the target language L_t or the ground state manifold $\mathcal{G}$, its words $\boldsymbol{x} \in \mathcal{G}$ are called the *ground states*. Conversely, the words of the same length which are not element of the target language are called the *excited states* and they define the excited state manifold $\mathcal{E} = \mathbb{F}_2^N \backslash \mathcal{G}$. The length of the ground state manifold will be denoted by $g = |\mathcal{G}|$ and the length of the excited state manifold will be denoted by $e = |\mathcal{E}|$. It is easy to see that $g + e = 2^N$. In the following we are particularly interested in two families of target languages: tessellated languages and Boolean languages. We start by introducing latter concept.

Boolean target Languages. Consider some Boolean function $v : \mathbb{F}_2^k \to \mathbb{F}_2^m$ of arity $k \in \mathbb{N}$ with $m \in \mathbb{N}_{\geq 1}$. For $m = 1$ the Boolean function v is scalar, for $m > 1$ it is vector-valued. It naturally defines a *Boolean language*

$$L[v] = \{(x_1, \dots\ x_k, y_1, \dots\ y_m) \mid \boldsymbol{x} \in \mathbb{F}_2^k,\ \boldsymbol{y} = v(\boldsymbol{x})\} \subset \mathbb{F}_2^{k+m} \tag{2.3}$$

where each word equals one row of its truth table. Languages of this family possess 2^k words. Note that there exist a total of $2^{2^k m}$ Boolean functions with dimension m of the codomain and arity k of which $2^{(k+1)m}$ are symmetric (this will become important later).

Tessellated target Languages. The second family of languages studied in this thesis are tessellated languages on lattices. Consider for simplicity a finite square lattice $\mathcal{L}$ with periodic boundary conditions and one vertex per lattice point. The set of vertices is denoted by $\mathcal{V}(\mathcal{L})$ and is of cardinality V, the set of the edges is denoted by $\mathcal{E}(\mathcal{L})$ and is of cardinality E. With each edge $e \in \mathcal{E}(\mathcal{L})$ we associate K classical bits (in the following usually $K = 1$) and which each vertex $v \in \mathcal{V}(\mathcal{L})$ we associate M classical bits. The number of bits on edges is called $k = KE$,

the number of bits on vertices is called $m = MV$. The generalization to non-square lattices, different boundary conditions or larger bases is straightforward.

The system is described by a bit configuration $\boldsymbol{x} \in \mathbb{F}_2^{k+m}$ assigning every bit $x_i \in \mathbb{F}_2$ a BOOLEAN value. For each vertex $v \in \mathcal{V}(\mathcal{L})$ we define a bit-projector $P_v : \mathbb{F}_2^{k+m} \to \mathbb{F}_2^{4K}$ which maps a bit configuration to the bits on the edges $e_1, \dots e_4 \in \mathcal{E}(\mathcal{L})$ emanating from vertex v: $P_v(\boldsymbol{x}) = (x_{e_1,1}, \dots x_{e_4,K})$. A *tessellated language* $L_{\mathcal{L}}[f_c] = L_{\mathcal{L}}[f_c; w]$ in some *realization* $w : \mathbb{F}_2^{4K} \to \mathbb{F}_2^M$ is defined as the set of words which locally fulfill the *check function* $f_c : \mathbb{F}_2^{4K} \to \mathbb{F}_2$ for each vertex $v \in \mathcal{V}(\mathcal{L})$:

$$L_{\mathcal{L}}[f_c] = \left\{ (x_{e_1,1}, \dots y_{v_V,M}) \;\middle|\; \forall v \in \mathcal{V}(\mathcal{L}) : \; f_c(P_v(\boldsymbol{x})) = 1, \; \boldsymbol{y}_v = w(P_v(\boldsymbol{x})) \right\}. \tag{2.4}$$

The first k letters correspond to the bit configuration on the edges, the last m letters correspond to the bit configuration on the vertices. Both the realization w and the check function f_c are BOOLEAN functions, however latter is scalar and former may be vectorial. The check function is effectively constraining the domain of w. The Hilbert space realized by a tessellated language is called a *tessellated Hilbert space* $\mathcal{H}_{\mathcal{L}}[f_c] = \mathcal{H}(L_{\mathcal{L}}[f_c])$. It is the state space of a system of $k+m$ *qubits* with K qubits placed on each edge $e \in \mathcal{E}(\mathcal{L})$ and M qubits placed on each vertex $v \in \mathcal{V}(\mathcal{L})$ locally realizing the check function f_c and the BOOLEAN function w.

Rydberg L-complexes. The structure $\mathcal{C}$ together with a tuple $(\mathcal{K}, \mathcal{Q})$ of disjoint sets of atoms defines a *(Rydberg) complex* $\mathcal{C}_{\mathcal{K}}^{\mathcal{Q}}$ (independent of any language). Consider a structure $\mathcal{C}$ of N atoms and a (Boolean or tessellated) language L with words of length $k+m = N$. For a BOOLEAN language we choose $q \in \mathbb{N}_{\leq m}$ (in the following usually $q \in \{1, 2, 3\}$), for a tessellated language choose $q = 0$. To connect the two notions of languages and complexes we define a *(bijective) labeling function*

$$\mathfrak{L} : \{1, \dots k+m\} \to \mathcal{N} \tag{2.5}$$

which identifies letter positions and atoms one-to-one. When given a labeling $\mathfrak{L}$ we can thus use the notions of atoms and indices interchangeably. We define $\mathcal{K} = \mathfrak{L}(\{1, \dots k\})$ and $\mathcal{Q} = \mathfrak{L}(\{1+k, \dots k+q\})$. This defines the complex $\mathcal{C}_{\mathcal{K}}^{\mathcal{Q}}$ with $|\mathcal{K}| = k$ and $|\mathcal{Q}| = q$. The triple $(\mathcal{C}_{\mathcal{K}}^{\mathcal{Q}}, L, \mathfrak{L})$ is called a *(Rydberg) L-complex*.

Further we define $\mathcal{P} = \dot{\bigcup}_{\mathcal{K},\mathcal{Q}}$ with $p = |\mathcal{P}|$ and $\mathcal{A} = \mathcal{N} \backslash \mathcal{P}$ with $a = |\mathcal{A}|$ accordingly. We call the atoms in $\mathcal{K}$ the *input ports*, the atoms in $\mathcal{Q}$ the *output ports*, the atoms in their union $\mathcal{P}$ the *ports* and the remaining atoms $\mathcal{A}$ the *ancillas*. The inverse labeling $\mathfrak{L}^{-1}$ associates with each set of atoms a set letter positions which we call *input bits*, *output bits*, *port bits* or *ancillary bits* respectively. Via $\mathfrak{L}$ the bits define the states of their atoms.

As the $m = q + a$ output and ancillary bits of the languages are (Boolean) functions of the k input bits they do not introduce additional degrees of freedom (DOFs) in the language. In the L-complex of a BOOLEAN language v we can define the projection of v on the output bits,

$$f_b : \mathbb{F}_2^k \to \mathbb{F}_2^q : \boldsymbol{x} \mapsto (v_1(\boldsymbol{x}), \dots v_q(\boldsymbol{x})), \tag{2.6}$$

and on the ancillary bits,

$$w : \mathbb{F}_2^k \to \mathbb{F}_2^a : \boldsymbol{x} \mapsto (v_{1+q}(\boldsymbol{x}), \dots v_{q+a}(\boldsymbol{x})). \tag{2.7}$$

In the reverse we write

$$v \equiv (f_b, w) : \mathbb{F}_2^k \to \mathbb{F}_2^m : \boldsymbol{x} \mapsto ((f_b)_1(\boldsymbol{x}), \dots (f_b)_q(\boldsymbol{x}), w_1(\boldsymbol{x}), \dots w_a(\boldsymbol{x})) \tag{2.8}$$

as the concatenation of f_b and w. The projected (vectorial) BOOLEAN f_b is called the *logical connective* (of the L-complex) and the L-complex is called the *logic gate* (of the BOOLEAN v). Its orthogonal projection w is called the *realization* (just as with tessellated languages), it determines the state of the ancillas. The ancillas are (often) needed to adjust the energy structure of the L-complex. For simplicity of notation we sometimes write $L[f_b] = L[f_b; w] \equiv L[v]$ to denote a BOOLEAN language and $L_{\mathcal{L}}[f_c] = L_{\mathcal{L}}[f_c; w]$ to denote a tessellated language. The projected BOOLEAN f_b and the check function f_c are jointly called *target functions* f_t. For one target function f_t there exist many different realizations w.

At this point it is to stress that that the introduced terminology is inspired from the common usage in electronic circuits. However in the present context there is no dynamics involved (we never wrote down any equation of motion) in the sense that information is flowing into the input ports and exits the output ports. Secondly, although the definitions and notation is closely related to the formalism introduced by STASTNY *et al.* [38], it slightly deviates at some points (e.g. the definitions of the languages in (2.3) and (2.4) include ancillary bits which makes the labeling function (2.5) is bijective).

2.3 | Setting the Objective

With the newly defined concepts we can summarize the main goal of this thesis as following:

> Given some uniform target language L_t we want to construct L-complexes $(\mathcal{C}^{\mathcal{Q}}_{\mathcal{K}}, L_t, \mathfrak{L})$ such that the Hamiltonian $H[\mathcal{C}]$ (cf. eq. (2.1)) realizes the target Hilbert space $\mathcal{H}_t = \mathcal{H}(L_t)$ (cf. eq. (2.2)) as its gapped low-energy eigenspace $\mathcal{H}_0 = \mathcal{H}_0[H; \mathcal{C}]$:
>
> $$\mathcal{H}_0 \overset{!}{\cong}_{\mathfrak{L}} \mathcal{H}_t \tag{2.9}$$
>
> The languages we are particularly interested in are BOOLEAN languages $L[w]$ (cf. eq. (2.3)) and tessellated languages $L_{\mathcal{L}}[f_c]$ (cf. eq. (2.4)) given by some target function f_t (and a grid $\mathcal{L}$).

If eq. (2.9) is fulfilled by the the complex we say the complex '*implements*' the target Hilbert space, the target language or the target function. To keep track of the different quantities and steps in the construction it is important to stick to a precise language. Thus we are strictly separating the notion of a *realization* w which defines the L-manifold $\mathcal{H}_t = \mathcal{H}(L[f_t; w])$, and the notion of an *implementation* $\mathcal{C}^{\mathcal{Q}}_{\mathcal{K}}$ of $\mathcal{H}_t$.

Loosely speaking the construction (2.9) can be understood as a 'reverse-engineering' process where we want to construct the inverse of the mapping $\mathcal{H}_0[H; \bullet]$ on the structure $\mathcal{C}$ (with labeling $\mathfrak{L}$) for a given target Hilbert space $\mathcal{H}_t$. However this mapping is neither injective and nor surjective. Before we can start the construction we have to think about what realizations w could be eligible and why others are not. Then we have to find a structure of length $N = p + a$

with an g-fold gapped low-energy eigenspace and determine a fitting labeling such that the L-complex implements the target L-manifold, i.e. that the words in the target language map one-to-one to the low-energy eigenstates. Obviously not every g-fold gapped low-energy eigenspace can be interpreted by a labeling can be interpreted by some labeling as a given language L. However a structure might be interpreted as different languages by different labelings. Hence the construction of an L-complex for a given target poses a highly non-trivial question. Especially for large target languages this makes a *reductionist approach* most promising.

2.4 | A reductionist Approach

We are going to start by constructing (small) '*primitives*' of L-complexes and we construct larger ones by gluing the primitives together. This process is called *amalgamation* and was first introduced by Stastny *et al.* in [38] for the PXP model. In the following we are going to introduce the mathematical framework to this process for the VdW model.

Consider two L-complexes $(\mathcal{C}_1{}^{\mathcal{Q}_1}_{\mathcal{K}_1}, L_1, \mathfrak{L}_1)$ and $(\mathcal{C}_2{}^{\mathcal{Q}_2}_{\mathcal{K}_2}, L_2, \mathfrak{L}_2)$. In the following the subscripts $l \in I = \{1, 2\}$ index the languages and structures and their properties. We start by introducing a concept to combine their languages.

The γ-Product of Languages. Let $\gamma \subset \{(n_1, n_2) \mid \forall_{l\in I} : n_l \in \{1, \dots p_l\}\}$ be a set of tuples of port indices where the tuples are pairwise distinct in *both* arguments. Let $\gamma_l = \{n_l \mid (n_1, n_2) \in \gamma\}$ such that $|\gamma| = |\gamma_l|$ for $l \in I$. For a word $\boldsymbol{x}_l \in L_l$, let $\boldsymbol{x}_l/\gamma_l$ denote the word where the bits at the indices in γ_l are removed.

We define the γ-*product* of L_1 and L_2 as

$$L_\gamma = L_1 \otimes_\gamma L_2 = \{\boldsymbol{x}_1 \otimes_\gamma (\boldsymbol{x}_2/\gamma_2) \mid \boldsymbol{x}_l \in L_l, \forall_{(n_1,n_2)\in\gamma} : (x_1)_{n_1} = (x_2)_{n_2}\}. \tag{2.10}$$

This is a language with words of length $N_\gamma = N_1 + N_2 - |\gamma|$. The construction restricts to pairs of words from L_1 and L_2 fulfilling the *compatibility condition*: $(x_1)_{n_1} = (x_2)_{n_2}$ for every $(n_1, n_2) \in \gamma$. Then $\otimes_\gamma : \mathbb{F}_2^{N_1} \times \mathbb{F}_2^{N_2-|\gamma_2|} \to \mathbb{F}_2^{N_\gamma}$ concatenates the words and orders the letters such that the first letters are the input bits followed by the output bits and the last letters are the ancillary bits. Therefore the lengths of the words are *added* (up to the number $|\gamma|$ of redundant letters) while the lengths of the languages are *multiplied* (up to the words not fulfilling compatibility condition).

The bits $(x_1)_{n_1} = (x_2)_{n_2}$ of $(n_1, n_2) \in \gamma$ are identified as input bits or ancillary bits depending on the context:

1 | If we concatenate two Boolean languages where γ_l are output bit indices and γ_{3-l} are input bit indices then the concatenated bits provide redundant information (they functions of the input bits of L_l). Thus they should be interpreted as ancillary bits. Thus the number of input and output port for the γ-product is $k_\gamma = k_l + k_{3-l} - |\gamma|$ and $q_\gamma = q_l + q_{3-l} - |\gamma|$ respectively.

2 | If we concatenate two tessellated languages where γ_l and γ_{3-l} are input bit indices then the bits of the concatenated language are still interpreted as input bits. This defines the number of input and output ports $k_\gamma = k_l + k_{3-l} - |\gamma|$ and $q_\gamma = 0$.

L-manifold. The L-manifold defined by L_γ is $\mathcal{H}(L_\gamma) = \mathcal{H}(L_1 \otimes_\gamma L_2) \leq (\mathbb{C}^2)^{\otimes N_\gamma}$. It is isomorphic to a quotient space of the tensor product:

$$\mathcal{H}(L_\gamma) \cong [\mathcal{H}(L_1) \otimes \mathcal{H}(L_2)]/\mathrm{span}(\{|\boldsymbol{x}_1\rangle|\boldsymbol{x}_2\rangle \mid \boldsymbol{x}_l \in L_l, \exists_{(n_1,n_2)\in\gamma} : (x_1)_{n_1} \neq (x_2)_{n_2}\}). \tag{2.11}$$

The isomorphism corresponds to the projection of vectors fulfilling the compatibility condition to vectors with the (redundant) components removed, and a relabeling of the basis vectors. In that sense the γ-product can be understood as the 'partial product' of languages constraint by the compatibility condition.

The Amalgamation of Structures. The definition of the γ-product of L_1 and L_2 is useful because it is paralleled by the combination of their structures $\mathcal{C}_l = (\boldsymbol{r}_\mathfrak{i}^{(l)}, \Delta_\mathfrak{i}^{(l)} \mid \mathfrak{i} \in \mathcal{N}_l)$ called *amalgamation*. Consider a set γ of tuples of port indices such that $L_\gamma \neq \emptyset$. We assume that the ports $\mathfrak{L}_l(\gamma_l)$ are located at the boundary of their structure $\mathcal{C}_l$. Further we assume that the structures do not overlap in their geometry but that the ports identified by γ are at the same position: $\boldsymbol{r}^{(1)}_{\mathfrak{L}_1(n_1)} = \boldsymbol{r}^{(2)}_{\mathfrak{L}_2(n_2)}$ for each $(n_1, n_2) \in \gamma$.

We can then combine the two structures by identifying the atoms paired in γ, i.e. for all $(n_1, n_2) \in \gamma$ we consider $\mathfrak{L}_1(n_1) = \mathfrak{L}_2(n_2)$ the same atom. Thus $\mathcal{N}_1$ and $\mathcal{N}_2$ have the intersection $\mathcal{N}_1 \cap \mathcal{N}_2 = \mathfrak{L}_l(\gamma_l)$ of length $|\gamma|$. We label $\mathcal{N}_\gamma = \mathcal{N}_1 \cup \mathcal{N}_2$ the amalgamated set of atom which is now of length $N_\gamma = |\mathcal{N}_\gamma| = N_1 + N_2 - |\gamma|$. The amalgamated structure $\mathcal{C}_\gamma = (\boldsymbol{r}_\mathfrak{i}^{(\gamma)}, \Delta_\mathfrak{i}^{(\gamma)} \mid i \in \mathcal{N}_\gamma)$ consists of positions $\boldsymbol{r}_\mathfrak{i}^{(\gamma)} = \boldsymbol{r}_\mathfrak{i}^{(l)}$ for $\mathfrak{i} \in \mathcal{N}_l$[1] and detunings $\Delta_\mathfrak{i}^{(\gamma)} = \Delta_\mathfrak{i}^{(l)}$ for $\mathfrak{i} \in \mathcal{N}_l \triangle \mathcal{N}_{3-l}$ and

$$\Delta_\mathfrak{i}^{(\gamma)} = \Delta_\mathfrak{i}^{(1)} + \Delta_\mathfrak{i}^{(2)} \tag{2.12}$$

for $\mathfrak{i} \in \mathcal{N}_1 \cap \mathcal{N}_2$.

The labeling $\mathfrak{L}_\gamma : \{1, \dots N_\gamma\} \to \mathcal{N}_\gamma$ is naturally defined by the labelings $\mathfrak{L}_1$ and $\mathfrak{L}_2$ (and the ordering in $\otimes_\gamma$). Again, the labeling defines the set of input ports $\mathcal{K}_\gamma = \mathfrak{L}_\gamma(\{1, \dots k_\gamma\})$, the set of output ports $\mathcal{Q}_\gamma = \mathfrak{L}_\gamma(\{1 + k_\gamma, \dots k_\gamma + q_\gamma\})$, the set of ports $\mathcal{P}_\gamma = \dot{\bigcup}_{\mathcal{K}_\gamma, \mathcal{Q}_\gamma}$ with $p_\gamma = |\mathcal{P}_\gamma|$ and the set of ancillaries $\mathcal{A}_\gamma = \mathcal{N}_\gamma \backslash \mathcal{P}_\gamma$ with $a_\gamma = |\mathcal{A}_\gamma|$. This yields the *amalgamated L-complex* $(\mathcal{C}_{\gamma\mathcal{K}_\gamma}^{\mathcal{Q}_\gamma}, L_\gamma, \mathfrak{L}_\gamma)$.

The interaction Hamiltonian. The Hamiltonian of the amalgamated structure is the sum of the Hamiltonians of the subcomplexes plus an additional correction term:

$$H[\mathcal{C}_\gamma] = (H[\mathcal{C}_1] + H[\mathcal{C}_2] + H_{\mathrm{int}}[\mathcal{C}_1; \mathcal{C}_2])_{\mathfrak{L}_{1,2}(\gamma)}\,. \tag{2.13}$$

The index formally notes that atoms $\mathfrak{L}_1(n_1)$ and $\mathfrak{L}_2(n_2)$ associated by their indices $(n_1, n_2) \in \gamma$ are identified. For $\mathfrak{i} \in \mathcal{N}_1 \cap \mathcal{N}_2$, the eigenenergies of the terms $-\Delta_\mathfrak{i}^{(1)} n_\mathfrak{i}$ and $-\Delta_\mathfrak{i}^{(2)} n_\mathfrak{i}$ add up

[1] It is $\boldsymbol{r}_\mathfrak{i}^{(1)} = \boldsymbol{r}_\mathfrak{i}^{(2)}$ for $\mathfrak{i} \in \mathcal{N}_1 \cap \mathcal{N}_2$ by assumption thus this is well-defined.

as defined previously; this yields $-\Delta_{\mathfrak{i}}^{(\gamma)} n_{\mathfrak{i}}$. H_{int} denotes the additional interactions arising in-between atoms of different subcomplexes minus the double-counted interactions in-between ports of their intersection:

$$H_{\text{int}} = \left(\sum_{\mathfrak{i}\in\mathcal{N}_1\setminus\mathcal{N}_2,\ \mathfrak{j}\in\mathcal{N}_2\setminus\mathcal{N}_1} - \frac{1}{2} \sum_{\mathfrak{i}\neq\mathfrak{j}\in\mathcal{N}_1\cap\mathcal{N}_2} \right) U_{\text{VdW}}(r_{\mathfrak{ij}}) n_{\mathfrak{i}} n_{\mathfrak{j}}. \tag{2.14}$$

In the PXP model $H_{\text{int}} = 0$ vanishes and the Hamiltonian $H[\mathcal{C}_\gamma]$ splits into the Hamiltonians of its parts. Lets assume that $\mathcal{C}_l {}^{\mathfrak{Q}_l}_{\mathcal{K}_l}$ implements L_l via $\mathfrak{L}_l$ in the PXP model. Then for the PXP model the amalgamated complex $\mathcal{C}_\gamma {}^{\mathfrak{Q}_\gamma}_{\mathcal{K}_\gamma}$ implements the amalgamated language L_γ with the derived labeling $\mathfrak{L}_\gamma$: The eigenenergies of $H[\mathcal{C}_\gamma]$ are lower bounded by the lowest eigenenergies of its summands $H[\mathcal{C}_l]$. This lower bound is only realized by the words $\boldsymbol{x} \in L_\gamma \neq \emptyset$.

In the VdW model the interaction term $H_{\text{int}} \neq 0$ does not vanish and is in general different for each eigenstate. This poses new challenges: even though the VdW interactions decay quickly for large distances, the interaction term is in general sufficiently large such that it can not be neglected. By amalgamating multiple primitives their VdW interactions might add up and disarrange the energy structure. For BOOLEAN languages and for tessellated languages this will be discussed in sec. 7 and sec. 6 respectively. For the moment however, we are going to ignore this issue and continue formalizing the mathematical framework.

2.5 | Measures of Quality

We have now formulated a mathematical framework to construct (large) L-complexes from (small) primitives by the process of amalgamation as a reductionist approach to solve eq. (2.9). However it is interesting for academic reasons as well as relevant for an experimental implementation to minimize the number of atoms in the L-complex. In particular we are interested in determining the minimal primitives which realize a given target f_t. Secondly, we want to quantify (and possibly maximize) the quality of an implementation via the low-energy eigenspace $\mathcal{H}_0[\mathcal{C}]$. Thus we have to find some measure by which we determine the quality. Both goals, the minimization of the number of atoms and the maximization of the quality, might interfere with each other. In that cases the experimentalist has to choose the measure.

Counting Degrees of Freedom. The structure $\mathcal{C}$ possesses dN degrees of freedom (DOFs) in its geometry $\mathcal{G}_\mathcal{C}$ and further N DOFs in its detunings $\Delta_\mathcal{C}$. However, in the Hamiltonian only relative distances $\boldsymbol{r}_{\mathfrak{ij}}$ are relevant. Thus the energy structure remains invariant under $d(d-1)/2$ rotations and d translations. Furthermore for any $\alpha \in \mathbb{R}_{\neq 0}$ the mapping

$$f_\alpha \ : \ \mathcal{C} = (\boldsymbol{r}_{\mathfrak{i}}, \Delta_{\mathfrak{i}} \mid \mathfrak{i} \in \mathcal{N}) \mapsto \tilde{\mathcal{C}} = (\boldsymbol{r}_{\mathfrak{i}}/\alpha, \alpha^6 \Delta_{\mathfrak{i}} \mid \mathfrak{i} \in \mathcal{N}) \tag{2.15}$$

only rescales the Hamiltonian (and its energy eigenvalues) by a factor of α^6: $H[\tilde{\mathcal{C}}] = \alpha^6 H[\mathcal{C}]$. This does not impact the energy structure in any meaningful way and leaves ratios of energies invariant. Thus the energy structure is fully determined by only $(d+1)(N-d/2)-1$ DOFs. Formally speaking we have an equivalence class of $(d+1)d/2+1$ physically similar structures. As a representative we typically choose a structure where $\Delta_{\max} = \max_{\mathfrak{i}\in\mathcal{N}} \Delta_{\mathfrak{i}} = 1$, i.e. we choose $\alpha = 1/\Delta_{\max}^{1/6}$ as normalization, or we measure in units of $\Delta_{\max}$.

Lastly note that we did not yet fix the interaction strength C as a constant in the Hamiltonian. Choosing a different (repulsive) interaction strength $\tilde{C} = \alpha C$ for $\alpha \in \mathbb{R}_{>0}$ is equal to a simple rescaling of the geometry $\mathcal{G}_{\mathcal{C}}$ by $\alpha^{1/6}$. A useful notion of distance is given by the blockade radii. In the following we are often going to measure in units of $r_{B,\min} = (C/\Delta_{\max})^{1/6}$ or draw the blockade radii.

The Quality Factor. As the Hamiltonian is scale invariant (up to some factor) we should define unit-free quantities to describe and judge the quality of the implementation. It is intuitive to start by defining the *spectral width* or *energy splitting*

$$\delta E = \max_{\boldsymbol{x}\in\mathcal{G}} E(|\boldsymbol{x}\rangle) - \min_{\boldsymbol{x}\in\mathcal{G}} E(|\boldsymbol{x}\rangle) \tag{2.16}$$

and the *energy gap*

$$\Delta E = \min_{\boldsymbol{x}\in\mathcal{E}} E(|\boldsymbol{x}\rangle) - \max_{\boldsymbol{x}\in\mathcal{G}} E(|\boldsymbol{x}\rangle) \tag{2.17}$$

as two important characteristics of $\mathcal{H}_0$. $E(|\boldsymbol{x}\rangle) = \langle H[\mathcal{C}]\rangle_{\boldsymbol{x}}$ denotes the energy eigenvalue of the Hamiltonian with respect to the word $\boldsymbol{x} \in \mathbb{F}_2^N = \mathcal{G} \dot\cup \mathcal{E}$. By definition $\delta E \geq 0$ is non-negative but ΔE may become negative if there exists an eigenstate $|\boldsymbol{x}\rangle \notin \mathcal{H}(L_t)$ of lower energy than an eigenstate in $\mathcal{H}(L_t)$. We can now introduce their *ratio*

$$Q = \delta E/\Delta E. \tag{2.18}$$

The ratio is unit-free and thus scale invariant and it is crucial in latter discussion. It is in some sense the natural measure for the energy structure. However the ratio may still diverge and become negative for vanishing or negative energy gap. Thus a reasonable choice for a *quality factor* would be

$$\mathcal{Q} = \left\{ \begin{array}{ll} \exp -Q, & \text{if } Q \geq 0 \\ 0, & \text{if } Q < 0 \end{array} \right\} = \Theta(Q)\exp(-Q). \tag{2.19}$$

Here Θ denotes the Heaviside (unit) step function which is one if the argument is greater-equal zero and zero else. The quality factor is one if $\mathcal{H}_0 = \mathcal{H}_t$ is the degenerate and gapped low-energy eigenspace of the Hamiltonian. Note that this is independent of the size of the energy gap for a vanishing energy splitting. The larger the energy splitting compared to the energy gap the more the quality decreases. The quality converges to zero as the energy gap vanishes.

The Robustness. The quality factor is a useful measure of quality and we are going to use in many cases. However for the case of a degenerate and gapped low-energy eigenspace $\mathcal{H}_0 = \mathcal{H}_t$ it does not yields any information about the size of the energy gap relative to the energy scaling. Thus it is useful to define the unit-free *robustness*

$$r = \max_{\mathfrak{i} \in \mathcal{N}} \Delta E / \Delta_{\mathfrak{i}} \leq_L 1 \tag{2.20}$$

of the realization as the ratio of the energy gap to the smallest detuning. The robustness quantifies the stability of the structure against perturbations. If there are multiple structures of unit quality factor an experimentalist might prefer a realization of larger robustness even if non-minimal in the number of atoms. The robustness is upper-bounded by one for the families of target languages we are interested in for this thesis. This is formally noted by the index $_L$ of the inequality symbol (we refer to app. 2.A for a more detailed discussion):

Proof 1. (An upper Bound to the Robustness)

We may assume that every bit is excited at least once in the ground state manifold due to ass. 2. Consider an atom $\mathfrak{i} = \mathfrak{L}(i) \in \mathcal{N}$ with the smallest detuning $\Delta_{\mathfrak{i}} = \Delta_{\min}$ and some word $\boldsymbol{x} \in L_t$ with $x_i = 1$. As we assume repulsive interactions between excited atoms the state $|\tilde{\boldsymbol{x}}\rangle = |x_1, \dots\ 0_i, \dots x_N\rangle$ is of energy $E(|\tilde{\boldsymbol{x}}\rangle) \leq E(|\boldsymbol{x}\rangle) + \Delta_{\mathfrak{L}(i)}$. We can now assume that the derived word $\tilde{\boldsymbol{x}} \notin_L L_t$ for some $\boldsymbol{x} \in L_t$ with $x_i = 1$ and formally note this by an index $_L$. Note that this is going to be fulfilled for the target languages of this thesis; for every BOOLEAN language and for most tessellated languages. This assumption is discussed in more detail in app. 2.A. Then the energy gap $\Delta E \leq_L \Delta_{\mathfrak{i}} = \Delta_{\min}$ is upper-bounded by the smallest detuning and thus the robustness $r \leq_L 1$ by one. □

The robustness is a particularly interesting quantity as in the PXP model every L-complex with quality factor $\mathcal{Q} = 1$ possesses robustness $r = 1$ due to the lack of long range interactions. In that sense the above inequality is sharp. Note that in Ref. [38, 37] STASTNY *et al.* choose $\Delta_{\min} = \min_{\mathfrak{i} \in \mathcal{N}} \Delta_{\mathfrak{i}} = 1$ as energy scaling for the PXP model. Thus they obtain a unit energy gap $r \equiv \Delta E = 1$ for every L-complex. In the PXP model the robustness is natural choice as a measurement for the energy gap.

The Effective Energy Gap. However, for an experimentalist it might be more interesting to consider the ratio of the energy gap to the largest detuning which determines the largest energy scale the experimentalist has to control. We thus define the *effective (energy) gap*

$$\Delta E_{\text{eff}} = \min_{\mathfrak{i} \in \mathcal{N}} \Delta E / \Delta_{\mathfrak{i}} \leq 1 \tag{2.21}$$

as the energy gap in units of the largest detuning. It is unit-free and thus scale invariant as well. The effective gap is smaller than the robustness by the ratio of the detunings. Therefore the effective gap is usually not one in the PXP model. More precisely STASTNY *et al.* showed that in the PXP model "all BOOLEAN functions can be realized by a complex with bounded detuning range $\{1\Delta, 2\Delta, 3\Delta\}$"[38] and thus $\Delta E_{\text{eff}} \geq 1/3$ for the PXP model[2]. The effective gap is upper-bounded by one as well.

[2] This however may contradict minimality in the number of atoms.

Proof 2. (An upper Bound to the effective Gap)

The effective gap is upper-bounded by the robustness which is upper-bounded by one for the target languages of this thesis; for any BOOLEAN language and most tessellated languages. We thus only have to discuss the tessellated languages where $r > 1$ is possible. $\Delta E > \Delta_{\max}$ could only be the case if the derived word $\tilde{\boldsymbol{x}} = (x_1, \dots\ 0_i, \dots x_N) \in L_t$ for any word $(\boldsymbol{x}\rangle \in L$ and any $i \in \{1, \dots N\}$. Then (if $L \neq \emptyset$) the zero-word $\mathbf{0} = (0, \dots 0) \in L$ would be element of the language. We do not consider such languages by ass. 4 as they can not be successfully realized in this model anyway. Therefore the energy gap $\Delta E \leq \Delta_{\mathfrak{L}(i)}$ is upper-bounded by the largest detuning and thus the effective energy gap $\Delta E_{\text{eff}} \leq 1$ by one. □

This inequality is generally less sharp than for the robustness as the effective gap is smaller and generally smaller one in the PXP model. However this inequality is valid for *every* language (which is not the case for the robustness). Thus we do not add an index to the inequality symbol.

At this point it is to note that the definition of the effective gap is not redundant to the definition of the robustness. There exist complexes which implement a language with unit quality $\mathcal{Q} = 1$ on a finite-size sub-manifold of the parameter space on which the effective gap and the robustness are maximized for disjoint sets of parameters (cf. fig. 4.3). Here the effective gap turns out the more useful measure because the robustness it artificially increased by arbitrarily suppressing the lowest detuning compared to the other detunings. This decreases the effective gap but still increases the robustness. As we are not interested in such limiting cases we generally stick to the effective gap as measure of quality (e.g. during optimization via algorithm 3.2). Still for all structures we mention the robustness as a comparison to the PXP case from Ref. [38].

2.6 | Some general Remarks

In the end of this section we want to make some general remarks and assumptions about the languages and structures we want to consider in the following thesis.

0 | We only consider *non-constant* target languages L_t of length $g = |L_t| \geq 2$ because target languages of length $g = 0, 1$ are physically not interesting. Such languages would be realizing e.g. constant BOOLEAN functions or tessellated languages without DOFs.

1 | We do not consider *factorizable languages*, i.e. languages $L_\emptyset = L_1 \otimes_\emptyset L_2$ that are amalgamations with $\gamma = \emptyset$. For such languages the associated L-manifolds $\mathcal{H}(L_\emptyset) = \mathcal{H}(L_1) \otimes \mathcal{H}(L_2)$ would describe a tensor product. Such languages are simply implemented by the complexes of their factor languages placed in sufficiently large distances to suppress interactions. Therefore such languages are physically not interesting.

2 | Furthermore, we can restrict ourselves to target languages $L_t = L[f_t]$ where *each bit is excited at least once*. Otherwise we could delete the bit and remove its corresponding atom and obtain a L-complex which implements the same target function f_t with fewer atoms and a greater-equal quality and effective gap. Remember that this assumption is the starting point for proof 1.

3 | Thirdly, we restrict ourselves to positive detunings: informally we write $\Delta_{\mathcal{C}} > 0$. For the moment assume that the detuning $\Delta_{\mathfrak{i}} \leq 0$ of some atom $\mathfrak{i} = \mathfrak{L}(i)$ is not positive. Then it is never energetically favorable to excite atom $\mathfrak{i}$. We may assume that there exists a word $\boldsymbol{x} \in L_t$ with $x_i = 1$ by remark 2. Then the state $|\tilde{\boldsymbol{x}}\rangle \equiv |x_1, \dots 0_i, \dots x_N\rangle$ where atom $\mathfrak{i}$ is not excited is energetically lower than state $|\boldsymbol{x}\rangle \in \mathcal{H}(L)$ by at least $\Delta_{\mathfrak{i}}$[3]. Thus if the $\tilde{\boldsymbol{x}} \notin L_t$ (as for languages of this thesis or if $\mathfrak{i} \notin \mathcal{K}$) this would yields a negative energy gap $\Delta E \leq 0$. If word $\tilde{\boldsymbol{x}} \in L_t$ for all $\boldsymbol{x} \in L_t$ with $x_i = 1$ then we would obtain a finite energy splitting $\delta E \geq \Delta_{\mathfrak{i}}$ and therefore no good quality factor.

4 | We restrict ourselves to target languages $L_t = L[f_t]$ with the word $\mathbf{0} = (0, \dots 0) \notin L_t$. For positive detunings $\Delta_{\mathfrak{i}} > 0$ (motivated by remark 3) the unit vector state $|\boldsymbol{e}_i\rangle = |0, \dots 1_i, \dots 0\rangle$ would be of lower energy than the zero-vector $|\mathbf{0}\rangle$ by $\Delta_{\mathfrak{i}}$. If there are any ancillaries or output ports they would need to be a function of the input ports. Then there would exist some unit vectors $\boldsymbol{e}_i \notin L_t$ which would not be element of the target language. Thus we would have a negative energy gap $\Delta E < 0$. Note that this is the case for all languages of this thesis and all BOOLEAN languages. Even if $\boldsymbol{e}_i \in L_t$ would be all elements of the target language then we still have a finite energy splitting $\delta E \geq \Delta_{\max}$. As $\Delta E \leq \Delta E_{\max}$ from proof 2 this would imply $\mathcal{Q} \leq 1/e$ for the quality. Thus even for such artificial languages we would obtain a bad quality factor.

5 | Finally, it is useful to restrict ourselves to target languages where each bit is not excited at least once (analogous to ass. 2). This can be justified as a corollary of ass. 1 and ass. 0: Such a language would be factorizable into a constant factor language with $g = 1$.

6 | Lastly, we assume that no two atoms are located at the same position. Instead one should physically motivate a minimal distance $\boldsymbol{r}_{\min}$ and constrain $\boldsymbol{r}_{\mathfrak{ij}} \geq \boldsymbol{r}_{\min}$ in numerical simulations.

[3] If $\mathbf{0} \notin L_t$ by remark 4 then $\tilde{\boldsymbol{x}} \neq \mathbf{0}$ and this is a strict inequality due to finite interaction energies

| Appendix

2.A | An upper bound for the Robustness

This section is dedicated to discussing the limits of the assumptions made in proof 1. Remember that the assumptions are fulfilled for all languages of this thesis which justifies them *a posteriori*. In this section we find that the assumptions are justified more generally for all BOOLEAN languages. However, they may be violated for general tessellated languages. We formulate an example language which violates the assumption and thus violates the upper bound.

Consider the smallest detuning $\Delta_{\min} = \min_{\mathfrak{i}\in\mathcal{N}} \Delta_{\mathfrak{i}}$. Proof 1 is based on the assumption that there exists an atom $\mathfrak{i} = \mathfrak{L}(i) \in \mathcal{N}$ with $\Delta_{\mathfrak{i}} = \Delta_{\min}$ which is excited in some ground state $\boldsymbol{x} = (x_1, \dots 1_i, \dots x_N)$ but the derived state $\tilde{\boldsymbol{x}} = (x_1, \dots 0_i, \dots x_N) \in \mathcal{E}$ is an excited state. This is the case for all languages of this thesis. In the following we want to discuss the validity of this assumption for general languages.
By remark 2 we can assume that every atom is excited in some ground state. Thus the assumption is always fulfilled if for some $\mathfrak{i} \in \mathcal{N}$ with $\Delta_{\mathfrak{i}} = \Delta_{\min}$, $\mathfrak{i} \in \mathcal{A} \cup \mathcal{Q}$ is an ancillary or an output port because their state is a function v of the state of the input ports. Thus for such an atom $\mathfrak{i}$ the derived state must be an excited state. The assumption might only be not fulfilled if for every $\mathfrak{i} = \mathfrak{L}(i) \in \mathcal{N}$ with $\Delta_{\mathfrak{i}} = \Delta_{\min}$, $\mathfrak{i} \in \mathcal{K}$ is an input port.

Consider a BOOLEAN language where $f_t = f_b$. Then $v = (f_b, w)$ would need to be independent

of x_i. Such a language would (trivially) factorize:

$$L[f_b; w] = \{(0), (1)\} \otimes_\emptyset L[f_b; w]/\{i\}.$$

As discussed in remark 1, we do not want to consider factorizable languages as they are physically not interesting. The factorized input port $\mathfrak{i}$ does not influence the states of remaining atoms at all and does not convey any information. Such a language would be hard (or usually impossible) to realize in the VdW model with degenerate ground states as atom $\mathfrak{i}$ would need to be placed at a position where it interacts equally strong with every ground state of $L[f_b; w]/\{i\}$.

Consider a tessellated language with check function $f_t = f_c$. Again any atom $\mathfrak{i} = \mathfrak{L}(i) \in \mathcal{N}$ with $\Delta_\mathfrak{i} = \Delta_{\min}$ needs to be a port and w needs to be independent of x_i. In any ground state $\boldsymbol{x} = (x_i, \dots 1_i, \dots x_N) \in \mathcal{G}$ we can always de-excite the i-th bit to obtain $\tilde{\boldsymbol{x}} = (x_i, \dots 0_i, \dots x_N) \in \mathcal{G}$. In other words: the bit x_i is never determined to be excited in any ground state $\boldsymbol{x}/\{i\}$ of the other atoms. Such BOOLEAN functions are called *negative unate* in the bits x_i whose atoms $\mathfrak{i} = \mathfrak{L}(i)$ possess the smallest detuning $\Delta_\mathfrak{i} = \Delta_{\min}$. Symmetric negative unate BOOLEAN functions are necessarily *antimonotonic* (i.e. their negation is monotonic). The only symmetric, antimonotonic check functions f_c contradicting the assumption are the ones representing an upper bound of the form $f_c(P_v(\boldsymbol{x})) = 1 \Leftrightarrow \|P_v(\boldsymbol{x})\|_1 \leq n \in \mathbb{N}$.

Example 2. (Minority-Model Unit-Cell (MINU))

As an example, consider on a honeycomb grid $\mathcal{L}$ with $p = 3$ (input) ports the 'minority language'

$$L_\mathcal{L}[\texttt{MINU}] = \{(0,0,0,1), (0,0,1,1), (0,1,0,1), (1,0,0,1)\}.$$

Here $f[\texttt{MINU}]$ is defined by $\|P_v(\boldsymbol{x})\|_1 \leq n$ with $n = 1$. We need one ancillary $0 \in \mathcal{A}$ to realize the check function. Fig. 2.1 portrays the minority-model unit-cell for $r \in \{1, 10, 100\}$.
We assume a D_3-symmetry in the structure, i.e. in particular $\Delta_\mathfrak{i} = \Delta_\mathfrak{j}$ for each port $\mathfrak{i}, \mathfrak{j} \in \mathcal{P}$. To achieve degeneracy in the ground states, we choose $I_{\mathfrak{i}0} = \Delta_\mathfrak{i}$ constant for $\mathfrak{i} \in \mathcal{P}$. Then each ground state $\boldsymbol{x} \in \mathcal{G}$ is of energy $E(|\boldsymbol{x}\rangle) = -\Delta_0$. *W.l.o.g.* by rescaling the energies using f_α from eq. (2.15) with $\alpha = \Delta_{\min}^{1/6}$, we can set $I_{\mathfrak{i}0} = \Delta_\mathfrak{i} = 1$ for $\mathfrak{i} \in \mathcal{P}$. We apply this choice of units in the following.
To maximize both r and ΔE_{eff} for a given value of Δ_0, we need to choose $I_{\mathfrak{i}\mathfrak{j}} \leq \max(\Delta_0, 2) - 1$ for $\mathfrak{i} \neq \mathfrak{j} \in \mathcal{P}$ sufficiently small. In fig. 2.1 this is denoted by the gray-shaded circles. For the portrayed structures we chose the limiting case $I_{\mathfrak{i}\mathfrak{j}} = \max(\Delta_0, 2) - 1$ which is most useful to decrease residual energies during tessellation. Then the excited states $\boldsymbol{x} \in \mathcal{E}$ are of energy $E(|\boldsymbol{x}\rangle) \geq -1$. Thus for $\Delta_0 > 1$ we obtain a positive energy gap $r = \Delta E > 0$. The robustness and the effective gap are given by $r = \Delta_0 - 1$ and $\Delta E_{\text{eff}} = 1 - 1/\Delta_0$ respectively; note that $\Delta E_{\text{eff}} = r/(r+1)$. We can send $r \to \infty$ by arbitrarily increasing Δ_0 (compared to $\Delta_\mathfrak{i}|_{\mathfrak{i}\in\mathcal{P}}$). In this limit $\Delta E_{\text{eff}} \to 1$. This is visualized in fig. 2.1 with $\Delta_0 = r + 1$ for $r \in \{1, 10, 100\}$. Of course, the upper bound $\Delta E_{\text{eff}} \leq 1$ still holds in the limit $r \to \infty$ as the proof is valid for all languages.

However remember that we are not very interested in such languages and for each other language of this thesis $r \leq_L 1$ holds. This example is merely of academic interest to visualize the limits of the upper bound. Note that this example can not be realized in the PXP model as it is heavily based on the intermediate energy regime which allows for the degeneracy of the ground states. Thus the equality $r = 1$ for all languages with $\mathcal{Q} = 1$ in the PXP model still holds.

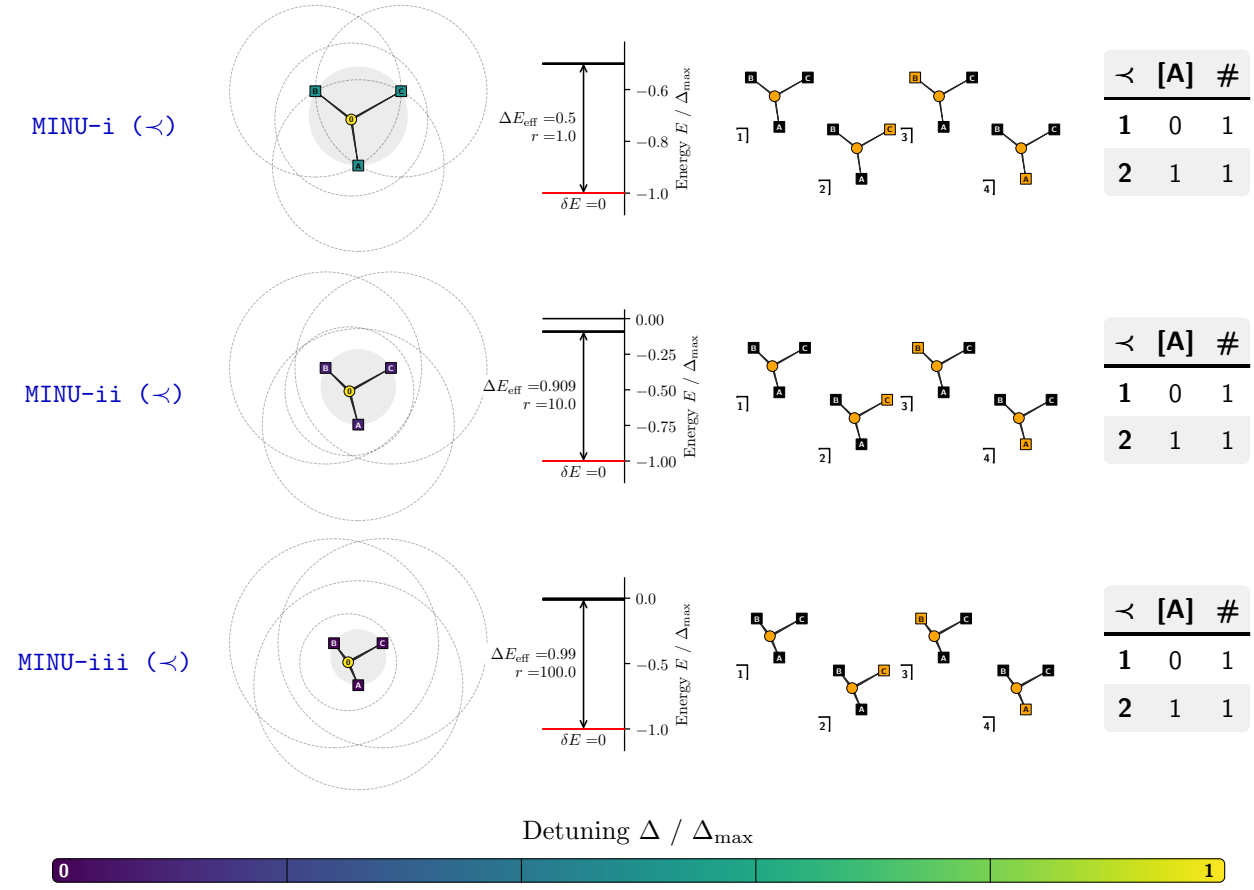

Figure 2.1: Realization of the minority-model unit-cell `MINU`. The language conflicts the assumptions of proof 1, thus we can achieve arbitrarily large r-values. The effective gap remains upper-bounded.

3 | The Problem and Methods

"Pure mathematics is, in its way, the poetry of logical ideas."

– A. Einstein in tribute to E. Noether, 'New York Times' (1935)

In chap. 2 we introduced the main goal of this thesis as to find solutions of eq. (2.9). We shortly discussed why this might be in general a non-trivial problem and we concluded that a reductionist approach would be most useful. For this purpose we created the mathematical framework for a process called *amalgamation*. Amalgamation is a useful tool to construct (larger) L-complexes by gluing (smaller) building blocks together.

In this thesis we focus particularly on the elementary building blocks of logical connectives, of the surface code and of the Fibonacci model. Within the PXP 'blockade-approximation' such elementary building blocks were already proposed in Refs. [38, 30, 23]. However, the VdW model more closely resembles the physical interactions between Rydberg atoms. Such 'long-range' interactions can behave qualitatively different than the PXP model with a finite cutoff-radius. On the one hand, the finite interaction energies between atoms can provide additional degrees of freedom to adjust the energy structure. On the other hand the physical interaction energies are a non-trivial function of the geometry. Therefore a natural question is whether it is possible to reconstruct the elementary building blocks from the PXP model within the VdW framework. Analogously, the question arises whether there are PXP-languages which can not be implemented in the VdW model. To answer these questions and to deal with the more complicated framework, we require appropriate tools and theory.

In this chapter we want to focus on developing the tools and the theory which allow us tackle these and further relevant questions in the following chapters 4, 5, ... We illustrate these tools in subsec. 3.1.2 and 3.2.6 exemplarily for the simplest elementary block of the logical connectives, namely the NOR. This is a particularly relevant example as the NOR is *functionally complete*: The singleton {NOR} is a universal gate set for Boolean logic.

3.1 | Rejection Sampling Algorithm

The implementation of the logical connectives for the PXP model were studied by Stastny *et al.* in Ref. [38]. Here multiple logic gates were found and proven to be minimal (in the number of atoms). The VdW model introduces additional interactions between atoms which are disconnected in the PXP blockade graph and it consider only finite interactions between atoms which are connected. This generally disarranges the energy structure.

Thus the first part of this thesis focuses on studying the known languages from the PXP model in the context of VdW interactions. The goal is to find out whether it is possible to implement these languages in the VdW model and if so to construct samples. This is studied by formulating a *rejection sampling algorithm* (also called *accept-reject algorithm*, a type of Monte Carlo Sampling):

Input (➔):	Target Language L_t
Output (➔):	L-complex $(\mathcal{C}^{\mathcal{Q}}_{\mathcal{K}}, L_t, \mathfrak{L})$ with gapped $\mathcal{H}_0[H;\mathcal{C}] \cong_{\mathfrak{L}} \mathcal{H}(L_t)$

The algorithm should consider the languages $L_t = L_v$ with $v \equiv (f_b, w)$ proposed by Stastny *et al.*[38] as input and outputs configurations with positive quality factors.

The following subsec. 3.1.1 formulates the problems in constructing such samples. It explains an ansatz for solving these problems via *linear programming*, *rejection sampling* and *graph embedding*. This outlines the steps of the rejection sampling algorithm which is summarized in flowchart 3.1. Readers only interest in the results of the algorithm can skip to the next subsec. 3.1.2. Here we exemplarily apply the algorithm to the PXP-minimal `NOR`-gates to illustrate the advantages and disadvantages of the algorithm.

3.1.1 | Construction of Samples

The goal of this subsection is to explain the problems which arise when constructing samples and to illustrate an ansatz for solving these problems. This outlines the rejection sampling algorithm presented in flowchart 3.1 which offers a quick overview over this subsection.

Consider the Hamiltonian (2.1). The goal is going to be to find a L-complex with a gapped low-energy eigenspace corresponding to the target Hilbert space. For simplicity, we start by ignoring the eigenstates $|\boldsymbol{x}\rangle$ for $\boldsymbol{x} \in \mathcal{E}$ of the excited state manifold and focus on the energy splitting δE of the eigenstates $|\boldsymbol{x}\rangle$ for $\boldsymbol{x} \in \mathcal{G}$. Ideally, we want to find a L-complex with a degenerate eigenspace $\delta E = 0$.

Definitions. Consider the target language $L = L_t$. In the following we label its words $\boldsymbol{x}_i \in L$ by indices $i \in \{1, \dots g\}$, thus fixing an arbitrary ordering. We start by defining the *language matrix* $\boldsymbol{L} \in \mathbb{F}_2^{g \times N}$ by $L_{ij} := (x_i)_j$ where the (i,j)-th index corresponds to the j-th bit of the i-th word. A different ordering would correspond to a permutation of the rows in $\boldsymbol{L}$ The labeling chooses

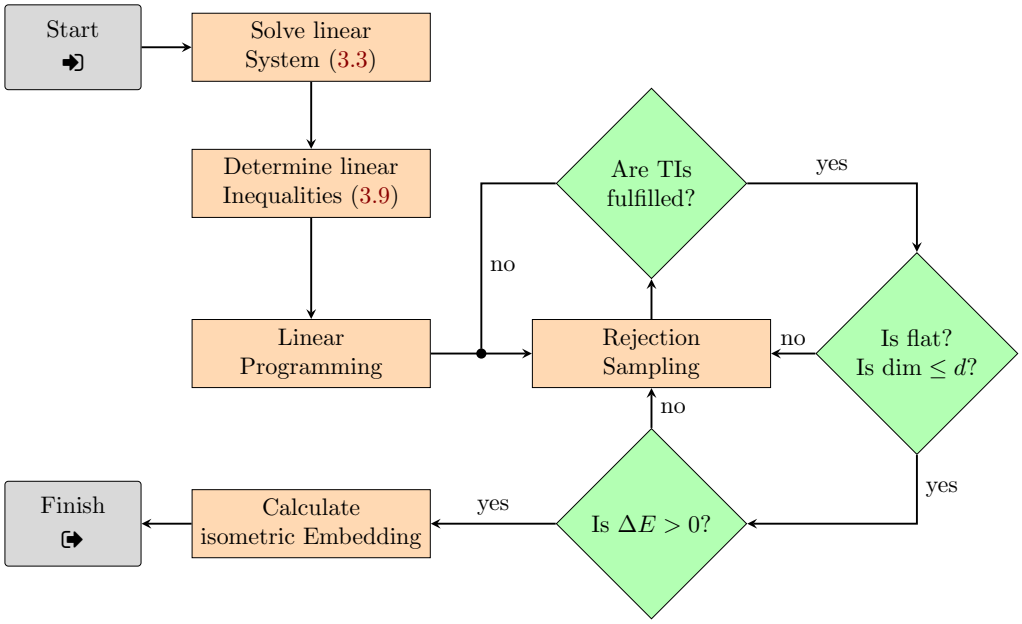

Algorithm 3.1: Flowchart of the Rejection Sampling Algorithm. The rejection sampling itself is applied to the solution space from linear programming. The constructed samples are checked for the triangle inequalities (TIs), for their curvature and dimension and for their energy gap. The accepted metric spaces are embeddable in Euclidean d-space.

a representative $\boldsymbol{L} \in [\boldsymbol{L}] \cong L$. We continue by defining another matrix $\boldsymbol{L}^2 \in \mathbb{F}_2^{g\times N(N-1)/2}$ by $(\boldsymbol{L}^2)_{i\alpha} := L_{ik}L_{il}$ with some (bijective) ordering $\alpha = \alpha(k,l)$ for $k < l$. We define the matrix $\boldsymbol{M} \in \mathbb{F}_2^{g\times[N+N(N-1)/2]}$ by concatenating $\boldsymbol{L}$ and $\boldsymbol{L}^2$ in the direction of the second index:

$$M_{ij} := \left\{ \begin{array}{ll} L_{ij}, & \text{if } j \leq N \\ (\boldsymbol{L}^2)_{i\alpha}, & \text{if } \alpha = j - N > 0 \end{array} \right\}. \tag{3.1}$$

Finally we define the *configuration vector* $\boldsymbol{c} \in \mathbb{R}^{N+N(N-1)/2}$ by rewriting the structure $\mathcal{C} = (\boldsymbol{r}_\mathfrak{i}, \Delta_\mathfrak{i} \mid \mathfrak{i} \in \mathcal{N})$ as a vector of the detunings $\Delta_\mathcal{C}$ and the interaction energies:

$$c_j := \left\{ \begin{array}{ll} -\Delta_{\mathfrak{L}(j)}, & \text{if } j \leq N \\ I_{\mathfrak{L}(k)\mathfrak{L}(l)}, & \text{if } \alpha(k,l) = j - N > 0 \end{array} \right\}. \tag{3.2}$$

For latter we introduce the shorter notation $I_{\mathfrak{i}\mathfrak{j}} \equiv U_{\mathrm{VdW}}(r_{\mathfrak{i}\mathfrak{j}})$ and we apply the labeling function $\mathfrak{L}$ to associate (bit) indices with the atoms. For the interaction energies we define their tuple $I_\mathcal{C} = (I_{\mathfrak{L}(k)\mathfrak{L}(l)} \mid \alpha(k,l) \in \{1, \dots N(N-1)/2\})$.

The linear System. We now want to find configuration vectors solving the linear system of equations[1]

$$M_{ij}c_j = E \tag{3.3}$$

[1]Here (and in the remaining thesis) we assume Einstein notation, i.e. we sum over paired bit indices.

for equal eigenenergies $E \in \mathbb{R}$. If $|E| > 0$ without loss of generality we may assume $E \in \pm 1$ by rescaling the energies using f_α with $\alpha = |E|^{-1/6}$, see eq. (2.15). In other words: we measure energies in 'units of the right-hand side'. Thus we have to consider only the three cases $E \in \{-1, 0, +1\}$ for the right-hand side of linear system (3.3).

In general the matrix $\boldsymbol{M}$ of the linear system (3.3) is non-invertible (it is in general not even a square matrix). The minimal norm solution (in Euclidean 2-norm) of such a system can easily be found using the MOORE–PENROSE pseudoinverse $\boldsymbol{M}^+$ of the matrix: $\boldsymbol{c}^* = E\boldsymbol{M}^+\mathbf{1}$ fulfills $\|\boldsymbol{c}^*\|_2 \leq \|\boldsymbol{c}\|_2$ for all solution vectors $\boldsymbol{c}$ of eq. (3.3). Here $\mathbf{1}$ is a vector with $1_i = 1$ in each component. The solution space of eq. (3.3) is an affine linear space:

$$\boldsymbol{M}\boldsymbol{c} = E\mathbf{1} \qquad \Leftrightarrow \qquad \boldsymbol{c} \in \boldsymbol{c}^* + \ker \boldsymbol{M}. \tag{3.4}$$

The dimension of the solution space is the corank of $\boldsymbol{M}$.

A semimetric Space. The linear system (3.3) formulates a a *necessary condition* to implement the target Hilbert space as the *degenerate*, low-energy eigenspace (2.9), however it is sufficient. It treats the $N(N-1)/2$ interaction energies $I_\mathcal{C}$ as independent variables, however they are functions of $d(N-(d+1)/2)$ *physical* DOFs, given by the geometry $G_\mathcal{C}$ and the potential U_{VdW}. Physical interaction energies should thus be positive, we (informally) write $I_\mathcal{C} > 0$.
As mentioned shortly in the beginning, we are interested in physical geometries with some finite distance between atoms. This distance may be motivated from experimental limitations or simply because the VdW model for interactions between Rydberg atoms breaks down at short distances. We can now formalize this notion by introducing a (unit-free) minimal radius $\hat{d}_{\min}$ such that $d_{\min} = \hat{d}_{\min} r_{\text{B, min}}$[2] is the minimal distance between atoms. Thus the interaction energies should be upper-bounded by some maximal interaction energy $I_{\max} \equiv U_{\text{VdW}}(d_{\min})$, we (informally) write $I_\mathcal{C} \leq I_{\max}$.

If both conditions are met, then the solutions of eq. (3.3) introduce a semimetric[3]

$$d(\mathfrak{i}, \mathfrak{j}) \equiv U_{\text{VdW}}^{-1}(I_{\mathfrak{ij}}) = (C/I_{\mathfrak{ij}})^{1/6} \tag{3.5}$$

between two atoms $\mathfrak{i}, \mathfrak{j} \in \mathcal{N}$. Thus $(\mathcal{N}, d)$ denotes a semimetric space. In general $(\mathcal{N}, d)$ will not be a metric space as is does not fulfill the *triangle inequalities*. The triangle inequalities are additional necessary conditions for $(\mathcal{N}, d)$ to be embeddable in Euclidean space, i.e. to correspond to a physical structure of atoms. However they will be discussed later as they are *nonlinear inequalities* on the interaction energies. We first want to focus on formulating further necessary *linear inequalities* in the detunings $\Delta_\mathcal{C}$ and the interaction energies $I_\mathcal{C}$.

A lower Bound. We now again incorporate the excites states into the discussion to find necessary linear conditions for a positive energy gap. From remark 3 we know that useful detunings should be positive, we (informally) write $\Delta_\mathcal{C} > 0$. However we can sharpen this inequality by including the interactions: Consider any atom $\mathfrak{i} = \mathfrak{L}(i) \in \mathcal{N}$ with bit index i. Consider any word $\boldsymbol{x} \in L$ where $x_i = 1$. Such a word always exists as discussed by remark 2. Let

$$\mathcal{N}_1(|\boldsymbol{x}\rangle) := \{\mathfrak{i} \in \mathcal{N} \mid x_i = 1, \mathfrak{i} = \mathfrak{L}(i)\} \subseteq \mathcal{N} \tag{3.6}$$

[2] Remember that $r_{\text{B, min}} = \min_{\mathfrak{i} \in \mathcal{N}} r_{B,\mathfrak{i}}$.
[3] A semimetric fulfills (similarly as a metric) the conditions of positivity, positive definiteness and symmetry but in general does not fulfill the triangle inequality.

be the subset of atoms excited in eigenstate $|\boldsymbol{x}\rangle$ and correspondingly $\mathcal{N}_0(|\boldsymbol{x}\rangle) := \mathcal{N}\backslash\mathcal{N}_1(|\boldsymbol{x}\rangle)$ the subset of atoms not excited in eigenstate $|\boldsymbol{x}\rangle$. We define its magnitudes $N_1(|\boldsymbol{x}\rangle) := |\mathcal{N}_1(|\boldsymbol{x}\rangle)|$ and $N_0(|\boldsymbol{x}\rangle) := |\mathcal{N}_0(|\boldsymbol{x}\rangle)|$. Again we consider the derived state $|\tilde{\boldsymbol{x}}\rangle = |x_1, \dots 0_i, \dots x_N\rangle$. It is of energy $E(|\tilde{\boldsymbol{x}}\rangle) = E(|\boldsymbol{x}\rangle) + \Delta_{\mathfrak{i}} - \sum_{\mathfrak{j}\in\mathcal{N}_1(|\boldsymbol{x}\rangle)\backslash\{\mathfrak{i}\}} I_{\mathfrak{ij}}$. If $\tilde{x} \in L$ as well, as we want the linear system (3.3) to be fulfilled we conclude $\Delta_{\mathfrak{i}} = \sum_{\mathfrak{j}\in\mathcal{N}_1(|\boldsymbol{x}\rangle)\backslash\{\mathfrak{i}\}} I_{\mathfrak{ij}}$. If on the other hand $\tilde{x} \notin L$, as we want $\Delta E > 0$ to be fulfilled we conclude $\Delta_{\mathfrak{i}} > \sum_{\mathfrak{j}\in\mathcal{N}_1(|\boldsymbol{x}\rangle)\backslash\{\mathfrak{i}\}} I_{\mathfrak{ij}}$. To summarize we require the inequality

$$\Delta_{\mathfrak{i}} \geq \sum_{\mathfrak{j}\in\mathcal{N}_1(|\boldsymbol{x}\rangle)\backslash\{\mathfrak{i}\}} I_{\mathfrak{ij}} \tag{3.7}$$

for every atom $\mathfrak{i} \in \mathcal{N}$ in every state $|\boldsymbol{x}\rangle \in L$ with $x_i = 1$. Informally we write $\Delta_{\mathcal{C}} \geq \Sigma_{I_{\mathcal{C}}}$.

An upper Bound. Now consider some ground state $\boldsymbol{x} \in L$. Let $\mathfrak{i} = \mathfrak{L}(i)$, $\mathfrak{j} = \mathfrak{L}(j)$ and $\mathfrak{k} = \mathfrak{L}(k)$ denote the atoms associated by $\mathfrak{L}$ with the indices i, j and k. Consider any atom $\mathfrak{k} \in \mathcal{N}_1(|\boldsymbol{x}\rangle)$ (it is $\mathcal{N}_1(|\boldsymbol{x}\rangle) \neq \emptyset$ by remark 4. The eigenenergy of state $|\boldsymbol{x}\rangle \in \mathcal{H}(L)$ can be rewritten as

$$E(|\boldsymbol{x}\rangle) = \langle H[\mathcal{C}]\rangle_{\boldsymbol{x}} = -\sum_{\mathfrak{i}\in\mathcal{N}_1(|\boldsymbol{x}\rangle)\backslash\{\mathfrak{k}\}} \left(\Delta_{\mathfrak{i}} - \sum_{\mathfrak{j}\in\mathcal{N}_1(|\tilde{\boldsymbol{x}}_{\mathfrak{i}}\rangle)\cup\{\mathfrak{k}\}} I_{\mathfrak{ij}}\right) - \Delta_{\mathfrak{k}}. \tag{3.8}$$

where $|\tilde{\boldsymbol{x}}_{\mathfrak{i}}\rangle \equiv |0_1, \dots 0_i, x_{i+1}, \dots x_N\rangle$. As $\mathcal{N}_1(|\tilde{\boldsymbol{x}}_{\mathfrak{i}}\rangle) \cup \{\mathfrak{k}\} \subseteq \mathcal{N}_1(|\boldsymbol{x}\rangle)\backslash\{\mathfrak{i}\}$, we may apply eq. (3.7) to obtain $E(|\boldsymbol{x}\rangle) \leq -\Delta_{\mathfrak{k}}$. This inequality is valid for all atoms $\mathfrak{k} \in \mathcal{N}$ excited in some eigenstate $|\boldsymbol{x}\rangle \in \mathcal{H}(L)$ (such an eigenstate exists for all $\mathfrak{k} \in \mathcal{N}$ by remark 2). For $\Delta_{\mathcal{C}} > 0$ is positive (by remark 3) we have negative eigenenergies $E(|\boldsymbol{x}\rangle) < 0$. W.l.o.g. we may thus choose $E = E(|\boldsymbol{x}\rangle) = -1$ on the right-hand side of linear system (3.3). As $\Delta_{\mathfrak{i}} \leq -E(|\boldsymbol{x}\rangle)$, we obtain an upper bound $\Delta_{\mathfrak{i}} \leq 1$ for every atom $\mathfrak{i} \in \mathcal{N}$: informally we write $\Delta_{\mathcal{C}} \leq 1$.

Linear Inequalities. To summarize, we have now derived a linear system of equations (3.3) and several linear inequalities

$$I_{\mathcal{C}} > 0, \quad I_{\mathcal{C}} \leq I_{\max}, \quad \Delta_{\mathcal{C}} \geq \Sigma_{I_{\mathcal{C}}} \quad \text{and} \quad \Delta_{\mathcal{C}} \leq 1 \tag{3.9}$$

in the energies of the system with constrain the affine linear solution space (3.4). In general there might be interaction energies $I_{\mathfrak{L}(k)\mathfrak{L}(l)} \in I_{\mathcal{C}}$ which correspond to zero-columns in $\boldsymbol{M}$, i.e. $M_{ij} = 0$ for $j = N + \alpha(k,l)$ and $i \in \{1, \dots g\}$. Such interactions do not contribute to the energy of the system in any ground state because the atoms $\mathfrak{L}(k)$ and $\mathfrak{L}(l)$ are never excited simultaneously. Such interaction energies are only upper-bounded by $I_{\max}$, i.e. their distance is only lower-bounded by $d_{\min}$. In particular such atoms may lie within each others blockade radii (i.e. be in blockade), however they do not need to.

Example 3. (`NOT1`-Gate)

> As the simplest example we anticipate the `NOT1`-gate from fig. 4.1 with $N = 2$ atoms in blockade. Its language $L_{\texttt{NOT1}} = \{(0,1), (1,0)\}$ with $g = 2$ is based on two bits which are each others negatives. Thus they are not excited simultaneously in any ground state. Their interaction energy in the third column of $\boldsymbol{M} \in \mathbb{F}_2^{2\times 3}$ is zero in every ground state.

For any other interaction energy $I_{\mathfrak{kl}} \in I_{\mathcal{C}}$ which is contributing to the energy of the system in some ground state $\boldsymbol{x} \in L$ with $x_k, x_l = 1$, the upper-bound to the interaction energies can be sharpened: $I_{\mathfrak{kl}} \leq \Delta_{\mathfrak{k}}, \Delta_{\mathfrak{l}} \leq 1$. Otherwise both atoms would be located within each others

blockade radii and it would be energetically not favorable to excite them simultaneously in $\boldsymbol{x}$. In the case of an equality in eq. (3.7) the two states with the atom (not) excited can be of the same energy. This is a feature of the VdW model which is excluded by the PXP-approximation. This ansatz is going to be useful in many cases to achieve degeneracy using fewer ancillary atoms and to construct elementaries of higher quality or larger effective gap.

Linear Programming. The solution space of the linear system is the affine linear space given in eq. (3.4). The linear inequalities constrain the physical (and useful) solutions within a bounded convex subspace. The goal of this algorithm is to sample (physical) solutions from this subspace. The idea is to construct the minimal *hyperrectangle* of dimension corank($\boldsymbol{M}$) in $N + N(N-1)/2$-dimensional parameter space which encloses the space of physical solution. As we restrict ourselves to linear inequalities (for now), the construction of the hyperrectangle is a problem solved by *linear programming*:

Input (➔):	Vectors $\boldsymbol{a} \in \mathbb{R}^m$, $\boldsymbol{b}_{\text{eq}} \in \mathbb{R}^{n_{\text{eq}}}$, $\boldsymbol{b}_{\text{in}} \in \mathbb{R}^{n_{\text{in}}}$,
	Matrices $\boldsymbol{A}_{\text{eq}} \in \mathbb{R}^{n_{\text{eq}} \times m}$, $\boldsymbol{A}_{\text{in}} \in \mathbb{R}^{n_{\text{in}} \times m}$
Output (➔):	Vector $\boldsymbol{x} \in \mathbb{R}^m$ which minimizes $\boldsymbol{a}^T \boldsymbol{x}$
	w.r.t. $\boldsymbol{A}_{\text{eq}} \boldsymbol{x} = \boldsymbol{b}_{\text{eq}}$ and $\boldsymbol{A}_{\text{in}} \boldsymbol{x} \leq \boldsymbol{b}_{\text{in}}$

In our case we use $\boldsymbol{A}_{\text{eq}} = \boldsymbol{M}$, $\boldsymbol{b}_{\text{eq}} = E\boldsymbol{1}$ and $\boldsymbol{x} = \boldsymbol{c}$. The inequalities of eq. (3.9) are summarized in the linear system $\boldsymbol{A}_{\text{in}} \boldsymbol{x} \leq \boldsymbol{b}_{\text{in}}$. We may now sample this hypercube to construct random solutions of the linear system and check the linear inequalities for these solutions (Rejection Sampling). However not every solution constructed by this algorithm yields a valid physical implementation yet.

Triangle Inequalities. We continue with the (nonlinear) *triangle inequalities*: For N atoms there are in total $3\binom{N}{3}$ triangle inequalities we need to check. We eliminate the samples which do not fulfill all triangle inequalities. The remaining samples now each define a metric space $(\mathcal{N}, d)$ with d defined in (3.5).

Isometric Embeddings of Metric Spaces. We are interested in the isometric embeddings of these finite metric spaces into the d-dimensional Euclidean space. Embeddings of metric spaces into other metric spaces are well studied in mathematics[27]. Not every finite metric space can be isometrically embedded in Euclidean space[5] and in general finding an embedding is NP-hard[7, 8]. A necessary and sufficient condition for the isometric embeddability of a given metric space in a Euclidean space of any dimension d was discovered by C. L. Morgan in Ref. [28]. C. L. Morgan introduced the notions of flatness and dimension for the metric spaces and proved that a metric space can be embedded in Euclidean d-space if and only if the metric space is flat and of dimension less than or equal to d.

By random chance it is likely that some sampled metric space of cardinality N will be of dimension $d = N - 1$ and not quite flat. However we want to consider two- or three-dimensional Euclidean spaces which generally not allows the embedding of such metric spaces. To solve this issue we introduce some finite tolerance radius l_t in the orthogonal directions to some two- or three-dimensional flat subspace. If the constructed metric space lies within the tolerance radius it is almost two- or three-dimensional and flat and we project it onto two- or three-dimensional hyperplane. This of course will slightly modify the interaction energies and thus shift the energy levels and cause some finite energy splitting $\delta E > 0$. The upper bound to the energetic shift of

the states can be controlled by setting the tolerance l_t. A smaller tolerance l_t implies a smaller energy splitting δE which comes at the cost of increasing the runtime.

The output is a structure in two- or three-dimensional Euclidean space. It remains to check whether the energy gap $\Delta E > 0$ is finite. If this is the case then the structure is a valid implementation of the target language in the VdW model with some finite quality.

3.1.2 | Application of the Algorithm

The last subsec. 3.1.1 offered a rejection sampling algorithm 3.1 which takes a target language as input and outputs samples of structures which realize the target language. In this subsection we apply this algorithm exemplary to the target languages of the NOR-gates introduced by Stastny *et al.* [38] in the PXP model. The objective is to generate samples which implement the same logic connectives with the same language but in the VdW model.

Families of Languages. In general there can exist more than one minimal language for the same logical connective which can be implemented. There are groups of such minimal logic gates which differ by only a single amalgamation but they possess the same general structure. We call such a group of such languages a *(logic) family of languages*. In the PXP model there are three families of minimal logic languages for the logic elementaries and this list is proven to be exhaustive[37]. We are going to label such families by arabic indices $\mathtt{1}, \mathtt{2}, \ldots$ in this thesis.

Using the rejection sampling algorithm 3.1 we are able to rediscover all PXP-realizations of the logic elementaries in the VdW model. For the NOR-gate there exist three PXP-minimal realizations (one for each family). Fig. 3.1 portrays one sample generated by the rejection sampling algorithm for each of the three realizations in the VdW model. Such samples are going to be labeled by lower case roman numerals $\mathtt{i}, \mathtt{ii}, \ldots$ in the following thesis. If there is only one sample in the whole thesis we leave-out this index to streamline the notation.

Interpretation of the Figures. The three samples NOR-0, NOR-1i and NOR-2i of the different realizations of the NOR-gate are presented in the second column. The black lines represent the edges of the blockade graph from the PXP model. The dashed circles correspond to the blockade radii $r_{B,\mathtt{i}}$ which are possibly different for each atom $\mathtt{i} \in \mathcal{N}$. They define the length scale of the geometry. The detunings are denoted by the color of each atom (see colorbar). Energies are measured in units of the largest detuning $\Delta_{\max} := \max_{\mathtt{i}\in\mathcal{N}} \Delta_{\mathtt{i}}$. Ancillaries are denoted by circles and they are indexed by integers $\mathtt{0}, \mathtt{1}, \mathtt{2}, \ldots$. The input ports are denoted by squares and labeled by the letters $\mathsf{A}, \mathsf{B}, \ldots$ and the output ports are denoted by diamonds and labeled by the letters $\mathsf{Q}, \mathsf{R}, \ldots$. The third column shows the energy structure of each realization with its energy splitting δE (in units of $\Delta_{\max}$), its (effective) energy gap ΔE_{eff} and its robustness r. Note that by choice of the energy scaling the energy gap equals the effective energy gap[4]. The fourth column presents the ground state configurations of each gate. The ground states are labeled by indices $\mathtt{1}, \mathtt{2}, \ldots$. Excited atoms are colored in orange while atoms which are not excited are colored in black. Again, the ancillaries, input ports and output ports are denoted by circles, squares and diamonds respectively. The last column portrays the language matrix of each realization. In the following chapters of this thesis we continue to use this representation and these labels for other gates.

[4] This differs from the choice of the energy scaling in Ref. [38] where energies are measured in units of the *smallest* detuning such that the energy gap equals the robustness.

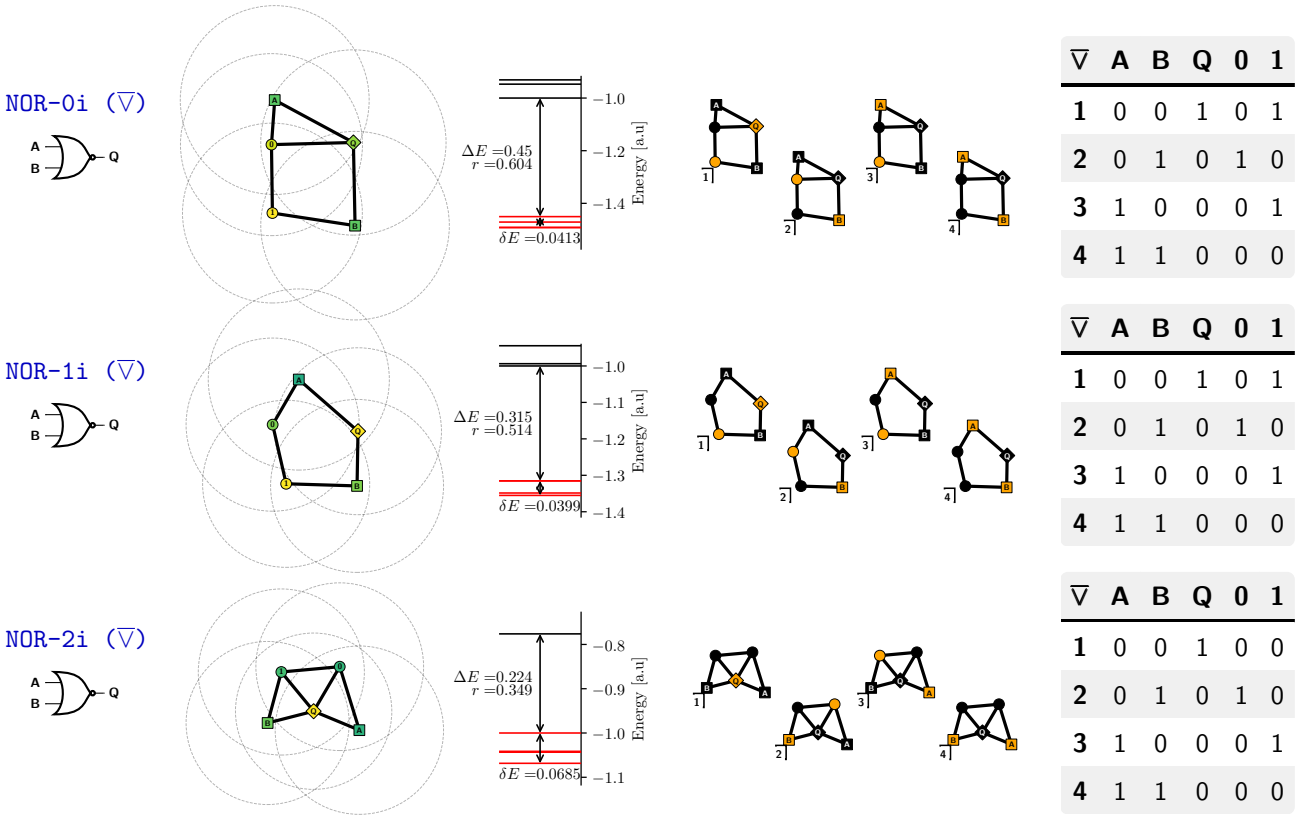

▽	A	B	Q	0	1
1	0	0	1	0	1
2	0	1	0	1	0
3	1	0	0	0	1
4	1	1	0	0	0

▽	A	B	Q	0	1
1	0	0	1	0	1
2	0	1	0	1	0
3	1	0	0	0	1
4	1	1	0	0	0

▽	A	B	Q	0	1
1	0	0	1	0	0
2	0	1	0	1	0
3	1	0	0	0	1
4	1	1	0	0	0

Figure 3.1: Three PXP-minimal NOR-realizations implemented in the VdW-model. The structures are constructed using the rejection sampling algorithm 3.1. The languages were introduced by Stastny *et al.* in Ref. [38, 37]. In the PXP model the realizations are minimal in their number of atoms and the list of minimal realizations is proven exhaustive[37].

Analysis of the Samples. For each realization the ratio is of magnitude $Q \approx 1/10$ leaving a quality factor $\mathcal{Q} \approx 90\%$. There is a finite splitting $\delta E > 0$ due to the projection onto the 2D-Euclidean plane as explained in the previous subsec. 3.1.1. As the black lines only represent the edges of the blockade graph from the PXP model, they do not posses much physical significance in the VdW model. In the VdW model there exists no clear distinction between atoms in blockade and atoms which are not in blockade. Nevertheless, they present a helpful tool for a clearer visualization and they offer an intuition about vicinity. We see that realization NOR-0 and realization NOR-1 differ only in their unphysical blockade graph but they possess the same language (see tables in the last column of fig. 3.1). They are therefore actually two implementations of the same realization w which makes them redundant in the VdW formalism.

In the PXP model the additional blockade in realization NOR-0 connects the two atoms 0 and Q which are not simultaneously excited in the language. In realization NOR-1 in the PXP model,

we could thus just move these two atoms closer and add the blockade as well. The advantage of realization NOR-0 and the additional blockade in the PXP model is however that it removes the need for the larger detunings of the atoms 1 and B. A circular graph of five vertices with equal weights would have five *maximum weight independent sets* (MWISs). Thus such a blockade graph with equal detunings possesses five ground states in the PXP model. In realization NOR-1 the larger detunings of atom 1 and atom B secure that the words $\boldsymbol{x} \in L$ are energetically lower than the fifth *maximum independent set* (MMIS) $(0_\mathsf{A}, 0_\mathsf{B}, 1_\mathsf{Q}, 1_0, 0_1) \notin L$. The equal detunings of all atoms in realization NOR-0 in the PXP model could be considered an experimental advantage as they are simpler to implement. At this point we want to note that such 'equi-detuned' implementations of the NOR0-gate are also possible in the VdW model. However we are not going to focus further on such implementations as this restriction yields a smaller energy gap.
In the PXP model realization NOR-2 can be derived from realization NOR-0 by introducing an additional blockade between atom Q and atom 1. Then it is energetically not favorable anymore to excite these two atoms simultaneously. We achieve degeneracy with the new ground state $|0_\mathsf{A}, 0_\mathsf{B}, 1_\mathsf{Q}, 0_0, 0_1\rangle$ by doubling the detuning of atom Q.

The remaining elementary Gates. Using the rejection sampling algorithm we were also able to rediscover all PXP-minimal realizations of the remaining logical connectives in the VdW model. However we do not want to discuss them at this point. They are presented and discusses in chapter 4 with an optimized structure. The reason for that is that the energy structure in fig. (3.1) is far from perfect: although the quality factor $\mathcal{Q} \approx 90\%$ is already quite large there remains a finite energy splitting $\delta E > 0$. It remains an open question for now whether it is possible to achieve perfect ground state degeneracy for these realizations. Furthermore we want to maximize the effective energy gap and robustness as much as possible. Although the current rejection sampling algorithm is useful to generate samples for the realization of gates, the samples are generally not quite optimal for a finite runtime. In the following subsec. 3.2 we want to discuss this problem and introduce a minimization algorithm for the optimization of the quality measures.

3.2 | Minimization Algorithm

The previous sec. 3.1 introduces the *rejection sampling algorithm* which solves the problem of constructing samples realizing a given target language in the VdW model. In the final subsec. 3.1.2 we exemplarily apply this algorithm to the PXP-minimal target languages of the logic elementaries to construct their logic gates. The constructed samples possess a positive quality factor however they are not yet optimal.

Given such a L-complex in this section we are now interested in optimizing its energy structure, i.e. in maximizing its quality factor, its effective energy gap and/or its robustness. This is generally a complicated problem of *multivariate global optimization* in the variables of the structure $\mathcal{C} = (\boldsymbol{r}_i, \Delta_i \mid i \in \mathcal{N})$. The relevant quantities are generally highly non-linear functions of the structure and usually possess multiple local optima.

We going to solve this problem numerically by implementing a *minimization algorithm*:

Input (🡒):	L-complex, Settings
Output (🡓):	Optimized L-complex

In the following subsec. 3.2.1 we are going to discuss this minimization algorithm 3.2. We formulate an important lemma I which makes an argument about the energy structure on very general ground. We formulate an algorithm 3.3 for the efficient calculation of the relevant quantities. This algorithm is based on the efficient calculation of *maximal independent sets* (MISs) of the blockade graph for amalgamated L-complexes for which we formulate lemma III. Readers only interested in the results can skip to subsec. 3.2.6 where we exemplarily apply the minimization algorithm to the sample logic gates from fig. 3.1.

3.2.1 | Numerical Optimization of Samples

In the following we start by introducing the general ideas of the minimization algorithm. The algorithm is summarized in the flowchart 3.2.

Libraries. The minimization algorithm in this thesis is based on the external global optimization functions `scipy.optimize` provided by the `SciPy` library. Specifically we apply the `SciPy` implementation `scipy.optimize.dual_annealing`[34] of the *dual annealing* (DA) algorithm which consists of a *generalized simulated annealing* (GSA) algorithm coupled to the local search '*L-BFGS-B*' algorithm. GSA is a stochastic approach first introduced by Tsallis *et al.*[41] and developed and tested by Xiang *et al.*[47, 46]. It combines classical simulated annealing (CSA) with fast simulated annealing (FSA) and is especially efficient for large number of variables in the objective function[46]. In this thesis the DA algorithm proved to be very efficient compared to other global optimization algorithms.

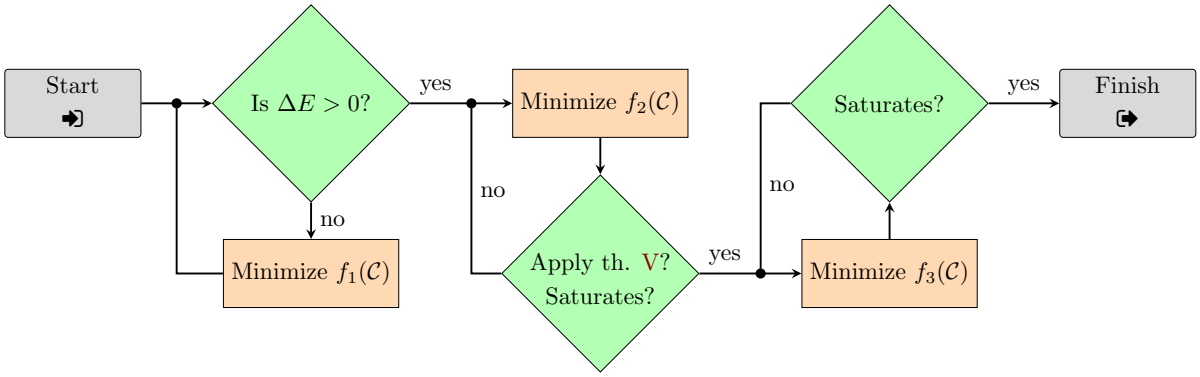

Algorithm 3.2: Flowchart of the minimization algorithm. f_1 and f_3 may vary whether we focus on maximizing ΔE_{eff} or r.

The Objective Functions. Depending on the context it is useful to minimize different *cost functions* $f_i : \mathcal{C} \to \mathbb{R}$. In the beginning we have to check whether the initial L-complex possesses a positive energy gap. If this is not the case it is useful to start by minimizing the first cost function

$$f_1(\mathcal{C}) = -\Delta E_{\text{eff}} \qquad (\text{ or } f_1(\mathcal{C}) = -r\ ) \tag{3.10}$$

until reaching the threshold $f_1(\mathcal{C}) < 0$. Otherwise we can directly continue by minimizing the second cost function

$$f_2(\mathcal{C}) = \left\{ \begin{array}{ll} Q, & \text{if } Q > 0 \\ \infty, & \text{if } Q \leq 0 \end{array} \right\}. \tag{3.11}$$

Here it is useful to punish negative energy gaps by some large value to prevent a relapse in the regime of negative energy gaps. We minimize f_2 until:

1 | we may apply the theorem V (or one of its corollaries) from sec. 3.3. This requires $f_2(\mathcal{C}) < Q^*$ where the target quality Q^* is given by theorem V (or its corollaries). Then we define the constraint $Q_c \ll Q^*$ and we apply theorem V (or its corollaries).

2 | f_2 saturates. It may be that f_2 saturates at some value Q_{sat} and we can not apply theorem V (or its corollaries). This may be because the minimization saturates due to numerical limitations (e.g. because $f_2 \lll 1$ or because the minimizer is stuck in a too large local minimum) or because f_2 possesses no zero in the parameter space of structures. In this case we define $Q_c \gtrsim Q_{\text{sat}}$.

Now we want to maximize the effective energy gap ΔE_{eff} (or the robustness r) while (approximately) constraining the value of f_2. We define the third cost function

$$f_3(\mathcal{C}) = -\Delta E_{\text{eff}} + R^+(Q/Q_c - 1) \qquad \big(\text{ or } f_3(\mathcal{C}) = -r + R^+(Q/Q_c - 1)\ \big) \tag{3.12}$$

which equals $-\Delta E_{\text{eff}}$ (or $-r$) if the constraint $Q \leq Q_c$ implied by the *unit ramp function* (or *rectifier function*) $R^+(x) := x\Theta(x)$ is fulfilled. Here $\Theta : \mathbb{R} \to \{0, 1\}$ is the HEAVISIDE unit step function. Otherwise f_3 is punished by the cost $R^+(Q/Q_c - 1) \propto Q/Q_c$ linearly depending on the magnitude of the violation. We minimize f_3 until it saturates and then we terminate. The algorithm outputs the final structure $\mathcal{C}$. This algorithm is summarized in the flowchart in fig. 3.2.

General Remarks. For this algorithm we have to *input the L-complex* consisting of an initial complex and a target language connected via a labeling. Besides that we have to input some *settings*:

1 | We have to choose the *mode*, i.e. whether to maximize ΔE_{eff} or r. This defines the minimization function f_1 and f_3.

2 | We should input a *maximum number of iterations* after which the algorithm terminates as a halting condition.

3 | We have to choose reasonable *bounds* for the variables. In particular the linear inequalities from eq. (3.9) should be fulfilled. We quantify upper bounds of the 'jumping distances' by (inverse) variances in the energy scaling.

4 | For unit-cells of tessellated languages we should decide whether we want to constrain the ports on the corners of a C_2-symmetric *parallelogram* (and the ancillaries within the parallelogram) to allow for tessellation. We can also choose *periodic boundary conditions* (PBCs) for the unit-cell.

5 | We have to decide whether we want to *constrain variables* and if so which ones. This is going to be discussed in more detail in the following

3.2.2 | Exponential Time Complexity

One execution of the minimization algorithm requires a multitude of iterations and thus a multitude of calculations of f_i. As the number of states 2^N increases exponentially with the number of atom N, the *asymptotic time complexity* $T = O(2^{\text{poly}(N)})$ for the 'brute-force' calculation of the energy gap (and thus the ratio, the effective gap and the robustness) increases exponentially as well. Furthermore as the number of DOFs increases polynomially with the number of atoms, the dimension of the parameter space increases polynomially. This requires the minimization algorithm to perform more iterations to find the global minimum which again increases the runtime. For large number of atoms (from $N \gtrsim 10$ atoms upwards) the runtime for one calculation of the energy structure becomes too slow and the minimization algorithm becomes infeasible. In the following we are going to discuss four ansatzes to tackle this issue:

1 | One simple ansatz would be not to calculate the energies of the whole manifold $\mathcal{E}$ but only of some random set $\mathcal{S} \subset \mathcal{E}$ of sample states. The hope would be that there always is some sample state sufficiently close to the (energetically) *lowest excited state* (LES) which allows us to *approximate the energy gap*. However this ansatz turns out to be not very promising: The excited state manifold seems to be *not dense enough* in its low-energy regime. The probability that the sample manifold includes a sample energetically close to the LES seems to be too small such that the fluctuations in the approximation of ΔE are too large.

2 | Another ansatz is to constrain the number of variables in a useful way to reduce the DOFs and the dimension of the parameter space in the algorithm. For tessellated languages, the language is approximately[5] transnational invariant. Thus it is intuitive to tessellate one unit-cell to construct the tessellated structure. In the following for tessellated languages we minimize only the unit-cell in the minimization algorithm and constrain that the atoms in the other unit-cells differ only by a lattice translation vector. This constrains the ports of the unit-cell on a parallelogram.

3 | We can additionally constrain the number of variables by imposing a symmetry on the structure. This is useful as many useful languages are symmetric (e.g. in their ports) and symmetric eigenstates are degenerate in a symmetric structure. However this also artificially reduces the DOFs which could prevent finding the global minimum (cf. the `ICRS2`-gate in fig. 4.8). It can also be useful to constrain the variables in a different way e.g. by minimizing primarily only the detunings or only the geometry.

4 | This last point is arguably the most important ansatz: The intuitive way to calculate the energy gap is to 'brute-force' calculate the energy of each excited state and each ground state and to take the difference of their respective minimum and maximum. This algorithm follows directly the definition (2.17) of the energy gap. With this naive algorithm we have to calculate the eigenenergy for each of the 2^N states which is infeasible for large number of atoms N. As a first ansatz we note that usually the number of ground states $g \ll e \sim 2^N$ is way smaller than the number of excited states. In the first point we mentioned that the excited state manifold is not very dense in the low-energy regime. This suggests that it is actually not necessary to calculate the eigenenergy for each excited state. In the following we derive a *more efficient algorithm to compute the LES*. The energy gap can then be calculated directly by evaluating only the energies of the $g \ll e$ ground states.

3.2.3 | The Energy Structure in the VdW Model

Consider a ground state manifold $\mathcal{G}$ and an excited state manifold $\mathcal{E}$. We start by calculating the eigenenergies of each ground state. The difference of its maximum and its minimum yields the energy splitting as defined in eq. (2.16). To calculate the energy gap we require the energy of the (energetically) *lowest excited state* (LES). A naive ansatz would be to consider only '*bit-flipped*' excited states $\tilde{\boldsymbol{x}} \in \mathcal{E}$ which emerge by single bit-flips of some bit $j \in \{1, \dots N\}$ from the ground states $\boldsymbol{x} \in \mathcal{G}$:

$$\tilde{x}_i = x_i(1 - \delta_{ij}) + (1 - x_i)\delta_{ij} \tag{3.13}$$

However it can be seen easily that even if the ground states are energetically lower than the bit-flipped excited states, there still might exist other excited states which are energetically lower than the ground states implying a negative energy gap:

Example 4. (A minimal Counterexample)

Consider the singleton $\mathcal{G} = \{(0_\mathsf{A}, 1_\mathsf{B})\}$. Its bit-flipped excited states are $(0_\mathsf{A}, 0_\mathsf{B}),\ (1_\mathsf{A}, 1_\mathsf{B}) \in \mathcal{E}$. However for $(1_\mathsf{A}, 0_\mathsf{B}) \in \mathcal{E}$ in a structure $\mathcal{C}$ with $I_{\mathsf{AB}} > \Delta_\mathsf{A} > \Delta_\mathsf{B} > 0$ it is

$$E(|1_\mathsf{A}, 0_\mathsf{B}\rangle) < E(|0_\mathsf{A}, 1_\mathsf{B}\rangle) < E(|0_\mathsf{A}, 0_\mathsf{B}\rangle),\ E(|1_\mathsf{A}, 1_\mathsf{B}\rangle).$$

[5] Up to boundary effects, i.e. depending on the boundary conditions and the size of the lattice

> Therefore the bit-flipped excited states are gapped-out while the energy gap $\Delta E < 0$ remains negative.

The bit-flipped excited states do not contain sufficient information to calculate the energy of the LES (and thus the energy gap or even the sign of the energy gap). To calculate the energy of the LES we start with two important observations:

Observation 1. In the PXP model the energetically lowest states are given by *maximum weight independent sets* (MWISs) of the blockade graph. However the kinematic constraint of the PXP blockade-approximation does not fully incorporate the effect of the VdW interactions. Due to finite long-range interactions it might be energetically favorable to excite less atoms compared to a *maximal independent set* (MIS). However in the VdW model it is remains energetically disfavourable to excite pairs of atoms which are in blockade. This allows us to formulate a weaker, analogue statement for the VdW model:

Remark 1. (A necessary Condition)

> The energetically lowest states are *independent sets* (ISs) of the blockade graph from the structure.

This directly excludes large sets of states as candidates for the energetically lowest state. We perform rough estimation: For a blockade graph $\mathcal{B} = (V, E)$ of degree Δ, the magnitude of the *maximum independent sets* (MMISs) is given by the *independence number* $\alpha(\mathcal{B}) \leq |V| - |E|/\Delta$[6]. This bound is credited to P. K. Kwok[44]. Thus we can exclude *at least* $\sum_{n=0}^{|E|/\Delta-1} \binom{|V|}{n}$ states where less than $|E|/\Delta$ atoms are *not* excited.

Obervation 2. The energetically lowest states in the PXP model are given by the MWISs of the unit-disk blockade graph. Thus the words in PXP-languages need to correspond to these MWISs to achieve unit quality. In particular the words of PXP-languages need to be *maximal* with respect to the blockade graph, i.e. no ground state can be a substate of any other ground state.
In the following we want to transfer this idea to the VdW model. However this is non-trivial because in the VdW model the energetically lowest states are generally not maximal on (and in particular no MWISs of) the blockade graph. Before formulating the second observation we first have to introduce some new concepts:

Definition 1. (Substates and Adjacency)

1 | We define $\boldsymbol{x}'\backslash\boldsymbol{x}$ as the *set of indices* $i \in \{1, \dots N\}$ with $x_i = 0$ and $x'_i = 1$. Further, we say $\boldsymbol{x} \subseteq \boldsymbol{x}'$ for $\boldsymbol{x}, \boldsymbol{x}' \in \mathbb{F}_2^N$ if $\boldsymbol{x}\backslash\boldsymbol{x}' = \emptyset$.

2 | If additionally $\boldsymbol{x}'\backslash\boldsymbol{x} \neq \emptyset$, then we define $\boldsymbol{x} \subset \boldsymbol{x}'$. If $\boldsymbol{x} \subset \boldsymbol{x}'$, we call $\boldsymbol{x}$ a *subword* of $\boldsymbol{x}'$ and $\boldsymbol{x}'$ a *superword* of $\boldsymbol{x}$. Correspondingly we call $|\boldsymbol{x}\rangle$ a *substate* of $|\boldsymbol{x}'\rangle$ and $|\boldsymbol{x}'\rangle$ a *superstate* of $|\boldsymbol{x}\rangle$.

3 | We call two words $\boldsymbol{x}, \boldsymbol{x}' \in \mathbb{F}_2^N$ with $\boldsymbol{x} \subset \boldsymbol{x}'$ (or their corresponding states) *adjacent* if there exists no third word $\tilde{\boldsymbol{x}} \in \mathbb{F}_2^N$ such that $\boldsymbol{x} \subset \tilde{\boldsymbol{x}} \subset \boldsymbol{x}'$. If $\boldsymbol{x} \subset \boldsymbol{x}'$ is a non-adjacent subword we also write $\boldsymbol{x} \Subset \boldsymbol{x}'$.

[6] There are multiple possible upper-bounds on the independence number α of a graph $\mathcal{B}$. For sharper bounds on $\alpha(\mathcal{B})$, see [45].

In other words: if $\boldsymbol{x} \subset \boldsymbol{x}'$ but $\boldsymbol{x} \notin \boldsymbol{x}'$ is an *adjacent substate* then $\boldsymbol{x}$ emerges from $\boldsymbol{x}'$ by *one bit flip* from 1 to 0. Note that $\subseteq$ (and $\subset$) introduces a *(strict) partial order* on the set of all uniform words $\mathbb{F}_2^N$. We can now formulate the second observation:

Lemma I (Transitivity of Energies)**.**

Consider three words $\boldsymbol{x}_1, \boldsymbol{x}_2, \boldsymbol{x}_3 \in \mathbb{F}_2^N$ *with* $\boldsymbol{x}_1 \subset \boldsymbol{x}_2 \subset \boldsymbol{x}_3$*. For* $n := \|\boldsymbol{x}_2\|_2^2$ *we define the intermediate states*

$$S_{\boldsymbol{x}_1, \boldsymbol{x}_3}(n) := \{\boldsymbol{x} \in \mathbb{F}_2^N \mid \boldsymbol{x}_1 \subset \boldsymbol{x} \subset \boldsymbol{x}_3 \ \wedge \|\boldsymbol{x}\|_2^2 = n\}.$$

Then we formulate:

1 | *If* $E(|\boldsymbol{x}_1\rangle) \leq E(|\boldsymbol{x}_2\rangle)$ *for all* $\boldsymbol{x}_2 \in S_{\boldsymbol{x}_1, \boldsymbol{x}_3}(\|\boldsymbol{x}_1\|_2^2 + 1)$*, then* $E(|\boldsymbol{x}_1\rangle) \leq E(|\boldsymbol{x}_2\rangle) < E(|\boldsymbol{x}_3\rangle)$*.*

2 | *If* $E(|\boldsymbol{x}_3\rangle) \leq E(|\boldsymbol{x}_2\rangle)$ *for all* $\boldsymbol{x}_2 \in S_{\boldsymbol{x}_1, \boldsymbol{x}_3}(\|\boldsymbol{x}_3\|_2^2 - 1)$*, then* $E(|\boldsymbol{x}_3\rangle) \leq E(|\boldsymbol{x}_2\rangle) < E(|\boldsymbol{x}_1\rangle)$*.*

In the above sense the energies of the subsets of words are *transitive*. The number of *intermediate states* is $|S_{\boldsymbol{x}_1, \boldsymbol{x}_3}(n)| = \binom{\|\boldsymbol{x}_3\|_2 - \|\boldsymbol{x}_1\|_2}{n - \|\boldsymbol{x}_1\|_2}$, thus $|S_{\boldsymbol{x}_1, \boldsymbol{x}_3}(n)| = \|\boldsymbol{x}_3\|_2 - \|\boldsymbol{x}_1\|_2$ *in both cases* 1 and 2. If the energies of some states fulfill the conditions of lemma I, the transitivity allows us to exclude further states as candidates for the energetically lowest state.

Proof.

Statements 1 and 2 are *dual*, their proof is very similar:

1 | As $E(|\boldsymbol{x}_1\rangle) \leq E(|\boldsymbol{x}_2\rangle)$ for all $\boldsymbol{x}_2 \in S_{\boldsymbol{x}_1, \boldsymbol{x}_3}(\|\boldsymbol{x}_1\|_2^2 + 1)$, it is $\Delta_{\mathfrak{i}} \leq \sum_{\mathfrak{j} \in \mathfrak{L}(\boldsymbol{x}_1 \setminus \boldsymbol{0})} I_{\mathfrak{i}\mathfrak{j}}$ for all $\mathfrak{i} \in \mathfrak{L}(\boldsymbol{x}_3 \setminus \boldsymbol{x}_1)$. Thus $\Delta_{\mathfrak{k}} < \sum_{\mathfrak{j} \in \mathfrak{L}(\boldsymbol{x}_1 \setminus \boldsymbol{0}) \cup \{\mathfrak{i}\}} I_{\mathfrak{k}\mathfrak{j}}$ for all $\mathfrak{i} \in \mathfrak{L}(\boldsymbol{x}_3 \setminus \boldsymbol{x}_1), \mathfrak{k} \in \mathfrak{L}(\boldsymbol{x}_3 \setminus \boldsymbol{x}_1) \setminus \{\mathfrak{i}\}$. Now we fix some $\boldsymbol{x}_2 \in S_{\boldsymbol{x}_1, \boldsymbol{x}_3}(\|\boldsymbol{x}_1\|_2^2 + 1)$ and thus $\{\mathfrak{i}\} = \mathfrak{L}(\boldsymbol{x}_2 \setminus \boldsymbol{x}_1)$. This yields $E(|\boldsymbol{x}_3\rangle) - E(|\boldsymbol{x}_2\rangle) \geq \sum_{\mathfrak{k} \in \mathfrak{L}(\boldsymbol{x}_3 \setminus \boldsymbol{x}_2)} [-\Delta_{\mathfrak{k}} + \sum_{\mathfrak{j} \in \mathfrak{L}(\boldsymbol{x}_2 \setminus \boldsymbol{0})} I_{\mathfrak{k}\mathfrak{j}}] = \sum_{\mathfrak{k} \in \mathfrak{L}(\boldsymbol{x}_3 \setminus \boldsymbol{x}_1) \setminus \{\mathfrak{i}\}} [-\Delta_{\mathfrak{k}} + \sum_{\mathfrak{j} \in \mathfrak{L}(\boldsymbol{x}_1 \setminus \boldsymbol{0}) \cup \{\mathfrak{i}\}} I_{\mathfrak{k}\mathfrak{j}}] > 0$ and thus $E(|\boldsymbol{x}_1\rangle) \leq E(|\boldsymbol{x}_2\rangle) < E(|\boldsymbol{x}_3\rangle)$.

2 | As $E(|\boldsymbol{x}_3\rangle) \leq E(|\boldsymbol{x}_2\rangle)$ for all $\boldsymbol{x}_2 \in S_{\boldsymbol{x}_1, \boldsymbol{x}_3}(\|\boldsymbol{x}_3\|_2^2 - 1)$, it is $\Delta_{\mathfrak{i}} \geq \sum_{\mathfrak{j} \in \mathfrak{L}(\boldsymbol{x}_3 \setminus \boldsymbol{0}) \setminus \{\mathfrak{i}\}} I_{\mathfrak{i}\mathfrak{j}}$ for all $\mathfrak{i} \in \mathfrak{L}(\boldsymbol{x}_3 \setminus \boldsymbol{x}_1)$. Thus $\Delta_{\mathfrak{k}} > \sum_{\mathfrak{j} \in \mathfrak{L}(\boldsymbol{x}_3 \setminus \boldsymbol{0}) \setminus \{\mathfrak{i}, \mathfrak{k}\}} I_{\mathfrak{k}\mathfrak{j}}$ for all $\mathfrak{i} \in \mathfrak{L}(\boldsymbol{x}_3 \setminus \boldsymbol{x}_1), \mathfrak{k} \in \mathfrak{L}(\boldsymbol{x}_3 \setminus \boldsymbol{x}_1) \setminus \{\mathfrak{i}\}$. Now we fix some $\boldsymbol{x}_2 \in S_{\boldsymbol{x}_1, \boldsymbol{x}_3}(\|\boldsymbol{x}_3\|_2^2 - 1)$ and thus $\{\mathfrak{i}\} = \mathfrak{L}(\boldsymbol{x}_3 \setminus \boldsymbol{x}_2)$. This yields $E(|\boldsymbol{x}_2\rangle) - E(|\boldsymbol{x}_1\rangle) \leq \sum_{\mathfrak{k} \in \mathfrak{L}(\boldsymbol{x}_2 \setminus \boldsymbol{x}_1)} [-\Delta_{\mathfrak{k}} + \sum_{\mathfrak{j} \in \mathfrak{L}(\boldsymbol{x}_2 \setminus \boldsymbol{0}) \setminus \{\mathfrak{k}\}} I_{\mathfrak{k}\mathfrak{j}}] = \sum_{\mathfrak{k} \in \mathfrak{L}(\boldsymbol{x}_3 \setminus \boldsymbol{x}_1) \setminus \{\mathfrak{i}\}} [-\Delta_{\mathfrak{k}} + \sum_{\mathfrak{j} \in \mathfrak{L}(\boldsymbol{x}_3 \setminus \boldsymbol{0}) \setminus \{\mathfrak{i}, \mathfrak{k}\}} I_{\mathfrak{k}\mathfrak{j}}] < 0$ and thus $E(|\boldsymbol{x}_3\rangle) \leq E(|\boldsymbol{x}_2\rangle) < E(|\boldsymbol{x}_1\rangle)$. □

At this point we want to formulate the corollary II of lemma I which becomes very important later to exclude realizations as candidates for target functions:

Corollary II (Transitivity of Energies)**.**

Consider two ground states $\boldsymbol{x}_1, \boldsymbol{x}_3 \in \mathcal{G}$ *where* $\boldsymbol{x}_1 \Subset \boldsymbol{x}_3$ *is s non-adjacent substate.*

1 | *Then the quality* $\mathcal{Q} < 1$ *is necessarily not perfect.*

2 | *If* $S_{\boldsymbol{x}_1,\boldsymbol{x}_3}(n) \not\subset \mathcal{G}$ *for any* $n \in \mathbb{N}_{(\|\boldsymbol{x}_1\|_2^2, \|\boldsymbol{x}_3\|_2^2)}$*, then the quality* $\mathcal{Q} = 0$ *vanishes.*

Note that corollary II is valid on general ground for any intermediate states $S_{\boldsymbol{x}_1,\boldsymbol{x}_3}(n)$ with $n \in \mathbb{N}_{(\|\boldsymbol{x}_1\|_2^2, \|\boldsymbol{x}_3\|_2^2)}$. However this is not necessary for most relevant cases: If $\boldsymbol{x}_1 \Subset \boldsymbol{x}_3$ differ by at most three bit flips then $n \in \{\|\boldsymbol{x}_1\|_2^2 + 1, \|\boldsymbol{x}_3\|_2^2 - 1\}$ implies an *adjacent* intermediate state. This is the case for every target function of this thesis. Even if $\boldsymbol{x}_1 \Subset \boldsymbol{x}_3$ differ by more than three bit flips then some adjacent intermediate state is generally an excited state. For these cases the proof simplifies to only its first part as it removes the need for the recursion.

Proof.

Corollary II is a direct consequence of lemma I when considering ground states $\boldsymbol{x}_1, \boldsymbol{x}_3 \in \mathcal{G}$:

1 | Consider $S_{\boldsymbol{x}_1,\boldsymbol{x}_3}(\|\boldsymbol{x}_1\|_2^2 + 1) \subset \mathcal{G}$. To achieve $\delta E = 0$ it must be $E(|\boldsymbol{x}_1\rangle) = E(|\boldsymbol{x}_2\rangle)$. Then we can apply statement 1 from lemma I such that $E(|\boldsymbol{x}_1\rangle) < E(|\boldsymbol{x}_2\rangle)$ and thus $\delta E > 0$.

2 | The following two cases are dual and we apply the dual statements 1 and 2 from lemma I respectively:

a | If $S_{\boldsymbol{x}_1,\boldsymbol{x}_3}(\|\boldsymbol{x}_1\|_2^2 + 1) \not\subset \mathcal{G} = \mathbb{F}_2^N \backslash \mathcal{E}$ then there exists an $\boldsymbol{x}_2 \in S_{\boldsymbol{x}_1,\boldsymbol{x}_3}(\|\boldsymbol{x}_1\|_2^2 + 1)$ which is an excited state $\boldsymbol{x}_2 \in \mathcal{E}$. To achieve $\Delta E > 0$ it must be $E(|\boldsymbol{x}_1\rangle) < E(|\boldsymbol{x}_2\rangle)$. Then we can apply statement 1 from lemma I such that $E(|\boldsymbol{x}_1\rangle) < E(|\boldsymbol{x}_2\rangle) < E(|\boldsymbol{x}_3\rangle)$ and thus $\Delta E < 0$.

b | If $S_{\boldsymbol{x}_1,\boldsymbol{x}_3}(\|\boldsymbol{x}_3\|_2^2 - 1) \not\subset \mathcal{G} = \mathbb{F}_2^N \backslash \mathcal{E}$ then there exists an $\boldsymbol{x}_2 \in S_{\boldsymbol{x}_1,\boldsymbol{x}_3}(\|\boldsymbol{x}_3\|_2^2 - 1)$ which is an excited state $\boldsymbol{x}_2 \in \mathcal{E}$. To achieve $\Delta E > 0$ it must be $E(|\boldsymbol{x}_3\rangle) < E(|\boldsymbol{x}_2\rangle)$. Then we can apply statement 2 from lemma I such that $E(|\boldsymbol{x}_3\rangle) < E(|\boldsymbol{x}_2\rangle) < E(|\boldsymbol{x}_1\rangle)$ and thus $\Delta E < 0$.

Thus if there exists an adjacent, intermediate excited state then the quality $\mathcal{Q} = 0 < 1$ vanishes (in particular it is not perfect). The only way to circumvent this case is if *all* adjacent, intermediate states would be ground states.

If *every* adjacent, intermediate state is a ground state, then we could apply the argument to these ground states as well. This implies that the only way to achieve a positive energy gap is that $S_{\boldsymbol{x}_1,\boldsymbol{x}_3}(n) \not\subset \mathcal{G}$ for *every* $n \in \mathbb{N}_{(\|\boldsymbol{x}_1\|_2^2, \|\boldsymbol{x}_3\|_2^2)}$. This proves the second statement of corollary II.

If $S_{\boldsymbol{x}_1,\boldsymbol{x}_3}(n) \not\subset \mathcal{G}$ for every $n \in \mathbb{N}_{(\|\boldsymbol{x}_1\|_2^2, \|\boldsymbol{x}_3\|_2^2)}$ then we can still follow the argument from the first point to conclude $\delta E > 0$. Then we can again conclude $\mathcal{Q} < 1$ not perfect which proves the first statement of corollary II. □

Corollary II is going to be very useful later as it allows us to exclude multiple realizations for the VdW model which do not need to be tested. For these realization we already know that the quality must vanish for *every* possible implementation. In contrast we find that for the

the elementary target functions we consider in this thesis, *every* realization allowed by corollary II can be implemented at least on three-dimensional Rydberg platform with finite quality. In most cases we are actually able to achieve unit quality. The simple elementaries can be also implemented on the two-dimensional Rydberg platform although this sometimes impedes the (effective) energy gap. This illustrates that the necessary condition for a positive energy gap introduced by corollary II is actually really sharp for elementary languages in the sense that we can always implement the elementary languages allowed by corollary II.

3.2.4 | Efficient Computation of LESs

Combining observation (1) (cf. remark 1) and observation (2) (cf. lemma I) we want to compute the LES efficiently. We interpret this as a *global minimization problem* on N bits subject to the constraint of excluding ground states. The constraint determines the finite *feasible set* $\mathcal{E}$ of words. In the following we shortly outline the key ideas of the algorithm which is formulated in fig. 3.3.

A Trickle-Down Ansatz. We only need to consider ISs as candidates for the energetically lowest states according to observation (1). Each IS is a subset of a MIS of the graph by definition, thus we start by considering the set of MISs on the blockade graph. The MISs include in particular the MWISs which are the energetically lowest states in the PXP-limit $\gamma \to \infty$. We *trickle-down* from the MISs by flipping excited bits to construct new ISs as subwords. This can be roughly interpreted as an 'expansion around the PXP solutions'.
We trickle-down until reaching an IS where the flip of any excited bit would increase the energy. This IS is energetically lower than any of its subwords according to observation (2). We call such an IS a *local minimum* (of the MIS)[7]. For each MIS we obtain a set of such local minima. Now, we want to exclude the ground states as candidates. For that we iterate through the ordered set of local minima. If a state we consider is a ground state we instead consider its adjacent states. Finally, we compare the energies of the excited states until finding the energetically lowest one which is the *local LES* of the MIS. This procedure is somewhat similar to the naive ansatz we attempted in subsec. 3.2.3 (cf. example 4) where we considered only the bit-flipped excited states. However now the local minima include potentially excited states.
We perform this 'trickle-down' algorithm separately for each MIS. In the end we compare the local LESs of each MIS. This guarantees to find the global energetic minimum of $\mathcal{E}$, i.e. the LES.

This algorithm is formulated rigorously in fig. 3.3. We want to illustrate this (abstract) algorithm via example 5 and fig. 3.2:

Example 5. (Cycle graph C_6)

> As an example of alg. 3.3 consider the cycle graph $\mathcal{B}' = C_6$. There are *five MISs* given by the states in the boxes in fig. 3.2. Note that the tree only comprises the 18 *ISs* of $\mathcal{B}'$ for a clearer visualization. Thanks to observation (1) we may directly exclude the 46 *non-independent sets* (NISs) as candidates for the energetically lowest state. Adjacent substates are connected by arrows in tree 3.2.

[7] The notion of a local minimum is mathematically not fully correct as there might still exist an adjacent superstate of lower energy. It can be interpreted as a 'local minimum' with respect to only its substates.

Starting with a MIS (boxes) the alg. 3.3 compares the eigenenergies of the adjacent substates (arrows) trickling down the tree 3.2. It stops as soon as every substate is energetically higher.

Consider an L-complex $(\mathcal{C}^{\mathcal{Q}}_{\mathcal{K}}, L, \mathfrak{L})$ of the target language $L = \{\boldsymbol{e}_1 + \boldsymbol{e}_3 + \boldsymbol{e}_5, \boldsymbol{e}_2 + \boldsymbol{e}_4 + \boldsymbol{e}_6\}$ with a D_6-symmetric structure $\mathcal{C}$ of equal detunings $\Delta = \Delta_i$ and equal distances d between the atoms. Note that the ground states are the MMISs (or equivalently the MWISs) of $\mathcal{B}'$. In the following we assume that $\mathcal{B}'$ is a *spanning subgraph*[a] of $\mathcal{B}[\mathcal{C}]$, i.e. that $d < (C/\Delta)^{1/6}$, such that we may apply the alg. 3.3:

1 | In case $d > (2C/3^3\Delta)^{1/6}$, the MISs are energetically favorable compared to their (adjacent) substates. Then the algorithm compares the adjacent excited states (including the adjacent non-independent superstates) of the ground states with the MISs $|\boldsymbol{e}_1 + \boldsymbol{e}_4\rangle$, $|\boldsymbol{e}_2 + \boldsymbol{e}_5\rangle$ and $|\boldsymbol{e}_3 + \boldsymbol{e}_6\rangle$ to find the LES. In this case latter would be the LESs.

2 | For distance $(C/3^3\Delta)^{1/6} < d < (2C/3^3\Delta)^{1/6}$ the six non-maximal substates with two excited bits are energetically lower than the two ground states and the words with one excited bit. In this case the algorithm would compare the words with two excited bits. Again, the LESs would be the MISs of two atoms.

3 | In case $(C/2^6\Delta)^{1/6} < d < (C/3^3\Delta)^{1/6}$ the MISs of two atoms remain favourable compared to their substates but the states $|\boldsymbol{e}_i\rangle$ are favourable compared to the six non-maximal ISs of two atoms. Thus again, we determine the LESs as the MISs of two atoms.

4 | Lastly consider the case $d < (C/2^6\Delta)^{1/6}$. Here $\mathcal{B}' \neq \mathcal{B}$ as $E' \subset E$. We may still apply alg. 3.3 and the algorithm trickles-down to the ISs of one atom. Each of these states $|\boldsymbol{e}_i\rangle$ is of equal energy, thus there are six LESs.

[a] A spanning subgraph $\mathcal{B}' = (V', E')$ of $\mathcal{B}[\mathcal{C}] = (V, E)$ includes the same set of vertices $V' = V$ but a subset $E' \subseteq E$ of the edges. Due to the D_6-symmetry of $\mathcal{C}$, this assumption only excludes only the *edgeless* blockade graph $\mathcal{B}[\mathcal{C}] = \overline{K}_6$ with $E = \emptyset$.

Especially for 'large' (inverse) exponents $\gamma \gg 1$ of the interaction potential this 'trickle-down' alg. 3.3 is far more efficient than the brute-force calculation of the energy for all 2^N eigenstates. For $\gamma = 6$ in the VdW model, the VdW potential $U_{\mathrm{VdW}}(r_{ij}) \sim 1/r_{ij}^6$ decays fast and the PXP model is a reasonable approximation. This makes the MISs good approximations of the energetically lowest states and alg. 3.3 converges fast.

3.2.5 | Efficient Computation of the MISs

Note that this alg. 3.3 requires the calculation of *all* MIS which is a well-known NP-hard problem[24]. This means that for large number of atoms this algorithm remains slow. Luckily, many interesting L-complexes are constructed from smaller ones using amalgamation: Tessellated languages are realized by amalgamating unit-cells on a lattice and complex Boolean functions can be decomposed into small primitives. This allows for a more efficient calculation of the MISs which we are going to discuss in this subsection. In the following we often denote a word $\boldsymbol{x}$ as an IS when formally $\mathfrak{L}(\boldsymbol{x}\backslash\boldsymbol{0}) \cong \boldsymbol{x}$ is the IS (the labeling is a one-to-one mapping).

Input: Blockade Graph $\mathcal{B}[\mathcal{C}] = (V, E)$

Output: Energetically lowest excited state $\boldsymbol{x} \in \mathcal{E}$ and its energy $E(|\boldsymbol{x}\rangle)$

1 | We fix a spanning subgraph $\mathcal{B}' = (V, E')$ where $E' \subseteq E$. Calculate the set of words $\boldsymbol{x} \in \mathbb{F}_2^N$ where $\mathfrak{L}(\boldsymbol{x} \backslash \mathbf{0})$ is a MIS of $\mathcal{B}'$.

2 | Continue the algorithm for each MIS separately (using multiprocessing). We want to substitute the word $\boldsymbol{x}$ of the MIS by its the sub- or superword with the lowest eigenenergy:

- **a** | Calculate the eigenenergy $E(|\boldsymbol{x}\rangle)$.
- **b** | For general IS, $B(\boldsymbol{x})$ is going to be the set of indices of excited bits for which it is potentially energetically favourable not to excite them. Initially, we define $B(\boldsymbol{x}) := \boldsymbol{x} \backslash \mathbf{0}$.
- **c** | We want to construct a list l of (locally minimal) IS. Initially, we define $l := \{\boldsymbol{x}\}$.
- **d** | For word $\boldsymbol{x}$, eigenenergy $E(|\boldsymbol{x}\rangle)$ and bit indices $B(\boldsymbol{x})$, perform the following loop:
  - **i** | For each bit $i \in B(\boldsymbol{x})$ it is $x_i = 1$ by construction. Consider the bit-flipped subwords $\boldsymbol{x}^{(i)} = (x_1, \ldots 0_i, \ldots x_N)$ of $\boldsymbol{x}$.
  - **ii** | Check whether we have already examined the word $\boldsymbol{x}^{(i)}$ by comparing with a global Hashlist. If we have already examined $\boldsymbol{x}^{(i)}$, break this loop and continue. Otherwise add this word to the global Hashlist and continue this loop.
  - **iii** | Calculate the eigenenergy $E(|\boldsymbol{x}^{(i)}\rangle)$.
  - **iv** | Start with $B' = \emptyset$. For each subword $\boldsymbol{x}^{(i)}$ with $E(|\boldsymbol{x}^{(i)}\rangle) < E(|\boldsymbol{x}\rangle)$, we add i to B'.
  - **v** | If $B' \neq \emptyset$, we discard $\boldsymbol{x}$ from l. For each $i \in B'$, we add $\boldsymbol{x}^{(i)}$ to l and restart this loop with $\boldsymbol{x}^{(i)} \mapsto \boldsymbol{x}$, $E(|\boldsymbol{x}^{(i)}\rangle) \mapsto E(|\boldsymbol{x}\rangle)$ and $B' \mapsto B(\boldsymbol{x})$. Otherwise we continue.
- **e** | Sort l by the energy of its states. Consider the first state of the sorted list (the state of lowest energy), we define it as $\tilde{\boldsymbol{x}}$. Initially, we set $E(|\hat{\boldsymbol{x}}\rangle) = \infty$.
- **f** | Consider two cases: (i) If $\tilde{\boldsymbol{x}}$ is an excited state: If $E(|\tilde{\boldsymbol{x}}\rangle) < E(|\hat{\boldsymbol{x}}\rangle)$ we define $\hat{\boldsymbol{x}} := \tilde{\boldsymbol{x}}$; else we continue. (ii) If $\tilde{\boldsymbol{x}}$ is a ground state we calculate its adjacent sub- or superstate of lowest energy and define it as $\tilde{\boldsymbol{x}}$ (if any of the adjacent states are ground states we also consider their adjacent states and so on), such that $\tilde{\boldsymbol{x}}$ is an excited state. If $E(|\tilde{\boldsymbol{x}}\rangle) < E(|\hat{\boldsymbol{x}}\rangle)$, we define $\hat{\boldsymbol{x}} := \tilde{\boldsymbol{x}}$.
- **g** | Consider the next state of l and define it as $\tilde{\boldsymbol{x}}$. If $E(|\hat{\boldsymbol{x}}\rangle) < E(|\tilde{\boldsymbol{x}}\rangle)$, we continue. Otherwise we restart previous point with the new $\tilde{\boldsymbol{x}}$.
- **h** | Return $\hat{\boldsymbol{x}}$ and $E(|\hat{\boldsymbol{x}}\rangle)$.

3 | For each word $\boldsymbol{x}$ of a MIS, we identified an excited state $\hat{\boldsymbol{x}}$ with eigenenergy $E(|\hat{\boldsymbol{x}}\rangle)$. Now for all MIS, we pick the word with the lowest eigenenergy and return it.

Algorithm 3.3: Algorithm for the efficient calculation of the energy gap. As input the algorithm requests the blockade graph $\mathcal{B}[\mathcal{C}]$ of the structure. It returns the energetically lowest excited state (LES).

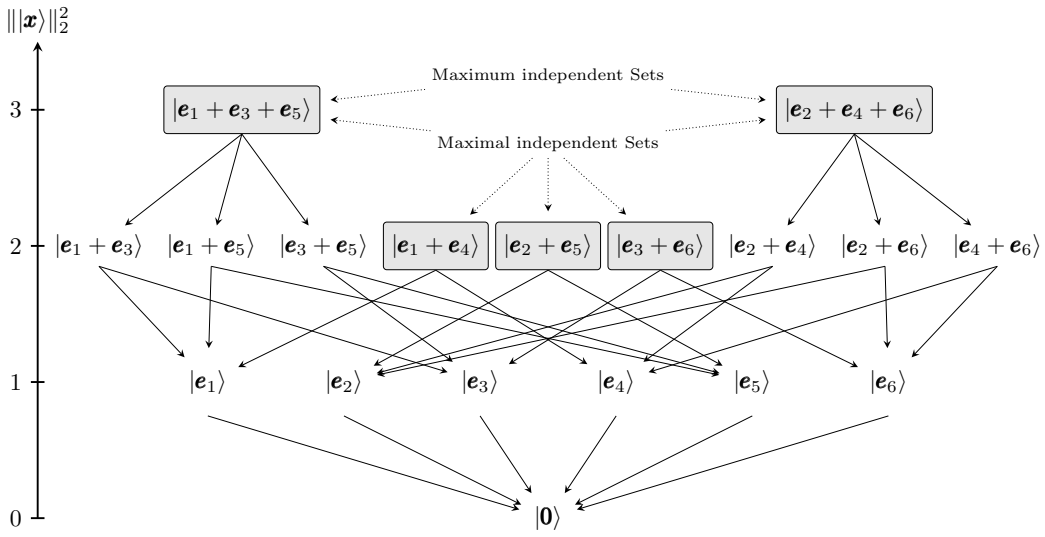

Figure 3.2: Tree of ISs for the cycle graph C_6. Adjacent substates are connected via arrows. The boxed states are the MISs of C_6. The axis denotes the number of atoms in the IS. The remaining 46 states corresponding to non-independent sets (NISs) are not noted in this tree as they are excluded by observation (1). The alg. 3.3 starts with the MISs and trickles down the tree following the arrows until finishing at the energetically lowest substate.

MISs of a Tessellated System. Consider the L-complex complex $([\mathcal{C}_\mathcal{L}]^\mathcal{Q}_\mathcal{K}, L_\mathcal{L}, \mathfrak{L})$ of a tessellated language $L_\mathcal{L}$ on a lattice $\mathcal{L}$[8]. The structure $\mathcal{C}_\mathcal{L}$ is constructed by placing a unit-cells $\mathcal{C}$ on each vertex $v \in \mathcal{V}(\mathcal{L})$. By amalgamating the corresponding ports of adjacent unit-cells this yields a structure $\mathcal{C}_v$ with modified detunings for each vertex $v \in \mathcal{V}(\mathcal{L})$.

Lemma III (MISs of a Tessellated System)**.**

We assume that no two ports are connected in the blockade graph $\mathcal{B}[\mathcal{C}]$ and that no two atoms of different unit-cells are connected in $\mathcal{B}[\mathcal{C}_\mathcal{L}]$. For each vertex $v \in \mathcal{V}(\mathcal{L})$ we assign a MIS $\boldsymbol{x}_v$ from of the blockade graph $\mathcal{B}[\mathcal{C}_v]$ with the following restriction:

> *''If an excited port and a ground-state port are identified, then each nearest neighbour of the excited port must have an excited nearest neighbour itself, besides any excited ports which are identified with a ground-state ports.''* (3.14)

Then, for each tuple $(\boldsymbol{x}_v \mid v \in \mathcal{V}(\mathcal{L}))$ of MISs on $\mathcal{B}[\mathcal{C}_v]$ following restriction (3.14), we can identify exactly one MIS $\boldsymbol{x}$ on $\mathcal{B}[\mathcal{C}_\mathcal{L}]$.

[8] Possibly finite or with PBCs

Proof.

We proof this statement constructively by constructing a bijection between the set of tuples and the set of MISs on $\mathcal{B}[\mathcal{C}_\mathcal{L}]$. Consider an arbitrary tuple $(\boldsymbol{x}_v \mid v \in \mathcal{V}(\mathcal{L}))$ of MISs on $\mathcal{B}[\mathcal{C}_v]$ following restriction (3.14). We define the γ-product of MISs by the following rules:

0 | *Ancillary bits* are excited in the amalgamated MIS if and only if they are excited in the MIS $\boldsymbol{x}_v$ of their vertex v.

1 | If *two excited bits* are identified during amalgamation, then the result is an *excited bit*.

2 | If *two ground-state bits* are identified during amalgamation, then the result is a *ground-state bit*.

3 | If *an excited bit and a ground-state bit* are identified during amalgamation, then the result is a *ground-state bit*.

Note that no two atoms of different unit-cells are connected in $\mathcal{B}[\mathcal{C}_\mathcal{L}]$. Thus $\mathcal{B}[\mathcal{C}_\mathcal{L}]$ is constructed from $\mathcal{B}[\mathcal{C}_v]|_{v\in\mathcal{V}(\mathcal{L})}$ by identifying the ports but we do not need to add further edges. As the tuple $(\boldsymbol{x}_v \mid v \in \mathcal{V}(\mathcal{L}))$ consisted of ISs on $\mathcal{B}[\mathcal{C}_v]|_{v\in\mathcal{V}(\mathcal{L})}$, the resulting (amalgamated) word $\boldsymbol{x}$ is an IS on $\mathcal{B}[\mathcal{C}_\mathcal{L}]$ by construction. $\boldsymbol{x}$ is maximal, if every ground-state atom possesses an excited nearest neighbour. This is trivially true for any port and for ancillaries adjacent only to ancillaries. Condition 3.14 secures that this remains true for ancillaries adjacent to ports subject to the 3rd rule, where an excited bit is flipped to its ground state. Thus this construction yields a MIS on $\mathcal{B}[\mathcal{C}_\mathcal{L}]$ for any initial tuple of MISs on $\mathcal{B}[\mathcal{C}_v]$ following restriction (3.14).
Now we have a construction which identifies a MIS on $\mathcal{B}[\mathcal{C}_\mathcal{L}]$ with each tuple $(\boldsymbol{x}_v \mid v \in \mathcal{V}(\mathcal{L}))$ of MISs on $\mathcal{B}[\mathcal{C}_v]$ following restriction (3.14). It remains to prove that this function is bijective. As no two ports are connected in $\mathcal{B}[\mathcal{C}]$, there are no connected ports in $\mathcal{B}[\mathcal{C}_v]|_{v\in\mathcal{V}(\mathcal{L})}$ and $\mathcal{B}[\mathcal{C}_\mathcal{L}]$ either. In a MIS $\boldsymbol{x}$ any bit i can be viewed as a function of its adjacent bits:

$$x_i = \prod_{j\in\mathbb{N}(i)} (1 - x_j). \tag{3.15}$$

Here $\mathfrak{L}(\mathbb{N}(i))$ denotes the set of nearest neighbours of vertex $\mathfrak{L}(i) \in V$. Thus for any MIS of a blockade graph where no two ports are adjacent, the states of the ports are a function of the states of their adjacent ancillaries. This means in a MIS of such a graph, the states of the ancillaries store the full information. As the states of the ancillaries is conserved (according to the 0th rule), there is no information lost during the construction. We can uniquely identify each tuple with each MIS on $\mathcal{B}[\mathcal{C}_\mathcal{L}]$ using the ancillaries. Thus no two different tuples yield the same MIS of $\mathcal{B}[\mathcal{C}_\mathcal{L}]$ and vice versa. Therefore, the described function is an bijection. □

Note that the 3rd rule in the proof of lemma III and the constraint (3.14) is what distinguishes the 'product' of MISs from the γ-product of languages where we instead consider the *compatibility condition*.

In the proof of lemma III we have constructed the bijection

$$\{\boldsymbol{x} \mid \boldsymbol{x} \text{ is MIS of } \mathcal{B}[\mathcal{C}_\mathcal{L}]\} \cong \big\{(\boldsymbol{x}_v \mid v \in \mathcal{V}(\mathcal{L})) \mid (3.14) \ \wedge \ \forall_{v\in\mathcal{V}(\mathcal{L})} : \boldsymbol{x}_v \text{ is MIS of } \mathcal{B}[\mathcal{C}_v]\big\} \tag{3.16}$$

between the MISs of the tessellated system and the MISs on every vertex following condition (3.14). By calculating the MIS of $\mathcal{B}[\mathcal{C}_v]$ for any vertex $v \in \mathcal{V}(\mathcal{L})$, this allows for the efficient calculation of every MIS of the tessellated system. If $\mathcal{L}$ has PBCs then the system is transnational invariant and $\mathcal{C}_v$ is identical for all $v \in \mathcal{V}(\mathcal{L})$. Otherwise $\mathcal{C}_v$ may differ at the boundary.

Closing Remarks. At this point I want to make some closing remarks on alg. (3.3) and lemma III:

1 | In lemma III we assume that no two ports are connected in the blockade graph $\mathcal{B}[\mathcal{C}]$. Note that this is a very weak assumption. If two ports were in blockade, it would be energetically disfavourable to excite them simultaneously. However in most interesting target functions (in particular the ones considered in this thesis) any two ports are excited simultaneously in some ground state. Such a ground state would be energetically gapped out if the ports were in blockade. Thus such a structure would be no good choice as a unit cell.

2 | Furthermore, in lemma III we assume that no two atoms of different unit cells are connected in the blockade graph. This is for general unit-cells not the case. However alg. (3.3) requests only the MISs of a *spanning subgraph* as its input. We can thus apply lemma III to calculate the MISs of the spanning subgraph which excludes edges between atoms of different unit-cells. This algorithm turned out to be very useful and is heavily used for the calculation of the energy structure throughout this thesis.

3 | A disadvantage of alg. (3.3) compared to the direct 'brute-force' calculation is that it only yields the lowest excited state but not the full energy structure. This is sufficient for the minimization algorithm and alg. (3.3) *heavily* used in the minimization of structures throughout this thesis. For the figures with the full energy structure we have to apply the slow direct algorithm calculating the energy of every state. This is still quite acceptable as now we only need to calculate the full structure just once but not in every minimization iteration.

4 | We can directly generalize lemma III to calculate MISs of amalgamated BOOLEAN L-complexes. In fact in the proof of lemma III we never really use that $\mathcal{C}_{\mathcal{L}}$ is a tessellated structure and the structures $\mathcal{C}_v$ of each vertex $v \in \mathcal{L}$ differ (in the detunings) anyway. However we do not require such an algorithm for this thesis.

This concludes the theoretical part of this section. In the following we want to apply the derived tools exemplary to logic elementaries from fig. 3.1.

3.2.6 | Optimization of the NOR-Gates

The last subsections 3.2.1 - 3.2.5 focused on the problem of optimizing a given L-complex for its measures of quality, namely $\mathcal{Q}$, ΔE_{eff} and r. For that purpose we introduced a numerical minimization algorithm 3.2 in subsec. 3.2.1. In this subsection we want to illustrate this algorithm by applying it exemplarily to the NOR-gates 3.1 from subsec. 3.1.2 which were constructed by the rejection sampling algorithm. The goal is to optimize the structures such that they implement their languages with a larger quality factor. We do not yet want apply theorem V (or its corollaries) which we are going to introduce in the following sections 3.3 and 3.4. Here we only want to illustrate the numerical optimization.

We apply the minimization algorithm to the three samples presented in fig. 3.1 which were constructed by the *rejection sampling algorithm* 3.1. The samples implement the PXP-minimal NOR-realizations. The samples optimized by the minimization algorithm are portrayed in fig. 3.3. Again we measure the energy scaling in units of the largest detuning $\Delta_{\max}$ thus the energy gap equals the effective energy gap. For a detailed explanation of this presentation we refer to subsec. 3.1.2.

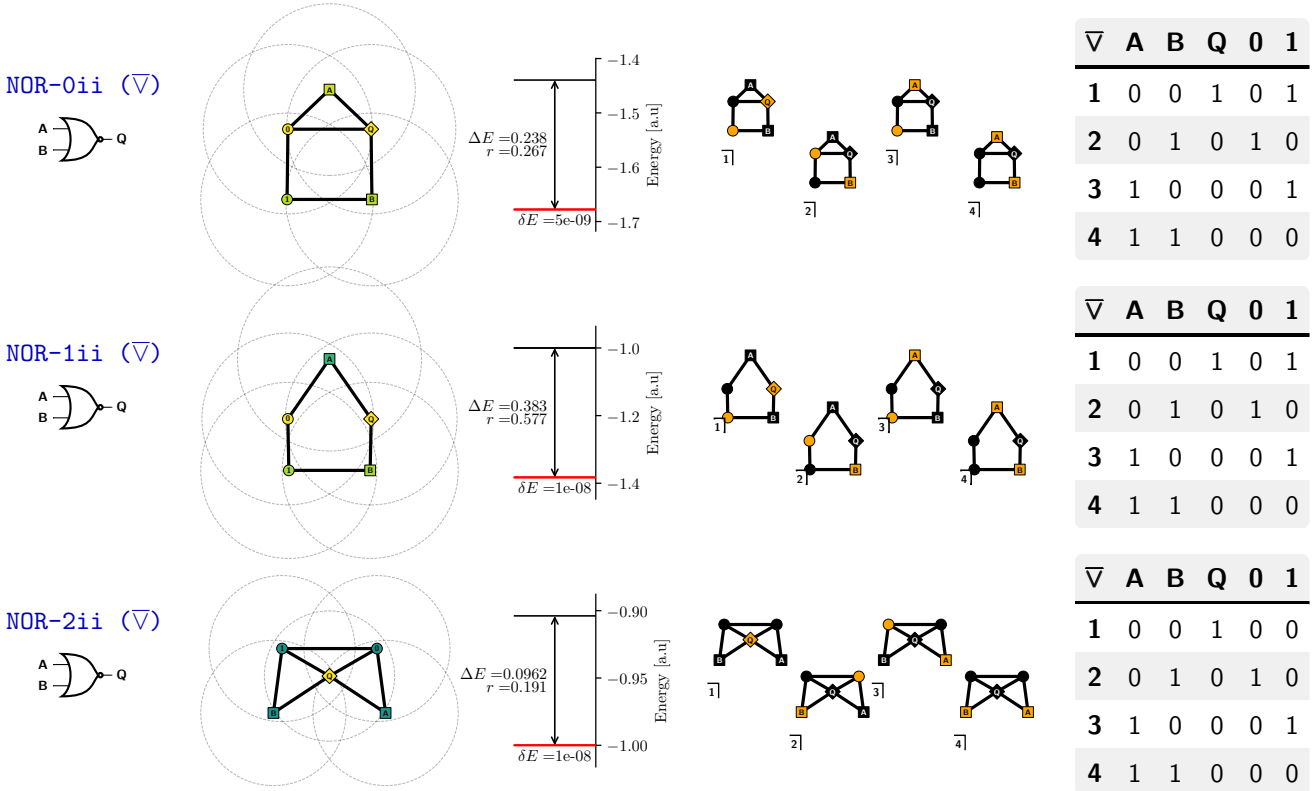

∇	A	B	Q	0	1
1	0	0	1	0	1
2	0	1	0	1	0
3	1	0	0	0	1
4	1	1	0	0	0

∇	A	B	Q	0	1
1	0	0	1	0	1
2	0	1	0	1	0
3	1	0	0	0	1
4	1	1	0	0	0

∇	A	B	Q	0	1
1	0	0	1	0	0
2	0	1	0	1	0
3	1	0	0	0	1
4	1	1	0	0	0

Figure 3.3: Three PXP-minimal NOR-realizations implemented in the VdW-model. The structures are optimized for the quality factor using the minimization algorithm 3.2. The languages were introduced by Stastny *et al.* in Ref. [38, 37]. In the PXP model the realizations are minimal in their number of atoms and the list of minimal realizations is proven exhaustive[37].

Symmetry Constraints. For fig. 3.3 we apply a D_1-symmetry as a constraint during minimization for all three samples. In the following we shortly motivate this ansatz. Remember that the languages $L_{\texttt{NOR0}} \equiv L_{\texttt{NOR1}}$ are identical and in particular they are the same realization: they differ only in their (unphysical) blockade graph. The generated permutation group $\Sigma_{\mathcal{N}}[\texttt{NOR1}] = \langle (0\ Q) \circ (1\ B) \rangle \subset S_{\mathcal{N}}$ is the symmetry group of $L_{\texttt{NOR1}}$ acting on the atoms via $\mathfrak{L}$. For $L_{\texttt{NOR2}}$ the symmetry group on the atoms is the permutation group $\Sigma_{\mathcal{N}}[\texttt{NOR2}] = \langle (A\ B) \circ (0\ 1) \rangle \subset S_{\mathcal{N}}$. Here $(\mathfrak{i}\ \mathfrak{j}\ \mathfrak{k})$ denotes the cyclic permutation of the atoms $\mathfrak{i}, \mathfrak{j}, \mathfrak{k} \in \mathcal{N}$.

The energy structure remains invariant under $\Sigma_{\mathcal{N}}$ if and only if we request the D_1-symmetry. This is in particular sufficient to achieve degeneracy between the symmetric ground states. Note that the logic gates in the PXP model possess a D_1-symmetry in their detunings and their blockade graph[9] as well[38]. Numerically we find that the symmetry constraint does not impede the

[9] In the PXP model we can modify the geometry in some small region without modifying the energy structure.

optimization (it supports the optimization) which legitimizes the constraint *a posteriori*.
Note that in contrast to $L_{\texttt{NOR1}}$ and $L_{\texttt{NOR3}}$, the language $L_{\texttt{NOR2}}$ is symmetric in the input ports: $\Sigma_{\mathcal{N}}[\texttt{NOR2}]$ does not permute ports with ancillaries. Thus in the second realization the symmetry between the ports in target function is conserved. This is going to help us in chapter 3.3 to define an effective language matrix.

A finite Energy Splitting. We find that the minimization algorithm successfully achieves almost perfect ground degeneracy $\delta E \lesssim 10^{-8}\Delta_{\max}$. Nevertheless, even though the energy splitting is very small it is not *exactly* zero and thus the quality is not quite perfect. Only by applying the minimization algorithm we are not going to achieve such a *perfect* energy splitting within a finite runtime.
In the following want to find a systematic way to determine whether it is possible to achieve a vanishing energy splitting. If so, we want to find a way to modify the samples such that they possess perfect quality. Furthermore, ideally we do not want to use the minimization algorithm until reaching $Q \lesssim 10^{-7}$ as this becomes very time-expensive for larger L-complexes. We want to find a criterion to determine just how long we have to apply the minimization algorithm to secure that we can achieve degeneracy in the ground states.
These issues are are going to be discussed in the following sec. 3.3. There we introduce theorem V which is a conceptually important and very helpful theorem in this thesis. Further, we introduce new concepts such as the extended language matrix which we are going use to derive corollary VII. In sec. 3.4 we are going to continue with a discussion about symmetries and we introduce the effective description.

Thus here consider the blockade graph instead.

3.3 | Achieving Ground State Degeneracy

The two previous sections 3.1 and 3.2 discuss the problems of implementing L-complexes in the VdW model. As a solution in each section we propose an algorithm: Sec. 3.1 discusses a *rejection sampling algorithm* 3.1 to construct samples of Rydberg complexes for a given target language. Sec. 3.2 discusses a *minimization algorithm* 3.2 to efficiently optimize a given L-complex for the measures of quality. In both sections we exemplarily apply the algorithms to the PXP-minimal `NOR`-languages which allows to construct and optimize their Rydberg complexes. This yields high-quality implementations as presented in fig. 3.3.

However these algorithms will for a finite runtime always terminate in L-complexes with a finite energy splitting and thus non-optimal quality. In the following we are interested in whether it is possible to achieve perfect degeneracy of the low-energy eigenspaces for these samples. This is not only interesting for academic reasons: Firstly, finite energy splittings can add up under amalgamation. We are going to see that this can disarrange the energy structure for large amalgamated complexes, e.g. in the case of tessellated loop models in chap. 6. Furthermore such energy splittings introduce a phase shift in the state when introducing quantum fluctuations by ramping up the Rabi frequencies $\Omega_{\mathfrak{i}} > 0$ in the Hamiltonian. This motivates the following chapter.

An introductory Remark. It is easy to see that we can not achieve ground state degeneracy for every target language in the VdW-model, even if that target language possesses an L-complex with a positive energy gap:

Example 6. (A minimal Counterexample)

> An simple example is $L_t = \mathbb{F}_2^3 \backslash \{(0,0,0)\}$ which has $\delta E \geq \Delta E/3$, i.e. $\mathcal{Q} \lesssim 71\%$. This can be easily seen with corollary II because the ground states are non-adjacent substates without intermediate excited states. Equality $Q = 1/3$ is only achieved in the D_3-symmetric configuration with $I_{\mathfrak{ij}} = 2\Delta_{\mathfrak{k}}/3$ for $\mathfrak{i}, \mathfrak{j}, \mathfrak{k} \in \mathcal{N}$. In this case it is $E(|1,1,1\rangle) = E(|1,0,0\rangle)$ and $E(|1,1,0\rangle) = 4/3E(|1,0,0\rangle)$.

We are going to discover more such target languages later in chap. 5 or chap. 6 where we prove the absence of a structure with vanishing energy splitting. In particular we encounter target languages which possess a L-complex with maximal quality factor in the PXP model but where no L-complex of unit quality factor exists in the VdW model. Nevertheless such languages might remain physically useful if their quality if sufficiently large.

On Ground State Degeneracy. To achieve degeneracy we search for *physical* solutions of the linear system (3.3). As it is not easy to check whether any given solution (3.4) is physical (cf. the rejection sampling algorithm 3.1), we instead start by considering a physical L-complex which *approximately* solves eq. (3.3), i.e. which possesses a (small) finite energy splitting $\delta E > 0$. Such a complex may for example be constructed using the algorithms from previous sections 3.1 and 3.2. We now formulate the lemma IV:

Lemma IV (Existence of Degeneracy)**.**

Consider some L-complex $(\mathcal{C}^{\mathcal{Q}}_{\mathcal{K}}, L_t, \mathfrak{L})$ *with target language* $L = L_t$ *of length* $g = |L_t|$*. If the eigenvectors* $|\boldsymbol{x}\rangle$ *of the words* $\boldsymbol{x} \in L_t$ *are linear independent, then there exists a L-complex* $(\tilde{\mathcal{C}}^{\mathcal{Q}}_{\mathcal{K}}, L_t, \mathfrak{L})$ *where* $\mathcal{H}_t = \mathcal{H}(L_t)$ *is a g-dimensional eigenspace of the Hamiltonian* $H[\tilde{\mathcal{C}}]$*.*

In other words: in Hamiltonian $H[\tilde{\mathcal{C}}]$ each vector $|\boldsymbol{x}\rangle \in \mathcal{H}_t$ possesses equal energy (in particular each vector $|\boldsymbol{x}\rangle$ with $\boldsymbol{x} \in L_t$), thus the energy splitting $\delta E = 0$ vanishes. For the following proof(s) we again denote the set of atoms by $\mathcal{N}$ and its magnitude by N, then the target language is $L_t \subseteq \mathbb{F}_2^N$.

Proof.

To proof lemma IV, we rewrite the problem as a linear system similar as in (3.3):

$$L_{ij}\tilde{\Delta}_j \stackrel{!}{=} \tilde{b}_i \qquad \text{with} \qquad \tilde{b}_i = -\tilde{E} + \sum\nolimits_{j,k=1}^{N} L_{ij} I_{\mathfrak{L}(j)\mathfrak{L}(k)} L_{ik}, \tag{3.17}$$

Here $\boldsymbol{L} \in \mathbb{F}_2^{g\times N}$ is the language matrix of $L = L_t$ as defined above. The solution vector $\tilde{\boldsymbol{\Delta}}$ is defined via the labeling $\tilde{\Delta}_j := \tilde{\Delta}_{\mathfrak{L}(j)}$ and the parameter $\tilde{E} \in \mathbb{R}$ is the new eigenenergy in Hamiltonian $H[\tilde{\mathcal{C}}]$. There are N *independent* variables in this linear system.

According to the Rouché–Capelli theorem a system of linear equations has no solution if the rank of the augmented matrix is greater than the rank of the coefficient matrix. If on the other hand the ranks of these two matrices are equal the system must have at least one solution. As the words are linear independent we know that the matrix $\boldsymbol{L}$ has full row rank, i.e. $\operatorname{rank}(\boldsymbol{L}) = g$. Thus the augmented matrix with the augmented rows must be of rank g as well. Therefore the linear system from eq. (3.17) has at least one solution $\tilde{\boldsymbol{\Delta}} = \boldsymbol{L}^{+}\boldsymbol{b}$ for any energy $\tilde{E} \in \mathbb{R}$, independent of the geometry. Here again $\boldsymbol{L}^{+}$ denotes Moore–Penrose pseudoinverse of the matrix $\boldsymbol{L}$.

Thus for structure $\tilde{\mathcal{C}} = (\boldsymbol{r}_{\mathfrak{i}}, \tilde{\Delta}_{\mathfrak{i}} \mid \mathfrak{i} \in \mathcal{N})$ the eigenstates $|\boldsymbol{x}\rangle$ with $\boldsymbol{x} \in L$ possess equal eigenenergy $\langle H[\tilde{\mathcal{C}}]\rangle_{\boldsymbol{x}} = \tilde{E}$ for any word $\boldsymbol{x} \in L$. □

It should be mentioned that solutions of this linear system might not be physically *useful* (yet). Solutions of this linear system might include negative detunings which we do not consider (by remark 3). Further, the lemma IV does not yet consider the energy gap ΔE and the new eigenenergy $\tilde{E} \in \mathbb{R}$ is still left a parameter. As discussed in sec. 3.1 (see eq. (3.8) *eq* seq.) we may restrict ourselves to $\tilde{E} > 0$ to achieve $\Delta E > 0$. Nevertheless, in general $\mathcal{H}_t$ is no gapped low-energy eigenspace of the Hamiltonian $H[\tilde{\mathcal{C}}]$ for any choice $\tilde{E} \in \mathbb{R}_{>0}$ because the energy gap becomes negative. This might even be the case if the target Hilbert space has been a gapped low-energy eigenspace of the L-complex $(\mathcal{C}^{\mathcal{Q}}_{\mathcal{K}}, L, \mathfrak{L})$ (with $\delta E > 0$), i.e. if the condition $\mathcal{H}_0[H; \mathcal{C}] \cong_{\mathfrak{L}} \mathcal{H}_t$ from eq. (2.9) is met: By shifting the detunings the states shift as well and thus the energetic arrangement of the states might get corrupted in the process.

Securing positive Quality. However the energy structure is a continuous, linear function of the detunings. Thus for a finite change in the detunings the states are shifted energetically only by a finite amount (depending on the magnitude of the change in the detunings). This allows for an upper bound on the energetic disarrangement and thus a lower bound on the energy gap. This solves the issues we discussed above for lemma IV. We formalize this argument in the following central theorem V of this thesis:

Theorem V (Degenerate Ground States 1)**.**

Consider some L-complex $(\mathcal{C}_{\mathcal{K}}^{\mathcal{Q}}, L, \mathfrak{L})$ *with target language* $L = L_t$ *of length* $g = |L_t|$*. If the eigenvectors* $|\boldsymbol{x}\rangle$ *of the words* $\boldsymbol{x} \in L_t$ *are linear independent and if the quality factor* $\mathcal{Q} > \exp\left[-2/(g\|\boldsymbol{L}^{+}\|_1)\right]$ *is sufficiently large, then there exists a L-complex* $(\tilde{\mathcal{C}}_{\mathcal{K}}^{\mathcal{Q}}, L, \mathfrak{L})$ *where* $\mathcal{H}_t = \mathcal{H}(L_t)$ *is a g-dimensional gapped low-energy eigenspace of the Hamiltonian* $H[\tilde{\mathcal{C}}]$*.*

In other words: $\mathcal{H}_0[H; \tilde{\mathcal{C}}] \cong_{\mathfrak{L}} \mathcal{H}_t$ with $\mathcal{Q} = 1$. The eigenstates $|\boldsymbol{x}\rangle$ with $\boldsymbol{x} \in L$ are degenerate and energetically lower than the eigenstates $|\boldsymbol{x}\rangle$ with $\boldsymbol{x} \in \mathbb{F}_2^N \backslash L$. To proof this statement, we start with previous lemma IV and derive an upper bound on the energetic shift.

Proof.

In structure $\mathcal{C} = (\boldsymbol{r}_{\mathfrak{i}}, \Delta_{\mathfrak{i}} \mid \mathfrak{i} \in \mathcal{N})$, the linear system

$$L_{ij}\Delta_j = b_i \qquad \text{with} \qquad b_i = -E_i + \sum\nolimits_{j,k=1}^{N} L_{ij} I_{\mathfrak{L}(j)\mathfrak{L}(k)} L_{ik} \tag{3.18}$$

is solved by the detunings $\Delta_j = \Delta_{\mathfrak{L}(j)}$. Here $E_i \equiv \langle H[\mathcal{C}]\rangle_{\boldsymbol{x}_i}$ is the eigenenergy of the i-th state associated with the i-th row of the language matrix $\boldsymbol{L} \in \mathbb{F}_2^{g\times N}$. From lemma IV, we know that there exists a structure $\tilde{\mathcal{C}} = (\boldsymbol{r}_{\mathfrak{i}}, \tilde{\Delta}_{\mathfrak{i}} \mid \mathfrak{i} \in \mathcal{N})$ with constant energy $\tilde{E} = \langle H[\tilde{\mathcal{C}}]\rangle_{\boldsymbol{x}_i}$ for all $\boldsymbol{x}_i \in L$ for any parameter $\tilde{E} \in \mathbb{R}$. By subtracting eq. (3.18) from eq. (3.17), we obtain the new linear system $L_{ij}\delta_j = \delta E_i$, where we defined $\delta_j \equiv \tilde{\Delta}_j - \Delta_j$ and $\delta E_i \equiv E_i - \tilde{E}$.
For any two words $\boldsymbol{x}, \boldsymbol{y} \in \mathbb{F}_2^N$, we can identify their energy difference in structure $\mathcal{C}$ as

$$\Delta E_{\boldsymbol{xy}} \equiv E_{\boldsymbol{y}} - E_{\boldsymbol{x}} = -\Delta_i\,(y_i - x_i) + \sum\nolimits_{i,j=1}^{N} I_{\mathfrak{L}(i)\mathfrak{L}(j)}\,(y_i y_j - x_i x_j)\,. \tag{3.19}$$

In $\tilde{\mathcal{C}}$ the energy difference is then modified by

$$\delta(\Delta E_{\boldsymbol{xy}}) \equiv \Delta\tilde{E}_{\boldsymbol{xy}} - \Delta E_{\boldsymbol{xy}} = -\delta_i\,(y_i - x_i) \tag{3.20}$$

as the geometries $\mathcal{G}_{\tilde{\mathcal{C}}} = \mathcal{G}_{\mathcal{C}}$ and thus the interactions $I_{\tilde{\mathcal{C}}} = I_{\mathcal{C}}$ are identical by construction. Choosing $\boldsymbol{x} \in L$ and $\boldsymbol{y} \in \mathbb{F}_2^N \setminus L$, we want to show $\Delta\tilde{E}_{\boldsymbol{xy}} > 0$. As $\Delta E_{\boldsymbol{xy}} \geq \Delta E$, this is fulfilled in particular if $\Delta E > -\delta(\Delta E_{\boldsymbol{xy}})$. An upper bound on $-\delta(\Delta E_{\boldsymbol{xy}})$ is given by

$$-\delta(\Delta E_{\boldsymbol{xy}}) = \delta_i\,(x_i - y_i) \leq |\delta_i\,(x_i - y_i)| \leq |\delta_i|\,|x_i - y_i| \leq |\delta_i| = \|\boldsymbol{\delta}\|_1, \tag{3.21}$$

where $\|\cdot\|$ denotes the 1-norm of the $\boldsymbol{\delta}$-vector. By definition $\boldsymbol{\delta}$ is the solution of the linear system $L_{ij}\delta_j = \delta E_i$. The minimal solution (with respect to the 2-norm[a]) can be constructed

using the Moore–Penrose pseudoinverse $\boldsymbol{L}^+$. Hence its 1-norm respects the upper bound

$$\|\boldsymbol{\delta}\|_1 = \|\boldsymbol{L}^+ \cdot \delta\boldsymbol{E}\|_1 \leq \|\boldsymbol{L}^+\|_1 \|\delta\boldsymbol{E}\|_1, \tag{3.22}$$

where the operator 1-norm is the norm induced by the vector 1-norm. We may now *choose* $\tilde{E}$ as the arithmetic mean $\bar{E} = 1/g \cdot \sum_{i=1}^{g} E_i$. Given some arbitrary but fixed ground state splitting $\delta E = \max_{i\in\{1,\dots g\}} \delta E_i - \min_{i\in\{1,\dots g\}} \delta E_i$, then $\|\delta\boldsymbol{E}\|_1$ is maximized for ground state energies $\delta E_i \in \{\max_{i\in\{1,\dots g\}} \delta E_i, \min_{i\in\{1,\dots g\}} \delta E_i\}$ in (approximately) equal number. This yields

$$-\delta(\Delta E_{\boldsymbol{xy}}) \leq \|\boldsymbol{\delta}\|_1 \leq \|\boldsymbol{L}^+\|_1 \frac{\delta E}{2} \left\{ \begin{array}{ll} g, & \text{if } g \text{ even} \\ g - 1/g, & \text{if } g \text{ odd} \end{array} \right\} \leq \|\boldsymbol{L}^+\|_1 \frac{g}{2} \delta E. \tag{3.23}$$

Thus it is $\Delta E > -\delta(\Delta E_{\boldsymbol{xy}})$ in particular fulfilled if $\Delta E > \|\boldsymbol{L}^+\|_1 g\delta E/2$ or equivalently $\mathcal{Q} > \exp\left[-2/(g\|\boldsymbol{L}^+\|_1)\right]$. Latter is fulfilled by assumption, hence we obtain $\Delta\tilde{E}_{\boldsymbol{xy}} > 0$ for all $\boldsymbol{x} \in L$ and $\boldsymbol{y} \in \mathbb{F}_2^N \setminus L$. Thus the L-complex $(\tilde{\mathcal{C}}_{\mathcal{K}}^{\mathcal{Q}}, L, \mathfrak{L})$ with the structure $\tilde{\mathcal{C}} = (\boldsymbol{r}_{\mathfrak{i}}, \tilde{\Delta}_{\mathfrak{i}} \mid \mathfrak{i} \in \mathcal{N})$ constructed in lemma IV possesses a positive energy gap. Therefore $(\tilde{\mathcal{C}}_{\mathcal{K}}^{\mathcal{Q}}, L, \mathfrak{L})$ realizes the target language with a degenerate ground state manifold. □

[a] Unfortunately, there is no *linear* operator creating the minimal solution of the 1-norm for general right-hand sides, see [10].

The target quality factor condition $\mathcal{Q} > \exp\left[-2/(g\|\boldsymbol{L}^+\|)\right]$ is generally very different for different target languages $L = L_t$. Here the operator 1-norm $\|\boldsymbol{L}^+\|_1$ can be computed from the language directly. This is easily done numerically. However analytically this computation is generally cumbersome and the condition $\mathcal{Q} > \exp\left[-2/(g\|\boldsymbol{L}^+\|)\right]$ above offers little intuition yet.

Rephrasing the Theorem. Thus it might be very useful to rephrase this condition in terms of the *dimensions* of the language matrix $\boldsymbol{L} \in \mathbb{F}_2^{g\times N}$, i.e. the number of the ground states $g = |L|$ and the number of atoms $N = |\mathcal{N}|$. We formulate corollary VI:

Corollary VI (Degenerate Ground States 2)**.**

Consider some L-complex $(\mathcal{C}_{\mathcal{K}}^{\mathcal{Q}}, L, \mathfrak{L})$ with target language $L = L_t$ of length $g = |L_t|$. If the eigenvectors $|\boldsymbol{x}\rangle$ of the words $\boldsymbol{x} \in L_t$ are linear independent and if the quality factor $\mathcal{Q} > \exp\left[-2/\sqrt{N^{2g-1}g^{g+2}}\right]$ is sufficiently large, then there exists a L-complex $(\tilde{\mathcal{C}}_{\mathcal{K}}^{\mathcal{Q}}, L, \mathfrak{L})$ where $\mathcal{H}_t = \mathcal{H}(L_t)$ is a g-dimensional gapped low-energy eigenspace of the Hamiltonian $H[\tilde{\mathcal{C}}]$.

Proof.

Using the *singular value decomposition* (SVD), we can decompose the language matrix $\boldsymbol{L} \in \mathbb{F}_2^{g\times N}$ in $\boldsymbol{L} = UDV^T$ for some (real) orthogonal matrices $U \in \mathbb{R}^{g\times g}$ and $V \in \mathbb{R}^{N\times N}$ and diagonal non-negative matrix D. The diagonal elements are the (up to permutations uniquely determined) singular values of $\boldsymbol{L}$. As $\operatorname{rank}(\boldsymbol{L}) = g$, there are g singular values and all of them

are positive. We are going to denote them by $\sigma_i = \sigma_i(\boldsymbol{L}) > 0$ with $i \in \{1, \dots g\}$ and we assume the usual ordering $\sigma_1 \geq \dots, \geq \sigma_g$. Using the SVD, the Moore–Penrose pseudoinverse of the language matrix can be written as $\boldsymbol{L}^+ = VD^+U^T$ where D^+ is constructed from D by inverting the (positive) diagonal elements. The natural matrix norm induced by the 1-norm is the maximum absolute column sum norm. The matrix 1-norm of D^+ is therefore given by the inverse of the smallest (positive) singular value: $\|D^+\|_1 = 1/\sigma_g$. As $U^T \in \mathbb{R}^{g\times g}$ and $V \in \mathbb{R}^{N\times N}$ are orthogonal, the vector 2-norm of its columns are one. Thus their matrix 1-norm is maximized for equal elements (up to a phase) in one column: $\|U\|_1 \leq g/\sqrt{g} = \sqrt{g}$ and $\|V\|_1 \leq N/\sqrt{N} = \sqrt{N}$. From the proof of previous theorem V we know that if $Q < 2/g\|\boldsymbol{L}^+\|_1$, then the energy gap $\Delta\tilde{E} > 0$ of $(\tilde{\mathcal{C}}^{\mathcal{Q}}_{\mathcal{K}}, L, \mathfrak{L})$ is positive. We reformulate this inequality by introducing a new lower-bound:

$$\frac{2}{g\|\boldsymbol{L}^+\|_1} = \frac{2}{g\|VD^+U^T\|_1} \geq \frac{2}{g\|V\|_1\|D^+\|_1\|U^*\|_1} \geq \frac{2\sigma_g}{\sqrt{Ng^3}}. \tag{3.24}$$

Note that as $\sigma_g = \sigma_g(\boldsymbol{L}) > 0$, it is $\exp\left[-2\sigma_g/\sqrt{Ng^3}\right] < 1$.
A lower bound on the minimal singular value of a binary matrix $\boldsymbol{L} \in \mathbb{F}_2^{g\times N}$ may be found in the following way: The Gramian matrix $\boldsymbol{A} = \boldsymbol{L}\boldsymbol{L}^T \in \mathbb{F}_N^{g\times g}$ is symmetric and possesses eigenvalues $\lambda_i(\boldsymbol{A}) = \sigma_i(\boldsymbol{L})^2$ for $i \in \{1, \dots g\}$. As $\sigma_i > 0$ it is $\lambda_i > 0$ and $\boldsymbol{A}$ is positive definite. As $\boldsymbol{L}$ is binary, $\boldsymbol{A}$ is constructed from natural number $n \in \mathbb{F}_N$. As the determinant of $\boldsymbol{A}$ is a polynomial function of integers with coefficients ± 1, it must be an integer as well. However we know that the eigenvalues are positive thus the determinant (which is their product) must be positive as well. Thus we follow $\det(\boldsymbol{A}) \geq 1$. The largest eigenvalue of an integer matrix $\boldsymbol{A} \in \mathbb{F}_N^{g\times g}$ may be upper-bounded by $\sqrt{g}N$. Thus the smallest eigenvalue λ_g must fulfill

$$\sigma_g(\boldsymbol{L})^2 = \lambda_g(\boldsymbol{A}) = \det \boldsymbol{A} / \prod\nolimits_{i\in\{1,\dots g-1\}} \lambda_i \geq 1/(\sqrt{g}N)^{g-1} \tag{3.25}$$

We may apply this lower bound to reformulate

$$\frac{2}{g\|\boldsymbol{L}^+\|_1} \geq \frac{2\sigma_g}{\sqrt{Ng^3}} \geq \frac{2}{\sqrt{N^{2g-1}g^{g+2}}}. \tag{3.26}$$

Thus $\mathcal{Q} > \exp\left[-2/(g\|\boldsymbol{L}^+\|)\right]$ is fulfilled in particular if $\mathcal{Q} > \exp\left[-2/\sqrt{N^{2g-1}g^{g+2}}\right]$ and we may apply theorem V. □

Note that this inequality $\mathcal{Q} > \exp\left[-2/\sqrt{N^{2g-1}g^{g+2}}\right]$ of corollary VI is *less sharp* than the previous inequality of theorem V. However corollary VI offers a very simple algebraic expression consisting of only the matrix dimensions g and N which can be evaluated easily by hand to get an intuition on the target quality factor.

An exponential Decay. We find that the lowest singular value σ_g (and thus the inverse of the 1-norm $\|\boldsymbol{L}^+\|_1^{-1}$) in general decays exponentially in the dimension g of the matrix. Here we derived the correct asymptotic behavior as proven in Ref. [1] for the more special case of binary square matrices $\boldsymbol{A} \in \mathbb{F}_2^{g\times g}$. There is a simple and clear argument in '*Matrix Computations*' by Golub *et al.*[16] (cf. section 2.4.2.) with explains why increasing the matrix dimension generally decreases the lowest singular value:

Remark 2. (The intuitive Argument behind Corollary VI)

For $\boldsymbol{L}^T = VDU^T \in \mathbb{F}_2^{N\times g}$ we label by $\boldsymbol{u}_g$ the last column of the orthogonal matrix $U \in \mathbb{R}^{g\times g}$. It is $\text{rank}(\boldsymbol{L}) = g$ thus $N \geq g$, by assumption. We augment the matrix $\boldsymbol{L}^T$ by an arbitrary column $b \in \mathbb{F}_2^N$ and call it $\boldsymbol{L}^T_{\text{Aug}} = \left[\boldsymbol{L}^T \mid b\right]$. Then we obtain

$$\sigma_{\min}(\boldsymbol{L}) = \|\boldsymbol{L}^T\boldsymbol{u}_g\|_2 = \left\|\boldsymbol{L}^T_{\text{Aug}}\begin{bmatrix}\boldsymbol{u}_g\\0\end{bmatrix}\right\|_2 \geq \sigma_{\min}(\boldsymbol{L}^T_{\text{Aug}})\left\|\begin{bmatrix}\boldsymbol{u}_g\\0\end{bmatrix}\right\|_2 = \sigma_{\min}(\boldsymbol{L}_{\text{Aug}}), \tag{3.27}$$

i.e. in a nutshell $\sigma_{\min}(\boldsymbol{L}) \geq \sigma_{\min}(\boldsymbol{L}_{\text{Aug}})$ for any augmentation $b \in \mathbb{F}_2^N$.

However this implies that for large languages of length $g = |L|$ it is exponentially hard in g to achieve degeneracy, because the ratio Q needs to be exponentially small in g for theorem V to apply.

General Remarks. In the following thesis we prefer to apply theorem V instead of corollary VI as we evaluate the 1-norm of the pseudoinverse of the language matrix numerically to obtain a sharper bound. It should be mentioned that theorem V (and thus corollary VI) only offer a *sufficient but not a necessary condition* to achieve a positive energy gap when applying lemma IV. We find numerically that in general if we violate the inequalities only slightly but still apply lemma IV we still obtain a positive energy gap in $(\tilde{\mathcal{C}}^{\mathcal{Q}}_{\mathcal{K}}, L, \mathfrak{L})$. In the following we conclude these proofs with a few remarks and discuss generalizations of theorem V.

In lemma IV we assumed that the eigenvectors $|\boldsymbol{x}\rangle$ of the words $\boldsymbol{x} \in L = L_t$ are linear independent, i.e. that the language matrix $\boldsymbol{L}$ is of rank $\text{rank}(\boldsymbol{L}) = g$. In particular this restricts to specific ground-state manifolds with $g \leq N$. Luckily, this condition will be fulfilled by for logic elementaries. For the remaining more complex languages we have to generalize this concept.

Generalizations. It is in general not necessary to fulfill $\text{rank}(\boldsymbol{L}) = g$ for the linear system (3.17) to be consistent, it is only sufficient. According to the Rouché-Capelli theorem a linear system of equations is consistent if and only if the rank of the augmented matrix $\boldsymbol{L}_{\text{Aug}} := [\boldsymbol{L} \,|\, \tilde{\boldsymbol{b}}]$ equals the rank of the coefficient matrix $\boldsymbol{L}$. This means that if the eigenvectors $|\boldsymbol{x}\rangle$ of the words $\boldsymbol{x} \in L_t$ are linear dependent, then the right-hand side $\tilde{\boldsymbol{b}}$ of the linear system must share this linear dependency.

In the following we denote the rank of the coefficient matrix by $r := \text{rank}(\boldsymbol{L})$. This allows us to generalize lemma IV and theorem V[10]:

> It is not necessary to assume that the eigenvectors $|\boldsymbol{x}\rangle$ of the words $\boldsymbol{x} \in L_t$ are linear independent. It is sufficient (and necessary) to assume $\text{rank}(\boldsymbol{L}_{\text{Aug}}) = r$.

In the case $r = g$ we recover the previous consistency condition of lemma IV. The new generalized consistency condition is explicitly dependent on the right-hand side $\tilde{\boldsymbol{b}}$, i.e. it is determined by the geometry $\mathcal{G}_{\mathcal{C}}$ and possibly by $\tilde{E}$. Still however for a given target language with $r < g$, a general geometry (possibly sampled and optimized using the algorithms from sections 3.1 and 3.2) does

[10]The generalization of corollary VI is more subtle. We denote it as corollary X and attach it in the app. 3.A.

not fulfill this consistency condition. If we optimize the quality factor using the minimization algorithm 3.2, a geometry solving the consistency condition is at best *approximated* due to numerical errors. Thus we can not yet profit from this generalization.

In the following we consider two cases: In case (1) the *cokernel is orthogonal* to the **1**-vector, i.e. the vector elements from the cokernel sum to zero, and in case (2) the cokernel is *not* orthogonal to the **1**-vector. We start with the former case:

1 | If the cokernel is orthogonal to the **1**-vector, the consistency condition can be reformulated as an equality of linear functions on the interaction energies (independent of $\tilde{E}$). Such a condition can not be solved for d-dimensional Euclidean geometries in every case[11]. If the language possesses a permutation symmetry in its bits[12] such a condition might correspond only to a *symmetry constraint* on the structure. It might therefore be useful to constrain this symmetry in the structure during the optimization to fulfill $\operatorname{rank}(\boldsymbol{L}_{\mathrm{Aug}}) = r$.

2 | Consider now the case where the vector elements of the cokernel do not sum to zero: Then the consistency condition is a function of $\tilde{E}$. In theorem V we made the choice for $\tilde{E} = \bar{E}$ as the arithmetic mean of the current eigenenergies in order to express $\|\delta\boldsymbol{E}\|_1$ as a linear function of the energy splitting δE. As it turns out however there are cases where this is not the most useful choice, i.e. where for $\tilde{E} = \bar{E}$ the linear system is inconsistent but by some other choice of $\tilde{E}$ one can make the linear system consistent. Thus sometimes we can profit from the additional DOF in the choice of $\tilde{E} - \bar{E}$ and we want to incorporate this additional DOF in the linear system. In a nutshell this corresponds to a substitution of $\boldsymbol{L}$ by an *extended language matrix* $\tilde{\boldsymbol{L}} := [\boldsymbol{L} \,|\, \mathbf{1}] \in \mathbb{F}_2^{g\times(N+1)}$ in the proof of theorem V. This of course will then change (more precisely worsen) the upper bound requested in theorem V.

Let $\tilde{r} = \operatorname{rank}(\tilde{\boldsymbol{L}})$ denote the rank of the extended language matrix. We can now formulate a generalized version of theorem V:

Corollary VII (Generalization of Theorem V)**.**

Consider some L-complex $(\mathcal{C}^{\mathcal{Q}}_{\mathcal{K}}, L, \mathfrak{L})$ *with target language* $L = L_t$ *of length* $g = |L_t|$. *If rank*$(\tilde{\boldsymbol{L}}_{Aug}) = \tilde{r}$ *and if the quality factor* $\mathcal{Q} > \exp\left[-2/(g\|\tilde{\boldsymbol{L}}^{+}\|_1)\right]$ *is sufficiently large, then there exists a L-complex* $(\tilde{\mathcal{C}}^{\mathcal{Q}}_{\mathcal{K}}, L, \mathfrak{L})$ *where* $\mathcal{H}_t = \mathcal{H}(L_t)$ *is a g-dimensional gapped low-energy eigenspace of the Hamiltonian* $H[\tilde{\mathcal{C}}]$.

Proof.

The proof in analogous to the proof of theorem V, we only note the differences. Analogous to eq. (3.17) we formulate a linear system

$$\tilde{L}_{ij}\tilde{\Delta}_j \stackrel{!}{=} \tilde{b}_i \qquad \text{with} \qquad \tilde{b}_i = -\bar{E} + \sum\nolimits_{j,k=1}^{N} L_{ij} I_{\mathfrak{L}(j)\mathfrak{L}(k)} L_{ik}, \tag{3.28}$$

[11] E.g. consider app. 5.A.1 or app. 5.B.2 or simply the introductory exmpl. 6

[12] E.g. if the (vectorial) Boolean function v is symmetric.

now using the extended language matrix $\tilde{\boldsymbol{L}}$. This linear system is consistent by assumption; its solution is given by the MOORE-PENROSE pseudoinverse. The solution vector is now defined via $\tilde{\Delta}_j \equiv \Delta_{\mathfrak{L}(j)}$ for $j \in \{1, \dots N\}$ and $\tilde{\Delta}_{N+1} \equiv \tilde{E} - \bar{E}$. By subtracting (3.18) from eq. (3.28), we obtain the new linear system $\tilde{L}_{ij}\tilde{\delta}_j = \delta E_i$, where we defined $\tilde{\delta}_j \equiv \tilde{\Delta}_j - \Delta_j$ for $j \in \{1, \dots N\}$, $\tilde{\delta}_{N+1} \equiv \tilde{E} - \bar{E}$ and $\delta E_i \equiv E_i - \bar{E}$. We can proceed similarly as in theorem V with the new upper bound

$$-\delta(\Delta E_{\boldsymbol{xy}}) \leq \|\boldsymbol{\delta}\|_1 \leq \|\tilde{\boldsymbol{\delta}}\|_1 \leq \|\tilde{\boldsymbol{L}}^+ \cdot \delta \boldsymbol{E}\|_1 \leq \|\tilde{\boldsymbol{L}}^+\|_1 \|\delta \boldsymbol{E}\|_1 \leq \|\tilde{\boldsymbol{L}}^+\|_1 \frac{g}{2} \delta E. \tag{3.29}$$

This yields a substitution of $\boldsymbol{L}$ by $\tilde{\boldsymbol{L}}$ in the final term. Thus it is $\Delta E > -\delta(\Delta E_{\boldsymbol{xy}})$ in particular fulfilled if $\Delta E > \|\tilde{\boldsymbol{L}}^+\|_1 g \delta E/2$ or equivalently $\mathcal{Q} > \exp\left[-2/(g\|\tilde{\boldsymbol{L}}^+\|_1)\right]$. □

Note that corollary VII is more general than theorem V. This comes at the cost that the rank of $\tilde{\boldsymbol{L}}_{\text{Aug}}$ and thus the condition is now explicitly dependent on the geometry. Furthermore the extended language matrix $\tilde{\boldsymbol{L}}$ possesses a smaller singular value $\sigma_{\min}$ following remark 2. This makes the target quality factor larger and thus the bound less sharp compared to theorem V.

Note that corollary VII includes *two generalizations*, via the effective language matrix *and* via the rank. It is clear that one could also consider only one generalization of theorem V at the time. Here we only note corollary VII including directly both generalizations *to avoid redundancies*.

Generalization of Corollary VI. We want to conclude with some remarks on the generalization of corollary VI: Although the generalization of theorem V to corollary VII is quite straight-forward this is not the case for corollary VI. The proof of corollary VI is heavily based on the assumption that $\text{rank}(\boldsymbol{L}) = g \leq N$ such that all singular values $\sigma_i(\boldsymbol{L}) > 0$ are positive. It may be generalized to the condition $\text{rank}(\boldsymbol{L}) = \text{rank}(\boldsymbol{L}_{\text{Aug}})$ by substituting the determinant by the *pseudodeterminant*, accounting for the (possibly) reduced number of eigenvalues. The detailed and rigorous (and beautiful) proof is attached in the app. 3.A.

3.4 | Exploiting Symmetries

This section is based directly on previous sec. 3.3. There we already mentioned that, if the language possesses permutation symmetries in the bits then the *consistency condition* might *impose symmetry constraints* on the structure. To fulfill the consistency condition and apply corollary VII it is useful to constrain these symmetries on the structure. In this section we want to continue on this ides and derive an effective description which is equivalent for structures respecting the symmetries.

Reformulation of the Consistency Condition. For any matrix $\boldsymbol{A} \in \mathbb{F}_2^{g\times n}$ it is $\operatorname{rank}(\boldsymbol{A}) = \operatorname{rank}(\boldsymbol{A}^T) = g - \operatorname{def}(\boldsymbol{A}^T) = g - \operatorname{codef}(\boldsymbol{A})$. Here 'def' denotes the *defect* (or *nullity*), i.e. the rank of the kernel, and 'codef' denotes the *codefect* (or *corank*), i.e. the rank of the cokernel[13]. With $\boldsymbol{A} = \tilde{\boldsymbol{L}} \in \mathbb{F}_2^{g\times N}$ and $\boldsymbol{A} = \tilde{\boldsymbol{L}}_{\text{Aug}} \in \mathbb{F}_2^{g\times(N+1)}$, the consistency condition $\operatorname{rank}(\tilde{\boldsymbol{L}}_{\text{Aug}}) = \operatorname{rank}(\tilde{\boldsymbol{L}})$ can be reformulated as $\operatorname{codef}(\tilde{\boldsymbol{L}}_{\text{Aug}}) = \operatorname{codef}(\tilde{\boldsymbol{L}})$. As $\operatorname{coker}(\tilde{\boldsymbol{L}}_{\text{Aug}}) \subseteq \operatorname{coker}(\tilde{\boldsymbol{L}})$ are vector spaces, we can further reformulate the consistency condition as

$$\operatorname{coker}(\tilde{\boldsymbol{L}}_{\text{Aug}}) = \operatorname{coker}(\tilde{\boldsymbol{L}}). \tag{3.30}$$

In other words: if $|\boldsymbol{y}\rangle \in \operatorname{coker}(\tilde{\boldsymbol{L}})$ then $\langle \boldsymbol{y}|\tilde{\boldsymbol{b}}\rangle = 0$ where $|\tilde{\boldsymbol{b}}\rangle$ is the right-hand side of the linear system (3.28). This means that $|\tilde{\boldsymbol{b}}\rangle$ should share the linear dependencies of the states of $\tilde{\boldsymbol{L}}$. Note that this reformulation is equal to the initial consistency condition.

As $|\tilde{\boldsymbol{b}}\rangle$ is a linear function of $I_{\mathcal{C}}$ and $\bar{E}$, this imposes linear constraints on the interactions. In the following we are interested in the *effect of symmetries* on these constraints. We want to know whether symmetries can help us to strengthen theorem V (and its corollaries). In the following we leave the tilde of the extended language matrix for a more streamline notation. The following arguments are similarly true for the extended and the non-extended language matrix.

Symmetries and Constraints. Consider a language L possessing some symmetry group Σ, i.e. $\sigma(L) = L$ for $\sigma \in \Sigma$. Here the symmetry σ acts element wise on each word $\boldsymbol{x} \in L$ by permuting the bit indices. As σ leaves L invariant this means that each word is either projected onto itself or to another word in L:

$$\forall \boldsymbol{x} \in L : \ \sigma(\boldsymbol{x}) \in L \qquad \text{with} \qquad (\sigma(\boldsymbol{x}))_i = x_{\sigma(i)}. \tag{3.31}$$

If L possesses a symmetry group Σ, it is not surprising that (some of) the linear constraints on $I_{\mathcal{C}}$ can correspond to symmetry constraints. The symmetry constraints request that the interactions respect (some of) the symmetries of the language under permutation (i.e. relabeling) of the atoms. Thus just by imposing these symmetry constraints on the interactions (e.g. while

[13] The cokernel is the kernel of the transpose.

applying the minimization algorithm 3.2) we are able to fulfill (some of) the constraints on the interactions. In the following we assume that we impose some symmetry constraints Σ on the complex, i.e. on the subspace $\mathcal{H}(L)$ the complex remains invariant to the Hamiltonian under a relabeling of atoms according to $\sigma \in \Sigma$. The goal of this section now is to find a simpler consistency condition (3.30) for such symmetric cases.

An effective Description. We define an *effective language* L_{eff} by identifying bits which are projected onto each other under σ. These bits of L construct equivalence classes:

$$x_i \sim x_j \quad \Leftrightarrow \quad \exists \sigma \in \Sigma : \; x_j = x_{\sigma(i)}. \tag{3.32}$$

We associate an effective bit $\tilde{x} \cong [x]$ in L_{eff} with their equivalence class and define its value in some state i as the sum of the values of all bits in the equivalence class: $\tilde{x}_i = \sum_{x \in \tilde{x}} x_i$. If the bit $x \in [x] \cong \tilde{x}$ of L is associated with the effective bit $\tilde{x}$ of L_{eff}, we write symbolically $x \in \tilde{x}$ to streamline notation. The new effective language we just constructed is *non-binary* as its letters can possess integer values larger one. However for simplicity we still call the letters of the effective language its bits. The effective language generally consists of fewer words $g_{\text{eff}} := |L_{\text{eff}}| \leq g$ and each word possess a smaller bit length $N_{\text{eff}} \leq N$.

The *effective language matrix* defined by the effective language is denoted by $\boldsymbol{L}_{\text{eff}} \in \mathbb{N}_0^{g_{\text{eff}} \times N_{\text{eff}}}$. In the following we denote the indices of the effective language matrix $\tilde{i}, \tilde{j}, \ldots$ with a tilde to distinguish them visually from indices of the actual language matrix. For the $\tilde{i}$-th row $\tilde{\boldsymbol{x}}_{\tilde{i}}$ in $\boldsymbol{L}_{\text{eff}}$ there is an equivalence class $[i]$ of rows $\boldsymbol{x}_i$ in $\boldsymbol{L}$ which projects to $\tilde{\boldsymbol{x}}_{\tilde{i}}$ under previous construction. Again we identify $\tilde{i} \cong [i]$ and we write symbolically $i \in \tilde{i}$ to streamline notation. This induces a *(linear) 'projection'*[14]

$$P : \; \mathbb{R}^g \to \mathbb{R}^{g_{\text{eff}}} : \; (P(|\boldsymbol{y}\rangle))_{\tilde{i}} = \sum_{i \in \tilde{i}} y_i \tag{3.33}$$

on the states. In the following we write $\tilde{y}_{\tilde{i}} := (P(|\boldsymbol{y}\rangle))_{\tilde{i}}$.

Now we need to show that these constructions are useful. We formulate lemma VIII:

Lemma VIII (Projection to effective Languages)**.**

Consider some $|\boldsymbol{y}\rangle \in coker(\boldsymbol{L})$*. Then it is:*

1 | $P(coker(\boldsymbol{L})) = coker(\boldsymbol{L}_{eff})$.

2 | $\langle \boldsymbol{y} | \tilde{\boldsymbol{b}} \rangle = 0$ *by the symmetry of the interactions if and only if* $|\boldsymbol{y}\rangle \in ker(P)$.

This means that under the projection P precisely the constraints for the consistency of the linear system which are fulfilled by the symmetry of the interactions are discarded and the remaining ones are conserved.

[14] P is not a projection in the mathematical definition as P is a linear function between *different* vector spaces. We just call it that way as it projects to a vector space of lower dimension.

Proof.

We start by showing (1) that $P:\ \mathrm{coker}(\boldsymbol{L}) \to \mathrm{coker}(\boldsymbol{L}_{\mathrm{eff}})$ is a well-defined Surjection. Consider some $|\boldsymbol{y}\rangle \in \mathrm{coker}(\boldsymbol{L})$. Then for any bit x we have $\sum_{i=1}^{g} y_i x_i = 0$. Here x_i is the bit-value of x in the i-th state. We now sum over the elements of the same equivalence class of bits:

$$0 = \sum_{\tilde{x}} \sum_{x \in \tilde{x}} \sum_{i=1}^{g} y_i x_i = \sum_{i=1}^{g} y_i \underbrace{\left(\sum_{x \in \tilde{x}} x_i \right)}_{\text{equal for } i_1, i_2 \text{ if } i_1 \sim i_2} = \sum_{\tilde{i}=1}^{g_{\mathrm{eff}}} \left(\sum_{i \in \tilde{i}} y_i \right) \tilde{x}_{\tilde{i}} = \sum_{\tilde{i}=1}^{g_{\mathrm{eff}}} \tilde{y}_{\tilde{i}} \tilde{x}_{\tilde{i}}. \tag{3.34}$$

As this is true for all bits $\tilde{x}$, we obtain $|\tilde{\boldsymbol{y}}\rangle = P(|\boldsymbol{y}\rangle) \in \mathrm{coker}(\boldsymbol{L}_{\mathrm{eff}})$. It is easy to see that this projection is surjective by constructing its right inverse: $y_i \equiv (P^+(|\tilde{\boldsymbol{y}}\rangle))_i = \tilde{y}_{\tilde{i}}/|\tilde{i}|$ fulfills $(P(P^+(|\tilde{\boldsymbol{y}}\rangle)))_{\tilde{i}} = \sum_{i \in \tilde{i}} \tilde{y}_{\tilde{i}}/|\tilde{i}| = \tilde{y}_{\tilde{i}}$. Thus (1) is proven.

As the projection is in general *not injective*, the construction of the right-inverse is *not unique*. The reason is that the kernel of P may be nontrivial: $\tilde{y}_{\tilde{i}} = \sum_{i \in \tilde{i}} y_i$ may vanish for all $\tilde{i}$ even if $y_i \neq 0$. As P is linear, we could add any element of its kernel to P^+ and obtain a different right inverse. We find that $\ker(P)$ consists of the vectors $|\boldsymbol{y}\rangle$ with $\sum_{i \in \tilde{i}} y_i = 0$ for all $\tilde{i}$:

$$|\boldsymbol{y}\rangle \in \ker(P) \qquad \Leftrightarrow \qquad \forall_{\tilde{i}}: \sum_{i \in \tilde{i}} y_i = 0. \tag{3.35}$$

However due to the symmetry of the interactions, for each state $i_1, i_2 \in \tilde{i}$ the right-hand side $\tilde{b}_{i_1} = \tilde{b}_{i_2} \equiv \tilde{b}_{\tilde{i}}$[a] is constant because each state 'looks the same' to the Hamiltonian. Thus the vectors $|\boldsymbol{y}\rangle$ with $\sum_{i \in \tilde{i}} y_i = 0$ for all $\tilde{i}$ are the vectors which are orthogonal to general symmetric $|\tilde{\boldsymbol{b}}\rangle$:

$$\langle \boldsymbol{y} | \tilde{\boldsymbol{b}} \rangle = \sum_{i=1}^{g} y_i \tilde{b}_i = \sum_{\tilde{i}=1}^{g_{\mathrm{eff}}} \left(\sum_{i \in \tilde{i}} y_i \right) \tilde{b}_{\tilde{i}} = 0 \qquad \Leftrightarrow \qquad \forall_{\tilde{i}}: \sum_{i \in \tilde{i}} y_i = 0 \tag{3.36}$$

Combined with eq. (3.35), this proves (2). □

[a] Note that $\tilde{b}_{\tilde{i}}$ is *not* defined as the *sum* of its $\tilde{b}_i$ with $i \in \tilde{i}$ but it *equals* them.

We find that the vectors $|\boldsymbol{y}\rangle \in \mathrm{coker}(\boldsymbol{L}) \cap \ker(P)$ of the intersection subspace are exactly the vectors with which the right-hand side of the linear system is already consistent due to the symmetry of the interactions. The remaining vectors $|\boldsymbol{y}\rangle \in \mathrm{coker}(\boldsymbol{L}) \backslash \ker(P)$ convey the remaining consistency conditions and they are translated into non-zero vectors $|\tilde{\boldsymbol{y}}\rangle \in \mathrm{coker}(\boldsymbol{L}_{\mathrm{eff}})$ surjectively. Thus (only) the relevant consistency conditions are conserved in the effective description via $\boldsymbol{L}_{\mathrm{eff}}$ and the effective description is equivalent to the description via the full language matrix $\boldsymbol{L}$ modulo symmetries. We want to illustrate this abstract concept via an example:

Example 7. (The ternary NOR-function)

As an example consider the BOOLEAN language matrix $\boldsymbol{L}$[`NOR3a`] of the (symmetric) 3-bit

NOR-function in realization a and its effective language matrix $\boldsymbol{L}_{\text{eff}}[\texttt{NOR3a}]$:

$$\boldsymbol{L}[\texttt{NOR3a}] = \begin{bmatrix} 0&0&0&0&1&1&1&1 \\ 0&0&1&1&0&0&1&1 \\ 0&1&0&1&0&1&0&1 \\ 1&0&0&0&0&0&0&0 \\ 0&1&1&0&1&0&0&0 \end{bmatrix}^T \quad \longleftrightarrow \quad \boldsymbol{L}_{\text{eff}}[\texttt{NOR3a}] = \begin{bmatrix} 0&1&0 \\ 1&0&1 \\ 2&0&0 \\ 3&0&0 \end{bmatrix}. \tag{3.37}$$

Here the input port bits are lumped together into one effective input port bit and the states $\{2,3,5\}$ and $\{4,6,7\}$ are lumped together in the effective states $\tilde{2}$ and $\tilde{3}$ respectively. Thus $g_{\text{eff}} = 4 < g = 8$ and $N_{\text{eff}} = 3 < N = 5$. The geometry is assumed to be D_3-symmetric. We can represent the linear projection P by a matrix

$$\boldsymbol{P} = \begin{bmatrix} 1&0&0&0&0&0&0&0 \\ 0&1&1&0&1&0&0&0 \\ 0&0&0&1&0&1&1&0 \\ 0&0&0&0&0&0&0&1 \end{bmatrix} \in \mathbb{F}_2^{g_{\text{eff}} \times g}. \tag{3.38}$$

For the matrices of eq. (3.37) we find the cokernels

$$\operatorname{coker}(\boldsymbol{L}[\texttt{NOR3a}]) = \operatorname{span}\left(\left\{ \begin{bmatrix} 0&0&1&-1&-1&1&0&0 \end{bmatrix}^T, \begin{bmatrix} 0&2&-1&-1&-1&-1&2&0 \end{bmatrix}^T, \begin{bmatrix} 0&0&0&-1&0&-1&-1&2 \end{bmatrix}^T \right\}\right), \tag{3.39}$$

$$\operatorname{coker}(\boldsymbol{L}_{\text{eff}}[\texttt{NOR3a}]) = \operatorname{span}\left(\left\{ \begin{bmatrix} 0&0&-3&2 \end{bmatrix}^T \right\}\right). \tag{3.40}$$

We find that the last basis vector in the spanning set of $\operatorname{coker}(\boldsymbol{L}[\texttt{NOR3a}])$ projects to the spanning vector of $\operatorname{coker}(\boldsymbol{L}_{\text{eff}}[\texttt{NOR3a}])$ under P:

$$\begin{bmatrix} 0&0&-3&2 \end{bmatrix}^T = \boldsymbol{P} \begin{bmatrix} 0&0&0&-1&0&-1&-1&2 \end{bmatrix}^T. \tag{3.41}$$

The condition imposed by these vectors requests that $I_{\mathfrak{i}\mathfrak{j}} = -\bar{E}/3$ where $\mathfrak{i} \neq \mathfrak{j}$ are input ports. This constraint has to be fulfilled in addition to the symmetry constraints. Using $\bar{E} = -3\Delta_{\mathfrak{i}}/2$ we can rephrase this as $I_{\mathfrak{i}\mathfrak{j}} = \Delta_{\mathfrak{i}}/2$, which is just what we expect to degenerate the third and fourth effective state.
The remaining two vectors (and their span) lie in the kernel of P and project to zero. This is just what we want as their constraints are trivial for a symmetric geometry:

$$\langle \boldsymbol{y} | \tilde{\boldsymbol{b}} \rangle = \sum_{\tilde{i}=1}^{4} \left(\sum_{i \in \tilde{i}} y_i \right) \tilde{b}_{\tilde{i}} = 0 \quad \text{for} \quad |\boldsymbol{y}\rangle \in \operatorname{span}\left(\left\{ \begin{bmatrix} 0&0&1&-1&-1&1&0&0 \end{bmatrix}^T, \begin{bmatrix} 0&2&-1&-1&-1&-1&2&0 \end{bmatrix}^T \right\}\right).$$

Here $\tilde{b}_{\tilde{1}} = b_2 = b_3 = b_5$ and $\tilde{b}_{\tilde{2}} = b_4 = b_6 = b_7$. The equivalence classes of the states are $\tilde{1} \cong \{1\}$, $\tilde{2} \cong \{2,3,5\}$, $\tilde{3} \cong \{4,6,7\}$ and $\tilde{4} \cong \{8\}$.

We conclude this discussion with a few remarks on symmetries and then use the above definitions and lemma VIII to reformulate corollary VII:

1 | In the following we are going to call a L-complex symmetric under some symmetry σ, if its language is symmetric under σ and if the interactions and detunings are symmetric under σ *for the ground states*. Latter means that the structure looks identical to the Hamiltonian for the ground states under σ. Note that this does not necessarily imply that the geometry is symmetric as the interactions may still be asymmetric under σ for the excited states (cf. the `ICRS2`-gate in fig. 4.8). However this is more the exception than the rule and usually the geometry also obeys the symmetry σ.

2 | It is possible that for a symmetric language there only exist (partially) asymmetric implementations on the d-dimensional Rydberg platform, i.e. where the L-complex is not symmetric (cf. the `CRS2`-gates in fig. 4.8). Thus one has to be cautious when assuming symmetries (e.g. during optimization via the minimization algorithm 3.2).

3 | In the remaining thesis we are going to use the effective description of symmetric L-complexes frequently as most interesting target languages L_t are symmetric (often they are symmetric in the ports). A symmetric (vectorial) BOOLEAN function v of k input ports possesses $g = 2^k$ words and thus 2^k rows in its language matrix. The visualization of the symmetric language matrix can be improved enormously by discarding redundant rows and reducing the rows to only $g_{\text{eff}} = k + 1$ in the effective language matrix.

4 | It should be noted that there are symmetric target functions f_t where it is useful to choose a (partially) asymmetric realization w to be able to construct $\mathcal{H}(L_t)$ as a gapped low-energy eigenspace. This is a known phenomenon as the atom-efficient realizations in the PXP model are (partially) asymmetric[38].[15] This means in particular that it is *a priori* not obvious whether it is useful to search for a (partially) symmetric realization and if so with which symmetries. Introducing more symmetries generally helps to achieve ground state degeneracy but at the cost of reducing available DOFs. It turns out that for small L-complexes it is often useful to obey the symmetries but for larger L-complexes it is more useful to break symmetries.

In the following we denote $\tilde{r}_{\text{eff}} = \text{rank}(\tilde{\boldsymbol{L}}_{\text{eff}})$ the rank of the effective extended language matrix. Now we can reformulate corollary VII within the effective description:

Corollary IX (Degenerate Ground States of Symmetric languages)**.**

Consider some symmetric L-complex $(\mathcal{C}_{\mathcal{K}}^{\mathcal{Q}}, L, \mathfrak{L})$ *with target language* $L = L_t$ *of length* $g = |L_t|$*. If rank*$(\tilde{\boldsymbol{L}}_{\text{eff, Aug}}) = \tilde{r}_{\text{eff}}$ *and if the quality factor* $\mathcal{Q} > \exp\left[-2/(g\|\tilde{\boldsymbol{L}}^{+}_{\text{eff}}\|_1)\right]$ *is sufficiently large, then there exists a symmetric L-complex* $(\tilde{\mathcal{C}}_{\mathcal{K}}^{\mathcal{Q}}, L, \mathfrak{L})$ *where* $\mathcal{H}_t = \mathcal{H}(L_t)$ *is a* g*-dimensional gapped low-energy eigenspace of the Hamiltonian* $H[\tilde{\mathcal{C}}]$*.*

[15] A relevant example is the PXP-minimal surface code unit-cell `SCUI-1` in fig. 5.1 whose language is fully symmetric in the ports which is partially broken by its ancillaries.

Proof.

The proof is analogous to the proof of corollary VII, we only note the differences. In the following when indexing the effective language matrix when are going to use tilde-indices $\tilde{i}, \tilde{j}, \ldots$ but we leave the subscript $_{\text{eff}}$ for a more streamline notation. We keep the subscript when denoting the effective matrix. Analogous to eq. (3.28) we formulate a linear system

$$\tilde{L}_{\tilde{i}\tilde{j}}\tilde{\Delta}_{\tilde{j}} \stackrel{!}{=} \tilde{b}_{\tilde{i}} \qquad \text{with} \qquad \tilde{b}_{\tilde{i}} \equiv \tilde{b}_i|_{i\in\tilde{i}} = -\bar{E} + \sum\nolimits_{j,k=1}^{N} L_{ij} I_{\mathfrak{L}(j)\mathfrak{L}(k)} L_{ik}, \tag{3.42}$$

now using the effective language matrix $\tilde{\boldsymbol{L}}_{\text{eff}}$. This linear system is consistent by assumption and equivalent to the linear (3.28) due to the symmetry as proven above. The solution to eq. (3.42) is given by the Moore-Penrose pseudoinverse. The solution vector is defined via $\tilde{\Delta}_{\tilde{j}} \equiv \Delta_{\mathfrak{L}(j)}$ for $j \in [j] \cong \tilde{j} \in \{1, \ldots N_{\text{eff}}\}$ and $\tilde{\Delta}_{N_{\text{eff}}+1} \equiv \tilde{E} - \bar{E}$. Similarly we can reformulate eq. (3.18) as

$$L_{\tilde{i}\tilde{j}}\Delta_{\tilde{j}} = b_{\tilde{i}} \qquad \text{with} \qquad b_{\tilde{i}} \equiv b_i|_{i\in\tilde{i}} = -E_i + \sum\nolimits_{j,k=1}^{N} L_{ij} I_{\mathfrak{L}(j)\mathfrak{L}(k)} L_{ik}. \tag{3.43}$$

By subtracting eq. (3.43) from eq. (3.42), we obtain the new linear system $\tilde{L}_{\tilde{i}\tilde{j}}\tilde{\delta}_{\tilde{j}} = \delta E_{\tilde{i}}$, where we defined $\tilde{\delta}_{\tilde{j}} \equiv \tilde{\Delta}_{\tilde{j}} - \Delta_{\tilde{j}}$ for $\tilde{j} \in \{1, \ldots N_{\text{eff}}\}$, $\tilde{\delta}_{N_{\text{eff}}+1} \equiv \tilde{E} - \bar{E}$ and $\delta E_{\tilde{i}} \equiv E_i - \bar{E}$ for $i \in [i] \cong \tilde{i} \in \{1, \ldots g_{\text{eff}}\}$. We can proceed similarly as in theorem V with the new upper bound

$$-\delta(\Delta E_{\boldsymbol{xy}}) \leq \|\boldsymbol{\delta}\|_1 \leq \|\tilde{\boldsymbol{\delta}}\|_1 \leq \|\tilde{\boldsymbol{L}}^{+}_{\text{eff}} \cdot \delta \boldsymbol{E}_{\text{eff}}\|_1 \leq \|\tilde{\boldsymbol{L}}^{+}_{\text{eff}}\|_1 \|\delta \boldsymbol{E}_{\text{eff}}\|_1 \leq \|\tilde{\boldsymbol{L}}^{+}_{\text{eff}}\|_1 \frac{g}{2} \delta E. \tag{3.44}$$

In the last inequality we used that $\|\delta \boldsymbol{E}_{\text{eff}}\|_1 \leq \|\delta \boldsymbol{E}\|_1$ as $\delta \boldsymbol{E}_{\text{eff}}$ possesses the same components as $\delta \boldsymbol{E}$ but (some) identical components from symmetric states are removed. This yields a substitution of $\tilde{\boldsymbol{L}}$ by $\tilde{\boldsymbol{L}}_{\text{eff}}$ in the final term. Thus it is $\Delta E > -\delta(\Delta E_{\boldsymbol{xy}})$ in particular fulfilled if $\Delta E > \|\tilde{\boldsymbol{L}}^{+}_{\text{eff}}\|_1 g \delta E/2$ or equivalently $\mathcal{Q} > \exp\left[-2/(g\|\tilde{\boldsymbol{L}}^{+}_{\text{eff}}\|_1)\right]$. □

This concludes the introductory part of this thesis. In the following part 4 and 5 we consider the elementary building blocks of logical connectives and tessellated languages.

| Appendix

3.A | The Generalization of Corollary VI

In the following let $\tilde{\boldsymbol{L}} := [\boldsymbol{L} \,|\, \tilde{\mathbf{1}}]$ denote the effective language matrix. Let $\tilde{r} \equiv \text{rank}(\tilde{\boldsymbol{L}})$ denote the rank of the effective language matrix and $m \equiv \min(g, N)$, $n \equiv \max(g, N)$ its dimensions. By $\tilde{\boldsymbol{L}}_{\text{Aug}} := [\tilde{\boldsymbol{L}} \,|\, \tilde{\boldsymbol{b}}]$ we denote the effective language matrix augmented by the right-hand side of the linear system.

Corollary X (Generalization of Corollary VI)**.**

Consider some L-complex $(\mathcal{C}^{\mathcal{Q}}_{\mathcal{K}}, L, \mathfrak{L})$ *of the target language* $L = L_t$ *with length* $g = |L_t|$*. If rank*$(\tilde{\boldsymbol{L}}_{Aug}) = \tilde{r}$ *and if the quality factor* $\mathcal{Q} > \exp\left[-2/n^{\tilde{r}-1}\sqrt{Ng^3m^{\tilde{r}-1}}\right]$ *is sufficiently large, then there exists a L-complex* $(\tilde{\mathcal{C}}^{\mathcal{Q}}_{\mathcal{K}}, L, \mathfrak{L})$ *where* $\mathcal{H}_t = \mathcal{H}(L_t)$ *is a g-dimensional gapped low-energy eigenspace of the Hamiltonian* $H[\tilde{\mathcal{C}}]$*.*

The assumption $\text{rank}(\tilde{\boldsymbol{L}}_{\text{Aug}}) = \tilde{r}$ is explicitly dependent on $\tilde{\boldsymbol{b}}$ and thus on the geometry. Note that in the case $\tilde{r} = m = g$ and $n = N$ we recover corollary VI.

Proof.

There exist $m \equiv \min(g, N)$ singular values $\sigma_1 \geq \ldots \sigma_{\tilde{r}} > \sigma_{\tilde{r}+1} = \ldots \sigma_m = 0$ and exactly $m - \tilde{r}$ of them are zero. Again we can use the SVD to derive $2/g\|\boldsymbol{L}^+\|_1 \geq 2\sigma_{\tilde{r}}/\sqrt{Ng^3}$, analog eq. (3.24). If $g \leq N$ we define the Gramian matrix $\boldsymbol{A} = \boldsymbol{L}\boldsymbol{L}^T \in \mathbb{F}_N^{g\times g}$, else if $g > N$ we define the Gramian matrix $\boldsymbol{A} = \boldsymbol{L}^T\boldsymbol{L} \in \mathbb{F}_g^{N\times N}$.

$\boldsymbol{A}$ possesses m eigenvalues $\lambda_i(\boldsymbol{A}) = \sigma_i(\boldsymbol{L})^2$ with the first $\tilde{r}$ of them positive and the last $m - \tilde{r}$ of them zero. Thus $\boldsymbol{A}$ is positive *semi*definite. By $\det^+(\boldsymbol{A}) := \lim_{\alpha\to 0} \alpha^{\tilde{r}-m}|\boldsymbol{A} + \alpha\mathbb{I}_m|$ we denote the *pseudo*determinant of $\boldsymbol{A}$. The pseudodeterminant corresponds to the product of the *non-zero* eigenvalues of $\boldsymbol{A}$. Before we apply the limit $\alpha \to 0$, the function in the limit is is polynomial function of integers and α with coefficients ± 1. We can interpret this as a polynomial function of α with integer coefficients. As $\operatorname{rank}(\boldsymbol{A}) = \tilde{r}$, the coefficients of each monomial of degree smaller $m-\tilde{r}$ vanish. For $\alpha \to 0$ the term $|\boldsymbol{A}+\alpha\mathbb{I}_m|$ decays with $\alpha^{m-\tilde{r}}$ thus the pseudodeterminant converges to the lowest non-zero *integer* coefficient. As the non-zero eigenvalues of $\boldsymbol{A}$ are positive, the *integer* pseudodeterminant (which is their product) must be positive as well: therefore $\det^+(\boldsymbol{A}) \geq 1$.

Let $n \equiv \max(g, N)$, then $\boldsymbol{A} \in \mathbb{F}_n^{m\times m}$ and the largest eigenvalue of $\boldsymbol{A}$ may be upper-bounded by $\sqrt{mn}$. We can now proceed similarly as in eq. (3.25) and eq. (3.26):

$$\frac{2}{g\|\boldsymbol{L}^+\|} \geq \frac{2\sigma_{\tilde{r}}}{\sqrt{Ng^3}} \geq \frac{2}{\sqrt{Ng^3}}\frac{1}{(\sqrt{mn})^{\tilde{r}-1}} = \frac{2}{n^{\tilde{r}-1}\sqrt{Ng^3m^{\tilde{r}-1}}}. \tag{3.45}$$

Thus $\mathcal{Q}(L) > \exp[-2/(g\|\boldsymbol{L}^+\|)]$ is fulfilled in particular if $\mathcal{Q}(L) > \exp[-2/n^{\tilde{r}-1}\sqrt{Ng^3m^{\tilde{r}-1}}]$ and we may apply theorem V. □

4 | Logic Elementaries

"Computers are composed of nothing more than logic gates stretched out to the horizon in a vast numerical irrigation system."

– Stan Augarten, 'State of the Art' (1983)

This chapter presents the first part of the results of this thesis. We apply the theory derived in the previous chapters and apply it to logical connectives in two dimensions. In sec. 4.1 we present the optimized results for all the PXP-minimal logic elementaries, and in particular for those we used as a motivation in the previous chap. 3. For each PXP-minimal elementary gate we are able to achieve a perfect quality. We complete the list of PXP-minimal gates proposed by Stastny *et al.* in Ref. [38].

We find that the additional DOFs introduced in the VdW model offer the possibility to construct new logic gates using fewer atoms. Such gates are based on the intermediate and low energy regime which is excluded in the more simple PXP model. We present and discuss such VdW-specific gates in sec. 4.2 and sec. 4.3. In particular we present a complete list of minimal elementary gates for the VdW model in subsec. 4.2.
For each VdW-specific gate we are able to achieve (almost) perfect quality. Especially the VdW-specific gates based on the intermediate-energy regime are of interest because they possess a similarly large or larger energy gap compared to their PXP-minimal analogue. Other gates which are based on the low-energy regime generally possess only a small energy gap. For these gates it might be preferable to consider non-minimal implementations with more atoms and a larger ennergy gap instead. Such non-minimal elementary gates are discussed in subsec. 4.3. Some of the minimal gates, namely the `XNOR3`-gate from fig. 4.9, also profit from embedding them in three-dimensional space. For the discussion of such three-dimensional logic gates we refer to chap. 8.

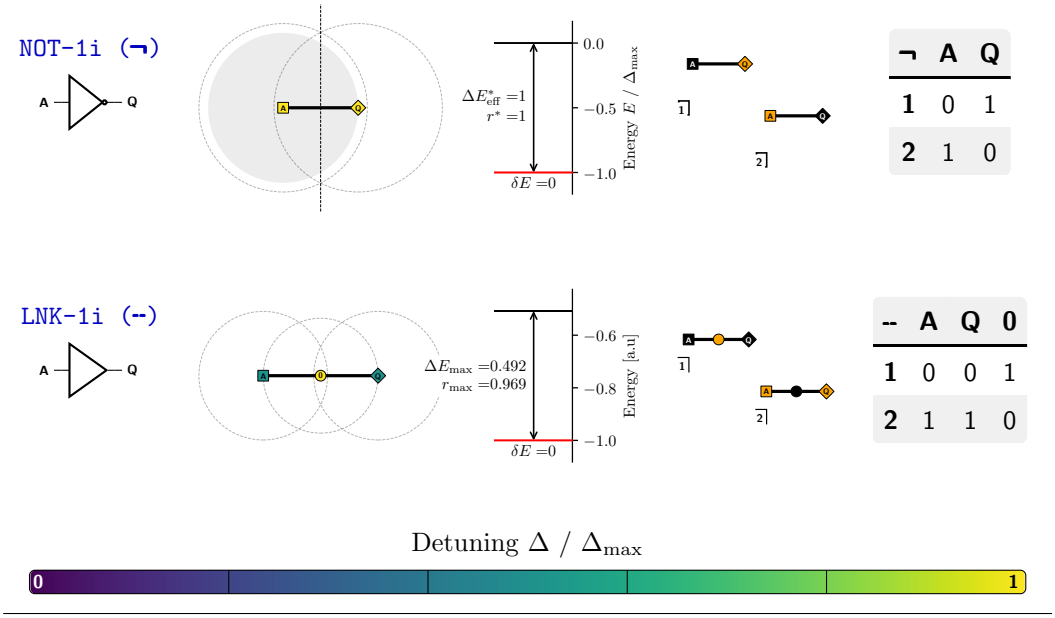

Figure 4.1: Minimal logic primitives optimal in ΔE_{eff} and r. The LNK1-gate is constructed by amalgamating two NOT1-gates. The logic primitives are necessary to construct logic circuits on the Rydberg platform using the gates introduced later.

4.1 | PXP-minimal logic Elementaries

We are going to start this chapter by presenting the results for the PXP-minimal logic elementaries, some of which were used as a motivation in the previous chap. 3. Most of the PXP-minimal elementaries discussed in this chapter were first introduced by Stastny *et al.* in Ref. [38]. As an introduction and for completeness we start which the somewhat trivial *logic primitives*.

4.1.1 | PXP-minimal Primitives

In this subsection we want to present the primitive PXP-minimal logic gates. They are somewhat trivial but they are necessary for the construction of any logic circuit. They include the NOT1-gate and the LNK1-gat presented in fig. 4.1 and the CPY- and ICPY-gates presented in fig. 4.2.

The NOT1-Gate. Just like in the PXP model, we see that the NOT1-gate is the natural building block on the Rydberg platform corresponding to a simple Rydberg blockade. The two atoms should be of equal detuning to achieve degeneracy between the two ground states, i.e. $\Delta_i = \Delta_j$ for $i, j \in \mathcal{N}$. The symmetry between the two atoms is denoted by the dashed symmetry axis in fig. 4.1. In the following we always draw the axes of symmetry iff the ground state manifold is degenerate thanks to the symmetry of the structure.

Without loss of generality we can choose $\Delta_i = \Delta_j = 1$ by rescaling the energies using f_α with $\alpha = \Delta_i^{-1/6}$, see eq. (2.15). Thus for the NOT1-gate the robustness and the effective gap are equal. If the two atoms are closer than their blockade radii then two atoms are in blockade and the energy gap is positive. To maximize the effective gap (and simultaneously the robustness) we need to choose $r_{ij} \leq (C/2\Delta_i)^{1/6}$. Then $E(|1,1\rangle) \geq 0$ and $r = \Delta E_{\text{eff}} = 1$. Note that for such a structure the effective gap and the robustness not only are maximized but they also equal the theoretical upper bound derived in (2.20) and (2.17). This confirms our intuition that the NOT1-gate is the most natural gate on the Rydberg platform. If we fix the position of atom A and vary the position of atom Q then the solutions to the above inequality describe a d-ball around atom A. In fig. 4.1 for $d = 2$ the d-ball is the disk shaded in gray. For most practical purposes it is going to be useful to maximize the distance between atoms to suppress residual interactions. Thus in the portrayed realization we choose the position of atom Q on the boundary of the disk. By the above construction the given L-complex is maximized for both the effective gap and for the robustness. We note this by the superscript * to ΔE_{eff} and r in the energy structure. In the following we always add this superscript to the quantity which is optimized. For sufficiently simple L-complexes we derive the optimal structure analytically.

The LNK1-Gate. To physically realize the edges in logic circuits we can interpret them as a unary logic function (the identity function) LNK which returns its input. Although edges are the fundamental building block of logic circuits the LNK-gates are not the natural building block on the Rydberg platform. They must be constructed by amalgamating an even number of NOT1-gates where we can choose the length of the LNK-gate depending on the application. In any amalgamation of two structures we can amalgamate a realization of the LNK-gate in-between the structures. This reduces residual long-rang interactions without modifying the target function. If we are not able to achieve degeneracy in the amalgamated L-complex (e.g. using theorem V) this can be used to artificially decrease the energy splitting thus increasing the quality. If we can achieve degeneracy this may be used to increase the effective gap or the robustness. This ansatz comes at the cost of a larger number of atoms for the realization. Such a realization of more atoms is less useful for the physicist as it is harder to implement experimentally and more intensive to simulate numerically.

Fig. 4.1 presents the ΔE_{eff}- and r-optimal realization of the LNK1-gate with $N = 3$ atoms. This realization is not just PXP-minimal but also minimal in the VdW model as we require the ancillary such that $\mathbf{0} \notin L_t$ (following remark 4). To achieve degeneracy in the ground states we set $\Delta_0 = \Delta_A + \Delta_Q - I_{AQ}$. For L_{LNK1} the symmetry group on the atoms is the permutation group $\Sigma_{\mathcal{N}}[\text{LNK1}] = \langle(\mathsf{A}\ \mathsf{Q})\rangle$. To achieve a positive energy gap we request that the blockade graph consists of edges $E = \{\{\mathsf{A}, 0\}, \{0, \mathsf{Q}\}\}$ and that $\Delta_0 > \Delta_A, \Delta_Q$. Then, candidates for LESs are $(1_A, 0_Q, 1_0)$, $(1_A, 0_Q, 0_0)$ and its permutations $(0_A, 1_Q, 1_0)$, $(0_A, 1_Q, 0_0)$. The remaining states are energetically larger following alg. 3.3. The energy gap is given by

$$\Delta E = \min(\Delta_0 - \Delta_A, \Delta_0 - \Delta_Q, I_{A0} - \Delta_A, I_{Q0} - \Delta_Q).$$

To maximize the effective gap (and simultaneously the robustness) we want to achieve degeneracy between the states. This implies a D_1-symmetry constraint $\Delta_A = \Delta_Q$ and $I_{A0} = I_{Q0} = \Delta_0$ on the

structure (as expected). Introducing the angle $\alpha = \angle(\mathsf{Q},\mathsf{0},\mathsf{A})$ this determines $r_{\mathsf{AQ}} = 2r_{\mathsf{A0}}\sin\alpha/2$. To maximize the energy gap $E(|1_\mathsf{A},1_\mathsf{Q},0_0\rangle) - E(|1_\mathsf{A},0_\mathsf{Q},0_0\rangle) = \Delta_\mathsf{Q} - I_{\mathsf{AQ}}$, we want to minimize I_{AQ} leaving $\alpha = \angle(\mathsf{Q},\mathsf{0},\mathsf{A}) = \pi$. This leaves essentially one DOF (and one corresponding to a rescaling of the structure). This is determined via

$$C/r_{\mathsf{A0}}^6 = I_{\mathsf{A0}} = \Delta_0 = 2\Delta_\mathsf{A} - I_{\mathsf{AQ}} = 2\Delta_\mathsf{A} - C/(2r_{\mathsf{A0}})^6.$$

For $\Delta_0 = 1$ this construction yields the structure of fig. 4.1. We confirm numerically that the structure is optimal. We note this again via the superscript * to ΔE_{eff} and r in the energy structure. Note that her we derived the symmetry of the structure from scratch. In the following we often assume that the structure respects the symmetries of the language. This reduces the number of DOFs which we have to determine in the numerical optimization process or the analytical derivation. Then in retrospect we check numerically that the symmetric structure is the global optimum in the parameter space.

The Family of (inverted) Copies. In logic circuits the splitting of edges is usually not considered a gate but fundamentally assumed. To physically realize such a copy operation on the Rydberg platform we interpret the branching of an edge as a unary logic function `CPY` which copies the input to q outputs.

In $d = 2$ dimensions on the Rydberg platform with only one ancillary we can realize $q \leq 4$ copies with a positive energy gap[1]. The `CPY`-gate with q copies is constructed by amalgamating $q+1$ `NOT`-gates at the same atom into a star-shape (for $q = 0, 1$ we essentially recover the `NOT`- and the `LNK`-gate respectively). Stastny *et al.*[38] mentioned only the `CPY`-gate with $q = 2$, here for completeness we generalize to gates with $q \in \{2,3,4\}$. Further, for completeness we introduce the logic function `ICPY` which realizes q inverted copies of the input bit. The ΔE_{eff}-optimal minimal realizations of the `ICPY`- and `CPY`-gates in the VdW model are portrayed in fig. 4.2. We find that for both families the maximal effective gap decreases with increasing q as the residual interaction strength increases.

Note that the ΔE_{eff}-optimal realization of the `ICPY`-gate of q copies is constructed by relabeling of the `CPY`-gate with $q-1$ copies. The input port is relabeled as the q^{th} output port and the ancillary is relabeled as the input port:

$$\mathcal{C}_\mathcal{K}^\mathcal{Q} \mapsto \mathcal{C}_{\mathcal{N}\setminus\{\mathcal{K}\cup\mathcal{Q}\}}^{\mathcal{K}\cup\mathcal{Q}}.$$

Thus for minimal `ICPY`-gates we do not need any ancillaries. The `ICPY`-gates are in that sense more natural to realize on the Rydberg platform. However the realizations of `ICPY`-gates in fig. 4.2 are no useful building blocks for logic circuits in two dimension. For each `ICPY`-gate the input port is in the center of the complex thus we can not address it via an `LNK`-link or another gate in two dimensions. These gates are onlz useful to implement logic circuits on the three-dimensional Rydberg platform.

The realizations in fig. 4.2 are not just PXP-minimal but they are also minimal in the VdW model. For the `ICRS`-gates this is trivial as they possess no ancillaries. For the `CPY`-gates we need the ancillary such that $\mathbf{0} \notin L_t$ (as required by remark 4). We want to note that the robustness is *not* maximal for these gates. We could pull out one of the ports while decreasing its detuning. This is shown in fig. 4.3 for $q = 2$. This decreases the effective gap but still 'artificially' increases the robustness by suppressing the smallest detuning. In the following we will stumble across

[1] For $q \geq 5$ output ports the $q+1 \geq 6$ ports would either be in blockade with each other or not in blockade with the ancillary.

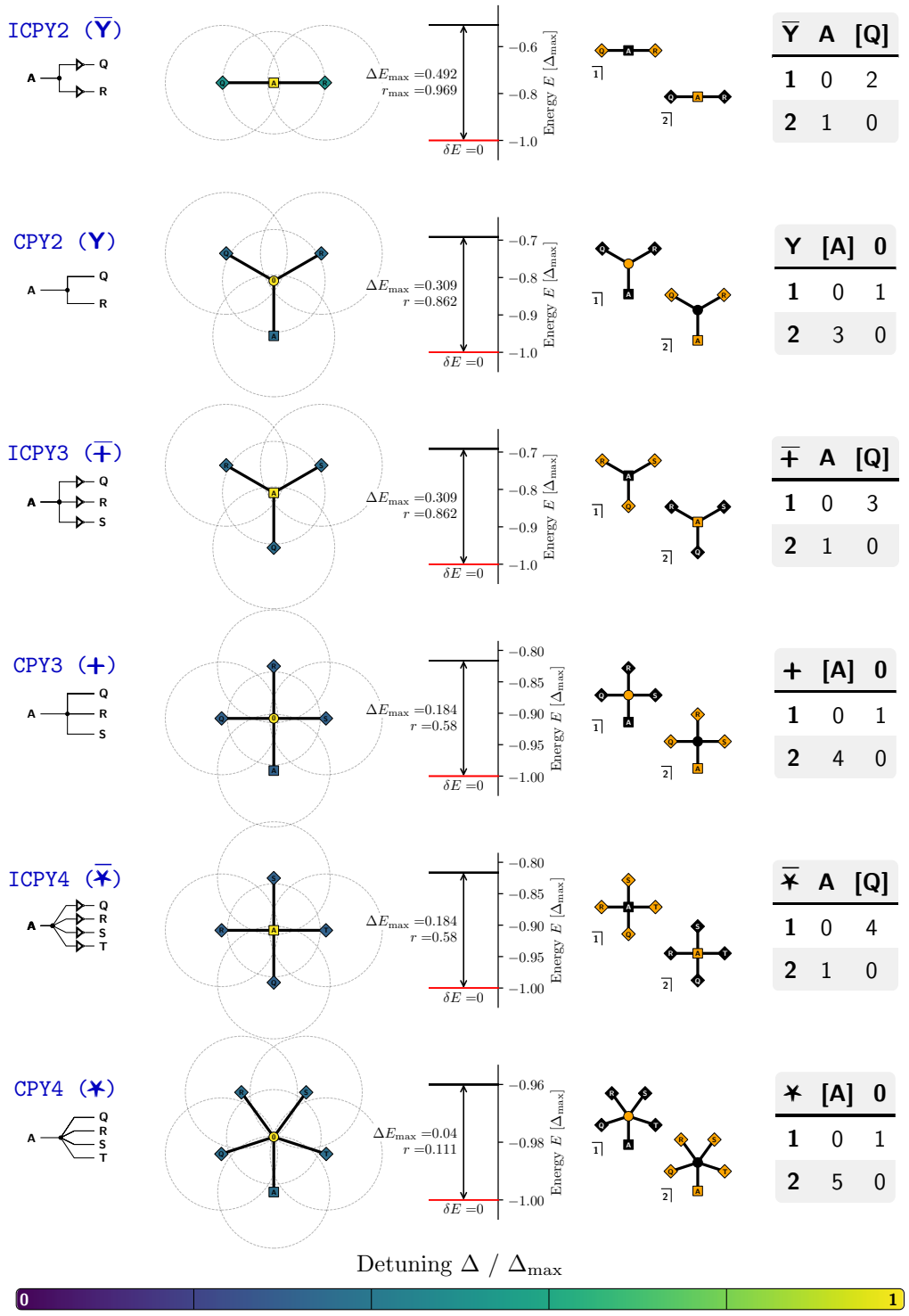

Figure 4.2: Family of ΔE_{eff}-optimal minimal ICPY- and CPY-gates. All gates of this family are constructed by amalgamating $1-5$ NOT-gates at the same atom. The L-complexes are symmetric in the (output) ports. This allows for a description via the effective language matrix which summarizes the (output) ports in one equivalence class (see tables in the right column).

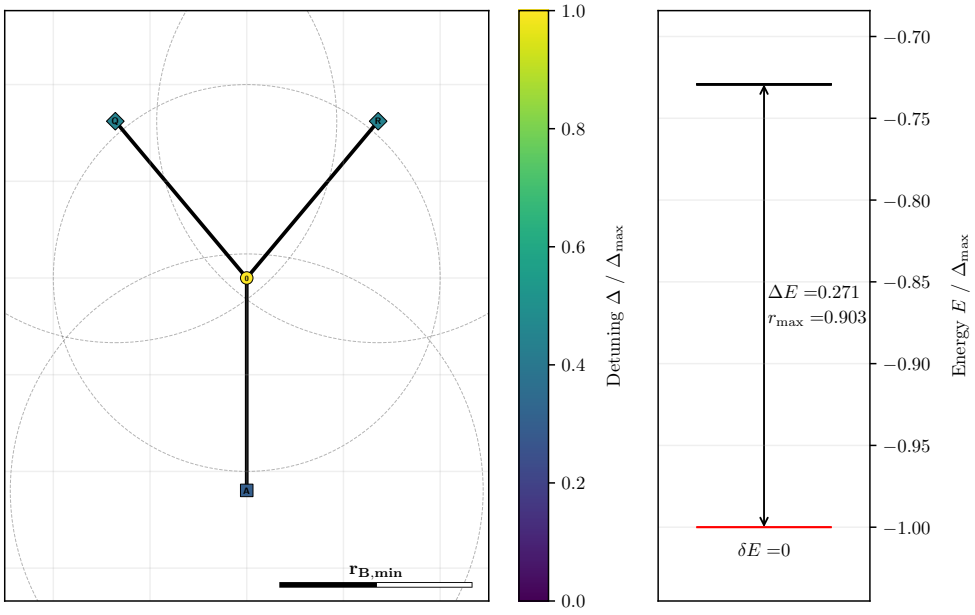

Figure 4.3: r-optimal realization of the CPY2-gate. This structure is found numerically. Note that we increased the robustness compared to fig. 4.2 by decreasing Δ_0 and I_{A0}. Thus the structure is not D_3-symmetric anymore.

more such languages where we can artificially increase r. We conclude that the robustness might be for some languages less suitable as a measure for the size of the energy gap as the effective gap. Thus in the following we mainly focus on the effective gap and optimize for ΔE_{eff}.

4.1.2 | The Crossing of Edges

Before we continue with the PXP-minimal logic gates we first have to discuss the crossing of edges. Just like CPY, the crossing of edges is usually not considered a gate in logic circuits but fundamentally assumed. To implement such a crossing on the $d = 2$-dimensional Rydberg platform we interpret it as a binary BOOLEAN function CRS with two outputs. The CRS-function just copies its inputs to its outputs. Such a function would be trivially realized by two LNK-gates. The point is that we want an implementation via an L-complex in the 2D-plane where the output bits are exchanged compared to the input bits. Secondly, we also consider the inverted crossing ICRS which inverts and exchanges the input bits. The CRS- and ICRS-gates were first introduced in Ref. [38] for the PXP model. The PXP-minimal ICRS1- and the CRS1-gate are portrayed in fig. 4.4. We are able to implement both gates with perfect quality $\mathcal{Q} = 1$. The portrayed structures are optimized for ΔE_{eff} and r. We see that the PXP-minimal realization of the inverted crossing ICRS1 requires less ancillaries than the PXP-minimal realization of the non-inverted crossing CRS1. In fact the CRS1-gate emerges from the ICRS1-gate by amalgamating two more NOT-gates. This is no surprise as the Rydberg platform is based on the Rydberg blockade with the NOT-gate as its fundamental building block. Thus the ICRS1-gate is more natural to realize than the CRS1-gate.

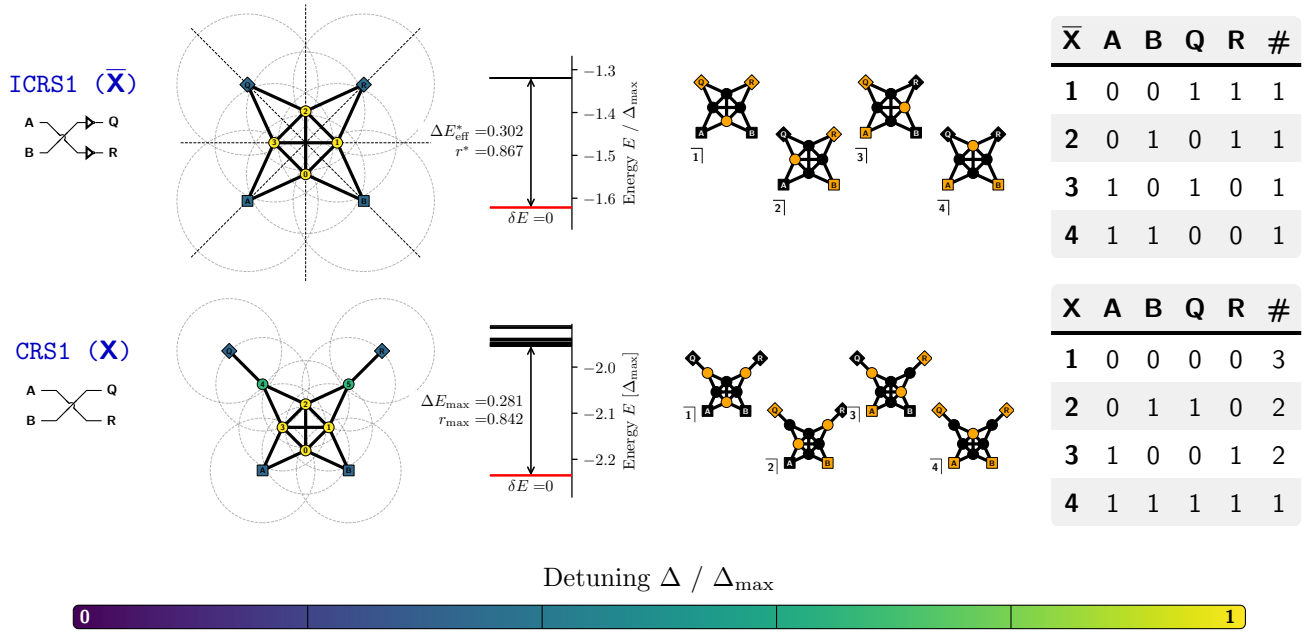

X̄	A	B	Q	R	#
1	0	0	1	1	1
2	0	1	0	1	1
3	1	0	1	0	1
4	1	1	0	0	1

X	A	B	Q	R	#
1	0	0	0	0	3
2	0	1	1	0	2
3	1	0	0	1	2
4	1	1	1	1	1

Figure 4.4: PXP-minimal (inverted) crossing optimal in ΔE_{eff} and r. The CRS1-gate emerges from the ICRS1-gate by amalgamating two NOT-gates to the output or input atoms. For a clearer visualization we summarize the ancillaries in one column portraying only their number of excitations.

In the ICRS1-gate there always the same number of ports and ancillaries excited. This helps to achieve a positive energy gap. In contrast in the CRS1-gate the number of excited ports varies thus we need more ancillaries to balance the energies of the ports. Note that the language $L_{\texttt{ICRS1}}$ of the inverted crossing is highly symmetric via

$$\Sigma_{\mathcal{N}}[\texttt{ICRS1}] = \langle (\mathsf{A}\,\mathsf{B}) \circ (\mathsf{Q}\,\mathsf{R}) \circ (1\,3),\ (\mathsf{A}\,\mathsf{B}\,\mathsf{R}\,\mathsf{Q}) \circ (0\,1\,2\,3) \rangle. \tag{4.1}$$

This is reflected in the D_4-symmetry of the ICRS1-gate. Thanks to this symmetry the effective language consists of only one word. Thus if we respect the symmetry during optimization the ground states are trivially degenerate. The axes of symmetry of the ICRS1-gate are drawn as dashed lines in fig. 4.4. For the ICRS1-gate it only remains to optimize the effective energy gap and the robustness. In the optimized ICRS1-gate of fig. 4.4 the LESs are $(0_{\mathsf{A}}, 0_{\mathsf{B}}, 0_{\mathsf{C}}, 0_{\mathsf{D}}, 1_0, 0_1, 1_2, 0_3)$, $(1_{\mathsf{A}}, 0_{\mathsf{B}}, 0_{\mathsf{C}}, 0_{\mathsf{D}}, 0_0, 1_1, 0_2, 0_3)$, $(1_{\mathsf{A}}, 1_{\mathsf{B}}, 1_{\mathsf{C}}, 0_{\mathsf{D}}, 0_0, 1_1, 0_2, 0_3)$ and $(1_{\mathsf{A}}, 1_{\mathsf{B}}, 1_{\mathsf{C}}, 1_{\mathsf{D}}, 0_0, 0_1, 0_2, 0_3)$ and its 15 permutations under $\sigma \in \Sigma_{\mathcal{N}}[\texttt{ICRS1}]$. The CRS1-gate is harder to optimize as it lacks the C_4-symmetry. We can not use symmetry arguments to achieve degeneracy in the ground state thus we have to apply theorem V.

4.1.3 | Family 1 of Elementary Logic Gates

In this subsection we want to continue with the PXP-minimal elementary logic gates. There exist three families of minimal logic gates in the PXP model for the logic elementaries[37]. We continue to label these families by indices $1, 2, 3$ as done previously. As discussed in chapter 3.1.2, the families 1 and 3 differ only by an additional blockade but their languages are identical. Therefore they are are only different *implementations* (via different structures) but not different *realizations*. Thus in this chapter and in the following we only consider the families 1 and 2 of languages.

The gates of family 1 are presented in fig. 4.5. We are able to implement each elementary gate with perfect quality $\mathcal{Q} = 1$. The gates are optimized for the effective energy gap.

The NOR1-Gate. The realization `NOR1` is an interesting case: The language $L_{\texttt{NOR1}}$ possesses the symmetry group $\Sigma_{\mathcal{N}}[\texttt{NOR1}] = \langle(\mathsf{Q}\,0)\circ(\mathsf{B}\,1)\rangle \subset S_{\mathcal{N}}$ acting on the atoms via $\mathfrak{L}$. If we constrain the D_1-symmetry corresponding to the central dashed symmetry axis the energy structure remains invariant under application of $\Sigma_{\mathcal{N}}[\texttt{NOR1}]$. This is the symmetry which was already constrained in fig. 3.3. Then two pairs of symmetric ground states are of equal energy leaving two effective ground states. We can set each ground state energetically equal by introducing one more symmetry corresponding to the two remaining dashed axes. Note that these symmetries are only fulfilled on $\mathcal{G}$ but not on $\mathcal{E}$.

Let d_{i} denote the distance of atom i from the intersection point of the symmetry axes. Then we have essentially three DOFs left: $\Delta_{\mathsf{Q}} = \Delta_{\mathsf{A}} = \Delta_0$, $\Delta_{\mathsf{B}} = \Delta_1$, $d_{\mathsf{Q}} = d_{\mathsf{A}} = d_0$ and $d_{\mathsf{B}} = d_1$ (one DOF corresponds to a rescaling of the structure). Note that we do not constrain the relation between Δ_{Q} and Δ_{B} as $(0_{\mathsf{A}}, 0_{\mathsf{B}}, 1_{\mathsf{Q}}, 1_0, 0_1) \notin L_{\texttt{NOR1}}$ is no ground state. Here we use the same labeling $\mathfrak{L}$ as in the right column of fig. 4.5. We want to determine solutions of the (symmetric) parameter space maximizing ΔE_{eff} and/ or r. The solution spaces maximizing ΔE_{eff} and r are finite dimensional subspaces and incomparable, however they intersect. The `NOR1`-gate presented in fig. 4.5 maximizes both ΔE_{eff} and r. In this implementation there are three LESs: $(0_{\mathsf{A}}, 0_{\mathsf{B}}, 1_{\mathsf{Q}}, 1_0, 0_1)$, $(0_{\mathsf{A}}, 1_{\mathsf{B}}, 0_{\mathsf{Q}}, 0_0, 0_1)$ and $(1_{\mathsf{A}}, 1_{\mathsf{B}}, 0_{\mathsf{Q}}, 0_0, 1_1)$. If we loosen the above constraints varying all variables the optimizer is able to improve neither ΔE_{eff} nor r any further. This is reason to assume that we actually found the global optimum in the structure for the `NOR1`-gate.

The remaining Gates. The other gates of the family are constructed by amalgamating one or multiple NOT-gates to some atom and relabeling the structure. In contrast to the `NOR1`-gate we can not apply symmetry arguments to achieve degeneracy, thus we apply theorem V.

Firstly, it is noticeable that the effective gap of the other gates is slightly smaller than the effective gap of the `NOR1`-gate. This might be partially for numerical reasons as they lack symmetries and thus are harder to optimize. Hence they might only be approximately ΔE_{eff}-optimal. This can be seen in the low-energy subspace of $\mathcal{E}$ which remain energetically slightly spread-out (e.g. for the `NAND1b`-gate). Nevertheless, we can not expect much more improvement. It is expected that they possess a smaller effective gap as they have more residual interactions between distant atoms. This is especially true for the `NAND1a`- and the `AND1a`-gate as their additional atom is in blockade with two atoms. Even though we did not optimize the robustness for the remaining gates (only the `NOR1`-gate is r-optimal), the robustness can profit from adding further atoms. The additional detunings can be smaller thus artificially increasing r.

Secondly, we want to note that for the connectives `AND` and `NAND` only realization `b` was found by Stastny in [38, 37]. In Ref. [37] it was claimed that the portrayed list is exhaustive. Nevertheless realization `a` is an equally valid PXP-minimal realization.

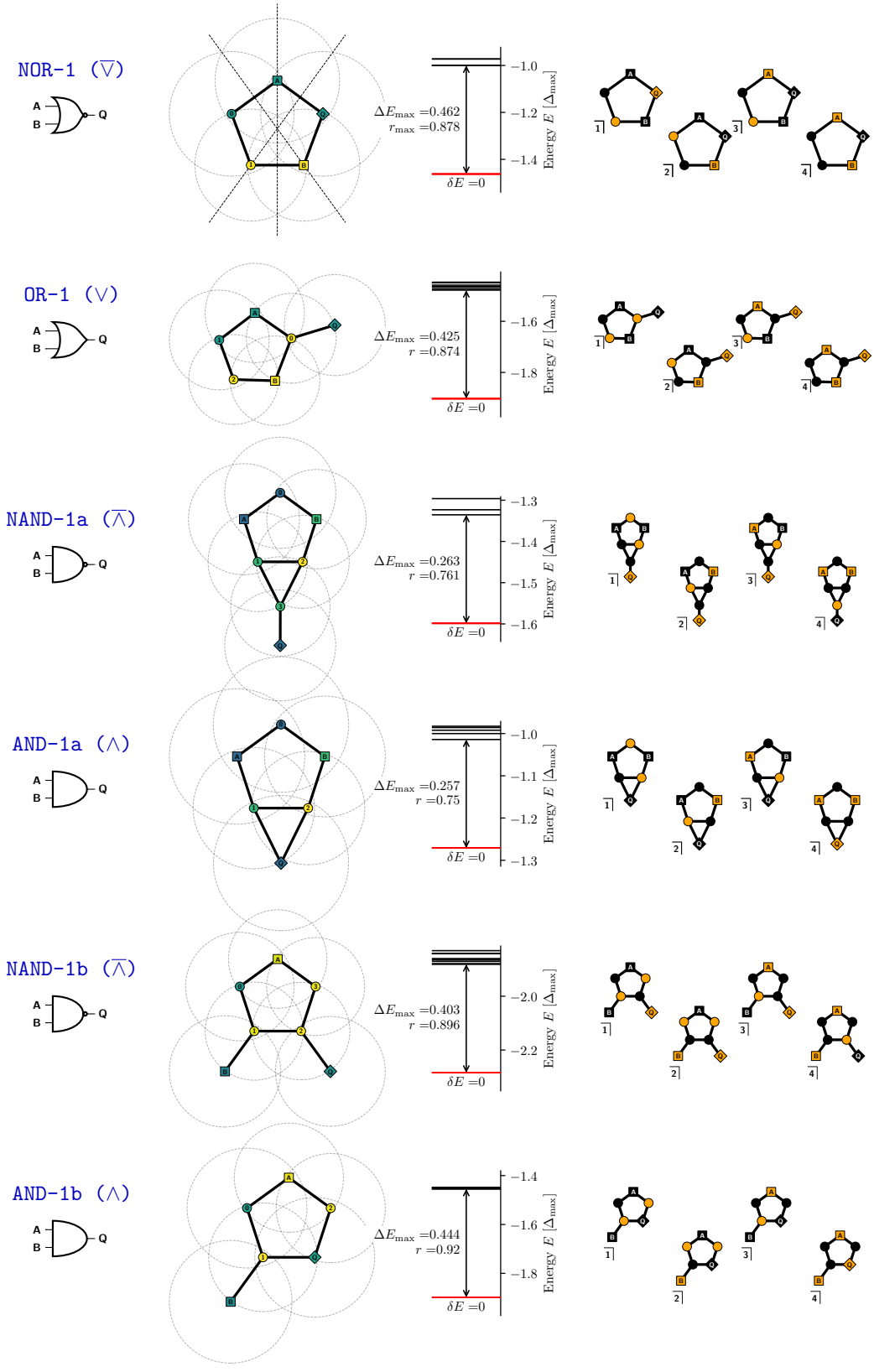

⊽	A	B	Q	0	1
1	0	0	1	0	1
2	0	1	0	1	0
3	1	0	0	0	1
4	1	1	0	0	0

∨	A	B	Q	0	1	2
1	0	0	0	1	0	1
2	0	1	1	0	1	0
3	1	0	1	0	0	1
4	1	1	1	0	0	0

⊼	A	B	Q	0	1	2	3
1	0	0	1	1	0	1	0
2	0	1	1	0	1	0	0
3	1	0	1	0	0	1	0
4	1	1	0	0	0	0	1

⊼	A	B	Q	0	1	2
1	0	0	0	1	0	1
2	0	1	0	0	1	0
3	1	0	0	0	0	1
4	1	1	1	0	0	0

⊼	A	B	Q	0	1	2	3
1	0	0	1	0	1	0	1
2	0	1	1	1	0	0	1
3	1	0	1	0	1	0	0
4	1	1	0	0	0	1	0

⊼	A	B	Q	0	1	2
1	0	0	0	0	1	1
2	0	1	0	1	0	1
3	1	0	0	0	1	0
4	1	1	1	0	0	0

Figure 4.5: Family 1 of PXP-minimal logic elementaries optimal in ΔE_{eff}. In family 1 there are two realizations of the NAND- and AND-gate but no realizations of the XOR- and XNOR-gate.

The realizations AND1a and NAND1a can be interpreted as somewhat analogous to the realizations of the XOR- and XNOR-gates in family 2 in fig. 4.6. As discussed in subsec. 3.1.2 we can construct family 3 from family 1 simply by adding an additional blockade between atom Q and atom 0. Family 2 is constructed from family 3 by connecting atom Q and atom 1 in the blockade graph modifying the first ground state such that only atom Q is excited: $(0_A, 0_B, 1_Q, 0_0, 1_1) \leftrightarrows (0_A, 0_B, 1_Q, 0_0, 0_1)$. Applying this construction to NAND1a and AND1a we obtain the XOR- and XNOR-gates of family 2. In that sense realization 1 (and 3) can be interpreted as inefficient or redundant in the choice of the ground state manifold. In $L_{\texttt{NOR1}} = L_{\texttt{NOR3}}$ there is no ancillary bit which is only excited if atom A is excited but atom B is not. In realization 2 the new output port is amalgamated to ancillary 2 to construct an XOR- and XNOR-gate. Instead in realization 1 (and 3) the ancillary 2 negates the state of atom B yielding only somewhat redundant information.

4.1.4 | Family 2 of Elementary Logic Gates

Fig. 4.5 presents the optimized gates of family 2. For each gate we are able to achieve perfect quality $\mathcal{Q} = 1$. Again only the effective gap but not the robustness is optimized. The effective gaps are of similar magnitude as in realization 1. Family 2 allows for the realization of a PXP-minimal XOR- and XNOR-gate. The realization w of the NOR-, OR-, XNOR- and XOR-gate is symmetric in the ports whereas in family 1 every gate was asymmetric in the ports (even $L_{\texttt{NOR1}}$ which was highly symmetric). This allows for a description via the effective language matrix in the right column. In particular the XNOR2-gate is D_3-symmetric; it respects the full permutation symmetry between the ports of the target function. This helps in the numerical optimization process which is probably the reason for the slightly larger effective gap (compared to the NOR2-gate).

4.1.5 | An additional PXP-minimal XOR-gate

At this point for completeness we should also mention the second PXP-minimal realization 2b of the XOR-gate portrayed in fig. 4.7. The XOR2b-gate differs from the XOR2a-gate not only in its structure and its blockade graph but also in the language. This makes it a new realization (and not just a new implementation with different blockade graph). This realization was also not mentioned by Stastny *et al.* in Refs. [37, 38].

The XOR2b-gate is D_3-symmetric, i.e. it respects the full permutation symmetry between the ports of the target function. Thus thanks to its symmetries it particularly easy to construct and optimize (similarly as the XNOR2-gate). The implementation portrayed in fig. 4.7 is optimized for ΔE_{eff} and r. Note that the optimized effective gap of the XOR2b-gate is slightly smaller than the effective gap of the XOR2a-gate because it is more compact and thus possesses larger residual interactions.

The XOR2b-gate differs from the other PXP-minimal logic gates in the sense that its blockade graph is not planar (its edges overlap). This however is only a mathematical peculiarity of the blockade graph but of no physical significance.
At this point one should refer to the FMS2-site from fig. 5.5. This FMS2-site is somewhat analogous to the XOR2b-gate as can be seen in their structure. Similarly, we can draw the analogy between the FMS1-site and the XOR2a-gate (which is less apparent in their optimized structures). For a discussion about the origin of this similarities we refer to sec. 4.1.

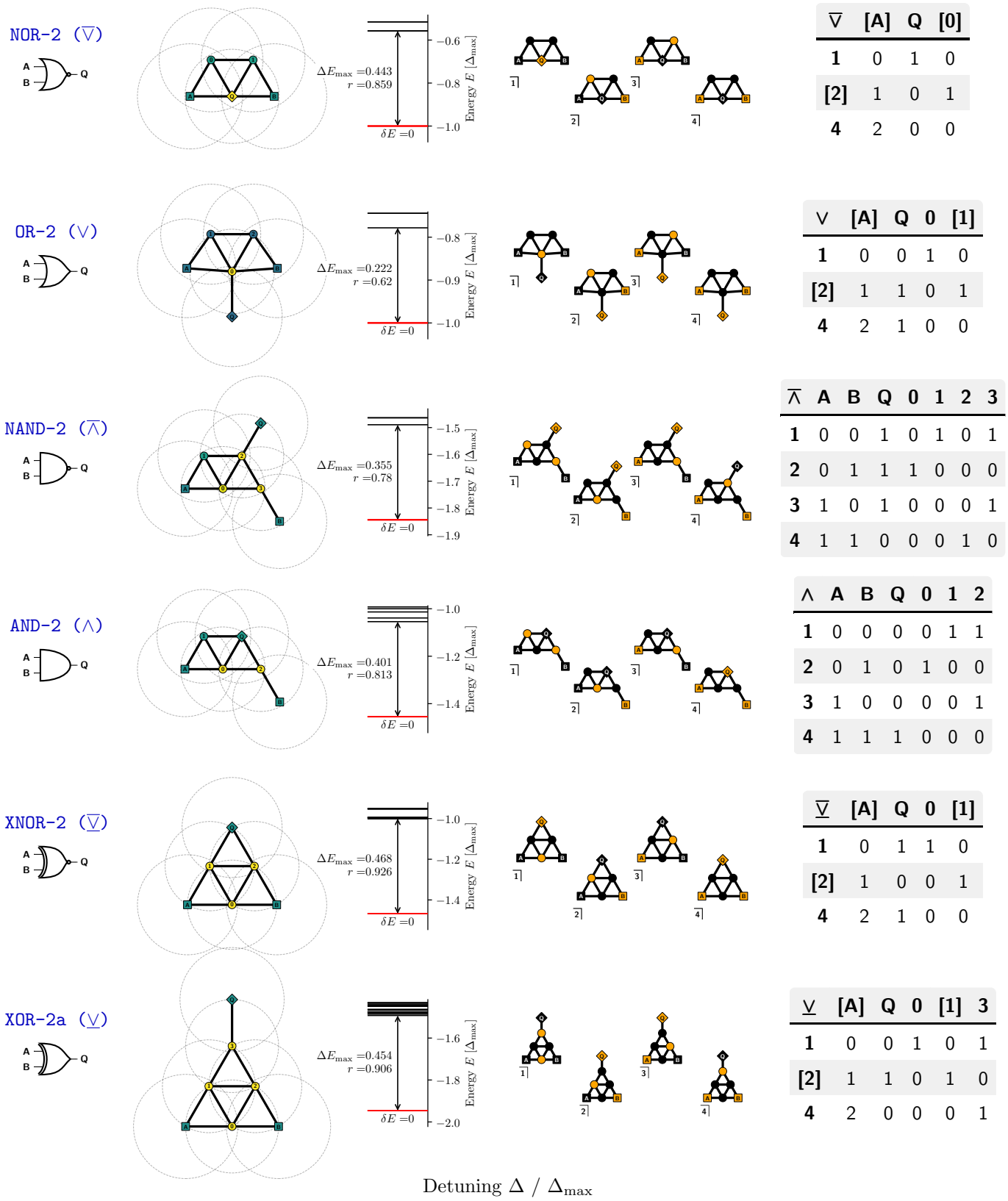

⊽	[A]	Q	[0]
1	0	1	0
[2]	1	0	1
4	2	0	0

∨	[A]	Q	0	[1]
1	0	0	1	0
[2]	1	1	0	1
4	2	1	0	0

⊼	A	B	Q	0	1	2	3
1	0	0	1	0	1	0	1
2	0	1	1	1	0	0	0
3	1	0	1	0	0	0	1
4	1	1	0	0	0	1	0

∧	A	B	Q	0	1	2
1	0	0	0	0	1	1
2	0	1	0	1	0	0
3	1	0	0	0	0	1
4	1	1	1	0	0	0

⊻	[A]	Q	0	[1]
1	0	1	1	0
[2]	1	0	0	1
4	2	1	0	0

⩒	[A]	Q	0	[1]	3
1	0	0	1	0	1
[2]	1	1	0	1	0
4	2	0	0	0	1

Figure 4.6: Family 2 of PXP-minimal logic elementaries optimal in ΔE_{eff}. Family 2 offers a realization of the NAND- and AND-gate but no realizations of the XOR- and XNOR-gate.

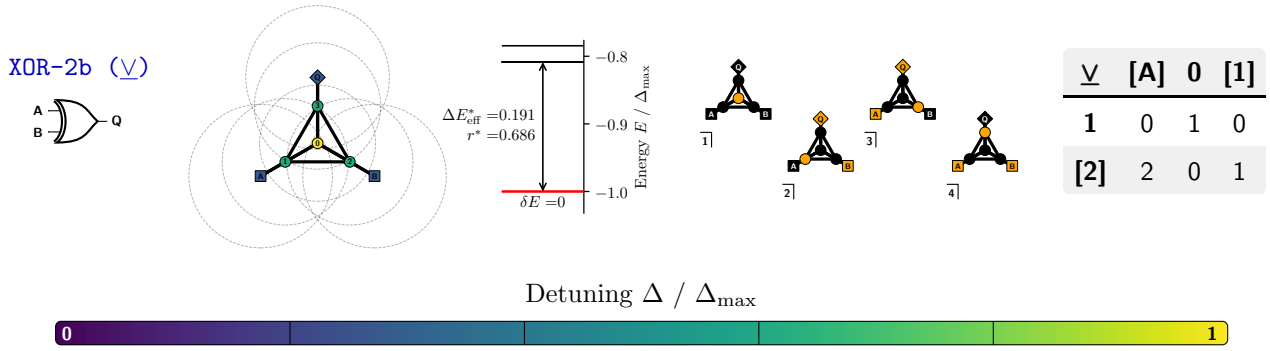

∨	[A]	0	[1]
1	0	1	0
[2]	2	0	1

Figure 4.7: XOR2b-Gate optimal in ΔE_{eff} and r. This is an additional PXP-minimal realization of the XOR-gate from family 2.

Conclusion. This concludes our list of PXP-minimal logic gates and primitives. We were able to reconstruct every PXP-minimal gate proposed by Stastny *et al.* with perfect quality factor $\mathcal{Q} = 1$ and with an effective gaps $\Delta E_{\text{eff}} \gtrsim 20\%$ in the VdW model. In some cases we were able to exploit symmetries to achieve a vanishing energy splitting or to simplify the optimization process. However in most cases we had to apply theorem V to achieve ground state degeneracy. We find that inversion gates of all kinds (i.e. NOT, ICRS, NOR1, NOR2) are natural to realize on the Rydberg platform. Amalgamating NOT-gates to obtain other gates of the same family in general decreases the effective gap due to additional residual interactions.

4.2 | VdW-minimal logic Elementaries

So far we only discussed PXP-derived logic elementaries. Many of the PXP-derived gates were introduced by Stastny *et al.* in [38, 37]. We completed these lists with further PXP-minimal gates. The VdW model possesses *finite* interaction energies and *long-range* interactions. Nevertheless we were able to reconstruct every PXP-minimal gate in the VdW model with perfect quality factor $\mathcal{Q} = 1$. For these elementary PXP-derived gates the finite and residual interactions do not impede the reconstruction in the VdW model.

In the following section we want to study whether we can exploit this intermediate and low energy regime to construct more atom-efficient gates in the VdW model. In particular we are interested in determining the VdW-minimal logic gates. This is interesting for academic reasons but also simplifies an experimental implementation or a numerical simulation of the gate.

4.2.1 | VdW-minimal Primitives

It is easy to see that the logic primitives in fig. 4.1 and 4.2 are VdW-minimal: they possess either no ancillary in the first place or only one ancillary which is necessary such that $\mathbf{0} \notin L_t$ (we exclude such languages by ass. 4). For those gates which require an ancillary the choice of the ancillary is *unique* to achieve a positive energy gap. This is shown in the following quick proof:

Proof 3. (Minimality and Uniqueness of Logic Primitives)

We follow the argument from corollary II. In a nutshell corollary II forbids ground states which are non-adjacent substates (with any intermediate excited state) because they imply a finite energy splitting (a negative energy gap).

Now each primitive of fig. 4.1 or fig. 4.2 with one ancillary possesses two states: In $\boldsymbol{x}_1$ we require an excited ancillary to prevent $\mathbf{0} \in L_t$ (which we exclude by remark 4). Thus the primitives are minimal for the number of atoms in the VdW model. In $\boldsymbol{x}_2$ for each primitive there are at least two excited ports. The ancillary can not be excited in $\boldsymbol{x}_2$ because otherwise $\boldsymbol{x}_1 \Subset \boldsymbol{x}_2$ is a non-adjacent substate. □

Thus the list of VdW-minimal gates for the above primitives is *complete*. The goal of this chapter is to find all VdW-minimal gates for the (inverted) crossing `ICRS` and `CRS` and the elementary logic gates. As in previous chapter we start with the (inverted) crossings.

4.2.2 | VdW-minimal (inverted) Crossings

The VdW-minimal realizations of the (inverted) crossings `ICRS` and `CRS` are portrayed in fig. 4.8. We were able to reduce the number of ancillaries by four atoms compared to the PXP-minimal realization. The `ICRS2`-gate does not require any ancillaries at all in the VdW model. Thus the `ICRS2`-gate is trivially VdW-minimal and unique in that attribute. The `CRS2`-gates possesses two ancillaries. In the following we show that the realizations are VdW-minimal and that the list of VdW-minimal realizations is complete:

Proof 4. (Minimality and Completeness of $L_{\texttt{CRS2}}$)

As above we argue with corollary II. In a nutshell corollary II forbids ground states which are non-adjacent substates (with any intermediate excited state) because they imply a finite energy splitting (a negative energy gap).

To circumvent that $\boldsymbol{x}_1 \Subset \boldsymbol{x}_2, \boldsymbol{x_3}, \boldsymbol{x_4}$ there must exist an ancillary which is excited in $\boldsymbol{x}_1$ but not excited in state $\boldsymbol{x}_2$, $\boldsymbol{x_3}$, $\boldsymbol{x_4}$. Furthermore to prevent $\boldsymbol{x}_2, \boldsymbol{x}_3 \Subset \boldsymbol{x_4}$ there must exist an ancillary which is excited in $\boldsymbol{x}_2$ and $\boldsymbol{x}_3$ but not in $\boldsymbol{x}_4$. Thus we require two ancillaries which makes the `CRS2`-gates from fig. 4.8 *VdW-minimal*. Up to a permutation of the ancillaries there exist only four possible choices for two ancillaries which respect the above condition: $w[\texttt{CRS2a}] = (\texttt{NOT}_\texttt{A}, \texttt{NOT}_\texttt{B})$, $w[\texttt{CRS2b}] = (\texttt{NAND}, \texttt{NOR})$, $w[\texttt{CRS2c}] = (\texttt{XOR}, \texttt{NOR})$ and $w[\texttt{CRS2d}] = (\texttt{NAND}, \texttt{XNOR})$. These realizations determine the languages presented in fig. 4.8. This makes the portrayed list of realizations *complete*. □

Thus we need at least two ancillaries to achieve a positive energy gap and fig. 4.8 presents all possible `CRS`-gates with two ancillaries in the VdW model. The four possible gates are labeled

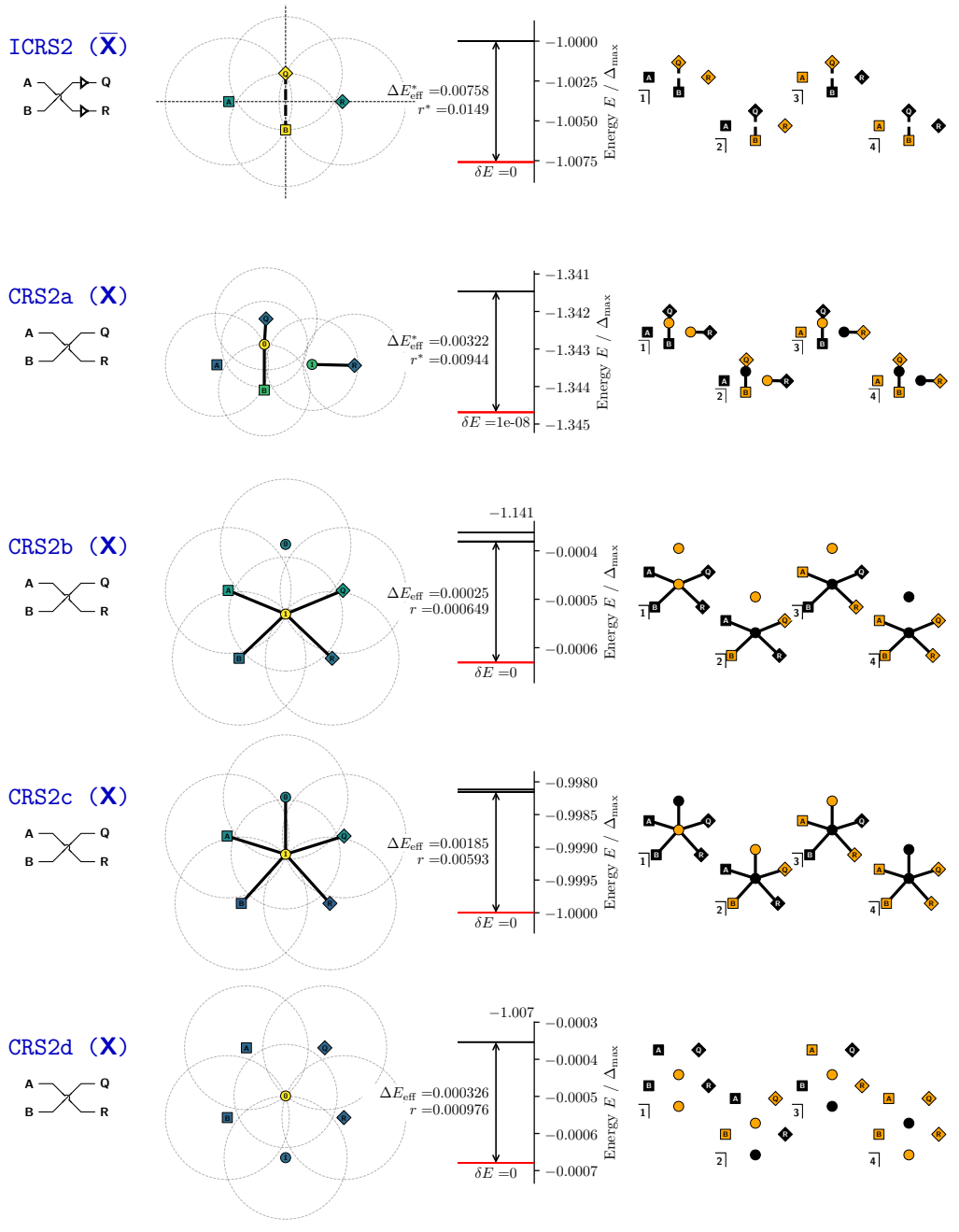

$\overline{X}$	A	B	Q	R
1	0	0	1	1
2	0	1	0	1
3	1	0	1	0
4	1	1	0	0

X	A	B	Q	R	0	1
1	0	0	0	0	1	1
2	0	1	1	0	0	1
3	1	0	0	1	1	0
4	1	1	1	1	0	0

X	A	B	Q	R	0	1
1	0	0	0	0	1	1
2	0	1	1	0	1	0
3	1	0	0	1	1	0
4	1	1	1	1	0	1

X	A	B	Q	R	0	1
1	0	0	0	0	0	1
2	0	1	1	0	1	0
3	1	0	0	1	1	0
4	1	1	1	1	0	0

X	A	B	Q	R	0	1
1	0	0	0	0	1	1
2	0	1	1	0	1	0
3	1	0	0	1	1	0
4	1	1	1	1	0	1

Figure 4.8: Complete list of VdW-minimal (inverted) crossings optimal in ΔE_{eff} and r. The crossings require only two ancillaries in VdW model, the inverted crossing does not require any ancillaries.

by the letters a, b, c, d respectively. In the following we discuss some interesting properties of the gates.

Necessary but not Sufficient. First note that the condition mentioned in proof 4 is *only necessary but not sufficient*. Specifically for the crossings we have the additional constraint on the geometry that we want to interchange the ports (that is why we construct such a CRS-gate in the first place). Without the numerical simulation it very unclear whether there exists such an implementation (on the $d = 2$-dimensional Rydberg platform) which realizes the CRS-languages with a positive energy gap. It is somewhat surprising that here and in the following we are always able to construct such implementations.

The ICRS2-Gate. The inverted crossing ICRS2 is optimal for ΔE_{eff} and r. The portrayed structure was *derived analytically* but an almost optimal structure was also found numerically. Similar to $L_{\texttt{ICRS1}}$ the language $L_{\texttt{ICRS2}}$ is highly symmetric via $\Sigma_{\mathcal{N}}[\texttt{ICRS1}] = \langle(\mathsf{A}\,\mathsf{B}) \circ (\mathsf{Q}\,\mathsf{R}),\ (\mathsf{A}\,\mathsf{B}\,\mathsf{R}\,\mathsf{Q})\rangle$. Contrary to the ICRS1-gate the ICRS2-gate is not D_4-symmetric. More precisely the ICRS2-gate can not be D_4-symmetric without destroying the energy gap. The ground state manifold consists of the four states where two neighboring atoms of one edge of the quadrilateral are excited. In a D_4-symmetric (i.e. square) geometry of the atoms with equal detunings it would be energetically favorable to excite the non-adjacent atoms from opposite corners.

In the structure $\mathcal{C}[\texttt{ICRS1}]$ the symmetry between the two input atoms (the two output atoms) is broken. However the constructed structure D_2-symmetric: the geometry is rhomboidal where opposite atoms possess equal detunings. The distance between neighboring atoms is equal. Thus for each ground state there is an equal contribution by the interaction energies and detuning energies to the Hamiltonian. In that sense the structure respects the symmetries of the language on the level of the ground state manifold. This is not true for excited states where opposite atoms of the rhomboid may be excited. By constraining the D_2-symmetry, the effective language of the ICRS2-gate consists of only one word. Thus the D_2-symmetry is sufficient to achieve degeneracy in the ground states. The axes of symmetry of the ICRS2-gate are drawn as dashed lines in fig. 4.8.

The CRS2a-Gate. The CRS2a-gate emerges from the ICRS2-gate by amalgamating two NOT-gates to the output or input atoms. Its structure in fig. 4.8 is optimized for ΔE_{eff} and r. Note that the the structure is fully asymmetric (even when restricted to the ground state manifold) while the language $L_{\texttt{CRS2}}$ is symmetric via $\Sigma_{\mathcal{N}}[\texttt{CRS2a}] = \langle(\mathsf{A}\,\mathsf{B}) \circ (\mathsf{Q}\,\mathsf{R}) \circ (\mathsf{0}\,\mathsf{1}), (\mathsf{A}\,\mathsf{R}) \circ (\mathsf{B}\,\mathsf{Q})\rangle$. We can not symmetrize the structure without destroying the energy gap. This is a consequence of the asymmetry of the ICRS2-gate on which the CRS2-gate is based on. This is conceptually interesting: naively one could have assumed that for a symmetric language there always exists a symmetric structure which optimally realizes the language on the Rydberg platform. However this counterexample illustrates that a symmetric structure is in general not optimal and might even imply a negative energy gap while there may exist an asymmetric structure which successfully realizes the language. Furthermore, the ICRS2-gate illustrates that a permutation symmetry of the language might only be conserved on the level of the interactions and detunings which contribute to eigenenergies of ground states. Here the symmetry is broken for interactions and detunings which contribute only to excited states and in particular for the structure. Therefore we have to be cautious when assuming symmetries: When constraining symmetries during numerical optimization we always have to check retrospectively whether the constructed symmetric structure is truly an optimal structure (with respect to $\mathcal{Q}$, ΔE_{eff} or r). Furthermore, the optimal structures for the simple, highly symmetric gates in this thesis are constructed analytically; usually by assuming that the structure respects the symmetry of the language to reduce the

number of DOFs. These analytical derivations can not be considered proofs for optimality in full parameter space but only in the symmetric subspace. Here again we have to check numerically whether these structures are optimal in the full parameter space.

Note that for the CRS2a-gate the energy splitting $\delta E \approx 10^{-8}$ is very small but non-zero and thus the quality factor is $\mathcal{Q} \approx 0.999995858$ is almost but not exactly one. This is due to the fact that the CRS2a-gate is the first structure we encounter where we can neither apply theorem V nor its corollaries nor we can exploit any symmetries. The lack of symmetries of the structure is a direct consequence from the breaking of the symmetries of the language (which was discussed above). It seems however that there does exist a structure with perfect degeneracy and the numerical optimization algorithm approximated in to very good precision. Only due to numerical error we can not achieve an energy splitting of precisely zero just with the optimization algorithm. If such a structure exists then its geometry fulfills $\operatorname{rank}(\tilde{\boldsymbol{L}}_{\text{Aug}}) = \operatorname{rank}(\tilde{\boldsymbol{L}}) = 3$. Here the augmented column of $\tilde{\boldsymbol{L}}_{\text{Aug}}$ is a function of the interaction energies an thus of the geometry. We can use the smallest singular value σ_4 of $\tilde{\boldsymbol{L}}_{\text{Aug}}$ as a measure for how strongly the above condition is broken in the CRS2a-gate of fig. 4.8: The singular value $\sigma_4 \approx 2.95967587 \cdot 10^{-9} \gtrsim 0$ is very small thus the condition $\operatorname{rank}(\tilde{\boldsymbol{L}}_{\text{Aug}}) \overset{!}{=} 3$ from corollary VII is just barely broken. The geometry is a very good approximation of an optimal geometry. To achieve perfect ground state degeneracy, we can add an additional *virtual ancillary* to achieve full row-rank for the language matrix and then apply V. This idea is discussed thoroughly in chapter 7.1, the optimized structure with the virtual ancillary is portrayed in fig. 7.1.

The remaining CRS2-Gates. The remaining CRS2-gates b, c and d portrayed in fig. 4.8 possess similar star-like structures which are D_1-symmetric in the vertical direction. Thus in contrast to the ICRS2- and CRS2a-gate they conserve the symmetry between input and output ports in their structure. Again, the symmetry between the two input (output) ports broken in the implementation but not in the realization. For these CRS2-gates we can achieve perfect degeneracy using V. In principle the gates are optimized for both ΔE_{eff} *and* r (just like the others). However this is not noted by an asterisk in fig. 4.8 as they are numerically hard to optimize (probably due to their partially asymmetric star-like structure). Thus we can not claim confidently that the portrayed structures are optimal for the gates.

4.2.3 | Family 3 of Elementary Logic Gates

Now we continue with the elementary logic gates in the VdW model. Fig. 4.9 portrays the minimal logic elementaries in the VdW-model optimal in ΔE_{eff} and r. We are able to reduce the number of ancillaries by up to four atoms (for the NAND3-gate) compared to the PXP-minimal case. The logic gates of family 3 possess *at most one ancillary*. In the following we briefly show that these logic gates are VdW-minimal and that the list of VdW-minimal realizations is complete:

Proof 5. (Minimality and Uniqueness of the Logic Elementaries)

Again, we argue with corollary II. In a nutshell corollary II forbids ground states which are non-adjacent substates (with any intermediate excited state).

1 | The NOR3- and the NAND3-gates possess no ancillary at all. Thus they are trivially VdW-minimal and unique in that attribute.

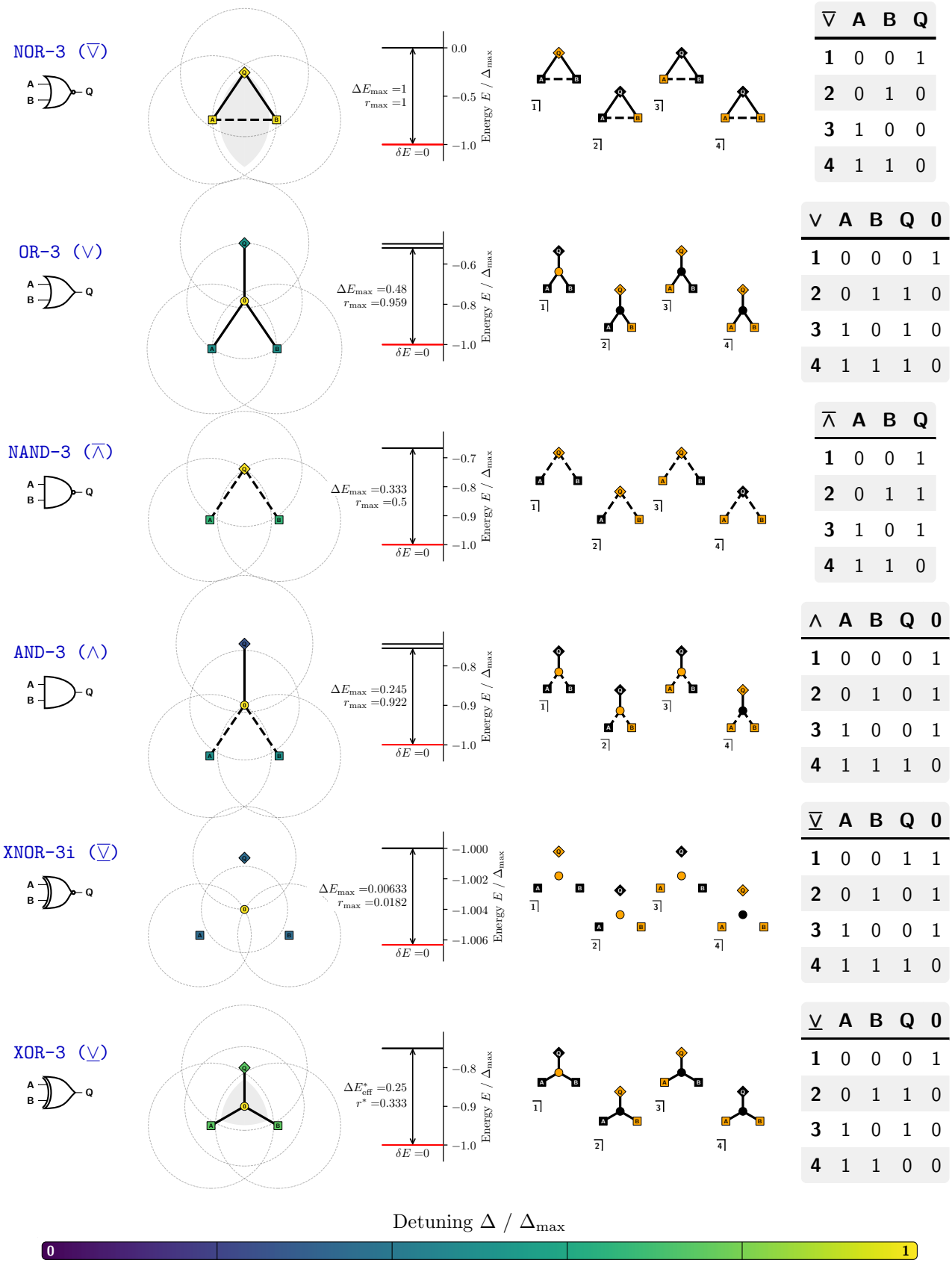

⊽	A	B	Q
1	0	0	1
2	0	1	0
3	1	0	0
4	1	1	0

∨	A	B	Q	0
1	0	0	0	1
2	0	1	1	0
3	1	0	1	0
4	1	1	1	0

⊼	A	B	Q
1	0	0	1
2	0	1	1
3	1	0	1
4	1	1	0

∧	A	B	Q	0
1	0	0	0	1
2	0	1	0	1
3	1	0	0	1
4	1	1	1	0

⊻	A	B	Q	0
1	0	0	1	1
2	0	1	0	1
3	1	0	0	1
4	1	1	1	0

⊻	A	B	Q	0
1	0	0	0	1
2	0	1	1	0
3	1	0	1	0
4	1	1	0	0

Figure 4.9: Family 3 of VdW-minimal logic elementaries optimal in ΔE_{eff}. Each elementary logic gate requires at most one ancillary in the VdW model.

2 | The OR3-, AND3- and XOR3-gate require one ancillary such that $\mathbf{0} \notin L_t$ (which we exlude by remark 4). They are the only possible VdW-minimal realizations of their connective by corollary II: For the OR3- and the XOR3-gate to circumvent that $\boldsymbol{x}_1 \Subset \boldsymbol{x}_2, \boldsymbol{x}_3, \boldsymbol{x}_4$ there must exist an ancillary which is excited in $\boldsymbol{x}_1$ but not excited in $\boldsymbol{x}_2$, $\boldsymbol{x}_3$ and $\boldsymbol{x}_4$. This determines the realizations $w[\texttt{OR3}] = w[\texttt{XOR3}] = \texttt{NOR}$. For the AND3-gate to circumvent that $\boldsymbol{x}_1, \boldsymbol{x}_2, \boldsymbol{x}_3 \Subset \boldsymbol{x}_4$ there must exist an ancillary which is not excited in $\boldsymbol{x}_4$ but which is excited in $\boldsymbol{x}_1$, $\boldsymbol{x}_2$ and $\boldsymbol{x}_3$. This determines $w[\texttt{AND3}] = \texttt{NAND}$.

3 | Similarly, for the XNOR3i-gate to circumvent that $\boldsymbol{x}_1, \boldsymbol{x}_2, \boldsymbol{x}_3 \Subset \boldsymbol{x}_4$ there must exist an ancillary which is not excited in $\boldsymbol{x}_4$ but which is excited in $\boldsymbol{x}_1$, $\boldsymbol{x}_2$ and $\boldsymbol{x}_3$. Thus we can not realize XNOR without ancillaries which makes the XNOR3i-gate is VdW-minimal. The condition fixes the realization $w = \texttt{NAND}$.

Thus the realizations portrayed in fig. 4.9 are VdW-minimal and the list is complete. □

In the proof above we frequently exploited corollary II. We want to illustrate the argument behind corollary II via an example:

Example 8. (Non-adjacent ground States of XNOR)

Consider the language $L[v = \texttt{XNOR}]$ without ancillaries consisting of the four 3-bit words with either one or three excited port bits. Let $\mathsf{i}, \mathsf{j}, \mathfrak{k} \in \mathcal{P}$ denote any pairwise different ports. For $\Delta E > 0$ it must be $E(|1_\mathsf{i}, 1_\mathsf{j}, 1_\mathfrak{k}\rangle) < E(|0_\mathsf{i}, 1_\mathsf{j}, 1_\mathfrak{k}\rangle)$. Thus its is $\Delta_\mathsf{i} > I_{\mathsf{ij}} + I_{\mathsf{i}\mathfrak{k}} > I_{\mathsf{ij}}$. This implies $E(|1_\mathsf{i}, 1_\mathsf{j}, 0_\mathfrak{k}\rangle) < E(|0_\mathsf{i}, 1_\mathsf{j}, 0_\mathfrak{k}\rangle)$ and hence $\Delta E < 0$. Thus we can not realize $f_b = \texttt{XNOR}$ without ancillaries in the VdW model with a positive energy gap.

Binary Gates without Ancillaries. We can also reverse the above reasoning and ask the question which further (symmetric) binary gates without any ancillary are allowed by corollary II in the VdW model. To prevent that $\boldsymbol{x}_1 \Subset \boldsymbol{x}_4$ the output port needs to be excited in $\boldsymbol{x}_1$ but not in $\boldsymbol{x}_4$. If we want to construct a symmetric language in the input ports we only have two choices for Q where it is or is not excited in states $\boldsymbol{x}_2$ and $\boldsymbol{x}_3$. This yields the NOR3- and the NAND3-gate from fig. 4.9. The asymmetric choices would yields the unary negations $\texttt{NOT}_\mathsf{A}$ and $\texttt{NOT}_\mathsf{B}$ of the input ports. Latter languages are factorizable and we are not interested in factorizable languages (by remark 1).

Binary Gates with one Ancillary. The next logical step would be to ask what symmetric binary connectives with one ancillary are allowed by corollary II. There are three effective words in the effective language thus for vectorial v with $m = 2$ there are $2^{2\cdot 3} = 64$ languages. We exclude languages with non-adjacent ground states by corollary II. This reduces the number to only $2 \cdot 10 = 20$ VdW-realizable languages (the factor of two emerges from the relabeling $\mathsf{Q} \leftrightarrows \mathsf{A}$).

1 | We recover six realizations for both Boolean connectives $f_b = \texttt{NOR}, \texttt{NAND}$ with one ancillary: For $f_b = \texttt{NOR}$ there is $w = \texttt{True}, \texttt{False}, \texttt{NAND}, \texttt{NOR}, \texttt{OR}, \texttt{XOR}$ and for $f_b = \texttt{NAND}$ there is $w = \texttt{True}, \texttt{False}, \texttt{NOR}, \texttt{NAND}, \texttt{AND}, \texttt{XNOR}$. These are realizations not interesting as we can implement the connectives NOR and NAND without any ancillary with perfect quality and large energy gap.

2 | There are two realizations for both constant Boolean functions $f_b = \texttt{True}, \texttt{False}$ via $w = \texttt{NOR}, \texttt{NAND}$ which are not interesting.

3 | The four remaining languages of f_b = `OR`, `AND`, `XNOR` and `XOR` are the languages portrayed in fig. 4.9.

In the following we shortly want to summarize the most important findings of this subsection:

1 | The logic gates in the VdW model need at most one ancillary.

2 | The `NOR3`- and the `NAND3`-gate do not require any ancillary. They are the only binary gates which can be realized in the VdW model without ancillaries.

3 | The logic gates portrayed in fig. 4.9 are VdW-minimal, i.e. minimal in their number of atoms.

4 | The list of VdW-minimal logic gates in fig. 4.9 is complete for the logic elementaries. For each logic elementary there exists only one unique VdW-minimal realization which allows for a positive energy gap.

This concludes the discussion of the minimal realizations for the logic elementaries in the VdW model. We want to continue by discussing some important properties of the portrayed gates.

The NOR3-Gate. It is interesting that the `NOR3`- and the `NAND3`-gate do not require any ancillaries at all. In particular in the `NOR3`-gate the effective gap and the robustness both equal their theoretical upper bound derived in the proofs 2 and 1. In that sense the upper bounds introduced for the effective gap and the robustness are *sharp*. The only other gate in this thesis where we maximize the theoretical bound is the somewhat trivial unary `NOT1`-gate. In that sense the `NOR3`-gate is the most natural binary logic gate on the Rydberg platform in the VdW model. This result parallels the finding of Stastny *et al.* for the PXP model.

The possibility of the `NOR3`-gate in the VdW model with only three atoms was already mentioned by Stastny *et al.* in [38] and independently found here. In contrast to what Stastny *et al.* noted such a `NOR3`-gate does *not* require an arrangement "in a triangle with precisely defined shape". When fixing the positions of the input ports A and B the `NOR3`-gate possesses a finite-size volume in which we may position the output port Q. The volume is the intersection of the two d-balls enclosed by the $d-1$-spheres of radii $(C/2\Delta_{\mathfrak{i}})^{1/6}$ around the input ports $\mathfrak{i} \in \mathcal{K}$. Inside this volume the interaction between the input and output port is sufficiently strong such that the excited states $(0_\mathsf{A}, 1_\mathsf{B}, 1_\mathsf{0})$, $(1_\mathsf{A}, 0_\mathsf{B}, 1_\mathsf{0}) \in \mathcal{E}$ are energetically larger-equal than the excited state $\mathbf{0} \in \mathcal{E}$ (which upper bounds the energy gap). The surface of the volume is the subspace where the energy of one of these excited states becomes zero. In the shell between the $d-1$-spheres and the blockade radii ΔE_{eff} and r remain positive but they are smaller than one. In fig. 4.9 for $d = 2$ the volume is the 'lens' shaded in gray.
In particular the `NOR3`-gate can be realized by a one-dimensional geometry and the output port does not even need to be centered between the input ports. For fig. 4.9 we chose a realization with maximal distance between the output port and the input ports because this geometry minimizes residual interactions when amalgamating further gates (e.g. `LNK`-gates).

We require equal detunings $\Delta_{\mathfrak{i}}$ in all three atoms $\mathfrak{i} \in \mathcal{N}$ such that the first three states are degenerate. The only constraint for the geometry of the `NOR3`-gate is the distance $r_{AB} \overset{!}{=} r_{B,\mathfrak{i}}$ between the two input ports $\mathfrak{i} \in \mathcal{K}$. This secures that it is energetically indifferent to excite the second input port if the first input port is already excited adjusting that the fourth ground state

to the same energy. In other words: the input ports must be just barely (not) in blockade. In fig. 4.9 this is visualized by a dashed line.

The intermediate-energy regime is lost in the simplified PXP approximation thus the NOR3-gate is not possible in the PXP model. In general the PXP model forbids ground states which are substates of other ground states as each ground state must be a MWIS (and thus in particular as MIS). This directly forbids binary, scalar logic gates without ancillaries in the PXP model. Here, the PXP model is more restrictive.

The NAND3-Gate. The NAND3-gate is also based on the intermediate-energy regime, now between the input ports $\mathsf{i} \in \mathcal{K}$ and the output port Q: $r_{\mathsf{iQ}} \overset{!}{=} r_{B,\mathsf{i}}$. This secures that it is energetically indifferent to excite one input port when only the output port is excited such that the first three states are degenerate. To achieve degeneracy with the fourth ground state we need to choose $\Delta_{\mathsf{Q}} = \Delta_{\mathsf{A}} + \Delta_{\mathsf{B}} - I_{\mathsf{AB}}$. Here, the NAND3-gate differs from the NOR3-gate by exploiting the long-range interactions: The input ports need to be sufficiently distant such that it is energetically disfavourable to excite only one input port, but they need to be sufficiently close such that if both input ports are excited it is energetically disfavourable to excite the output port. The optimal realization is somewhere in-between and needs to be fine-tuned to maximize ΔE_{eff} and r. It is defined by requiring the LESs $(1_{\mathsf{A}}, 0_{\mathsf{B}}, 0_{\mathsf{Q}})$, $(0_{\mathsf{A}}, 1_{\mathsf{B}}, 0_{\mathsf{Q}})$ and $(1_{\mathsf{A}}, 1_{\mathsf{B}}, 1_{\mathsf{Q}})$ to be of equal energy. This implies equal detunings $\Delta_{\mathsf{A}} = \Delta_{\mathsf{B}}$ of the input ports and determines the optimal angle $\alpha = \angle(\mathsf{A}, \mathsf{Q}, \mathsf{B})$ between the input ports by $I_{\mathsf{AB}} = \Delta_{\mathsf{Q}} - \Delta_{\mathsf{A}}$. This yields the NAND3-gate of fig. 4.9. We check numerically that ΔE_{eff} and r are truly optimal for NAND3.

The effective gap and the robustness of the NAND3-gate are smaller than of the NOR3-gate (smaller than one). This is a direct consequence of exploiting 'long-range' interaction energies which are smaller than the detunings. Nevertheless, the effective gap $\Delta E_{\text{eff}} = 33.3\%$ is still of order one and comparable with the effective gaps of the NAND1a,b- and NAND2-gates. The robustness is less useful to compare as NAND1 and NAND2 possess four more ancillaries than NAND3 and thus naturally a larger range in the detunings which increases the robustness.

The OR3- and the AND3-Gate. We continue with some remarks to the remaining gates in fig. 4.9. First we note that the OR3- and the AND3-gate emerge by simply amalgamating a NOT1-gate to the NOR3- and NAND3-gate respectively. In the OR3-gate there is no dashed blockade anymore: $r_{\mathsf{AB}} > r_{\mathsf{B},\mathsf{i}}$ is now slightly larger than blockade radius of input port $\mathsf{i} \in \mathcal{K}$ because the amalgamated atom Q introduces additional interactions which need to be included in the detuning $\Delta_{\mathsf{i}} = I_{\mathsf{AB}} + I_{\mathsf{iQ}} > I_{\mathsf{AB}}$.

The XOR3- and the XNOR3-Gate. The languages $L_{\texttt{XOR3}}$ and $L_{\texttt{XNOR3}}$ are inverses of each other (up to permutations of words). They are realized via $w = \texttt{NOR}$ and $w = \texttt{NAND}$ respectively. They are highly symmetric via $\Sigma_{\mathcal{N}}[\texttt{XOR3}] = \Sigma_{\mathcal{N}}[\texttt{XNOR3}] = \langle(\mathsf{A}\,\mathsf{B}),\ (\mathsf{A}\,\mathsf{B}\,\mathsf{Q})\rangle$. Correspondingly we find that the optimal implementations of both languages are D_3-symmetric.

The XOR3-gate is based on the long-range interactions between the ports: The interactions between the ports should be sufficiently small such that they are not in blockade with each other but the ports need to interact sufficiently strong such that it is energetically disfavourable to excite all of them simultaneously. The LESs are the words $(1_{\mathsf{A}}, 0_{\mathsf{B}}, 0_{\mathsf{Q}}, 0_0)$, $(1_{\mathsf{A}}, 1_{\mathsf{B}}, 1_{\mathsf{Q}}, 0_0)$ and the cyclic permutations under $\Sigma_{\mathcal{N}}[\texttt{XOR3}]$ where only one or all three ports are excited.

In the XNOR3i-gate we exploit the long-range interactions between the ports and the ancillary. The complex needs to be sufficiently large such that it is energetically favorable to excite all three ports at once. However in such such a large complex the residual VdW interactions between the

ports are suppressed with the sixth power of their distance. This is the reason for the extremely small effective gap of the XNOR3i-gate. The XNOR3i-gate is realized via $w = \texttt{NAND}$ which is less natural to implement on the Rydberg platform than $w[\texttt{XOR3}] = \texttt{NOR}$. Again, the optimal size of the complex is determined by its lowest excited states: the interaction of the ancillary with a port should be small enough such that they are not in blockade but large enough such that it is energetically disfavourable to excite a second port simultaneously. In the optimum the LESs of XNOR3i are the states $(0_\texttt{A}, 1_\texttt{B}, 1_\texttt{Q}, 1_0)$, $(0_\texttt{A}, 0_\texttt{B}, 0_\texttt{Q}, 1_0)$ and the cyclic permutations under $\Sigma_\mathcal{N}[\texttt{XNOR3}]$ where only one or all three ports are *not* excited (the LESs of the XOR3-gate inverted).

Note that the XNOR3i-gate is essentially constructed from the XNOR2-gate by unifying the three ancillaries into one ancillary. The ancillary in XNOR3 is excited in the states where any of the three ancillaries was excited for realization XNOR2. In the PXP model the three ancillaries were necessary to block the two other ports from being excited while not blocking one ancillary. In the VdW model the blockade is achieved via the long-range interactions.

Similarly, the XOR3-gate is constructed from the XOR2a- and the XOR2b-gate essentially by removing the three ancillaries 1, 2 and 3. In the PXP model these ancillaries were necessary to block the third port from excitation, in the VdW model this is achieved via the long-range interactions. Thus in the VdW model we only need one ancillary which is excited iff no port is excited.

4.3 | Non-minimal VdW-Elementaries

The previous chapter portrayed the VdW-minimal realizations for the (inverted) crossings 4.8 and the elementary logical connectives 4.9. We were able to achieve perfect quality for almost[2] all gates and drastically reduce the number of ancillaries. For most elementary logic gates the optimized effective gap of the VdW-minimal gate is of similar magnitude as for the PXP-minimal gates in fig. 4.5 and 4.6 and sometimes even larger. However for the XNOR3i-gate and the (inverted crossings) the optimal effective gaps turned out very small (about two orders of magnitude smaller than for the PXP-minimal realizations) as these gate are based on the long-range interaction between distant atoms. As proven above, the portrayed realizations are the only VdW-minimal realizations. Therefore for an experimentalist implementing a logic circuit on the Rydberg platform it might be useful to consider other non-minimal realizations as a building blocks to achieve a larger effective gap. In the following we are going to focus on $f_b = \texttt{XNOR}$. The non-minimal NOT- and LNK-gates (which are essential to amalgamate logic circuits) are discussed in app. 6.A.1.

4.3.1 | The XNOR4-Gate

As a reasonable ansatz we restrict ourselves to languages symmetric in the input ports as this reduces the number of effective ground states to only three. Constraining we permutation sym-

[2] Except for the CRS2a-gate which had $1 \approx \mathcal{Q} \gg 0$.

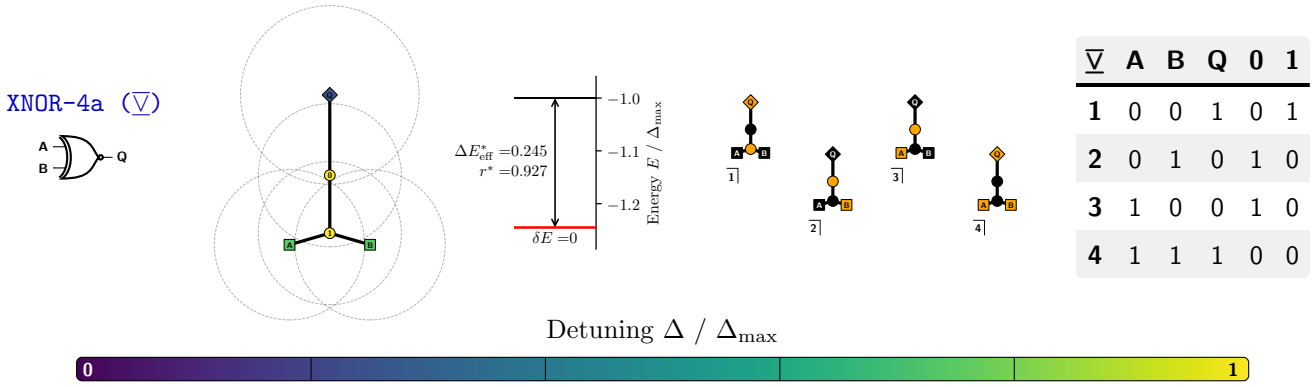

▽	A	B	Q	0	1
1	0	0	1	0	1
2	0	1	0	1	0
3	1	0	0	1	0
4	1	1	1	0	0

Figure 4.10: XNOR4a-gate optimal in ΔE_{eff} and r. This realization is based on two ancillaries which makes it non-minimal. The VdW-minimal XNOR3-gate in fig. 4.9 requires one ancillary less but possesses possesses a 40 times smaller effective gap. The PXP-minimal XNOR2-gate in fig. 4.6 requires one more ancillary and possesses a similar effective gap. Realization 4a is just one seven possible realizations with two ancillaries which are noted in the app. 4.A.

metry between all ports would be too strict of a constraint. Then the realization must be a symmetric (vectorial) BOOLEAN function with $w(0,1) \equiv w(1,0)$. The unique VdW-minimal realization XNOR3 possesses one ancillary and the PXP-minimal realization possesses three ancillaries. Thus we want to determine the realizations of XNOR with two ancillaries which can be implemented in the VdW model with a large effective energy gap. We are not interested in realizations which differ only by a relabeling/ permutation of the two ancillaries as they correspond to the same *physical* L-complex. Up to a permutation of the ancillaries at most *seven* realizations qualify for an implementation in the VdW model. The proof of this statement is in app. 4.A.

Arguably the most promising realization is $w_{\texttt{XOR4a}} = (w_{\texttt{XOR3}}, \overline{w_{\texttt{XOR3}}})$ which is constructed by the γ-product $L_{\texttt{XOR3}} \otimes_\gamma L_{\texttt{NOT1}}$. We present the XNOR4a-gate in fig. 4.10. The XNOR4a-gate corresponds simply to the XOR3-gate with a NOT1-gate amalgamated to the output port. Therefore its effective energy gap is of the same order of magnitude as for the XOR3-gate. The robustness is significantly larger as the amalgamated new output port possesses a small detuning which artificially increases the robustness.

The remaining six realizations are denoted by 4b – 4g. Surprisingly, we are able to find implementations on the two-dimensional Rydberg platform with unit quality for each of these realizations. They are discussed in app. 4.A. They do not profit from the additional ancillary. They possess essentially the same structure as the XNOR3i-gate with some additionally ancillary 'glued' somewhere. This ancillary is not used to mediate information between other atoms. Instead it somewhat separately realizes an additional gate. Without this ancillaries we would simply recover the XNOR3i-gate. Therefore the effective gap of these gates is of similar magnitude as the effective gap of XNOR-3i. These realizations are not useful to construct a XNOR-gate with a larger effective gap.
Nevertheless, these gates are conceptually interesting as they shows that we can implement multiple logic gates with the same two input ports without using additional CPY-gates. This is very efficient in the number of atoms.

| Appendix

4.A | The VdW-specific XNOR-Gates with two Ancillaries

In subsec. 4.3.1 we introduced the `XNOR4a`-gate as an alternative to the VdW-minimal `XNOR3`-gate from fig. 4.9 and the PXP-minimal `XNOR2`-gate from fig. 4.6. The idea is to construct a `XNOR`-gate in the VdW-model with similarly good effective gap as the `XNOR2`-gate but only two ancillaries. In this section we want rigorously categorize the possible `XNOR`-gates with two ancillaries to complete the list and exclude further candidates. As mentioned in subsec. 4.3.1 there exist *seven* viable realization for the `XNOR`-gate with two ancillaries in the VdW model:

Proof 6. (Completeness of `XNOR4`)

We consider the case of two ancillaries for which there are in total there exist $2^{2\cdot 3} = 64$ symmetric realizations. In the following we are interested only in the realizations modulo permutation of the two ancillaries. The proof is again based on corollary II. In a nutshell corollary II forbids ground states which are non-adjacent substates (with an intermediate excited state).

To circumvent that $\boldsymbol{x}_1, \boldsymbol{x}_2, \boldsymbol{x}_3 \Subset \boldsymbol{x}_4$ there must exist an ancillary which is not excited in $\boldsymbol{x}_4$ but which is excited in $\boldsymbol{x}_1$, $\boldsymbol{x}_2$ and $\boldsymbol{x}_3$. This forbids in particular $w(\boldsymbol{x}_4) = (1,1)$. Thus *w.l.o.g.* we can restrict ourselves to $w(\boldsymbol{x}_4) = (0,0)$ and $w(\boldsymbol{x}_4) = (1,0)$. If $w(\boldsymbol{x}_4) = (0,0)$ we can choose $w(\boldsymbol{x}_1), w(\boldsymbol{x}_2) \in \{(1,0),(0,1),(1,1)\}$. If $w(\boldsymbol{x}_4) = (1,0)$ we can choose $w(\boldsymbol{x}_1), w(\boldsymbol{x}_2) \in \{(0,1),(1,1)\}$ independently. We exclude the realizations $w = (\texttt{NAND}, \texttt{False})$ and $w = (\texttt{NAND}, \texttt{True})$ and it permutations where one ancillary is constant. This is legitimated by 2 and 5 respectively. This yields (modulo permutation of the ancillaries) exactly the seven realizations from fig. 4.10, fig. 4.11 and fig. 4.12. □

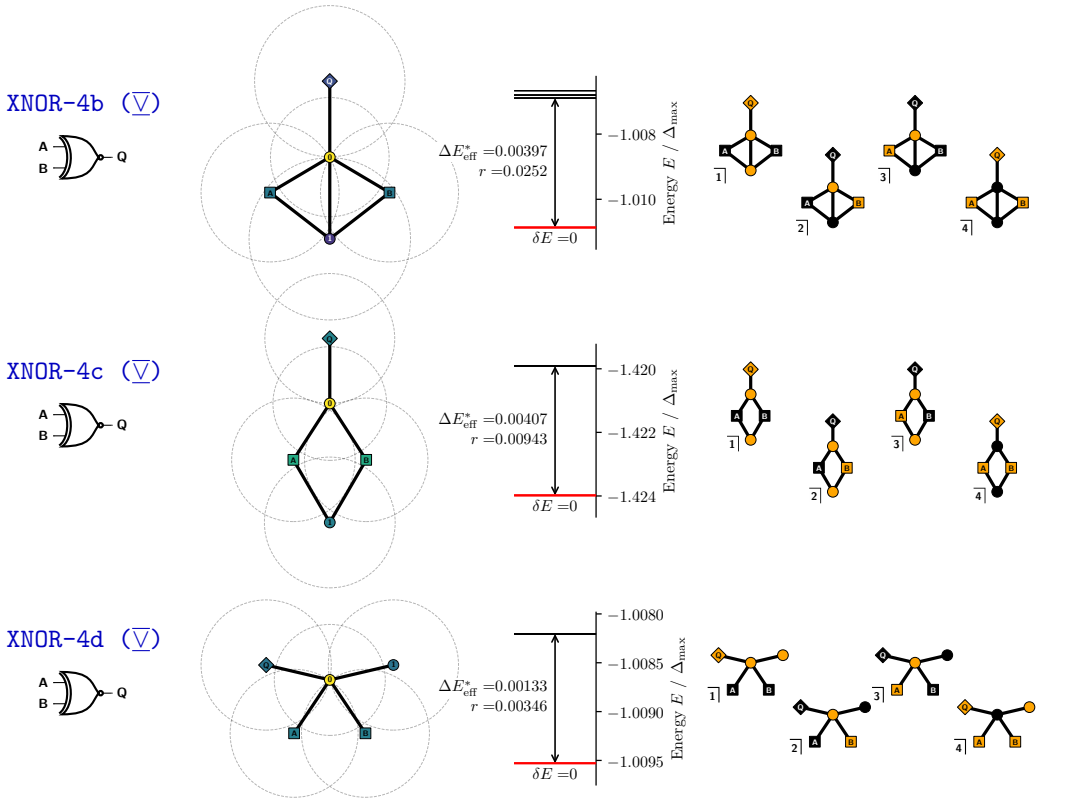

▽	A	B	Q	0	1
1	0	0	1	1	1
2	0	1	0	1	0
3	1	0	0	1	0
4	1	1	1	0	0

▽	A	B	Q	0	1
1	0	0	1	1	1
2	0	1	0	1	1
3	1	0	0	1	1
4	1	1	1	0	0

▽	A	B	Q	0	1
1	0	0	1	1	1
2	0	1	0	1	0
3	1	0	0	1	0
4	1	1	1	0	1

Figure 4.11: The non-minimal realizations XNOR-4b – 4d optimal in ΔE_{eff}. These realizations use two ancillaries, i.e. more than the VdW-minimal XNOR3i-gate in fig. 4.9 but less than the PXP-minimal XNOR2-gate in fig. 4.6. Realization XNOR4a possesses a larger effective gap and is portrayed in chap. 4.3 in fig. 4.10.

The seven realizations we derived above are $w = (\texttt{NOR}, \texttt{XOR})$ and $w = (\texttt{NAND}, \texttt{NOR})$, (NAND, NAND), (NAND, XNOR), (NAND, OR), (NAND, AND), (NAND, XOR). We denote these realizations by 4a – 4g respectively.

Note that $w_{\texttt{XOR3}} = \texttt{NOR}$ and $w_{\texttt{XNOR3}} = \texttt{NAND}$. Thus the first realization is $w_{\texttt{XOR4a}} = (w_{\texttt{XOR3}}, \overline{w_{\texttt{XOR3}}})$ which is studied in subsec. 4.3.1. Its language $L_{\texttt{XOR4a}}$ simply corresponds to the γ-product $L_{\texttt{XOR3}} \otimes_\gamma L_{\texttt{NOT1}}$ where γ includes the output bit of $L_{\texttt{XOR3}}$ and the input bit of $L_{\texttt{NOT1}}$ as a tuple. The XOR4a-gate is portrayed in fig. 4.10.

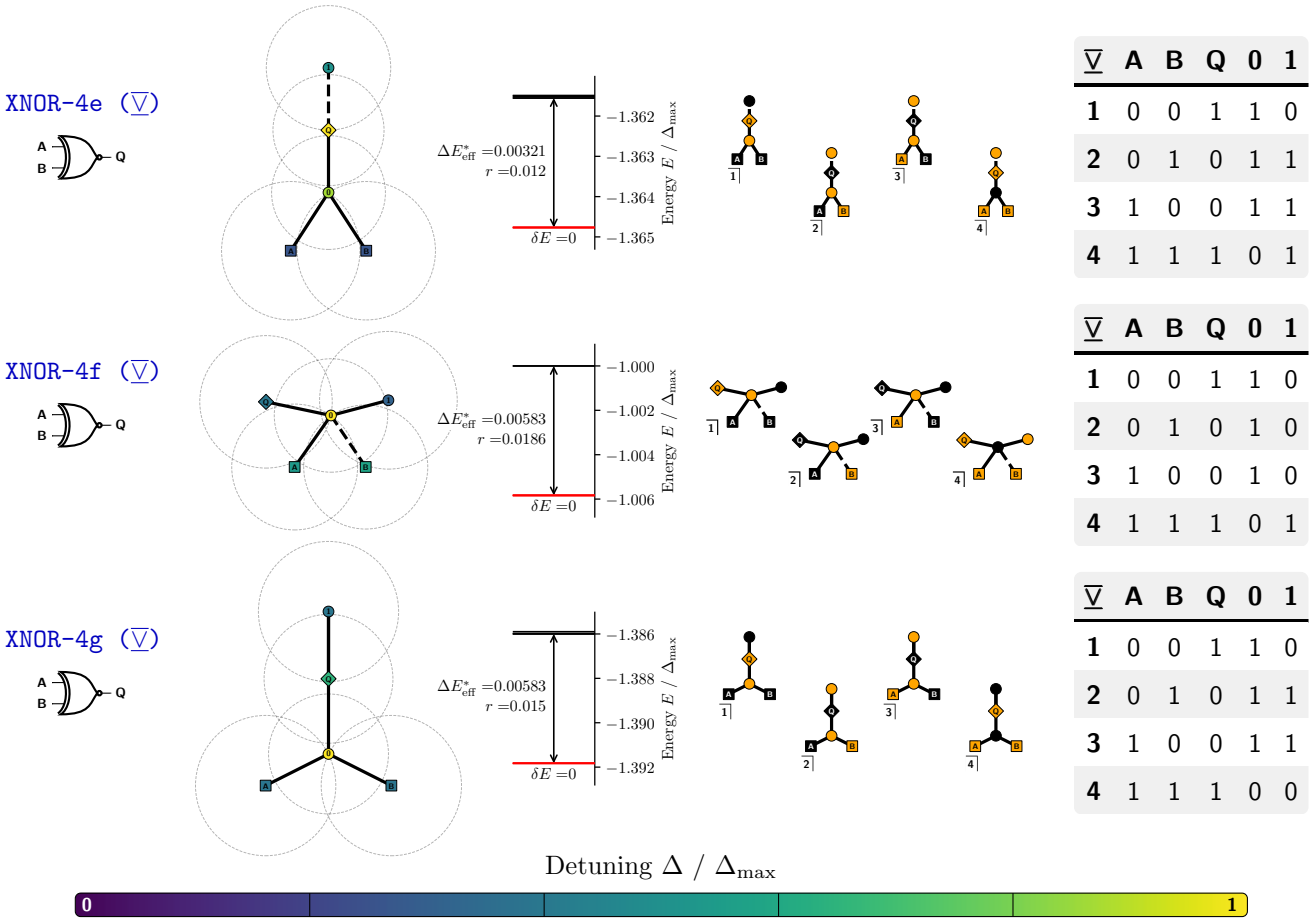

▽	A	B	Q	0	1
1	0	0	1	1	0
2	0	1	0	1	1
3	1	0	0	1	1
4	1	1	1	0	1

▽	A	B	Q	0	1
1	0	0	1	1	0
2	0	1	0	1	0
3	1	0	0	1	0
4	1	1	1	0	1

▽	A	B	Q	0	1
1	0	0	1	1	0
2	0	1	0	1	1
3	1	0	0	1	1
4	1	1	1	0	0

Figure 4.12: The non-minimal realizations `XNOR-4d` – `4g` optimal in ΔE_{eff}. These realizations use two ancillaries, i.e. more than the VdW-minimal `XNOR3i`-gate in fig. 4.9 but less than the PXP-minimal `XNOR2`-gate in fig. 4.6. Realization `XNOR4a` possesses a larger effective gap and is portrayed in chap. 4.3 in fig. 4.10.

The remaining six realizations are essentially $(w_{\texttt{XNOR3}}, f_b)$ where f_b is any of the six non-constant[3], symmetric, binary logical connectives. We are able to find implementations on the two-dimensional Rydberg platform with unit quality for each of these realizations. These gates are presented in fig. 4.11 and 4.12. They are optimized for the effective gap however their effective gap are only of the same order of magnitude as for the `XNOR3i`-gate. They essentially correspond to `XNOR3i`-gate with some ancillary 'glued' somewhere. This is discussed in the main text 4.3.1.

[3] i.e. neither `True` nor `False`

5 | Elementaries of tessellated Languages

"I call our world Flatland, not because we call it so, but to make its nature clearer to you, my happy readers, who are privileged to live in Space."

– Edwin A. Abbott, 'Flatland', Chap. 1, Line 1 (1884)

So far we only considered Boolean languages of the form $L[f_b; w]$. As discussed in sec. 2.2 this is only one of the two interesting classes of languages which we want to study in this thesis. In the following chapter we focus on tessellated languages of the form $L_{\mathcal{L}}[f_c; w]$ defined in eq. 2.4. Here $\mathcal{L}$ is a lattice, f_c is the local check function and w is the realization. The goal is the implementation of tessellated target Hilbert spaces of systems characterized by local gauge constraints on the Rydberg platform. We focus exemplary on two important models which were already studied by Stastny *et al.* in their paper [38] for the PXP model: The *surface code* `SC` and the *Fibonacci model* `FM`.

In this chapter we first introduce the two models and discuss the local mapping on the Rydberg platform. Then we focus on the implementation of their elementary building blocks in the VdW model. We apply the theory introduced in chap. 3 to construct the optimal structures of the elementaries. As results we present the PXP-minimal realizations and the VdW-minimal realizations for both systems. We are going to find that the VdW model allows for more efficient realizations of the elementaries.

The theory for tessellated system is not studied in this chapter but in the next chap. 6. The elementaries on the $d = 3$-dimensional Rydberg platform are studied in chap. 8.

5.1 | Surface Code

We are going to start by introducing the surface code SC. The surface code describes a gapped phase with $\mathbb{Z}_2$ topological order by the mechanism of string-net condensation[26]. Its local excitations are Abelian anyons[20] which lead to ground-state degeneracies on topologically nontrivial surfaces. The prime example of a spin-liquid with long-range entangled ground states is the *toric code* on the two-dimensional plane with periodic boundary conditions[6, 14]. Surface codes present a promising candidate for fault-tolerant quantum computation[19] by storing local qubits in topological delocalized DOFs[9]. Thus the implementation of the surface code is interesting not only from an academic but also from an applied perspective[35, 2].

In the following subsec. 5.1.1 we recapitulate the main concepts of the surface code and discuss viable mappings to the Rydberg platform. The reader only interested in the results may skip to the subsequent subsections 5.1.2, 5.1.3 and 5.1.4 where we discuss the implementations of the surface code elementaries in the VdW model.

5.1.1 | General Theory

In the following we start by briefly recalling the definition and the properties of the surface code. We introduce the Hamiltonian and derive the ground state. In the the subsequent paragraph we discuss the implementation of the Hamiltonian on the Rydberg platform. We find two different local mappings for the surface code.

Summary of the Surface Code. We consider the surface code on a finite square lattice $\mathcal{L}$ with either *open boundary conditions (OBCs)* or *periodic boundary conditions (PBCs)*. On each edge $e \in \mathcal{E}(\mathcal{L})$ we place $K = 1$ qubits. We denote the set of *plaquettes* of the lattice as $\mathcal{P}(\mathcal{L})$. To each vertex $v \in \mathcal{V}(\mathcal{L})$ and each plaquette $p \in \mathcal{P}(\mathcal{L})$ we assign a *stabilizer operator*

$$A_v = \prod_{e \in \mathrm{star}(v)} \sigma_e^{(z)} \qquad \text{and} \qquad B_p = \prod_{e \in \mathrm{bound}(p)} \sigma_e^{(x)}. \tag{5.1}$$

The stabilizer operator are called *star and plaquette operators* respectively. Here $\mathrm{star}(v) \subseteq \mathcal{E}(\mathcal{L})$ denotes the set of edges emanating from v and $\mathrm{bound}(p) \subseteq \mathcal{E}(\mathcal{L})$ denotes the set of edges bounding p. $\sigma_e^{(\alpha)}$ for $\alpha \in \{x, y, z\}$ denotes the PAULI matrix acting on the qubit placed on edge e. With the stabilizer operators we can write down the Hamiltonian

$$H_{\mathrm{SC}} = -J_B \sum_{v \in \mathcal{V}(\mathcal{L})} A_v - J_B \sum_{p \in \mathcal{P}(\mathcal{L})} B_p \tag{5.2}$$

which operates on the qubits of the edges $e \in \mathcal{E}(\mathcal{L})$.

As the stabilizer operators overlap on an even number of edges they commute: $[A_v, B_p] = 0$. Assuming $J_A, J_B > 0$, the ground state $|G\rangle$ of the Hamiltonian 5.2 is characterized by $A_v|G\rangle =$

$|G\rangle = B_p|G\rangle$ for all $v \in \mathcal{V}(\mathcal{L})$ and $p \in \mathcal{P}(\mathcal{L})$. To construct an invariant eigenvector of A_v for all $v \in \mathcal{V}(\mathcal{L})$ one can choose the product state $|\mathbf{0}\rangle$ characterized by $\sigma_e^{(z)}|\mathbf{0}\rangle = |\mathbf{0}\rangle$ for all edges $e \in \mathcal{E}(\mathcal{L})$. This state however is no invariant eigenvector of B_p. Thus we construct the superposition

$$|G\rangle \propto \sum_{C_B \in B} C_B|\mathbf{0}\rangle \tag{5.3}$$

by summing the full (multiplicative) group $B := \mathrm{span}\left(\{B_p \mid p \in \mathcal{P}(\mathcal{L})\}\right)$ generated by the plaquette operators B_p. This is an invariant eigenvector of B_p by construction as the sum of the group elements is invariant under the application of B_p. This construction is useful because the commutativity of A_v and B_p secures that the superposition (5.3) remains an invariant eigenvector of A_v. Thus $|G\rangle$ is a ground state of the Hamiltonian. Assuming OBCs there is no ground-state degeneracy and $|G\rangle$ is (up to normalization) the unique ground state.

The states $|C_B\rangle := C_B|\mathbf{0}\rangle$ correspond to the product states with closed loops of flipped qubits on the lattice[1]. The state $|\mathbb{1}\rangle = |\mathbf{0}\rangle$ without any flipped qubits is interpreted as the loop-free state. Each C_B imprints its closed loops on $|\mathbf{0}\rangle$. The qubits are flipped on edges $e \in \mathrm{bound}(p)$ bounding the plaquettes p where the plaquette operators B_p act. Thus $|G\rangle$ is the equal-weight superposition of all closed-loop configurations on the square lattice which makes it a string-net condensate[26] with long-range entanglement.

Implementation of the Hamiltonian. The goal is to prepare the ground state $|G\rangle$ in a physical system. Straightforwardly, one could try to implement the Hamiltonian (5.2) in a physical system and cool the system to its ground state. However the four-body interaction between the qubits of adjacent edges is notoriously hard to realize. On the Rydberg platform an alternative and more promising approach is introduced in Ref. [38]. This approach is summarized in the following.

The idea is to prepare the invariant eigenspace of the star operators

$$\mathcal{H}_0[H;\mathcal{C}_{\mathrm{loop}}] \overset{!}{\cong}_{\mathrm{loc}} \mathcal{H}_{\mathrm{loop}} := \bigcap_{v\in\mathcal{V}(\mathcal{L})} \mathrm{Eig}(A_v, 1) = \mathrm{span}\left(\{|C_B\rangle \mid C_B \in B\}\right) \tag{5.4}$$

by locally mapping it one-to-one to the low-energy manifold of a Rydberg structure $\mathcal{C}_{\mathrm{loop}}$ of atoms (cf. eq. (2.9)). The eigenspace of the star operators is spanned by the states with an even number of flipped qubits for each vertex, i.e. the states of all closed-loop configurations on the square lattice. For the surface code $\mathcal{H}_0[H;\mathcal{C}_{\mathrm{loop}}]$ is a Hilbert space of dimension $\dim \mathcal{H}_{\mathrm{loop}} \sim 2^{V}$[2] (up to boundary effects) which can not be decomposed into factors of local Hilbert spaces. $\mathcal{H}_{\mathrm{loop}}$ is the Hilbert space of a $\mathbb{Z}_2$ lattice gauge theory on a charge-free (i.e. divergence-free) background[21]. This is the ground state manifold of Hamiltonian H_{SC} from eq. (5.2) for $J_A > 0$ and $J_B = 0$. For $J_B > 0$, the B_p-terms introduces quantum fluctuations on $\mathcal{H}_{\mathrm{loop}}$ which gaps-out the string-net condensate $|G\rangle$ as the (unique) ground state. On the Rydberg platform quantum fluctuations are introduced perturbatively by ramping up the Rabi frequencies Ω_{i} of the atoms in Hamiltonian (2.1). This motivates the construction of the structure $\mathcal{C}_{\mathrm{loop}}$.

[1] We consider loops terminating at dangling edges at an open boundary as closed.
[2] Recall that $V = |\mathcal{V}(\mathcal{L})|$.

Introduction of Edge Levels. Before we can start with the construction of the Rydberg structure $\mathcal{C}_{\text{loop}}$ we first need to specify the *local mapping* denoted by the isomorphism $\cong_{\text{loc}}$. We want to map the closed-loop Hilbert space $\mathcal{H}_{\text{loop}}$ locally, one-to-one to the derived L-manifold $\mathcal{H}(L_{\mathcal{L}}[f_c])$ of a tessellated language $L_{\mathcal{L}}[f_c]$ with check function f_c to define our target Hilbert space:

$$\mathcal{H}_0[H;\mathcal{C}_{\text{loop}}] \overset{!}{\cong}_{\mathfrak{L}} \mathcal{H}_t = \mathcal{H}(L_{\mathcal{L}}[f_c]) \cong_{\text{loc}} \mathcal{H}_{\text{loop}}. \tag{5.5}$$

Here the lattice of the language is the same lattice $\mathcal{L}$ as for the surface code. The construction for the first isomorphism is studied in the next three subsections 5.1.2, 5.1.3 and 5.1.4. The local mapping $\cong_{\text{loc}}$ will in general be not unique. This allows for the definition of multiple equally valid target functions which represent the same physical closed-loop Hilbert space.

This parallels the concept of logic levels in logic circuits: In binary logic the two levels are logical high and logical low. On the Rydberg platform we want to represent the logical levels via the states of the Rydberg ports. This leaves for binary logic circuits two definitions of the *active state*: *active high* (positive logic) associates the excited Rydberg state with the logical high and analogously *active low* (negative logic) associates the electronic ground state with the logical high. For the logic gates above we (arbitrarily but intuitively) chose the active high representation[3] of the logic. We could have similarly chosen the active low representation which would have shuffled the logic gates. When implementing a logic circuit it might be useful to choose a suitable active level or to mix active levels in a circuit. The appropriate choice might simplify the logic design (following the De Morgan laws) and the appropriate gates might be more natural to implement in the blockade formalism of the Rydberg platform.

Similarly, in loop models such as the surface code with $\mathbb{Z}_2$ DOFs we identify two *edge levels*: *edge high* is called an excited edge and *edge low* is called an edge which is not excited. Consider a loop model where each vertex possesses p adjacent edges and $g \leq 2^p$ valid edge states. Then we can choose either the edge high or the edge low representation for each edge. This leaves in total 2^p possible representations for the edges. They define a equivalence class $[f_c]$ of 2^p equally valid check functions $f_c : \mathbb{F}_2^p \to \mathbb{F}_2$.
For the surface code on a square lattice there are $p = 4$ edges adjacent to each vertex and $g = 8$ edge states where an even number of edges is excited. Thus we search for uniform languages of length $g = 8$ to represent the surface code states, i.e. check functions $f_c : \mathbb{F}_2^4 \to \mathbb{F}_2$ with Hamming weight[4] $w_H[f_c] = g = 8$. There are in total $\binom{2^4}{8} = 12.870$ such check functions of which only $2^4 = 16$ define valid candidates for the surface code. As in the surface code the valid vertex states are permutation symmetric in the edges this boils down to only 6 check functions (up to rotations). The eigenspace $\mathcal{H}_{\text{loop}}$ is highly symmetry as it contains all states with an *even* number of excited edges for each vertex. If we choose for all edges the *edge high representation* this projects the states to check function

$$f_c[\texttt{SC-I}] : \boldsymbol{x} \mapsto \overline{\bigvee}_{i=1}^{4} x_i \equiv 1 - \bigvee_{i=1}^{4} x_i \tag{5.6}$$

which is one iff the number of excited port bits is *even*. Thus any *even* number of additional bit flips maps to the same check function. Here $\overline{\vee}$ is the logical `XNOR` and $\vee$ is the logical `XOR` as

[3] The label representation is commonly used for *logic levels* and we expand this notion to the *edge levels*. In this thesis we use the label *representation* for the local mapping between the physical setup and the target function f_t, while the label *realization* is reserved for the function w defining the ancillary bits. The label *implementation* is reserved for the Rydberg complex $\mathcal{C}_{\mathcal{K}}^{\mathcal{Q}}$ which implements the derived L-manifold of a language as its low-energy eigenspace via the labeling $\mathfrak{L}$. Thus the representation determines the states of the port bits while the realization determines the states of the ancillary bits.

[4] The Hamming weight of a Boolean function is the magnitude of its support.

defined[5] in chap. 4. Note that this is the representation of the surface code with was discussed in by Stastny *et al.* in Ref. [38] for the PXP model. In contrast any *odd* number of bit flips maps to the check function

$$f_c[\texttt{SC-II}] \,:\, \boldsymbol{x} \mapsto \bigvee_{i=1}^{4} x_i \equiv 1 - \overline{\bigvee}_{i=1}^{4} x_i \tag{5.7}$$

which is one iff the number of excited port bits is *odd*. Thus in the end there are essentially only two check functions representing the surface code. Here and in the following we label representations by roman numeral $\texttt{I}, \texttt{II}, \ldots$.

Interpretation of the Check Functions. We find that $f_c[\texttt{SC-I}]$ can be interpreted as a 4-ary generalization of XNOR ($\overline{\vee}$) while $f_c[\texttt{SC-II}]$ can be interpreted as a 4-ary generalization of XOR ($\vee$). As we want to restrict ourselves to the support of the check function this yields the constraint $f_c[\texttt{SC}](\boldsymbol{x}) = 1$ for both representations.

As a naive ansatz one could treat $f_b = f_c[\texttt{SC-I}]$ as a Boolean function to define a Boolean language $L[f_b] = L_{\texttt{XNOR}}^{\otimes_\gamma 3}$ as the γ-product of three XNOR-languages. We can construct the L-complex by amalgamating the three corresponding XNOR-gates while adding LNK-gates in-between to connect the ports. As gates we could utilize the elementaries portrayed in chap. 4. Finally, to enforce $f_c[\texttt{SC-I}](\boldsymbol{x}) = 1$ we increase the detuning of the final output port. This yields a valid implementation $\mathcal{C}_{\texttt{SCU-I}}$ of a surface code unit-cell in representation I. This construction can be done similarly for representation II using XOR-gates. However such realizations would be highly non-minimal and require an enormous amount of ancillaries.

Instead we can use that the logical connectives XNOR and XOR are invertible. This allows us to rewrite the constraint $f_c[\texttt{SC}](\boldsymbol{x}) = 1$ as

$$\text{(I)} \quad x_4 = \bigvee_{i=1}^{3} x_i \equiv \overline{\bigvee}_{i=1}^{3} x_i \qquad \text{and} \qquad \text{(II)} \quad x_4 = 1 - \bigvee_{i=1}^{3} x_i = 1 - \overline{\bigvee}_{i=1}^{3} x_i \tag{5.8}$$

for representation I and representation II respectively. This suggests the interpretation of any bit as a ternary Boolean function of the three remaining bits. Similarly, we can rewrite the constraint as

$$\text{(I)} \qquad x_1 \vee x_2 = x_3 \vee x_4 \qquad \Leftrightarrow \qquad x_1 \overline{\vee} x_2 = x_3 \overline{\vee} x_4, \tag{5.9}$$

$$\text{(II)} \qquad x_1 \vee x_2 = 1 - x_3 \vee x_4 \qquad \Leftrightarrow \qquad x_1 \overline{\vee} x_2 = 1 - x_3 \overline{\vee} x_4, \tag{5.10}$$

which suggests the interpretation of the constraint as an equality. Such an equality is realized on the languages by the γ-product of the output bits. A concatenation of two logical connectives is realized by the γ-product of the output bit with an input bit of the other language. This yields a more efficient recipe for the construction of surface code unit-cells by utilizing only two logic elementaries of XNOR or XOR (e.g. the elementaries from chap. 4). Surprisingly[6], for the PXP model in representation I using the PXP-minimal XNOR2-gate from fig. 4.6 it turns out that this realization is minimal for the PXP model[38]. Note that as the XNOR2-gate is symmetric in all ports, both of the above interpretations (as a concatenation and as an equality) are equal. As in the PXP model there are no long-range interactions perturbing the energy structure of the amalgamated L-complex this constructing yields $\mathcal{Q} = 1 = r$ for the PXP model. For the VdW model we can expect a more efficient realization with less ancillaries using the VdW-minimal

[5] Note that the above iteration is well-defined due to the associativity of XNOR and XOR.
[6] Usually amalgamated L-complexes are no minimal realizations.

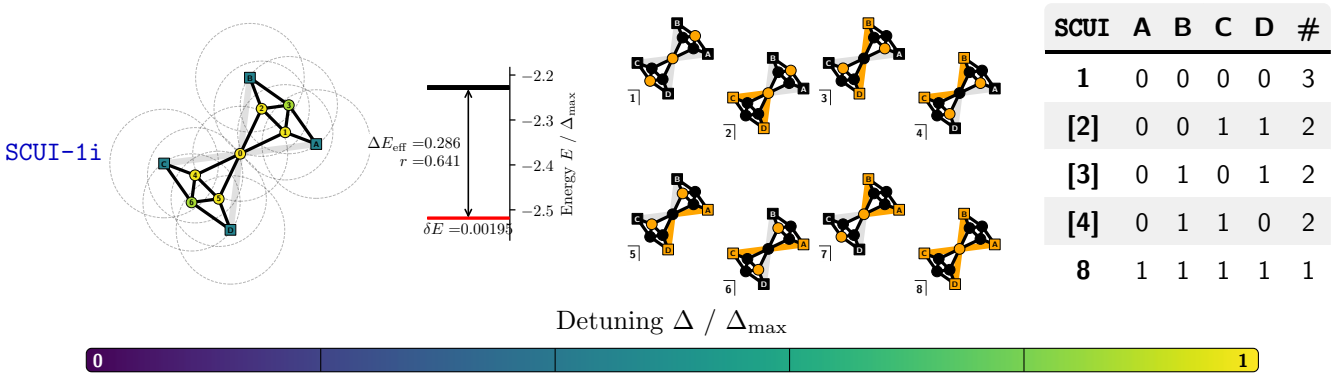

SCUI	A	B	C	D	#
1	0	0	0	0	3
[2]	0	0	1	1	2
[3]	0	1	0	1	2
[4]	0	1	1	0	2
8	1	1	1	1	1

Figure 5.1: Optimized PXP-minimal surface code unit-cell in the VdW model. The unit-cell is optimized for the quality achieving $\mathcal{Q} \approx 99.3\% < 1$. The underlying edges are colored in gray, the excited edges are colored in orange. The tables in the last column portray only the number # of excited ancillaries for a clearer visualization.

`XNOR3i`-gate from fig. 4.9. The `XNOR3i`-gate is symmetric in all ports too, thus again both of the above interpretations are equal. However such an amalgamated L-complex is perturbed by the long-range interactions (2.14) between the atoms of different gates in the VdW model. This can decrease the quality factor and the robustness. Such effects are going to be discussed in the next two subsections 5.1.2 and 5.1.3.

5.1.2 | PXP-minimal Surface Code Elementaries

In this subsection and the two following subsections 5.1.3 and 5.1.4 we discuss implementations of the surface code unit-cell in $d = 2$ dimensions. We present the optimized results for the PXP-minimal realization in the VdW-model and we introduce new VdW-specific realizations which are more atom-efficient. For that we apply the theory derived in chap. 3. Some of the presented realizations are based on amalgamations of the logic elementaries introduced in chap. 4.

Quasiplanar[7] and tetrahedral unit-cells on the $d = 3$-dimensional Rydberg platform are not discussed in this chapter, for that we refer to chap. 8. Tessellated structures are discussed in chap. 6.

Following the PXP Model. Like for the logic elementaries of chap. 4 it is natural to start by reconstructing the PXP-minimal elementaries found by Stastny *et al.* in Ref. [38]. These PXP-minimal elementaries are based only representation `I` thus we consider the check function f_c[`SC-I`] from eq. (5.6). Fig. 5.1 presents the PXP-minimal unit-cell of the surface code optimized in the VdW model. We label such unit cells of the surface code by `SCU`, followed by the representation `I`, the realization `1` and the implementation `i`. In the second and fourth column the underlying lattice of the unit-cell is colored in gray. In representation `I` the excited ports are mapped locally one-to-one to excited edges of $\mathcal{H}_{\text{loop}}$. The excited edges are colored orange in the states represented in the fourth column.

[7] Only the ports lie in a two-dimensional plane.

Remember that the PXP-minimal language $L_{\texttt{SCUI-1}}$ is constructed as the γ-square of the XNOR2-language. Thus the overall structures looks like a distorted amalgamation of two PXP-minimal XNOR2-gates from fig. 4.6. The distortion is caused by the optimization due to the minimization algorithm 3.2. Note that due to residual long-range interactions there remains a finite energy splitting $\delta E \approx 0.2\%\ \Delta_{\max} > 0$. Thus the quality factor $\mathcal{Q} \approx 99.3\% < 1$ is not perfect. The optimization algorithm was not able to improve the ratio any further even with intensive computation. This suggests that even though the quality is not perfect, the portrayed structure is (almost) optimal and that there exists no structure with perfect quality. We are not able to apply theorem V (or its corollaries) as there are not sufficient DOFs in the detunings for this language. The consistency condition $\operatorname{rank}(\tilde{\boldsymbol{L}}_{\text{Aug}}) = \operatorname{rank}(\tilde{\boldsymbol{L}})$ is not fulfilled. This is not surprising as the γ-product of two languages parallels the tensor product of their Hilbert spaces (2.11) (up to the compatibility constraint). Thus for general amalgamations of gates we can not expect to achieve perfect quality (via theorem V).

Symmetries. Note that the check function is symmetric under any permutation of the ports. However the chosen realization of the language partially breaks this symmetry. The symmetry group of the language $L_{\texttt{SCUI-1}}$ is given by

$$\Sigma_{\mathcal{N}}[\texttt{SCUI-1}] = \langle (\mathsf{A\ B}) \circ (\mathsf{D\ C}) \circ (\mathsf{1\ 5}) \circ (\mathsf{2\ 4}) \circ (\mathsf{3\ 6}),\ (\mathsf{A\ D}) \circ (\mathsf{B\ C}) \circ (\mathsf{1\ 2}) \circ (\mathsf{5\ 4}) \rangle.$$

The structure in fig. 5.1 possesses two D_2-symmetries respecting the symmetries of the language. Thus the ports of the portrayed structure lie on some rectangle and construct a centered rectangular (orthorhombic) lattice. As the realization partially breaks the symmetry between the ports it is no surprise that the rectangle traced-out by the ports of the optimized structure is no square, i.e. that the underlying lattice of the unit-cell is non-square but angled.
In particular the ports of the unit-cell lie on the corners of some parallelogram with the ancillaries inside the parallelogram. This is necessary for the tessellation of the structure such that we can amalgamate adjacent ports. This property should be constrained during the numerical optimization. Numerically we find that breaking the D_2-symmetries (i.e. only conserving the C_2-symmetry of any unit-cell) does not help to further improve the quality factor.

A Finite Quality Factor. At this point it is reasonable question whether the finite energy splitting is only caused by numerical difficulties or whether it is a fundamental feature of this language. This is studied in app. 5.A.1. Here we summarize the main observations:

1 | It is *not* possible to achieve a perfect quality factor $\mathcal{Q} = 1$ for the SCUI-1 unit cell (in any symmetric implementation).

2 | There exist PXP-derived languages which can *not* be implemented in the VdW model with degenerate ground states. In particular such languages possess only imperfect quality $\mathcal{Q} < 1$.

Realization SCUI-1 is an example of a PXP-minimal language which can not be implemented in the VdW model with degenerate ground states. To be precise for the proof of this statements we assumed the D_2-symmetry of the SCUI-1 unit cell. This is ('only') legitimized via intensive numerical simulation where we find that breaking the D_2-symmetries does not help to improve the quality. We are going to find an additional, less simple example of such a PXP-derived languages which are necessarily imperfect in the VdW model later with tessellated loop structures in chap. 6.

The finite energy splitting seems to be consequence of the amalgamation of the gates which causes residual interactions between the product states. These residual interactions can not be compensated by the given DOFs in the detunings. To maximize the quality the numerical optimization algorithm suppresses the residual interactions by maximizing the distances between the atoms of the two amalgamated gates. This decreases the ratio but decreases the effective energy gap as well. We can circumvent this issue by adding additional DOFs with *virtual ancillaries*. This concept is discussed in sec. 7.1.

Surface Code on the square Lattice. In the PXP model there always is some wiggle-room in which the blockade graph does not change. Thus in the PXP model one can always slightly customize the geometry. In particular in the PXP model it is possible to implement the surface code on a square grid[38]. This freedom of choice is lost in the VdW model as the interaction energies are highly sensitive on the geometry with the (inverse) exponent $\gamma = 6$. It is therefore a natural question whether we can implement the surface code unit-cell on a square grid in the VdW model as well. This is studied in the app. 5.A.2 with implementation `SCUI-1iii`. Here we optimized a `SCUI-1` unit cell while constraining the ports on a square grid reducing the parameter space. This impaired the quality factor by $\sim 12.8\%$ compared to the `SCUI-1i` unit cell from fig. 5.1.

Local Minima. Furthermore, in app. 5.A.2 we add the implementation `SCUI-1ii`. The `SCUI-1ii` unit cell possesses a slightly worse quality factor than implementation `SCUI-1i` from fig. 5.1 (by $\sim 5.4\%$) however a very different structure. This is an illustrative example of two quite different local minima in parameter space. Such local minima make it sometimes difficult to determine the true global minimum in parameter space.

5.1.3 | VdW-specific SC Elementaries in Representation I

As discussed in chap. 4, in the VdW model we can reduce the number of ancillaries compared to the PXP model by exploiting the intermediate and low-energy regime. In fig. 4.9 the VdW-minimal realizations of the logic elementaries are portrayed with only one ancillary. The PXP-minimal `SCUI-1` unit-cell is constructed by amalgamating two PXP-minimal XNOR2-gates[38].

SCUI-2a Unit Cell. Similarly, in the VdW model we can realize a more atom-efficient `SCUI` unit-cell by amalgamating the VdW-minimal XNOR3I-gates. The constructed unit-cell is portrayed as realization `2a` in fig. 5.2. As the `XNOR3i`-gate is based on the low-energy regime is possess only a small the effective gap. This also impedes the effective gap of the `SCUI-2a` unit cell. Here $\Delta E_{\text{eff}}[\texttt{SCUI-2a}] \approx 0.1\%$ is more than two orders of magnitude smaller than for the `SCUI-1i` unit cell.

SCUI-2b Unit Cell. As discussed in the previous subsec. 5.1.1 we can interpret the check function $f_c[\texttt{SC-I}]$ as an equality or a concatenation of either two `XNOR`- *or* two `XOR`-functions. In a nutshell the two negations we introduce in `XNOR` cancel themselves out. Thus we can also amalgamate two `XOR3`-gates to construct the `SCU-I` unit-cell. This realization `SCUI-2b` is portrayed in the second row of fig. 5.2. The advantage of this realization compared to realization `SCUI-2a` is clearly that the `XOR3`-gate possesses a way larger effective gap than the `XNOR3i`-gate. This also assists the effective gap $\Delta E_{\text{eff}}[\texttt{SCUI-2bi}] \approx 1.7\%$ of the `SCUI-2b` unit cell which is more than an order of magnitude lager than for the `SCUI-2a` unit cell. Nevertheless, the effective gap remains relatively small compared to the PXP-minimal implementation `SCUI-1i`. The main

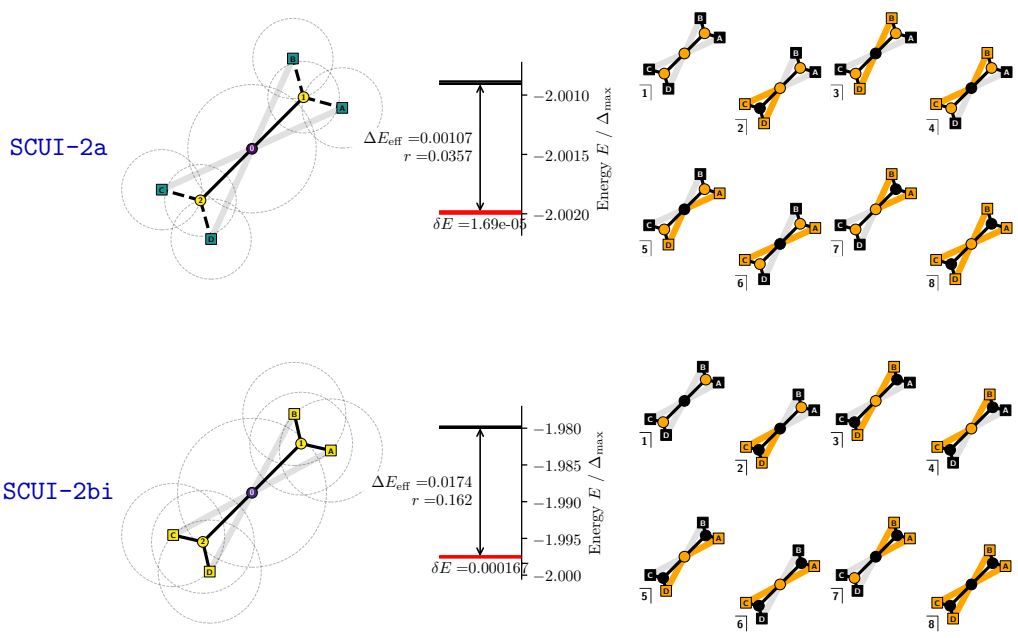

SCUI	A	B	C	D	#
1	0	0	0	0	3
[2]	0	0	1	1	2
[3]	0	1	0	1	2
[4]	0	1	1	0	2
8	1	1	1	1	1

SCUI	A	B	C	D	#
1	0	0	0	0	2
[2]	0	0	1	1	1
[3]	0	1	0	1	1
[4]	0	1	1	0	1
8	1	1	1	1	0

Figure 5.2: Optimized VdW-specific surface code unit-cell. The unit-cell is optimized for the quality achieving $\mathcal{Q}_{\texttt{SCUI-2a}} \approx 98.4\%$ and $\mathcal{Q}_{\texttt{SCUI-2b}} \approx 99.0\%$. The underlying edges are colored in gray, the excited edges are colored in orange. The tables in the last column portray only the number # of excited ancillaries for a clearer visualization

reason is that the smaller `XOR3`-gate needs to be heavily distorted to suppress the distance between the atoms of the amalgamated gates. This also decreases the advantage of the `XOR3`-based `SCUI-2bi` unit cell compared to the realization via the larger `XNOR3`-based `SCUI-2a` unit cell. The larger `XNOR3`-gate naturally possesses smaller residual interactions under amalgamation.

Finite Energy Splitting. All of the presented unit cells possess a finite energy splitting $\delta E > 0$ and thus an imperfect quality. For realization `2a` it is $\mathcal{Q}_{\texttt{SCUI-2a}} \approx 98.4\%$, for realization `2b` it is $\mathcal{Q}_{\texttt{SCUI-2bi}} \approx 99.0\%$. There are residual long-rang interactions which impede us from achieving perfect degeneracy. We can not apply theorem V or its corollaries to compensate for the residual interactions as we have not sufficient DOFs in the detunings of this language. During optimization the residual interactions are suppressed by maximizing the distance between the two gates. This is achieved in the minimization algorithm by decreasing the detuning of the central ancillary 0. This comes at the cost of increasing the energy range of the detunings and decreasing the effective energy gap. Thus increasing the quality factor comes at the cost of decreasing effective energy gap. At this point it is a legitimate question whether it is theoretically possible to achieve $\delta E = 0$ but numerically we are not able to find such a structure. This is discussed in the app. 5.A.1. We summarize the main results proven in app. 5.A.1:

It is *not* possible to achieve a perfect quality factor $\mathcal{Q} = 1$ for the unit cells `SCUI-2a` and `SCUI-2b` (in any symmetric implementation).

The structures of the `SCUI-2a` and `SCUI-2bi` unit cells are D_2-symmetric conserving the symmetries of the target language (similar as for the `SCUI-1i` unit cell). For the proof in app. 5.A.1 we assume this D_2-symmetry to reduce the number of DOFs. Numerically we find that we do not profit from breaking the symmetries of the language. This legitimizes the assumption for the prove.

Elongation of the Unit Cells. The underlying grid of the D_2-symmetric unit cells `SCUI-2a` and `SCUI-2bi` is a non-square centered-rectangular (orthorhombic) lattice now with a narrow angle. In the app. 5.A.2 we add two more implementation `SCUI-2bii` and `SCUI-2biii` (fig. 5.9) with larger effective gaps at the cost of a smaller quality factor. To optimize the quality the minimization algorithm suppresses the residual interactions between the atoms by elongating the unit cell which causes the narrow angle. In fig. 5.9 the unit-cells are less angled and less elongated which causes stronger residual interactions. Interestingly the detunings of implementation `2b-iii` seem somewhat inverted compared to implementation `2bi` where the detuning of the central ancillary is suppressed.

On Minimality. The realizations `SCUI-2a` and `SCUI-2b` possess only three ancillaries. They emerge somewhat naturally by amalgamating their respective logic elementaries. At this point a reasonable question is whether they are minimal in the VdW model or whether we could theoretically construct a more atom-efficient unit cell for representation `SCU-I`. As it turns out representation `SCU-I` requires only two ancillaries for a realization:

Proof 7. (Minimality in Representation `I`)

> We argue with corollary II. Corollary II forbids ground states which are non-adjacent substates with any intermediate excited state. Without ancillaries it would be $\boldsymbol{x}_1 \Subset \boldsymbol{x}_i$ for $i > 1$ and $\boldsymbol{x}_i \Subset \boldsymbol{x}_8$ for $i < 8$. Thus we require two ancillaries: Firstly, in $\boldsymbol{x}_2, \dots \boldsymbol{x}_7$ there must be one ancillary which is excited and which is not excited in $\boldsymbol{x}_8$. Secondly in $\boldsymbol{x}_1$ there must be one ancillary which is excited and which is not excited in $\boldsymbol{x}_2, \dots \boldsymbol{x}_7$. Thus in particular for each $\boldsymbol{x}_i$ with $i \in \{2, \dots 7\}$ there needs to be one ancillary excited and one which is not excited. □

However numerically it seems that such a language with two ancillaries can not be implemented as the low-energy eigenspace on the $d = 2$-dimensional Rydberg platform. Remember that the ports need to construct some C_2-symmetric parallelogram to yield a valid unit cell. This heavily constrain the structure of only six atoms. The six states with two excited ports (and one excited ancillary) necessarily look different to the Hamiltonian because the interaction energies are different if two diagonal or two adjacent ports are excited. This explains also why for quasiplanar structures on the three dimensional Rydberg platform (cf. fig. 8.15) we observe a large energy splitting. However here we have sufficient DOFs in the positioning of the ancillaries to achieve a positive energy gap with two ancillaries. For truly three-dimensional, tetragonal structures we are successful in implementing the surface code unit cell with only two ancillaries (fig. 8.17). This observation is not quite surprising: the argument of proof. 7 is based on corollary II which considers only the energy gap (i.e. the ordering of the energy structure). It does not include any consideration of the energy splitting or of the embeddability in smaller dimensions. Such higher dimensional structures are going to be studied in chap. 8.

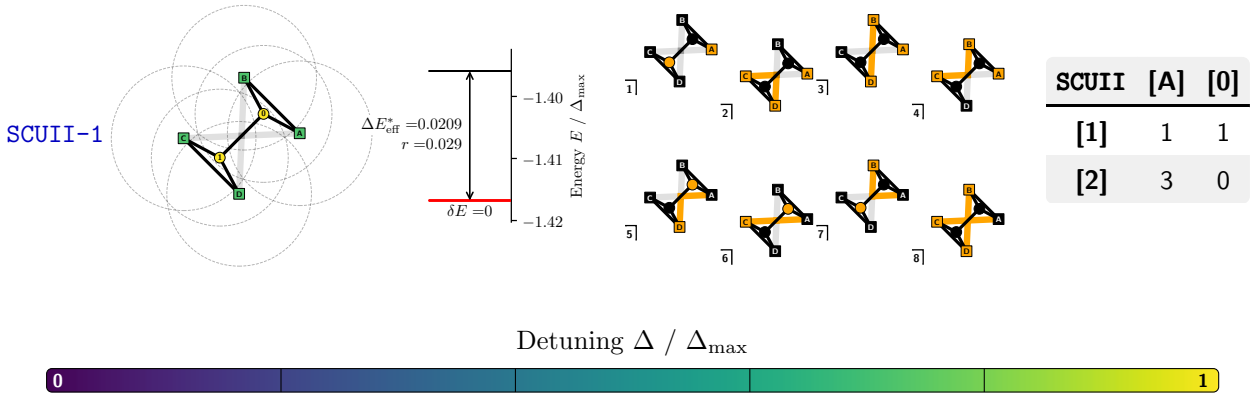

SCUII	[A]	[0]
[1]	1	1
[2]	3	0

Figure 5.3: SCUII-1 unit cell. In representation II we can construct a unit-cell with $\mathcal{Q} = 1$ with only two ancillaries.

5.1.4 | VdW-specific SC Elementaries in Representation II

So far we only considered the representation SCU-I which is the one studied for the PXP model by Stastny *et al.*[38]. In the following we want to focus on the second representation SCU-II. Representation SCU-II possesses *only two effective ground states* (in a D_2-symmetric L-complex) where only one of the ports is (not) excited[8]. Here the ground states of similar number of excited ports look identical to the Hamiltonian[9]. This turns out as an advantage compared to representation SCU-I as it is easier to achieve a positive energy gap and degeneracy when considering fewer effective ground states.

On Minimality. Following a similar argument as in proof 7 we find that for representation II we require at least only one ancillary:

Proof 8. (Minimality of Representation II)

> Again, we argue with corollary II. Corollary II forbids ground states which are non-adjacent substates with any intermediate excited state. We follow the labeling of the ground states from fig. 5.3, i.e. the lexicographic order of the edge states. Without ancillaries it would be $\boldsymbol{x}_1 \Subset \boldsymbol{x}_2, \boldsymbol{x}_3, \boldsymbol{x}_4$, $\boldsymbol{x}_5 \Subset \boldsymbol{x}_2, \boldsymbol{x}_3, \boldsymbol{x}_8$, $\boldsymbol{x}_6 \Subset \boldsymbol{x}_2, \boldsymbol{x}_8, \boldsymbol{x}_8$ and $\boldsymbol{x}_7 \Subset \boldsymbol{x}_3, \boldsymbol{x}_4, \boldsymbol{x}_8$ non adjacent substates. Thus representations SCU-II requires an ancillary. If we assume only one ancillary it needs to be excited in $\boldsymbol{x}_1, \boldsymbol{x}_5, \boldsymbol{x}_6, \boldsymbol{x}_7$ and not excited in $\boldsymbol{x}_2, \boldsymbol{x}_3, \boldsymbol{x}_4, \boldsymbol{x}_8$. □

Thus a reasonable goal would be to construct a SCU-II unit cell with only *one* ancillary which is only excited in the ground states where only one port is excited. We call this realization SCUII-2. It is studied for the $d = 2$-dimensional Rydberg platform in app. 5.A.3. Here we summarize the main results:

[8] Remember that representation SCU-I possesses *five effective states*.

[9] This is not the case for representation SCU-I if two ports are excited: if two diagonal ports are excited they experience different interaction energies compared to when two adjacent ports are excited.

1 | It is *not* possible to achieve perfect quality $\mathcal{Q} = 1$ with $a = 1$ ancillary in $d = 2$ dimensions.

2 | Numerically we find that it is *not* possible to achieve even a positive energy gap $\Delta E > 0$ with $a = 1$ ancillary in $d = 2$ dimensions.

The ancillary needs to be sufficiently distant from the ports such that both can be excited in simultaneously. On the other hand the ports need to interact sufficiently strong such that the states where two ports are excited alongside the ancillary are gapped-out. It seems that there are simply too few DOFs left with only one ancillary in $d = 2$ dimensions to fulfill both conditions simultaneously. Thus we have two possibilities of lowering our requirements: The first is to consider a *quasiplanar*[10] structure in $d = 3$ dimensions where the ancillary may be placed outside the plane of the ports. This adds an extra DOF which is useful to achieve a positive energy gap $\Delta E > 0$ (and even perfect quality $\mathcal{Q} = 1$). This is studied in chap. 8. This again illustrates that the argument of corollary II on which (proof 8 is based) is on very general ground and does not take the dimensionality of the space in consideration.

With two Ancillaries. In the following we consider the other ansatz where we choose $a = 2$ ancillaries to construct a realization of the `SCU-II` unit cell in $d = 2$ dimension. This is portrayed in fig. 5.3. Compared to the one-ancillary case we effectively split the ancillary such that only one of the two ancillaries is excited iff only one of the ports is excited. This elongates the unit-cell such that the geometry is only D_2- but not D_4-symmetric. Thus the underlying grid is a non-square centered-rectangular (orthorhombic) lattice. However the permutation symmetries of the ports remain conserved on the level of the ground states (cf. the `ICRS2`-gate from fig. 4.8) thus we only have two effective ground states. This is in contrast to the `SCUI`-realizations where the permutation symmetry of the ports was broken by the realization. For this D_2-symmetric unit cell we are even able to achieve perfect quality $\mathcal{Q} = 1$. The effective gap $\Delta E_{\text{eff}} \approx 2.1\%$ is larger than for the `SCUI-2a` and `SCUI-2bi` unit cells however it remains smaller than for the `SCUI-1` unit cell. Nevertheless, for these unit cells of representation `SCU-I` it is not possible to achieve ground state degeneracy.

[10] With 'quasiplanar' we denote that we constrain only the ports in one plane. The ancillary may be shifted outside the plane of the ports.

5.2 | Fibonacci Model

Topological quantum computation has emerged as one of the most promising approaches for constructing a fault-tolerant quantum computer. The proposal relies on topological states of matter whose quasiparticle excitations are anyons (i.e. neither bosons nor fermions) obeying non-Abelian statistics. Here unitary gate operations are implemented by *braiding* of localized excitations. The fault-tolerance arises from the nonlocal encoding of the quasiparticle states which makes them immune to local perturbations. Quantum information is stored in states with multiple quasiparticles which have topological degeneracy[29].

The surface code studied in chap. 5.1 only supports *Abelians anyons* which are not sufficient to achieve universal *topological quantum computation*. The simplest model with non-Abelian anyons supporting universal quantum computation by braiding is known as the FIBONACCI model `FM`. The FIBONACCI model was examined in the Rydberg PXP-blockade formalism by STASTNY *et al.* in Ref. [38]. This motivates us to study the FIBONACCI MODEL on the Rydberg platform with VdW interactions.

In the following subsec. 5.2.1 we recapitulate the key concepts of the FIBONACCI model and discuss possible target functions. The reader only interested in the results may skip to the subsequent subsections 5.2.2 and 5.2.3 where we discuss the implementations of the FIBONACCI model elementaries in the VdW model.

5.2.1 | General Theory

In the following we briefly recall the definition and the properties of the FIBONACCI model. We write down the ground state and discuss its preparation. Then we introduce the local mappings to the Rydberg platform.

The Fibonacci Model Ground State. The properties of the FIBONACCI model quasiparticles are a consequence of the entanglement patterns of the ground state. The ground state can be represented as a string-net condensate with weights[26]. In the following we consider a honeycomb lattice with qubits on the edges. Then the ground state of the FIBONACCI model is given by the superposition

$$|G\rangle = \sum_{\boldsymbol{s}\in\boldsymbol{S}} \Phi(\boldsymbol{s})|\boldsymbol{s}\rangle \tag{5.11}$$

where we sum over the set $\boldsymbol{S}$ of all string-net patterns on the edges where no single string ends at any site[12]. Note that the string-net patterns of the FIBONACCI model differ from the closed-loop patterns of the surface code (cf. eq. (5.3)) as they allow for a fusion of three strings at any site. The coefficients $\Phi(\boldsymbol{s})$ are nontrivial functions of the string-net pattern $\boldsymbol{s}$ such that the condensate is no equal-weight superposition like for the surface code.

Preparation of the Ground State. The goal is to prepare the ground state $|G\rangle$. Straightforwardly we could write down a solvable, local Hamiltonian for the FIBONACCI model with exact ground state $|G\rangle$ (like for the surface code, see eq. (5.2)). Then we could try to implement the Hamiltonian in a physical system and cool the system to its ground state. Such a solvable, local Hamiltonian does in fact exist, however it is very complicated and thus essentially useless for an implementation of the ground state[26].

This motivates us to follow the approach from previous chap. 5.1.1 on the Rydberg platform[38]. We want to prepare the string-net Hilbert space

$$\mathcal{H}_0[H;\mathcal{C}_{\text{loop}}] \overset{!}{\cong}_{\text{loc}} \mathcal{H}_{\text{loop}} := \text{span}\left(\{|\boldsymbol{s}\rangle \mid \boldsymbol{s} \in \boldsymbol{S}\}\right) \tag{5.12}$$

by locally mapping it one-to-one to the low-energy manifold of a Rydberg structure $\mathcal{C}_{\text{loop}}$ of atoms (cf. eq. (5.4)). The Hilbert space $\mathcal{H}_{\text{loop}}$ is now spanned by the string-net patterns where no single edge ends on any site. Note that on the honeycomb grid every unit cell vertex consists of two sites. By $V = |\mathcal{V}|$ we still denote the number of vertices of the underlying hexagonal lattice. Then $\mathcal{H}_0[H;\mathcal{C}_{\text{loop}}]$ is a Hilbert space of dimension[33] $\dim \mathcal{H}_{\text{loop}} \sim (1+\varphi^2)^V + (1+\varphi^{-2})^V$ which can not be decomposed into factors of local Hilbert spaces (similar to the surface code). Here $\varphi = (1+\sqrt{5})/2$ is the golden ratio. On the honeycomb grid each site is now trivalent with $K = 1$ logical bits associated with each edge. This redefines the bit projector $P_s : \mathbb{F}_2^N \to \mathbb{F}_2^{3K}$ which maps the bit configuration to the bits on the edges emanating from site s. Again, we can perturbatively introduce quantum fluctuations on the Rydberg platform by ramping up the RABI frequencies Ω_i of the atoms in Hamiltonian (2.1). To construct the structure $\mathcal{C}_{\text{loop}}$ we first have to define the check function f_c on the Rydberg platform.

Definition of the Check Functions. To define the check function we need to specify the local mapping denoted by the isomorphism $\cong_{\text{loc}}$. For a detailed introduction to these concepts and to avoid repetitiveness we refer to subsec. 5.1.1.

For the FIBONACCI model on the honeycomb grid there are $p = 3$ edges adjacent to each site and $g = 5$ states: The two states where either no or all three edges are excited and the three states where two edges are excited. There exist in total $\binom{2^3}{5} = 56$ check function with HAMMING weight $w_H = g = 5$. For each adjacent edge we can choose one of two representations. This makes $2^3 = 8$ possible representations for the edges defining an equivalence classes $[f_c]$ of 8 check functions. Like for the surface code, for the FIBONACCI model the valid states of a site are symmetric under permutations of the edges. This effectively boils down the number check functions to only *four*[11] (up to rotations):

$$f_c[\texttt{FM-I}] : \boldsymbol{x} \mapsto \overline{(x_1 \underline{\vee} x_2 \underline{\vee} x_3)} \vee (x_1 \wedge x_2 \wedge x_3) = \overline{(x_1 \underline{\vee} x_2 \underline{\vee} x_3)} \vee (x_1 \wedge x_2 \wedge x_3) \tag{5.13}$$

$$f_c[\texttt{FM-II}] : \boldsymbol{x} \mapsto (x_1 \underline{\vee} x_2 \underline{\vee} x_3) \vee (x_1 \wedge x_2 \wedge \overline{x_3}) = (x_1 \underline{\vee} x_2 \underline{\vee} x_3) \vee (x_1 \wedge x_2 \wedge \overline{x_3}) \tag{5.14}$$

$$f_c[\texttt{FM-III}] : \boldsymbol{x} \mapsto \overline{(x_1 \underline{\vee} x_2 \underline{\vee} x_3)} \vee (\overline{x_1} \wedge \overline{x_2} \wedge x_3) = \overline{(x_1 \underline{\vee} x_2 \underline{\vee} x_3)} \vee (\overline{x_1} \wedge \overline{x_2} \wedge x_3) \tag{5.15}$$

$$f_c[\texttt{FM-IV}] : \boldsymbol{x} \mapsto (x_1 \underline{\vee} x_2 \underline{\vee} x_3) \vee (\overline{x_1} \wedge \overline{x_2} \wedge \overline{x_3}) = (x_1 \underline{\vee} x_2 \underline{\vee} x_3) \vee (\overline{x_1} \wedge \overline{x_2} \wedge \overline{x_3}) \tag{5.16}$$

Here we chose two equivalent, simple BOOLEAN expressions which manifestly respect the permutation symmetries of the check functions. The expressions consist of a disjunction of two terms:

1 The first term is a ternary `XNOR`- or `XOR`-function which implements the closed-loop constraint. Note that the two negations when exchanging $\underline{\vee}$ and $\underline{\vee}$ cancel out. We can also

[11] In contrast to the surface code the FIBONACCI model has no additional internal symmetries which further reduce the number of representations.

reformulate the term as an equivalence condition in the ports by breaking their manifest permutation symmetry:

$$\overline{x_1 \underline{\vee} x_2 \underline{\vee} x_3} = (x_1 \underline{\vee} x_2 \equiv x_3), \qquad \overline{x_1 \underline{\overline{\vee}} x_2 \underline{\overline{\vee}} x_3} = (x_1 \underline{\overline{\vee}} x_2 \not\equiv x_3) \tag{5.17}$$

Here $\underline{\overline{\vee}}$, $\equiv$ denotes both the exclusive nor but latter suggests the interpretation as an *equivalence condition*. The reformulation (5.17) suggests the interpretation of the closed-loop constraint on the trivalent site as the binary logic function `XOR`.

2 The second term is a *minterm*. The minterm adds an additional word to the language which allows for the fusion of three strings. Without the minterm the model would only contain closed loops and would essentially correspond to the surface code on the honeycomb grid. For the natural representations all edge high `FM-I` and all edge low `FM-IV` the minterm includes the word where all three bits are (not) excited. The other two representations `FM-II` and `FM-III` partially break the permutation symmetry between the edges. Here the minterm describes a state where two bits are (not) excited.

Due to the minterm there are in total $g = 5$ ground states. Thus the `FM` site can not be realized by a single logic gate (like the surface code on the honeycomb grid via the `XOR`-gate). As a first, naive ansatz we could decompose the check function into a circuit of logic elementaries. A concatenation of an even number of logic elementaries always yields an even number of ports, thus we would need at least three logic elementaries. This comes at the cost of gaining a lot of ancillaries which we deem to much overhead for a single site. Instead a more promising approach is to directly implement the L-complex for a single site as a fundamental building block. This is studied in the following subsec. 5.2.2 and the subsequent subsec. 5.2.3.

5.2.2 | PXP-derived Fibonacci Model Elementaries

In this subsection and the following subsec. 5.2.3 we present implementations of the Fibonacci model site and the Fibonacci model unit cell for the honeycomb grid optimized in the VdW model. In this subsection we start by reconstructing the Fibonacci model site and unit-cell of representation `FM-I` which was first introduced by Stastny *et al.* for the PXP model[38]. We introduce a more atom-efficient realization of the `FM` site in the PXP-model which we also implement in the VdW model. In the next subsec. 5.2.3 we construct a VdW-minimal realizations of the `FM-I` site.

In both subsections we exemplarily consider only the representation `FM-I`. The other three representations partially profit from embedding them on the three-dimensional Rydberg platform. Thus we want to discuss them collectively in sec. 8.6 in a comparative study with their three-dimensional counterparts.

Reconstruction of the PXP-model Elementaries. Like for the surface code elementaries of subsec. 5.1.2, we start by reconstructing the elementaries introduced by Stastny *et al.* for the PXP-model[38]. These PXP-model elementaries only use the all edge high representation `I` thus we consider the check function f_c[`FM-I`] from eq. (5.13). Fig. 5.4 presents the elementaries of the Fibonacci model for realization `FMI-1` optimized in the VdW model. In the all edge high representation excited ports are mapped locally one-to-one to excited edges of $\mathcal{H}_{\text{loop}}$. In the second and the fourth column the underlying honeycomb grid is colored in gray. Excited edges are colored in orange in the foruth column.

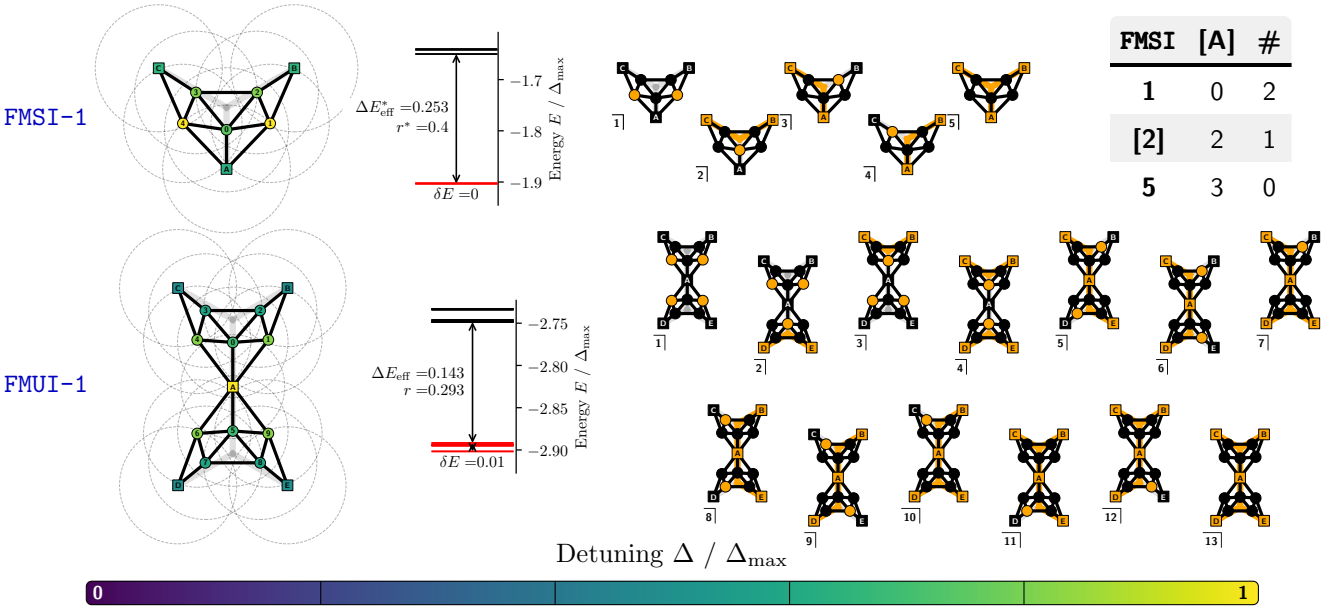

Figure 5.4: Optimized PXP-elementaries of the FIBONACCI model. The `FMSI-1` site is optimized for ΔE_{eff} and r. The `FMUI-1` unit cell is optimized for the quality $\mathcal{Q} \approx 93.2\% < 1$. The underlying edges are colored in gray, the excited edges are colored in orange.

The first row shows the `FMSI-1` site. Here we can apply theorem V to achieve a vanishing energy splitting of the ground states. Both the effective gap $\Delta E_{\text{eff}}[\texttt{FMSI-1}] \approx 25.3\%$ and the robustness $r_{\texttt{FMSI-1}} \approx 40.0\%$ are optimized. In the table of the last column we summarized the number of excited ancillaries # in one column. Note that the check function $f_c[\texttt{FM-I}]$ is symmetric under any permutation of the ports but realization `FMSI-1` breaks this symmetry. The structure possesses only a D_2-symmetry.

The second row portrays the amalgamation of two `FMSI-1` sites constructing a unit-cell of the hexagonal lattice. The structure is optimized for its quality factor $\mathcal{Q} \approx 93.2\% < 1$. It possesses a finite energy splitting $\delta E \approx 1\%\Delta_{\max}$. Due to the relatively high number of ancillaries the unit-cell is computationally intensive to optimize thus its quality might only be almost optimal. Like for the `SCUI-1`- and `SCUI-2`-unit cells we can not apply theorem V. There are not sufficient DOFs in the detunings of the language to compensate the residual interactions between the amalgamated sites. This comes as no surprise as the language a the γ-square (of $L_{\texttt{FMSI-1}}$).

Non-Minimality. In Ref. [38] STASTNY *et al.* claimed that they proved that realization `FMSI-1` is PXP-minimal, i.e. optimal in the number of atoms for the PXP model. However this turns out as *not correct* as fig. 5.5 presents a PXP-model realization `FMSI-2` of the site with only 7 atoms of which 4 are ancillaries. This makes one ancillary less than in realization `FMSI-1`. Note that the blockade graph for this realization is *not planar*. This however is only a mathematical peculiarity of the blockade graph and of no physical significance (as the blockade graph is unphysical).

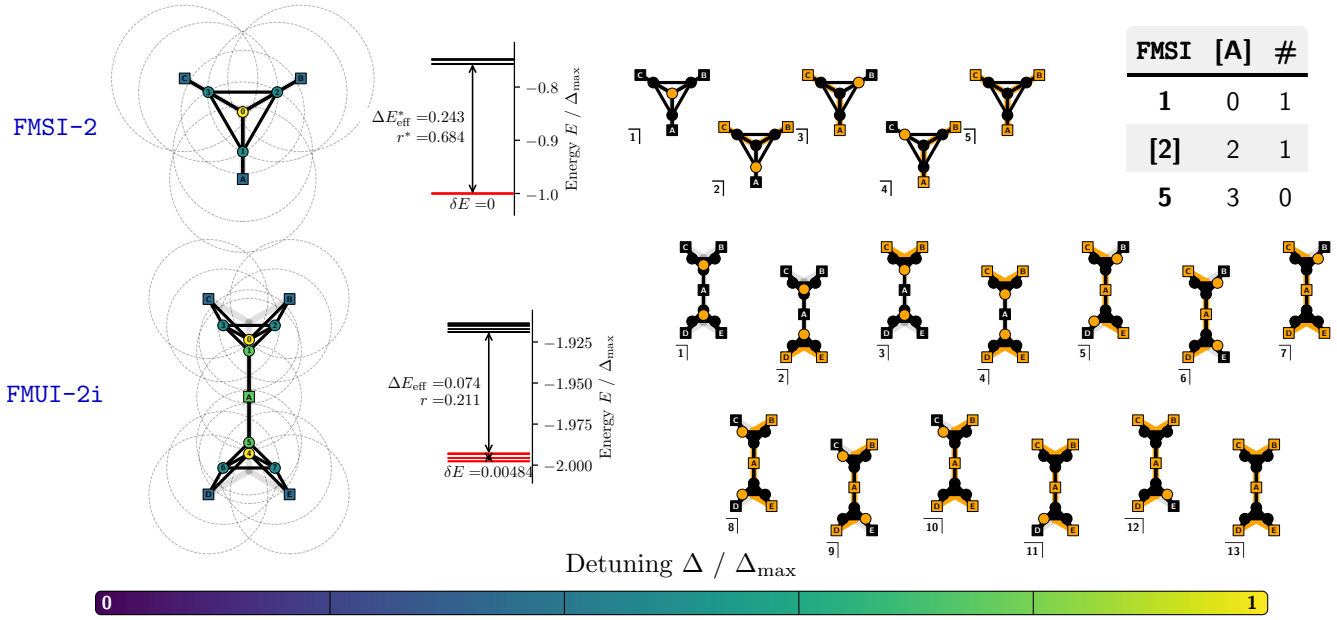

FMSI	[A]	#
1	0	1
[2]	2	1
5	3	0

Figure 5.5: Optimized PXP-minimal elementaries of the FIBONACCI model. The `FMSI-2` site is optimized for ΔE_{eff} and r, the `FMUI-2` unit cell is optimized for the quality $\mathcal{Q} \approx 93.6\%$. The underlying edges are colored in gray, the excited edges are colored in orange.

On Uniqueness and PXP-Minimality. Now again it arises the question whether the newly constructed atom-efficient PXP-realization is PXP-minimal and whether it is the only PXP-minimal solution. Otherwise it would be interesting to construct (further) PXP-minimal solutions. This is discussed in app. 5.B.1. In the following we summarize the main results:

1 | Realization `FMSI-2` is PXP-minimal for representation `FM-I`.

2 | It is the *only* PXP-minimal realization of representation `FM-I`.

Thus there exist no further PXP-minimal realizations which could be added to the 'list' from fig. 5.5; `FMSI-2` is *unique*.

Construction. The construction of this `FMSI-2` site from the `FMSI-1` site can be interpreted quite intuitively: First note that in the `FMSI-1` site the ancillaries 1 and 4 are excited simultaneously iff no other atom is excited (i.e. in state $\boldsymbol{x}_1$). This allows us to combine them into one ancillary. This ancillary is excited iff no other atom is excited thus it needs to be in blockade with all other atoms.

The advantage of this construction compared to realization `FMSI-1` is (besides fewer ancillaries) its symmetry in the ports: It respects the permutation symmetries of the target function

f_c[FM-I]. Thus the optimized structure is D_3-symmetric. This helps with the construction and the optimization. Furthermore, as the central ancillary needs to be in blockade with all other atoms the FMSI-2 site is more compact than the FMSI-1 site. Note that the effective gap ΔE_{eff}[FMSI-2] $\approx 24.3\%$ and the robustness r[FMSI-2] $\approx 68.4\%$ of the FMSI-2 site are similar as for the FMSI-1 site.

Analogies to other Structures. At this point we should draw the analogy of the FMSI-2 site to the XOR2b-gate from fig. 4.7. Their similarity is not only apparent in their structure but also in their language: The language L_{FMSI2} emerges from the XOR2b-language by additionally including the word where all port bits are excited simultaneously but no ancillary bits. This reflects eq. (5.13) where the minterm modified the ternary XOR-function implementing the fusion of three strings. In the PXP-model this is achieved by setting the detunings of the ports equal to the detunings of the ancillaries 1, 2 and 3.
Similarly, the FMSI-1 site from fig. 5.4 and the XOR2a-gate from fig. 4.6 are somewhat analogous. This however is less apparent in their optimized structure. The FMSI-1 site emerges from the XOR2a-gate by adding an additional ancillary 4 between the ports B and Q with the additional blockades {4, B}, {4, Q}, {4, 2}, {4, 3}. This ancillary is only excited in simultaneity with ancillary 0 (in state $\boldsymbol{x}_1$). As discussed above this ancillary is somewhat redundant as we can construct realization FMSI-2.

Unit-Cells. The second row portrays the FMUI-2i unit cell. Here the D_3-symmetry of both sites is distorted by the residual interactions with the other site. The quality factor is $\mathcal{Q}_{\text{FMUI-2i}} \approx 93.6\% < 1$ which is similar as for the FMUI-1 unit cell. Again, we are not able to apply theorem V. It arises the question whether there exists a structure with degenerate ground states which we simply are not able to find numerically. This is discussed in app. 5.B.2. We summarize that:

> It is impossible to achieve a perfect quality factor $\mathcal{Q} = 1$ for the PXP-minimal realization FMUI-2 in any symmetric implementation.

The assumption for a symmetric implementation is legitimized numerically as we find that breaking the D_2-symmetry does not help to improve the quality factor. This means that the FMUI-2 unit cell is another example for a PXP-derived (even PXP-minimal) structure which we can not implement in the VdW model with perfect quality.
The effective gap ΔE_{eff}[FMUI-2i] $\approx 7.4\%$ of the FMUI-2i unit cell is a little smaller than for the FMUI-1 unit cell. This is not quite surprising as we already mentioned that the FMSI-2 site is necessarily more compact than the FMSI-1 site. This increases residual interactions with the neighboring unit cell decreasing the effective gap.

Note that the FMUI-2i unit cell is D_2-symmetric and it is distorted along the axis of symmetry. The reason is that the optimization algorithm suppresses residual interactions by increasing the distances between the atoms of different sites. However, we would not expect such a distortion of the D_3-symmetry to be of advantage when constructing the D_3-symmetric tessellated structure on the hexagonal honeycomb grid. Therefore, in app. 5.B.3 we introduce implementation FMUI-2ii where we constrain the D_3-symmetry of each site. This constrains the parameter space thus impeding the quality factor to $\mathcal{Q} \approx 72.2\%$.

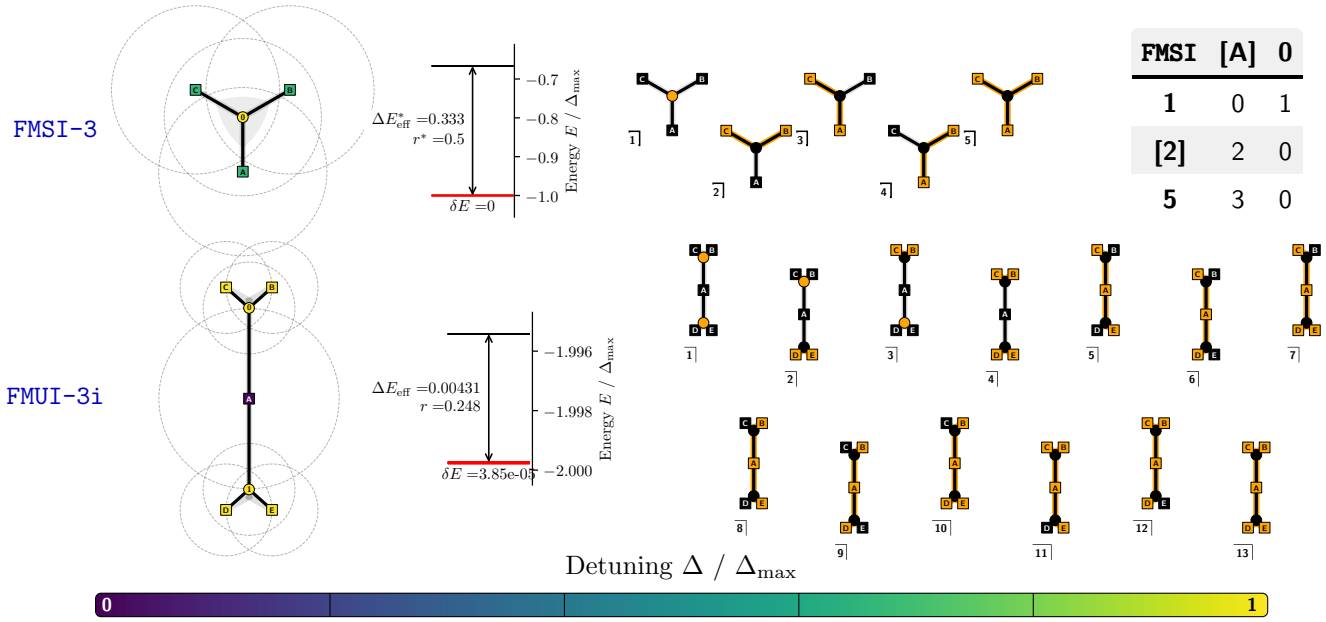

FMSI	[A]	0
1	0	1
[2]	2	0
5	3	0

Figure 5.6: Optimized VdW-minimal elementaries of the FIBONACCI model. The `FMSI-3` site is optimized for ΔE_{eff} and r, the `FMUI-3` unit cell is optimized for the quality $\mathcal{Q} \approx 99.1\% < 1$. The underlying edges are colored in gray, the excited edges are colored in orange.

5.2.3 | VdW-specific Fibonacci Model Elementaries

In the following we discuss whether we are able to construct a more atom-efficient realization in the VdW model. Again, in this subsection we want to consider only representation `FM-I` defined by check function (5.13). For the remaining three representations we refer to sec. 8.6.

The VdW-minimal `FMI`-elementaries are presented in fig. 5.6.

On Minimality. This realization `FMI-3` is VdW-minimal and it is the only VdW-minimal realization of representation `I`:

Proof 9. (Minimality and Uniqueness of Realization `FMI-3`)

> We follow the argument of corollary II. Corollary II forbids the existence of ground states which are non-adjacent substates with an intermediate excited state. Without ancillaries it would be $\boldsymbol{x}_1 \Subset \boldsymbol{x}_i$ for $i > 1$ (and it would be $\mathbf{0} \in L_t$ which we exclude by remark 4). Thus this representation requires one ancillary. The ancillary needs to be excited in $\boldsymbol{x}_1$ but not excited in $\boldsymbol{x}_i$ for $i > 1$. This is the only choice for one ancillary to circumvent non-adjacent substates with intermediate excited states. □

Note that we can also argue differently following the reformulation (5.17) of the check function to proof minimality: the check function f_c[`FMS-I`] is one in particular if one ports is equivalent to the `XOR` of the other two ports. However for `XOR` we know from proof 5 that it requires at least one

ancillary in the VdW model. The minterm adds an additional ground state which only tightens the constraints. Thus a realization with one ancillary must be necessarily VdW-minimal.

Construction of the Site. In implementation `FMSI3` we exploit the intermediate energy regime to achieve degeneracy between the four ground states where two or three ports are excited simultaneously. This is very efficient compared to the PXP-model where we already need three ancillaries only to achieve degeneracy between these four ground states. The ancillary `0` is then required to additionally achieve degeneracy with the first ground state $\boldsymbol{x}_1$. It is excited iff no other atom is excited. Thus the position of the ancillary is not fixed but can be chosen freely is some finite volume where it interacts sufficiently strong with the ports. In this volume the quality factor and the energy gap are constant. This region is shaded gray in the `FMSI3` site in fig. 5.6. This might be considered an additional advantage compared to the PXP-minimal `FMSI2`-site as it simplifies an experimental construction. For the structure in fig. 5.6 we *choose* the D_3-symmetric implementation which is most useful for tessellation to minimize residual interactions.

Analogies. Note that the VdW-minimal `FMSI3` site mirrors the VdW-minimal `XOR3`-gate the same way the PXP-minimal `FMSI2` site mirrored the PXP-minimal `XOR2b`-gate. The VdW-minimal `FMSI3` site can be constructed from the PXP-minimal `FMSI2` site by removing the three non-central ancillaries `1`, `2` and `3`. In the PXP model these ancillaries were vital to block the third port from excitation. In the VdW model this is achieved via the intermediate-range interactions between the ports. As the `FMSI3` site is based on relatively strong interactions between the ports its effective gap $\Delta E_{\text{eff}} = 33.3\%$ is relatively large. In particular the effective gap is larger than the effective gap of both PXP-derived realizations `FMSI1` and `FMSI2`.

Compared to the `XOR3`-language the `FMSI3`-language additionally includes the word where all three port bits are excited. This is described by the minterm of the check function (5.13). In the VdW model this is accomplished simply by appropriately increasing the distance between the ports. This reduces the interaction energy between the ports (compared to their detunings) and thus the energy of the fifth ground state until achieving degeneracy. This explains the apparent similarity between the `FMSI3` site and the `XOR3`-gate.

Unit Cell. The second row presents the `FMUI-3` unit cell. Similarly to the surface code unit cells `SCUI-2` from fig. 5.2 the optimization algorithm elongates the unit cell to minimize residual interactions between the sites. Intuitively, by elongating the unit cell the interaction energies between two diagonal ports approach the interaction energies between two ports on its long side. This achieves a high quality factor $\mathcal{Q} \approx 99.1\% < 1$. Again, there are not sufficient DOFs in the detunings to apply theorem V to achieve ground state degeneracy because the language is a γ-square (of $L_{\texttt{FMSI-3}}$).
It arises the question whether there exists a structure with degenerate ground states which we simply are not able to find numerically. This is discussed in app. 5.B.2. Here we summarize the main result:

> It is impossible to achieve a perfect quality factor $\mathcal{Q} = 1$ for the VdW-minimal realization `FMUI-3` in any symmetric implementation.

Again, the assumption for a symmetric implementation is legitimized numerically as we find that breaking the D_2-symmetry does not help to improve the quality factor.

To elongate the unit cell the detuning of the central ancillary is suppressed which decreases the effective gap $\Delta E_{\text{eff}} \approx 0.4\%$. In app. 5.B.2 we add implementation `FMU-3ii` with a larger effective gap at the cost of a smaller quality factor. Here the unit cell is less elongated which causes stronger residual interactions. Interestingly the detunings seem somewhat inverted compared to the `FMU-3i` unit cell because the detuning of the central ancillary is now significantly larger.

D3-symmetric Unit Cells. We would not expect such an elongation of the unit cell to be optimal in a tessellated structure as here the honeycomb grid is D_3-symmetric. Thus we add implementation `FMU-3iii` in app. 5.B.2. Here we constrain the parameter space only allowing for D_3-symmetric sites. This impedes the quality factor $\mathcal{Q} \approx 88.4\%$. Note that this quality is still significantly larger than for the `FMUI-2ii` unit cell. It is interesting to note that for the VdW-minimal `FMU-3iii` unit cell with D_3-symmetric sites tessellated on the hexagonal honeycomb grid there would be precisely one ancillary centered on every site and one port centered on every edge in-between the sites.

| Appendix

5.A | Surface Code Unit Cells

This first section of the appendix is dedicated to the surface code. In subsec. 5.A.1 we proof that the `SCUI` unit cells from sec. 5.1 possess a finite ground state splitting for every symmetric structure. We continue presenting further implementations of the `SCUI` unit cells in subsec. 5.A.2. Finally, in subsec. 5.A.3 we proof the non-existence of two-dimensional `SC` unit cells with one ancillary.

For the FIBONACCI model we refer to the second sec. 5.B of this appendix.

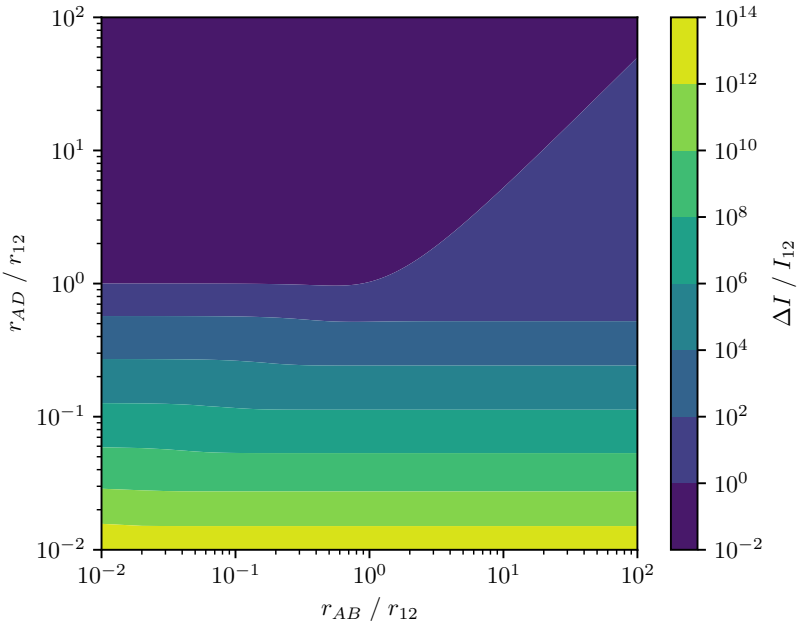

Figure 5.7: The measure ΔI as a function of the parameters r_{AB} and r_{AD}. We measure in units of I_{12} and r_{12}. Note that the graph remains positive in the full parameter space.

5.A.1 | Finite Energy Splitting of the SC-I Unit Cells

In the following we show that:

> For any D_2-symmetric implementation of the realization `SCUI-1`, `SCUI-2a` and `SCUI-2b`, we can not achieve a vanishing energy splitting and therefore only an imperfect quality $\mathcal{Q} < 1$.

The assumption about symmetry is legitimized via intensive numerical optimization because we find that breaking the symmetries does not help to improve the quality factor.

Proof 10. (Finite Energy Splitting)

In general we use the labeling of ports and ancillaries as in fig. 5.1 and 5.2 with one exception: To parallel the labeling of the ancillaries in realizations `2a,b`, we relabel in realization `1` the ancillaries

$$3, 6 \qquad \mapsto \qquad 1, 2$$

respectively. Here we do not need to define new labels for the remaining ancillaries as we are

only going to consider the ground states $\boldsymbol{x}_1, \boldsymbol{x}_2, \boldsymbol{x}_7$ and $\boldsymbol{x}_8$ where none of these ancillaries are excited.

As mentioned above, we assume that the unit-cell is D_2-symmetric to reduce the number of DOFs. The ports construct a rectangle of side lengths r_{AD} and r_{AB}. The diagonal is denoted by r_{AC}.

To achieve a vanishing energy splitting, each ground state $\boldsymbol{x} \in \mathcal{G}$ should be of the same energy. In the following we consider the ground states $\boldsymbol{x}_1, \boldsymbol{x}_2, \boldsymbol{x}_7$ and $\boldsymbol{x}_8$. Then in particular it should be

$$\texttt{(1)} \quad E(|1,1,0,0;1,0,1\rangle) + E(|0,0,1,1;1,1,0\rangle) \stackrel{!}{=} E(|1,1,1,1;1,0,0\rangle) + E(|0,0,0,0;1,1,1\rangle),$$

$$\texttt{(2a)} \quad E(|1,1,0,0;1,0,1\rangle) + E(|0,0,1,1;1,1,0\rangle) \stackrel{!}{=} E(|1,1,1,1;1,0,0\rangle) + E(|0,0,0,0;1,1,1\rangle),$$

$$\texttt{(2b)} \quad E(|1,1,0,0;0,0,1\rangle) + E(|0,0,1,1;0,1,0\rangle) \stackrel{!}{=} E(|1,1,1,1;0,0,0\rangle) + E(|0,0,0,0;0,1,1\rangle)$$

for the sum of their energies in realization `1`, `2a` and `2b` respectively. Here for realization `1` for a clearer visualization we left out the remaining ancillaries which are not excited in any of the four ground states anyway. This illustrates the analogy between realization `1` and realization `2a`. Thus we find that the constraint induced for realization `1` and realization `2a` is the same while the constraint for realization `2b` differs as here the ancillary zero is excited in addition in every of the four ground states.

By exploiting the D_2-symmetries, this can be rewritten for all three realizations as the same constraint:

$$4I_{A2} \stackrel{!}{=} 2(I_{AC} + I_{AD}) + I_{12}. \tag{5.18}$$

Here we cancelled all detunings[a] and some interaction energies on both sides. Note that even though the initial ground states differed between realization `2a` and `2b` they yield the same constraint. The interaction energies $I_{AC} = U_{\mathrm{VdW}}(r_{AC})$, $I_{AD} = U_{\mathrm{VdW}}(r_{AD})$ and $I_{12} = U_{\mathrm{VdW}}(r_{12})$ on the right-hand side are functions of the distance between their atoms. *W.l.o.g* we can choose our energy scaling such that $I_{12} = 1$ by applying f_α with $\alpha = |I_{12}|^{-1/6}$, see eq. (2.15). We rewrite $r_{AC}(r_{AB}, r_{AD}) = \sqrt{r_{AB}^2 + r_{AD}^2}$ such that we can choose the two remaining distances r_{AB} and r_{AD} on the right-hand side independently. The interaction energy $I_{A2} = U_{\mathrm{VdW}}(r_{A2})$ on the left-hand side is a function of the distance r_{A2}. We can express the distance $r_{A2}(r_{AB}, r_{AD}) = \sqrt{r_{AB}^2 + (r_{AD} + r_{12})^2}/2|_{r_{12}=C^{1/6}}$ as a function of the distances on the right-hand side.

Now we can simply plug in $r_{AC} = r_{AC}(r_{AB}, r_{AD})$ and $r_{A2} = r_{A2}(r_{AB}, r_{AD})$ in eq. (5.18) and define the measure

$$\Delta I(r_{AB}, r_{AD}) := 2I_{AC}|_{r_{AC}(r_{AB},r_{AD})} + 2I_{AD}|_{r_{AD}} + 1 - 4I_{A2}|_{r_{A2}(r_{AB},r_{AD})}. \tag{5.19}$$

We are interested in the solution space where $\Delta I(r_{AB}, r_{AD}) \stackrel{!}{=} 0$. Fig. 5.7 shows the contour graph of $\Delta I(r_{AB}, r_{AD})$ in logarithmic scaling. It is almost constant in r_{AB} and decays exponentially in r_{AD}. Thus for large r_{AD} our measure ΔI can become very small. However ΔI remains positive and in particular non-zero in the full parameter space. Thus the solution space is empty and $\delta E > 0$ remains positive. This means that for all realizations `SCUI` the quality factor is $\mathcal{Q} < 1$. □

[a] We chose the above equation such that the detunings cancel.

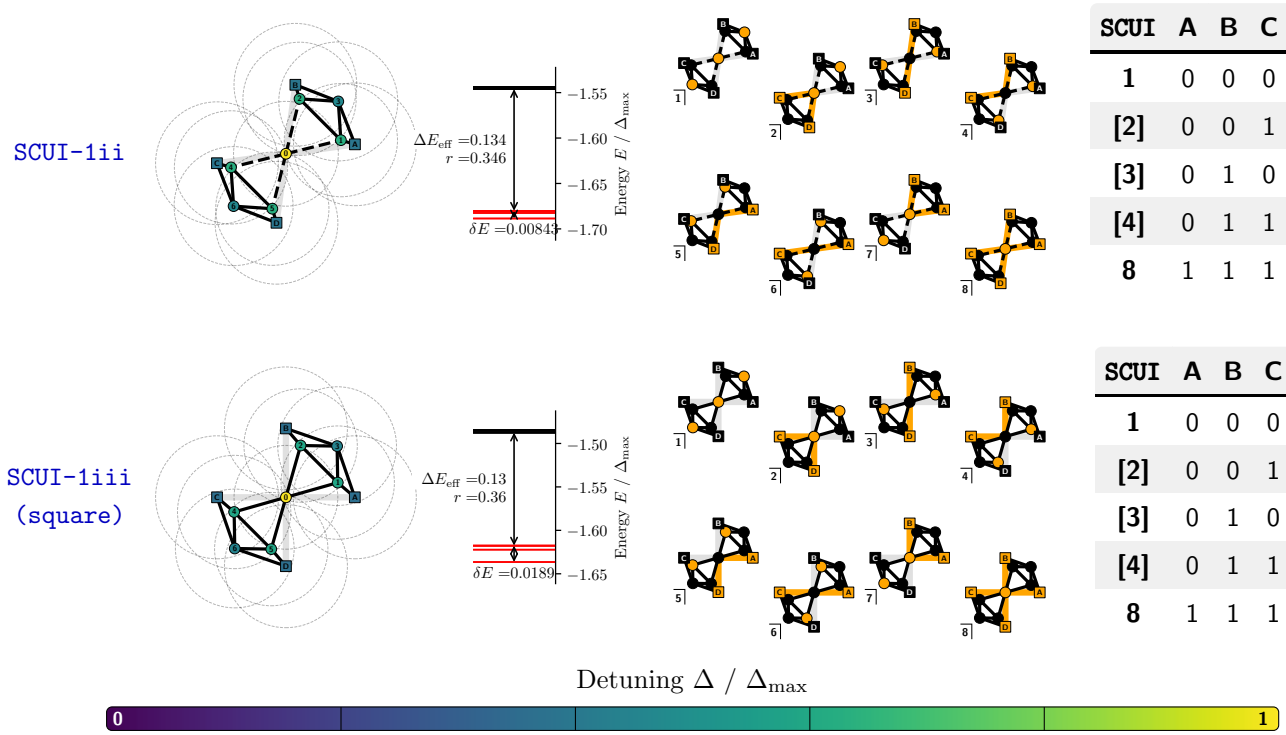

SCUI	A	B	C	D	#
1	0	0	0	0	3
[2]	0	0	1	1	2
[3]	0	1	0	1	2
[4]	0	1	1	0	2
8	1	1	1	1	1

SCUI	A	B	C	D	#
1	0	0	0	0	3
[2]	0	0	1	1	2
[3]	0	1	0	1	2
[4]	0	1	1	0	2
8	1	1	1	1	1

Figure 5.8: PXP-minimal `SCUI-1` unit cells. The tables in the last column portray only the number # of excited ancillaries for a clearer visualization. Implementation `SCUI-1ii` is not optimal but visualizes another local minimum. Implementation `SCUI-1iii` is optimized while constraining the port on a square lattice.

5.A.2 | Additional SC-I Unit Cells

In this subsection we present additional surface code unit cells in representation `I`.

PXP-minimal SCUI-1 Unit-Cells. In fig. 5.8 we present two additional implementations of the PXP-minimal realization `SCUI-1`. The optimized `SCUI-1i` unit cell is presented in fig. 5.1. The `SCUI-1ii` unit cell visualizes a different local minimum of the ratio in parameter space. The `SCUI-1iii` unit cell is optimized while constraining the ports on a square such that they trace-out a square lattice. In the VdW model constraining the implementation to the square grid impedes the quality factor $\mathcal{Q}[\texttt{SCUI-1iii}] \approx 86.5\%$.

For such a square lattice we can arbitrarily choose the orientations of each D_2-symmetric unit cells under tessellation. However in each unit cell only the two diagonal quadrants are occupied by ancillaries. Thus it is quite clear that the translational symmetric choice minimizes residual interaction energies between atoms of adjacent unit cells. Thus this choice might be preferable to maximize the quality of the tessellated structure.

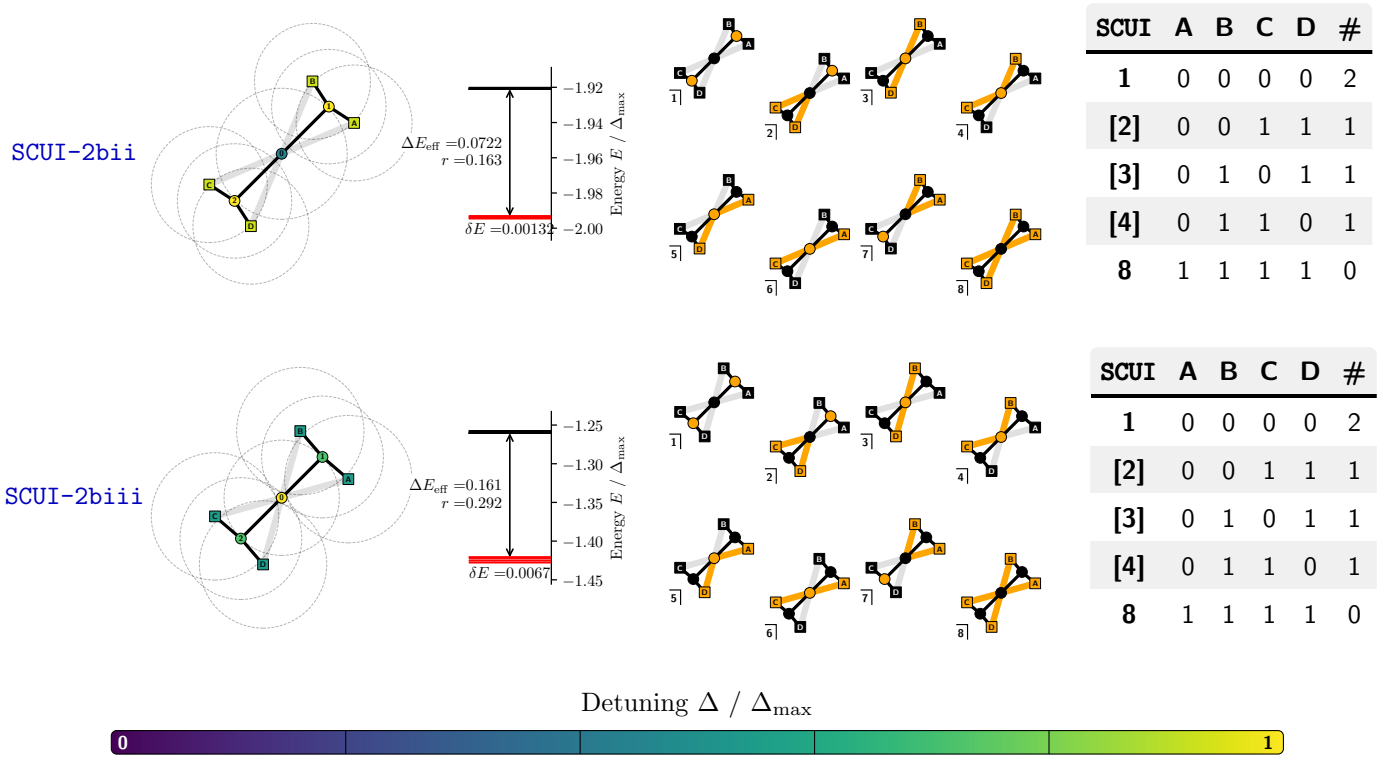

SCUI	A	B	C	D	#
1	0	0	0	0	2
[2]	0	0	1	1	1
[3]	0	1	0	1	1
[4]	0	1	1	0	1
8	1	1	1	1	0

SCUI	A	B	C	D	#
1	0	0	0	0	2
[2]	0	0	1	1	1
[3]	0	1	0	1	1
[4]	0	1	1	0	1
8	1	1	1	1	0

Figure 5.9: Two additional `SCUI-2b` unit cells. The tables in the last column portray only the number # of excited ancillaries for a clearer visualization. The $\mathcal{Q}$-optimized `SCUI-2bi` unit cell is presented in fig. 5.10. Both unit cells presented here posses a larger effective gap at the cost of a reduced quality.

VdW-specific SCUI-2b Unit-Cells. In fig. 5.9 we present two additional implementations of the VdW-specific `SCUI-2b` unit cells. The optimized `SCUI-2bi` unit cell is presented in fig. 5.10. However the `SCUI-2bi` unit cell possesses a significantly smaller effective gap. The quality factor is maximized by 'stretching' the unit cell to suppress residual interactions. This decreases the effective gap is the process. Thus there is a trade-off between optimizing the quality factor and the effective gap. If an experimentalist requires a large effective gap this suggests an implementation of fig. 5.9.

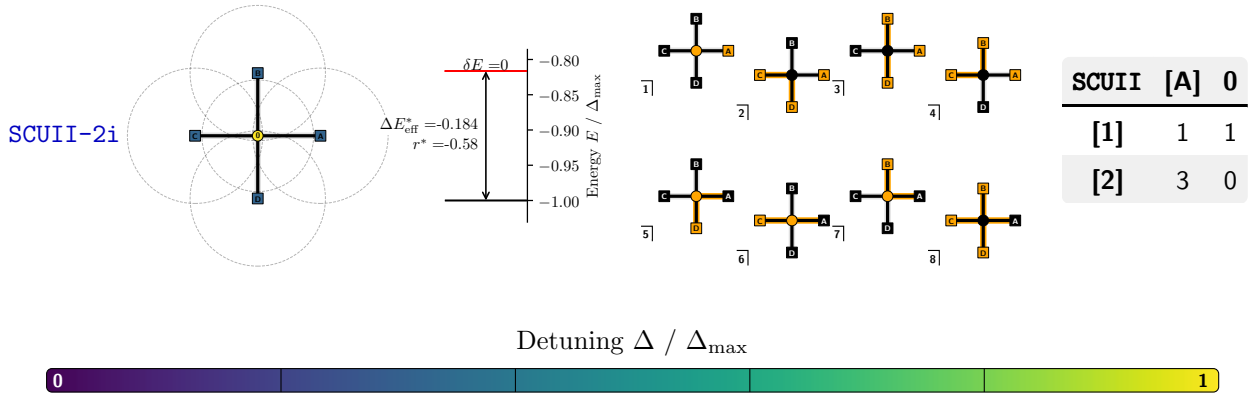

SCUII	[A]	0
[1]	1	1
[2]	3	0

Figure 5.10: Ansatz for a SCII unit cell in $d = 2$ dimensions with one ancillary. The energy gap is negative.

5.A.3 | Impossibility of two-dimensional the SC Unit Cells with one Ancillary

In the following we show that:

> It is impossible to achieve $\mathcal{Q} = 1$ for a Surface Code unit cell unit in $d = 2$ dimensions with only $a = 1$ ancillary.

For representation SCU-I this proven in proof 7. The proof for representation SCU-II needs to include the geometry and thus is more complex. It is based on the fact that any valid unit cell should be C_2-symmetric to allow for tessellation.

Proof 11. (Finite Energy Splitting of SCU-II with one Ancillary)

We use the same labeling as in fig. 5.10. Note that any unit cell must be C_2-symmetric thus $r_{0\mathsf{A}} = r_{0\mathsf{C}}$ and $r_{0\mathsf{B}} = r_{0\mathsf{D}}$. Note that we do not make any assumptions about the detunings. Let $i \in \mathcal{P}$ denote any port of the unit cell. To achieve degeneracy between the states $\boldsymbol{x}_1$, $\boldsymbol{x}_5$, $\boldsymbol{x}_6$ and $\boldsymbol{x}_7$ it must be $\Delta_{\mathfrak{i}} - I_{0\mathfrak{i}} \stackrel{!}{=} \text{const}_{\mathfrak{i}}$. This directly implies that the two opposite atoms each must possess the same detunings: $\Delta_{\mathfrak{i}} = \Delta_{\tilde{\mathfrak{i}}}$. By $\tilde{\mathfrak{i}}$ we denote the port which is projected to port $\mathfrak{i}$ when inverting the unit cell. Similarly, to achieve degeneracy between the states $\boldsymbol{x}_2$, $\boldsymbol{x}_3$, $\boldsymbol{x}_4$ and $\boldsymbol{x}_8$ it must be

$$0 \stackrel{!}{=} \Delta_{\mathfrak{i}} - \sum_{\mathfrak{j} \in \mathcal{P} \setminus \{\mathfrak{i}\}} I_{\mathfrak{j}\mathfrak{i}} - \text{const}_{\mathfrak{i}} = \Delta_{\mathfrak{i}} - I_{\tilde{\mathfrak{i}}\mathfrak{i}} - \text{const}_{\mathfrak{i}} = \Delta_{\mathfrak{i}} - I_{0\mathfrak{i}}/2^6 - \text{const}_{\mathfrak{i}}.$$

Here in both equalities we applied the C_2 symmetry constraint. In the first equality due to the C_2 symmetry the other two interaction energies are constant for all ports and thus can

be pushed into const_i. In the second equality due to the C_2 symmetry the distance $d_{\mathsf{i}\tilde{\mathsf{i}}} = 2d_{0\mathsf{i}}$ is inserted. Thus we obtain $\Delta_\mathsf{i} - I_{0\mathsf{i}}/2^6 \stackrel{!}{=} \text{const}_\mathsf{i}$. By subtracting the first constraint (times $1/2^6$) we obtain $I_{0\mathsf{i}} = \text{const}_\mathsf{i}$ (and $\Delta_\mathsf{i} = \text{const}_\mathsf{i}$). Thus the structure must be D_4-symmetric and we only have two effective ground states.

Now *w.l.o.g.* we choose $\Delta_0 = 1$ for the only ancillary by rescaling the energies by f_α with $\alpha = \Delta_0^{-1/6}$, see eq. (2.15). The detunings $\Delta_\mathsf{i} = (\Delta_0 + I_{\mathsf{AC}} + 2I_{\mathsf{AB}} - I_{0\mathsf{A}})/2$ of the ports $\mathsf{i} \in \mathcal{P}$ are fixed to achieve degeneracy between the two effective states. This reduces the number of DOFs to only one: the radius $r_{0\mathsf{A}}$ of the ports which also fixes the distances between the ports. However the energy gap $\Delta E < 0$ remains negative for all choices of $r_{0\mathsf{A}}$. This can be understood as follows: We can choose $r_{0\mathsf{A}} = [C(1 + 2^{-2} + 2^{-6})/2]^{1/6} =: r$ which maximizes the (negative) effective gap and the robustness simultaneously. This optimal implementation is portrayed in fig. 5.10. Here the LESs $(\bar{4}_\mathsf{A}, 0_0)$ and $(\bar{0}_\mathsf{A}, 1_0)$ where all ports are (not) excited are of equal energy. If we would choose $r_{0\mathsf{A}} > r$ then the LES $(\bar{4}_\mathsf{A}, 0_0)$ would energetically fall faster than any ground state thus further decreasing the energy gap. Similarly, if we would choose $r_{0\mathsf{A}} < r$ then the ground states would energetically rise faster than the LES $(\bar{0}_\mathsf{A}, 1_0)$ (which would not change energetically) thus further decreasing the energy gap. Because the energy gap in fig. 5.10 is negative and because every modification of the structure further decreases the energy gap, the energy gap of every structure (without energy splitting) must be negative. □

The assumptions about the vanishing energy splitting only seems to be useful for the calculation to reduce the number of DOFs. Numerically we find that the energy gap $\Delta E < 0$ is always negative even if we allow a finite energy splitting. For a rigorous proof in the D_4-symmetric case we could proceed similarly as proof 10: In the D_4-symmetric case we only have only two DOFs in the structure. This would allow us to construct a contour plot of the energy gap.

As the energy gap of two-dimensional structures seems to be necessarily negative, in subsec. 5.1.4 we study the `SCUII-1` unit cell with $a = 2$ ancillaries in $d = 2$ dimensions. If we allow for a *quasiplanar* structure in $d = 3$ dimensions where the ancillary may be placed outside the plane of the ports this adds an additional DOF. Then we can actually achieve a perfect quality factor $\mathcal{Q} = 1$ (i.e. and in particular a positive energy gap) with only one ancillary. This is studied in chap. 8.

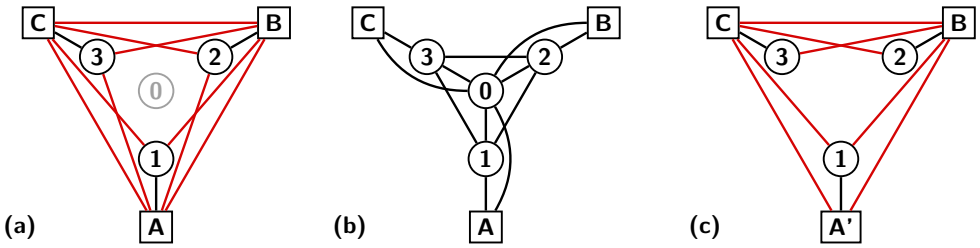

Figure 5.11: Sketch of the blockade graph. Ports are drawn as squares, ancillaries are drawn as circles. **(a)** `FMS-I`-site with three or four ancillaries. Black edges have to be in the blockade graph (the atoms are in blockade), red edges can not be in the blockade graph (the atoms are not in blockade). Edges which are not drawn are not yet determined to be (not) in the blockade graph. **(b)** Non-planar blockade graph of realization `FMSI-2`. **(c)** `FMS-II`-site with three ancillaries. Again, black edges have to be in the blockade graph, green edges can not be in the blockade graph.

5.B | Fibonacci Model Elementaries

This second section of the appendix is dedicated to the FIBONACCI model. In subsec. 5.B.1 we proof that the `FMSI-2` site from subsec. 5.2.2 is PXP-minimal and that it is unique in the sense that it is the only PXP-minimal structure. We continue in subsec. 5.B.2 by proving that the `FMI-2` and `FMI-3` unit cells from subsec. 5.2.2 and 5.2.3 possess a finite ground state splitting for every symmetric structure. Lastly, in subsec. 5.B.3 we present further implementations of the `FMI-2` and `FMI-3` unit cells from subsec. 5.2.2 and 5.2.3.

For the surface code we refer to the first sec. 5.A of this appendix.

5.B.1 | Minimality and Uniqueness for the FMSI-2 Site

As portrayed in fig. 5.5 we found a more atom-efficient PXP-realization compared to realization `FMSI-1` introduced in Ref. [38]. Thus naturally it arises the question whether this realization is PXP-minimal and whether it is the only PXP-minimal realization. In the following we show that:

1 | Realization `FMSI-2` is PXP-minimal for representation `FM-I`.

2 | It is the *only* PXP-minimal realization of representation `FM-I`.

Proof 12. (Uniqueness and Minimality of the FMSI1-site)

Consider representation I with check function f_c[FMSI]. It includes the state where all three ports are excited. We label the ports as A, B and C in the following. Thus no two ports may be in blockade with each other. Further f_c[FMSI] includes the three words where two ports $\mathfrak{j}, \mathfrak{k} \in \mathcal{P}$ are excited but one port $\mathfrak{i} \in \mathcal{P}$ is not excited. For each of these words to be a MIS there needs to exist one excited ancillary $i \in \mathcal{A}$ which is in blockade with port $\mathfrak{i}$ but not in blockades with ports $\mathfrak{j}, \mathfrak{k} \in \mathcal{P}$. Thus we need three ancillaries 1, 2 and 3 where each one is in blockade with exactly one port A, B and C. This is summarized in sketch 5.11a. In the following we only consider blockade graphs of this form.
Lets assume that we only have these three ancillaries 1, 2 and 3 (i.e. we ignore the grayed-out ancillary 0 in fig. 5.11a). Then each port is in blockade with precisely one atom. In the ground state with no excited ports, the ports can only be blocked if all of the three ancillaries are excited simultaneously. This fully defines the language:

$$L_{\texttt{FMSI}^*} = \{(0,0,0;1,1,1),(0,1,1;1,0,0),(1,0,1;0,1,0),(1,1,0;0,0,1),(1,1,1;0,0,0)\}$$

Here the labeling is such that the first three bits are mapped to the ports A, B, C while latter three bits are mapped to the ancillaries 0, 1, 2 respectively. In particular no two ancillaries can be in blockade with each other. This fully defines the blockade graph. The language factorizes in the product of three primitive NOT1-languages and the corresponding blockade graph is disconnected. Such an blockade graph obviously can not realize the language as all three ports are independent.
Thus we need at least four ancillaries (this was already proven in Ref. [38]) which makes the realization FMSI-2 PXP-minimal. As we are only interested in PXP-minimal realizations, in the following we consider the case of four ancillaries. We label the additional ancillary as 0. It is drawn grayish in fig. 5.11a. Remember that the three ancillaries 1, 2 and 3 are in blockade with precisely one port each and that any two ports can not be in blockade with each other. Thus every port is only in blockade with at least one but at most two atoms/ ancillaries. In the following we distinct these two cases:

1 | Consider the case where each port is in blockade with two ancillaries: Then the ancillary 0 needs to be in blockade with all three ports. Hence it can only be excited in the ground state where no ports are excited. In the remaining ground states there are two or three ports excited. To achieve degeneracy between these ground states the detunings $\Delta_A = \Delta_1$, $\Delta_B = \Delta_2$, $\Delta_C = \Delta_3$ must be pairwise equal. To gap-out the excited states where two ancillaries and one port is excited, any two ancillaries need to be in blockade. This fully defines the blockade graph of realization FMSI-2 in fig. 5.11b.

2 | Now we consider we three remaining cases where three, two or one ports are connected to only one ancillary each:

a | Consider the case where all *three* ports are connected to only one ancillary each. Then the language is the γ-product of *three* primitive NOT1-languages multiplied with a kernel language of four-bit words. The kernel language is of the form FMS-IV and possesses only one ancillary bit. In this language some ground state would be a subword of another ground state. This makes it impossible to implement in the PXP model.

b | Consider the case where *two* ports are connected to only one ancillary each. This language is the γ-product of *two* primitive NOT1-languages multiplied with a kernel

language of five-bit words. The kernel language is of the form `FMS-III` and possesses two ancillary bits. It includes the three words where two ports are excited. However as discussed above to realize these ground states in the PXP model we need three ancillaries where each one is connected to precisely one port. Thus this language is impossible to implement in the PXP model.

c | Lastly, consider the case where *one* port is connected to only one ancillary. *W.l.o.g.* we label this port as A. Then the other two ports B and C are connected to two ancillaries each. This language is the γ-product of *one* primitive `NOT1`-language multiplied with a kernel language of six-bit words. The kernel language is of the form `FMS-II` and possesses three ancillary bits. It possesses three ports A', B and C. It includes the three states where only one port is excited, the state where three ports are excited and the state where the two ports B and C are excited. In latter state there must exist one excited ancillary 1 which is in blockade with port A but not in blockade with the ports B and C. Consider the state where only the port B is excited. There must exist one excited ancillary 3 which in blockade with port C but not in blockade with port B. This can not be ancillary 1 because ancillary 1 is only in blockade with port A but not with the ports B and C. Similarly, in the state where only the port C is excited, there must exist one excited ancillary 2 which in blockade with port B but not in blockade with port C. This is sketched in fig. 5.11c. As there are only three ancillaries, the ports B and C can only connected via a blockade to the ancillaries 2 and 3 respectively but to no other atom. This contradicts the initial assumption that port A is connected to one ancillary but that ports B and C are connected to two ancillaries each.

Thus languages of this form are impossible to implement in the PXP model.

To summarize, we find that realization `FMSI-2` is PXP-minimal and the only PXP-minimal realization in representation `I`. □

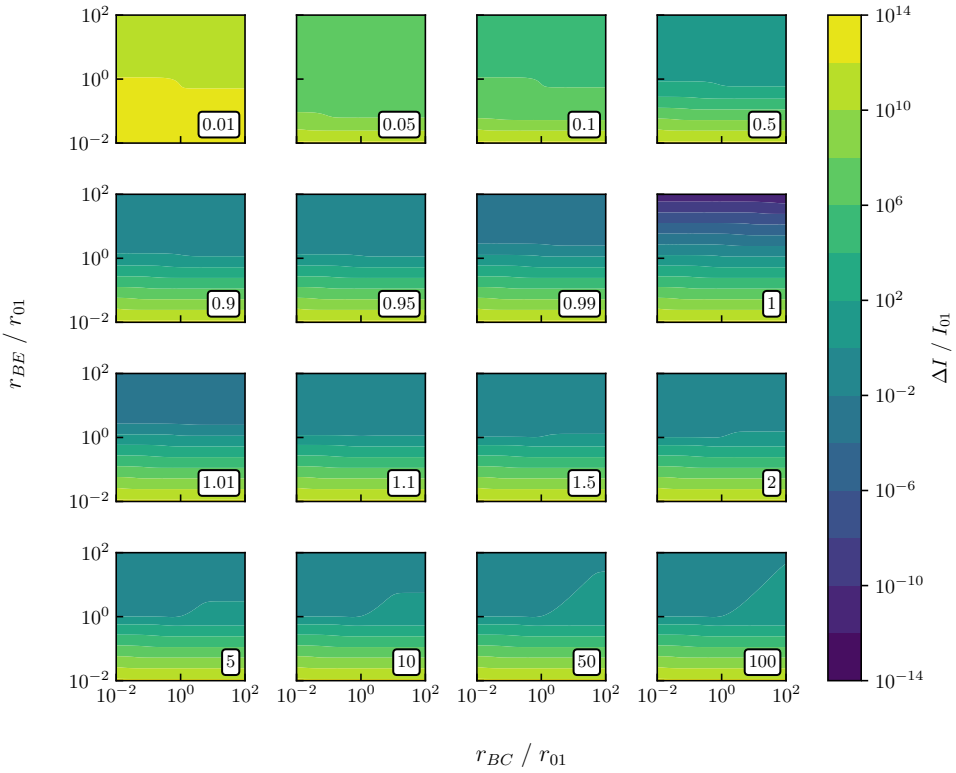

Figure 5.12: The measure ΔI as a function of the parameters r_{BC} and r_{BE}. The inset box is the value r_{23}. We measure in units of I_{01} and r_{01}. Note that the graph remains positive in the full parameter space.

5.B.2 | Finite Energy Splitting of the FMUI Unit Cells

In the following we show that:

> For any D_2-symmetric implementation of the realizations `FMUI-2` and `FMUI-3` we can not achieve a vanishing energy splitting.

This implies in particular that the quality $\mathcal{Q} < 1$ can not be perfect. The assumption about symmetry is legitimized numerically because we find that breaking the symmetries does not help to improve the quality factor.

Note that the following proof is analogous to proof 10 from app. 5.A.1: For `FMUI-2` we are able to recover the same argument as for `SCUI` but for `FMUI-3` we need to consider its additional DOFs. This makes the proof more complex than proof 10.

Proof 13. (Finite Energy Splitting of FMUI Unit Cells)

We follow the labeling of ports as in fig. 5.5 and 5.6. For the ancillaries of realization FMUI-2 we choose a different labeling to parallel the labeling of the ancillaries in realization FMUI-3 and SCUI. We relabel the ancillaries

$$0, 4, 1, 5 \qquad \mapsto \qquad 0, 1, 2, 3$$

respectively. Here we do not need to define a new label for the remaining ancillaries as we are only going to consider the ground states $\boldsymbol{x}_1, \boldsymbol{x}_2, \boldsymbol{x}_3$ and $\boldsymbol{x}_4$ where none of these ancillaries are excited.

As mentioned above, we assume that the unit-cell is D_2-symmetric to reduce the number of DOFs. The ports construct a rectangle of side lengths r_{BC} and r_{BE}. The diagonal is denoted by r_{BD}.

To achieve a vanishing energy splitting, each ground state $\boldsymbol{x} \in \mathcal{G}$ should be of the same energy. In the following we consider the ground states $\boldsymbol{x}_1, \boldsymbol{x}_2, \boldsymbol{x}_3$ and $\boldsymbol{x}_4$. Then in particular it should be

(2) $E(|0,1,1,0,0;0,1,1,0\rangle) + E(|0,0,0,1,1;1,0,0,1\rangle)$
$\stackrel{!}{=} E(|0,1,1,1,1;0,0,1,1\rangle) + E(|0,0,0,0,0;1,1,0,0\rangle),$

(3) $E(|0,1,1,0,0;0,1\rangle) + E(|0,0,0,1,1;1,0\rangle) \stackrel{!}{=} E(|0,1,1,1,1;0,0\rangle) + E(|0,0,0,0,0;1,1\rangle),$

for the sum of their energies in realization 2 and 3 respectively. Here for realization 2 for a clearer visualization we left out the remaining ancillaries which are not excited in any of the four ground states anyway. This illustrates the analogy to realization 3.

By exploiting the D_2-symmetries, this can be rewritten as the constraints:

(2) $$4I_{B1} + 2I_{03} \stackrel{!}{=} 2(I_{BD} + I_{BE}) + I_{01} + 4I_{B3} + I_{23}. \tag{5.20}$$

(3) $$4I_{B1} \stackrel{!}{=} 2(I_{BD} + I_{BE}) + I_{01}. \tag{5.21}$$

Here we cancelled all detunings[a] and some interaction energies on both sides. Note that the second eq. (5.21) is essentially the same constraint as eq. (5.18) only with a different labeling. As proven in app. 5.A.1 we can not fulfill this constraint in the parameter space which completes the proof for the FMUI-3 unit cell.

The proof for the FMUI-2 unit cell is a little more subtle. Here we have additional DOFs in the distance r_{23} which could theoretically help us achieve degeneracy. Thus just like in proof. 10 we rewrite the interactions energies $I_{ij} = U_{VdW}(r_{ij})$ as functions of the variables r_{BC}, r_{BE}, r_{01} and r_{23} by exploiting the D_2-symmetry:

$$r_{BD} = \sqrt{r_{BC}^2 + r_{BE}^2}, \qquad r_{B1} = \sqrt{r_{BC}^2 + (r_{BE} + r_{01})^2}/2,$$
$$r_{03} = (r_{01} + r_{23})/2, \qquad r_{B3} = \sqrt{r_{BC}^2 + (r_{BE} + r_{23})^2}/2.$$

W.l.o.g we can choose our energy scaling such that $I_{01} = 1$ by applying f_α with $\alpha = |I_{01}|^{-1/6}$,

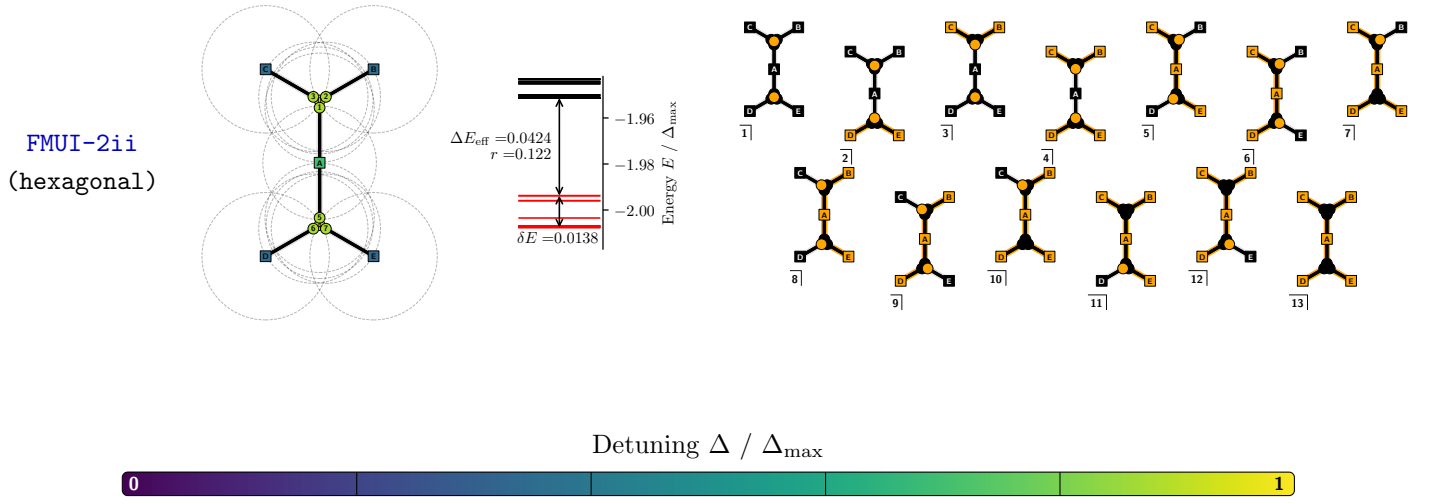

Figure 5.13: PXP-minimal FMUI-2 unit cell. The FMUI-2ii unit cell possesses quality $\mathcal{Q} \approx 72.2\%$. The unit cell is optimized while constraining the D_3-symmetry of the hexagonal honeycomb grid on each site.

see eq. (2.15). We plug in these expressions in eq. (5.20) and define the measure

$$\begin{aligned}\Delta I(r_{BC}, r_{BE}, r_{23}) \; &:= 2I_{BD}|_{r_{BD}(r_{BC},r_{BE})} + 2I_{BE}|_{r_{BE}} + 1 - 4I_{B1}|_{r_{B1}(r_{BC},r_{BE})} \\ &\quad + 4I_{B3}|_{r_{B3}(r_{BC},r_{BE},r_{23})} + I_{23}|_{r_{23}} - 2I_{03}|_{r_{03}(r_{01},r_{23})}.\end{aligned} \tag{5.22}$$

We are interested in the solution space where $\Delta I(r_{BC}, r_{BE}, r_{23}) \overset{!}{=} 0$. Fig. 5.12 shows the contour graph of $\Delta I(r_{BC}, r_{BE})$ in logarithmic scaling for multiple choices of the parameter r_{23}. It is almost constant in r_{BC} and decays exponentially in r_{BE} and r_{23}. The measure ΔI can become very small in parameter small but remains positive and in particular non-zero for the whole parameter space. Note that for $r_{23} = 1 = r_{01}$ the atoms 0 and 1 are at the same positions as the atoms 2 and 3 respectively. This case is unphysical but mathematically many terms in ΔI cancel causing interesting behaviour in the limit.

Thus we find that for both the FMUI-2 and the FMUI-3 unit cell the solution space is empty and $\delta E > 0$ remains positive. This means that for both realizations FMUI-2 and FMUI-3 the quality factor $\mathcal{Q} < 1$ remains smaller one. □

[a] We chose the above equation such that the detunings cancel.

5.B.3 | Additional FMUI Unit Cells

Figures 5.13 and 5.14 portray three additional FMUI unit cells.

Fig. 5.13 presents implementation FMUI-2ii. Implementation FMUI-2ii is optimized for the quality factor while constraining the D_3-symmetry of the underlying honeycomb grid on each site.

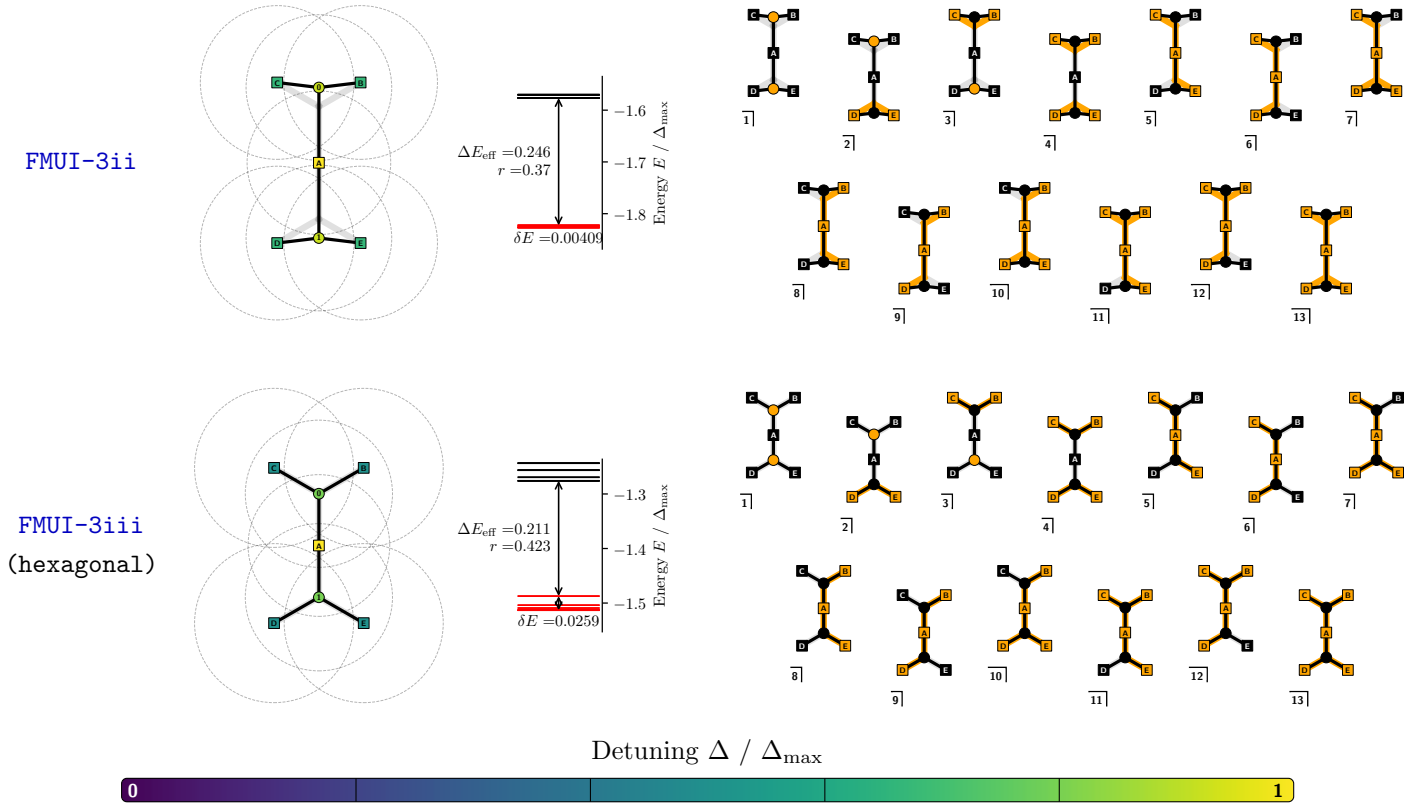

Figure 5.14: VdW-minimal FMUI unit cells. The FMUI-3ii unit cell possesses quality $\mathcal{Q} \approx 98.4\%$ and the FMUI3-iii unit cell possesses quality $\mathcal{Q} \approx 88.4\%$. Implementation FMUI-3ii possesses a larger effective gap $\Delta E_{\text{eff}} \approx 24.6\%$ at the cost of a smaller quality than FMUI-3i. FMUI-3iii is optimized while constraining the D_3-symmetry of the hexagonal honeycomb grid on the structure.

This restricts the parameter space reducing the optimal quality factor to $\mathcal{Q} \approx 72.2\%$. We expect this D_3-symmetric FMUI-2ii site to be more optimal in a D_3-symmetric tessellated structure. Note that the optimized implementation FMUI-2ii emerges not simply by an amalgamation of two optimized FMSI2-implementations.

The first row of fig. 5.14 presents a less elongated version FMUI-3ii of the unit cell compared to implementation FMUI-3i in fig. 5.6. This comes with a larger effective gap $\Delta E_{\text{eff}} \approx 24.6\%$ but at the cost of a smaller quality factor $\mathcal{Q} \approx 98.4\%$ (however this is still very good). Therefore it might be preferable to choose this implementation.

The second row portrays implementation FMUI-3iii. Similar to the FMUI-2ii unit cell it is optimized for the quality factor while constraining the D_3-symmetry of the underlying honeycomb grid on each site. Note that by tessellating this implementation FMUI-3iii on the hexagonal lattice there would be precisely one ancillary centered on every site and one port centered on every edge in-between the sites.

6 | Tessellated Theory

"Equations are just the boring part of mathematics. I attempt to see things in terms of geometry."

– Stephen Hawking, 'A Biography' (2005)

In the previous chap. 5 we introduced and discussed the elementaries of two string-net models: the surface code and the Fibonacci model. In this chapter we want to discuss these models more broadly: We consider non-elementary loop structures and we formulate a key no-go theorem about tessellating loop structures to large scales. Afterwards we consider local excitations on these loop structures. In the following sec. 6.1 we want to start by introducing non-elementary loop-structures.

6.1 | Non-elementary loop Structures

In this section we want to study *non-elementary loop structures* exemplarily with the PXP-minimal `SCUI-1` unit cell. For each structure we consider both *open boundary conditions* (OBCs) and *periodic boundary conditions* (PBCs).

The Energy Structure. The SCUI-1 unit cell consists of 11 atoms, 7 of which are ancillaries. By tessellating a $m \times n$ grid of unit cell we obtain $N \sim 11mn$ atoms and thus $2^N \sim 2^{11mn}$ excited states (up to the number of amalgamations and the number of ground states). The runtime increases exponentially in the total number of atoms N. To optimize the energy structure we would need to calculate the quality factor a *multitude* of times. This makes it computationally very intensive to simulate such tessellated Rydberg structures for the VdW model.

Example 9. **(2×2 SCI-1 Lattice)**

> As an example consider a tessellated SCI-1 structure on a 2×2 grid. This is the minimal structure which includes a *full loop* as a ground state. Here we have already $N = 40$ atoms (36 atoms) with OBCs (with PBCs) implying $e \sim 2^{40}$ ($\sim 2^{36}$) excited states. In contrast there are only $g = 2^8$ (2^5) ground states.

Note that there are way fewer ground states that excited states, thus we can simply 'brute-force' calculate their energies. This defines the energy splitting (2.16) and the energetically highest ground state. Both quantities are necessary to calculate the quality factor (2.19). Thus in the energy structures presented in this thesis we always plot all the ground state energies (red lines).

As discussed in sec. 3.2 we are not interested in the full energy structure of the excited states but only in the energy of its *lowest excited state* (LES). The LES allows for the calculation of the energy gap (2.17) and thus defines the quality factor. In sec. 3.2 we introduce alg. 3.3 which allows for the efficient calculation of the LESs. This allows for the optimization of such tessellated structures with up to *four* SCI-1 unit cells in a reasonable runtime. Without alg. 3.3 it would be computationally too intensive to optimize such loop structures which are presented in this section.

The 1x1-Grid. In the following we consider three grids with $m \times n = 1 \times 1$, 1×2 and 2×2 respectively. Fig. 6.1 presents the SCI-1 unit cell on a 1×1 grid *with PBCs*. For completeness we also included the SCI-1i unit cell with OBCs from fig. 5.1. For clearer visualization (and to reflect the D_2-symmetry) of the SCI-1 unit cell with PBCs, we also portrayed the two ports of the adjacent unit cells (without labels). Due to the PBCs they are excited if and only if their opposite counterpart is excited. Thus the SCI-1 unit cell with PBCs includes *only four ground states* and three effective ground states. As the (effective) ground states are linearly independent we can apply theorem V to achieve *ground state degeneracy* and unit quality $\mathcal{Q} = 1$. Note that this is not possible for OBCs (see app. 5.A.1) and we can not apply theorem V for larger tessellated structures. The unit cell is optimized for the effective gap $\Delta E_{\text{eff}} \approx 8.5\%$. Interestingly the optimized SCI-1 unit cell with PBCs looks very different from the SCI-1 unit cell with OBCs due to the additional residual interactions with its neighboring unit cells.

The unit cell with PBCs simulates the ground states and excited states with fundamental period one[1] on an infinite grid. Its energies correspond to the energy densities of the 1-periodic states on the infinite grid. Note that as we consider only the 1-periodic states, there are no independent loop DOFs and the theorem XI from chap. 6 does not apply. Thus the ground state degeneracy in fig. 6.1 is not that surprising.

[1] In units of the unit cell scaling.

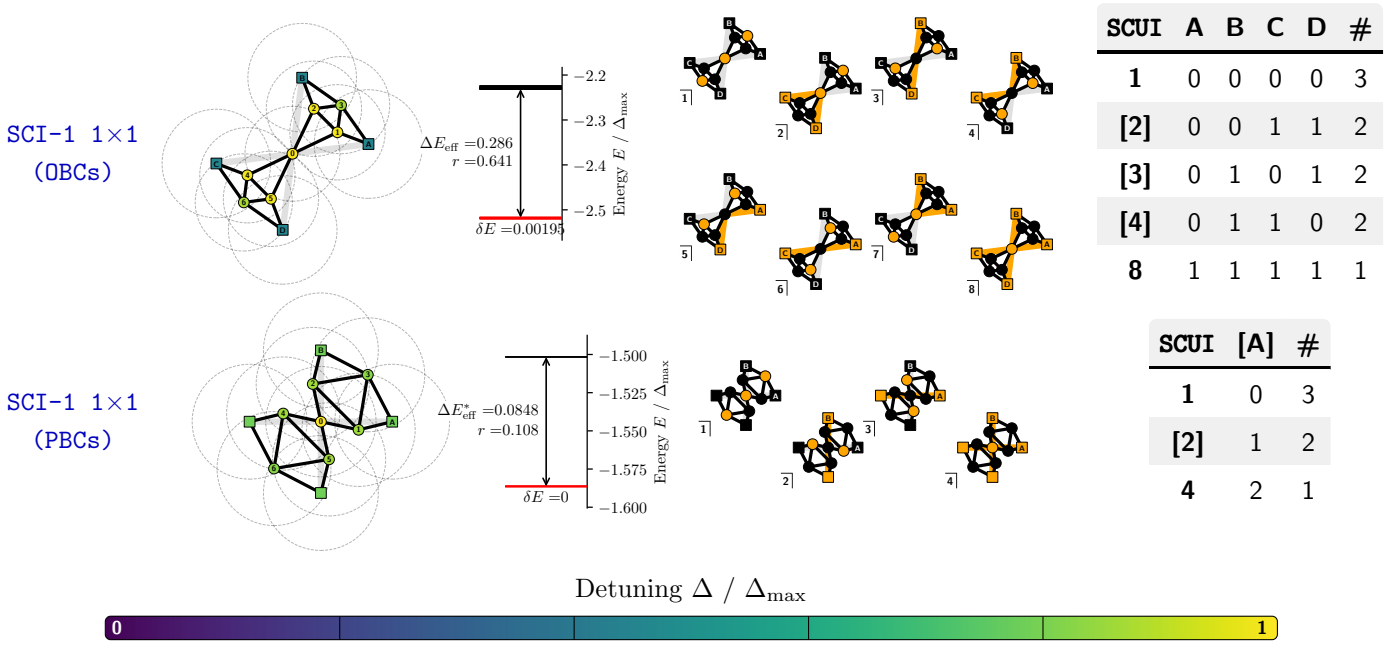

SCUI	A	B	C	D	#
1	0	0	0	0	3
[2]	0	0	1	1	2
[3]	0	1	0	1	2
[4]	0	1	1	0	2
8	1	1	1	1	1

SCUI	[A]	#
1	0	3
[2]	1	2
4	2	1

Figure 6.1: SCI-1 unit cell on a 1×1 grid with OBCs and PBCs respectively. The SCI-1 unit cell with OBCs from the first row is the structure from fig. 5.1. The second row we portrays the SCI-1 unit cell with PBCs. We added two atoms from the adjacent unit cell (without labels) for a clearer visualization. Note that for the SCI-1 unit cell with PBCs we obtain $\mathcal{Q} = 1$, it is optimized for $\Delta E_{\text{eff}} \approx 8.5\%$.

The 1x2-Grid. A natural next step is to consider 1×2 grids of SCI-1 unit cells. This is portrayed in the first two rows of fig. 6.2. Here $g = 2^5$ and $g = 2^3$ for OBCs and PBCs respectively. To optimize such a tessellated 1×2 structure with the minimization algorithm 3.2 it turns out efficient to start with the structure of the smaller 1×1 grid as input. Then the states are energetically clumped into '*bands*' of similar energy. The excited states of the shorter period are already sorted and the ground states of the shorter period are already of similar (or the same) energy. The optimization algorithm only needs to sort and optimize the additional states with the larger fundamental period which is computationally less intensive. The optimization seems to accentuate the energy bands. During the optimization process for the 1×2 grids the ground states energetically *condensate on two levels*. This can be seen in the energy structures in the first two rows of fig. 6.2. If we initially start the optimization process with an arbitrary structure which is not yet optimized such clumping naturally arises. This can be seen in the unit cells of figs. 5.1, 5.2, 5.4, 5.5 and 5.6 where the ground states also seem to condensate on two energy levels during optimization. For the ground state-degenerate logic gates of chap. 4, the ΔE_{eff}-optimal structures are characterized by the LESs condensing on equal energies. Thus the *energetic clumping* of ground states and excited states seems to be a general phenomenon which optimizes the effective gap or the quality factor in (amalgamated) structures throughout this thesis. This is an interesting phenomenon which can not be resolved by the relatively coarse measures $\mathcal{Q}$ and ΔE_{eff} studied in this thesis. The measures $\mathcal{Q}$ and ΔE_{eff} only consider the ground and excited states of extremal energies which can not quantify a clumping of the remaining states.

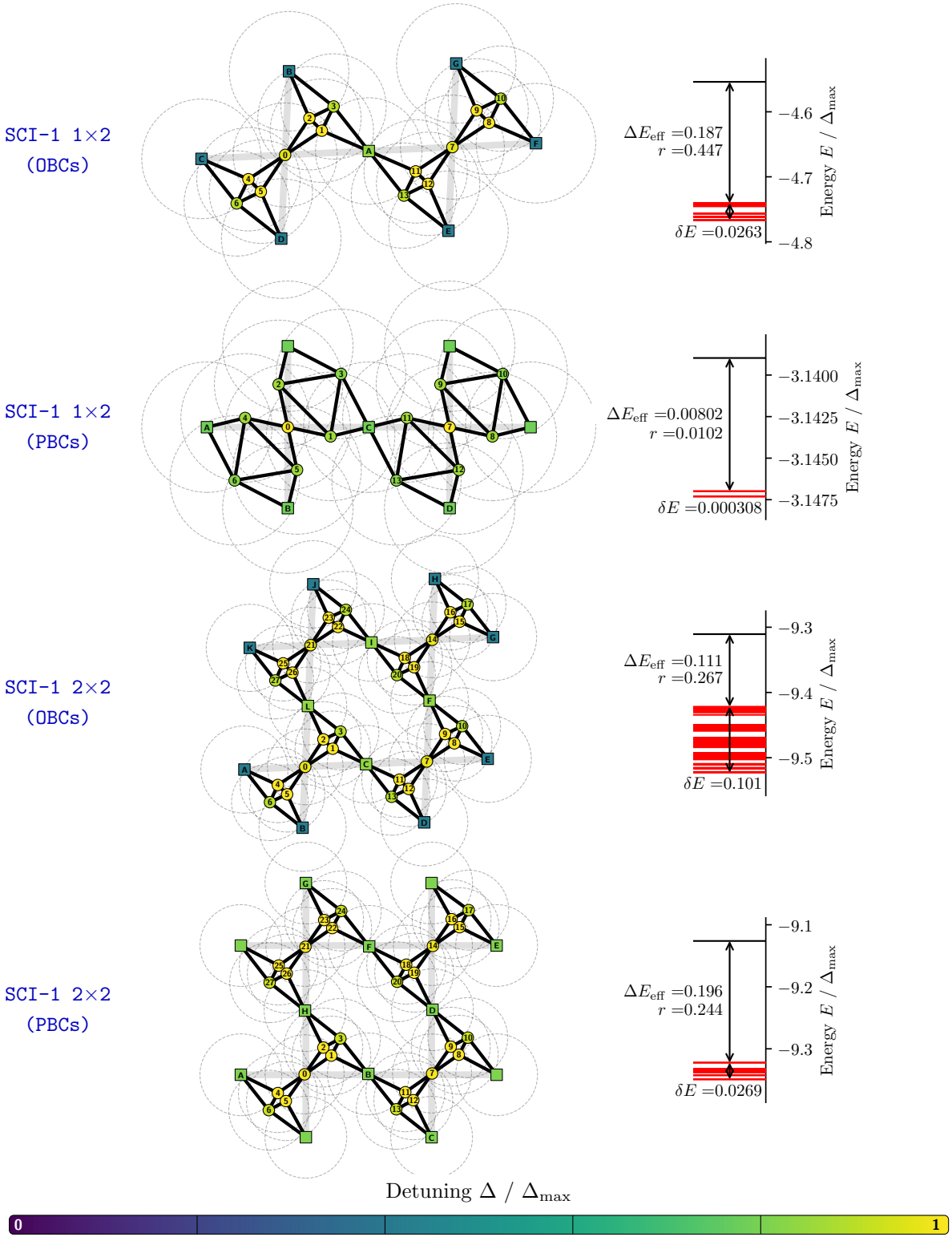

Figure 6.2: `SCI-1` 2×1 and 2×2 grid with OBCs and PBCs respectively. Note that again we added the atoms from the adjacent unit cell (without labels) for a clearer visualization. One can notice a clumping of the ground states in the energy structure.

This suggests that possibly a *finer measure* for such structures is necessary. This leaves room for further studies and is discussed in the outlook 9.

For the optimization of the 1×2 grid (and later for the 2×2 grid) we constrain the unit cells to the same D_2-symmetric structure. This assumption reduces the number of DOFs and thus the runtime. The translational symmetry is reasonable to assume to allow for further tessellation on larger grids. Physically we are mainly interested in large tessellated structures which allow for the excitation of many loops. In the bulk of such a tessellated structure (e.g. with PBCs) the language is translational, inversion and reflection symmetric thus one can reasonably expect identical D_2-symmetric unit cells to be optimal.

The 2x2-Grid. For the optimization of the 2×2 `SCI-1` grid we use the optimized 1×2 grid as input. The 2×2 grids with OBCs and PBCs are presented in the third and fourth row of fig. 6.2 respectively. As mentioned in the example above, the 2×2 grid is particularly interesting as it is the *minimal grid including a full loop*. The case with OBCs is harder to optimize. This may be partly due to the a little larger number of atoms which increases the runtime but mainly due to the larger number of ground states. There are $g = 2^8$ and $g = 2^5$ ground states for OBCs and PBCs respectively. Especially for the 2×2 grid with OBCs we can notice a *strong clumping* of the ground states into multiple bands of states with similar energy. For the 2×2 grid with PBCs it is interesting to note that the unit cells actually looks quite different from the unit cells in the 1×2- and the 1×1-grid with PBCs. This suggests that the 2×2 grid with PBCs is in a different local minimum of the ratio in parameter space.

A choice for Tesselation. At this point it should be noted that we made a(n arbitrary) choice during the amalgamation of the unit cells: To construct the tessellated language as the ground state manifold of a tessellated structure we translated and amalgamated the same D_2-symmetric unit cells of fig. 6.1. These unit cells are slightly skewed because the realization `SCUI-1` breaks the permutation symmetry between the ports in the check function (5.6). In the VdW model the quality factor of the unit cell profits from breaking the rotational symmetry of the underlying grid yielding a non-square centered rectangular grid. In contrast in the PXP model we can implement a rotational symmetric, square grid without modifying the blockade graph[38]. This can be also accomplished in the VdW model at the cost of impeding the quality factor, see in app. 5.A.2 the `SCUI-1iii` unit cell (fig. 5.8). If we consider such a non-D_4-symmetric unit cell for a square grid, then there are *multiple possibilities to tessellate the structure*: each unit cell could be rotated by 90° without modifying the language. This constructs a different structure which implements the same language. In particular within the PXP model such structures are equally valid because the PXP model excludes long-range interactions. Within the VdW model the residual long-range interactions in different implementations are generally different. Here it seems reasonable that the 1-periodic tessellated structure suits best for an implementation of the surface code as it minimizes residual interactions in-between neighboring unit cells. As in each unit cell the atoms are only positioned within two diagonal quadrants, a 1-periodic 'checkerboard-pattern' of such quadrants is the only implementation which prevents adjacent (i.e. strongly-interacting) quadrants. This motivates us to stick to this implementation for this section.

6.2 | On Tessellated Loop Structures

In the previous sec. 6.1 we simulated small, finite `SCI-1` grids with OBCs and with PBCs. We are computationally very limited in the number of atoms which we can simulate because the number of states increases exponentially. This limits the size of the grid which we can study numerically. Nevertheless, we want to make some statements about large tessellated grids which are not accessible computationally. Such large grids are studied in this chapter.

We start with an important and central theorem of this thesis:

Theorem XI (Energy Levels of States with Loop DOFs)**.**

Consider a tessellated L-complex $([\mathcal{C}_\mathcal{L}]^{\mathfrak{Q}}_{\mathcal{K}}, L_\mathcal{L}, \mathfrak{L})$ *on a grid* $\mathcal{L}$ *in the VdW-model. For any tessellated language* $L_\mathcal{L}$ *with loop-DOFs, the energy splitting* $\delta E \to \infty$ *diverges and the effective gap* $\Delta E_{\mathit{eff}} \to -\infty$ *is negative and diverges.*

Proof.

Consider the state where no port is excited and tessellate it on the periodic grid $\mathcal{L}$ with $V \to \infty$. In the following, this state of the tessellated language with no loops is denoted by $|0\rangle \in L_\mathcal{L}$. We define a one-loop state $|1\rangle \in L_\mathcal{L}$, where just one loop is excited. Similarly, we define a two-loop state $|2\rangle \in L_\mathcal{L}$, where two *non-adjacent*[a] loops are excited. We start with some short comments on the notation used in the following calculation:

1 | By E_{loop} (E_{noloop}) we denote the 'self-energy' of a loop-cell (of a no-loop-cell). This includes its detunings and its internal interactions. It excludes interactions with the surrounding grid, i.e. it considers the loop in empty space.

2 | By $I_{\text{loop,noloops}}$ ($I_{\text{noloop,noloops}}$), we denote the interaction energy of a loop-cell (of a no-loop-cell) with the surrounding grid (which has no loops).

3 | Lastly, by $I_{\text{loop,loop}}$ ($I_{\text{noloop,noloop}}$, $I_{\text{loop,noloop}}$) we denote the interaction energy of a loop-cell (no-loop-cell, loop-cell) with some other loop-cell (no-loop-cell, no-loop-cell) of the surrounding grid.

We measure the energies relative to $E_0 \equiv E(|0\rangle)$. We obtain the relative energies of the states

$$\Delta E_0 = E_0 - E_0 = 0, \tag{6.1a}$$
$$\Delta E_1 = E(|1\rangle) - E_0 = E_{\text{loop}} - E_{\text{noloop}} + I_{\text{loop,noloops}} - I_{\text{noloop,noloops}} =: -\Delta, \tag{6.1b}$$
$$\begin{aligned}\Delta E_2 &= E(|2\rangle) - E_0 \\ &= -2\Delta + (I_{\text{loop,loop}} + I_{\text{noloop,noloop}} - 2I_{\text{loop,noloop}}) =: -2\Delta + I,\end{aligned} \tag{6.1c}$$

Each loop state $|n\rangle$ for $n \in \{0, 1, 2\}$ needs to possess equal energy to obtain a vanishing energy splitting $\delta E = 0$, thus $\Delta E_2 = \Delta E_1 = \Delta E_0 = 0$. Then the linear system (6.1) implies that $\Delta = 0 = I$, i.e.

$$\Delta = 0 \quad \Leftrightarrow \quad E_{\text{loop}} + I_{\text{loop,noloops}} = E_{\text{noloop}} + I_{\text{noloop,noloops}}, \tag{6.2a}$$
$$I = 0 \quad \Leftrightarrow \quad I_{\text{loop,loop}} + I_{\text{noloop,noloop}} = 2I_{\text{loop,noloop}}. \tag{6.2b}$$

Note that eq. (6.2b) is a constraint on the interaction energies and thus on the geometry of the structure but it includes no detunings. Furthermore eq. (6.2b) needs to be fulfilled for all possible distances between the two cells.

We denote the set of atoms in a cell excited during a loop as $\mathcal{N}_{\text{loop}}$ and the set of atoms excited if there is no loop as $\mathcal{N}_{\text{noloop}}$. Depending on the representation any port $\mathfrak{p} \in \mathcal{P}$ is excited (not excited) if and only if its edge is excited. Thus the ports $\mathfrak{p} \in \mathcal{P}$ are either elements of $\mathcal{N}_{\text{loop}}$ or of $\mathcal{N}_{\text{noloop}}$ but can not be elements of both sets. The set of ports $\mathcal{P} \subseteq \mathcal{N}_{\text{loop}} \triangle \mathcal{N}_{\text{noloop}}$ of the cell needs to be a subset of the symmetric difference. We choose two cells which are next-nearest neighbours and denote the vector between those cells as $\boldsymbol{x}_1$. The vector $\boldsymbol{x}_n = n\boldsymbol{x}_1$ with $n \in \mathbb{N}$ points to another cell due to translational invariance. W.l.o.g. we choose the x-axis of our coordinate system parallel to $\boldsymbol{x}_1$, i.e. $\boldsymbol{e}_x \parallel \boldsymbol{x}_1$. We can rephrase eq. (6.2b) as

$$\begin{aligned}\sum_{\mathfrak{i},\mathfrak{j}\in\mathcal{N}_{\text{loop}}} \|x\boldsymbol{e}_x + \boldsymbol{r}_\mathfrak{i} - \boldsymbol{r}_\mathfrak{j}\|^{-6} + \sum_{\mathfrak{i},\mathfrak{j}\in\mathcal{N}_{\text{noloop}}} \|x\boldsymbol{e}_x + \boldsymbol{r}_\mathfrak{i} - \boldsymbol{r}_\mathfrak{j}\|^{-6} \\ \overset{\substack{x=x_n \\ n\in\mathbb{N}}}{=} 2 \sum_{\mathfrak{i}\in\mathcal{N}_{\text{loop}}} \sum_{\mathfrak{j}\in\mathcal{N}_{\text{noloop}}} \|x\boldsymbol{e}_x + \boldsymbol{r}_\mathfrak{i} - \boldsymbol{r}_\mathfrak{j}\|^{-6}.\end{aligned} \tag{6.3}$$

Here $\boldsymbol{r}_\mathfrak{i}$ for $\mathfrak{i} \in \mathcal{N}_{\text{loop}}$ ($\mathfrak{i} \in \mathcal{N}_{\text{noloop}}$) denotes the position of the $\mathfrak{i}$-th atom in the (no)loop. Both sides of eq. (6.3) are rational functions on $x \in \mathbb{R}$ which have to be equal for a countably infinite number of points $x_n = nx_1 \in$ for $n \in \mathbb{N}$. This is only possible if both sides are the same rational function[b]. Two rational functions (without any polynomial part) are equal if and only if their poles have the same position and are of equal amplitude. In particular the sum of the amplitudes on both sides must be equal, thus

$$|\mathcal{N}_{\text{loop}}|^2 + |\mathcal{N}_{\text{noloop}}|^2 \overset{!}{=} 2|\mathcal{N}_{\text{loop}}||\mathcal{N}_{\text{noloop}}| \quad \Leftrightarrow \quad |\mathcal{N}_{\text{loop}}| = |\mathcal{N}_{\text{noloop}}|. \tag{6.4}$$

We find that the number of atoms excited in a loop and without a loop must be equal; we denote it by N^*.

In any physical case, two different atoms $\mathfrak{i}, \mathfrak{j} \in \mathcal{N}_{\text{loop}} \cup \mathcal{N}_{\text{noloop}}$ with $\mathfrak{i} \neq \mathfrak{j}$ should not occupy the same position, i.e. $\boldsymbol{r}_\mathfrak{i} \neq \boldsymbol{r}_\mathfrak{j}$. Thus the left side has a pole at $x = 0$ of amplitude $2N^*$. The right side should have the same pole of the same amplitude. However, this means that there are N^*

atoms $\mathfrak{i} \in \mathcal{N}_{\text{loop}}$ occupying the same position $\boldsymbol{r}_\mathfrak{i} = \boldsymbol{r}_\mathfrak{j}$ as an atom in $\mathfrak{j} \in \mathcal{N}_{\text{noloop}}$; they must be the same atoms. As there are only N^* atoms in $\mathcal{N}_{\text{loop}}$ and $\mathcal{N}_{\text{noloop}}$ (by definition), it is $\mathcal{N}_{\text{loop}} = \mathcal{N}_{\text{noloop}}$. However this would imply that their symmetric divergence $\mathcal{N}_{\text{loop}} \triangle \mathcal{N}_{\text{noloop}} = \emptyset$ is empty. This contradicts the above observation that $\emptyset \neq \mathcal{P} \subseteq \mathcal{N}_{\text{loop}} \triangle \mathcal{N}_{\text{noloop}}$. Thus the two sets $\mathcal{N}_{\text{loop}}$ and $\mathcal{N}_{\text{noloop}}$ can not be equal and therefore eq. (6.2b) has no solution. However eq. (6.2b) is *necessary* condition for a vanishing energy splitting $\delta E = 0$ of the states of the language $L_\mathcal{L}$. Therefore we always have $\delta E > 0$.

Now assume that $I = \varepsilon \neq 0$, possibly small but non-zero[c]. Then $\Delta = \varepsilon/2$ minimizes the energy splitting $\delta E_\mathcal{L} \geq |\varepsilon|/2$[d] for the states $|n\rangle$ with $n \in \{0, 1, 2\}$. We consider $N_L \in \mathbb{N}$ of such n-loop states which are sufficiently distant from each other such that their interactions may be neglected. This is possible as for large distances any interaction between the atoms of both cells decays as the potential decays. The relative energy of such a ground state is then given by $\Delta E_n(N_L) = N_L \Delta E_n$ with ΔE_n given by eq. (6.1). With $I = \varepsilon \neq 0$ finite, the energy splitting $\delta E_\mathcal{L}(N_L) \geq N_L|\varepsilon|/2$ again is minimized for $\Delta = \varepsilon/2$. We find that the energy splitting diverges for configurations with $N_L \to \infty$.
Consider the energetically lowest state $|\boldsymbol{x}\rangle \in L_\mathcal{L}$ of the tessellated language $L_\mathcal{L}$. We choose one arbitrary site and construct a state $|\boldsymbol{x}^*\rangle \in \mathbb{F}_2^N \backslash L_\mathcal{L}$ by de-exciting and exciting some atoms (including amalgamated ports) of this site. As any two different atoms are in different positions, the energy of the constructed state $|\boldsymbol{x}^*\rangle$ is shifted from the energy of $|\boldsymbol{x}\rangle$ by some finite difference. However the energy splitting $\delta E_\mathcal{L}(N_L)$ between $|\boldsymbol{x}\rangle$ and the energetically highest state of $L_\mathcal{L}$ diverges for $N_L \to \infty$. Thus the constructed state $|\boldsymbol{x}^*\rangle \in \mathbb{F}_2^N \backslash L_\mathcal{L}$ is of (infinitely) lower energy than the energetically highest state of $L_\mathcal{L}$. Thus we have a diverging energy splitting $\delta E_\mathcal{L} \to \infty$ between the states of $L_\mathcal{L}$ and a negative diverging energy gap $\Delta E_\mathcal{L} \to -\infty$. □

[a] No unit cell should be part of both loops.

[b] This can be seen by multiplying each side by every denominator to obtain a polynomial on both sides. Both polynomials possess the same values at countably infinite number of points, thus they must be the same polynomial. Hence the rational functions on both sides must have been the same function.

[c] Note that it can be $I < 0$ and $\Delta < 0$. This is not ill-defined as Δ and I are a mesoscopic quantities composed of differences in detunings and interaction energies.

[d] For $\Delta = I/2$ it is $\Delta E_0 = \Delta E_2 = 0$ and $\Delta E_1 = -I/2$, i.e. $\delta E_\mathcal{L} = |I|/2$. Consider $\Delta = I/2 > (<) 0$: By decreasing (increasing) Δ, $\Delta E_2 = -2\Delta + I \propto -2\Delta$ increases (decreases) faster than $\Delta E_1 = -\Delta$, i.e. $\delta E > I/2$. By increasing (decreasing) Δ, $\Delta E_1 = -\Delta$ decreases (increases) faster than $\Delta E_0 = 0$, i.e. $\delta E > I/2$.

The intuition behind the Argument. We shortly want to summarize the argument of the proof in an intuitive way: In a nutshell we interpret loops as *independent local excitations* for which we can associate some *mesoscopic 'self-energy'* Δ and some *mesoscopic interaction energy* I. We find that such independent BOOLEAN DOFs can only be degenerate if their self-energy and their interaction energy vanishes. The interaction energy is independent of the detunings thus $I = 0$ imposes a *constraint on the geometry*. In a periodic structure the interaction energy must vanish for all possible distances between the loops. However I is a non-trivial function of the distance and we only have finitely many DOFs in the geometry of the unit cell. Thus we find that the I only vanishes for all possible distances if the loop-state is the same state as the no-loop-state. Obviously we do not want them to be the exactly same state which implies that we *can not achieve degeneracy* in the ground states. By tessellating such loop states on the (infinitely) large grid we sum up their energy splittings and obtain an (infinitely) large energy splitting: $\delta E \nearrow \infty$. The LES is at most by $\Delta_{\max}$ energetically higher than the energetically lowest ground state thus for large tessellated structures the energy gap must be (infinitely) negative: $\Delta E \searrow -\infty$.

Some concluding Remarks. We conclude theorem XI with a few remarks:

1 | Theorem XI is *valid for all loop models* and thus in particular for the FIBONACCI model and the surface code. Thus the (infinite) FIBONACCI model and the (infinite) surface code both are exemplary systems which can be implemented in the PXP model but which can not be implemented in the VdW-model for any L-complex. Here the finite residual interaction energies cause *qualitatively different physics*. Further examples of PXP-languages which can not be implemented perfectly in the VdW model are the `SCUI-1,2a,2b` and the `FMUI-2,3` unit cells which are discussed in the appendices 5.A.1 and 5.B.2.

2 | The argument behind theorem XI is *very general*. Thus theorem XI can be generalized to any tessellated system with any *independent* BOOLEAN DOFs in the ground state manifold. This result can be understood intuitively: For any tessellated system with independent BOOLEAN DOFs we have $\sim 2^p$ ground states but only $\sim \text{poly}(p)$ DOFs in the structure of the unit cell. This prevents from achieving a sufficiently small energy splitting to 'sort' the excited states.

3 | Furthermore, theorem XI can be generalized to any model with *algebraically decaying interactions* (e.g. to γ-model with power-law potential) following similar reasoning: Then $I(x_n)$ is a general algebraic function of the distance x_n between the loops. Any algebraic function is either *aperiodic or constant*. Then the condition $I(x_n) = 0$ for countably infinite $n \in \mathbb{N}$ implies again that the mesoscopic interaction energy $I = 0$ must vanish (is constant) and we can continue like for the VdW-case for $\gamma = 6$.

4 | The theorem XI remains valid if one considers only the physically relevant *excitations in some local environment* of the grid. The proof of theorem XI considers the global *ground* states of the tessellated structure and derives their *energy splitting*. However the local energy gap is still upper bounded by $\Delta_{\max}$. Thus the (infinitely) large energy splitting still causes a(n infinitely) large negative energy gap.

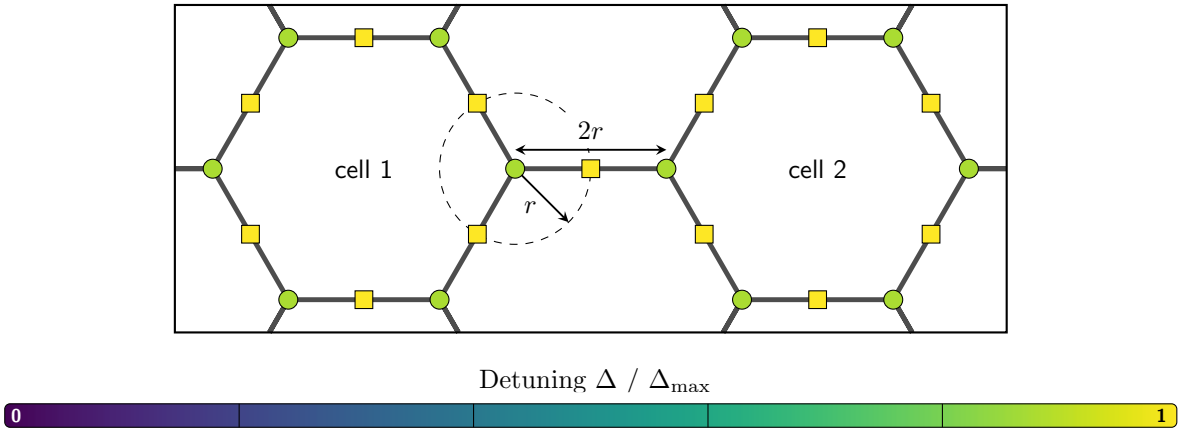

Figure 6.3: Hexagonal FIBONACCI model grid with hexagonal cells 1 and 2. The length scale of the cells is $2r$ where r is the radius of each site.

Example 10. (Energy Splitting of the Fibonacci Model)

For an illustrative example of theorem XI and the mesoscopic interaction energies we consider the FIBONACCI model. We want to calculate a lower bound on the mesoscopic loop interaction energy $I = \varepsilon$ from eq. (6.1) in the VdW-model. We consider the (simple) D_3-symmetric `FMSI3`-site from fig. 5.6 and we amalgamate adjacent sites directly without adding interstitial `LNK`-gates on the edges: $N_E = 0$. A section of this structure is visualized in the sketch 6.3. We choose two hexagonal cells which are next-nearest neighbors such that their unit cells do not overlap and linear system (6.1) is valid. Numerically[18] we find

$$I \geq \frac{C}{(2r)^6}(\underbrace{0.306872}_{I_{\text{loop,loop}}} + \underbrace{0.390862}_{I_{\text{noloop,noloop}}} - 2 \cdot \underbrace{0.327425}_{I_{\text{loop,noloop}}}) = 0.042884\frac{C}{(2r)^6}. \tag{6.5}$$

Here r denotes the radius of the `FMSI3` site and thus $2r$ the length scale of the hexagonal cells. In the optimal `FMSI3` site from fig. 5.6 it is $r/r_{\min} = 3^{-1/3}$ which yields $I \geq 0.4523\%\Delta_{\max}$. Considering that we only included two cells of the grid, this is actually quite large because we assumed no interstitial `LNK`-gates.

6.3 | A lower bound on the Quality Factor

In the previous section we showed that we can not implement the surface code or the FIBONACCI model on arbitrarily large grids, even if we consider only local excitations. Depending on the size of the system there seems to be a general upper bound to the quality factor for all systems with loop-DOFs. Therefore naturally the analogous question arises how good of a quality factor we can achieve (as a function of the size of the grid). In sec. 6.1 we implemented the surface code grid with one loop. In this section we want to study larger tessellated structures which are not accessible via a numerical simulation. We start by introducing lemma XII (subsec. 6.3.1) which is necessary to formulate lemma XIII (subsec. 6.3.2). Finally in subsec. 6.3.3 we formulate theorem XIV.

6.3.1 | A Chain of Atoms

By $\mathcal{C}_{N_E}$ we denote a chain of $N = N_E + 1$ equidistant atoms where the ports (at the boundary) and ancillaries (in the bulk) possess equal detunings Δ and $\tilde{\Delta}$ respectively. The distance between adjacent atoms is denoted by a, the length of $\mathcal{C}_{N_E}$ is denoted by $d = N_E a$. We define the language $L_{N_E} := L_{\texttt{NOT1}}^{\otimes_\gamma N_E}$. We can formulate lemma XII:

Lemma XII (N_E-Chain of arbitrary Length)**.**

The language L_{N_E} can be implemented as the low-energy eigenspace of a structure $\mathcal{C}_{N_E}$ with quality factor $\mathcal{Q} = 1$, robustness $r \gtrsim 91.23\%$ and effective energy gap $\Delta E_{eff} \gtrsim 46.66\%$ for any $N_E \in \mathbb{N}$.

First we want to emphasize that the lower bound introduced in lemma XII is valid *for all number of links* $N_E \in \mathbb{N}$, i.e. in particular for $N_E \nearrow \infty$. If the number of links $N_E = 2m-1$ with $m \in \mathbb{N}$ is *odd* the L-complex implements a $\texttt{NOT}m$-gate in realization m. If the number of links $N_E = 2m$ with $m \in \mathbb{N}$ is *even* the L-complex implements a $\texttt{LNK}m$-gate in realization m. In the following we unify the notion of both gates as N_E-chains $([\mathcal{C}_{N_E}]_{\{\texttt{A}\}}^{\{\texttt{Q}\}}, L_{N_E}, \mathfrak{L})$ with $N = N_E + 1$ atoms.

The Proof. The proof of lemma XII is noted and discussed in app. 6.A.1. Here were only want to give an short overview and mention a few important points. The proof is *constructive* and formulates an algorithm which generates N_E-chains of arbitrary length. In the proof we derive a *lower bound* to the energy gap independent of N_E. Then we choose the parameters of $\mathcal{C}_{N_E}$ such that the ground states become degenerate and such that the lower bound becomes maximal. Afterwards in app. 6.A.1 we introduce and discuss exemplary four N_E-chains with $N_E \in \{1, 2, 9, 10\}$ links for $m = 1$ and $m = 5$. They are portrayed in fig. 6.11. We find that

the lower bound derived in the proof is *very tight* for large N_E. Note that $\Delta E_{\text{eff}} \gtrsim 46.66\%$ and $r \gtrsim 91.23\%$ of the N_E-chains are exceptionally large compared to other gates in the VdW model because the linear geometry of the N_E-chains maximizes the distance between non-adjacent atoms which minimizes residual interactions. As a comparison, in the PXP model such a chain trivially possesses $\Delta E_{\text{eff}}|_{\text{PXP}} = 50\%$ and $r|_{\text{PXP}} = 1$.

6.3.2 | Appendage of atomic Chains

In the following we want to apply lemma XII to derive lemma XIII. We consider a kernel structure $\mathcal{C}_k$ of N_k atoms and some uniform language L_k of N_k bits. We assume that the atoms of $\mathcal{C}_k$ are placed inside some *circular area* of radius r with $p_k \leq 4$ ports spaced equally around the circumference. One could think of any D_{p_k}-symmetric site of a tessellated language, for example the `FMSI-3` site with $p_k = 3$.
We define the structure $\mathcal{C}_{k\cup N_E}$ where a N_E-chain $\mathcal{C}_{N_E}$ is amalgamated radially to each port of $\mathcal{C}_k$. In the following we assume that $\mathcal{C}_{k\cup N_E}$ implements the γ-product $L_{k\cup N_E} = L_k \otimes_\gamma L_{N_E}^{\otimes_\gamma p_k}$ as its low-energy eigenspace with $\mathcal{Q}[\mathcal{C}_{k\cup N_E}] = 1$. Here each γ associates one port bit of L_k with the input port bit of one L_{N_E}.

Now we consider a N'_E-chain with structure $\mathcal{C}_{N'_E}$ constructed from lemma XII with equal distances $a' = a$ between the atoms. We can now formulate lemma XIII:

Lemma XIII (Appendage of N_E-Chains)**.**

We assume that the energy gap of the amalgamated structure $\mathcal{C}_{k\cup N_E}$ fulfills the condition

$$0 < \Delta E_{lb}(N_E) := \min\left(\Delta E[\mathcal{C}_{k\cup N_E}],\ 20\frac{C}{(2a)^6}\right) - \frac{C}{(2a)^6}\left[2\zeta(5)P + \left(1 + \|\mathbf{L}_k^+\|_1 \frac{|L_k|}{2}\right) \times \frac{P(P-1)}{(N_E+1)^4}\left(4.8 + \frac{25.6 + 6.4N_k/(P-1)}{N_E+1} + \frac{65.3 + 110.7N_k/(P-1)}{(N_E+1)^2}\right)\right]. \tag{6.6}$$

Then $\mathcal{C}_{k\cup(N_E+N'_E)}$ implements $L_{k\cup(N_E+N'_E)}$ as its low-energy eigenspace with $\mathcal{Q}[\mathcal{C}_{k\cup(N_E+N'_E)}] = 1$ for any $N'_E \in \mathbb{N}_0$. The energy gap is $\Delta E[\mathcal{C}_{k\cup(N_E+N'_E)}] \geq \Delta E_{lb}(N_E)$.

First note that for essentially *every relevant case* it is $\Delta E[\mathcal{C}_{k\cup N_E}] < 20C/(2a)^6 \lesssim \Delta E[\mathcal{C}_{N'_E}]$ because the energy gap of a N'_E-chain is exceptionally large compared to other gates in the VdW model (see subsec. 6.3.1). This means the min(•)-term of ΔE_{lb} generally evaluates as $\Delta E[\mathcal{C}_{k\cup N_E}]$.

In a nutshell lemma XIII argues that one can amalgamate a N'_E-chain for any $N'_E \in \mathbb{N}_0$ to every port of $\mathcal{C}_{k\cup N_E}$ and still achieve $\mathcal{Q} = 1$ if the energy gap $\Delta E[\mathcal{C}_{k\cup N_E}]$ of the initial kernel structure is sufficiently large. The energy gap after amalgamation is lower-bounded by $\Delta E_{\text{lb}}(N_E)$. The proof of this lemma is quite straightforward: the idea is to determine an upper-bound to the interactions energies which distort the energy structure. This requires evaluating multiple series. This makes the proof lengthy, hence we note it in app. 6.A.2.

6.3.3 | Tessellated Languages on the Honeycomb Grid

Given lemma XIII we now focus on the main theorem XIV of this section.

The Formalism. Consider a honeycomb grid of $S = |\mathcal{S}(\mathcal{L})| = 2V$ sites $s \in \mathcal{S}(\mathcal{L})$ on a hexagonal lattice $\mathcal{L}$ with $V = |\mathcal{V}(\mathcal{L})|$ vertices $v \in \mathcal{V}(\mathcal{L})$. With each site $s \in \mathcal{S}(\mathcal{L})$ we want to associate an identical structure $\mathcal{C}_s$ of N_s atoms and some uniform language L_s of N_s bits. The atoms of $\mathcal{C}_s$ are placed inside some circular area of radius r with $p_s = 3$ ports spaced equally around its circumference.
The amalgamated structure $\mathcal{C}_{s\cup N_E}$ is constructed by radially amalgamating N_E-chains $\mathcal{C}_{N_E}$ with an *even* number of links $N_E = 2m$ for $m \in \mathbb{N}$ to each port. In the following we assume that $\mathcal{C}_{s\cup N_E}$ implements the language $L_{s\cup N_E} = L_s \otimes L_{N_E}^{\otimes_\gamma 3}$ as its low-energy eigenspace with $\mathcal{Q}[\mathcal{C}_{s\cup N_E}] = 1$. The tessellated structure $\mathcal{C}_\mathcal{L}$ is constructed by amalgamating the sites *at their full edge*[2]. The tessellated language is denoted by $L_\mathcal{L} = L_{s\cup N_E}^{\otimes_\gamma S}$.
By $N_A(s)$ we denote the number of amalgamated edges which connect site s with another site $s' \in \mathcal{S}(\mathcal{L})$, i.e. the number of edges in the bulk emanating from site s[3]. As a useful mathematical construct we define the local Hamiltonian $H_{\text{loc}}[\mathcal{C}_{s\cup N_E}] := H[\mathcal{C}_{s\cup N_E}] - H_{\text{sr}}[\mathcal{C}_{s\cup N_E}]/2$. The 'short-range' Hamiltonian $H_{\text{sr}}[\mathcal{C}_{s\cup N_E}]$ corresponds to the second term (the correction term) of the interaction Hamiltonian (2.14). It includes only the interactions between the atoms of *the same edge* which connects site s with another site $s' \in \mathcal{S}(\mathcal{L})$. Thus in $H_{\text{sr}}[\mathcal{C}_{s\cup N_E}]$ the atoms of $N_A(s)$ edges contribute.

The Theorem. With this formalism we can now formulate the following theorem:

Theorem XIV (Tessellated Languages on the Honeycomb-Grid)**.**
We assume that the local energy gaps fulfill the condition

$$0 < \Delta E_\infty := \min_{N_A \in \{1,\dots p_s\}} \left\{ \min\left(\Delta E_{loc}[\mathcal{C}_{s\cup N_E^{(0)}}],\ 10\frac{C}{(2a)^6} \right) - \frac{C}{(2a)^6} \left[2\zeta(5)P - \zeta(5)N_A + \left(1 + \|\mathbf{L}_s^+\|_1 \frac{|L_s|}{2}\right) \frac{P(P-1)}{(N_E^{(0)}+1)^4} \left(4.8 + \frac{25.6 + 6.4N_s/(P-1)}{N_E^{(0)}+1} + \frac{65.3 + 110.7N_s/(P-1)}{(N_E^{(0)}+1)^2} \right) \right] \right\} \tag{6.7}$$

for some $N_E^{(0)} \in \mathbb{N}_0$. Then for any target $\mathcal{Q}_t \in \mathbb{R}_{(0,1)}$ and any size S of the grid there exists a $N_E^* \in \mathbb{N}$ such that for all $N_E \geq N_E^*$ the quality factor is $\mathcal{Q}[\mathcal{C}_\mathcal{L}] > \mathcal{Q}_t$.

This means that there is a balance between the size $S = 2V$ of the grid, the number of links N_E in the chain between adjacent sites and the quality factor $\mathcal{Q}[\mathcal{C}_\mathcal{L}]$ of the tessellated grid. To achieve the target $\mathcal{Q}[\mathcal{C}_\mathcal{L}] > \mathcal{Q}_t$, the ratio S/N_E^4 needs to be sufficiently small. This means that:

> *Twice* the number of links between adjacent sites can achieve the same quality factor for a lattice of (at least) *16-times* the size.

[2] That is why we assumed that $N_E = 2m$ for $m \in \mathbb{N}$ is even.
[3] For PBCs every site is in the bulk of the tessellated structure thus it necessarily is $N_A = p_s = 3$

There is an *interplay* between the size of the grid S, the number of links N_E between sites and the quality factor $\mathcal{Q}[\mathcal{C}_\mathcal{L}]$. We can also interpret theorem XIV differently:

> For some fixed implementation $\mathcal{C}_{s\cup N_E}$ of the sites (with fixed $N_E < \infty$) we can formulate an *upper bound to the number of sites* S below which we can achieve the target quality factor $\mathcal{Q}[\mathcal{C}_\mathcal{L}] > \mathcal{Q}_t$.

The theorem XIV does not make any statements for larger tessellated structures. In fact we expect that the bound is not that sharp as the derivation requires a lot of approximations. In particular we do not specify a language for theorem XIV but only the underlying grid. Thus the results are more of conceptual than of quantitative interest: They describe the correct qualitative behavior and they offer an estimate for the orders of magnitude.

The idea behind theorem XIV can be transferred straightforwardly to other grids, but this requires evaluating different series in the proof. This yields a quantitatively different condition (6.7) in theorem XIV. In this thesis we exemplary restrict ourselves to the honeycomb grid.

Note that theorem XIV (of course) does not contradict the results from theorem XI: In theorem XI we also consider some fixed implementation $\mathcal{C}_{s\cup N_E}$ and consider the limit $S/N_E^4 \nearrow \infty$. In theorem XIV for this limit, the lower bound on the energy gap diverges to negative infinity consistent with theorem XI.

The Proof. The proof of theorem XIV is very lengthy as it includes the evaluation of multiple series, thus we note it in app. 6.A.3. We shortly want to summarize the main ideas of the proof: As already mentioned above we *amalgamate the full edge* and we introduce the concept of the *local Hamiltonian*. This allows us to treat the tessellated structure similarly to the PXP model as the sum of its parts with some additional *perturbation Hamiltonian* $H_{\text{lr}}[\mathcal{C}_\mathcal{L}]$. Without the perturbation term the low-energy eigenspace would be degenerate and the energy gap would be given by the minimal local energy gap of the sites. The perturbation term introduces a finite energy splitting and may reduce the energy gap. Thus we determine an *upper bound to the perturbation* term which monotonically decreases as S/N_E^4. To determine a lower bound to the local energy gaps (which now depend on $N_A(s)$) we need to apply some modified version of lemma XIII. This introduces condition (6.7) in theorem XIV. If condition (6.7) is fulfilled we can arbitrarily suppress the perturbation term by increasing the number of links N_E.

Example 11. (Fibonacci Model Grid)

We want to conclude this subsection with an illustrative example. We consider the FIBONACCI model site with $p_s = 3$ ports and $|L_s| = 5$ ground states. For realization `FMSI-3` (see fig. 5.6) we have $\|\mathbf{L}_s^+\|_1 = 10/7$. In the following we assume $N_E^{(0)} = 4$, then we obtain the lower bound $\Delta E[\mathcal{C}_{s\cup(N_E^{(0)}+N_E)}] > 5.7\%\Delta E[\mathcal{C}_{s\cup N_E^{(0)}}]$ for any $N_E \in \mathbb{N}$ similar to lemma XIII.

1 | If we choose $S = 100$ sites for $N_E = 8$, then we have $\mathcal{Q}[\mathcal{C}_\mathcal{L}] > 48.9\%$.

2 | For $S = 1000$ sites, we need $N_E = 14$ to obtain $\mathcal{Q}[\mathcal{C}_\mathcal{L}] > 46.44\%$.

6.4 | Local Languages on the Honeycomb Grid

In the previous sections of this chapter we studied the possibilities and the limits for implementing tessellated languages with loop-DOFs in the VdW model.
In sec. 6.2 we proved it impossible to implement (infinitely) large tessellated languages with loop-DOFs on very general ground. Afterwards we shortly argued that this argument also holds in the case where we only consider locally excited states. However the reasoning of theorem XI yields only a *qualitative statement* for (infinitely) large grids but makes no statements about the *interplay* between the size S of the grid, the number of links N_E between sites and the quality factor $\mathcal{Q}$.
In sec. 6.3 we answered the analogous question how good of a quality factor we are able to achieve. For that we exemplary focused on the honeycomb-grid. For the honeycomb-grid we made *quantitative statements about the interplay* between S, N_E and $\mathcal{Q}$.

6.4.1 | The local Energy Structure

In this section we are interested in the *local energy structure*, i.e. we want to compare only the states which differ locally on the Rydberg platform. This can be understood an the logical continuation of global languages (with locally excited states).

Locality is characterized by some 'support' on the Rydberg platform. For simplicity we consider a *circular support* $\mathcal{U}_{\text{loc}}(R)$ defined by some radius $R \in \mathbb{R}_{>0}$. The area of $\mathcal{U}_{\text{loc}}(R)$ is denoted by $A_{\text{loc}}(R) := |\mathcal{U}_{\text{loc}}(R)| = \pi R^2$. The number of atoms located in $\mathcal{U}_{\text{loc}}(R)$ is denoted by N_R, the total number of atoms is denoted by N. We define the *local language*/ the *local ground state manifold*

$$L_R(\boldsymbol{x}) \equiv \mathcal{G}_R(\boldsymbol{x}) := \left\{ \tilde{\boldsymbol{x}} \in \mathcal{G} \mid \forall_{\boldsymbol{r}_{\mathfrak{L}(i)} \notin \mathcal{U}_R(\boldsymbol{x})} : \ \tilde{x}_i = x_i \right\} \subseteq \mathcal{G}, \tag{6.8}$$

and similarly the *local excited state manifold*

$$\mathcal{E}_R(\boldsymbol{x}) := \left\{ \tilde{\boldsymbol{x}} \in \mathcal{E} \mid \forall_{\boldsymbol{r}_{\mathfrak{L}(i)} \notin \mathcal{U}_R(\boldsymbol{x})} : \ \tilde{x}_i = x_i \right\} \subseteq \mathcal{E}. \tag{6.9}$$

The argument $\boldsymbol{x}$ fixes some arbitrary state $|\boldsymbol{x}\rangle$ as 'background' outside of the local environment. Thus $\mathcal{G}_R(\boldsymbol{x})$ and $\mathcal{E}_R(\boldsymbol{x})$ are languages with a 'large' number N of bits which differ only within the 'small' local support of N_R bits.

For the local energy structure we now want to define our *measures of quality*. We associate the *local energy splitting*

$$\delta E_R[\mathcal{C}_\mathcal{L}] := \max_{\boldsymbol{x}\in\mathcal{G}} \delta E[\mathcal{C}_\mathcal{L}]|_{\mathcal{G}_R(\boldsymbol{x})} = \max_{\boldsymbol{x}\in\mathcal{G}} \left[\max_{\tilde{\boldsymbol{x}}\in\mathcal{G}_R(\boldsymbol{x})} E(|\tilde{\boldsymbol{x}}\rangle) - \min_{\tilde{\boldsymbol{x}}\in\mathcal{G}_R(\boldsymbol{x})} E(|\tilde{\boldsymbol{x}}\rangle) \right]. \tag{6.10}$$

Similarly we define the *local energy gap*

$$\Delta E_R[\mathcal{C}_\mathcal{L}] := \min_{\boldsymbol{x}\in\mathcal{G}} \Delta E[\mathcal{C}_\mathcal{L}]\Big|_{\substack{\mathcal{G}_R(\boldsymbol{x})\\ \mathcal{E}_R(\boldsymbol{x})}} = \min_{\boldsymbol{x}\in\mathcal{G}} \left[\min_{\tilde{\boldsymbol{x}}\in\mathcal{E}_R(\boldsymbol{x})} E(|\tilde{\boldsymbol{x}}\rangle) - \max_{\tilde{\boldsymbol{x}}\in\mathcal{G}_R(\boldsymbol{x})} E(|\tilde{\boldsymbol{x}}\rangle) \right]. \tag{6.11}$$

Note that we restrict ourselves to $\boldsymbol{x} \in \mathcal{G}$ such that $\mathcal{G}_R(\boldsymbol{x}) \neq \emptyset$. Thus $\tilde{\boldsymbol{x}} \in \mathcal{E}_R(\boldsymbol{x})$ are locally excited states which are only excited on the support of the local language. Intuitively we now associate the *local ratio* $Q_R[\mathcal{C}_\mathcal{L}] = \delta E_R[\mathcal{C}_\mathcal{L}]/\Delta E_R[\mathcal{C}_\mathcal{L}]$ which defines the *local quality factor*

$$\mathcal{Q}_R[\mathcal{C}_\mathcal{L}] = \Theta(Q_R[\mathcal{C}_\mathcal{L}]) \exp\left(-Q_R[\mathcal{C}_\mathcal{L}]\right). \tag{6.12}$$

6.4.2 | A lower Bound on the Honeycomb Grid

As in subsec. 6.3 we consider in the following a tessellated *honeycomb grid* on the hexagonal lattice $\mathcal{L}$. We continue with the notation introduced in the previous sections. The relevant quantities are sketched in fig. 6.4. The goal is to make quantitative statements about the interplay between the R, N_E and $\mathcal{Q}$. We formulate corollary XV:

Corollary XV (Lower Bounds to local Languages on the Honeycomb Grid)**.**
We assume that the local energy gaps fulfill the condition

$$\begin{aligned}\Delta E_\infty := \min\Big(\Delta E_{loc}[\mathcal{C}_{s\cup N_E^{(0)}}],\ 10\frac{C}{(2a)^6} \Big) - \frac{C}{(2a)^6}\Bigg[(2P-3)\zeta(5) + \left(1 + \|\mathbf{L}_s^+\|_1 \frac{|L_s|}{2}\right) \\ \times \frac{P(P-1)}{(N_E^{(0)}+1)^4} \left(4.8 + \frac{25.6 + 6.4N_s/(P-1)}{N_E^{(0)}+1} + \frac{65.3 + 110.7N_s/(P-1)}{(N_E^{(0)}+1)^2} \right) \Bigg] > 0\end{aligned} \tag{6.13}$$

for some $N_E^{(0)} \in \mathbb{N}_0$. Then for any target $\mathcal{Q}_t \in \mathbb{R}_{(0,1)}$ and any radius R of $\mathcal{U}_{loc}(R)$ there exists a $N_E^* \in \mathbb{N}$ such that for all $N_E \geq N_E^*$ the local quality factor is $\mathcal{Q}_R[\mathcal{C}_\mathcal{L}] > \mathcal{Q}_t$.

We denote this statement only the rank of a corollary because it can be essentially reduced to theorem XIV. Corollary XV essentially argues that the local energy structure on a local environment with S_{loc} sites behaves similarly to the energy structure of $S = S_{\text{loc}}$ sites. There is an interplay between the size $S_{\text{loc}}(R)$ of the local environment, the number of links in the N_E-chain between adjacent sites and the local quality factor $\mathcal{Q}_R[\mathcal{C}_\mathcal{L}]$. To achieve the target $\mathcal{Q}_R[\mathcal{C}_\mathcal{L}] > \mathcal{Q}_t$ the ratio R/lN_E^2 needs to be sufficiently small. This means that:

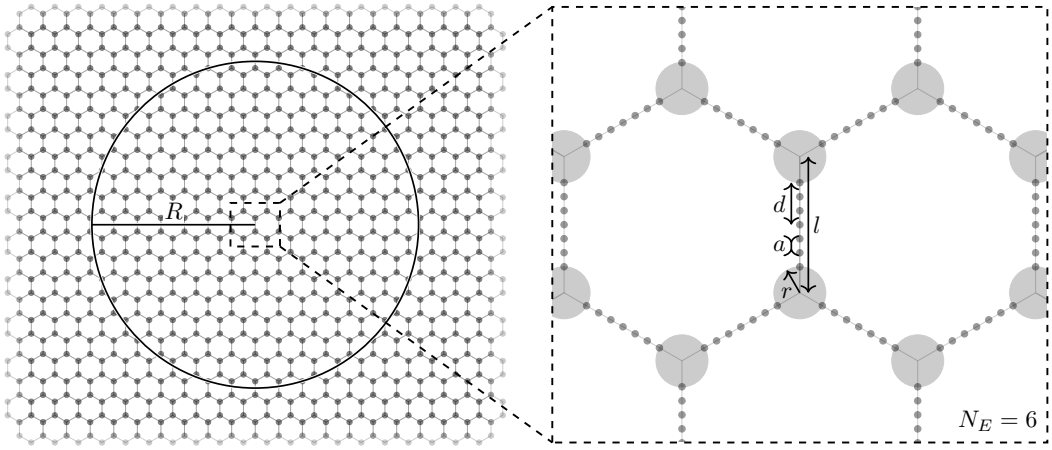

Figure 6.4: Sketch of the honeycomb grid. Left: $\mathcal{U}_{\text{loc}}(R)$ is sketched by its circumference. The radius of the circular local environment is denoted by R. Right: Zoom on two adjacent cells of the grid inside $\mathcal{U}_{\text{loc}}(R)$. For visualization we chose $N_E = 6$ links between adjacent sites. The length of each link (i.e. the distance between adjacent atoms on the edge) is denoted by a. The length of the amalgamated N_E-chains (per site) is denoted by $d = N_E a/2$. By r we denote the radius of $\mathcal{C}_s$. The length of each edge is denoted by $l = 2(d + r)$.

Twice the number of links between adjacent sites allow for the same quality factor in a local environment of (at least) *four-times* the radius.

As for the previous lemmata and theorem XIV, the proof is noted in the app. 6.B.1. In the following we briefly want to illustrate the interplay between R, N_E and the *local ratio* Q_R exemplary for the FIBONACCI model in realization `FMI-2` on the honeycomb grid. Note that the *lower bound on the quality* now corresponds to an *upper bound on the ratio*. Here we consider the ratio as it is the more natural quantity than the quality (although arguably less intuitive).

Example 12. (Fibonacci Model Grid 2)

In this example we want to apply corollary XV to illustrate the interplay of the radius R, the number of links N_E and the local ratio Q_R. Exemplary we choose the FIBONACCI model in realization `FMI-2` on the honeycomb grid. The results are represented in tab. 6.1. We measure the radius R in units of l (cf. sketch 6.4). We consider three target ratios $Q_t \in \{0.01, 0.1, 1\}$ which are represented in tab. 6.1a, 6.1b and 6.1c respectively. Remember that ratio $Q = 0$ corresponds to unit quality $\mathcal{Q} = 1$. For the target Q_t we want that $Q_R[\mathcal{C}_\mathcal{L}] < Q_t$. We evaluate the upper bound $Q_{\text{ub}}(N_E, R) > Q_R[\mathcal{C}_\mathcal{L}]$ on the local ratio for $R/l \in \{2, 3, 5, 10, 20, 40, 80\}$ and choose N_E just large enough such that $Q_{\text{ub}}(N_E, R) < Q_t$.

R/l	$N_E/2$	Q_{ub}
2	7	0.0095
3	8	0.0099
5	10	0.0090
10	14	0.0077
20	19	0.0082

(a) $Q_t = 0.01$
$\mathcal{Q}_t = 99.0\%$

R/l	$N_E/2$	Q_{ub}
2	4	0.010
3	5	0.070
5	6	0.076
10	8	0.080
20	11	0.080
40	15	0.088
80	21	0.088

(b) $Q_t = 0.1$
$\mathcal{Q}_t = 90.5\%$

R/l	$N_E/2$	Q_{ub}
2	3	0.40
3	4	0.19
5	4	0.57
10	5	0.98
20	7	0.86
40	10	0.71
80	14	0.71

(c) $Q_t = 1$
$\mathcal{Q}_t = 36.8\%$

Table 6.1: Upper Bounds Q_{ub} on the ratio for multiple choices of the local radius R. We consider three target ratios $Q_t \in \{0.01, 0.1, 1\}$ which are represented in tab. 6.1a, 6.1b and 6.1c respectively. We choose the number of links N_E between two sites such that $Q_{\text{ub}} < Q_t$.

6.4.3 | A upper Bound on the Honeycomb Grid

In analogy to corollary XV we want to determine the limits for the construction of a local environment. We formulate corollary XVI:

Corollary XVI (Upper Bounds to local Languages on the Honeycomb Grid)**.**

Consider a tessellated L-complex $([\mathcal{C}_{\mathcal{L}}]^{\mathcal{Q}}_{\mathcal{K}}, L_{\mathcal{L}}, \mathfrak{L})$ *on a honeycomb grid of lattice* $\mathcal{L}$ *where* $L_{\mathcal{L}}$ *is a tessellated language with loop-DOFs. Then for any target* $\mathcal{Q}_t \in \mathbb{R}_{[0,1]}$ *there exists a finite critical radius* $R_c(\mathcal{Q}_t) < \infty$ *such that for all radii* $R \geq R_c(\mathcal{Q}_t)$ *the* local *quality factor is* $\mathcal{Q}_R[\mathcal{C}_{\mathcal{L}}] \leq \mathcal{Q}_t$ *in the local environment* $\mathcal{U}_{loc}(R)$*.*

We attach the proof in app. 6.B.2 of this thesis. We denote this statement only the rank of a corollary because the argument of the proof is similar to the proof of theorem XI. However there are some key differences: The proof from the 'no-go'-theorem XI works on *very general ground* for any system with loop-DOFs on any lattice. It offers a *qualitative argument* for (infinitely) large systems that they can not be implemented in the VdW model. In contrast the proof of corollary XVI is *constructive* as it derives the *interplay* between the size of the local environment (given by its radius R), the quality factor $\mathcal{Q}$ and the number of links N_E between the sites[4]. However for this derivation we need to *fix an underlying grid* to evaluate the series. In this proof we exemplary considered the honeycomb grid as used in the FIBONACCI model. However the argument of this proof can be generalized to other grids straightforwardly. Note that the exact evaluation of the parameters (see eq. (6.54) in app. 6.B.2) can only be done numerically for a specific implementations of a specific language. This allows for the discussion in the next sec. 6.5 which compares the lower bound from corollary XV and the upper bound from corollary XVI.

[4] N_E determines the mesoscopic loop-loop-interaction energy $I(l_+)$.

6.5 | A Comparative Study on the Bounds

In the previous sec. 6.4 we discussed the behavior of local tessellated languages defined by a circular support $\mathcal{U}_{\text{loc}}(R)$ of radius R. In a nutshell we traced-back the properties of local languages to the properties of global languages which are defined only within the local environment. We derived an upper and a lower bound to the quality factor as a function of the size of the local environment and of the length of the edges. Note that so far the discussion is based on *general* tessellated languages on the honeycomb grid although it would be straightforward to generalize these concept to other grids.

In this section we want to exemplarily apply the derived bounds to the FIBONACCI model on the honeycomb grid. More specifically we are interested in the VdW-minimal realization `FMI-3` presented in fig. 5.6. In the next subsec. 6.5.1 we want to visualize and compare the lower and the upper bounds on the local ratio for the VdW-minimal realization `FMI-3`. We continue in subsec. 6.5.2 with discussing the *asymptotic behavior* which we explain via a model based on the multipole expansion from electrodynamics. Here we compare with the `FMI2`-realization (see fig. 5.5) of the FIBONACCI model.

6.5.1 | Visualizing the Bounds

In this subsection we want to visualize and study the bounds on the quality factor (2.19). More precisely we are interested in the *ratio* $Q_R = \delta E_R / \Delta E_R$ which is the more natural quantity as it only includes the energy splitting and the inverse of the energy gap (while the quality is its negative exponent). Remember that a ratio $Q_R = 0$ means unit quality $\mathcal{Q}_R = 1$ and the larger the ratio the smaller the quality which becomes zero as the ratio diverges.

Upper Bounds on the Ratio. We want to start by comparing the *upper bounds on the ratio* (i.e. lower bounds on the quality) for realization `FMS3`. The upper bounds presented in this subsection are based on corollary XV. Fig. 6.5 presents the upper bounds on the ratio as a contour plot of the radius R and the number of links N_E. Remember that $A_{\text{loc}}(R) = \pi R^2$ is the size of the local environment $\mathcal{U}_{\text{loc}}(R)$. $d = N_E a$ is the length of the N_E-chain which is amalgamated to each site and $l = 2d + 2r$ is the distance between adjacent sites characterized by N_E `LNK2`-gates on the edges (cf. sketch 6.4).

The calculations are based on numerical simulations of sites with $N_E = 4$, 6 attached `LNK1`-gates. This is visualized via the horizontal dashed black line in fig. 6.5. For larger $N_E > 4$, 6 we require lemma XIII as discussed in corollary XV. This introduces additional uncertainties and makes the bound less tight. For smaller N_E we do not require lemma XIII thus the final bound on Q_R is tighter for $N_E < 6$. This causes the cut in the ratio at $N_E = 4$, 6 at the dashed black line.

In fig. 6.5 one can clearly see that for large N_E, $R/l \gg 1$ the curves $N_E \propto \sqrt{R/l}$ possess constant local ratio as it was predicted in previous sec. 6.4. This asymptotic behavior is studied in more detail in the next subsec. 6.5.2. In general, by increasing N_E we can arbitrarily suppress

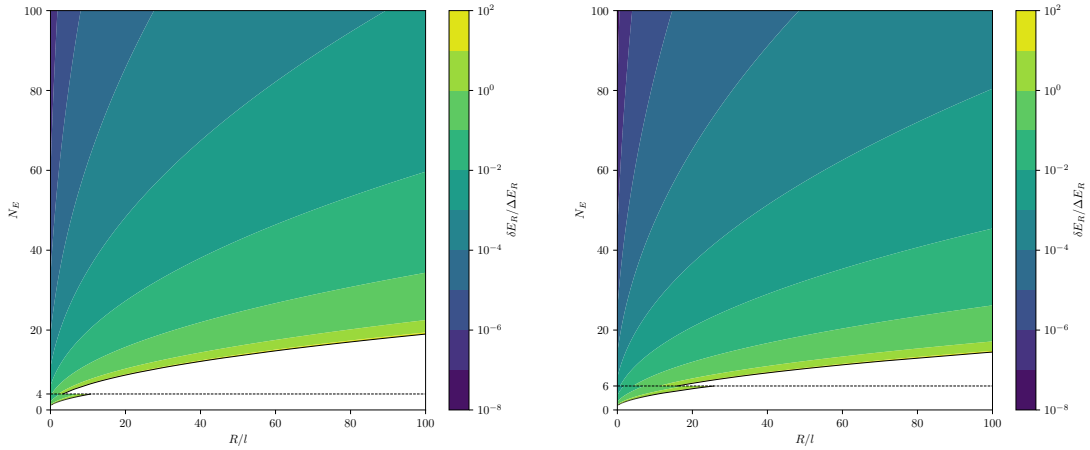

(a) Based on $N_E = 4$.

(b) Based on $N_E = 6$.

Figure 6.5: Upper bounds on the local ratio $Q_R = \delta E_R/\Delta E_R$ for the FIBONACCI model in realization `FMI-3` as a function of the radius R and the number N_E of `LNK1`-gates on the edges. The calculations for fig. 6.5a and fig. 6.5b are based on numerical simulations of the `FMSI-3` sites with $N_E = 4$ and $N_E = 6$ attached `NOT1`-gates respectively. The value with $N_E = 4$ and $N_E = 6$ is marked by a dashed black line respectively. The continuous black line separates the region with a negative lower bound on the local energy gap where corollary XV makes no statement.

the ratio increasing the quality. In contrast by choosing N_E too low the upper bound on Q_R becomes negative (as the lower bound on ΔE_R becomes negative) and corollary XV does not make any useful statement anymore. This is visualized via the continuous black line separating the white-colored regime without upper bound. Similarly by choosing R too large the upper bound becomes negative and we again fall into the white-colored regime.

For $N_E = 6$ in subplot 6.5b one can see that the upper bound of the ratio decreases as the bound becomes tighter compared to subplot 6.5a with $N_E = 4$. Here the calculation is based on a larger initial value of N_E which sharpens the inequalities. With more extensive simulations we could increase the number N_E on which the calculation is based and further tighten the bound provided by corollary XV. This illustrates the interplay between the *numerical simulations* (on which the proof is based) which we can improve to tighten the bound provided by the *analytical corollary XV*.

Lower Bounds on the Ratio. We continue by discussing the *lower bounds on the ratio* (i.e. upper bounds on the quality) for realization `FMSI-3`. These bounds are provided by corollary XVI. Fig. 6.6 presents the lower bounds on the ratio as a contour plot of the radius R and the number of links N_E. Again the calculations are based on numerical simulations of sites with $N_E = 4$ and $N_E = 6$ attached `NOT1`-gates.

Firstly we want to emphasize that this plot is *linear-log* to allow the presentation of larger values for the radius: $R/l \leq 10^{10}$. We want to include the white-colored regime on the right of the plot. Here the *lower bound on the ratio diverges* implying a negative energy gap and a vanishing quality. We can not implement such large local environments with the given number N_E of

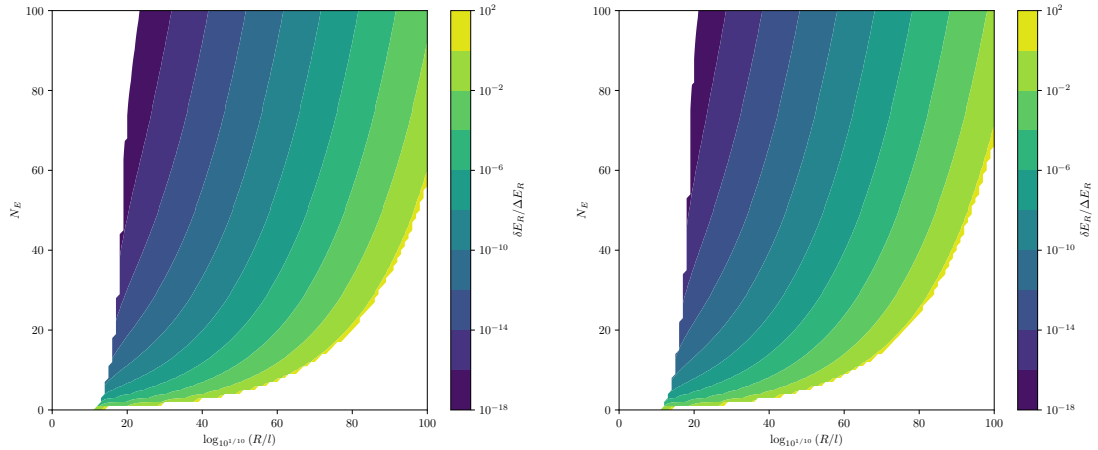

(a) Based on $N_E = 4$. **(b)** Based on $N_E = 6$.

Figure 6.6: Lower bounds on the local ratio $Q_R = \delta E_R/\Delta E_R$ for the FIBONACCI-model in realization `FMI-3` as a function of the radius R and the number N_E of `LNK1`-gates on the edges. The calculations for fig. 6.6a and fig. 6.6b are based on numerical simulations of the `FMSI-3` sites with $N_E = 4$ and $N_E = 6$ attached `NOT1`-gates respectively.

`LNK1`-gates on the edges. However for any given radius R/l we can always *choose* N_E sufficiently large to obtain an arbitrarily small lower bound on the ratio.
In the white-colored regime on the left corollary XVI makes no statement about the ratio. We require a sufficiently large local environment to obtain loops and loop-loop interactions (and to exclude boundary effects) such that the lower bound on Q_R does not vanish. Here we find that for $N_E = 6$ in fig. 6.6b the lower bound on the ratio increases as the bound becomes tighter compared to subplot 6.5a with $N_E = 4$.

Comparing the Bounds. To compare the upper an the lower bounds we consider one-dimensional 'slices' of the N_E, R/l-plane. Fig. 6.7a and fig. 6.7b present the upper and the lower bounds on the ratio as a function of N_E and R/l respectively. The other variable is given parametrically by the selected values portrayed in the legend. Both figures are based on the `FMSI-3` site with $N_E = 4$ attached `NOT1`-gates. Again we want to emphasize that fig. 6.7a is a *log-linear* plot while fig. 6.7b is a *log-log* plot. Fig. 6.7a possesses a linear x-axis because N_E is given by integer values. In both plots the upper bound is visualized by a *dotted line* and the lower bound is visualized by a *dashed line*. The intervals allowed by the inequalities are colored. One can see that there are quite large discrepancies between the upper and the lower bound as we made quite 'rough' approximations in the derivation. One could improve these derivations by fixing a language and an implementation if this is deemed necessary. Especially for the log-log plot 6.7b one can see that both bounds follow the same qualitative behavior.

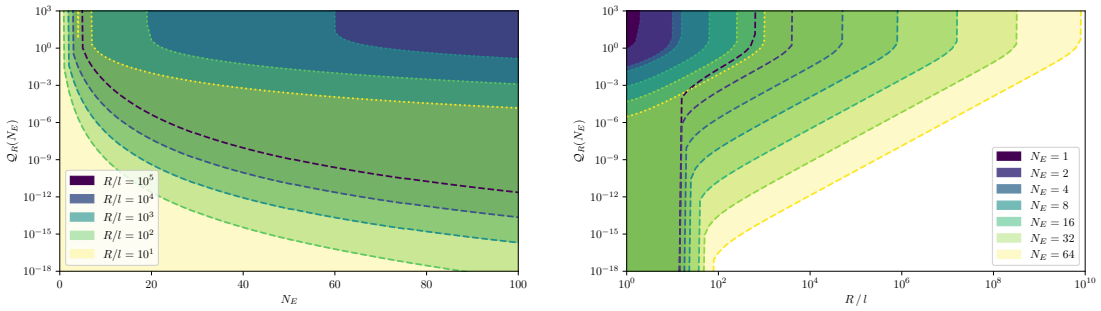

(a) Function of N_E. **(b)** Function of R/l.

Figure 6.7: The bounded interval of the local ratio $Q_R = \delta E_R/\Delta E_R$ for the FIBONACCI-model in realization FMI-3. The calculations are based on numerical simulations of the FMSI-3 sites with $N_E = 4$ attached NOT1-gates. Fig. 6.7a and fig. 6.7b portray the interval as a function of the number N_E of LNK1-gates on the edges and of the radius R/l respectively. The lower bound is represented by the dashed line, the upper bound is represented by the dotted line. The colored area describes possible values for the local quality factor.

6.5.2 | The asymptotic behavior of the Bounds

In this subsection we want to study the *asymptotic behavior* of the upper bound (see corollary XVI) and of the lower bound (see corollary XV) on the local quality. For that we employ an analogy to the *multipole expansion* from electrodynamics.

The multipole Analogy. As a starting point we realize that the mesoscopic loop-loop-interaction energy

$$I = I_{\text{loop,loop}} + I_{\text{noloop,noloop}} - 2I_{\text{loop,noloop}} \tag{6.14}$$

consists of three parts (cf. eq. (6.1c)): It includes the interactions between the atoms excited in (no-)loops with a positive sign and the interactions excited between loops and no-loops with a negative sign. This allows us to interpret the atoms excited in a loop as possessing a positive charge $+1$, and the atoms excited in a 'no-loop' as possessing a negative charge -1. Such a charged atomic (no-)loop structure with VdW interactions would precisely reproduce the mesoscopic interaction energy I.

Realization FMI-3. In realization FMI-3 there are as many atoms excited in a loop as when there is no loop. Both the loop and the no-loop state possess a discrete D_6-rotational symmetry. This means the loop-loop interaction energy (6.14) is neither a monopole nor a dipole interaction but needs to be interpreted as the interaction energy of a *quadrupole in a quadrupole field*. The *quadrupole VdW-potential* decays as the eighth power of the distance to the quadrupole, i.e. as $\sim 1/N_E^8$. A quadrupole in a field has a potential energy proportional to the derivative of the field, i.e. the second derivative of the potential. Thus we expect the interaction energy between the two loops to decay by the tenth power of their distance. However the number of atoms for each loop grows linearly with $\sim N_E$ as well. Thus the number of interactions grows quadratically as $\sim N_E^2$. Therefore we expect the loop-loop interaction energy to behave asymptotically as $I \sim \text{const}_{N_-,R}/N_E^8$.

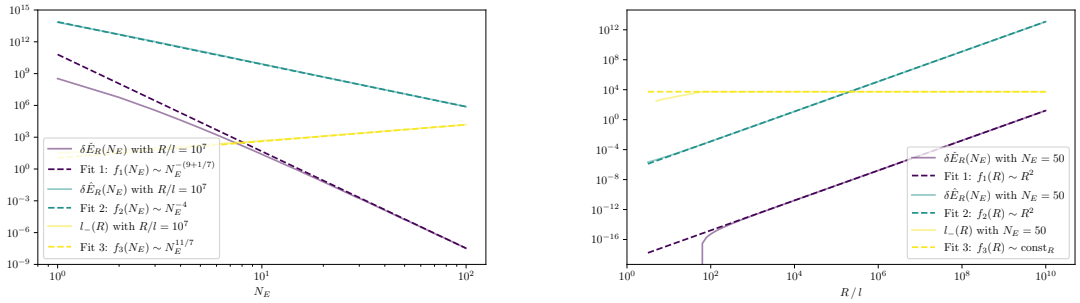

(a) Fit of N_E. **(b)** Fit of R.

Figure 6.8: Asymptotic behavior of the local energy splitting $\delta E_R(N_E)$ and the distance $l_-(R, N_E)$ between loops in state $|-\rangle$ for realization `FMI-3`. The fit functions are represented by dashed lines. The continuous lines correspond to selected slices of fig. 6.5a and fig. 6.6a.

The asymptotic behavior of the Upper Bound. For the asymptotic behavior as a function of R we refer to the proof of corollary XVI in app. 6.B.2. To maximize the local energy splitting δE_R, the condition (6.54) should be fulfilled for all N_E:

$$I'_{-,\text{ub}}(N_-)|_{R,N_E} \overset{!}{\sim} \varepsilon \sim \text{const}_{N_-,R}/N_E^8. \tag{6.15}$$

We can reasonably expect that $x \approx 4N_E a/l_- \ll 1$[5] (for large N_E) because $l_+ \gtrsim 6N_E a$ and $l_- > l_+$ should grow faster in N_E. This allows us to expand $I_{-,\text{ub}}(N_-) \sim N_-(N_E^2/l_-^6) \cdot N_E/l_-$ (the second term) and solve eq. (6.15) in first order. This yields $l_- \sim \text{const}_R N_E^{11/7}$[6] which retrospectively confirms that asymptotically the expansion is justified. The area per excited loop is a hexagon of side-length $l_-/\sqrt{3}$ which yields the area $A_{\text{loop}} = \sqrt{3}l_-^2/2 \sim l_-^2$. Thus up to boundary effects (e.g. in the continuum limit $R \nearrow \infty$) it is

$$N_- \approx A_{\text{loc}}(R)/A_{\text{loop}} = 2\pi R^2/\sqrt{3}l_-^2 \sim (R/l)^2 N_E^2/l_-^2 \sim (R/l)^2/N_E^{8/7}.$$

We obtain for the local energy splitting $\delta E_R \sim N_-\varepsilon \sim (R/l)^2/N_E^{9+1/7}$ asymptotically in N_E and R/l. We verify this asymptotic behavior in fig. 6.8. All four fit functions for $l_- \sim \text{const}_{R/l} N_E^{11/7}$ and for $\delta E_R \sim (R/l)^2/N_E^{9+1/7}$ are portrayed and fit *perfectly* for large N_E and R. Therefore the curves of constant local energy splitting (and thus constant local quality factor[7]) follow the behavior $N_E \sim (R/l)^{7/32}$ for large N_E and R/l.

Realization FMI-2. In realization `FMI-2` the number of atoms excited in a loop is larger than the number of atoms excited when there is no loop: In a loop there is one additional atom excited per site , i.e. in total six additional atoms in the cell, independent N_E. We can thus interpret the loop-loop interaction as the *monopole-monopole-interaction between two VdW-charges* which are independent of N_E. Therefore we expect the loop-loop interaction energy to decay as $I \sim \text{const}_{N_-,R}/N_E^6$. We can now follow analogous arguments as for realization `FMI-3`: With $I'_{-,\text{ub}}(N_-)|_{R,N_E} \sim \text{const}_{N_-,R}/N_E^6$ we obtain $l_- \sim \text{const}_R N_E^{9/7}$ and $N_- \sim (R/l)^2/N_E^{4/7}$. This

[5] This is also confirmed numerically.
[6] Remember that $l_- = \text{const}_R$ is proven in app. 6.B.2. However this is also quite intuitive as for large R, l_- should only depend on l_+ and thus on N_E.
[7] The local energy gap can be upper bounded simply by the (constant) detuning $\Delta_{\max}$.

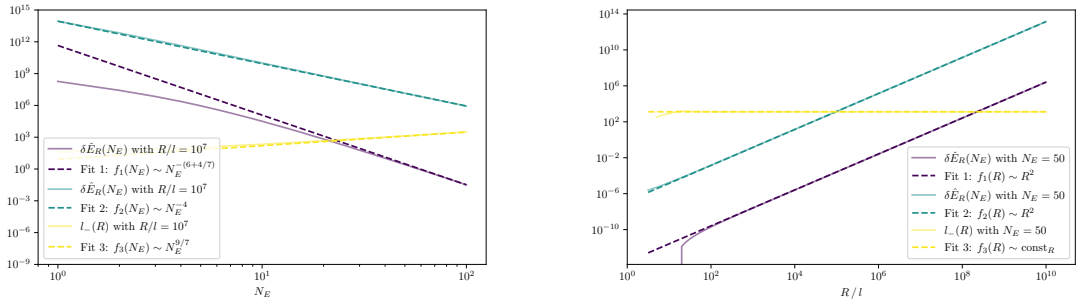

(a) Fit of N_E. **(b)** Fit of R.

Figure 6.9: Asymptotic behavior of the local energy splitting $\delta E_R(N_E)$ and the distance $l_-(R, N_E)$ between loops in state $|-\rangle$ for realization `FMI-2`. The fit functions are represented by dashed lines.

yields the asymptotical behavior $\delta E_R \sim N_- \varepsilon \sim (R/l)^2/N_E^{6+4/7}$ of the local energy splitting for large N_E and R/l. Again, we verify this asymptotic behavior in fig. 6.9. Both fit functions for $l_- \sim \text{const}_{R/l} N_E^{9/7}$ and for $\delta E_R \sim (R/l)^2/N_E^{6+4/7}$ are portrayed and fit well for large N_E and R. We find that the curves of constant δE_R follow the behavior $N_E \sim (R/l)^{7/23}$ for large N_E and R/l.

Comparison. Note that the lower bound of the local quality factor for realization `FMI-3` decays faster than the lower bound of the local quality factor for realization `FMI-2` as its loops interact via *higher-order interactions*. Furthermore the number of atoms per site in realization `FMI-2` is larger than in realization `FMI-3` which also contributes to a larger lower bound on the energy splitting. Both facts suggest that realization `FMI-3` is better suited to implement the FIBONACCI-model because it allows (if implemented correctly) for smaller local energy splittings. This adds to the advantage of realization `FMI-3` that is a simpler structure with only one atom per site/edge.

The asymptotic behavior of the Lower Bound. Note that the *upper* bound on the local energy splitting follows a different asymptotic behavior. The reason is that its derivation is valid on more general ground; independent of the L-complex. For some realizations (such as `FMI-2`) there may be a monopole term contributing to the loop-loop interactions. If one further assumes that the monopole charge is linear $\sim N_E$ (as the number of atoms is linear in N_E), one obtains $I \sim \text{const}_{N_-,R}/N_E^4$ which yields $l_- \sim \text{const}_R N_E$ and $N_- \sim (R/l)^2 \text{const}_{N_E}$. This explains the asymptotical behavior $\delta E_R \sim N_- \varepsilon \sim (R/l)^2/N_E^4$ which is found by the fits in fig. 6.8 and fig. 6.9.

| Appendix

6.A | Proofs for the lower bound on the Quality

This appendix is denoted to sec. 6.3. Here we include the proofs for lemma XII, lemma XIII and theorem XIV.

6.A.1 | Proof for the N_E-Chain

In this subsection we present the proof of lemma XII. The proof is constructive and describes an algorithm to construct N_E-chains of arbitrary length. Afterwards we illustrate this algorithm via four examples. First we briefly recapitulate lemma XII:

Lemma XII (N_E-Chain of arbitrary Length)**.**

The language L_{N_E} can be implemented as the low-energy eigenspace of a structure $\mathcal{C}_{N_E}$ with quality factor $\mathcal{Q} = 1$, robustness $r \gtrsim 91.23\%$ and effective energy gap $\Delta E_{eff} \gtrsim 46.66\%$ for any $N_E \in \mathbb{N}$.

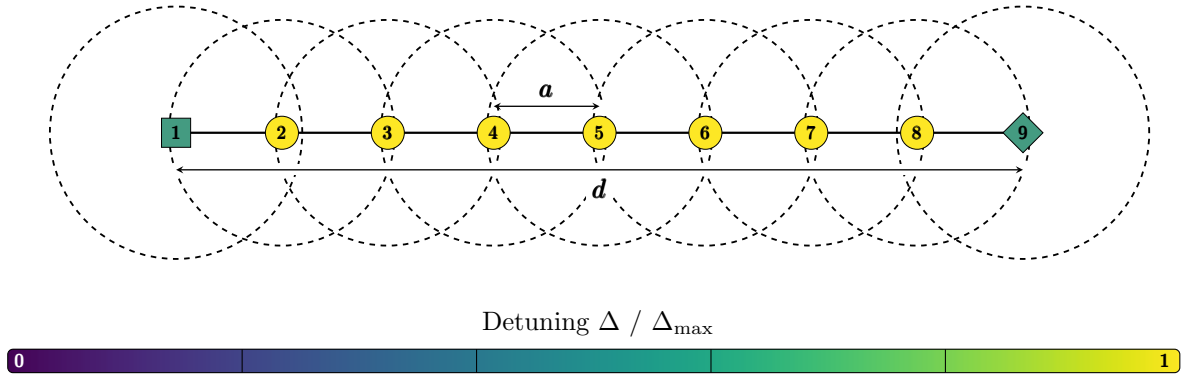

Figure 6.10: Sketch of the LNK4-gate with $N = 9$ atoms. We assume equal distances a between the atoms and equal detunings for the ports and the ancillaries respectively. The detunings are visualized by the coloring of the atoms. The blockade radii are drawn as dashed circles. The length and the color scaling fits with the construction in the proof of lemma XII.

Proof.

We proof lemma XII constructively by formulating an algorithm which constructs the structure $\mathcal{C}_{N_E}$ for any $N_E \in \mathbb{N}$. We assume that the chain consists of $N = N_E+1$ atoms $1, \ldots N$ of equal distance a. Further we assume equal detunings $\Delta_1 = \Delta_N =: \Delta$ and $\Delta_2 = \ldots = \Delta_{N-1} =: \tilde{\Delta}$. The length of the chain is denoted by $d = N_E a$. This is sketched in fig. 6.10. W.l.o.g. we can set the detuning $\Delta = 1$ choosing the energy scaling using f_α with $\alpha = \Delta^{-1/6}$ (see eq. (2.15)). We define $\varepsilon := 2\Delta - \tilde{\Delta}$ for the atoms of the bulk.

Note that $g = |L^N_{\mathrm{LNK}}| = 2$. The ground states are the two alternating states where every second atom is excited. In the following the state where atom 0 is *not* excited is denoted by state 1 and the state where atom 0 is excited is denoted by state 2. In the PXP-model with blockade radii $r_{B,\mathrm{i}} = 1$ we would need to choose $\varepsilon = 0$ to achieve ground state degeneracy and $1/2 < a < 1$ to obtain the correct blockade graph. Here the energy gap would be $\Delta E = \Delta$, i.e. $r = 1$ and $\Delta E_{\mathrm{eff}} = 1/2$. In the VdW-model there are residual interactions between distant atoms. We have to distinguish two cases: (1) If the number of atoms $N = 2m$ with $m \in \mathbb{N}_1$ is *even*, then the two alternating states are of equal energy thanks to the symmetry of the structure. Thus the ground state manifold is degenerate for any choice of ε. We denote this L-complex as a NOTm-gate in realization m^a. (2) If the number of atoms $N = 2m + 1$ with $m \in \mathbb{N}_1$ is *odd*, then the two alternating states possess a different number of excited atoms and thus different interaction energies. We denote this L-complex as a LNKm-gate in realization m^b. Consider case (2), i.e. the LNKm-gate with $N = 2m + 1$ atoms. To achieve ground state

degeneracy the difference in the interaction energies needs to be compensated by a finite $\varepsilon > 0$. For state 1 and state 2 the total interaction energies are

$$I_1(N) = \sum_{i=1}^{m-1}\sum_{j=1}^{m-i}\frac{C}{(2aj)^6} = \frac{C}{(2a)^6}\sum_{i=1}^{m-1} H_{i,6} = \frac{C}{(2a)^6}\left[mH_{m-1,6} - H_{m-1,5}\right], \tag{6.16a}$$

$$I_2(N) = \sum_{i=0}^{m-1}\sum_{j=1}^{m-i}\frac{C}{(2aj)^6} = \frac{C}{(2a)^6}\sum_{i=1}^{m} H_{i,6} = \frac{C}{(2a)^6}\left[(m+1)H_{m,6} - H_{m,5}\right] \tag{6.16b}$$

respectively. Here $H_{m,\gamma} \equiv \sum_{k=1}^{m} 1/k^\gamma$ is the m^{th} generalized harmonic number of order γ. $H_{m,\gamma}$ is monotonic growing in m and upper-bounded by the Euler–Riemann zeta-function $H_{\infty,\gamma} \equiv \zeta(\gamma)$. The interaction energies (6.16) yield the energy splitting of the ground states

$$\delta E[\mathcal{C}_{2m}] = |\langle H[\mathcal{C}_{2m}]\rangle_2 - \langle H[\mathcal{C}_{2m}]\rangle_1| = |-2\Delta + I_2 + \tilde{\Delta} - I_1| = \left|\frac{C}{(2a)^6}H_{m,6} - \varepsilon\right|. \tag{6.17}$$

Thus for both cases (1) and (2) we choose $\varepsilon_m = H_{m,6}C/(2a)^6$ for $m = \lfloor N/2 \rfloor$ to obtain a vanishing energy splitting $\delta E[\mathcal{C}_{2m}] = 0$.

This leaves only one DOF which we need to fix to fully define the structure: the distance a between adjacent atoms of the chain. We want to determine an implementation which approximates the optimal effective energy gap and the optimal robustness. For that we derive a lower bound to the energy gap and optimize it by gapping-out all excited states. First note that the set of excited states $\mathcal{E} = \mathcal{E}_1 \cup \mathcal{E}_2$ can be split into two (overlapping) subsets: There are excited states $\boldsymbol{x} \in \mathcal{E}_1$ where two adjacent atoms are *excited* and there are excited states $\boldsymbol{x} \in \mathcal{E}_2$ where two adjacent atoms are *not excited*. Both sets together include every state except for the two alternating ground states. In a nutshell the goal is to choose C/a^6 sufficiently large such that the excited states $\boldsymbol{x} \in \mathcal{E}_1$ do not impair the energy gap but as small as possible to maximally gap-out the excited states $\boldsymbol{x} \in \mathcal{E}_2$.

First we consider set $\mathcal{E}_1$: To gap-out the excited states $\boldsymbol{x} \in \mathcal{E}_1$ it is sufficient to request that it is energetically never favourable to excite adjacent atoms. By exciting an atom we gain at most $\tilde{\Delta}$ energy. By setting the interaction energy between adjacent atoms as

$$C/a^6 = \tilde{\Delta} + \Delta E_1 = 2\Delta - H_{m,6}C/(2a)^6 + \Delta E_1 \leq 2\Delta - C/(2a)^6 + \Delta E_1 \tag{6.18}$$

we secure any excited state $\boldsymbol{x}_1 \in \mathcal{E}_1$ is energetically at least ΔE_1 higher than the lowest state $\boldsymbol{x}_{\min} \in \mathbb{F}_2^N \backslash \mathcal{E}_1 = \mathcal{G} \sqcup (\mathcal{E}_2 \backslash \mathcal{E}_1)$. If we would choose a such that $\Delta E|_{\mathcal{E}_2\backslash\mathcal{E}_1} > 0$ then it would be $\boldsymbol{x}_{\min} \in \mathcal{G}$ and $\Delta E|_{\mathcal{E}_1} \gtrsim \Delta E_1$. Here $\Delta E|_{\mathcal{E}_i}$ denotes the energy gap where the excited state manifold is restricted to its subset $\mathcal{E}_i \subset \mathcal{E}$. Solving eq. (6.18) yields $C/a^6 = (2\Delta + \Delta E_1)/(1+2^{-6})$ (independent of m). This fixes a as a function of ΔE_1 such that exciting adjacent atoms energetically costs at least ΔE_1 units of energy.

Secondly for set $\mathcal{E}_2$ it is now sufficient to consider only states $\boldsymbol{x} \in \mathcal{E}_2 \backslash \mathcal{E}_1$ not covered by case (1). If two adjacent atoms are not excited in the chain we call this a *defect*. In a defect the distance between the nearest excited atoms is $3a$. Adjacent defects[c] may cause even larger distances. Defects on the ground states may arise for two reasons: (2a) there are different atoms excited and/ or (2b) there are fewer atoms excited than in an alternating state. Firstly consider case (2a): To excite a defect while conserving the number of excited atoms without exciting adjacent atoms is only possible if at least one atom at the boundary is not excited.

In this case we can excite an atom at the boundary instead of an atom in the bulk. This costs $1-\varepsilon_m$ of detuning energy but generates one defect. The defect reduces the interaction energies between the atoms by

$$\begin{aligned}\Delta I &\leq \sum_{i,j=0}^{\infty}\left[\frac{C}{[(2i+1)+(2j+1)]^6}-\frac{C}{[(2i+1)+(2j+2)]^6}\right]\\ &\overset{n\equiv i+j}{\leq} \frac{C}{(2a)^6}\sum_{n=0}^{\infty}\left[\frac{n+1}{(n+1)^6}-\frac{n+3/2}{(n+3/2)^6}+\frac{1/2}{(n+3/2)^6}\right]\\ &= \frac{C}{(2a)^6}\left[\zeta(5)-\zeta(5,3/2)+\frac{\zeta(6,3/2)}{2}\right]=\frac{C}{(2a)^6}\left[\frac{\pi^6}{30}-30\zeta(5)\right]=:\Delta I_{\mathrm{Def}}.\end{aligned} \tag{6.19}$$

Here $\zeta(\gamma,\delta)\equiv\sum_{k=0}^{\infty}1/(k+\delta)^\gamma$ is the HURWITZ zeta-function which recovers the EULER-RIEMANN zeta-function $\zeta(\gamma)\equiv\sum_{k=1}^{\infty}1/k^\gamma$ for $\delta=1$. During the proof ΔI should be interpreted as a placeholder symbolizing the difference in the total interaction energies. Thus the total energetic cost for introducing such a defect is

$$\Delta-\varepsilon_m-\Delta I\geq\Delta-\zeta(6)\frac{C}{(2a)^6}-\Delta I_{\mathrm{Def}}=\Delta-\frac{C}{(2a)^6}\left[\zeta(6)+\frac{\pi^6}{30}-30\zeta(5)\right]=:\Delta E_2. \tag{6.20}$$

We want that $\Delta E_2>0$ to derive a useful lower bound on $\Delta E|_{\mathcal{E}_2}$.

Now consider case (2b): there may be fewer atoms excited either because we de-excited an atom in the bulk or because we de-excited an atom at the boundary. If we de-excite an atom in the bulk we loose $\tilde{\Delta}$ of detuning energy but we generate two defects. Thus the total energetic cost becomes $\tilde{\Delta}-2\Delta I\geq 2\Delta E_2+\varepsilon_m$. If we de-excite an atom at the boundary we loose Δ of detuning energy but we generate one defect. Here the total energetic cost becomes $\Delta-\Delta I\geq\Delta E_2+\varepsilon_m$. Thus for $\Delta E_2>0$ defects of type (2b) are energetically even more costly than defects of type (2a).

Thus the energetic cost of any defect can be lower-bounded by ΔE_2 for $\Delta E_2>0$. Any excited state $\boldsymbol{x}_2\in\mathcal{E}_2$ is energetically at least ΔE_2 higher than the lowest state $\boldsymbol{x}_{\min}\in\mathbb{F}_2^N\backslash\mathcal{E}_2=\mathcal{G}\cup(\mathcal{E}_1\backslash\mathcal{E}_2)$. Combining with case (1), if we choose $C/a^6=(2\Delta+\Delta E_1)/(1+2^{-6})$ with $\Delta E_1,\ \Delta E_2>0$ then this implies $\Delta E|_{\mathcal{E}_1}\gtrsim\Delta E_1$ and $\Delta E|_{\mathcal{E}_2}\gtrsim\Delta E_2$. We obtain the lower bound $\Delta E\gtrsim\min(\Delta E_1,\Delta E_2)$. Reasonably we can now set $\Delta E_1=\Delta E_2=:\Delta E_{\mathrm{lb}}$ to define the lower bound on the energy gap. Then eq. (6.20) with C/a^6 from (6.18) yields

$$\Delta E_{\mathrm{lb}}=\Delta-\frac{2\Delta+\Delta E_{\mathrm{lb}}}{2^6+1}\left[\zeta(6)+\frac{\pi^6}{30}-30\zeta(5)\right]. \tag{6.21}$$

Solving for the lower bound yields $\Delta E\gtrsim\Delta E_{\mathrm{lb}}\gtrsim 0.91236\,\Delta$. Note that

$$\tilde{\Delta}\leq 2\Delta-\frac{C}{(2a)^6}=\frac{2^7\Delta-\Delta E_{\mathrm{lb}}}{2^6+1}\lesssim 1.95520\,\Delta\equiv\Delta_{\max}$$

and $\Delta\equiv\Delta_{\min}$. Thus we obtain the robustness $r\gtrsim 91.236\%=:r_{\mathrm{lb}}$ and the effective gap

$\Delta E_{\text{eff}} \gtrsim 46.664\% =: \Delta E_{\text{eff, lb}}$. This defines the distance

$$a = \left[\frac{1+2^{-6}}{2+\Delta E_{\text{lb}}/\Delta}\right]^{1/6} r_{B,\max} \approx 0.83897\, r_{B,\max} \overset{N\geq 2}{\approx} 0.93817\, r_{B,\min}$$

between adjacent atoms. The construction of the LNK4-gate with $N = 9$ atoms is exemplary visualized in fig. 6.10 for $\Delta_{\max} = 1$. □

[a] Note that for $m = 1$ we recover the NOT1-gate from fig. 4.1.
[b] Note that for $m = 1$ we recover the LNK1-gate from fig. 4.1.
[c] To minimize the interaction energies between the atoms defects tend to center themselves and distribute equally along the chain.

In the following we want to illustrate the construction by the algorithm of the proof. We introduce and discuss four examples constructed for $m = 1$ and $m = 5$. We find that the lower bound on the energy gap introduced in the proof is *very tight* for large N_E-chains.

Example 13. (NOTm-Gates and LNKm-Gates for $m \in \{1, 5\}$)

Note that the optimal NOT1i- and the LNK1i-gate with $m = 1$ are already introduced in fig. 4.1. For comparison we introduce the NOT1ii- and the LNK1ii-gate constructed by following the algorithm of lemma XII. As another example we introduce the NOT5- and the LNK5-gate. We want to calculate the energy structure of the gates and compare the lower bound introduced in lemma XII. The constructed gates are portrayed in fig. 6.11. The lower bound $r_{\text{lb}} = 91.236\%$ is visualized as a dashed blue line in the energy structures.

The first row portrays the NOT1ii-gate. Here for $m = 1$ with $N_E = 1$ there are only $N = 2$ atoms of equal detunings $\Delta_{\max} = \Delta_{\min}$. This is a somewhat special case as there are no ancillaries of detuning $\tilde{\Delta}$ in this chain. As $a < 2^{-1/6}\, r_{B,\max}$, it is $r[\mathcal{C}_1] = \Delta E_{\text{eff}}[\mathcal{C}_1] = 1$. Note that here the algorithm actually yields an r- and ΔE_{eff}-optimal implementation, although the implementation is different from NOT1-i in fig. 4.1. For the LNK1ii-gate with $N_E = 2$ and $N = 3$ atoms in the second row the implementation is not quite optimal: $\Delta E_{\text{eff}}[\mathcal{C}_2] \approx 48.9\% < 49.2\%$ and $r[\mathcal{C}_2] \approx 95.5\% < 96.9\%$. However the algorithm yields a good approximation of the ΔE_{eff}- and r-optimal LNK1i-gate in fig. 4.1.

For $m = 5$ there are $N = 10,\ 11$ atoms in the NOT5- and LNK5-gate respectively. The effective gaps $\Delta E_{\text{eff}}[\mathcal{C}_9] \approx \Delta E_{\text{eff}}[\mathcal{C}_{10}] \approx 46.686\%$ and the robustness $r[\mathcal{C}_9] \approx \Delta r[\mathcal{C}_{10}] \approx 91.243\%$ are very similar. Note that for such longer chains with $N_E = 9,\ 10$ links the lower bounds from lemma XII $\Delta E_{\text{eff, lb}} = 46.664\%$ and $r_{\text{lb}} = 91.236\%$ are very tight. In the energy structures the lower bounds essentially coincide with the actual gaps. Note that (similar to the LNK1ii-gate) the NOT5- and LNK5-implementations are constructed by the proof and thus are only approximations of the ΔE_{eff}- and r-optimal gates. This main reason is that the condition (6.18) to gap-out $\mathcal{E}_1$ is very simple which causes $\Delta E_{\text{eff}}|_{\mathcal{E}_1} \approx 95.771\% > \Delta E_{\text{eff}} \approx 46.686\%$. To determine the optimal structures we would need to allow for varying distances and detunings along the chain.

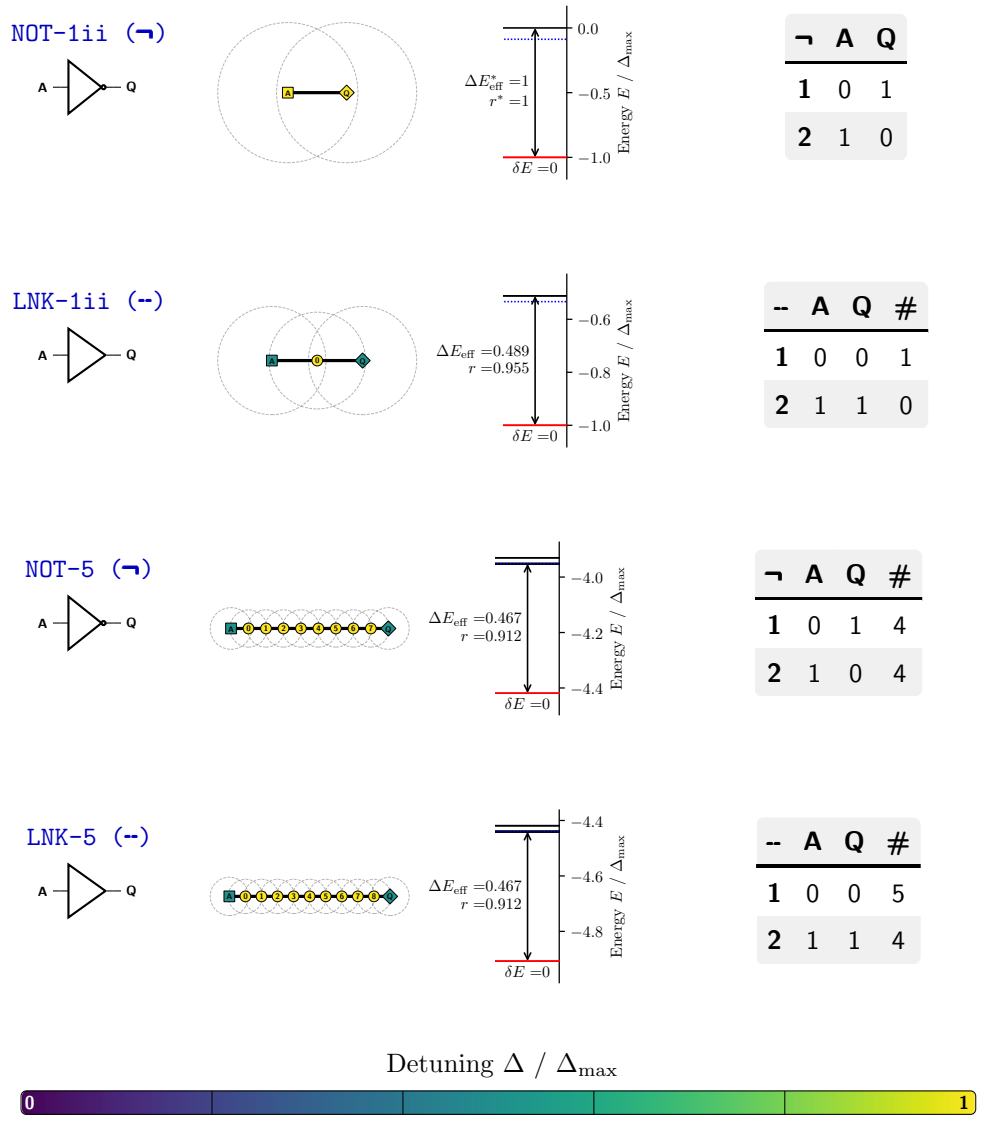

¬	A	Q
1	0	1
2	1	0

--	A	Q	#
1	0	0	1
2	1	1	0

¬	A	Q	#
1	0	1	4
2	1	0	4

--	A	Q	#
1	0	0	5
2	1	1	4

Figure 6.11: NOTm-Gates and LNKm-Gates for $m = 1$ and $m = 5$ constructed by the algorithm of lemma XII. The constructed chains are characterized by equidistant atoms and equal detunings of the ports and the ancillaries respectively. The lower bound $r_{\text{lb}} = 91.236\%$ is visualized as a dashed blue line in the energy structures. For long chains of atoms the lower bound becomes very tight (for $m = 5$ it lies on top of the lowest excited state in the energy structure). The tables in the third column portray the states of the ports and the number # of excited ancillaries.

6.A.2 | Proof for the Appendage of N_E-Chains

In this subsection we present the proof of lemma XIII. First we briefly recapitulate lemma XIII:

Lemma XIII (Appendage of N_E-Chains)**.**

We assume that the energy gap of the amalgamated structure $\mathcal{C}_{k\cup N_E}$ fulfills the condition

$$0 < \Delta E_{lb}(N_E) := \min\left(\Delta E[\mathcal{C}_{k\cup N_E}],\ 20\frac{C}{(2a)^6}\right) - \frac{C}{(2a)^6}\left[2\zeta(5)P + \left(1+\|\mathbf{L}_k^+\|_1\frac{|L_k|}{2}\right)\right.$$
$$\left.\times\frac{P(P-1)}{(N_E+1)^4}\left(4.8+\frac{25.6+6.4N_k/(P-1)}{N_E+1}+\frac{65.3+110.7N_k/(P-1)}{(N_E+1)^2}\right)\right]. \tag{6.22}$$

Then $\mathcal{C}_{k\cup(N_E+N'_E)}$ implements $L_{k\cup(N_E+N'_E)}$ as its low-energy eigenspace with $\mathcal{Q}[\mathcal{C}_{k\cup(N_E+N'_E)}]=1$ for any $N'_E\in\mathbb{N}_0$. The energy gap is $\Delta E[\mathcal{C}_{k\cup(N_E+N'_E)}]\geq\Delta E_{lb}(N_E)$.

Proof.

We consider the full Hamiltonian $H[\mathcal{C}_{\cup N_E\cup N'_E}]$ of the amalgamated structure. As discussed in eq. 2.13 there arise residual interactions

$$H_{\text{int}}[\mathcal{C}_{\cup N_E\cup N'_E}] = H_E[\mathcal{C}_{\cup N_E\cup N'_E}] + H_{KE}[\mathcal{C}_{\cup N_E\cup N'_E}] + H_{EE}[\mathcal{C}_{\cup N_E\cup N'_E}] \tag{6.23}$$

in-between the substructures during amalgamation. There are three contributions to the residual interactions: (1) There are edge (E) interactions between atoms of the same edge but different substructures, (2) there are kernel-edge (KE) interactions between atoms of the kernel structure and atoms of the amalgamated edge and (3) there are edge-edge (EE) interactions between atoms of an amalgamated edge and atoms of a different edge. If we would ignore this part of the Hamiltonian then the amalgamated structure would implement the γ-product $L_{\cup N_E\cup N'_E} = L_{\cup N_E}\otimes L_{N'_E}^{\otimes_\gamma p}$ as its low-energy eigenspace with quality factor $\mathcal{Q}[\mathcal{C}_{\cup N_E\cup N'_E}]=1$. The energy gap of the Hamiltonian would be given by the minimal energy gap of its parts:

$$\Delta E[\mathcal{C}_{\cup N_E\cup N'_E}] = \min\left(\Delta E[\mathcal{C}_{\cup N_E}],\ \Delta E[\mathcal{C}_{N'_E}]\right) =: \Delta E_\infty[\mathcal{C}_{\cup N_E\cup N'_E}]. \tag{6.24}$$

However in the VdW model the are finite residual interactions between the substructures. This may cause an energy splitting and reduce an energy gap. The idea of the proof is the following: First we want to upper bound the energy splitting. By assumption the language $L_{\cup N_E}$ is linearly independent. Thus $L_{\cup N_E\cup N'_E}$ is linearly independent as well and we can apply apply theorem V. This balances the energy splitting but may further reduce the energy gap. Then we want to derive a lower bound for the energy gap.

First note that $H_{\text{int}}[\mathcal{C}_{\cup N_E\cup N'_E}]>0$, thus

$$0 \leq \langle H_{\text{int}}[\mathcal{C}_{\cup N_E\cup N'_E}]\rangle_{\boldsymbol{x}\in\mathbb{F}_2^N} \tag{6.25}$$

yields a lower bound to the residual interaction energy. We still need to determine an upper-bound $\langle H_{\text{int}}[\mathcal{C}_{\cup N_E \cup N'_E}]\rangle_{\boldsymbol{x}\in\mathcal{G}} \leq I_{\text{int}}(N_E)$ to the residual interaction energies of the ground states. We want the upper bound to be only a function of N_E but to be independent of N'_E. As introduced in eq. (6.23) there are three contributions to $H_{\text{int}}[\mathcal{C}_{\cup N_E \cup N'_E}]$ which we have to calculate in the following:

1 | There are edge (E) interactions between the atoms of the same edge from different substructures for each edge:

$$\begin{aligned}\langle H_E[\mathcal{C}_{\cup N_E \cup N'_E}]\rangle_{\boldsymbol{x}\in\mathcal{G}} &\leq \sum_{p\in\mathcal{P}} \sum_{i=1}^{N_E//2} \sum_{j=1}^{N'_E//2} \frac{C}{\left((2i-1)a+(2j-1)a\right)^{-6}} \\ &\overset{\substack{n=i+j \\ \leq \\ N_E,N'_E\to\infty}}{} \frac{CP}{(2a)^6} \sum_{n=1}^{\infty} n^{-5} \leq \frac{CP}{(2a)^6}\zeta(5) =: I_E(N_E).\end{aligned} \tag{6.26}$$

Here $\zeta(s) \equiv \sum_{n=1}^{\infty} 1/n^s$ denotes the EULER–RIEMANN zeta-function. Note that $I_E(N_E) = \text{const}_{N_E}$ is a constant.

2 | There are kernel-edge (KE) interactions between the atoms of $\mathcal{C}$ and atoms of $\mathcal{C}_{N'_E}$ of each edge:

$$\begin{aligned}\langle H_{KE}[\mathcal{C}_{\cup N_E \cup N'_E}]\rangle_{\boldsymbol{x}\in\mathcal{G}} &\leq \sum_{p\in\mathcal{P}} \sum_{i=1}^{N'_E} \frac{CN_k}{(d+(2i-1)a)^{-6}} \\ &\overset{N'_E\to\infty}{\leq} \frac{CP}{(2a)^6} N_k \sum_{i=0}^{\infty} (x+i)^{-6}\Big|_{x=\frac{N_E+1}{2}} \leq \frac{CP}{(2a)^6}\frac{N_k}{120}\, S_2^{(6)}(x)\Big|_{x=\frac{N_E+1}{2}} \\ &\leq \frac{CP}{(2a)^6}\,\frac{N_k}{x^5}\left[\frac{1}{5}+\frac{2}{3x}+\frac{19}{24x^2}+\frac{427}{1728x^3}+\frac{847}{41472x^4}+\frac{7}{9216x^5}\right]\Bigg|_{x=\frac{N_E+1}{2}} \\ &\leq \frac{CP}{(2a)^6}\frac{6.4N_k}{(N_E+1)^5}\left(1+\frac{17.3}{N_E+1}\right) =: I_{KE}(N_E).\end{aligned} \tag{6.27}$$

Here we used STERLING's formula[a] in second order to upper bound the sixth logarithmic derivative of the gamma-function $\Gamma(z) \equiv \int_0^{\infty} t^{z-1}e^{-t}dt$. We find that $I_{KE}(N_E)$ decays as $1/N_E^5$.

3 | There are interactions edge-edge (EE) interactions between the atoms of $\mathcal{C}^{N'_E}$ of any edge and the atoms of all other edges. We only consider the case where the number of ports $P \leq 4$:[b]

$$\begin{aligned}
&\langle H_{EE}[\mathcal{C}_{\cup N_E \cup N'_E}]\rangle_{\boldsymbol{x}\in\mathcal{G}} \leq \sum_{\substack{p,p'\in\mathcal{P}\\ p\neq p'}} \sum_{i,j\in\mathbb{N}_0} C\left[(r+d+a+2ai)^2+(r+a+2aj)^2\right]^{-3} \\
&= \frac{CP(P-1)}{(2a)^6} \sum_{i,j\in\mathbb{N}_0} \left[j^2+n_i^2\right]^{-3}\Big|_{n_i=\frac{N+1}{2}+i} \\
&= \frac{CP(P-1)}{(2a)^6} \sum_{i\in\mathbb{N}_0} \left[-\frac{1}{n_i^6}+\frac{3\pi\coth n_i\pi}{16n_i^5}+\frac{3\pi^2}{16n_i^4\sinh^2 n_i\pi}+\frac{\pi^3\coth n_i\pi}{8n_i^3\sinh^2 n_i\pi}\right]\Big|_{n_i=\frac{N+1}{2}+i} \\
&\leq \frac{CP(P-1)}{(2a)^6} \sum_{i\in\mathbb{N}_0} \left[\frac{5\pi}{16n_i^5}\coth\left(\frac{N_E+1}{2}\pi\right)-\frac{13}{16n_i^6}\right]\Big|_{n_i=\frac{N+1}{2}+i} \qquad (6.28)\\
&\leq -\frac{C}{(2a)^6}\frac{P(P-1)}{20} S_2^{(5)}(x)\Big|_{x=\frac{N_E+1}{2}} \\
&\leq \frac{CP}{(2a)^6}\frac{(P-1)}{x^4}\left[\frac{3}{10}+\frac{4}{5x}+\frac{19}{24x^2}+\frac{61}{288x^3}+\frac{847}{55296x^4}+\frac{7}{13824x^5}\right]\Big|_{x=\frac{N_E+1}{2}} \\
&\lesssim \frac{CP}{(2a)^6}\frac{4.8(P-1)}{(N_E+1)^4}\left(1+\frac{5.\bar{3}}{N_E+1}+\frac{13.6}{(N_E+1)^2}\right) =: I_{EE}(N_E).
\end{aligned}$$

We find that $I_{EE}(N_E)$ decays as $1/N_E^4$.

Thus the residual interaction energies of the ground states are upper-bounded by

$$I_{\text{int}}(N_E) = I_E(N_E) + I_{KE}(N_E) + I_{EE}(N_E). \qquad (6.29)$$

With the lower bound (6.25) on the residual interaction energies, we obtain $\delta E[\mathcal{C}_{\cup N_E\cup N'_E}] \leq I_{\text{int}}(N_E)$ and $\Delta E[\mathcal{C}_{\cup N_E\cup N'_E}] \geq \Delta E_\infty[\mathcal{C}_{\cup N_E\cup N'_E}] - I_{\text{int}}(N_E)$. The idea is to use the detunings of different atoms to compensate for the different components of $I_{\text{int}}(N_E)$. As the languages L ($L_{N'_E}$) are linear independent, we may use the detunings of atoms in $\mathcal{C}$ ($\mathcal{C}_{N'_E}$) to correct the energy splitting introduced by $I_{KE}(N_E)+I_{EE}(N_E)$ ($I_E(N_E)$) following lemma IV. Then, the energy splitting vanishes: $\delta E[\mathcal{C}_{\cup N_E\cup N'_E}] = 0$. In the progress the energy gap may be reduced as described by theorem V:

$$\begin{aligned}
&\Delta E[\mathcal{C}_{\cup N_E\cup N'_E}] \overset{th.V}{\geq} \Delta E_\infty[\mathcal{C}_{\cup N_E\cup N'_E}] - I_{\text{int}}(N_E) - \sum\nolimits_i \|\mathbf{L}_i^+\|_1 \frac{|L_i|}{2} I_i(N_E) \\
&\geq \Delta E_\infty[\mathcal{C}_{\cup N_E\cup N'_E}] - \frac{C}{(2a)^6}\left[2\zeta(5)P + \left(1+\|\mathbf{L}^+\|_1\frac{|L|}{2}\right)\frac{P(P-1)}{(N_E+1)^4}\right. \qquad (6.30)\\
&\qquad \left.\times\left(4.8+\frac{25.6+6.4N_k/(P-1)}{N_E+1}+\frac{65.3+110.7N_k/(P-1)}{(N_E+1)^2}\right)\right] =: \Delta E_{\text{lb}}(N_E).
\end{aligned}$$

Here i symbolically iterates over the three contributions to $H_{\text{int}}[\mathcal{C}_{\cup N_E\cup N'_E}]$. Note that $\Delta E_{\text{lb}}(N_E)$ is independent of N'_E except for $\Delta E_\infty[\mathcal{C}_{\cup N_E\cup N'_E}]$. Applying lemma XII we can lower bound

$$\Delta E_\infty[\mathcal{C}_{\cup N_E\cup N'_E}] = \min\left(\Delta E[\mathcal{C}_{\cup N_E}],\ \Delta E[\mathcal{C}_{N'_E}]\right) \gtrsim \min\left(\Delta E[\mathcal{C}_{\cup N_E}],\ 20.36238\ C/(2a)^6\right) \qquad (6.31)$$

independent of N'_E. Note that the gap $\Delta E[\mathcal{C}_{N'_E}] \gtrsim 0.31816\ C/a^6$ will be larger than $\Delta E[\mathcal{C}_{\cup N_E}]$

for almost all relevant cases. If we assume that $\Delta E_{\text{lb}}(N_E) > 0$ for some N_E we obtain $\mathcal{Q}[\mathcal{C}_{\cup N_E \cup N'_E}] = 1$ independent of $N'_E \in \mathbb{N}$. □

[a] STERLING's formula: $\ln \Gamma(x) \lesssim S_2(x) \equiv \ln\left[\sqrt{2\pi/x}\,(x/e)^x \left(1 + 1/12x + 1/288x^2 + O\left(1/x^3\right)\right)\right]$ for $x > 2$
[b] Notation: $a//b \equiv \lfloor a/b \rfloor$ where $\lfloor \cdot \rfloor$ denotes the floor function.

6.A.3 | Proof for Tessellated Languages on the HC-Grid

In this subsection we present the proof of theorem XIV. First we briefly recapitulate theorem XIV:

Theorem XIV (Tessellated Languages on the Honeycomb-Grid)**.**
We assume that the local energy gaps fulfill the condition

$$0 < \Delta E_\infty := \min_{N_A \in \{1,\dots p_s\}} \left\{ \min\left(\Delta E_{loc}[\mathcal{C}_{s\cup N_E^{(0)}}],\ 10\frac{C}{(2a)^6}\right) - \frac{C}{(2a)^6}\left[2\zeta(5)P - \zeta(5)N_A + \left(1 + \|\mathbf{L}_s^+\|_1 \frac{|L_s|}{2}\right)\frac{P(P-1)}{(N_E^{(0)}+1)^4}\left(4.8 + \frac{25.6 + 6.4N_s/(P-1)}{N_E^{(0)}+1} + \frac{65.3 + 110.7N_s/(P-1)}{(N_E^{(0)}+1)^2}\right)\right]\right\} \tag{6.32}$$

for some $N_E^{(0)} \in \mathbb{N}_0$. Then for any target $\mathcal{Q}_t \in \mathbb{R}_{(0,1)}$ and any size S of the grid there exists a $N_E^* \in \mathbb{N}$ such that for all $N_E \geq N_E^*$ the quality factor is $\mathcal{Q}[\mathcal{C}_\mathcal{L}] > \mathcal{Q}_t$.

Proof.

Consider the full Hamiltonian $H[\mathcal{C}_\mathcal{L}]$ of the tessellated structure. As discussed in eq. 2.13 there arise residual interactions $H_{\text{int}}[\mathcal{C}_\mathcal{L}]$ during amalgamation which we need to consider. The residual interactions prevent us from treating amalgamated L-complexes of the VdW model as the sum of its parts like it is possible in the PXP model. This proof is based on two main ideas to circumvent this issue:
The first idea is to consider the amalgamation of the *full edge*, i.e. γ includes for each edge $N_E + 1$ atoms. The second idea is to split the residual interaction energies of the amalgamated system in the two sums from eq. (2.14). They correspond to a 'long-range' Hamiltonian $H_{\text{lr}}[\mathcal{C}_\mathcal{L}]$ a 'short-range' Hamiltonian $H_{\text{sr}}[\mathcal{C}_{s\cup N_E}]$ respectively:

$$H_{\text{int}}[\mathcal{C}_\mathcal{L}] = H_{\text{lr}}[\mathcal{C}_\mathcal{L}] - \frac{1}{2}\sum\nolimits_{s\in\mathcal{S}(\mathcal{L})} H_{\text{sr}}[\mathcal{C}_{s\cup N_E}]. \tag{6.33}$$

The short-range Hamiltonian is the correction term from eq. (2.14) which prevents double-counting of the interactions between atoms of amalgamated edges. Each edge in the bulk of the tessellated structure is adjacent to two sites. $H_{\text{sr}}[\mathcal{C}_{s\cup N_E}]$ includes the interactions between the atoms of same amalgamated edges emanating from site s. Edges at the boundary of $\mathcal{C}_\mathcal{L}$ emanate from only one site $s \in \mathcal{S}(\mathcal{L})$; they are not amalgamated thus do not contribute in

$H_{\mathrm{sr}}[\mathcal{C}_{s\cup N_E}]$. The 'long-range' Hamiltonian

$$H_{\mathrm{lr}}[\mathcal{C}_{\mathcal{L}}] = H_{EE}[\mathcal{C}_{\mathcal{L}}] + H_{SE}[\mathcal{C}_{\mathcal{L}}] + H_{SS}[\mathcal{C}_{\mathcal{L}}] \tag{6.34}$$

includes the remaining interaction energies which we did not account for in the Hamiltonian $H[\mathcal{C}_{s\cup N_E}]$ of each site s. It possesses three contributions: (1) There are edge-edge (EE) interactions between atoms of non-adjacent edges of the honeycomb grid, (2) there are site-edge (SE) interactions between atoms of sites and atoms of non-adjacent edges and (3) there are site-site (SS) interactions between atoms of any two sites. The point is that by increasing the number of atoms $2N_E$ on each edge the distance between the pairs of atom contributing to $H_{\mathrm{lr}}[\mathcal{C}_{\mathcal{L}}]$ increases as well. Thus we can arbitrarily suppress $H_{\mathrm{lr}}[\mathcal{C}_{\mathcal{L}}]$ by increasing N_E. This allows us to consider the 'long-range' Hamiltonian as a perturbation. However the 'short-range' Hamiltonian can not be suppressed by increasing N_E. The goal is to split the full Hamiltonian

$$H[\mathcal{C}_{\mathcal{L}}] = \sum\nolimits_{s\in\mathcal{S}(\mathcal{L})} H_{\mathrm{loc}}[\mathcal{C}_{s\cup N_E}] + H_{\mathrm{lr}}[\mathcal{C}_{\mathcal{L}}] \tag{6.35}$$

into a sum over local Hamiltonians $H_{\mathrm{loc}}[\mathcal{C}_{s\cup N_E}] = H[\mathcal{C}_{s\cup N_E}] - H_{\mathrm{sr}}[\mathcal{C}_{s\cup N_E}]/2$ plus the perturbation term. H_{loc} treats the $N_E + 1$ atoms of the amalgamated edge in the bulk differently as *'dummy'* atoms. The atoms of edges at the boundary are adjacent to only one site and thus are not treated as 'dummies'. A 'dummy' $\mathfrak{i}$ interacts via a *reduced interaction strength* $\tilde{C} := C/2$ with other 'dummies' $\mathfrak{j}$ *of the same edge*:

$$\tilde{U}_{\mathrm{VdW}}(\boldsymbol{r}_{\mathfrak{ij}}) := \tilde{C}/\boldsymbol{r}_{\mathfrak{ij}}^6 = U_{\mathrm{VdW}}(\boldsymbol{r}_{\mathfrak{ij}})/2. \tag{6.36}$$

A 'dummy' of an edge adjacent to a site s interacts normally via U_{VdW} with an atom of the site s or with a 'dummy'/ atom of a different edge adjacent to s. This prevents over-counting of the interaction energies between atoms of the same edge in the sum. Thus the local Hamiltonians $H_{\mathrm{loc}}[\mathcal{C}_{s\cup N_E}]$ of the sites $s \in \mathcal{S}(\mathcal{L})$ differ only in the number of amalgamated edges in the bulk which self-interact via the reduced interaction strength $\tilde{C}$.

The splitting of the full Hamiltonian (6.35) allows us to treat the structures similarly as used to in the PXP model: If for now we ignore $H_{\mathrm{lr}}[\mathcal{C}_{\mathcal{L}}]$ (e.g. by increasing $N_E \nearrow \infty$) then the energy gap of the full Hamiltonian is given by the minimal energy gap of the local Hamiltonians:

$$\Delta E[\mathcal{C}_{\mathcal{L}}] \overset{H_{\mathrm{lr}}=0}{=} \min_{s\in\mathcal{S}(\mathcal{L})} \Delta E_{\mathrm{loc}}[\mathcal{C}_{s\cup N_E}] =: \Delta E_\infty(N_E). \tag{6.37}$$

As the energy splittings of the local Hamiltonians vanish the energy splitting of the full Hamiltonian must vanish as well: $\delta E_\infty(N_E) := 0$. Note that *for OBCs* the local effective gap $\Delta E_{\mathrm{loc}}[\mathcal{C}_{s\cup N_E}]$ from sites at the boundary may differ from sites in the bulk due to a different number of amalgamated edges N_A. This means for p_s ports at each site site we need to calculate the energy gap of up to $p_s + 1$ local Hamiltonians with $N_A = 0, \dots p_s$ to determine the energy gap $\Delta E_\infty(N_E)$ of the tessellated structure. *For PBCs* due to the translational invariance we only need to calculate the energy of one local Hamiltonian where all $p_s = N_A$ adjacent edges are amalgamated.

However physically we are interested in a finite number $N_E < \infty$ of links. This introduces finite 'long-range' interactions which may cause a finite energy splitting and reduce the energy

gap. The goal is to determine an upper-bound to the energy splitting and a lower-bound to the energy gap. First note that $H_{\mathrm{lr}}[\mathcal{C}_{\mathcal{L}}] > 0$, thus

$$0 \leq \langle H_{\mathrm{lr}}[\mathcal{C}_{\mathcal{L}}] \rangle_{\boldsymbol{x} \in \mathbb{F}_2^N} \tag{6.38}$$

yields a lower bound to the 'long-range' interaction energy. We still need to determine an upper-bound $\langle H_{\mathrm{lr}}[\mathcal{C}_{\mathcal{L}}] \rangle_{\boldsymbol{x} \in \mathcal{G}} \leq I_{lr}(N_E, S)$ to the 'long-range' interaction energies of the ground states. As already noted in eq. 6.34, there are three contributions to the long-range Hamiltonian which we have to calculate in the following:

1 | There are edge-edge (EE) interactions between atoms of non-adjacent edges of the honeycomb grid:

$$\begin{aligned}
\langle H_{EE}[\mathcal{C}_{\mathcal{L}}] \rangle_{\boldsymbol{x} \in \mathcal{G}} &\leq \frac{E}{2} \frac{C}{a^6} \sum_{\substack{(i,j) \in \mathbb{Z}^2 \\ b \in \{0,1,2\} \\ \text{no nNs}}} \sum_{k,l=1}^{N_E} \left\| (N_E + r/a) \begin{bmatrix} 3(i+j) \\ \sqrt{3}(i-j) \end{bmatrix} + (2k - 1 + r/a) \begin{bmatrix} \cos 2\pi b/3 \\ \sin 2\pi b/3 \end{bmatrix} - (2l - 1 + r/a) \begin{bmatrix} 1 \\ 0 \end{bmatrix} \right\|^{-6} \\
&\overset{\substack{m=i+j \\ \leq \\ n=i-j}}{} \frac{3S}{4} \frac{C}{a^6} \frac{N_E^2}{(N_E + r/a)^6} \left[\left(\frac{8}{4^3} + \frac{14}{12^3} \right) + \sum_{\substack{(m,n) \in (2\mathbb{Z})^2 \cup (2\mathbb{Z}+1)^2 \\ b \in \{0,1,2\} \\ \text{higher orders}}} \left(\left\| \begin{bmatrix} 3m \\ \sqrt{3}n \end{bmatrix} + \begin{bmatrix} \cos 2\pi b/3 \\ \sin 2\pi b/3 \end{bmatrix} - \begin{bmatrix} 1 \\ 0 \end{bmatrix} \right\| - 1 \right)^{-6} \right] \\
&\overset{[18]}{\lesssim} \frac{CS}{a^6} \frac{0.09982635 + 0.00093604011}{(N_E + r/a)^4} \lesssim \frac{CS}{(2a)^6} \frac{6.4488}{(N_E + r/a)^4} =: I_{EE}(N_E, S).
\end{aligned} \tag{6.39}$$

We find that $I_{EE}(N_E, S)$ decays as S/N_E^4.

2 | There are site-edge (SE) interactions between atoms of sites and atoms of non-adjacent edges:

$$\begin{aligned}
\langle H_{SE}[\mathcal{C}_{\mathcal{L}}] \rangle_{\boldsymbol{x} \in \mathcal{G}} &\leq ECN_s \sum_{\substack{(i,j) \in \mathbb{Z}^2 \setminus \{\mathbf{0}\} \\ b \in \{0,1\}}} \sum_{l=1}^{N_E} \left(\left\| \begin{bmatrix} 3/2(i+j) + b \\ \sqrt{3}/2(i-j) \end{bmatrix} - \frac{2l - 1 + r/a}{N_E + r/a} \begin{bmatrix} 1/2 \\ 0 \end{bmatrix} \right\| (2d + 2r) - r \right)^{-6} \\
&\overset{\substack{m=i+j \\ \leq \\ n=i-j}}{} \frac{3S}{2} \frac{C}{a^6} \frac{N_s N_E}{(N_E + r/a)^6} \left[\left(\frac{4}{4^3} + \frac{8}{12^3} \right) + \sum_{\substack{(m,n) \in (2\mathbb{Z})^2 \cup (2\mathbb{Z}+1)^2 \\ b = \pm 1 \\ \text{higher orders}}} \left(\left\| \begin{bmatrix} 3m + b \\ \sqrt{3}n \end{bmatrix} \right\| - 1 \right)^{-6} \right] \\
&\overset{[18]}{\lesssim} \frac{CS}{a^6} \frac{(0.100694 + 0.002413936807) N_s}{(N_E + r/a)^5} \lesssim \frac{CS}{(2a)^6} \frac{6.5990 N_s}{(N_E + r/a)^5} =: I_{SE}(N_E, S).
\end{aligned} \tag{6.40}$$

We find that $I_{SE}(N_E, S)$ decays as S/N_E^5.

3 | There are site-site (SS) interactions between atoms of any two sites:

$$\begin{aligned}\langle H_{SS}[\mathcal{C}_{\mathcal{L}}]\rangle_{\boldsymbol{x}\in\mathcal{G}} &\leq \frac{S}{2}CN_s^2 \sum_{\substack{(i,j)\in\mathbb{Z}^2\\ b\in\{0,1\}\\ (i,j,b)\neq\mathbf{0}}} \left[\left\| i\begin{bmatrix}3/2\\ \sqrt{3}/2\end{bmatrix} + j\begin{bmatrix}3/2\\ -\sqrt{3}/2\end{bmatrix} + b\begin{bmatrix}1\\0\end{bmatrix}\right\|(2d+2r) - 2r\right]^{-6}\\ &\overset{\substack{m=i+j\\ n=i-j}}{\leq} \frac{S}{2}\frac{C}{a^6}\frac{N_s^2}{N_E^6} \sum_{\substack{(m,n)\in(2\mathbb{Z})^2\cup(2\mathbb{Z}+1)^2\\ b\in\{0,1\}\\ (m,n,b)\neq\mathbf{0}}} \left[(3m+2b)^2+3n^2\right]^{-3} \qquad (6.41)\\ &\overset{[18]}{\lesssim} \frac{CS}{(2a)^6}\frac{1.65300633N_s^2}{N_E^6} =: I_{SS}(N_E,S).\end{aligned}$$

We find that $I_{SS}(N_E,S)$ decays as S/N_E^6.

Thus the 'long-range' interaction energies of the ground states are upper-bounded by

$$\begin{aligned}I_{lr}(N_E,S) &= I_{EE}(N_E,S) + I_{SE}(N_E,S) + I_{SS}(N_E,S)\\ &= \frac{CS}{(2a)^6}\frac{6.4488 + 6.5990N_s/N_E + 1.6530N_s^2/N_E^2}{N_E^4} = O\left(S/N_E^4\right). \qquad (6.42)\end{aligned}$$

With the lower bound (6.38) on the 'long-range' interaction energies, we obtain $\delta E[\mathcal{C}_{\mathcal{L}}] \leq \delta E_\infty(N_E) + I_{lr}(N_E,S)$[a] and $\Delta E[\mathcal{C}_{\mathcal{L}}] \geq \Delta E_\infty(N_E) - I_{lr}(N_E,S)$.

Note that $\Delta E_\infty(N_E)$ is still a function of N_E. To obtain a lower bound $\Delta E_\infty \leq \Delta E_\infty(N_E)$ independent of $N_E \in \mathbb{N}$ we need to transfer lemma XIII to the local Hamiltonians. The local Hamiltonians $H_{\mathrm{loc}}[\mathcal{C}_{s\cup N_E}]$ may differ in the number of amalgamated edges $N_A(s)$ which are shared with another site. In the following we want to discuss the effects of the reduced interaction strength on lemma XIII parametrically dependent on N_A:
In lemma XIII we amalgamate an LNK-chain $\mathcal{C}_{N'_E}$ of length $d' = N'_E a$ to each port of $\mathcal{C}_{s\cup N_E}$ where a is defined by $\mathcal{C}_{s\cup N_E}$. In the local Hamiltonian the dummies of $\mathcal{C}_{N'_E}$ interact via $\tilde{C}$ with other dummies in $\mathcal{C}_{N'_E}$. For $\tilde{C}$ lemma XII of course remains valid by substituting $C \mapsto \tilde{C}$. This essentially corresponds to a rescaling of the chain.
The dummies in $\mathcal{C}_{N'_E}$ and the dummies in $\mathcal{C}_{s\cup N_E}$ of the same edge may interact via $\tilde{C}$ in the local Hamiltonian. In lemma XIII these interactions are upper-bounded by $I_E(N_E)$. Thus need to substitute $C \mapsto \tilde{C}$ in the upper bound $I_E(N_E)$. For residual interactions with the kernel structure and residual interactions between different edges the interaction strength is C and the upper bounds $I_{KE}(N_E)$ and $I_{EE}(N_E)$ introduced in the proof of lemma XIII remain valid.
Thus for general N_A we can reformulate the lower bound (6.6) as

$$\begin{aligned}\Delta E_\infty := \min_{N_A\in\{1,\dots p_s\}} \Bigg\{ &\min\left(\Delta E_{\mathrm{loc}}[\mathcal{C}_{s\cup N_E^{(0)}}],\ 10\frac{C}{(2a)^6}\right) - \frac{C}{(2a)^6}\Bigg[2\zeta(5)P - \zeta(5)N_A\\ &+ \left(1 + \|\mathbf{L}_s^+\|_1\frac{|L_s|}{2}\right)\frac{P(P-1)}{(N_E^{(0)}+1)^4}\left(4.8 + \frac{25.6+6.4N_s/(P-1)}{N_E^{(0)}+1} + \frac{65.3+110.7N_s/(P-1)}{(N_E^{(0)}+1)^2}\right)\Bigg]\Bigg\}. \qquad (6.43)\end{aligned}$$

independent of N_E. The lower-bound ΔE_∞ parametrically depends only on some $N_E^{(0)} < N_E$ for which we can calculate $\Delta E_{\mathrm{loc}}[\mathcal{C}_{s\cup N_E^{(0)}}]$ numerically. First note that for $N_A = 0$ we recover

the lower bound from lemma XIII. Secondly note that for almost all relevant L-complexes it is $\Delta E_{\mathrm{loc}}[\mathcal{C}_{s\cup N_E^{(0)}}] < 10C/(2a)^6$ as the energy gap of the LNK-chain is very large compared to other gates of this thesis (cf. lemma XII). Then the lower bound (6.32) is greater-equal than the lower bound (6.6) from lemma XIII. Then we can apply lemma XIII directly but this yields a less-sharp bound.

Note that $I_{lr}(N_E, S)$ decays monotonically as S/N_E^4 and becomes negligible for $N_E^4 \gg S$. Thus for any size $S \in \mathbb{N}$ of the grid and any gap $\Delta E_\infty > 0$, there exists an $N_E^* \in \mathbb{N}$ such that $I_{lr}(N_E, S) < \Delta E_\infty/2$ for all $N_E > N_E^*$. If we assume that $\Delta E_\infty > 2I_{lr}(N_E, S)$, we obtain a positive quality factor

$$\begin{aligned} \mathcal{Q}[\mathcal{C}_{\mathcal{L}}] = \exp\left[-\frac{\delta E[\mathcal{C}_{\mathcal{L}}]}{\Delta E[\mathcal{C}_{\mathcal{L}}]}\right] &\geq \exp\left[-\left(\frac{\Delta E_\infty}{I_{lr}(N_E, S)} - 1\right)^{-1}\right] \\ &\gtrsim 2 - \left[1 - \frac{I_{lr}(N_E, S)}{\Delta E_\infty}\right]^{-1} =: \mathcal{Q}_{\mathrm{lb}}(N_E, S). \end{aligned} \tag{6.44}$$

Note that latter approximation is only good for $I_{lr}(N_E^*, S) \ll \Delta E_\infty/2$. By choosing N_E^4/S sufficiently large we can achieve arbitrarily large lower bounds $\mathcal{Q}_{\mathrm{lb}}(N_E, S) > 1 - \varepsilon$ for any $\varepsilon \ll 1$. In the limit $N_E \nearrow \infty$ we recover $\mathcal{Q}_{\mathrm{lb}}(N_E, S) \nearrow 1$.

[a] Note that we can not apply theorem V to compensate for the energy splitting of the linear dependent tensor product states of the tessellated language.

6.B | Proofs for Local Languages on the HC-Grid

This appendix is denoted to sec. 6.4. Here we include the proofs to corollary XV and corollary XVI.

6.B.1 | Proof for Lower Bounds to local Languages on the HC-Grid

In this subsection we present the proof of corollary XV. First we briefly recapitulate corollary XV:

Corollary XV (Lower Bounds to local Languages on the Honeycomb Grid)**.**
We assume that the local energy gaps fulfill the condition

$$\begin{aligned}\Delta E_\infty := \min\left(\Delta E_{loc}[\mathcal{C}_{s\cup N_E^{(0)}}],\ 10\frac{C}{(2a)^6}\right) - \frac{C}{(2a)^6}\Bigg[(2P-3)\zeta(5) + \left(1+\|\mathbf{L}_s^+\|_1\frac{|L_s|}{2}\right) \\ \times \frac{P(P-1)}{(N_E^{(0)}+1)^4}\left(4.8 + \frac{25.6+6.4N_s/(P-1)}{N_E^{(0)}+1} + \frac{65.3+110.7N_s/(P-1)}{(N_E^{(0)}+1)^2}\right)\Bigg] > 0\end{aligned} \tag{6.45}$$

for some $N_E^{(0)} \in \mathbb{N}_0$. Then for any target $\mathcal{Q}_t \in \mathbb{R}_{(0,1)}$ and any radius R of $\mathcal{U}_{loc}(R)$ there exists a $N_E^* \in \mathbb{N}$ such that for all $N_E \geq N_E^*$ the local quality factor is $\mathcal{Q}_R[\mathcal{C}_\mathcal{L}] > \mathcal{Q}_t$.

Proof.

On the honeycomb grid there exist two sites per vertex. One site possesses the area

$$A_s = \frac{l^2}{2}\left|\begin{bmatrix} 3/2 & 3/2 \\ \sqrt{3}/2 & -\sqrt{3}/2\end{bmatrix}\right| = \frac{3^{3/2}}{4}l^2, \tag{6.46}$$

where $l := 2(d+r)$ denotes the distance between adjacent sites (cf. chap. 6.3 or fig. 6.4). The radius R can be directly identified with the number of sites $S_{\text{loc}}(R)$ in the local environment (and vice versa). We can upper-bound the number of sites in the local environment

$$S \lesssim \frac{A_{\text{loc}}(R+l)}{A_s} = \frac{4\pi}{3^{3/2}}\left(R/l+1\right)^2 =: S_{\text{loc}}(R). \tag{6.47}$$

We use a larger effective radius $R+l$ such that the area of each site near the boundary of the local environment is fully emerged inside the effective radius.

The main idea is to split the full Hamiltonian of the full tessellated system

$$H[\mathcal{C}_{\mathcal{L}}] = H_{\text{in}}[\mathcal{C}_{\mathcal{L}}] + H_{\text{out}}[\mathcal{C}_{\mathcal{L}}] + H_{\text{int}}[\mathcal{C}_{\mathcal{L}}] \tag{6.48}$$

into three parts: (1) $H_{\text{in}}[\mathcal{C}_{\mathcal{L}}]$ considers only the local contributions from inside the local environment, i.e. detunings from atoms inside the environment and interactions between atoms inside the environment. (2) Similarly, $H_{\text{out}}[\mathcal{C}_{\mathcal{L}}]$ considers only the detunings from atoms outside the environment and interactions between atoms outside the environment. (3) Lastly there are residual interactions $H_{\text{int}}[\mathcal{C}_{\mathcal{L}}]$ between atoms inside and outside the environment. As we are only interested in relative energies on some 'fixed background' of states outside the environment $H_{\text{out}}[\mathcal{C}_{\mathcal{L}}]$ only contributes to an absolute energy shift of the local states. Thus $H_{\text{out}}[\mathcal{C}_{\mathcal{L}}]$ neither influences the local energy splitting nor the local energy gap. Thus we essentially only need to consider $H_{\text{in}}[\mathcal{C}_{\mathcal{L}}]$ and the additional contribution by $H_{\text{int}}[\mathcal{C}_{\mathcal{L}}]$.

In the proof of theorem XIV we found that the energy splitting is caused only by the long-range interactions $H_{\text{lr}}[\mathcal{C}_{\mathcal{L}}]$. Without the long-range interactions the energy splitting (and thus in particular the local energy splitting) would vanish. Without the long-range interactions the energy gap of the tessellated structure would be the minimal energy gap of the local Hamiltonians. For the local energy gap the local environment is inside the bulk thus we only consider identical local Hamiltonians with $N_A = p_s = 3$. Thus given some initial structure $\mathcal{C}_{c\cup N_E^{(0)}}$ of each site with $N_E^{(0)}$ amalgamated links the local energy gap would be lower-bounded by (cf. eq. (6.43))

$$\begin{aligned}\Delta E_\infty := \min\left(\Delta E_{\text{loc}}[\mathcal{C}_{s\cup N_E^{(0)}}],\ 10\frac{C}{(2a)^6}\right) - \frac{C}{(2a)^6}\Bigg[(2P-3)\zeta(5) + \left(1 + \|\mathbf{L}_s^+\|_1\frac{|L_s|}{2}\right)\\ \times \frac{P(P-1)}{(N_E^{(0)}+1)^4}\left(4.8 + \frac{25.6+6.4N_s/(P-1)}{N_E^{(0)}+1} + \frac{65.3+110.7N_s/(P-1)}{(N_E^{(0)}+1)^2}\right)\Bigg].\end{aligned} \tag{6.49}$$

In the following we assume that the lower bound $\Delta E_\infty > 0$ is positive. Now for the local energy structure we only need to consider long-range interactions contributing in $H_{\text{in}}[\mathcal{C}_{\mathcal{L}}]$ or $H_{\text{int}}[\mathcal{C}_{\mathcal{L}}]$, i.e. long-range interactions which include an atom inside $\mathcal{U}_{\text{loc}}(R)$ (the second atom may be either inside or outside of $\mathcal{U}_{\text{loc}}(R)$). In the proof of theorem XIV the upper bound $I_{\text{lr}}(N_E, S)$ was calculated by considering the long-interactions of a section of S sites with the infinite honeycomb grid. Hence $I_{\text{lr}}(N_E, S_{\text{loc}}(R))$ can also be applied as an upper bound to the long-range interactions of the $S \lesssim S_{\text{loc}}(R)$ sites inside the local environment.

We obtain $\delta E[\mathcal{C}_{\mathcal{L}}] \leq I_{lr}(N_E, S)$ and $\Delta E[\mathcal{C}_{\mathcal{L}}] \geq \Delta E_\infty - I_{lr}(N_E, S)$ with $S = S_{\text{loc}}(R)$. Following this substitution, we obtain the upper-bound for the quality factor

$$\mathcal{Q}_R[\mathcal{C}_{\mathcal{L}}] \geq \exp\left[-\left(\frac{\Delta E_\infty}{I_{\text{lr}}(N_E, S_{\text{loc}}(R))} - 1\right)^{-1}\right] \geq \mathcal{Q}_{\text{lb}}(N_E, S_{\text{loc}}(R)) \tag{6.50}$$

where $\mathcal{Q}_{\text{lb}}(N_E, S_{\text{loc}}(R))$ is defined in chap. 6.A.3. If we choose $N_E^2 \gg R/l$ sufficiently large we suppress $I_{\text{lr}}(N_E, S_{\text{loc}}(R))$ and achieve an arbitrarily good lower bound $\mathcal{Q}_{\text{lb}}(N_E, S_{\text{loc}}(R))$ to the quality factor. □

6.B.2 | Proof for Upper Bounds to local Languages on the HC-Grid

In this subsection we present the proof of corollary XVI. First we briefly recapitulate corollary XVI:

Corollary XVI (Upper Bounds to local Languages on the Honeycomb Grid)**.**

Consider a tessellated L-complex $([\mathcal{C}_\mathcal{L}]_\mathcal{K}^\mathcal{Q}, L_\mathcal{L}, \mathfrak{L})$ *on a honeycomb grid of lattice* $\mathcal{L}$ *where* $L_\mathcal{L}$ *is a tessellated language with loop-DOFs. Then for any target* $\mathcal{Q}_t \in \mathbb{R}_{[0,1]}$ *there exists a finite critical radius* $R_c(\mathcal{Q}_t) < \infty$ *such that for all radii* $R \geq R_c(\mathcal{Q}_t)$ *the* local *quality factor is* $\mathcal{Q}_R[\mathcal{C}_\mathcal{L}] \leq \mathcal{Q}_t$ *in the local environment* $\mathcal{U}_{loc}(R)$*.*

Proof.

We want to proceed similarly as in the proof of theorem XI by calculating the energy splitting. However now we consider the *local splitting* and we want to quantify it as a function of the local radius R of $\mathcal{U}_{\text{loc}}(R)$ (the proof of theorem XI was qualitative for infinite grids). To determine a lower bound to the local energy splitting we consider the language $L_R(\mathbf{0})$ where no loops are excited outside of $\mathcal{U}_{\text{loc}}(R)$. We measure relative to the energy $E_0 := E(|0\rangle)$ of the state $|0\rangle$ where no loops are excited. Additionally we consider the two states $|\pm\rangle$ where $N_\pm$ loops are excited in $\mathcal{U}_{\text{loc}}(R)$. The loops are positioned on a hexagonal 'superlattice' with equal distances $l_- > l_+$ between adjacent loops. We assume that $l_+ \geq 3l$ such that two adjacent loops are not in adjacent cells. Further we assume that l_+ is sufficiently large such that the mesoscopic loop-loop-interaction energy $I(\tilde{l}) \equiv I_{\text{loop,loop}}(\tilde{l}) + I_{\text{noloop,noloop}}(\tilde{l}) - 2I_{\text{loop,noloop}}(\tilde{l})$ (cf. eq. (6.1c)) between two loops of distance $\tilde{l}$ decays monotonically for $\tilde{l} > l_+$[a]. Such a distance l_+ always exists as I is an algebraic function consisting of finitely many terms which themselves all monotonically decay to zero with (inverse) exponent γ.

For the three states $|0\rangle$, $|+\rangle$ and $|-\rangle$ we obtain the relative energies

$$\Delta E_0 = E(|0\rangle) - E(|0\rangle) = 0, \tag{6.51a}$$
$$\Delta E_+ = E(|+\rangle) - E(|0\rangle) = -N_+\Delta + I_+, \tag{6.51b}$$
$$\Delta E_- = E(|-\rangle) - E(|0\rangle) = -N_-\Delta + I_- \tag{6.51c}$$

respectively. In eqs. (6.51b) and (6.51c) $I_\pm$ denotes the sum of the loop-loop-interaction energies I between all pairs of loops. Note that $\text{sgn}(I_+) = \text{sgn}(I_-)$ because the summands I decay monotonically to zero. $\Delta \equiv E_{\text{noloop}} - E_{\text{loop}} + I_{\text{noloop,noloops}} - I_{\text{loop,noloops}}$ was already defined in eq. (6.1b) for the proof of theorem XI. It corresponds to the difference in the intrinsic energy of a cell embedded in an environment without loops. Thus Δ is a function of the geometry *and* the detunings while I and thus $I_\pm$ are only functions of the geometry. Note that state $|-\rangle$ has the same structure as state $|+\rangle$ however the distances $l_- > l_+$ between adjacent loops are larger. Thus for some fixed radius R state $|-\rangle$ possesses less excited loops than state $|+\rangle$: $N_- < N_+$. Further state $|-\rangle$ possesses less interaction energy per loop than state $|+\rangle$ due to the larger distances $l_- > l_+$ between the loops and due to the monotony of $I(\tilde{l})$ for $\tilde{l} > l_+$: $|I_-|/N_- < |I_+|/N_+$.

To minimize the splitting of the energies in eq. (6.51) we need to choose $\Delta = I_+/N_+$ [b] such that $\Delta E_+ = \Delta E_0 = 0$ and $\Delta E_- = -N_-(I_+/N_+ - I_-/N_-)$. We assume that $R \geq l_+ + 2l$ is sufficiently large such that $N_+ \geq 3$. Then we can lower-bound $|\Delta| = |I_+|/N_+ \geq |I(l_+)|$ [c]. Here $I(l_+)$ is the mesoscopic loop-loop-interaction energy between adjacent loops of distance l_+. Remember that $I(\tilde{l}) = 0$ can only be zero for finitely many values of $\tilde{l}$ as proven in theorem XI. As we chose l_+ sufficiently large such that $I(\tilde{l})$ decays monotonically to zero for $\tilde{l} > l_+$ it is $I(l_+) = \varepsilon \neq 0$. As state $|-\rangle$ has less interaction per loop than state $|+\rangle$, we obtain $\Delta E_- < (>)\, 0$ for $I_+ > (<)\, 0$. Thus the local energy splitting can be lower-bounded by

$$\delta E_R[\mathcal{C}_\mathcal{L}] \geq \delta E[\mathcal{C}_\mathcal{L}]|_{L_R(\mathbf{0})} \geq |\Delta E_-| = N_-(|I_+|/N_+ - |I_-|/N_-) \geq N_-|\varepsilon| - |I_-|. \tag{6.52}$$

Thus to make the lower bound useful we need to determine an upper bound to the interaction energy I_-:

$$\begin{aligned} I_\pm &\leq [6(N_s+N_E)]^2 \sum_{i,j\in\mathbb{Z}^2\setminus\mathbf{0}} \frac{N_\pm C}{2}\left(2\left[\left\|\begin{bmatrix} i+j/2 \\ \sqrt{3}j/2\end{bmatrix}\right\| l_\pm - 2(l+r)\right]^{-6} - 2\left[\left\|\begin{bmatrix} i+j/2 \\ \sqrt{3}j/2\end{bmatrix}\right\| l_\pm + 2(l+r)\right]^{-6}\right) \\ &\leq 36CN_\pm(N_s+N_E)^2\left([l_\pm - 2(l+r)]^{-6} - [l_\pm + 2(l+r)]^{-6}\right)\sum_{i,j\in\mathbb{Z}^2\setminus\mathbf{0}}\left[i^2+ij+j^2\right]^{-6} \\ &\overset{[18]}{\lesssim} 229.53\frac{N_\pm C}{l_\pm^6}(N_s+N_E)^2\left[(1-x)^{-6} - (1+x)^{-6}\right]\Big|_{x=2(l+r)/l_\pm} =: I_{\pm,\mathrm{ub}}(N_\pm, l_\pm). \end{aligned} \tag{6.53}$$

This now defines the lower bound $\delta E_{\mathrm{lb}}(N_-, l_-) := N_-|\varepsilon| - |I_{-,\mathrm{ub}}|$ to the energy splitting. For sufficiently large distances $l_- > l_+$ it is $|I_{-,\mathrm{ub}}|/N_- < |\varepsilon|$ and thus $\delta E_{\mathrm{lb}}(N_-, l_-) > 0$. In the following want to choose the distance $l_- = l_-^*(R) > l_+$ such that the lower bound $\delta E_{\mathrm{lb}}(N_-, l_-)$ becomes maximal for some fixed R (note that $N_- = N_-(R, l_-)$). This can be formulated as

$$I'_{-,\mathrm{ub}}(N_-)|_R \overset{!}{\approx} \varepsilon = \mathrm{const}_{N_-,\,R}. \tag{6.54}$$

Note that N_- is discrete thus this condition can in general be only be fulfilled in approximation. Further note that the local maxima are not at the boundaries because in the limiting cases $l_- = l_+,\ \infty$ it is $\delta E_{\mathrm{lb}}(R) \leq \mathrm{const}_R$.

Solving condition (6.54) can be easily done numerically (see sec. 6.5). In the following we want to derive the qualitative behavior to conclude this proof analytically. Note that the area per excited loop is a hexagon of side-length $l_\pm/\sqrt{3}$ and area $A_{\mathrm{loop}} := \sqrt{3}l_\pm^2/2$. Thus up to boundary effects [d] (e.g. in the continuum limit $N_\pm \ll R \nearrow \infty$) it is $N_\pm \approx A_{\mathrm{loc}}(R)/A_{\mathrm{loop}} = 2\pi R^2/\sqrt{3}l_\pm^2$. In eq. (6.53) it is $I_{\pm,ub} = N_\pm f(l_\pm) = N_\pm \bar{f}(N_\pm/R^2)$ with some functions $f, \bar{f} : \mathbb{R} \to \mathbb{R}$. Thus the derivative $I'_{-,ub}(N_-)|_R = f(N_-/R^2) + N_-/R^2 f'(N_-/R^2) =: \tilde{f}(N_-/R^2)$ yields some function $\tilde{f} : \mathbb{R} \to \mathbb{R}$ of N_-/R^2. Hence condition (6.54) implies $N_-^*(R) \propto R^2$ and therefore $l_-^*(R) = \mathrm{const}_R$. This means that $|I_-|/N_- = \mathrm{const}_R O(l_-^{-7})$ and we can choose $l_- = l_-^* = \mathrm{const}_R$ such that $\delta E_{\mathrm{lb}}(N_-, l_-) > 0$. Then the lower bound $\delta E_{\mathrm{lb}}(R) := \delta E_{\mathrm{lb}}(R)|_{l_-^*} \propto R^2$ on the energy splitting from eq. (6.52) diverges quadratically with the number of loops N_- in state $|-\rangle$.

As the local energy splitting diverges (quadratically) with the local radius R we can now argue similarly as in theorem XI. Consider a ground state $\boldsymbol{x} \in L$ for which the energy splitting $\delta E[\mathcal{C}_\mathcal{L}]|_{\mathcal{G}_R(\boldsymbol{x})}$ is maximized. Now consider the ground state $\tilde{\boldsymbol{x}}_{\min} \in L_R(\boldsymbol{x})$ of lowest energy $E_{\min} := E(|\tilde{\boldsymbol{x}}_{\min}\rangle)$. Note the locally modified ground state of largest energy $\tilde{\boldsymbol{x}}_{\max} \in L_R(\boldsymbol{x})$ is

of energy

$$E_{\max} := E(|\tilde{\boldsymbol{x}}_{\max}\rangle) = E_{\min} + \delta E_R[\mathcal{C}_{\mathcal{L}}] \geq E_{\min} + \delta E_{\mathrm{lb}}(R). \tag{6.55}$$

Consider any site $s \in \mathcal{S}$ of the grid inside $\mathcal{U}_{\mathrm{loc}}(R)$ with atoms $\mathcal{N}_s$. In ground state $|\tilde{\boldsymbol{x}}_{\min}\rangle$ we can always de-excite some atom(s) (e.g. one ancillary if there is one) to obtain an excited state $\tilde{\boldsymbol{x}}^* \notin L$. Exemplary consider the word $\tilde{\boldsymbol{x}}^*$ with $\tilde{x}^*_{\mathfrak{i}} = 0$ for $\mathfrak{i} \in \mathcal{N}_s$ and $\tilde{x}^*_i = (\tilde{x}_{\min})_i$ else[e]. In $\tilde{\boldsymbol{x}}^*$ all atoms (including the ports) of site s are not excited. As $\mathbf{0} \notin L$ (by remark 4) we know that $\tilde{\boldsymbol{x}}^* \in \mathcal{E}_R(\boldsymbol{x})$ is a locally excited state. The energy of $\tilde{\boldsymbol{x}}^*$ can be upper-bounded by

$$E^* := E(|\tilde{\boldsymbol{x}}^*\rangle) \leq E_{\min} + \sum_{\mathfrak{i}\in\mathcal{N}_s} \Delta_{\mathfrak{i}}. \tag{6.56}$$

Eq. (6.56) in combination with eq. (6.55) yields an upper bound $\Delta E_R[\mathcal{C}_{\mathcal{L}}] \leq \sum_{\mathfrak{i}\in\mathcal{N}_s} \Delta_{\mathfrak{i}} - \delta E_{\mathrm{lb}}(R) =: \Delta E_{\mathrm{ub}}(R)$. The ratio $Q_{\mathrm{lb}}(R) := \delta E_{\mathrm{lb}}(R)/\Delta E_{\mathrm{ub}}(R)$ defines the upper bound $\mathcal{Q}_{\mathrm{ub}}(R) := \Theta(Q_{\mathrm{lb}}(R)) \exp[-Q_{\mathrm{lb}}(R)]$ to the quality factor. As $\delta E_{\mathrm{lb}}(R) \propto R^2$ grows quadratically there exists some finite critical radius $R_{\mathrm{c}}(\mathcal{Q}_t)$ such that $\mathcal{Q}_{\mathrm{ub}}(R) < \mathcal{Q}_t$ for $R \geq R_{\mathrm{c}}(\mathcal{Q}_t)$. In particular for $\mathcal{Q}_t = 0$ there exists some finite critical radius $R_{\mathrm{c}}(\mathcal{Q}_t)$ such that $\Delta E_{\mathrm{ub}}(R) < 0$ for $R > R_{\mathrm{c}}(\mathcal{Q}_t)$. □

[a] Remember that I may be negative. $I(\tilde{l})$ may be zero for finitely many values of $\tilde{l}$.

[b] For $\Delta = I_+/N_+$ it is $\Delta E_0 = \Delta E_+ = 0$ and $\Delta E_- = -N_-(I_+/N_+ - I_-/N_-)$, i.e. $\delta E_R = N_-(|I_+|/N_+ - |I_-|/N_-)$. Consider $\Delta I_+/N_+ > (<)0$: By decreasing (increasing) Δ, $\Delta E_+ = -N_+\Delta + I_+ \propto -N_+\Delta$ increases (decreases) faster than $\Delta E_- = -N_-\Delta + I_- \propto -N_-\Delta$, i.e. δE_R increases. By increasing (decreasing) Δ, $\Delta E_- = -N_-\Delta + I_- \propto -N_-\Delta$ decreases (increases) faster than $\Delta E_0 = 0$, i.e. δE_R increases.

[c] In the limit $R \to \infty$ we would find $\Delta \gtrsim 3|I(l_+)|$

[d] The total number of loops can be upper-bounded (lower-bounded) by:
$N_\pm(R, l_\pm) \lesssim (\gtrsim)\ A_{\mathrm{loc}}(R + (-)\, l_\pm/\sqrt{3})/A_{\mathrm{loop}} = \pi(R + (-)\, l_\pm/\sqrt{3})^2/\sqrt{3}l_\pm^2/2$.

[e] This choice is possible for every language but arguably not the best choice for most languages.

7 | Boolean Theory

"Information is the resolution of uncertainty."

– C. Shannon, 'A Mathematical Theory of Communication'[36] (1948)

In chap. 4 we introduced the logic elementaries as building blocks for the amalgamation of larger Rydberg complexes. Here, for *all* PXP-minimal logic elementaries (sec. 4.1) we were able to achieve a perfect quality factor. Furthermore for *all* VdW-specific logic elementaries (sec. 4.2, sec. 4.2 and app. 4.A) *except for* the `CRS2a`-gate, we were able to achieve perfect quality. However for the asymmetric `CRS2a`-gate (see fig. 4.8) we were not able to apply theorem V (or its corollaries) therefore there remains a numerical error in the quality. Similarly for the `SCUI` unit cells from sec. 5.1 we showed in app. 5.A.1 that we can not achieve perfect ground state degeneracy. These are peculiar cases for which we would like to possess tools which guarantee us to achieve perfect quality. This motivates to introduce the concept of *virtual ancillaries* in the next sec. 7.1.

In the VdW model there arise residual interactions (2.14) between amalgamated structures. This leads us to generalize the concept of virtual ancillaries to general target functions in sec. 7.2. We derive theorem XVII which is a key result of this theses. It secures that any Boolean function or any check function can be constructed from the elementary building blocks with *perfect quality*. The downside is that theorem XVII requires generally *exponentially*[1] *many ancillaries*. This problem is discussed in outlook 7.3. Here we introduce a *counting argument* which suggests that we require in general exponentially many ancillaries to implement target functions on the Rydberg platform. However this is far from a rigorous proof and leaves room for future research.

[1] Exponential in the number of DOFs.

7.1 | Virtual Ancillaries

In the previous chapters we rarely stumbled across elementaries for which we were not able to achieve perfect quality. For most of them we were even able to achieve very good qualities. These were most notably the `CRS2a`-gate from fig. 4.8 and the amalgamated loop model unit cells `SCUI-1`, `SCUI-2a,b` and `FMUI-1,2,3` from figs. 5.1 - 5.6. Here we are not able to apply theorem V: There are too few DOFs in the detunings and too many ground states such that we are not able to compensate for the residual long-range interactions in the ground states. Furthermore there are too few intrinsic symmetries which could be exploited to effectively reduce the number of ground states for corollary IX. Thus restricts us to numerically optimizing the quality factor using the the minimization algorithm 3.2. For the `CRS2a`-gate this seems to work great as we can achieve almost perfect quality $\mathcal{Q} \approx 99.9996\%$. There seems to exist a structure with perfect degeneracy however numerically we can only approximate it (to good precision). For larger structures like the amalgamated loop model unit cells `SCUI-1`, `SCUI-2a,b` and `FMUI-2,3` the numeric optimization is computationally more intensive. It is problematic that for these unit cells a better quality factor seems to imply a smaller effective gap. In app. 5.A.1 and 5.B.2 we are able to proof that there can not exist a (symmetric) structure with a vanishing ground state splitting for these languages. Thus to achieve a vanishing energy splitting for such complexes we need to invent a new strategy which is introduced in the following.

The Concept. We want to start with an initial high-$\mathcal{Q}$ L-complex. The goal is to apply theorem V or its corollaries. The idea is to modify the languages by introducing *virtual ancillaries*. These ancillaries are not necessary to implement the language in the model but only serve the purpose to *introduce additional DOFs* to the complex (that why we call them virtual). Ideally the virtual ancillaries should not strongly modify or impede the energy structure and we want to introduce as few virtual ancillaries as possible. In the following we formalize this concept. Consider a(n effective and/or extended) language matrix $\boldsymbol{L}$ of rank $\operatorname{rank}(\boldsymbol{L}) = r$ with $g > r$ ground states. The issue is that $\operatorname{rank}(\boldsymbol{L}_{\text{Aug}}) = r + 1 > r$. The idea is to modify the language by appending ancillary bits such that the modified language matrix $\tilde{\boldsymbol{L}}$ is of rank $\operatorname{rank}(\tilde{\boldsymbol{L}}) = g$. Then the words are *linear independent* and we can apply theorem V. This concept is generalized in sec. 7.2 with theorem XVII to general Boolean functions.

Achieving perfect Quality. In the following we want to illustrate this concept by exemplary applying it to the VdW-minimal crossing `CRS-2a`, the PXP-minimal `SCUI-1` unit cell and the VdW-minimal `SCUI-2b` unit cell. As a *naive ansatz* one could try to append only a *single virtual ancillary* $\mathtt{i}$ finely tuning its detuning $\Delta_{\mathtt{i}}$ and position $\boldsymbol{r}_{\mathtt{i}}$ to its ground states. However this turns out as no useful ansatz: adding only one ancillary without modifying the other atoms *heavily* distorts the energy structure. Ground states where the virtual ancillary is excited would be energetically shifted by the detuning (plus additional interactions) whereas ground states where the virtual ancillary is not excited would not be shifted energetically. The energetic shift from the detuning can not be compensated by *strong interaction energies*, because then the state where the virtual ancillary is not excited would be energetically equally favorable. Furthermore the interaction energies would be generally very different for different ground states.

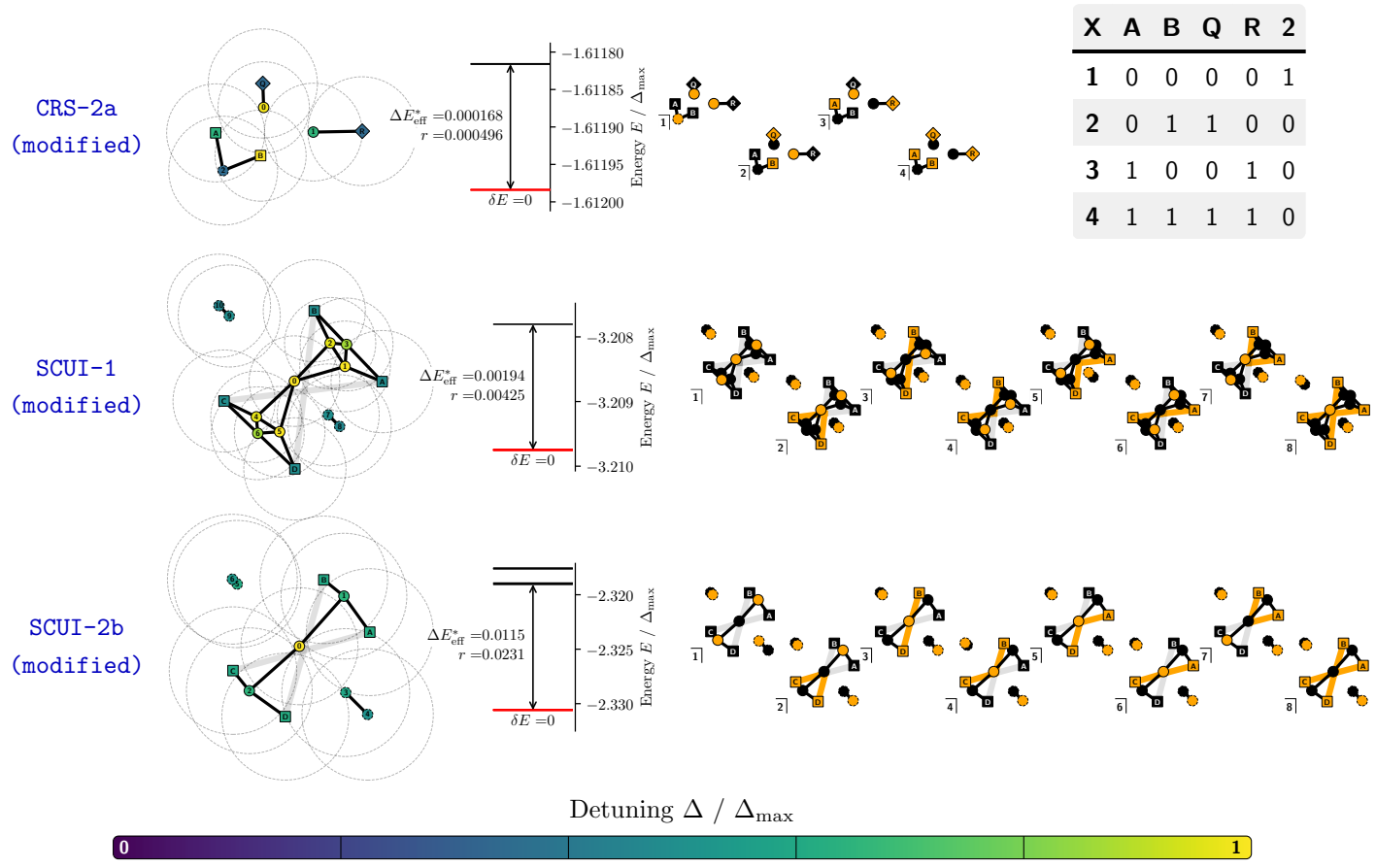

X	A	B	Q	R	2
1	0	0	0	0	1
2	0	1	1	0	0
3	1	0	0	1	0
4	1	1	1	1	0

Figure 7.1: Virtual ancillaries (dashed nodes) appended to the VdW-minimal CRS-2a-gate 4.8, the PXP-minimal SCUI-1 unit cell 5.1 and the VdW-minimal SCUI-2b unit cell 5.2. We only include the language matrix of the CRS-2a-gate as the other language matrices would be quite large. Here we note only the states of the appended ancillary. The L-complexes without the virtual ancillaries are displayed in figure 4.8, 5.1 and 5.2 respectively.

Instead, to minimize the distortion we have essentially two possibilities:

1 | We amalgamate a virtual logic gate $\mathcal{C}_2$ for which we can apply theorem V (e.g. a logic gate from chap. 4) to the initial structure $\mathcal{C}_1$. Here γ_2 should include the input ports of $\mathcal{C}_2$ such that no additional input ports are introduced in the appended language L_γ. Then the atoms of the virtual gate $\mathcal{C}_2$ are a function of the initial input ports of $\mathcal{C}_1$. Thus such an amalgamation does not change the number of the ground states.
Natural candidates for the amalgamation are the `NOR3`- and the `NAND3`-gates as they introduce only one additional ancillary (the output port of $\mathcal{C}_2$) and they possess a large effective gap. This ansatz is applied in the first row in fig. 7.1 by amalgamating a `NOR3`-gate to the input ports of the `CRS2a`-gate. The additional long-rang interactions between the amalgamated structures slightly distort the energy structure. The downside of this ansatz is that it may not be atom-efficient for every geometry. The virtual ancillary might need to be a function of atoms which are quite distant of each other. Then one would need to introduce additional `LNK`-gates which would create a large overhead of ancillaries. Therefore for the `SCUI` unit cells we choose the second ansatz.

2 | A second ansatz is to append a logic gate (e.g. a `NOT1`-gate) to the L-complex finely tuning its detuning and position such that the necessary ground states are gapped-out. This directly relies on exploiting the long-range interactions between atoms and is not based on amalgamation. Thus it can be expected that this ansatz in general yields smaller effective gaps. This ansatz might be more atoms-efficient but the fine-tuning might be complicated and numerically intensive for larger structures. This ansatz is applied in the second and third row where we appended two `NOT1`-gates to the `SCUI-1` and the `SCUI-2b` unit cell. Here the `NOT1`-gates are fine-tuned such that one of its atoms is excited in precisely one ground state. This increases the rank by one for each gate.

Using these methods we can construct a language matrix which is of full rank and which allows the application of theorem V. Thus all the elementaries portrayed in fig. 7.1 possess perfect quality $\mathcal{Q} = 1$. The elementaries are optimized for ΔE_{eff}. Note that the appended bits break some symmetries of the `SCUI`-languages, thus their optimized structures are not C_2-symmetric anymore. Furthermore the virtual ancillaries are positioned outside of the unit cell and would strongly interact with the atoms of a neighboring unit cell. Thus we can not directly tessellate the `SCUI`-structures. First we would need to add interstitial `NOT`- or `LNK`-gates to the ports.

7.2 | Implementability of Boolean Functions

In the following consider an arbitrary BOOLEAN function $f_t : \mathbb{F}_2^k \to \mathbb{F}_2^q$ with k input bits and q output bits. For $q > 1$ the BOOLEAN functions is vectorial. A corresponding L-complex possesses k input ports and q output ports. We formulate the theorem:

Theorem XVII (Implementability of BOOLEAN Functions)**.**

For every BOOLEAN *function* $f_t = f_b \in (\mathbb{F}_2^q)^{\mathbb{F}_2^k}$ *or for every check function* $f_t = f_c \in (\mathbb{F}_2)^{\mathbb{F}_2^k}$*, there exists an L-complex* $(\mathcal{C}_{\mathcal{K}}^{\mathcal{Q}}, L[f_t], \mathfrak{L})$ *which implements the target function* f_t *as its gapped low-energy eigenspace*

$$\mathcal{H}_0[\mathcal{C}] \cong_{\mathfrak{L}} \mathcal{H}(L[f_t]) \tag{7.1}$$

with quality factor $\mathcal{Q} = 1$ *in the VdW model on the* $d \geq 2$*-dimensional Rydberg platform.*

The Algorithm. The proof of this theorem is *constructive*, i.e. we formulate an algorithm which outputs the structure $\mathcal{C}$. We do not want to portray the proof in this section but instead attach it in the app. 7.A. The main idea for the construction is that we require a structure with sufficient DOFs such that we can apply theorem V. The algorithm is inspired from the proof from theorem XIV in app. 6.A.3: In the proof we split the Hamiltonian and argue that we can achieve an arbitrarily small ratios $Q[\mathcal{C}]$ for the structure choosing a sufficiently large edge-length N_E between adjacent gates. In this proof we are not interested in quantitative estimates but only in the conceptual argument thus we stick to qualitative reasoning. It would be straightforward however time-consuming to calculate a lower bound to the energy gap $\Delta E[\mathcal{C}]$ analogous to theorem XIV. We do not consider this as useful because such a construction would be in general far from minimal in the number of atoms. The argument is more of academic interest: It illustrates the possibility of the Rydberg platform to implement any target function. This is based on a 'beautiful' interplay between numerics and analytics: Numerically we calculate and optimize the energy structure of the logic elementaries we require to construct the target function. Analytically with theorem V we achieve degeneracy.

The Target Functions. Theorem XVII treats target functions defined by BOOLEAN functions $f_t = f_b$ and target functions defined by check functions $f_t = f_c$ equally, the statement is valid for both cases. This has been applied in sec. 7.1 where we added virtual ancillaries to known L-complexes to incorporate additional DOFs and achieve degeneracy. In fact the proof for check functions is inferred as a 'corollary' from the statement for BOOLEAN functions. We can treat target functions defined by check functions simply like BOOLEAN functions. Then theorem XVII

yields a structure which implements the BOOLEAN target function as its degenerate, gapped low-energy eigenspace. This includes some states where $f_c(\boldsymbol{x}) = 0$. By increasing the detuning of the output port we can lower the eigenenergy of the eigenstates with $f_c(\boldsymbol{x}) = 1$ by equal amount. This gaps-out the eigenstates with $f_c(\boldsymbol{x}) = 0$ and we obtain a positive energy gap while conserving the degeneracy of the ground states with $f_c(\boldsymbol{x}) = 1$. This yields theorem XVII for $f_t = f_c$.

Exponentially Many Ancillaries. At first glance it might come as a surprise that theorem XVII is valid for check functions as target functions because we know from theorem XI that we can not implement tessellated languages with loop-DOFs as the gapped low-energy eigenspace of a structure. However theorem XVII only makes claims about check functions which represent one site or vertex of the tessellated structure. Theorem XVII states that we can achieve degeneracy for any such vertex or site but makes no statement about how they behave under tessellation. This was exemplarily applied to the surface code unit-cells `SCUI-1` and `SCUI-2b` in fig. 7.1 from sec. 7.1. As proven in app. 5.A.1 we can not achieve degeneracy for these (symmetric) unit-cells but we can add the additional DOFs from the virtual ancillaries to apply theorem V. To make statements about the tessellated structure we would require to treat the full 'tessellated target functions' as one check function and apply theorem XVII. In such a way we could implement the language as the low-energy eigenspace of a structure. However such a structure constructed by theorem XVII would never be a tessellated structure. Theorem XVII requires *exponentially*[2] *many ancillaries* which is fundamentally incompatible with a tessellated structure which possesses *linearly many ancillaries* due to translational invariance. Therefore theorem XVII (of course) is perfectly compatible with theorem XI.

Independent Boolean DOFs. Similarly we can not simply generalize the argument of the 'no-go'-theorem XI to BOOLEAN functions. As a quick reminder in the proof of theorem XI we introduced mesoscopic 'loop-loop' interaction energies which were only functions of the geometry. As the loops are independent BOOLEAN DOFs, these mesoscopic interaction energies need to vanish such that we can achieve ground state degeneracy. Using the translational invariance of the tessellated structure we were able to proof that the mesoscopic interaction energies in general can not vanish. Then we argued that the energy splittings introduced by finite mesoscopic interactions energies add up such that they are always larger than the energy gap for large tessellated structures. We want to make some remarks why one can not simply generalize this argument to BOOLEAN functions:
Firstly we note that BOOLEAN functions possess in general no *independent* BOOLEAN DOFs. If we disassemble a BOOLEAN function into any concatenation of logic elementaries the independent inputs in general need to be evaluated multiple times. For simplicity we can consider the special case of a *read-once Boolean function* with a 'tree-level' realization. Still any input bits can modify the other bits on the same 'branch' below itself in the tree. Analogously to theorem XI we can now try to derive a mesoscopic interaction energy between these 'branches' (instead of loops) of the tree. However such branches of two bits always overlap somewhere down the tree. Thus the two bits are not independent DOFs iff the information of one bit is not annihilated in the branch before intersecting the other branch. This is in particular the case if the output is dependent on the state of both bits. In this case such a mesoscopic 'branch-branch' interaction energy always depends on the detunings of the atoms on the branch. Now we can assume that our BOOLEAN-function is *non-linear* such that there exist some bits in some state where the information of one bit is annihilated along the branch before intersecting the other branch. Then again the mesoscopic 'branch-branch' interaction energy is only dependent on the geometry and

[2] in the number of ports

we have *independent Boolean DOFs*. The mesoscopic interaction energy needs to vanish which yields a condition similarly to eq. (6.2b) which. However still BOOLEAN functions are *not translational invariant* which was applied in the proof of theorem XI to derive a contradiction. For some realizations of the BOOLEAN function where *every* other bit is fully independent of one input bit this actually yields a contradiction. However this only tells us that there exist some implementations of BOOLEAN functions for which we can not achieve ground state degeneracy (which is not very surprising). However this makes no statement at all about whether we can achieve ground state degeneracy in *any* realization of the BOOLEAN function (with polynomial many ancillaries). Thus in a nutshell, the ansatz of treating BOOLEAN functions analogous to the mesoscopic independent loop-DOFs from theorem XI turned out not very fruitful.

7.3 | Outlook: Sub-exponential Realizations

Note that for BOOLEAN target functions with k input bits there are $g = 2^k$ (exponentially) many ground states. Thus the construction from theorem XVII requires *exponentially many ancillaries*. For the $d = 2$-dimensional case the realization requires additional CRS- or ICRS-gates which further increases the number of required ancillaries. The construction 'blows up' the target function to obtain sufficient DOFs and sufficiently small residual interactions such that we can apply theorem V. Reasonably the question arises whether this upper bound to the number of required ancillaries is good or whether we can construct BOOLEAN functions with only polynomial many ancillaries. In this section we want to motivate that in general one does require exponentially many ancillaries. We start with a *counting argument* against such sub-exponential realizations (in the number of ancillaries) in the next subsec. 7.3.1. This is illustrated in subsec. 7.3.2 via limiting or high-dimensional examples for which the counting argument does not apply.

7.3.1 | A counting Argument against sub-exponential Realizations

In this subsection we want to introduce a counting argument which leads us to believe that for general target functions we do in fact require exponentially many ancillaries to implement a general BOOLEAN function on the Rydberg platform as a *degenerate*, gapped low-energy eigenspace. Note that this argument is *far from a rigorous proof*. Instead it should be understood as an outlook, a motivation or a starting point for possible future research.

Consider the Rydberg L-complex of a BOOLEAN function with a gapped, degenerate low-energy eigenspace. As the structure is degenerate the linear system (3.28) is solvable with $\tilde{\Delta}_i = \Delta_i$ and hence it must be $\operatorname{rank}(\tilde{\boldsymbol{L}}_{\text{Aug}}) = \operatorname{rank}(\tilde{\boldsymbol{L}})$. This implies that $\operatorname{coker}(\tilde{\boldsymbol{L}}_{\text{Aug}}) = \operatorname{coker}(\tilde{\boldsymbol{L}})$ where $\operatorname{coker}(\boldsymbol{A}) = \ker(\boldsymbol{A}^T)$ is the *cokernel* of a matrix $\boldsymbol{A}$. In other words: if the ground states in $\tilde{\boldsymbol{L}}$ are linear dependent via some vector $\boldsymbol{y} \in \operatorname{coker}(\tilde{\boldsymbol{L}})$, then the right-hand side of the linear system $\tilde{\boldsymbol{b}}$ must share this linear dependency:

$$\langle \boldsymbol{y} \mid \tilde{\boldsymbol{b}} \rangle \overset{!}{=} 0. \tag{7.2}$$

Now we assume that we have exponentially many ground states $g \sim 2^k$ but polynomial many ancillaries $a \sim p(k)$. Here $p \in \mathbb{R}[X]$ denotes some polynomial function. This implies that the structure possesses $N \sim p(k)$ atoms, thus the language matrix $\tilde{\boldsymbol{L}} \in \mathbb{F}_2^{g \times N}$ is very *tall-and-skinny* for large k. The rank of the language matrix is $r := \operatorname{rank}(\tilde{\boldsymbol{L}}) \leq N$ therefore the cokernel is of dimension $g - r \gtrsim 2^k - p(k) \sim 2^k$. This means that there exist $\sim 2^k$ linear independent vector $\boldsymbol{y} \in \operatorname{coker}(\tilde{\boldsymbol{L}})$ which need to be orthogonal to the right-hand side of the linear system $\tilde{\boldsymbol{b}}$. $\tilde{\boldsymbol{b}}$ is a function of the interaction energies and thus of the geometry but independent of the detunings. Thus for $g \sim 2^k$ (exponentially) many ground states there are exponentially many linear independent constraints of the form (7.2) on the geometry. However there are only $dN \sim p(k)$ (polynomial many) DOFs in the geometry which we can use to fulfill the exponentially many linear independent constraints.

Such exponentially many constraints can in fact be fulfilled with polynomial many ancillaries in *highly* symmetric L-complexes. For such L-complexes we can introduce effective ground states and the effective language matrix which effectively reduces the rows in the language matrix to $g_{\text{eff}} \sim p(k)$. However to achieve such high symmetries between k ports it seems that we require a Rydberg platform of dimension $d \sim k$. This is illustrated via brief examples in the next subsection. This leads us to believe that for general BOOLEAN functions f_b on the $d \leq 3$-dimensional Rydberg platform we can not choose a realization with polynomial many ancillaries which we can implement in the VdW model. The constraint on the dimension and thus on the symmetry seems to imply that a proof for this conjecture can not be formulated on general ground on the level of the linear system (3.28) (as done above). Instead it seems that this is a question about the *embeddability* of geometries fulfilling exponentially many constraints (7.2).

As a closing remark we want to note that if we do not require perfect degeneracy then this question becomes qualitatively different. In theorem XVII we require exponentially many ancillaries to apply theorem V and to achieve perfect degeneracy. However even without theorem V the algorithm from the proof of theorem XVII can achieve arbitrarily small energy-splitting by choosing sufficiently large distances between gates. However only for infinite distances (and therefore infinite number of ancillaries) this would yield perfect degeneracy.

7.3.2 | Examples in limiting cases

In this chapter we want to illustrate that there may exist unphysical or high-dimensional structures with *linearly*[3] many ancillaries for which it is possible to achieve a degenerate, gapped low-energy eigenspace.

The regular k-Polygon of NOT-Gates. As a simple but somewhat artificial (and unphysical) example consider the structure of k ports and $a = k$ ancillaries. The ports and ancillaries construct two concentric D_k-symmetric regular k-polygons of radii $r_{\mathcal{K}}$ and $r_{\mathcal{A}}$ respectively. Each atom possesses equal detuning. We consider the product language $L = L_{\text{NOT1}}^{\otimes_\emptyset k}$ where each port is in blockade with its nearest ancillary. It is easy to see that for $r_{\mathcal{A}} \approx r_{\mathcal{K}} \gg k r_{B,\mathrm{i}}$ the structure implements the language L as its gapped low-energy eigenspace. In this case the L-complex essentially reduces to k distant `NOT1`-gates. In the limit $r_{\mathcal{A}} \to r_{\mathcal{K}}$ the ground states are degenerate because each ground state looks the same to the Hamiltonian. This limit however is quite unphysical as it requires two different atoms to inhabit the same position. Nevertheless this illustrates that for almost-degenerate, gapped low-energy eigenspaces there may very well exist physical structures and that for fully-degenerate, gapped low-energy eigenspaces there may exist unphysical structures. The language above is constructed as a factorizable language. We are interested in whether we can construct a more physical, non-factorizable L-complex.

The Polytope of Ports. Consider a regular $2k-1$-polytope of k input ports and $a = k$ ancillaries of equal detunings $\Delta_{\mathrm{i}} < kC/r_{\mathrm{ij}}^6$ and $\Delta_{\mathrm{i}} > (k-1)C/r_{\mathrm{ij}}^6$. For such a polytope-structure on the $2k-1$-dimensional Rydberg platform each state where exactly k atoms are excited is degenerate and gapped-out. However, this is no well-defined BOOLEAN language.
Instead we consider a regular $k-1$-polytope of k input ports of equal detunings. The idea is to choose the structure highly symmetric such that we can reduce the language to $k+1$ effective ground states where $0, 1, \ldots k$ ports are excited. We add ancillaries along orthogonal directions to prevent breaking the symmetries between the ports. It turns out the most useful ansatz

[3] in the number k of input ports

to choose the (equal) distances between the input ports such that the effective ground states with $k-2n$ and $k-2n-1$ (for $n \in \mathbb{N}_0$) excited input ports are degenerate. Furthermore it turns out useful to choose the realization such that only the $n-1$-th ancillary is excited in the effective ground states with $k-2n$ and $k-2n-1$ (for $n \in \mathbb{N}_0$) excited input ports. In this way we are able to formulate an algorithm which constructs L-complexes of a BOOLEAN language with $\mathcal{Q} = 1$ as a function of the number of input ports k. This algorithm however has two important downsides: First it works only for $k \leq 9$ input ports because for larger numbers of port the energy gap seems to become negative. Secondly it requires an Rydberg platform of *large dimension* $d = N - 1 = k + \lfloor k/2 \rfloor - 1$ to achieve sufficiently many symmetries and to reduce the number of effective ground states. This illustrates that for high-dimensional structures it might be possible to choose linearly many ancillaries to achieve ground state degeneracy. However such structures are not embeddable in the three-dimensional Rydberg platform.

| Appendix

7.A | Proof of the Implementability of Boolean Functions

In this section we present the proof of theorem XVII. The proof is constructive and describes an algorithm to construct the structure $\mathcal{C}$. First we briefly recapitulate theorem XVII:

Theorem XVII (Implementability of Boolean Functions)**.**

For every Boolean *function* $f_t = f_b \in (\mathbb{F}_2^q)^{\mathbb{F}_2^k}$ *or for every check function* $f_t = f_c \in (\mathbb{F}_2)^{\mathbb{F}_2^k}$*, there exists an L-complex* $(\mathcal{C}_{\mathcal{K}}^{\mathcal{Q}}, L[f_t], \mathfrak{L})$ *which implements the target function* f_t *as its gapped low-energy eigenspace*

$$\mathcal{H}_0[\mathcal{C}] \cong_{\mathfrak{L}} \mathcal{H}(L[f_t]) \tag{7.3}$$

with quality factor $\mathcal{Q} = 1$ *in the VdW model on the* $d \geq 2$*-dimensional Rydberg platform.*

The following proof is based on the unique representation of each Boolean function as a *full disjunctive normal form (fDNF)*. Note that this choice for the proof is arbitrary and we could

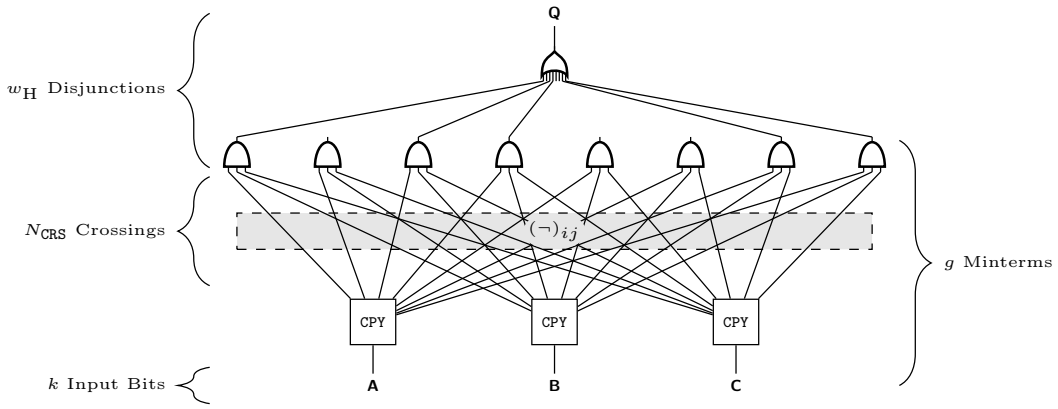

Figure 7.2: Sketch of the the construction for a scalar, ternary BOOLEAN function $f_t = f_b$ according to the proof of theorem XVII. There are $k = 3$ input ports and $g = 2^3$ ground states and minterms. The $q = 1$ fDNF of the BOOLEAN function is the disjunction of $w_H(f_b) = 5$ of these minterms. For a vectorial BOOLEAN function there would be multiple outputs.

similarly consider the DE MORGAN-dual realization with the *full conjunctive normal form (fCNF)* which is based on the *conjunction of maxterms*. Other normal forms are less natural to choose for the proof.

Proof.

We want to prove theorem XVII for general target functions either defined by a (vectorial) BOOLEAN function $f_t = f_b$ or by a check function $f_t = f_c$. Thus for $f_t = f_b$ we associate $f_c := 1$ and for $f_t = f_c$ we associate $f_b := f_c$. Then for k input bits there exist $g = w_H(f_c)$ ground states $\boldsymbol{x} \in L[f_t]$. Here w_H is the HAMMING weight which gives the cardinality of the support.

The idea is to consider the unique *full disjunctive normal form (fDNF)* of the check-function

$$f_c : \mathbb{F}_2^k \to \mathbb{F}_2 : \boldsymbol{x} \mapsto \bigvee_{i=1}^{g} \bigwedge_{j=1}^{k} (\neg)_{ij} x_j. \tag{7.4}$$

The fDNF consists of g disjunctions of pairwise different minterms. Each minterm is a conjunction of k literals including each variable precisely once. Note that the i-th minterm $Q_i := \bigwedge_{j=1}^{k} (\neg)_{ij} x_j$ of state $\boldsymbol{x}$ is one if and only if $\boldsymbol{x} = \boldsymbol{x}_i$ is the i-th ground state. The j-th literal of the i-th minterm $(\neg)_{ij} x_j$ is positive iff the j-th bit in the i-th ground state is positive. To realize the BOOLEAN functions f_b we construct its fDNF as the disjunction of the pairwise different minterms Q_i. If $f_t = f_b$ is vectorial then we construct one such fDNF for each component.

Now we want to implement each minterm Q_i for $i \in \{1, \dots g\}$ and f_b on the Rydberg platform in the VdW model. An example of the construction is sketched in fig. 7.2. The g minterms include in total at most $N_{\mathtt{AND}} = g(k-1)$ binary conjunctions `AND` (and negations `NOT`). The fDNF of f_b additionally includes at most $N_{\mathtt{OR}} = g-1$ binary disjunctions `OR`. We need $N_{\mathtt{CPY}} = k(g-1)$ `CPY2`-gates with two outputs to multiply the input ports for the `AND`-gates. For the $d = 2$-dimensional Rydberg platform we also need $N_{\mathtt{CRS}} = \delta_{d,2} N_{\mathtt{AND}}(N_{\mathtt{AND}} - 1)k(k-1)/4$ crossings

CRS. We denote the set of these AND-, OR-, CPY- and CRS-gates as $\mathcal{G}$. Thus the total number of (non-trivial[a]) gates is

$$|G| = N_{\texttt{AND}} + N_{\texttt{OR}} + N_{\texttt{CPY}} + N_{\texttt{CRS}} = O(gk) + \delta_{d,2} O(g^2 k^4), \tag{7.5}$$

linear (quadratic) in g for the $d \geq 3$ ($d = 2$)-dimensional Rydberg platform. Each gate $g \in \mathcal{G}$ is connected via at most $(k+1)g + 2N_{\texttt{CRS}}$ N_E-chains (this includes NOTm-gates[b]) such that the distance between gates scales with N_E. Each N_E-chain consists of $N_E + 1$ atoms, thus we can estimate the total number of atoms $N = O(gk)$ ($N = O(g^2k^4)$) for the two-dimensional (three-dimensional) Rydberg platform.

Now we follow the argument from the proof of theorem XIV in app. 6.A.3. We split the full Hamiltonian of the amalgamated system

$$H[\mathcal{C}] = \sum\nolimits_{g \in \mathcal{G}} H_{\text{loc}}[\mathcal{C}_{g \cup N_E}] + H_{\text{lr}}[\mathcal{C}] \tag{7.6}$$

in local Hamiltonians $H[\mathcal{C}_{g \cup N_E}]$ and a long-range Hamiltonians $H_{\text{lr}}[\mathcal{C}]$. Here $\mathcal{C}_{g \cup N_E}$ denotes gate g with $N_E + 1$ amalgamated dummies which (in a nutshell) interact with themselves via the reduced interaction strength $\tilde{C}$ (cf. eq. (6.36)). They are formally defined in app. 6.A.3. The introduction of dummies prevents over-counting of interaction energies between atoms of the same edge. Thus the local Hamiltonians may differ in the type of the gate g and in the number of edges which are associated with dummies. The idea of this artificial splitting (7.6) is the following: Ignoring the long-range Hamiltonian (i.e. for $N_E \nearrow \infty$) the energy gap of the amalgamated structure would be given by the minimal energy gap of the local Hamiltonians (cf. eq. (6.37)):

$$\Delta E[\mathcal{C}] \overset{H_{\text{lr}}=0}{=} \min_{g \in \mathcal{G}} \Delta E_{\text{loc}}[\mathcal{C}_{g \cup N_E}] =: \Delta E_\infty(N_E). \tag{7.7}$$

If condition (6.43) is fulfilled with $s \mapsto g$ for some $N_E^{(0)}$ and all $g \in \mathcal{G}$ (i.e. if $\Delta E_{\text{loc}}[\mathcal{C}_{g \cup N_E^{(0)}}]$ is sufficiently large) then there exists a lower bound $\Delta E_\infty(N_E) > \Delta E_\infty$ independent of length N_E of the chains. Note that for all the PXP-minimal elementaries from fig. 4.6 and for the VdW-minimal elementaries from fig. 4.9 we can construct such structures numerically such that $\Delta E_\infty > 0$. This allows us to assume that $\Delta E_\infty(N_E) > 0$ and $\mathcal{Q}[\mathcal{C}]|_{N_E \nearrow \infty} = 1$.

Now we need to include the long-range interactions. We constructed the structure above such that the distance between adjacent gates scales with N_E. As the number of atoms at the edges scales with N_E as well the long-range interactions energies $H_{\text{lr}}[\mathcal{C}] = O(1/N_E^4)$ are suppressed with N_E (cf. eq. (6.42)). If we choose N_E sufficiently large then we can arbitrarily suppress the perturbation introduced by $H_{\text{lr}}[\mathcal{C}]$. In particular $\Delta E[\mathcal{C}] \geq 0$ of the full Hamiltonian remains positive and $\delta E[\mathcal{C}] \ll 1$ of the full Hamiltonian is arbitrarily small.

Note that so far the proof treated target functions defined via Boolean functions $f_t \equiv f_b$ and target functions defined via check functions $f_t \equiv f_c$ equally. For latter case we treat the check function as a Boolean function $f_b \equiv f_c$. With sufficient ancillaries we are able to construct a structure which implements f_b as its gapped low-energy eigenspace. However this low-energy eigenspace includes every configuration $\boldsymbol{x} \in \mathbb{F}_2^N$ of the ports independent whether $f_c(\boldsymbol{x}) = 1$ or $f_c(\boldsymbol{x}) = 0$. To gap-out the support of the check-function we increase the detuning of the output port of $f_b \equiv f_c$. This energetically lowers the eigenenergy of the eigenstates with $f_c(\boldsymbol{x}) = 1$ by equal amount while conserving the energy splitting of the support and the energy gap to the

excited states of $f_b \equiv f_c$. We can gap-out the excited states $\boldsymbol{x}$ with $f_c(\boldsymbol{x}) = 0$ sufficiently much such that they do not impede the energy gap. Then we can again continue for both cases is similar way.

Thanks to our construction from above for each ground state $\boldsymbol{x}_i$ for $i \in \{1, \dots g\}$ there exists a minterm Q_i which is one if and only if the system is in state $|\boldsymbol{x}\rangle = |\boldsymbol{x}_i\rangle$. Thus the language matrix necessarily is of full row rank g and the ground states are linear independent. If we choose N_E sufficiently large such that $Q[\mathcal{C}]$ is sufficiently small, this allows us to apply theorem V to achieve $\mathcal{Q}[\mathcal{C}] = 1$.

[a] We do not consider the primitive gates `NOT` and `LNK` here. They are included in the N_E-chains below.

[b] For $N_E = 2m$ even with $m \in \mathbb{N}$ we obtain an `LNK`m-gate, for $N_E = 2m - 1$ odd with $m \in \mathbb{N}$ we obtain a `NOT`m-gate.

8 | Higher Dimensions

"In the history of science it happens not infrequently that a reductionist approach leads to a spectacular success. Frequently the understanding of a complicated system as a whole is impossible without an understanding of its component parts."

– Freeman Dyson, 'The Scientist as Rebel' (2006)

So far in this thesis we considered structures on the $d = 2$-dimensional Rydberg platform. In two dimensions we were able to reconstruct the PXP-minimal logic elementaries (sec. 4.1) and introduce new more atom-efficient VdW-specific elementaries (cf. sec. 4.2 and sec. 4.3) with degenerate ground states. For most of them the energy gap turned out sufficiently large with only few exceptions such as most notably the `XNOR3i`-gate. Thus one could reasonably question whether we are able to improve the `XNOR3i`-gate when including the third spatial dimension.
Afterwards in chap. 5 we studied the elementaries of two exemplary tessellated languages. For the surface code we found that we can not implement the unit cell on the $d = 2$-dimensional Rydberg platform with only one ancillary. Here the question arises whether we are able to implement the surface code unit cell in three dimensions with only one ancillary if we allow the ancillary to be located outside the plane of the ports.
These are two interesting examples which motivate us to study Rydberg structures in higher (mainly in three) dimensions. As it turns out including the additional DOFs offered by the additional spatial dimension is very fruitful to construct new and more efficient gates in the VdW model.

Constructing Rydberg structures in three dimensions can be considered the logical next step for constructing elementary Rydberg structures. However, controlling atoms in three dimensions is

experimentally much more demanding. In $d = 2$ dimensions one can exploit the third dimension to access and control the atoms. Quantum gas microscopes[22] allow for the preparation of two-dimensional lattices of hundreds of atoms. Another ansatz uses large arrays of optical tweezers[3, 31] which allow individual control of ~ 50 atoms. More recently individual control of ~ 100 atoms was achieved for arbitrarily shaped three-dimensional arrays in $d = 3$ dimensions[4]. Thus experimentally implementing the Rydberg structures portrayed in this chapter is within reach of state-of-the-art technology.

Quasiplanarity. In this context we want to introduce the concept of '*quasiplanarity*'. In the following Rydberg complexes or their geometries are called 'quasiplanar' if the ports of the complex lie within a two-dimensional plane. The ancillaries of the quasiplanar complex may be shifted outside the plane of the ports. Note that every complex with only three ports is necessarily quasiplanar, e.g. the elementary logic gates with two input ports and one output port or the FIBONACCI model sites. For complexes with four ports (e.g. for the (inverted) crossings or the surface code unit cells) requesting quasiplanarity restricts the DOFs of the ports. Such quasiplanar geometries allow for the amalgamation into large, 'thin' Rydberg complexes where only the elementary building blocks themselves are three-dimensional. The idea is that such quasiplanar geometries may be experimentally less demanding than true three-dimensional geometries with a bulk of atoms, and thus allow for the control of large numbers of atoms. Thus in this chapter we want to focus particularly on quasiplanar structures.

Visualizing three-dimensional Structures. Before we can start with the results we want to conclude this introduction with some remarks about the *visualization*. The Rydberg structures are now three-dimensional which which we need to visualize as a two-dimensional figure. For the following figures we use the *oblique graphical projection* which uses angled parallel rays to project onto the two-dimensional plane. This corresponds to the point of view of an infinitely distant observer looking at the structure under an angle. We choose the polar angle $\vartheta \approx 6.40°$[1] and the azimuthal angle $\varphi \approx 26.50°$ in spherical coordinates where the reference plane is the projection plane. This 'shifts' atoms with a positive z-coordinate to the bottom-left and atoms with a negative z-coordinate to the top-right. This prevents that atoms of the same x,y-coordinates 'hide' behind each other.
The orthographic-projected position of the atoms (with orthogonal rays where $\vartheta = 0$) is denoted by a dashed line from the oblique-projected position. For quasiplanar structures we choose the plane of the ports as the projection plane. For non-quasiplanar structures (with at least four ports) we choose the plane of three ports (usually defined by their D_3-symmetry). Black lines between the atoms are used for a clearer visualization. Note that they can *not* be interpreted as blockades anymore. Inspired from the NATTA *projection* we visualize atoms in the foreground with wedge-shaped bold bonds and atoms in the background with wedge-shaped thin bonds.
As for the two-dimensional structures we continue drawing the *blockade radii* as dashed circles around the oblique-projected positions of the atoms. Note that in three dimension the blockade radii now trace-out 2-spheres from which we draw only the projection of the equatorial great circle. Thus for three-dimensional structures one has to be even more cautious about the physical interpretation of the circles: they can only make clear statements about the blockade of two atoms if the atoms posses the same z-coordinate.

In this chapter we want to start (similarly as for the two-dimensional structures) with the logic elementaries in sections 8.1 – 8.4. Then we continue studying the surface code in sec. 8.5 and we finish with the FIBONACCI model in sec. 8.6.

[1] Note that the polar angle is relatively small. Thus the projection is *almost orthographic*.

8.1 | Binary Logic Elementaries

In this section we study implementations of the binary logic elementaries in three dimensions. Initially we consider the VdW-minimal logic gates and in particular the `XNOR3i`-gate (fig. 4.9) which was already mentioned above as an introductory example. Then we continue by introducing a family of gates based on the PXP-minimal `ICRS1`-gate from fig. 4.4. Ternary logic gates are studied in the next sec. 8.2.

8.1.1 | VdW-specific logic Elementaries

In this subsection we want to focus on the VdW-minimal realizations of the logic elementaries which were presented in sec. 4.2. Here we ignore the (inverted) crossings introduced in fig. 4.8. We need to introduce these crossing gates to implement logic circuits on the *two*-dimensional Rydberg platform. However for the three-dimensional Rydberg platform there is no necessity for introducing such gates. Here the edges may be skewed to exchange bits without a crossing. Thus it is of little use to discuss implementations for the (inverted) crossings in three dimensions.
For all the remaining VdW-specific gates presented in the sec. 4.2 and sec. 4.3 (and app. 4.A[2]) we are able to achieve ground state degeneracy. For all of them except for the `XNOR3i`-gate we obtained effective gaps of order $\Delta E_{\text{eff}} \sim 50\%$, i.e. similar as for the PXP-minimal logic gates from fig. 4.5 and 4.6. However for the `XNOR3i`-gate (see fig. 4.9) the effective gap $\Delta E_{\text{eff}}[\texttt{XNOR3i}] \approx 0.633\%$ is by *two orders of magnitude* smaller than for the PXP-minimal realization in fig. 4.6. Thus it is interesting to study whether the `XNOR3i`-gate can profit from the additional DOFs introduced by the additional spatial dimension.

The remaining VdW-specific logic Elementaries. For all the other VdW-specific logic gates from sec. 4.2 and sec. 4.3 except for the `XNOR3i`-gate we reasonably expect no improvement in the effective gap by embedding in three dimensions: the `NOR3`- and the `NAND3`-gate possess only three atoms which lie in a 2D-plane anyway. In the optimized `XOR3`-gate of fig. 4.9 the ports are located in an equilateral triangle of a fixed distance which optimizes the effective gap. The ancillary needs to be sufficiently close to the ports to remain in blockade but it can be located anywhere in the finite gray-shaded volume without modifying the effective gap. Here we can for simplicity just choose a planar structure without impeding the effective gap. The `OR3`-, the `AND3`- and the non-minimal `XNOR4a`-gate are constructed as a negation of the previous three gates by amalgamating a `NOT1`-gate to the output port. Here to maximize the effective gap we want to minimize the residual interactions. Thus reasonably the amalgamated output ports should be as distant as possible from the two input ports without breaking the blockade with the ancillary. This is achieved if the output port lies in-plane with the other three atoms respecting the reflection symmetry in the z-direction. This makes the `XNOR3i`-gate not only the

[2] In the following we ignore the VdW-specific non-minimal `XNOR4b-g`-gates with two ancillaries from app. 4.A because they are essentially the `XNOR3i`-gate from 4.9 with an additional ancillary 'glued' somewhere from which they do not profit. They are added in the appendix only for completeness.

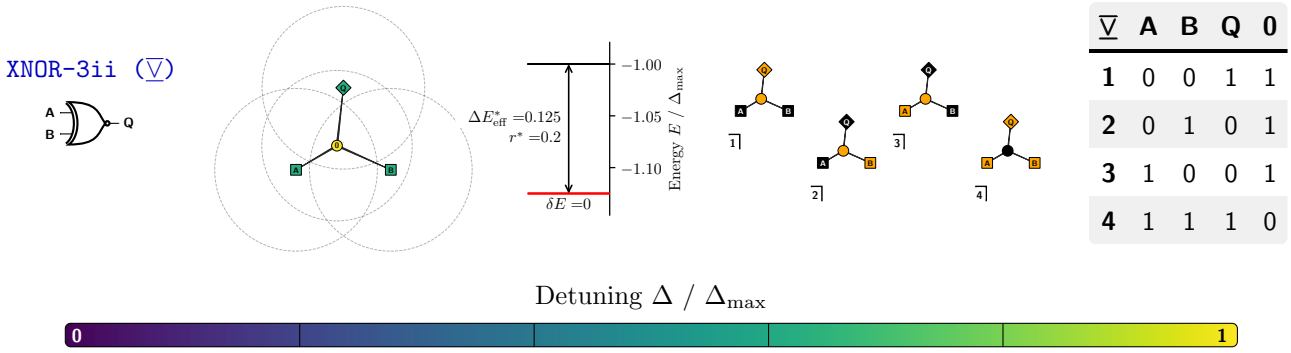

▽	A	B	Q	0
1	0	0	1	1
2	0	1	0	1
3	1	0	0	1
4	1	1	1	0

Figure 8.1: The XNOR3ii-gate optimal in ΔE_{eff} and r. The *quasiplanar* XNOR3ii-gate profits from the additional DOF for the ancillary: Its effective gap is more than one order of magnitude larger than for the planar XNOR3i-gate from fig. 4.9.

most interesting but also the only possible candidate which may profit from the additional DOFs in $d = 3$ dimensions.

The XNOR3-Gate. The XNOR3i-gate requires that the ports are sufficiently distant from the ancillary such that they are not in blockade however they should be sufficiently close such that exciting two ports alongside the ancillary is energetically not favorable. For a planar geometry the ports are necessarily distant from each other thus they possess only a small interaction energies which block the respective other ports. Here the advantage of a *quasiplanar* geometry on the $d = 3$-dimensional Rydberg platform comes into play. By shifting the ancillary outside the plane of the ports we can decrease the distance between the ports without modifying the distance with the ancillary. This allows for a greater interaction energy between the ports increasing the gap to the excited state where both ports are excited in simultaneity with the ancillary. This is portrayed in fig. 8.1 optimized in ΔE_{eff} and r. Here the effective gap $\Delta E_{\text{eff}}[\texttt{XNOR3ii}] \approx 23.5\%$ is *20 times larger* than for the two-dimensional XNOR3i-gate and of similar magnitude as the remaining logic gates in fig. 4.9. Remember that the VdW minimal realization XNOR3 is unique for $f_b = \texttt{XNOR}$. In the structure from fig. 8.1 the ports define the projection-plane and the ancillary 0 possesses a positive z-coordinate and is therefore shifted to the bottom-left.

8.1.2 | PXP-derived logic Elementaries

In this subsection we want to discuss the PXP-minimal logic elementaries from sec. 4.1. In particular we derive a family of gates based on the ICRS1-gate from fig. 4.4 which we call ICRS3.

Embeddings of PXP-blockade Graphs. In the previous subsec. 8.1.1 we discussed that the XNOR3-gate from fig. 4.9 profits from introducing the third spatial dimension. This was based on the residual interactions between the ports which needed to be *increased* to increase the effective gap. The remaining VdW-specific gates did not profit from an embedding in three dimensions because they need to *decrease* residual interactions to increase the effective gap. This already hints at what we expect for PXP-model elementaries: PXP-model elementaries are defined by a

blockade graph where atoms in blockade interact 'infinitely strong' and atoms without a blockade do not interact at all. Here $r = 1$ and the effective gap $\Delta E_{\text{eff}} = \Delta_{\min}/\Delta_{\max}$ profits from reducing the range of the detunings. When implementing such a PXP-model elementary in the VdW model the atoms in blockade possess only finite interaction energies and the atoms not in blockade possess residual interaction energies. Thus exciting an additional atom in blockade is punished by only a finite energy increase and de-exciting an atom is punished by the loss of detuning energy (as in the PXP-case) but supported by the residual interaction energies. Thus we need to *suppress the residual interactions* between the atoms which are not in blockade while keeping sufficiently *strong interactions between adjacent atoms* in the blockade graph[3]. For a two-dimensional PXP-elementary with a connected blockade graph it is now clear that this is achieved in the VdW model for a planar structure (without any bumps or curvature in the third dimension).

Symmetries. Therefore in this subsection we focus on PXP-model elementaries which are already three-dimensional in the PXP model. This subsection is based on the ideas introduced by Tobias Maier for the PXP model, transferred to the VdW model. As already noted in sec. 4.1 for the `ICRS1`-gate we can achieve ground state degeneracy just by exploiting the permutation symmetries (4.1) of the language[4]. For the D_4-symmetric implementation from fig. 4.4 the four ground states 'look identical' to the Hamiltonian and thus they trivially possess equal eigenenergies. Thus for such a D_4-symmetric structure it only remains to optimize the effective gap of the L-complex.
We can perturbatively introduce quantum fluctuations on the Rydberg platform by ramping up the Rabi frequencies Ω_i of the atoms in Hamiltonian (2.1). As the ground states still look identical to the Hamiltonian they obtain equal-weights in the superposition. This is rigorously proven by T. Maier for the PXP-model. This motivates the following study of the `ICRS1`-gate in the VdW model.

The ICRS3-Family of Gates. The `ICRS1`-gate from fig. 4.4 is of interest beyond realizing an inverted crossing on the two-dimensional Rydberg platform. As proposed by T. Maier we can relabel two ancillaries of the structure as output ports which yields the `ICRS3a`-gate. This is portrayed in the first row fig. 8.2. Here the black lines represent the blockade graph. The `ICRS3a`-gate is of course still two-dimensional and (as discussed above) does not profit from the third dimension. Still we include it in this chapter for completeness as it is the basis for the following gates `3b`, `3c` and `3d` of the same family. The two additional output ports `Q` and `R` of the `ICRS3a`-gate realize the connectives `NOR` and `AND` respectively. Thus the `ICRS3a`-gate unifies two (of in total six nontrivial) binary, scalar logical connectives as well as the inverted crossing in one gate with only two ancillaries. In the following we call such L-complexes whose output ports realize multiple logical connectives simultaneously a *multigate*. This makes the `ICRS3a`-gate the first example of a multigate we encounter.

Note that the output ports `Q` and `R` of the `ICRS3a`-gate are not quite at the boundary of the gate. This makes it impossible to amalgamate further gates (e.g. `LNK`m-gates) to the output ports in two dimensions. Therefore, even though the `ICRS3a`-gate is two-dimensional, this makes it only useful in three dimensions. To construct the negated gate we access the third dimension. We do not want to disrupt the symmetry of the structure by amalgamating `NOT1`-gates only to

[3] Think about two opposing 'forces' which need to be balanced: Connected atoms attract each other while disconnect atoms repel each other to optimize the energy gap. Although this model has its limits as the blockade graph is unphysical.

[4] Further examples of such 'degenerating symmetries' were found with the `NOR1`-gate and the `ICRS2`-gate (and trivially the `NOT1`-gate).

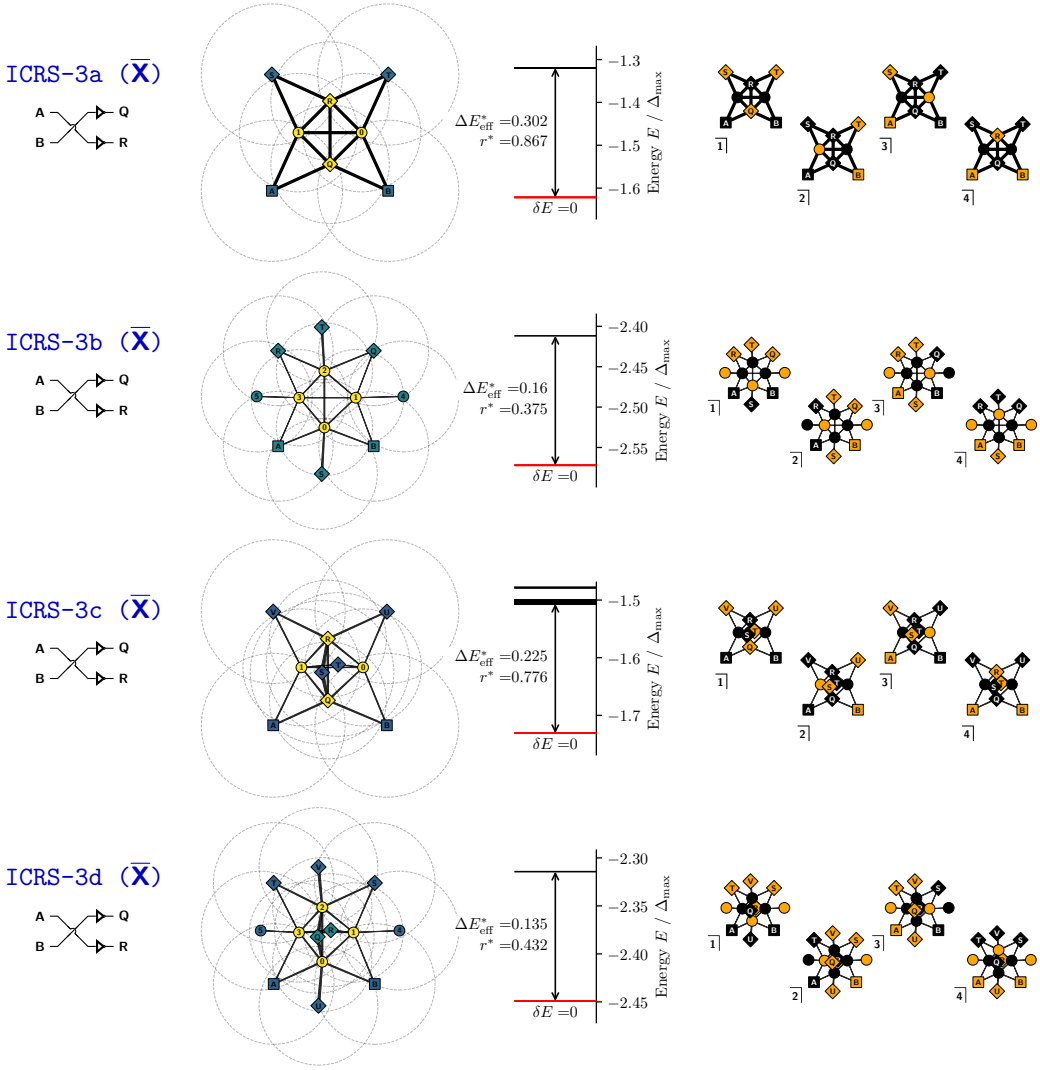

X̄	A	B	Q	R
1	0	0	1	0
2	0	1	0	0
3	1	0	0	0
4	1	1	0	1

X̄	A	B	S	T
1	0	0	0	1
2	0	1	1	1
3	1	0	1	1
4	1	1	1	0

X̄	A	B	Q	R	S	T
1	0	0	1	0	0	1
2	0	1	0	0	1	0
3	1	0	0	0	1	0
4	1	1	0	1	0	1

X̄	A	B	Q	R	U	V
1	0	0	0	1	0	1
2	0	1	1	0	1	1
3	1	0	1	0	1	1
4	1	1	0	1	1	0

Figure 8.2: Family of ICRS3-multigates optimized for ΔE_{eff} and r. For all gates the ports of the built-in ICRS-gate lie in a plane. The gates are based on the ICRS1-gate from fig. 4.4. The structures are (except for the the ICRS3a-gate) non-quasiplanar but truly three-dimensional. In this figure exceptionally the black lines *do* correspond to the blockade graph. In the tables of the right column we only show the additional/ relabeled output ports but leave out the ports and ancillaries of the ICRS1-gate.

the output ports as the symmetry is what motivates the study of this structure. Therefore we also amalgamate NOT1-gates to the two ancillaries as portrayed for the ICRS3b-multigate in the second row of fig. 8.2. Here the ground states are again degenerate by symmetry and the black lines correspond to the blockade graph. Note that the symmetry group is now the $D_{2\mathrm{d}}$ dihedral point group (this is the point group of a *tetragonal disphenoid*). The output ports S and T of the multigate realize the connectives OR and NAND respectively.

Amalgamating LNK-Gates. An interesting ansatz introduced by T. Maier for the PXP model is to amalgamate two LNK1-gates between opposite ancillaries of the ICRS1-gate. This makes the blockade graph non-planar and the Rydberg structure necessarily three-dimensional. In the VdW model the additional atoms introduce additional residual interactions which makes the construction *a priori* non trivial. It turns out that it is possible to implement this language in the VdW model by shifting adjacent ancillaries in opposite directions out of plane such that they trace-out a *tetragonal disphenoid*. The amalgamated atoms are then centered above and below the projection plane. The amalgamated structure ICRS3c is portrayed in the third row of fig. 8.2.

The amalgamation is paralleled on the languages by their γ-product. It is important to note that this γ-product conserves the permutation symmetries (4.1) of the language:

$$\Sigma_{\mathcal{N}}[\texttt{ICRS3c}] = \langle (\mathsf{A}\,\mathsf{B}) \circ (\mathsf{U}\,\mathsf{V}) \circ (0\,1),\ (\mathsf{A}\,\mathsf{B}\,\mathsf{U}\,\mathsf{V}) \circ (\mathsf{Q}\,0\,\mathsf{R}\,1) \circ (\mathsf{S}\,\mathsf{T}) \rangle.$$

In the ICRS3c-gate from fig. 8.2 this is reflected in its $D_{2\mathrm{d}}$ dihedral point group. In particular the structure is invariant under a 4-fold *improper* rotation in the plane of the ports. This implies that the four ground states of the amalgamated structure still look identical to the Hamiltonian. Thus the amalgamation conserves the ground state degeneracy and quantum fluctuation still produce equal-weights in the superposition of the ground states.

We label the amalgamated atoms as additional output ports. The amalgamation is of interest as the additional output ports S and T realize the connectives XOR and XNOR respectively. The output ports Q and R still realize the connectives NOR and AND respectively. Thus the ICRS3c-multigate unifies four (of in total six nontrivial) binary, scalar logical connectives as well as the inverted crossing in one gate with only two ancillaries. Note that the amalgamated output ports S and T make the complex non-quasiplanar but truly three-dimensional.

Similarly as for the ICRS3b-gate we can again amalgamate four NOT1-gates to negate the two output ports and construct the ICRS3d-gate. The ICRS3d-gate is portrayed in the last row of fig. 8.2. The new output ports U and V realize the connectives OR and NAND respectively. The output ports Q and R again realize the connectives XOR and XNOR respectively. Thus the ICRS3d-multigate unifies again four (of in total six nontrivial) binary, scalar logical connectives as well as the inverted crossing in one gate with six ancillaries.

Summary. In a nutshell with the ICRS3c-multigate and its negation the ICRS3d-multigate we can realize *every* logical elementary (including the inverted crossing) on a $D_{2\mathrm{d}}$-symmetric structure with equal-weight superposition. As a trade-off to conserve the symmetry we need to treat the atoms (at least in the vicinity) equally. Especially if we do not need every output this introduces an overload of ancillaries. Further the amalgamated output ports make the structure non-quasiplanar and logical circuits constructed with these gates live necessarily on the three-dimensional Rydberg platform. This makes the output of the built-in ICRS-gate not useful as in three spatial dimensions we do not require such a(n inverted) crossing implemented as a gate.

8.2 | Ternary Logic Elementaries

In this section we want to introduce ternary, scalar, symmetric logic elementaries.

The NOOR0-Gate. As an introductory, motivating example we start with the logic gate `NOOR-0` presented in fig. 8.3. It is constructed by amalgamating a `NOT1`-gate to a D_3-symmetric hexagon of atoms. The effective language matrix realized by `NOOR-0` is portrayed in the right column. The logical connective `NOOR` can be interpreted as follows:

"Q is Not excited iff any input bit A Or B OR C is excited".

This generalizes the binary `NOR`-connective to three input bits which motivates the label `NOOR` of the connective.

The `NOOR0`-gate is an example of a ternary logic gate on the *two*-dimensional Rydberg platform in the VdW model. The `NOOR0`-gate requires four ancillaries which is a lot considering that the binary `NOR3`-gate requires no ancillary at all in the VdW model. As the logic elementaries from fig. 4.9 are functionally complete we can also simply amalgamate these elementaries to construct another realization of the `NOOR`-function. For example the amalgamation of a `NOR3`-gate to the output of a `OR3`-gate possesses only two ancillaries. However such an amalgamation introduces additional residual interaction energies (2.14) which cause a finite energy splitting. In general we can not fully suppress such energy splittings (e.g. with theorem V).

Example 14. (Surface Code Unit-Cellls)

> For example the surface code unit cells `SCUI-1` and `SCUI-2a,b` from chap. 5.1 are constructed by amalgamating two binary `XNOR`- or `XOR`-gates. However as shown in proof 10 we can not achieve degeneracy for them in any (symmetric) structure.

In contrast the language matrix $\mathbf{L}_{\texttt{NOOR0}}$ is of full rank which allows us to apply theorem V to achieve ground state degeneracy in fig. 8.3.

More-advanced Building Blocks. Naturally the question arises whether we are able to construct further more atom-efficient, high-$\mathcal{Q}$ (and ideally high-ΔE_{eff}) ternary logic gates if we allow for three-dimensional geometries. Such building blocks would allow us to reduce the number of amalgamations between logic gates and simplify the logic circuit. This could help to reduce the energy splitting (i.e. increase the quality) and make the logic circuit more atom-efficient. Latter is relevant to reduce the requirements to the experimental setup. This motivates the following study of ternary logic gates on the three-dimensional Rydberg platform in this section.

The goal is to offer a list of more advanced building blocks which can be used to efficiently implement logic circuits and to visualize the possibilities introduced with the third spatial dimension. In this section we focus on *ternary, scalar and symmetric* logic elementaries. We are mainly interested in the *VdW-minimal* realizations of the functions.

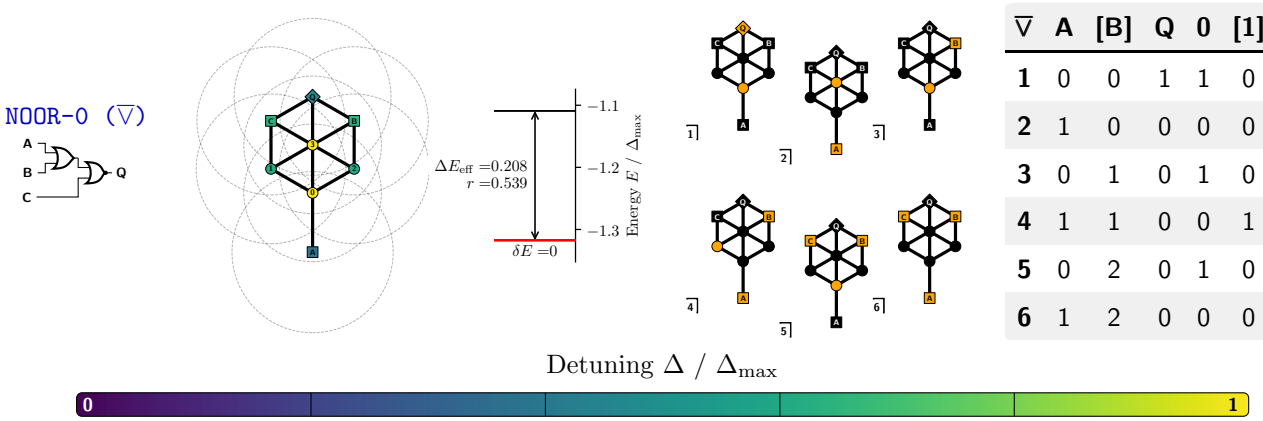

▽	A	[B]	Q	0	[1]	3
1	0	0	1	1	0	0
2	1	0	0	0	0	1
3	0	1	0	1	0	0
4	1	1	0	0	1	0
5	0	2	0	1	0	0
6	1	2	0	0	0	0

Figure 8.3: Two-dimensional, ternary NOOR0-gate with four ancillaries. The gate is constructed as an amalgamation of a hexagonal structure with a NOT1-gate.

For the symmetric BOOLEAN functions we consider only *symmetric realizations*. With $k = 3$ input bits there are $g = 2^3$ ground states which reduce to only $g_{\text{eff}} = 4$ effective ground states for symmetric implementations. With $q = 1$ output bit there exist in total $2^4 = 16$ symmetric BOOLEAN functions. Two of them are constant and thus trivial which makes *14 nontrivial* BOOLEAN *functions*. In the following for a clearer discussion we categorize the 14 nontrivial symmetric BOOLEAN function in sets distinguished by the number of *effective* ground states for which the output bit is excited. We call this the *effective Hamming weight* w_H of the BOOLEAN function (in analogy to the HAMMING weight[5] defined for general BOOLEAN functions). In a nutshell there exist four connectives with effective HAMMING weight $w_H = 1$ or $w_H = 3$ and there exist six connectives with effective HAMMING weight $w_H = 2$[6]. The first two sets of connectives are dual to each other under negation of the output bit while latter set is self-dual. In the following two subsections 8.2.1 and 8.2.2 we start with the first two sets of connectives.

Labels of the Connectives. Note that the names associated with the following BOOLEAN functions are not common in literature. They are either motivated from their binary counterparts or they are chosen such that they offer an interpretation of the function. The negation of a connective is usually denoted by the prefix 'N'. The functions are *defined* by their logic circuit (in the first column) or by their truth table (in the last column). We already encountered an example of this labeling with the NOOR0-gate in fig. 8.3. We want to illustrate the labeling scheme briefly via two more examples:

Example 15. (Nomenclature of the ternary logic Gates)

1 | The logical connective XXOR can be interpreted as: "iff eXclusively A or eXclusively B OR exclusively C is excited then Q is excited". Its negation is the logical connective NXXOR.

2 | The logical connective XXNOR can be interpreted as: "iff eXclusively A or eXclusively B OR exclusively C is Not excited then Q is excited". Its negation is the logical connective NXXNOR.

[5] The HAMMING weight of a BOOLEAN function is defined as the cardinality of its support.
[6] The two BOOLEAN functions with effective HAMMING weight $w_H = 0$ and $w_H = 4$ are the *constant* BOOLEANS.

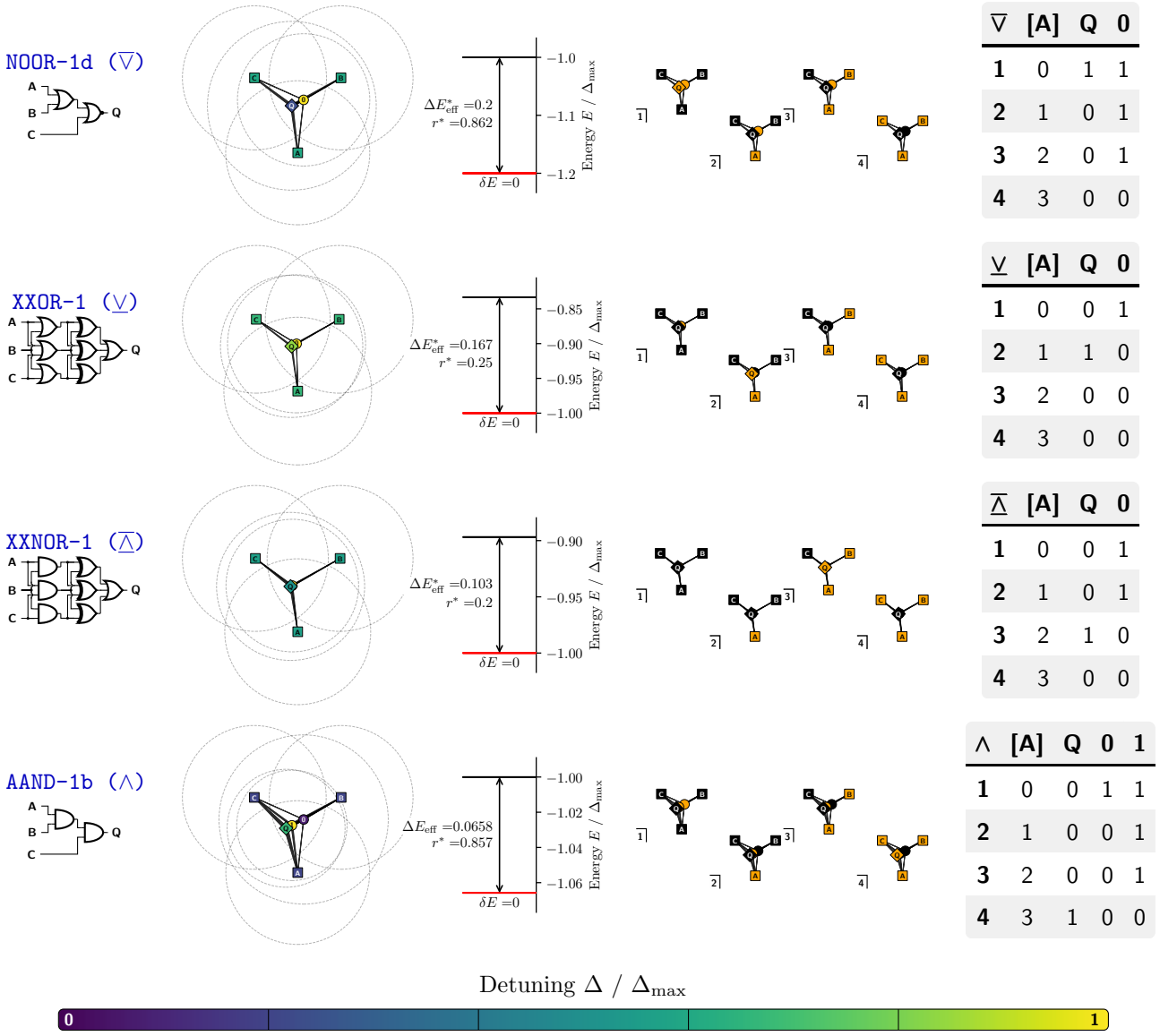

▽	[A]	Q	0
1	0	1	1
2	1	0	1
3	2	0	1
4	3	0	0

⩛	[A]	Q	0
1	0	0	1
2	1	1	0
3	2	0	0
4	3	0	0

⩓	[A]	Q	0
1	0	0	1
2	1	0	1
3	2	1	0
4	3	0	0

∧	[A]	Q	0	1
1	0	0	1	1
2	1	0	0	1
3	2	0	0	1
4	3	1	0	0

Figure 8.4: Family of ternary, scalar, symmetric logic gates with unit effective HAMMING weight $w_H = 1$. The portrayed connectives emerge from the connectives from fig. 8.5 via negation. Further gates are portrayed in fig. 8.22. Completeness and minimality are shown in proof 16.

8.2.1 | Unit effective Hamming Weight

First we consider the ternary, scalar, symmetric logic gates with effective HAMMING weight $w_H = 1$. Here the output bit is excited in precisely one *effective* ground state. This includes the four logical connectives `NOOR`, `XXOR`, `XXNOR` and `AAND` which are defined in fig. 8.4. Note that fig. 8.4 portrays only one representative of the possible realizations. Further realizations are attached in app. 8.A.1 (see fig. 8.22). There in proof 16 we show two important statements which we briefly want to summarize in the following:

1 | Every realization portrayed in fig. 8.4 and fig. 8.22 is *VdW-minimal*: The connectives `NOOR`, `XXOR` and `XXNOR` require only one ancillary. The `AAND`-gates require at least two ancillaries.

2 | For the connectives `NOOR`, `XXOR` and `XXNOR` the combined list of realizations in fig. 8.4 and fig. 8.22 is *exhaustive*. For `AAND` there exist in total *seven* possible realizations.

For `AAND` we restrict ourselves for simplicity to the two realizations which we identified as the most promising ones. The portrayed `AAND1a`- and `AAND1b`-gate are the negations of the `NAAND1a`- and the `NAAND1b`-gate from fig. 8.5 and fig. 8.23 respectively.

The `NOOR1`-gate is essentially constructed from the `NOOR0`-gate in fig. 8.3 by unifying the four ancillaries from which at most one is excited in any state.

8.2.2 | Effective Hamming Weight Three

In this subsection we consider the ternary, scalar, symmetric logic gates with effective HAMMING weight $w_H = 3$. It is natural to continue with these connectives because they are *dual* to the connectives with unit effective HAMMING weight: They emerge by a simple negation of the output from the gates of previous subsec. 8.2.1. Thus the output bit is *not* excited in precisely one *effective* ground state. This includes the four logical connectives `OOR`, `NXXOR`, `NXXNOR` and `NAAND` which are defined in fig. 8.5. They are the negations of the connectives `NOOR`, `XXOR`, `XXNOR` and `AAND` which is denoted by the prefix '`N`'. Again, fig. 8.5 portrays only one representative of the possible realizations. Further realizations are attached in app. 8.A.2 (see fig. 8.23). There in proof 17 we show two important statements which we briefly want to summarize at this point:

1 | Every realization portrayed in fig. 8.5 and fig. 8.23 is *VdW-minimal*. The connectives `NAAND`, `NXXNOR` and `NXXOR` require only one ancillary. The `OOR`-gates require at least two ancillaries.

2 | For the connectives `NAAND`, `NXXNOR` and `NXXOR` the combined list of realizations in fig. 8.5 and fig. 8.23 is *exhaustive*. For `OOR` there exist in total *seven* possible realizations.

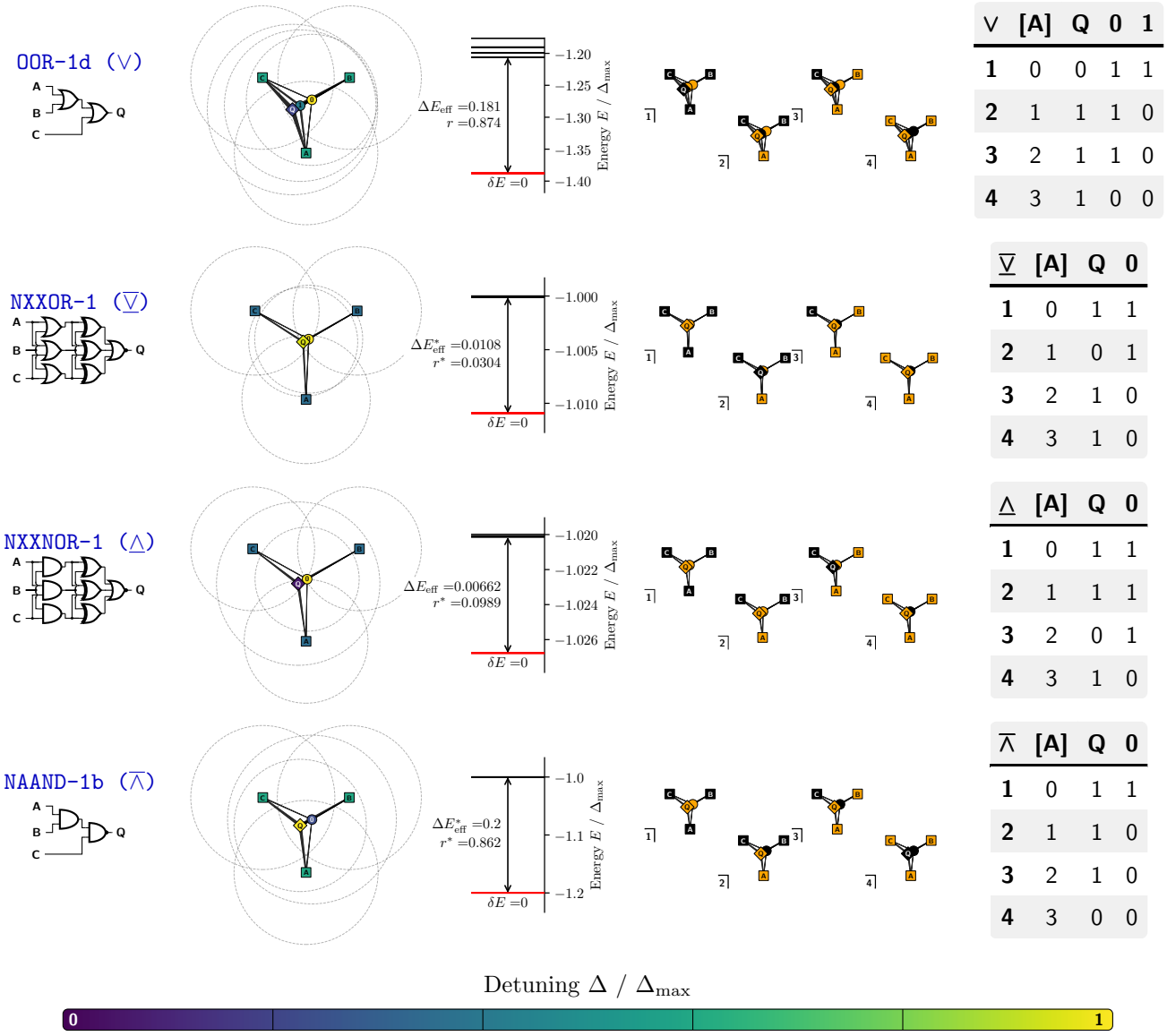

∨	[A]	Q	0	1
1	0	0	1	1
2	1	1	1	0
3	2	1	1	0
4	3	1	0	0

⊽	[A]	Q	0
1	0	1	1
2	1	0	1
3	2	1	0
4	3	1	0

△	[A]	Q	0
1	0	1	1
2	1	1	1
3	2	0	1
4	3	1	0

⊼	[A]	Q	0
1	0	1	1
2	1	1	0
3	2	1	0
4	3	0	0

Figure 8.5: Family of ternary, scalar, symmetric logic gates with effective HAMMING weight $w_H = 3$. The portrayed connectives emerge from the connectives from fig. 8.4 via negation. Further gates are portrayed in fig. 8.23. Completeness and minimality are shown in proof 17.

For OOR we restrict ourselves for simplicity to the four realizations which we identified as the most promising ones. The portrayed OORa,b,c,d-gates are the negations of the NOORa,b,c,d-gates from fig. 8.4 and fig. 8.22 respectively.

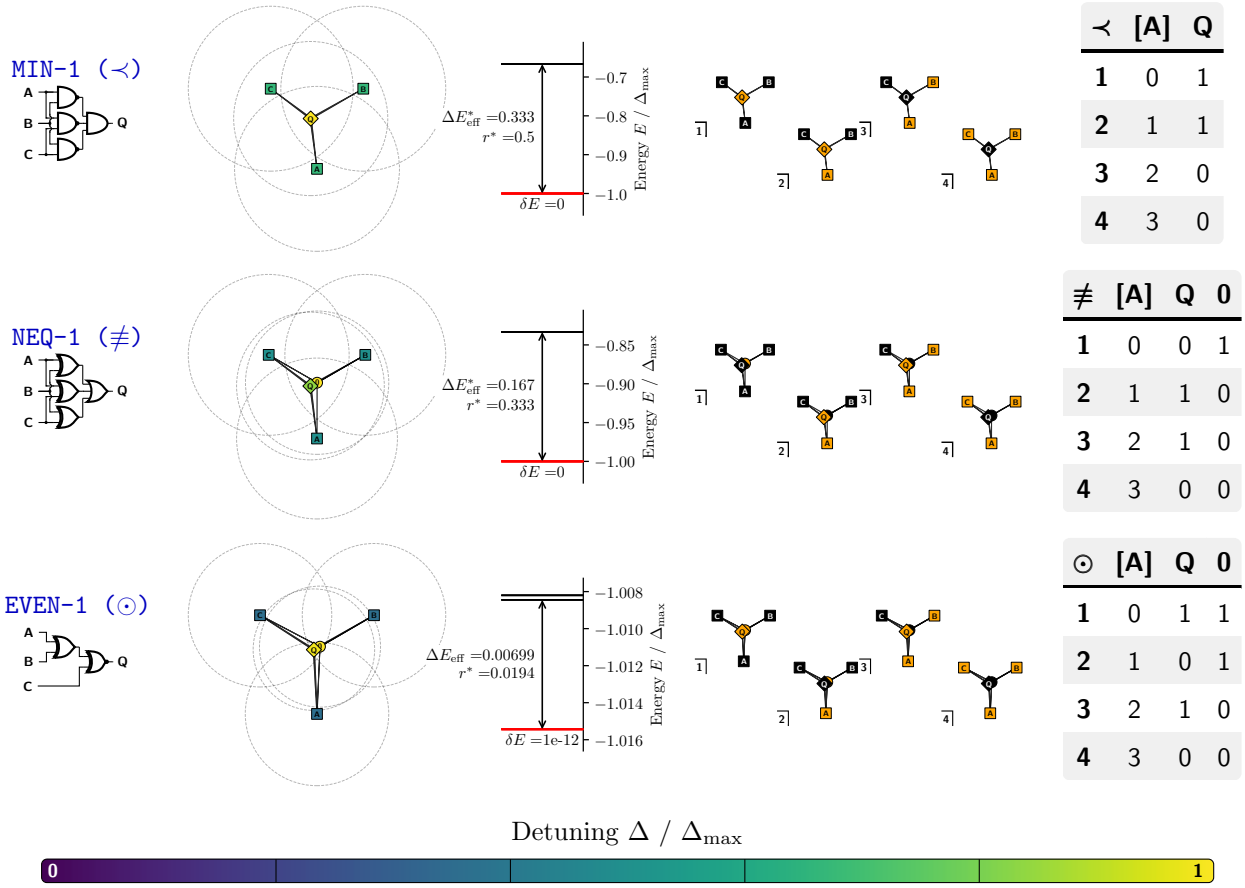

≺	[A]	Q
1	0	1
2	1	1
3	2	0
4	3	0

≠	[A]	Q	0
1	0	0	1
2	1	1	0
3	2	1	0
4	3	0	0

⊙	[A]	Q	0
1	0	1	1
2	1	0	1
3	2	1	0
4	3	0	0

Figure 8.6: Part 1 of the family of ternary, scalar and symmetric logic gates with effective HAMMING weight $w_H = 2$. The portrayed connectives emerge from the connectives in part 2 (see fig. 8.7). Completeness and Minimality are discussed in app. 8.A.3 (see proof 18).

8.2.3 | Effective Hamming Weight Two

Lastly we consider the ternary, scalar, symmetric logic gates with effective HAMMING weight $w_H = 2$. Here the output bit is (not) excited in precisely two *effective* ground states. This includes the three logical connectives `MIN`, `NEQ` and `EVEN` and their respective negations `MAJ`, `EQU` and `ODD`. The connectives are defined by the logic circuits (first column) or the effective language matrix (last column) in fig. 8.6 and fig. 8.7 respectively.

In app. 8.A.3 in proof 17 we show two important statements about these gates which we briefly want to summarize:

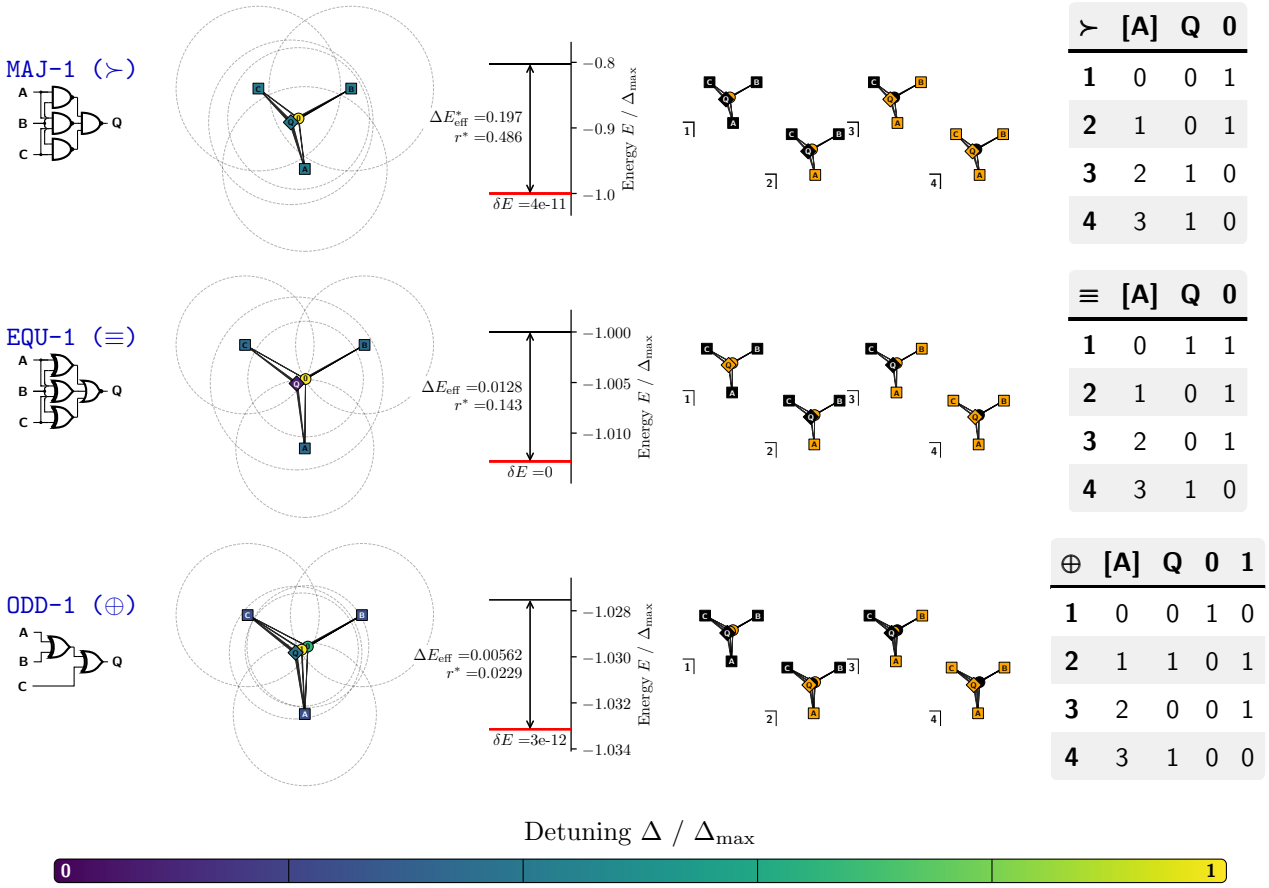

≻	[A]	Q	0
1	0	0	1
2	1	0	1
3	2	1	0
4	3	1	0

≡	[A]	Q	0
1	0	1	1
2	1	0	1
3	2	0	1
4	3	1	0

⊕	[A]	Q	0	1
1	0	0	1	0
2	1	1	0	1
3	2	0	0	1
4	3	1	0	0

Figure 8.7: Part 2 of the family of ternary, scalar and symmetric logic gates with effective HAMMING weight $w_H = 2$. The portrayed connectives emerge from the connectives in part 1 (see fig. 8.7). Completeness and Minimality are discussed in app. 8.A.3 (see proof 18).

1 | Every realization portrayed in fig. 8.6 and fig. 8.7 is *VdW-minimal*. The connectives require at most one ancillary. The `MIN`-gate requires no ancillary at all.

2 | The list of VdW-minimal realizations in fig. 8.6 and fig. 8.7 is *exhaustive*. For each gate there exists only one *unique* VdW-minimal realization.

The `MIN1`-gate ('minority'-gate) requires no ancillary at all which makes it the most 'natural' ternary gate on the three-dimensional Rydberg platform. In comparison even the `NOOR1`-gates (see fig. 8.4) require at least one ancillary[7].

[7] Remember that the `NOR`-gates were the most natural *binary* gates on the two-dimensional Rydberg platform (cf. subsections 4.1.3, 4.1.4 and 4.2.3).

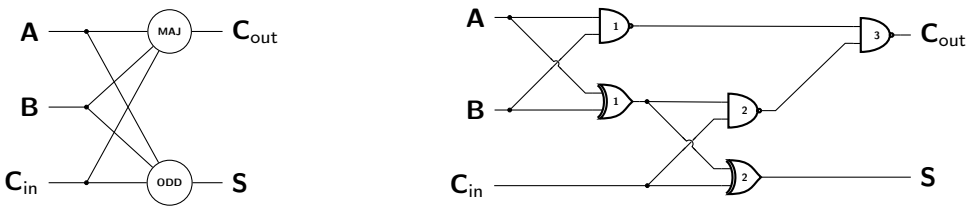

(a) Full adder based on ternary gates

(b) Standard XOR-based full adder

Figure 8.8: Full Adders based on different Gates. The ternary logic gates MAJ and ODD allow for a simpler implementation (left) than the standard XOR-based full adder (right).

8.2.4 | Interpretations of the Connectives

In the following we want to offer some brief interpretations and applications of the gates from the previous subsections 8.2.1, 8.2.2 and 8.2.3.

Full Adders. The negation of the MIN1-gate is the MAJ1-gate ('majority'-gate) which requires at least one ancillary. MAJ-gates are well-known for being used in *full adders*[17] to calculate the carry bit C_{out}:

$$\mathsf{C_{out}} = \mathtt{MAJ}(\mathsf{A},\mathsf{B},\mathsf{C_{in}}), \qquad \mathsf{S} = \mathtt{ODD}(\mathsf{A},\mathsf{B},\mathsf{C_{in}}). \tag{8.1}$$

The sum-bit S is evaluated as the ODD-gate of the inputs. This is visualized as a logic circuit in fig. 8.8a. This illustrates the possibilities introduced with ternary logic gates: With the ternary elementaries we require only *two gates* for the full adder, one for each output bit. In contrast, with the binary elementaries the calculation of the sum and the carry bit requires two and four gates respectively. The standard XOR-based implementation of the full adder requires in total *five gates* (plus additionally more CPY-gates):

$$\mathsf{C_{out}} = (\mathsf{A} \barwedge \mathsf{B}) \barwedge (\mathsf{C_{in}} \barwedge (\mathsf{A} \veebar \mathsf{B})), \qquad \mathsf{S} = (\mathsf{A} \veebar \mathsf{B}) \veebar \mathsf{C_{in}}. \tag{8.2}$$

The logic circuit for the standard XOR-based full adder is visualized in fig. 8.8b. The implementation of the full adder based only on the singleton {NOR} as the 'natural universal gate set' on the Rydberg platform requires *nine NOR-gates* (plus additionally a lot CPY-gates).

Additionally the MAJ1-gate is very robust with $\Delta E_{\text{eff}}[\mathtt{MAJ1}] \approx 19.7\%$. This is the disadvantage of the ODD1-gate which possesses a relatively low effective gap $\Delta E_{\text{eff}}[\mathtt{ODD1}] \approx 0.6\%$. Thus experimentally it might be preferable to instead implement the sum S instead via two binary XOR3-gates or to construct the full-adder only with MAJ- and/ or MIN-gates[17].

Generalizations of XOR. The connectives NEQ ('not-equal') and ODD ('odd') from fig. 8.6 can be interpreted as different generalizations of the binary XOR. NEQ generalizes the interpretation of XOR as *'non-equivalence'* ($\not\equiv$) which yields one if and only the inputs are *not equal*. Similarly, ODD generalizes the interpretation of XOR as a *linear parity function* ($\oplus$) which performs addition modulo 2 (i.e. in $\mathbb{Z}_2$). Here the output bit (*parity bit*) is one if and only if an *odd number* of input

bits is excited. Due to this interpretation XOR-gates are used to implement binary addition in computers. A simple *half adder* consists of an XOR-gate which outputs the *sum* and an AND-gate which output the *carry*[39].
The binary XOR can also be interpreted as a the logic gate analogous to the *'exclusive or'* from mathematical logic. This interpretation suggests the generalization as the XXOR-gate (see fig. 8.4) which is one if and only if *exclusively one* input bit is excited.
Lastly the binary XOR can also be interpreted as a *'programmable inverter'* or *'controlled not'* in which one input (the *switch* or *control*) determines whether to invert the other input (the *target*) or to pass it along. Such an interpretation suggests the generalization as an *asymmetric* Toffoli-gate or a SWITCH-gate which we are going to discuss in the following sec. 8.3.

For binary operations the XNOR-gate is the logical complement of the XOR-gate. Analogously the connectives EQU, EVEN and NXXOR (see fig. 8.7 and fig. 8.5) are the negations of NEQ, ODD and XXOR (see fig. 8.6 and fig. 8.4). They represent the generalizations of the binary XNOR following similar interpretations.

8.2.5 | Non-minimal Gates

The previous subsections 8.2.1, 8.2.2 and 8.2.3 presented a (complete) list of the VdW-minimal realizations for the ternary, symmetric logical connectives. The VdW-minimal gates require at most two ancillaries; the MIN1-gate requires no ancillary at all. We were able to achieve perfect quality for almost all gates except for MAJ-1, EVEN-1 and ODD-1 for which we were able to suppress the ground state splitting up to numerical errors. The effective gaps of most gates are at least of magnitude $\Delta E_{\text{eff}} \sim 10\%$ with some exceptions: The effective gaps of the gates NXXOR1, NXXNOR1, EVEN1, EQU1 and ODD1 are of order $\Delta E_{\text{eff}} \sim 1\%$. For the NXXOR1-, NXXNOR1- and EQU1-gates their negations XXOR1, XXNOR1 and NEQ1 possess a significantly larger effective gap. This suggests a realization based on these gates by amalgamating a NOT1-gate. Such a realization then possesses a significantly larger effective gap which comes at the cost of an additional ancillary. These gates then possess *two ancillaries* which makes them non-minimal in the VdW-model. The three amalgamated gates are denoted by NXXOR-2, NXXNOR-2 and EQU-2 respectively; they are presented in fig. 8.9. Note that the portrayed non-minimal gates are of course *not unique* in the sense that there exist further non-minimal realizations of the connectives with two ancillaries. However the portrayed realizations are the most promising ones for a large effective gap. The gates possess effective gaps of order $\Delta E_{\text{eff}} \sim 10\%$, i.e. one order of magnitude larger than their minimal realizations.

For the *linear* Boolean connectives EVEN-1 and ODD-1 it is of no use to express them via their negation as *both* gates possess a low effective gap. Note that the VdW-minimal ODD1-gate already requires two ancillaries. It seems that *linear* Boolean *functions* are inherently hard to implement on the Rydberg platform. It can be argued that this was already observed for the binary linear connectives XOR and XNOR: In the PXP-model (see sec. 4.1) these connectives posses fewer realizations and they require more ancillaries than the other binary gates. In the VdW model the two-dimensional XNOR3i-gate from fig. 4.9 possesses only a small effective gap which even in three dimensions for the XNOR-3ii-gate (see fig. 8.1) remains smaller than for the other two-dimensional binary gates in fig. 4.9.

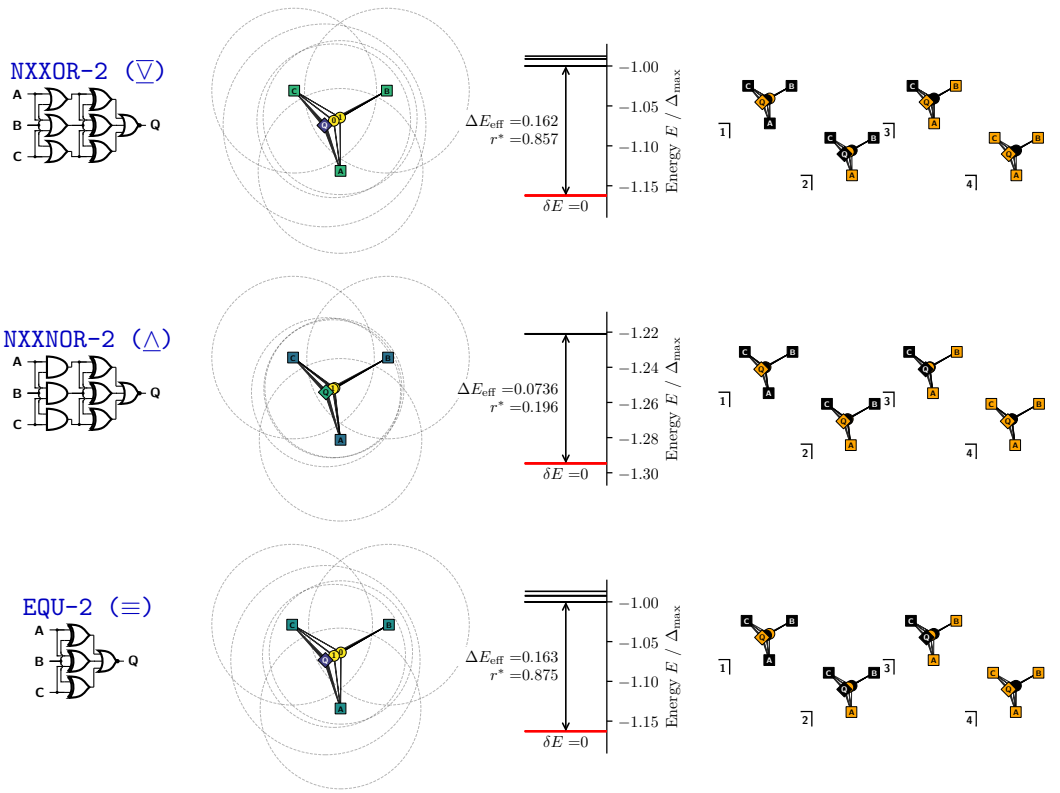

▽	[A]	Q	0	1
1	0	1	0	1
2	1	0	1	0
3	2	1	0	0
4	3	1	0	0

△	[A]	Q	0	1
1	0	1	1	0
2	1	1	1	0
3	2	0	0	1
4	3	1	0	0

≡	[A]	Q	0	1
1	0	1	1	0
2	1	0	0	1
3	2	0	0	1
4	3	1	0	0

Figure 8.9: Non-minimal ternary, scalar and symmetric logic gates with two ancillaries. The gates are constructed as negations of the XXOR1-, XXNOR1- and NEQ1-gate from fig. 8.4 and fig. 8.6 by amalgamating a NOT1-gate to the ouput port. The effective gaps of these non-minimal realizations is one order larger than for the VdW-minimal realizations from fig. 8.5 and fig. 8.7 with only one ancillary.

8.3 | Asymmetric Ternary Logic Gates

In previous sec. 8.2 we introduced a complete list of symmetric, ternary logic elementaries. For the symmetric, ternary logic gates there are only $g_{\text{eff}} = 4$ effective ground states and thus $2^4 = 16$ scalar, symmetric logical connectives; 14 of which are non-constant. For asymmetric logic gates we can not reduce the number of ground states by introducing effective ground states. Here we have to consider the full $g = 2^3 = 8$ ground states. Thus there exist in total $2^8 - 2^4 = 240$ asymmetric logical connectives. It is not practical to consider all of them. However most of them are not of interest for practical applications anyway. In this section we want to focus on three asymmetric connectives we identified as the most important ones. The paradigmatic *Toffoli-gate* `TOFF` and the *logical conditional* `SWITCH` were already mentioned in previous chapter as asymmetric generalizations of the binary `XOR`-gate. Additionally we want to introduce the *Fredkin-gate* `FRED`. In the following subsec. 8.3.1 we start with the Toffoli-Gate.

8.3.1 | The Toffoli-Gate

In this subsection we want to introduce the Toffoli-gate (also called 'controlled-controlled-not' gate) on the three-dimensional Rydberg-platform. In a Toffoli-gate the states of two *control bits* control whether to invert the third *target bit*. If both control bits are one then the target bit is inverted. Otherwise the Toffoli-gate outputs the target bit. The Toffoli-gate can be decomposed/ defined using two binary elementaries (see chap. 4):

$$\mathsf{Q} = \mathsf{A} \veebar (\mathsf{B} \wedge \mathsf{C}). \tag{8.3}$$

Commonly the two control bits are also passed along as output bits making the Boolean function $\texttt{CCNOT} := (\texttt{1}, \texttt{1}, \texttt{TOFF})$ vectorial. Such a `CCNOT`-gate is *reversible* because the concatenation $\texttt{CCNOT} \circ \texttt{CCNOT} = \texttt{1}$ is the identity. For a clear distinction in the following we denote by `TOFF` the scalar, controlled component of the vectorial `CCNOT`. Note that this slightly differs from common literature where the notions of the Toffoli- and `CCNOT`-gate are usually used interchangeably.

A reversible and universal Gate. The `CCNOT`-gate generalizes the binary *reversible* `CNOT`-gate ('controlled-not') on two input bits. The vectorial $\texttt{CNOT} := (\texttt{1}, \texttt{XOR})$-gate is just the well-known `XOR`-gate where the control bit is passed along to the output as well. The problem with the `CNOT`-gate is that the set $\{\texttt{NOT}, \texttt{CNOT}\}$ is no universal gate set, i.e. not every logical connective can be constructed just from `NOT` and `CNOT`. In contrast the singletons $\{\texttt{NOR}\}$ and $\{\texttt{NAND}\}$ while universal are not reversible. T. Toffoli proposed in 1980 the `CCNOT`-gate as a *universal and reversible gate*[40]. This allows to construct any *classical* logic circuit in a reversible way using only `CCNOT`-gates.

Implementation of the Toffoli-Gate. In this subsection we are interested in the scalar version `TOFF` with only one output bit. One could add `CPY`-gates to the control input ports to implement the vectorial `CCNOT`-gate discussed above. Fig. 8.10 presents the optimized `TOFF`-gate. Like

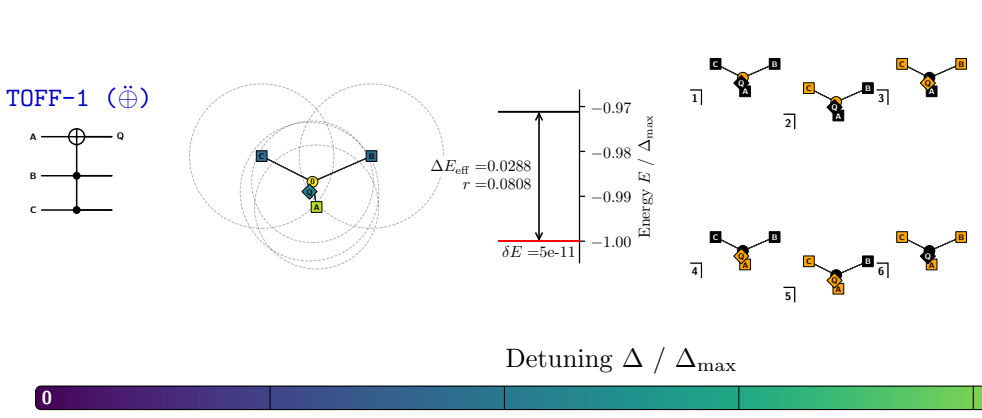

⊕	A	[B]	Q	0
1	0	0	0	1
2	0	1	0	1
3	0	2	1	0
4	1	0	1	0
5	1	1	1	0
6	1	2	0	0

Figure 8.10: TOFFOLI-gate (TOFF) with one ancillary. The implementation conserves the bilaterally symmetry between the control ports B and C. The output bit corresponds to (the negation of) the target bit (if both control bits are one).

for the previous three-dimensional gates the input ports lie in the projection plane. The input port A is the target bit, the input ports B and C are the control bits. For the TOFF-gate we require at least one ancillary such that $\mathbf{0} \notin L_{\texttt{TOFF}}$. For the realization in fig. 8.10 we choose the ancillary such that it is excited if no input bit is excited or if only one control bit is excited. This preserves the symmetry between the two control bits. The ports of the TOFF-gate in fig. 8.10 construct a *bilaterally symmetric tetrahedron*. In fig. 8.10 the plane of symmetry is the y, z-plane. The ancillary lies inside this tetrahedron on the y, z-plane. This allows us to reduce the ground states to *six effective ground states* presented in the table of the right column. We can not apply theorem V (or its corollaries) but we are able to achieve ground state degeneracy up to numerical errors. The effective gap is $\Delta E_{\text{eff}}[\texttt{TOFF-1}] \approx 2.9\%$.

Minimality and Completeness. Naturally the question arises whether there are further VdW-minimal realizations of the TOFFOLI-gate in the VdW-model:

> Realization TOFF-1 is *VdW-minimal* and *unique*, i.e. there exist no further TOFFOLI-gates with less than two ancillary in the VdW-model.

Thus the 'list' of realizations in fig. 8.10 is *complete*. We show this statement in the following proof 14:

Proof 14. (Uniqueness and Minimality)

We argue with corollary II. In a nutshell corollary II forbids ground states which are non-adjacent substates (with any intermediate excited state). This makes the statement is relatively straightforward: Realization TOFF-1 possesses one ancillary bit. The ancillary bit is necessary such that $\boldsymbol{x}_1 \notin \boldsymbol{x}_3, \boldsymbol{x}_4, \boldsymbol{x}_5, \boldsymbol{x}_6$ and such that $\boldsymbol{x}_2 \notin \boldsymbol{x}_3, \boldsymbol{x}_5, \boldsymbol{x}_6$ (and such that $\mathbf{0} \notin L_{\texttt{TOFF}}$). This makes realization TOFF-1 VdW-minimal. We need to choose the ancillary bit such that it is excited in $\boldsymbol{x}_1$ but not in $\boldsymbol{x}_3$, $\boldsymbol{x}_4$, $\boldsymbol{x}_5$ and $\boldsymbol{x}_6$ and such that it is excited in $\boldsymbol{x}_2$ but not in $\boldsymbol{x}_3$, $\boldsymbol{x}_5$ and $\boldsymbol{x}_6$. This uniquely determines realization TOFF-1. □

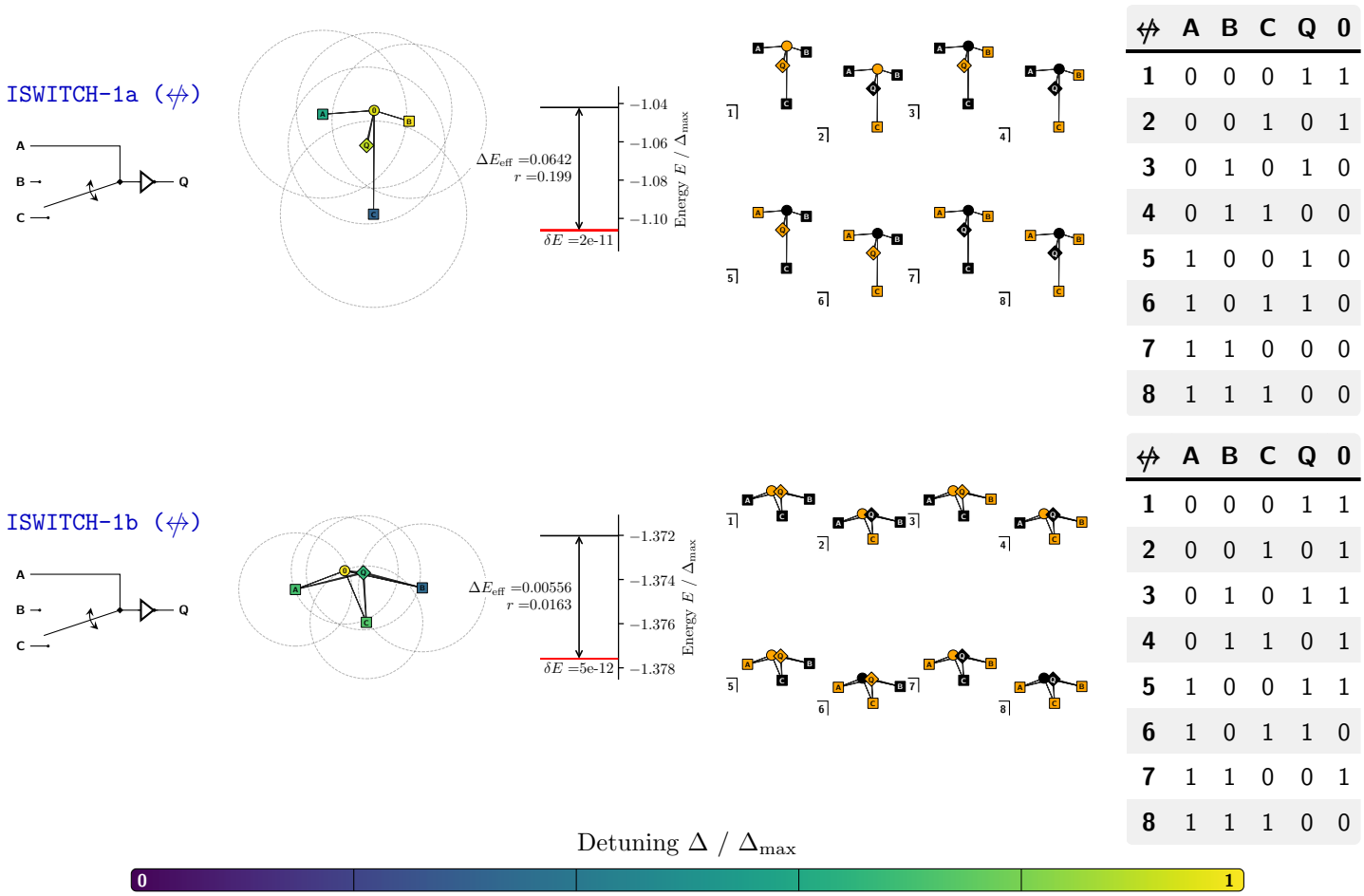

⇿	A	B	C	Q	0
1	0	0	0	1	1
2	0	0	1	0	1
3	0	1	0	1	0
4	0	1	1	0	0
5	1	0	0	1	0
6	1	0	1	1	0
7	1	1	0	0	0
8	1	1	1	0	0

⇿	A	B	C	Q	0
1	0	0	0	1	1
2	0	0	1	0	1
3	0	1	0	1	1
4	0	1	1	0	1
5	1	0	0	1	1
6	1	0	1	1	0
7	1	1	0	0	1
8	1	1	1	0	0

Figure 8.11: `ISWITCH`-gate with one ancillary defined in eq. (8.4). The *switch* A determines whether the gate outputs $\bar{\mathsf{B}}$ or $\bar{\mathsf{C}}$. The connective and the language are intrinsically asymmetric.

8.3.2 | Inverted SWITCH-Gate

A logical next step is to consider a switch between two of the inputs. More precisely we want to consider an *inverted* switch `ISWITCH` which is more natural to implement in the VdW model. From such an inverted switch we expect the following behavior:

$$\mathsf{Q} = (\mathsf{A} \wedge \bar{\mathsf{B}}) \vee (\bar{\mathsf{A}} \wedge \bar{\mathsf{C}}). \tag{8.4}$$

This can be interpreted as:

> "If the *switch* A is excited then the output inverts *target bit* B,
> otherwise the output inverts *target bit* C."

Note that such a switch is *inherently asymmetric* between the target bits, thus we can not expect a symmetric implementation. Two optimized `ISWITCH`-gates are presented in fig 8.11.

The implementations are asymmetric thus we can not introduce effective ground states. We claim that:

> Realizations `ISWITCH-1a` and `ISWITCH-1b` are *VdW-minimal*. There exist *at most* 2^4 possible VdW-minimal realizations for `ISWITCH`.

We show this statement in the following proof 15:

Proof 15. (Uniqueness and Minimality)

Again, we argue with corollary II which forbids ground states which are non-adjacent substates (with any intermediate excited state). Both realizations `ISWITCH-1a` and `ISWITCH-1b` posses one ancillary bit. The ancillary bit is necessary such that $\boldsymbol{x}_1 \notin \boldsymbol{x}_6$ and such that $\boldsymbol{x}_2 \notin \boldsymbol{x}_6, \boldsymbol{x}_8$. This makes the realizations `ISWITCH-1a,b` VdW-minimal. We need to choose the ancillary bit such that it is excited in $\boldsymbol{x}_1$ and $\boldsymbol{x}_2$ but not excited in $\boldsymbol{x}_6$ and $\boldsymbol{x}_8$. The state of the ancillary bit remains undetermined in the remaining ground states $\boldsymbol{x}_3$, $\boldsymbol{x}_4$, $\boldsymbol{x}_5$ and $\boldsymbol{x}_7$ by this criterion. This leaves up to 2^4 possibilities for the realizations in these four states. □

For the realizations in fig. 8.11 we choose two promising representatives where the ancillary is excited either in no or in all ground states where exactly two ports are excited. This list is of course *not complete*. We find that former realization `ISWITCH-1a` seems to work significantly better because here the effective gap $\Delta E_{\text{eff}}[\texttt{ISWITCH-1a}] \approx 6.5\%$ is by one order of magnitude larger than $\Delta E_{\text{eff}}[\texttt{ISWITCH-1b}] \approx 0.5\%$. We are not able to apply theorem V (or its corollaries) however for both gates we are able achieve ground state degeneracy up to numerical errors.

8.3.3 | Controlled SWAP-Gate

In previous subsec. 8.3.2 we introduced the `ISWITCH`-gate where the output inverts either target bit B or C depending on the state of the switch A. We add the *prefix* `I` to emphasize that the gate *inverts* the bits, otherwise the gate is simply a switch. A natural generalization of the (inverted) `SWITCH`-gate would be the (inverted) FREDKIN-gate (or 'controlled swap' gate) which outputs both target bits A and B in the outputs R and Q but swaps them if the switch/ control C is excited. The FREDKIN-gate can be decomposed/ defined using three (if one includes `NOT` four) of the binary elementaries (see chap. 4):

$$\mathsf{R} = (\bar{\mathsf{C}} \wedge \mathsf{A}) \vee (\mathsf{C} \wedge \mathsf{B}), \qquad \mathsf{Q} = (\bar{\mathsf{C}} \wedge \mathsf{B}) \vee (\mathsf{C} \wedge \mathsf{A}). \tag{8.5}$$

In the following we are interested in the negation of the FREDKIN-gate `FRED` which we call the `IFRED`-gate. The `IFRED`-gate additionally inverts the input bits which is more natural to implement on the Rydberg platform. One could recover the common FREDKIN-gate by amalgamating `NOT1`-gates to the output or input ports. By considering only one output port of the `IFRED`-gate one recovers the inverted switch `ISWITCH` from previous subsec. 8.3.2.

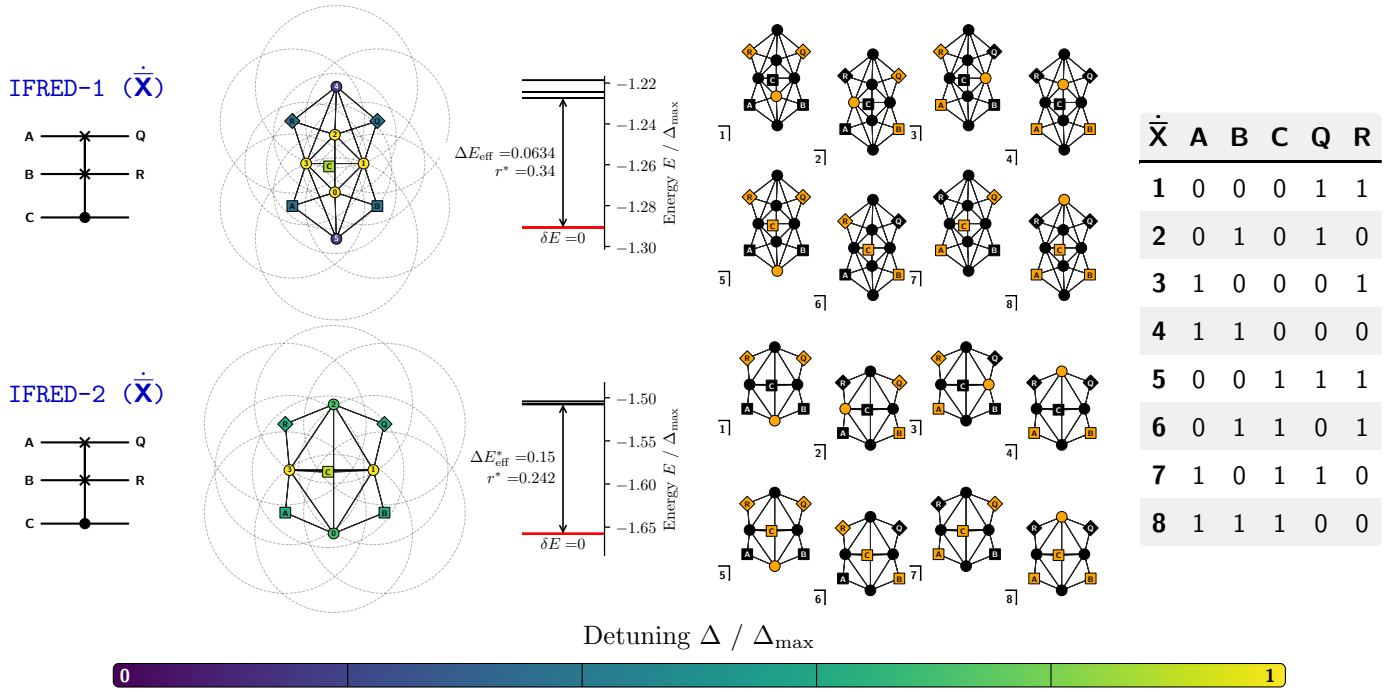

X̄	A	B	C	Q	R
1	0	0	0	1	1
2	0	1	0	1	0
3	1	0	0	0	1
4	1	1	0	0	0
5	0	0	1	1	1
6	0	1	1	0	1
7	1	0	1	1	0
8	1	1	1	0	0

Figure 8.12: Inverse FREDKIN-gate in two realizations. They are inspired from the inverted crossing ICRS1 from fig. 4.4. If the *switch* A is not excited the outputs are swapped (and inverted), if the *switch* A is excited the outputs are not swapped (but still inverted).

A reversible and universal Gate. Note that usually in common literature the notions of a FREDKIN-gate and a controlled-swap gate are used interchangeably. Here we specifically define the FRED-connective as a BOOLEAN function which outputs only the *two* (swapped) target bits. We reserve the label controlled-swap gate for the vectorial connective $\texttt{CSWAP} = (\texttt{1}, \texttt{FRED})$ which is usually also denoted as the FREDKIN-gate. Here the switch/ control bit C is also passed along in the output. This can be easily achieved on the Rydberg platform by amalgamating a CPY2-gate to the switch. Implementing such a CSWAP-gate on the Rydberg platform is of large interest because (like the CCNOT-gate in subsec. 8.3.1) the CSWAP-gate is a *universal* and *reversible* ternary logic gate. The CSWAP-gate is reversible because the concatenation $\texttt{CSWAP} \circ \texttt{CSWAP} = \texttt{1}$ is the identity. This means that any logic gate can be constructed entirely of CSWAP-gates in a reversible manner. The CSWAP-gate was first introduced by E. FREDKIN and T. TOFFOLI in 1982[13].

Implementation of the Fredkin-Gate. The construction of an inverted FREDKIN-gate is highly nontrivial on the Rydberg platform. The gate possesses five ports of which two are output ports. As a starting point we consider again the inverted crossing ICRS1 from fig. 4.4. Here the output ports are swapped (and inverted) compared to the input ports. We can 'conserve' these ground states if we assume that the switch or additional ancillaries are not excited. Then we only need to achieve degeneracy with the remaining four ground states where the switch is activated and the ground states are not swapped. This includes two ground states where either only the input or the output ports are excited and two ground states where the ports along a diagonal are excited.

An intuitive wat to implement the IFRED-gate is presented with realization IFRED-1: Here we conserve the D_4-symmetric structure of the planar ICRS1-gate and introduce two additional ancillaries. The switch is centered above the planar ICRS1-gate. If the switch is excited, one additional ancillaries is excited if either only the input or only the output ports are excited. In that sense the additional ancillaries substitute the two ancillaries from the swapped ground states. This leaves sufficient DOFs for the diagonal ground states to achieve ground state degeneracy. The IFRED1-gate is by construction D_2-symmetric. We are able to achieve perfect quality by applying theorem V. The IFRED1-gate was only optimized for $r_{\texttt{IFRED1}} \approx 34\%$ and it is computationally intensive (due to *six* ancillaries), thus it is probably not quite optimal in $\Delta E_{\text{eff}}[\texttt{IFRED1}] \approx 6.3\%$.

The IFRED2-Gate. The additional ancillaries of the IFRED1-gate are actually not necessary to implement the gate. Instead we can realize the IFRED-gate by exciting the ancillaries of the $L_{\texttt{ICRS1}}$-ground states and (heavily) modify the structure. This yields the IFRED2-gate from the second row of fig. 8.12. The IFRED2-gate is D_2-symmetric respecting the permutation symmetries of the language. The target and output ports remain in a plane (they trace-out a rectangle within the projection plane) while the ancillaries are shifted out of plane. We are able to achieve perfect quality by applying theorem V. The IFRED2-gate is *extensively* optimized such that we can confidently claim that it is optimal in $\Delta E_{\text{eff}}[\texttt{IFRED2}] \approx 15\%$ and $r_{\texttt{IFRED2}} \approx 24.2\%$. Note that the effective gap is surprisingly large for a language of this complexity.

8.4 | Binary Multi Logic Gates

In subsec. 8.1.2 we presented the ICRS3-multigates which are based on the ICRS1-gate from chap. 4.1. They implement multiple logic gates simultaneously, i.e. *vectorial* BOOLEAN functions with $q > 1$, without requiring additional CPY- or LNK-gates or any further elementary logic gates. We want to elaborate on this idea in this section. The goal is to find atom-efficient multigates in the VdW model for the binary logical connectives. Such gates expand out toolbox and allow us to implement logic circuits more efficiently on the Rydberg platform.

8.4.1 | Double Logic Gates

In this chapter we want to implement the vectorial logical connectives with $q = 2$ output bits where each component is a different scalar, symmetric, binary logical connective. We call the L-complexes implementing two logical connectives *double logic gates*. As a natural ansatz we start with the logic elementaries from chap. 4. Then we show that they do yield the VdW-minimal multigates.

The initial Ansatz. First consider the PXP-minimal elementary gates from sec. 4.1. Due to the positioning of the atoms we can not directly amalgamate two PXP-minimal gates without inheriting strong residual interactions which would heavily distort the energy structure. Furthermore these gates possess quite a large number of ancillaries and we are interested in atom-efficient implementations. Instead starting with the VdW-minimal logic gates from fig. 4.9 seems to be the more promising ansatz. Furthermore, for simplicity we can restrict ourselves to the three logical connectives NOR, NAND and XOR. The remaining connectives OR, AND and XNOR are obtained as the respective negations. We could obtain these multigates by amalgamating a NOT1-gate to the complexes introduced in the following.

Amalgamations of two elementary Gates. We can efficiently construct double logic gates by amalgamating the input ports of the VdW-minimal elementary gates from fig. 4.9. These amalgamated gates are portrayed in fig. 8.13. There are six combinations of the three elementary gates NOR3, NAND3 and XOR3. We label the amalgamated gates by the labels of their components from which they are constructed, i.e. for example NORNOR = (NOR, NOR) is the vectorial connectives where both components are a NOR. The gates are optimized for the effective energy gap (and except for the NORNAND3-gates they are also optimized for the robustness). The vectorial NORNOR1-gate is particularly natural to implement on the Rydberg platform because it consists of two NOR3-gates which are the natural binary, scalar logic gates. Nevertheless the remaining logic gates still posses large effective gaps $\Delta E > 16\%$.

Completeness and Minimality. Note that such amalgamations of VdW-minimal logic gates are in general not VdW-minimal. To complete the list with the VdW-minimal double logic gates we attach further gates in app. 8.B.1 (see fig. 8.24). This allows is to formulate the following statements:

NORNOR-1 $((\overline{\vee}, \overline{\vee}))$

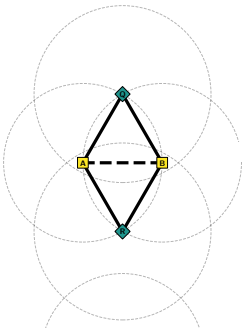

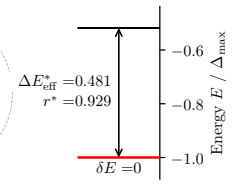

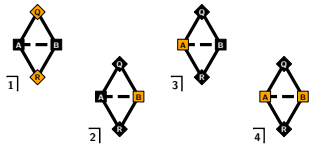

$\overline{\vee}$	[A]	Q	R
1	0	1	1
[2]	1	0	0
4	2	0	0

NANDNAND-1 $((\overline{\wedge}, \overline{\wedge}))$

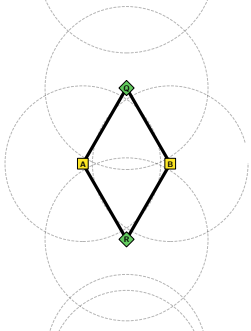

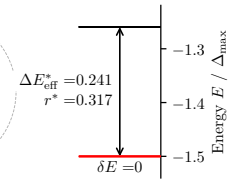

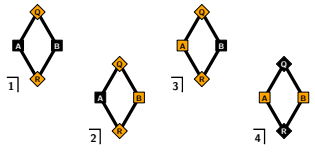

$\overline{\wedge}$	[A]	Q	R
1	0	1	1
[2]	1	1	1
4	2	0	0

XORXOR-1 $((\underline{\vee}, \underline{\vee}))$

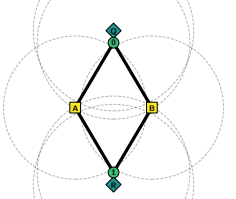

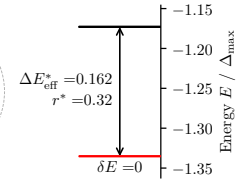

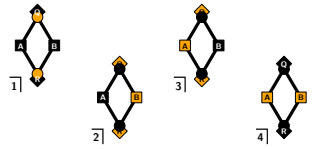

$\underline{\vee}$	[A]	Q	R	0	1
1	0	0	0	1	1
[2]	1	1	1	0	0
4	2	0	0	0	0

NORNAND-1 $((\overline{\vee}, \overline{\wedge}))$

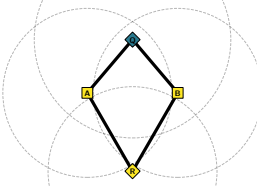

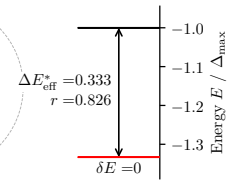

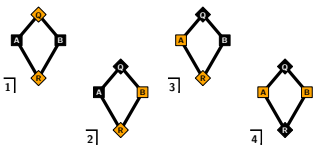

$\overline{\vee}$	[A]	Q	R
1	0	1	1
[2]	1	0	1
4	2	0	0

NANDXOR-1 $((\overline{\wedge}, \underline{\vee}))$

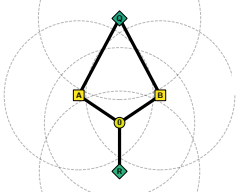

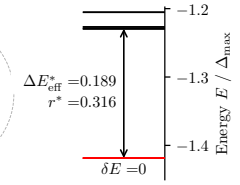

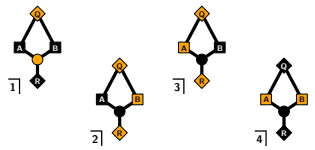

$\overline{\vee}$	[A]	Q	R	0
1	0	1	0	1
[2]	1	1	1	0
4	2	0	0	0

NORXOR-1 $((\overline{\vee}, \underline{\vee}))$

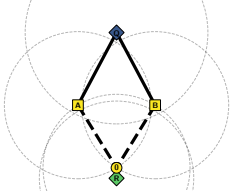

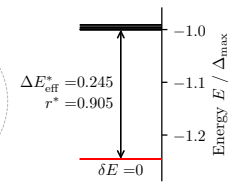

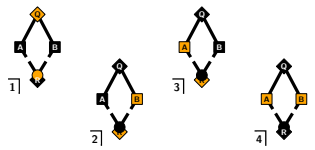

$\overline{\vee}$	[A]	Q	R	0
1	0	1	0	1
[2]	1	0	1	0
4	2	0	0	0

Figure 8.13: Double Logic Gates constructed by amalgamating two elementary gates from fig. 4.9 by their input ports.

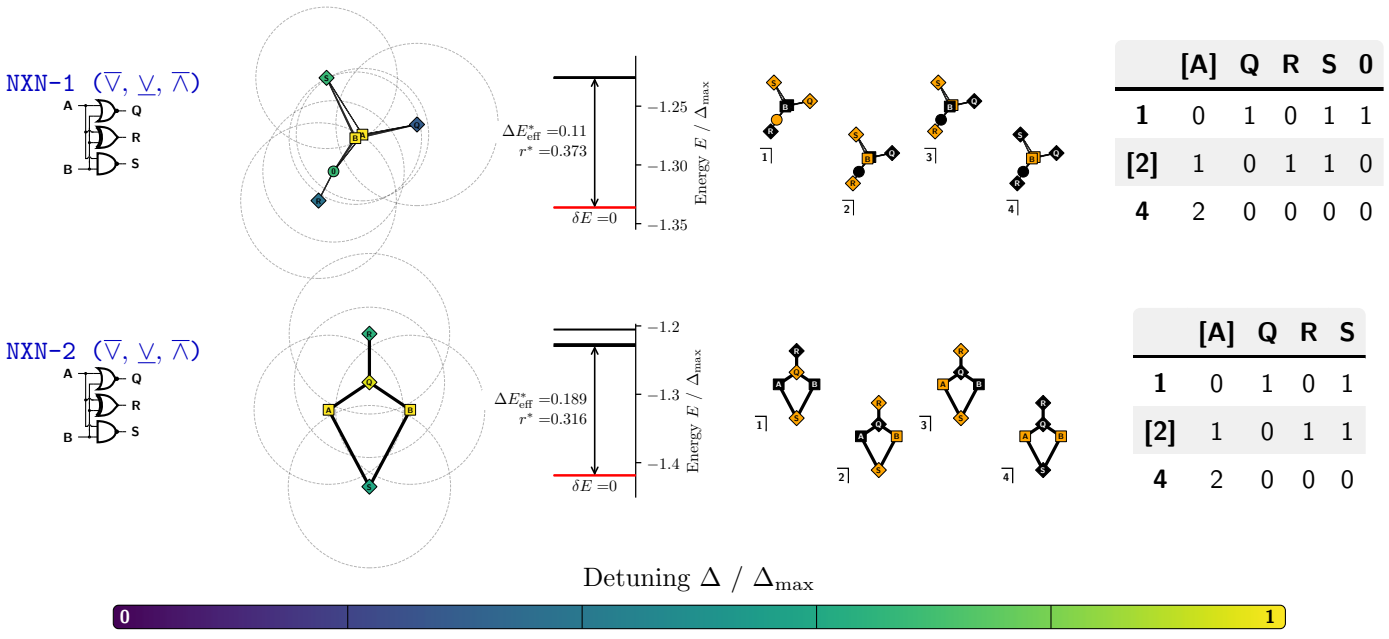

	[A]	Q	R	S	0
1	0	1	0	1	1
[2]	1	0	1	1	0
4	2	0	0	0	0

	[A]	Q	R	S
1	0	1	0	1
[2]	1	0	1	1
4	2	0	0	0

Figure 8.14: Triple Logic Gates constructed by amalgamating elementary gates from fig. 4.9. Realization NXN−2 is VdW-minimal and unique in that sense.

> The double logic gates NORNOR-1, NANDNAND-1, XORXOR-2, NORNAND-1 and NORXOR-2 are VdW-minimal and unique. The two gates NANDXOR1 and NANDXOR2 are both VdW-minimal and the only VdW-minimal realizations.

This statement is shown in proof 19. Nevertheless it might be preferable to rely on the logic gates presented in fig. 8.13 to implement a logic circuit as they possess significantly larger effective gaps. This concludes our discussion about double logic gates. In the next subsec. 8.4.2 we want to focus on *triple logic gates*.

8.4.2 | Triple Logic Gates

In this brief subsection we want to implement the vectorial logical connectives with $q = 3$ output bits where each component is a different scalar, symmetric, binary logical connective.

The NXN1-Gate. As an ansatz we consider again the VdW-minimal logic gates NOR-3, NAND-3 and XOR-3 from fig. 4.9. We can efficiently construct the triple logic gate by amalgamating the input ports of three VdW-minimal elementary gates. The amalgamated gate NORXORNAND-1 (NXN-1) is presented in the first row of fig. 8.14. Note that this amalgamated gate possesses only *one ancillary* but it implements *three logic elementaries* simultaneously with effective gap $\Delta E_{\text{eff}} \approx 11\%$. We require three dimensions to amalgamate the three logic elementaries. The

three output ports and the ancillary lie in the projection plane while the input ports are located orthogonally above and below the plane respectively. The input ports can be accessed by connecting them (e.g. via an N_E-chain) in the vertical dimension.

The NXN2-Gate. The NXN1-gate is not VdW-minimal because its ancillary is always in the same state as output port Q. In fact by relabeling the ancillary from the NANDXOR1-gate in fig. 8.13 as a third output port we obtain the VdW-minimal and unique NXN2-gate from the second row in fig. 8.14. Minimality and uniqueness are obvious as realization NXN-2 possesses *no ancillaries*. Note that the optimized structure is actually two-dimensional but the output port Q can only be accessed efficiently via the vertical dimension. Nevertheless it is possible to embed this gate in a logic circuit on the two-dimensional Rydberg platform. This is illustrated via the ORXORNAND2 (OXN2)-gate which is attached in the app. 8.B.2. However such a dimensionality constraint implies strong residual interactions which impairs the effective gap.

8.5 | Surface Code Unit Cells

The previous section concluded our discussion about three-dimensional gates for logical connectives. In the following two sections we want to focus again on tessellated languages, more precisely the unit cell of the surface code and the single site of the FIBONACCI model. In this section we want to start with the surface code unit cells. We split this subsection logically in two parts: in the first part we consider quasiplanar unit cells for the surface code. In the second part we discuss higher dimensional implementations.

8.5.1 | Quasiplanar Surface Code

In this subsection we want to consider quasiplanar unit cells of the surface code where the ports lie in one plane. Such quasiplanar structures can be tessellated on the *two-dimensional lattice* such that the tessellated structure possesses little extent in the vertical direction. Such (quasi) two-dimensional structures are experimentally less demanding as the atoms can be accessed via the third dimension. With state-of-the-art technology it is currently possible to prepare hundreds of atoms in a two-dimensional structure[22, 3, 31].

Representation `I`. We want to start by considering the check function (5.6) in representation `I`. In this representation for the VdW model we require at least *two ancillaries* to achieve a positive energy gap. This follows directly from corollary II: The two ancillaries are necessary such that the ground states $\boldsymbol{x}_1 \notin \boldsymbol{x}_i|_{i>1}$ and $\boldsymbol{x}_i|_{i<8} \notin \boldsymbol{x}_8$ are no non-adjacent substates. Fig. 8.15 exemplarily portrays two symmetric VdW-minimal realizations which we identified as the most promising ones. For both realizations we were able to achieve a positive energy gap however at a miserable ratio $Q \approx 14$[8] implying $\mathcal{Q} \approx 8.315 \times 10^{-7}$. Note that the portrayed structures are D_4-symmetric respecting the permutation symmetries of the ports. Breaking these symmetries (only constraining the C_2-symmetry in the ports) only seems to worsen the quality factor and even with extensive simulation we were not able to improve the quality factor. This is conceptually interesting as this is the first structure we encounter where we can achieve a positive energy gap but only at a miserable quality. Such a structure is not viable for tessellating the surface code. It seems that we require three ancillaries to construct a viable (quasi)planar unit cell in representation `I`. Examples for such realizations are the planar, non-VdW-minimal `SCUI-2a,b` unit cells presented in fig. 5.2. In the following we want want to consider representation `II` which already turned out more promising in the two-dimensional case.

Representation `II`. We continue by considering the check function (5.7) in representation `II`. As already mentioned in sec. 5.1 we require at least one ancillary in this representation to achieve a positive energy gap. For the two-dimensional case this was studied in app. 5.A.3. Here we found that it is impossible to achieve degeneracy (or a positive energy gap) with a planar structure.

[8] Astonishingly the ratio of both implementations seems to converge to exactly $Q \searrow 14$.

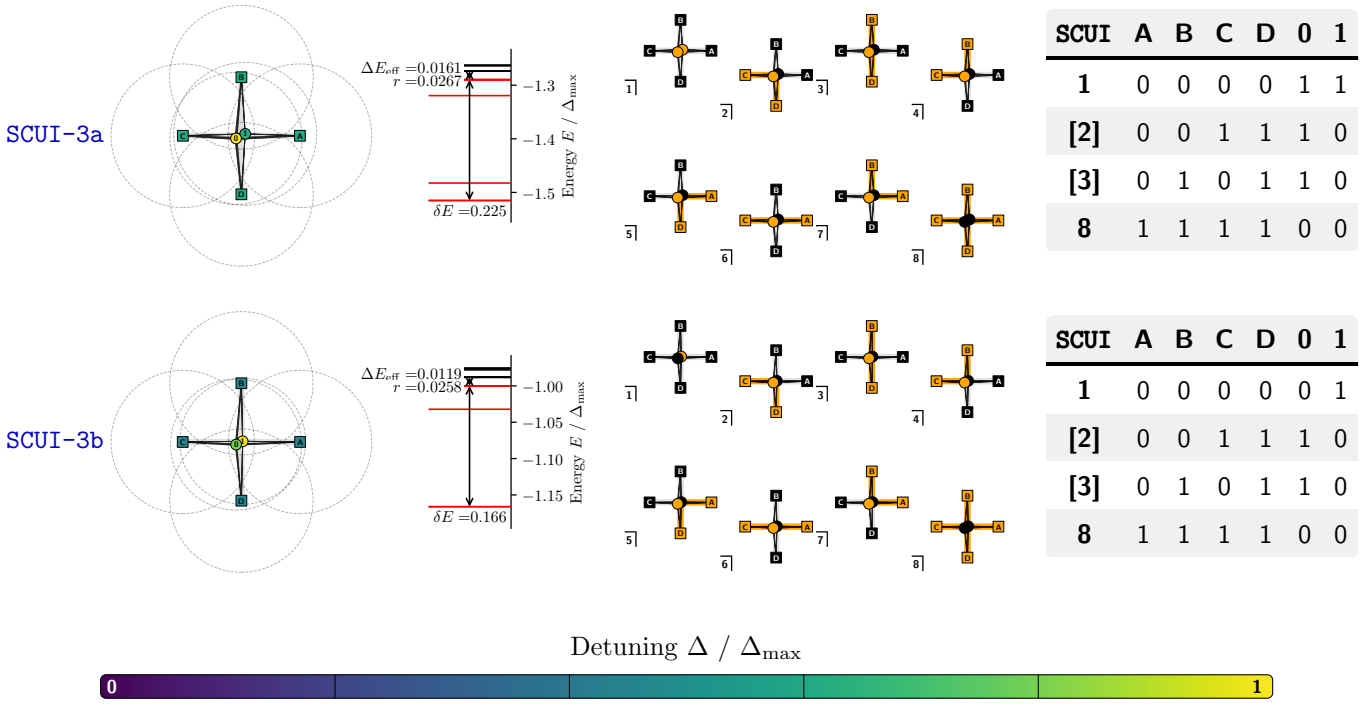

SCUI	A	B	C	D	0	1
1	0	0	0	0	1	1
[2]	0	0	1	1	1	0
[3]	0	1	0	1	1	0
8	1	1	1	1	0	0

SCUI	A	B	C	D	0	1
1	0	0	0	0	0	1
[2]	0	0	1	1	1	0
[3]	0	1	0	1	1	0
8	1	1	1	1	0	0

Figure 8.15: Quasiplanar SCUI unit cells in two realizations 3a,b. For these realizations of representation I we are not able to achieve a good quality factor.

We can introduce an additional DOF to the ancillary by embedding the structure in three-dimensional space constraining the ports in the projection plane. Implementation SCUII-2ii in fig. 8.16 portrays the quasiplanar surface code unit cell in representation II. The unit cell SCUII-2ii possesses unit quality $\mathcal{Q} = 1$ and $\Delta E_{\text{eff}} \approx 1.5\%$ *with only one ancillary*. This again illustrates that representation II is more natural to implement on the Rydberg platform. Note that the effective gap is of the same order of magnitude as in the planar unit cell SCUII-1 from fig. 5.3 with two ancillaries. The additional DOF in the ancillary turned out really useful to obtain a positive energy gap.

Note that the optimized unit cell SCUII-2ii is D_4-symmetric. This reduces ground states to only two effective ground states and the number of DOFs to only two. One DOF is required to achieve ground state degeneracy between the effective ground states while the last DOF is chosen such that the effective gap and the robustness are both maximized.

8.5.2 | Surface Code in higher Dimensions

In this brief subsection we want to introduce and discuss higher-dimensional unit cells in representation I. More precisely we consider the surface code unit cell in three dimensions and conclude with a short comment on four dimensions.

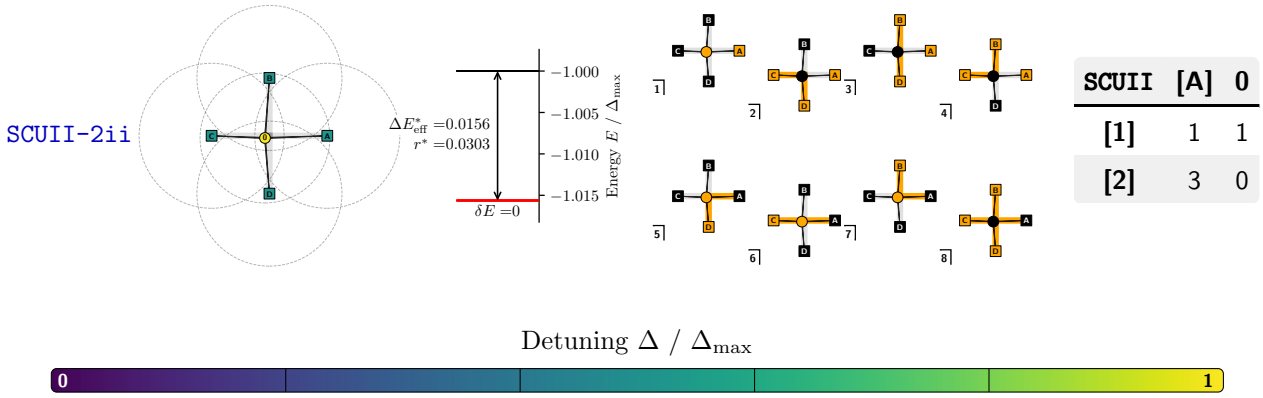

Figure 8.16: Quasiplanar `SCUII-2ii` unit cell with one ancillary. The optimized unit cell possesses unit quality and the optimized effective gap is similar to the effective gap of the `SCUII-1` unit cell in fig. 5.3. The planar implementation `SCUII-2i` is presented in fig. 5.10 and discussed in app. 5.A.3.

The tetrahedral SCUI-4 Unit Cell. We want to start by introducing the three-dimensional implementation `SCUI-4` of the surface code unit cell. The structure is presented in fig. 8.17. The ports B, C and D lie in the projection plane while the port A and the ancillaries are centered above the projection plane. The structure is D_3-symmetric thus there are four effective ground states (similarly as for the D_4-symmetric `SCUI3` unit cells in fig. 8.15). However the D_3-symmetry constrains fewer DOFs than the D_4-symmetry leading to two more useful DOFs. Thus in contrast to the quasiplanar `SCUI-3` unit cells we are able to achieve ground state degeneracy (up to numerical errors) with only two ancillaries. The effective gap is $\Delta E_{\text{eff}}[\texttt{SCUI-4}] \approx 0.6\%$ which is smaller than for the `SCUII-2ii` or the `SCUII-1` unit cell.

Such a tetrahedral surface code unit cells can be used to tessellate the surface code on the *diamond lattice*. Here each unit cell is placed on one site of the lattice and amalgamated with its four adjacent unit cells in a tetrahedral structure.

The four-dimensional Unit Cell. As a closing remark we want to note on a four-dimensional `SCUI` unit cell which would be somewhat trivial to construct.
Consider a *regular tetrahedron of ports*. We position the two ancillaries in the *orthogonal fourth dimension* equidistant to each port to conserve the S_4-symmetry of the ports. We choose the realization such that ancillary 0 is excited iff only two ports are excited, and ancillary 1 is excited iff no port is excited. One DOFs in the position and the detuning of ancillary 0 is fixed such that the ground states with two excited ports achieve degeneracy with the ground state where all four ports are excited. The second DOF is used to optimize the effective gap. The ports and the ancillary 0 now construct a 'squeezed' *tetrahedral pyramid*. Finally ancillary 1 is centered between the other atoms such that it is in blockade with all of them (this defines a finite volume). The detuning is fixed to achieve full ground state degeneracy.

This construction requires a *four-dimensional* Rydberg platform. The structure is actually 'quasi-planar' however the 'plane' is now a three-dimensional hyperplane in four-dimensional space. This is not quite surprising as four ports lie necessarily in a three-dimensional hyperplane. Nevertheless the construction requires four dimensions which makes it only conceptually interesting.

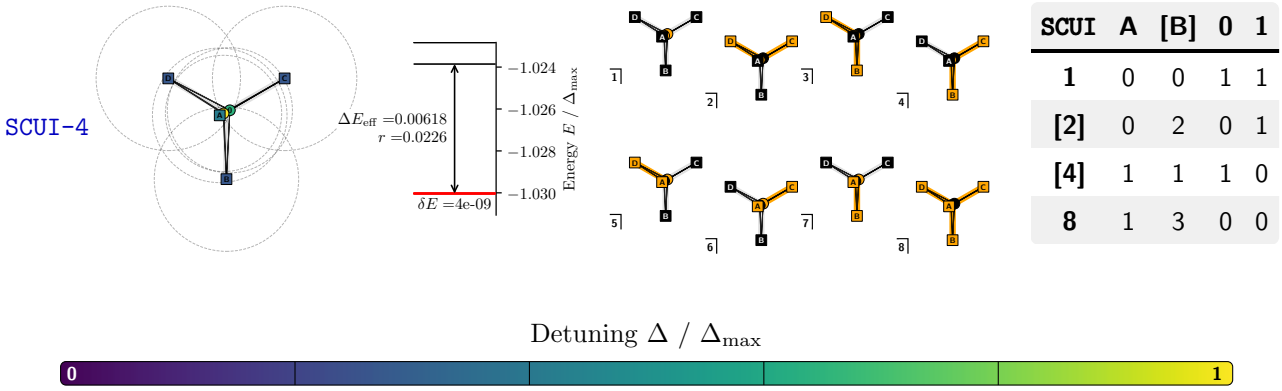

SCUI	A	[B]	0	1
1	0	0	1	1
[2]	0	2	0	1
[4]	1	1	1	0
8	1	3	0	0

Figure 8.17: VdW-minimal (inverted) crossings optimal in ΔE_{eff} and r. For a clearer visualization we summarize the ancillaries in one column portraying only their number of excitations.

It illustrates the advantage provided by additional dimensions: In higher dimensions we can construct *more-symmetric* structures which simplify the implementation of highly symmetric languages, such as the surface code in representation `I`.

8.6 | Fibonacci Model Sites

In this section we want to discuss FIBONACCI model sites on the three-dimensional Rydberg platform. Note that FIBONACCI model sites only possess three ports thus the following sites are necessarily quasiplanar. We are interested in constructing VdW-minimal realizations and compare them with the VdW-minimal `FMSI-3` site from fig. 5.6. In particular we are interested in realizations optimizing the effective gap.

The FMSI3-Site. First we recapitulate the `FMSI-3` site portrayed in fig. 5.6. Representation `I` is the *all edge high representation* where an excited port is identified with an excited edge. It is in some sense the natural representation and it is the only representation studied in Ref. [38] for the PXP model. For the `FMSI-3` site we were able to chose the ancillary anywhere inside the gray-shaded area without modifying the energy gap. The ancillary only needed to be sufficiently close to each port such that it does not impede the energy gap. This was founded in the similarity to the `XOR3`-gate from fig. 4.9 where we first encountered this behavior. On the three-dimensional Rydberg platform the gray-shaded area is a volume but we can still choose a planar structure. Thus the `FMSI-3` site does not profit from the additional DOF provided by three-dimensional space.

Other Representations. As an introductory example of this chapter we considered the `XNOR3ii`-gate (see fig. 8.1) which drastically improved by more than one order of magnitude compared to the two-dimensional case `XNOR-3i` from fig. 4.9. In sec. 5.2 we first introduced the four different representations of the FIBONACCI model. Analogously to how representation `FMSI` parallels `XOR3` (adding one more state) the representation `FMSIV` parallels `XNOR`. We only need to include the additional ground state where no port is excited. This motivates that for representation `FMSIV` we expect a significantly better effective gap in three-dimensional space. This is the reason why we directly study the remaining FIBONACCI model representations on the three-dimensional Rydberg platform. We compare the two-dimensional cases where we consider it relevant.

8.6.1 | Representation IV

Representation `IV` is the *all edge low representation* where an excited port is identified with a de-excited edge. It is *dual* to representation `I` and thus its check function (5.16) is also symmetric in the port bits. It includes the five ground states where zero, one or three port bits are excited.

Fig. 8.18 presents the two-dimensional (`i`) and three-dimensional (`ii`) ΔE_{eff}-optimized structures for the `FMSIV` site in realization `1`. The effective gap $\Delta E_{\text{eff}}[\mathcal{C}_{\texttt{ii}}] \approx 16.6\%$ of the quasiplanar structure `FMSIV-1ii` is more than one order of magnitude larger than the effective gap $\Delta E_{\text{eff}}[\mathcal{C}_{\texttt{i}}] \approx 1.3\%$ of the planar structure `FMSIV-1i`. Thus as reasoned above the structure profits from embedding it in three-dimensional space. Shifting the ancillary out-of-plane allows to

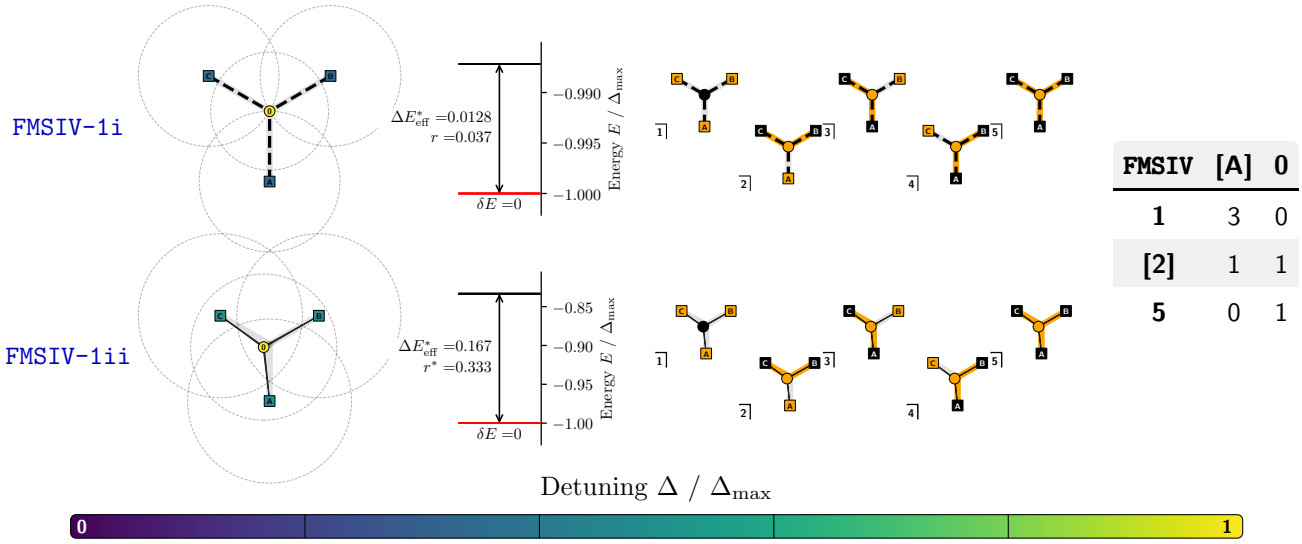

FMSIV	[A]	0
1	3	0
[2]	1	1
5	0	1

Figure 8.18: FIBONACCI model site with check function (5.16) in representation `IV`. `FMSIV-1i` is planar while `FMSIV-1ii` is quasiplanar. The effective gap profits from including the additional DOF in the ancillary because it allows to increase the interactions between pairs of ports (cf. `XNOR3ii`-gate from fig. 8.1).

increase the residual interaction energies between the ports without modifying the distance to the ancillary. This further gaps-out the excited state where two ports are excited simultaneously with the ancillary. Still the effective gap $\Delta E_{\text{eff}}[\mathcal{C}_{\texttt{ii}}]$ is only half as large as the effective gap of the planar structure `FMSI-3` from representation `I`. In that sense representation `I` is more natural to implement on the Rydberg platform than representation `IV`. This is similar to how the effective gap of the quasiplanar `XNOR3ii`-gate ($\Delta E_{\text{eff}} = 12.5\%$) remains half-as large as the effective gap of the planar `XOR3`-gate ($\Delta E_{\text{eff}} = 25\%$).

Realization `FMSIV-1` is *VdW-minimal* and the *only VdW-minimal realization* of representation `IV`. This follows directly from corollary II. We require the ancillary such that such that the ground states $\boldsymbol{x}_2, \boldsymbol{x}_3, \boldsymbol{x}_4, \boldsymbol{x}_5 \notin \boldsymbol{x}_1$ are no non-adjacent substates of $\boldsymbol{x}_1$ (and such that $\mathbf{0} \notin L_t$). Thus the ancillary needs to be excited in $\boldsymbol{x}_2, \boldsymbol{x}_3, \boldsymbol{x}_4, \boldsymbol{x}_5$ but not excited in $\boldsymbol{x}_1$ which defines the VdW-minimal realization `1`.

Note that realization w[`FMSIV-1`] = `MIN` is excited if at most one port is excited. This realization and both implementations `FMSIV-1i` and `FMSIV-1ii` are symmetric thus we can reduce the ground states to three effective ground states defined only by the number of excited input ports. Note that in the states of the fourth column in fig. 8.18 and in the table of the last column we stick to the lexicographic order of the edge states. As the edge states are now inverted compared to the ground states this shuffles the order of the ground states compared to the other figures throughout this thesis.

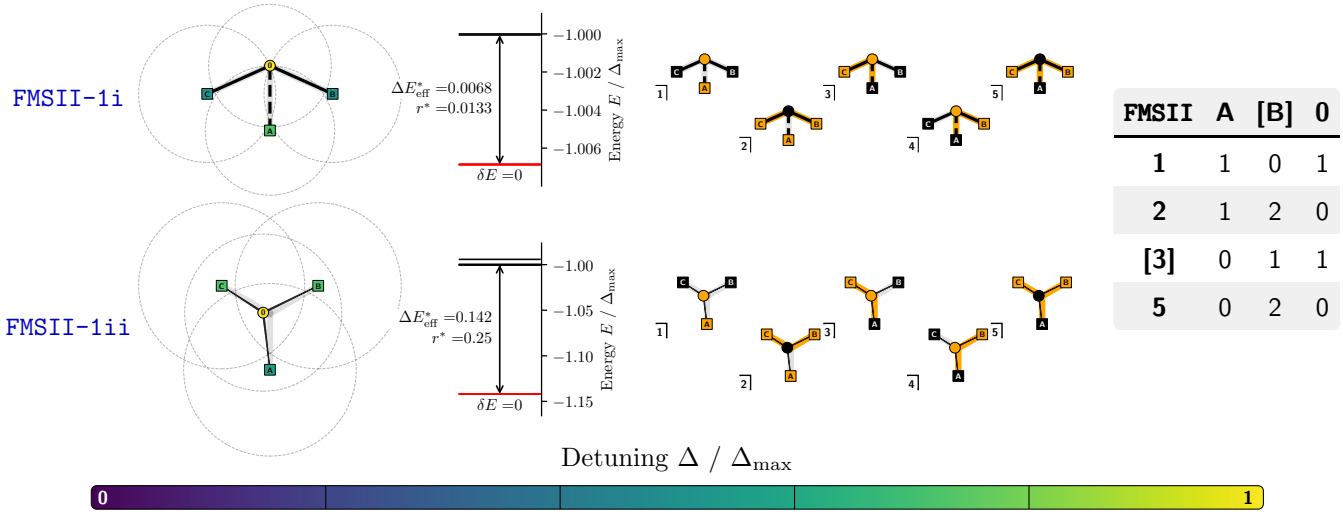

FMSII	A	[B]	0
1	1	0	1
2	1	2	0
[3]	0	1	1
5	0	2	0

Figure 8.19: FIBONACCI model site with check function (5.14) in realization `FMSII-1`. `FMSII-1i` is planar while `FMSIV-1ii` is quasiplanar. The effective gap profits from including the additional DOF in the ancillary because it allows to increase the interactions between pairs of ports (cf. `XNOR3ii`-gate from fig. 8.1).

8.6.2 | Representation II

Representation `II` is defined by the *edge low representation for one edge*. Thus the check function (5.14) is *intrinsically asymmetric* in the port bits. It includes the four words where either one or three port bits are excited but also the asymmetric word where only the two port bits associated with edges in positive representations are excited. In the following we associate the edge in negative representation with port A and the edges in positive representations with the ports B and C. Thus the permutation symmetry between the ports B and C remains conserved on the level of the check function.

For this representation we require at least one ancillary. Again, we follow the argument from corollary II. We require the ancillary such that such that the ground states $\boldsymbol{x}_1, \boldsymbol{x}_3, \boldsymbol{x}_4 \notin \boldsymbol{x}_2$ are no non-adjacent substates of $\boldsymbol{x}_2$ (and such that $\mathbf{0} \notin L_t$). Thus the ancillary needs to be excited in $\boldsymbol{x}_1, \boldsymbol{x}_3, \boldsymbol{x}_4$ but not excited in $\boldsymbol{x}_2$. This leaves two choices for the state of the ancillary in $\boldsymbol{x}_5$: Realization w[`FMSII-1`] = `MIN` and realization w[`FMSII-2`] = `NAAND` are presented in fig. 8.19 and fig. 8.20 respectively. This makes the realizations of figs. 8.19 and 8.20 *VdW-minimal* and the list of VdW-minimal realizations *complete*. For each realization we consider one planar (`i`) and one quasiplanar (`ii`) implementation.

As the check function is only permutation symmetric between two ports the four sites `FMSII-1i,ii` and `FMSII-2i,ii` are only D_1-symmetric as well. For the *quasiplanar* sites `FMSII-1ii` and `FMSII-2ii` we draw the underlying grid such that it conserves the angle 120° between the edges (but therefore not necessarily the equal lengths of the edges). The grid is visualized as the gray-shaded lines in the sites. For the *planar* implementations `FMSII-1i` and `FMSII-2i` the ports

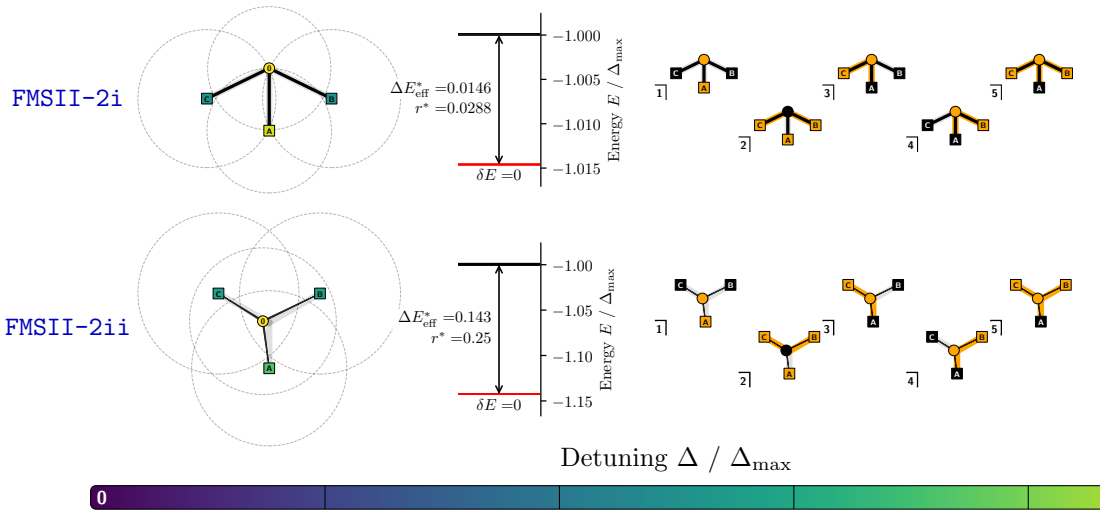

FMSII	A	[B]	0
1	1	0	1
2	1	2	0
[3]	0	1	1
5	0	2	1

Figure 8.20: FIBONACCI model site with check function (5.14) in realization `FMSII-2`. `FMSII-2i` is planar while `FMSIV-2ii` is quasiplanar. The effective gap profits from including the additional DOF in the ancillary because it allows to increase the interactions between pairs of ports (cf. `XNOR3ii`-gate from fig. 8.1).

enclose the angle $\angle(\mathsf{A},\mathsf{B},\mathsf{C}) > 120°$: Here we draw the edges such that they connect to the ancillary. The planar implementations `FMSII-1i` and `FMSII-2i` are too deformed such that we can not directly amalgamate two of such sites to construct a unit cell without corrupting the energy structure. Such an amalgamation would either require intermediate LNK-gates or a deformation of the structure. Additionally the planar site possesses only a small effective gap $\Delta E_{\text{eff}} \sim 1\%$ which is at least one order of magnitude smaller than the effective gap of the planar `FMSI-3` site. This realization seems not very natural to implement on the *two-dimensional* Rydberg platform.

The quasiplanar `FMSII-1ii` and `FMSII-2ii` sites possess an effective gap $\Delta E_{\text{eff}} \approx 14\%$ similarly as for the `FMSIV-1ii` site. Thus this realization profits heavily from the third dimension for the ancillary. Still, the energy gap is smaller than for the `FMSI-3` site. This behavior is very similar to the `XNOR3ii`-gate from fig. 8.1 as the language $L_{\texttt{FMSI1}} = \texttt{XNOR3} \cup \{(0_\mathsf{A}, 1_\mathsf{B}, 1_\mathsf{C}, 0_0)\}$ are identical up to the fifth ground state. If we constrain the structure to the two-dimensional Rydberg platform the effective gap suffers similarly as for `XNOR3i`. On the three-dimensional Rydberg platform the `XNOR3ii`-gate still possesses a smaller effective gap than the `XOR3`-gate which parallels the `FMSI-3` site.

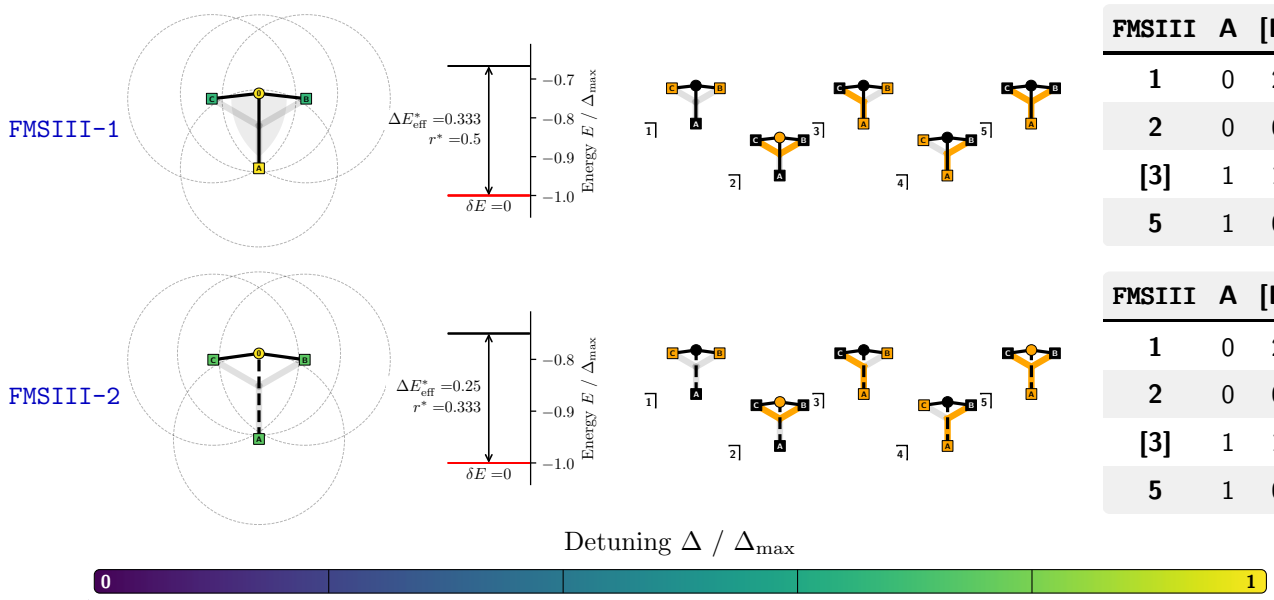

FMSIII	A	[B]	0
1	0	2	0
2	0	0	1
[3]	1	1	0
5	1	0	0

FMSIII	A	[B]	0
1	0	2	0
2	0	0	1
[3]	1	1	0
5	1	0	1

Figure 8.21: FIBONACCI model site with check function (5.15) in representation III. There exist two VdW-minimal realizations FMSIII-1 and FMSIII-2 which can both be chosen planar without impeding the effective gap (cf. XOR3-gate from fig. 4.9). The effective gaps are comparable to the FMSI-3 site from fig. 5.6.

8.6.3 | Representation III

Lastly, we consider representation III which is *dual* to representation II. Representation III is *edge low for two edges* which we identify with the ports B and C. Like for representation II the check function (5.15) is only permutation symmetric in the ports B and C. It includes the four words where either no or two port bits are excited but also the asymmetric word where only the port A is excited.

Again we require one ancillary for this representation. We argue with corollary II. We require the ancillary such that such that the ground state $\boldsymbol{x}_2 \notin \boldsymbol{x}_1, \boldsymbol{x}_3, \boldsymbol{x}_4$ is no non-adjacent substate of $\boldsymbol{x}_1$, $\boldsymbol{x}_3$ and $\boldsymbol{x}_4$ (and such that $\mathbf{0} \notin L_t$). Thus the ancillary needs to be excited in $\boldsymbol{x}_2$ but not excited in $\boldsymbol{x}_1, \boldsymbol{x}_3, \boldsymbol{x}_4$. This leaves two choices for the state of the ancillary in $\boldsymbol{x}_5$: Realization $w[\texttt{FMSIII-1}] = \texttt{NOOR}$ and realization $w[\texttt{FMSII-2}] = \texttt{MIN}$ are presented in the first and second row of fig. 8.21 respectively. This makes the realizations of fig. 8.21 *VdW-minimal* and the list of VdW-minimal realizations *complete*.

The FMSIII-1,2 site is similar to the XOR3-gate from fig. 4.9. The language $L_{\texttt{FMSI1}} = \texttt{XNOR3} \cup \{(0_\mathsf{A}, 1_\mathsf{B}, 1_\mathsf{C}, 0_0)\}$ are identical up to the fifth ground state. In the fifth ground state of realization FMSIII-1 the ancillary is not excited. Thus the ancillary only needs to be sufficiently close to the ports such that it does not impede the energy gap. Thus the FMSIII-1 site possesses again a gray-shaded volume in which we can arbitrarily position the ancillary to optimize the effective gap. We choose a planar implementation where the distance with the port A is maximal because this emphasizes the similarity with theFMSIII-2 site.

In the FMSIII-2 site the ancillary is excited in the fifth ground state. To optimize the energy gap for the FMSIII-2 site the distance between port A and the ancillary needs to be maximized. Here the only choice left is the positioning of the ancillary on the two-dimensional spherical cap between the ports B and C. We choose a planar and symmetric implementation for fig. 8.21. Note that for both realizations we *choose* a planar implementation within the solution space which optimizes the effective gap. This solution space includes quasiplanar structures as well.

8.6.4 | Summary and Conclusion

The effective gaps of both realizations FMSIII-1,2 are large and comparable with the FMSI-3 site in fig. 5.6. Especially the effective gap $\Delta E_{\text{eff}} \approx 33.3\%$ of realization FMSIII-1 is besides the FMSI-3 site the largest one we encountered. Similarly both sites possess tolerance in the positioning of the ancillary which supports an experimental implementation. In contrast the effective gaps of representations II and IV are smaller and require the third dimension. They possess no tolerance in the positioning of the ancillaries. This can be explained by the similarity of representations I and III to the XOR3-gate and from representations II and IV to the XNOR3-gate. Negating two edges maps the eigenstates of XOR/ XNOR with even/ odd number of excited ports to themselves. Thus the even/ odd representations differ only in their fifth ground states which seems to require only small modifications. In sec. 4.2 we already found that XOR3 can be implemented as a planar structure with choice left in the positioning of the ancillary. Instead the XNOR-gate possesses only a low effective gap for a planar structure and even with the third dimension the effective gap is only half as large as for XOR3.
For the even/ odd representations there is one representation with a symmetric and one with an asymmetric check function. The asymmetric check functions possess two VdW-minimal realizations each, the symmetric check functions possess only one VdW-minimal realization each.

In conclusion the most promising VdW-minimal realizations for the Fibonacci model seem to be the FMSI-3 *and* the FMSIII-1 site with one ancillary each. Tessellating the FMSI-3 site yields a hexagonal structure where one ancillary is positioned on each site and one port is positioned on each edge. Tessellating the FMSIII-1 sites constructs a similar honeycomb grid however 'squished' in the vertical direction.

| Appendix

8.A | Completeness and Minimality of the Ternary Logic Elementaries

In this appendix we want to include the remaining ternary, scalar, symmetric logic elementaries which were not yet mentioned in sec. 8.2. Furthermore we want to proof *minimality* and *completeness* of the portrayed lists. Again, we structure this section by the effective HAMMING weight.

8.A.1 | Unit effective Hamming Weight

In this subsection we prove the following statement:

1 | Every realization portrayed in fig. 8.4 and fig. 8.22 is *VdW-minimal*: The connectives `NOOR`, `XXOR` and `XXNOR` require only one ancillary. The `AAND`-gates require at least two ancillaries.

2 | For the connectives `NOOR`, `XXOR` and `XXNOR` the combined list of realizations in fig. 8.4 and fig. 8.22 is *exhaustive*. For `AAND` there exist in total *seven* possible realizations.

Proof 16. (Completeness and Minimality for unit effective Hamming Weight)

We follow the argument from corollary II. In a nutshell corollary II forbids ground states which are non-adjacent substates (with any intermediate excited state).
We start with $f_b = \texttt{NOOR}$. The realizations `NOOR-1a,b,c,d` posses one ancillary. The ancillary bit is necessary such that $\boldsymbol{x}_2 \notin \boldsymbol{x}_4$. Thus the realizations `NOOR-1a,b,c,d` are VdW-minimal. We need to choose the ancillary bit such that it is excited in $\boldsymbol{x}_2$ but not excited in $\boldsymbol{x}_4$. This leaves $2^2 = 4$ choices for $\boldsymbol{x}_1$ and $\boldsymbol{x}_4$ which are presented as `a`, `b`, `c` and `d` in fig. 8.4 and fig. 8.22. Thus the list of VdW-minimal realizations is complete.
We continue with $f_b = \texttt{XXOR}$. Realization `XXOR-1` possesses one ancillary. The ancillary bit is necessary such that $\boldsymbol{x}_1 \notin \boldsymbol{x}_2, \boldsymbol{x}_3, \boldsymbol{x}_4$ (and such that $\mathbf{0} \neq \boldsymbol{x}_1 \in \mathcal{G}$ which is excluded by remark 4). Thus realization `XXOR-1` is VdW-minimal. We need to choose the ancillary bit such that it is excited in $\boldsymbol{x}_1$ but not excited in $\boldsymbol{x}_2, \boldsymbol{x}_3, \boldsymbol{x}_4$. This leaves only one choices which is presented in fig. 8.4. Thus realization `XXOR-1` is VdW-minimal and unique.
Now consider $f_b = \texttt{XXNOR}$. Realization `XXNOR-1` possesses one ancillary. The ancillary bit is necessary such that $\boldsymbol{x}_1, \boldsymbol{x}_2 \notin \boldsymbol{x}_3, \boldsymbol{x}_4$ (and such that $\mathbf{0} \neq \boldsymbol{x}_1 \in \mathcal{G}$ which is excluded by remark 4). Thus realization `XXNOR-1` is VdW-minimal. We need to choose the ancillary bit such that it is excited in $\boldsymbol{x}_1, \boldsymbol{x}_2$ but not excited in $\boldsymbol{x}_3, \boldsymbol{x}_4$. This leaves only one choices which is presented in fig. 8.4. Thus realization `XXNOR-1` is VdW-minimal and unique.
Lastly consider $f_b = \texttt{AAND}$. The realizations `AAND-1a,b` posses two ancillaries. We need (an) ancillary bit(s) such that $\boldsymbol{x}_1 \notin \boldsymbol{x}_3$ and such that $\boldsymbol{x}_1, \boldsymbol{x}_2, \boldsymbol{x}_3 \notin \boldsymbol{x}_4$. Thus in particular (at least) one ancillary bit needs to be excited in $\boldsymbol{x}_1$ which is not excited in $\boldsymbol{x}_3$ and (at least) one ancillary bit needs to be excited in $\boldsymbol{x}_3$ but not excited in $\boldsymbol{x}_4$. This requires at least two ancillary bits which makes realizations `AAND-1a,b` VdW-minimal. As mentioned above the portrayed list of VdW-minimal `AAND`-gates is not complete. In the following we derive a complete list of candidates. W.l.o.g. assume that ancillary bit 0 is excited in $\boldsymbol{x}_1$ but not excited in $\boldsymbol{x}_3$ and ancillary bit 1 is excited in $\boldsymbol{x}_3$ but not excited in $\boldsymbol{x}_4$:

1 | First assume that bit 0 is excited in $\boldsymbol{x}_4$. Then bit 1 needs to be excited in $\boldsymbol{x}_1$ and $\boldsymbol{x}_2$ such that $\boldsymbol{x}_1, \boldsymbol{x}_2 \notin \boldsymbol{x}_4$. This leaves two possibilities for the realizations: $w = (\texttt{EQU}, \texttt{NAAND})$ and $w = (\texttt{NXXNOR}, \texttt{NAAND})$.

2 | Now consider the case where bit 0 is not excited in $\boldsymbol{x}_4$ (this is the case for both realizations `1a` and `1b`):

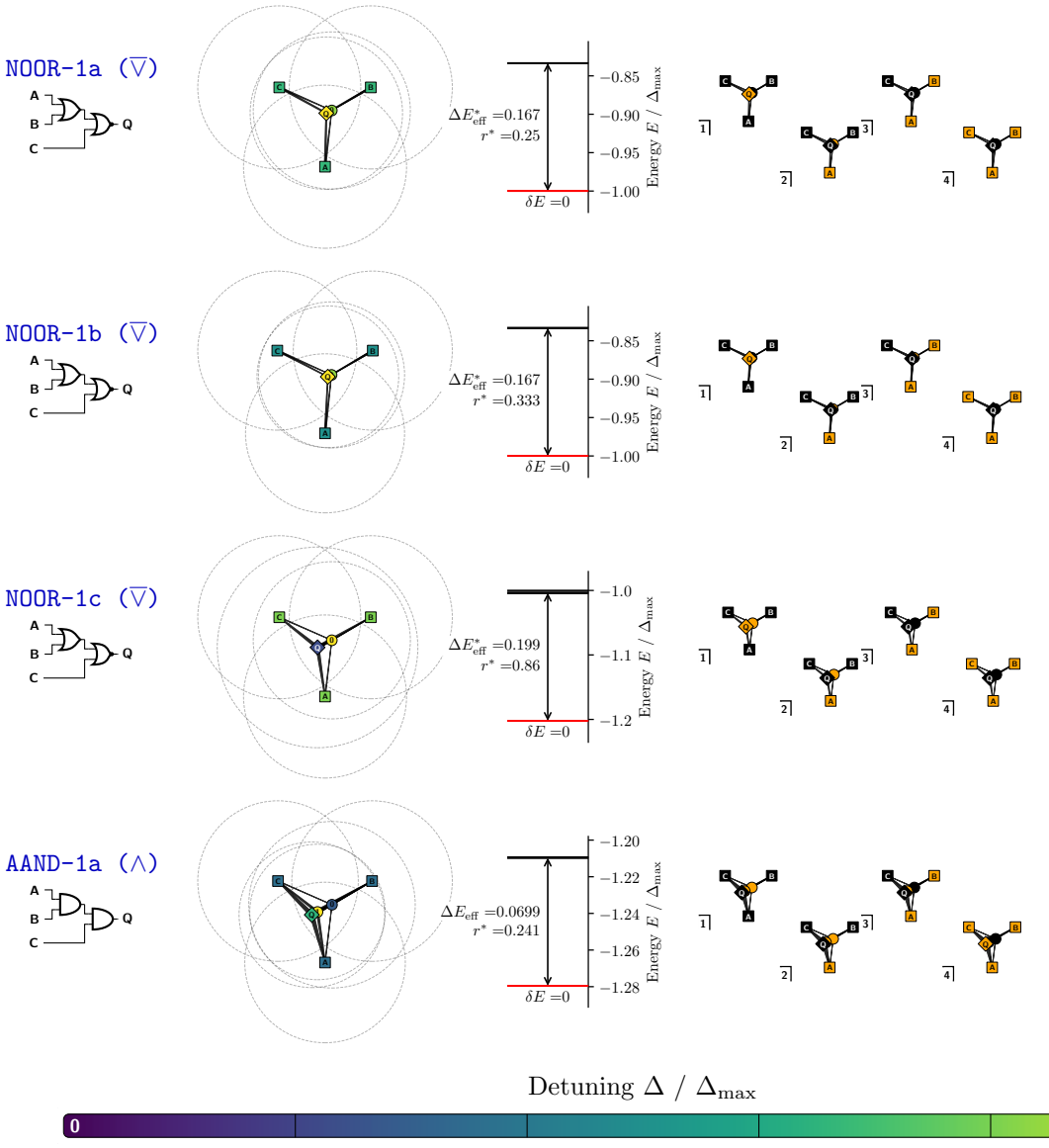

∇̄	[A]	Q	0
1	0	1	0
2	1	0	1
3	2	0	0
4	3	0	0

∇̄	[A]	Q	0
1	0	1	0
2	1	0	1
3	2	0	1
4	3	0	0

∇̄	[A]	Q	0
1	0	1	1
2	1	0	1
3	2	0	0
4	3	0	0

∧	[A]	Q	0	1
1	0	0	1	1
2	1	0	1	1
3	2	0	0	1
4	3	1	0	0

Figure 8.22: Additional ternary, scalar, symmetric logic gates with unit effective HAMMING weight $w_H = 1$. The portrayed connectives emerge from the connectives from fig. 8.23 via negation. Further gates are portrayed in fig. 8.4. Completeness and minimality are shown in proof 16.

a | If bit 1 is not excited in $\boldsymbol{x}_2$ then bit 0 needs to be excited $\boldsymbol{x}_2$ such that $\boldsymbol{x}_2 \notin \boldsymbol{x}_4$. This leaves two possibilities for the realizations: $w = (\texttt{MIN}, \texttt{XXNOR})$ and $w = (\texttt{MIN}, \texttt{EVEN})$.

b | If bit 1 is excited in $\boldsymbol{x}_2$ then bit 0 can be either excited or not excited in $\boldsymbol{x}_2$:

i | If bit 0 is excited in $\boldsymbol{x}_2$ then bit 1 needs to be excited in $\boldsymbol{x}_1$ such that $\boldsymbol{x}_1 \notin \boldsymbol{x}_2$. This yields realization $w[\texttt{AAND1a}] = (\texttt{MIN}, \texttt{NAAND})$.

ii | On the other hand if bit 0 is not excited in $\boldsymbol{x}_2$ this yields two possibilities for the realizations: $w[\texttt{AAND1b}] = (\texttt{NOOR}, \texttt{NAAND})$ and $w = (\texttt{NOOR}, \texttt{NEQ})$.

Thus in total we obtain seven realization for $f_b = \texttt{AAND}$ and recover the two realizations `1b` and `1a` from fig. 8.4 and fig. 8.22 respectively which are . □

8.A.2 | Effective Hamming Weight Three

In this subsection we prove the following statement:

1 | Every realization portrayed in fig. 8.5 and fig. 8.23 is *VdW-minimal*. The connectives NAAND, NXXNOR and NXXOR require only one ancillary. The OOR-gates require at least two ancillaries.

2 | For the connectives NAAND, NXXNOR and NXXOR the combined list of realizations in fig. 8.5 and fig. 8.23 is *exhaustive*. For OOR there exist in total *seven* possible realizations.

Proof 17. (Completeness and Minimality for effective Hamming Weight Three)

We follow the argument from corollary II. In a nutshell corollary II forbids ground states which are non-adjacent substates (with any intermediate excited state).
We start with $f_b = \texttt{NAAND}$. The realizations NAAND-1a,b,c,d posses one ancillary. The ancillary bit is necessary such that $\boldsymbol{x}_1 \notin \boldsymbol{x}_3$. Thus the realizations NAAND-1a,b,c,d are VdW-minimal. We need to choose the ancillary bit such that it is excited in $\boldsymbol{x}_1$ but not excited in $\boldsymbol{x}_3$. This leaves $2^2 = 4$ choices in bit 1 for $\boldsymbol{x}_2$ and $\boldsymbol{x}_4$ which are presented as a, b, c and d in fig. 8.4 and fig. 8.23. Thus the list of VdW-minimal realizations is complete.
We continue with $f_b = \texttt{NXXNOR}$. Realization NXXNOR-1 possesses one ancillary. The ancillary bit is necessary such that $\boldsymbol{x}_1, \boldsymbol{x}_2, \boldsymbol{x}_3 \notin \boldsymbol{x}_4$. Thus realization NXXNOR-1 is VdW-minimal. We need to choose the ancillary bit such that it is excited in $\boldsymbol{x}_1$, $\boldsymbol{x}_2$ and $\boldsymbol{x}_3$ but not excited in $\boldsymbol{x}_2, \boldsymbol{x}_3, \boldsymbol{x}_4$. This leaves only one choices which is presented in fig. 8.4. Thus realization NXXNOR-1 is VdW-minimal and unique.
Now consider $f_b = \texttt{NXXOR}$. Realization NXXOR-1 possesses one ancillary. The ancillary bit is necessary such that $\boldsymbol{x}_1, \boldsymbol{x}_2 \notin \boldsymbol{x}_4$ and such that $\boldsymbol{x}_1 \notin \boldsymbol{x}_3$. Thus realization NXXOR-1 is VdW-minimal. We need to choose the ancillary bit such that it is excited in $\boldsymbol{x}_1$ and $\boldsymbol{x}_2$ but not

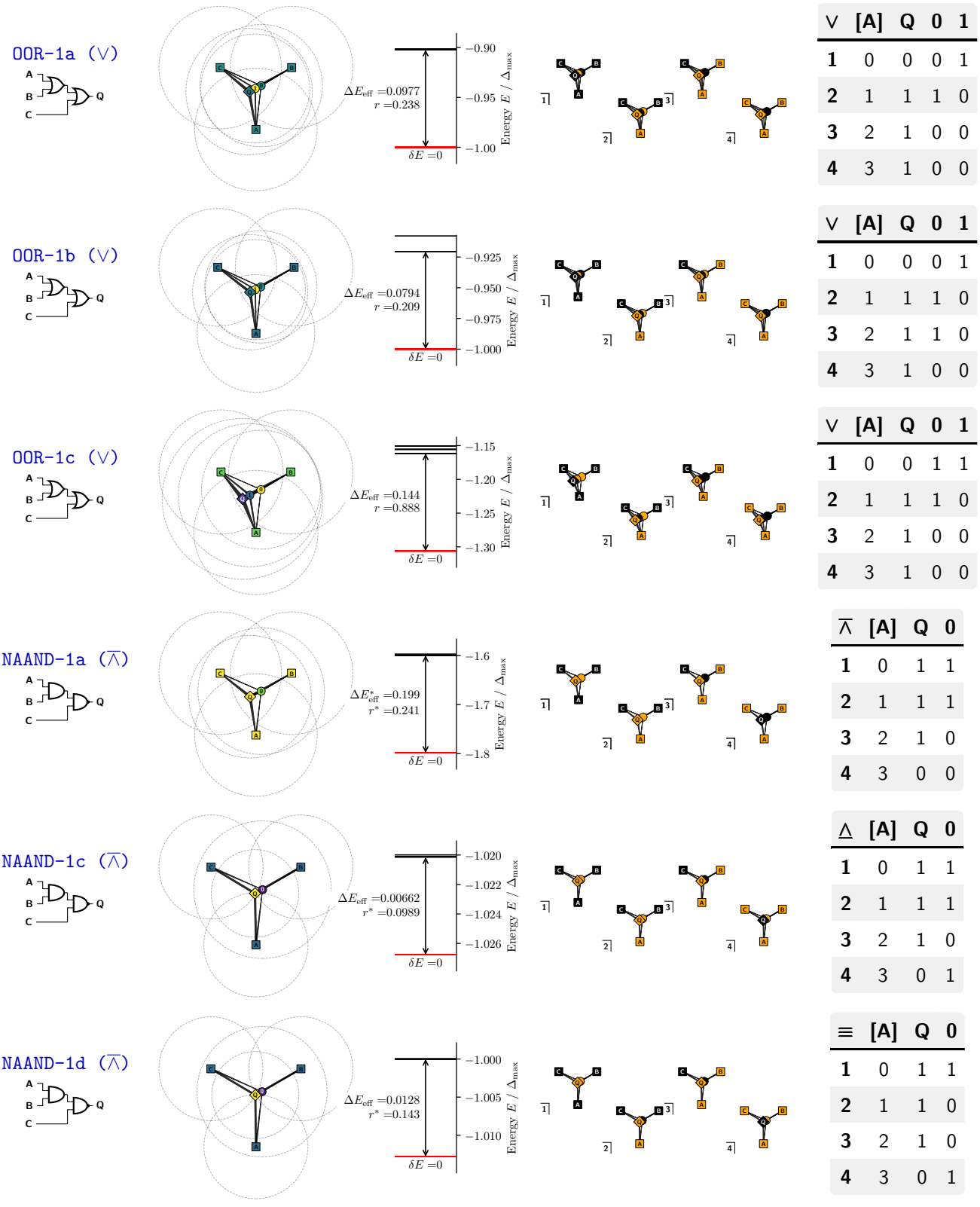

∨	[A]	Q	0	1
1	0	0	0	1
2	1	1	1	0
3	2	1	0	0
4	3	1	0	0

∨	[A]	Q	0	1
1	0	0	0	1
2	1	1	1	0
3	2	1	1	0
4	3	1	0	0

∨	[A]	Q	0	1
1	0	0	1	1
2	1	1	1	0
3	2	1	0	0
4	3	1	0	0

$\overline{\wedge}$	[A]	Q	0
1	0	1	1
2	1	1	1
3	2	1	0
4	3	0	0

$\wedge$	[A]	Q	0
1	0	1	1
2	1	1	1
3	2	1	0
4	3	0	1

≡	[A]	Q	0
1	0	1	1
2	1	1	0
3	2	1	0
4	3	0	1

Figure 8.23: Additional ternary, scalar, symmetric logic gates with effective HAMMING weight $w_H = 3$. The portrayed connectives emerge from the connectives from fig. 8.22 via negation. Further gates are portrayed in fig. 8.5. Completeness and minimality are shown in proof 17.

excited in $\boldsymbol{x}_3$ and $\boldsymbol{x}_4$. This leaves only one choices which is presented in fig. 8.4. Thus realization `NNXXOR-1` is VdW-minimal and unique.
Lastly consider $f_b = \texttt{OOR}$. The realizations `OOR-1a,b,c,d` posses two ancillaries. We need (an) ancillary bit(s) such that $\boldsymbol{x}_1 \notin \boldsymbol{x}_2, \boldsymbol{x}_3, \boldsymbol{x}_4$ and such that $\boldsymbol{x}_2 \notin \boldsymbol{x}_4$. Thus in particular (at least) one ancillary bit needs to be excited in $\boldsymbol{x}_1$ which is not excited in $\boldsymbol{x}_2$ and (at least) one ancillary bit needs to be excited in $\boldsymbol{x}_2$ but not excited in $\boldsymbol{x}_4$. This requires at least two ancillary bits which makes realizations `OOR-1a,b,c,d` VdW-minimal. As mentioned above the portrayed list of VdW-minimal `OOR`-gates is not complete. In the following we derive a complete list of candidates. W.l.o.g. assume that ancillary bit 0 is excited in $\boldsymbol{x}_1$ but not excited in $\boldsymbol{x}_2$ and ancillary bit 1 is excited in $\boldsymbol{x}_2$ but not excited in $\boldsymbol{x}_4$:

1 | First assume that bit 0 is excited in $\boldsymbol{x}_4$. Then bit 1 needs to be excited in $\boldsymbol{x}_1$ such that $\boldsymbol{x}_1 \notin \boldsymbol{x}_4$. In $\boldsymbol{x}_3$ the two bits must be different because for both bits (de-)excited it is $\boldsymbol{x}_1 \notin \boldsymbol{x}_3$ ($\boldsymbol{x}_3 \notin \boldsymbol{x}_4$). This leaves two possibilities for the realizations: $w = (\texttt{NXXOR}, \texttt{NAAND})$ and $w = (\texttt{EQU}, \texttt{NAAND})$.

2 | Now consider the case where bit 0 is not excited in $\boldsymbol{x}_4$ (this is the case for all realizations `1a,b,c,d`):

a | If bit 1 is excited in $\boldsymbol{x}_3$ then bit 0 needs to be not excited $\boldsymbol{x}_3$ such that $\boldsymbol{x}_2 \notin \boldsymbol{x}_3$. This leaves two possibilities for the realizations: $w = (\texttt{NOOR}, \texttt{NAAND})$ and $w = (\texttt{NOOR}, \texttt{NEQ})$.

b | If bit 1 is excited in $\boldsymbol{x}_3$ then bit 0 can be either excited or not excited in $\boldsymbol{x}_3$:

i | If bit 0 is excited in $\boldsymbol{x}_3$ then bit 1 needs to be excited in $\boldsymbol{x}_1$ such that $\boldsymbol{x}_1 \notin \boldsymbol{x}_3$. This yields realization $w = (\texttt{EVEN}, \texttt{MIN})$.

ii | On the other hand if bit 0 is not excited in $\boldsymbol{x}_3$ this yields two possibilities for the realizations: $w = (\texttt{NOOR}, \texttt{MIN})$ and $w = (\texttt{NOOR}, \texttt{XXOR})$.

Thus in total we obtain seven realization for $f_b = \texttt{OOR}$ and recover the two realizations `1a,b,c,d` from fig. 8.4 and fig. 8.22 respectively which are . □

8.A.3 | Effective Hamming Weight Two

In this subsection we prove the following statement:

1 | Every realization portrayed in fig. 8.6 and fig. 8.7 is *VdW-minimal*. The connectives require at most one ancillary. The `MIN`-gate requires no ancillary at all.

2 | The list of VdW-minimal realizations in fig. 8.6 and fig. 8.7 is *exhaustive*. For each gate there exists only one *unique* VdW-minimal realization.

Proof 18. (Completeness and Minimality for effective Hamming Weight Two)

Again, we follow the argument from corollary II. In a nutshell corollary II forbids ground states which are non-adjacent substates (with any intermediate excited state).
We start with $f_b = \texttt{MIN}$. The realization `MIN-1` presented in fig. 8.4 possesses no ancillary. This makes this realization trivially VdW-minimal and unique.
We continue with $f_b = \texttt{MAJ}$. Realization `MAJ-1` possesses one ancillary. The ancillary bit is necessary such that $\boldsymbol{x}_1, \boldsymbol{x}_2 \notin \boldsymbol{x}_3, \boldsymbol{x}_4$. Thus realization `MAJ-1` is VdW-minimal. We need to choose the ancillary bit such that it is excited in $\boldsymbol{x}_1$ and $\boldsymbol{x}_2$ but not excited in $\boldsymbol{x}_3$ and $\boldsymbol{x}_4$. This leaves only one choice which is presented in fig. 8.4. Thus realization `MAJ-1` is VdW-minimal and unique.
Thirdly consider $f_b = \texttt{NEQ}$. Realization `NEQ-1` possesses one ancillary. The ancillary bit is necessary such that $\boldsymbol{x}_1 \notin \boldsymbol{x}_2, \boldsymbol{x}_3, \boldsymbol{x}_4$. Thus realization `NEQ-1` is VdW-minimal. We need to choose the ancillary bit such that it is excited in $\boldsymbol{x}_1$ but not excited in $\boldsymbol{x}_2$, $\boldsymbol{x}_3$ and $\boldsymbol{x}_4$. This leaves only one choice which is presented in fig. 8.4. Thus realization `NEQ-1` is VdW-minimal and unique.
Now we consider $f_b = \texttt{EQU}$. Realization `EQU-1` possesses one ancillary. The ancillary bit is necessary such that $\boldsymbol{x}_1, \boldsymbol{x}_2, \boldsymbol{x}_3 \notin \boldsymbol{x}_4$. Thus realization `EQU-1` is VdW-minimal. We need to choose the ancillary bit such that it is excited in $\boldsymbol{x}_1$, $\boldsymbol{x}_2$ and $\boldsymbol{x}_3$ but not excited in $\boldsymbol{x}_4$. This leaves only one choice which is presented in fig. 8.4. Thus realization `EQU-1` is VdW-minimal and unique.
Finally consider $f_b = \texttt{EVEN}$. Realization `EVEN-1` possesses one ancillary. The ancillary bit is necessary such that $\boldsymbol{x}_1 \notin \boldsymbol{x}_3$ and such that $\boldsymbol{x}_2 \notin \boldsymbol{x}_4$. Thus realization `EVEN-1` is VdW-minimal. We need to choose the ancillary bit such that it is excited in $\boldsymbol{x}_1$ but not in $\boldsymbol{x}_3$ and such that is is excited in $\boldsymbol{x}_2$ but not in $\boldsymbol{x}_4$. This leaves only one choice which is presented in fig. 8.4. Thus realization `EVEN-1` is VdW-minimal and unique.
Lastly consider $f_b = \texttt{ODD}$. The realizations `OOR-1` posses two ancillaries. We need (an) ancillary bit(s) such that $\boldsymbol{x}_1 \notin \boldsymbol{x}_2, \boldsymbol{x}_3, \boldsymbol{x}_4$ and such that $\boldsymbol{x}_2, \boldsymbol{x}_3 \notin \boldsymbol{x}_4$. Thus in particular (at least) one ancillary bit needs to be excited in $\boldsymbol{x}_1$ which is not excited in $\boldsymbol{x}_2$ and (at least) one ancillary bit needs to be excited in $\boldsymbol{x}_2$ but not excited in $\boldsymbol{x}_4$. This requires at least two ancillary bits which makes realizations `ODD-1` VdW-minimal. As mentioned above the portrayed list of VdW-minimal `ODD`-gates is not complete. In the following we derive a complete list of candidates. W.l.o.g. assume that ancillary bit 0 is excited in $\boldsymbol{x}_1$ but not excited in $\boldsymbol{x}_2$ and ancillary bit 1 is excited in $\boldsymbol{x}_2$ but not excited in $\boldsymbol{x}_4$:

1 | First assume that bit 0 is excited in $\boldsymbol{x}_4$. Then bit 1 needs to be excited in $\boldsymbol{x}_1$ and $\boldsymbol{x}_3$ such that $\boldsymbol{x}_1, \boldsymbol{x}_3 \notin \boldsymbol{x}_4$. Further bit 0 needs to be not excited in $\boldsymbol{x}_3$ such that $\boldsymbol{x}_1 \notin \boldsymbol{x}_3$. This yields realization $w = (\texttt{EQU}, \texttt{NAAND})$.

2 | Now consider the case where bit 0 is not excited in $\boldsymbol{x}_4$ (this is the case for realization `1`):

a | If bit 1 is excited in $\boldsymbol{x}_1$ then in $\boldsymbol{x}_3$ either bit 0 or 1 needs to be (not) excited such that $\boldsymbol{x}_1 \notin \boldsymbol{x}_3$ and $\boldsymbol{x}_3 \notin \boldsymbol{x}_4$. This leaves two possibilities for the realizations: $w = (\texttt{EVEN}, \texttt{MIN})$ and $w = (\texttt{NOOR}, \texttt{NAAND})$.

b | If bit 1 is not excited in $\boldsymbol{x}_1$ then in $\boldsymbol{x}_3$ bit 1 (0) needs to be (not) excited such that $\boldsymbol{x}_1 \notin \boldsymbol{x}_3$ and $\boldsymbol{x}_3 \notin \boldsymbol{x}_4$. This yields realization $w = (\texttt{NOOR}, \texttt{NEQ})$.

Thus in total we obtain five realizations for $f_b = \texttt{ODD}$ and recover the two realizations `1` from fig. 8.5. □

8.B | Completeness and Minimality of the Multi Gates

In this appendix we want to include the remaining VdW-minimal binary, double and triple logic gates which were not yet mentioned in sec. 8.4. Furthermore we want to proof *minimality* and *completeness* for the double logic gates.

8.B.1 | Double Logic Gates

In this subsection in fig. 8.24 we present further double gates which complete the list portrayed in fig. 8.13. We claim that fig. 8.13 and fig. 8.24 together include the complete list of VdW-minimal double gates constructed from the three logical connectives `NOR`, `NAND` and `XOR`:

Proof 19. (Completeness and Minimality of Double Logic Gates)

> The double gates `NORNOR-1`, `NANDNAND-1`, `NORNAND-1` and `NORXOR-2` are trivially the unique VdW-minimal realizations because they possess no ancillaries. Thus we only need to show that for the two remaining connectives `NANDXOR` and `XORXOR` we found the complete list of VdW-minimal realizations. We follow the argument from corollary II. In a nutshell corollary II forbids that there are two ground states which are non-adjacent substates (with any intermediate excited state).
> The realizations `NANDXOR-1` and `NANDXOR-2` posses one ancillary each. The ancillary bit is necessary such that $\boldsymbol{x}_1 \notin \boldsymbol{x}_2, \boldsymbol{x}_3$. This makes both realizations VdW-minimal. We need to choose the ancillary bit such that it is excited in $\boldsymbol{x}_1$ but not excited in $\boldsymbol{x}_2, \boldsymbol{x}_3$. The state of the ancillary bit remains undetermined in $\boldsymbol{x}_4$. This leaves only 2 possibilities for the realizations: $w[\texttt{NANDXOR1}] = \texttt{NOR}$ and $w[\texttt{NANDXOR2}] = \texttt{XNOR}$. This makes the list of VdW-minimal `NANDXOR`-gates complete.
> Realizations `XORXOR-2` possesses one ancillary. The ancillary bit is necessary such that $\boldsymbol{x}_1 \notin \boldsymbol{x}_2, \boldsymbol{x}_3, \boldsymbol{x}_4$ (and such that $\mathbf{0} \notin L_t$), thus realization `XORXOR-2` is VdW-minimal. We need to choose the ancillary bit such that it is excited in $\boldsymbol{x}_1$ but not excited in $\boldsymbol{x}_2, \boldsymbol{x}_3, \boldsymbol{x}_4$. This fully determines the realizations $w[\texttt{XORXOR2}] = \texttt{NOR}$ which makes `XORXOR-2` the unique VdW-minimal realization. □

The `XORXOR2`-Gate. The `XORXOR1`-gate is not VdW-minimal because it includes two ancillaries in identical states. The VdW-minimal `XORXOR2`-gate in the first row of fig. 8.24 is constructed by removing one of the two ancillaries. Interestingly the $\Delta E_{\text{eff}}, r$-optimized L-complex seems to remain two-dimensional. However there are necessarily strong residual interaction between the two output ports which cause a small effective gap $\Delta E_{\text{eff}}[\texttt{XORXOR2}] \approx 3.8\%$. It might therefore be more useful to rely on realization `XORXOR-1` for the implementation of a logic circuit.

The `NANDXOR2`-Gate. Similarly the VdW-minimal realization `NANDXOR-1` is not unique. One could imagine an equally valid realization $w[\texttt{NANDXOR2}] = \texttt{XNOR}$ as presented in the second row of fig. 8.24. The effective gap is $\Delta E_{\text{eff}}[\texttt{NANDXOR2}] \approx 9.4\%$.

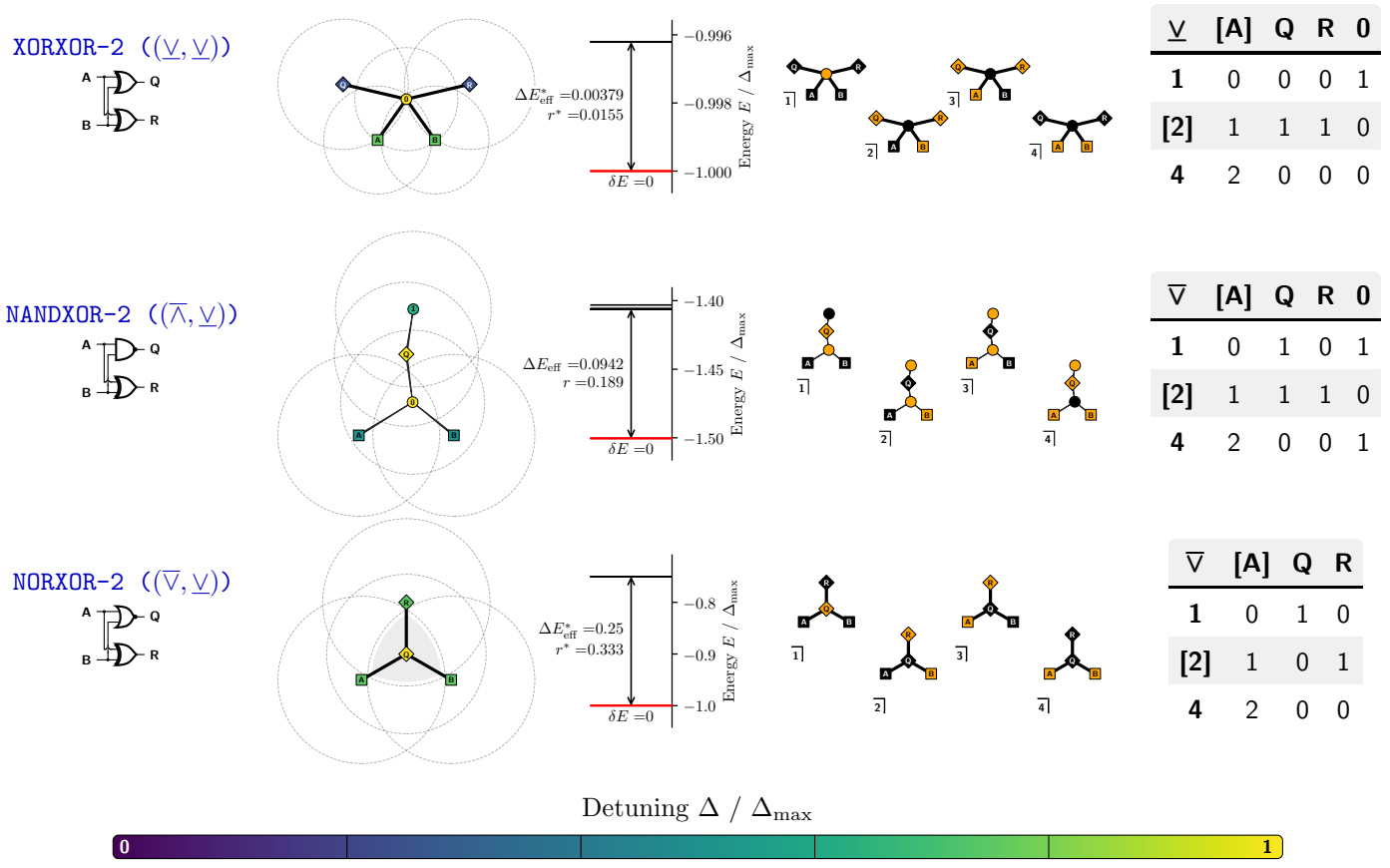

⩒	[A]	Q	R	0
1	0	0	0	1
[2]	1	1	1	0
4	2	0	0	0

⩑	[A]	Q	R	0
1	0	1	0	1
[2]	1	1	1	0
4	2	0	0	1

⩒	[A]	Q	R
1	0	1	0
[2]	1	0	1
4	2	0	0

Figure 8.24: Further double logic Gates which implement vectorial connectives with $q = 2$. The remaining gates are portrayed in fig. 8.13.

The NORXOR2- and the ORXOR2-Gate. Lastly realization NORXOR-1 is not VdW-minimal either because here the ancillary 0 is always in the same state as output port Q. In fact by relabeling the ancillary from the XOR3-gate in fig. 4.9 as another output port we obtain the VdW-minimal and unique NORXOR2-gate from the third row in fig. 8.24. Note that we can choose the output port Q inside the gray-shaded volume freely without modifying the effective gap. In particular we can choose the optimized structure as two-dimensional. However the output port Q can only be accessed efficiently via the third dimension. Nevertheless it is possible to embed this gate in a logic circuit on the two-dimensional Rydberg platform. This is illustrated via the ORXOR2-gate in the first row of fig. 8.25. Here we amalgamated a NOT1-gate to output port Q such that it lies in-plane with the remaining atoms. Such an amalgamation on the two-dimensional Rydberg platform introduces strong residual interactions between the output ports. This impairs the effective gap $\Delta E_{\text{eff}} \approx 0.6\%$ of the ORXOR2-gate.
The ORXOR2-gate is actually VdW-minimal and unique. Here the ancillary bit is necessary such that $\boldsymbol{x}_1 \notin \boldsymbol{x}_2, \boldsymbol{x}_3, \boldsymbol{x}_4$ thus the ancillary needs to be excited in $\boldsymbol{x}_1$ but not excited $\boldsymbol{x}_2, \boldsymbol{x}_3, \boldsymbol{x}_4$. This fully determines realization $w[\text{ORXOR2}] = \text{NOR}$.

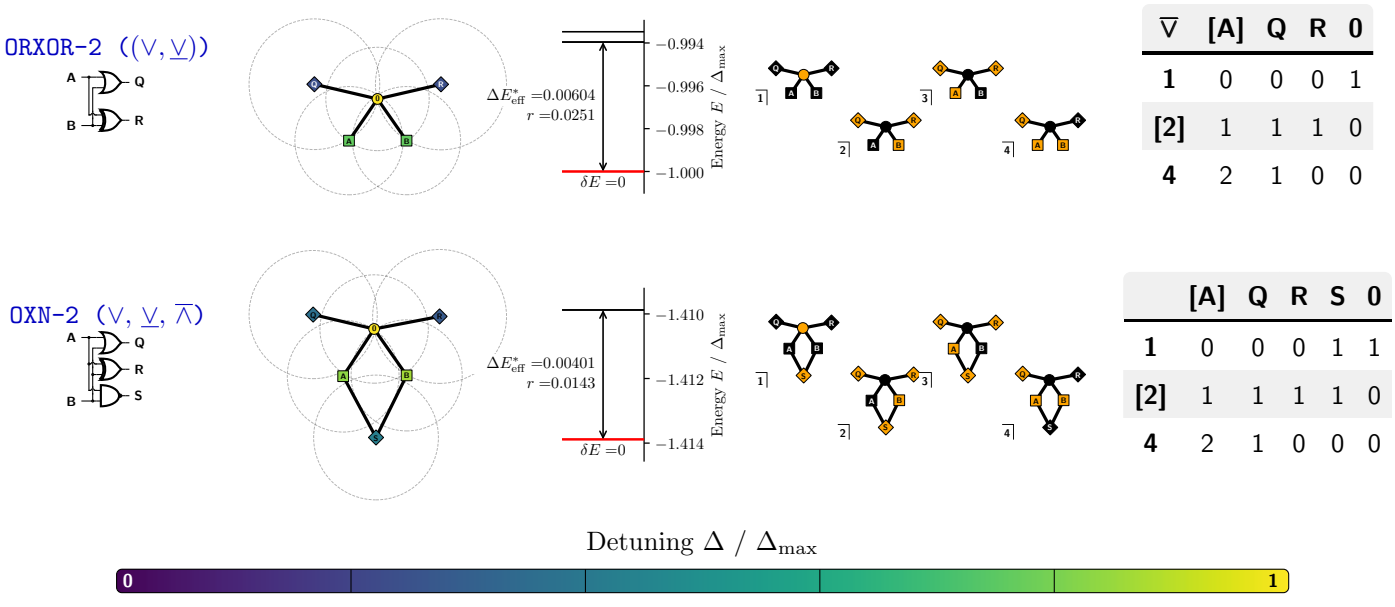

⩒	[A]	Q	R	0
1	0	0	0	1
[2]	1	1	1	0
4	2	1	0	0

	[A]	Q	R	S	0
1	0	0	0	1	1
[2]	1	1	1	1	0
4	2	1	0	0	0

Figure 8.25: Two-dimensional multi gates which include OR. They are constructed by amalgamating a NOT1-gate in-plane with the other atoms to the NORXOR2- and NXN2-gate from fig. 8.24 and fig. 8.14 respectively.

8.B.2 | Triple Logic Gates

In fig. 8.25 in the second row we portray the OXN2-gate. Here we amalgamated a NOT1-gate to output port Q of the NXN2-gate in fig. 8.14 such that it lies in-plane with the remaining atoms. Such an amalgamation on the two-dimensional Rydberg platform introduces strong residual interactions between the output ports which impairs the effective gap $\Delta E_{\text{eff}} \approx 0.4\%$ of the OXN2-gate. This illustrates that it is possible to construct a logic circuit with the NXN2-gate on the two-dimensional Rydberg platform however the dimensionality constraint impairs the effective gap.
We can also interpret the OXN2-gate as a ORXOR2-gate where an additional NAND3-gate amalgamated to the input ports. As the effective gap of the ORXOR2-gate is very small this also explains why the effective gap of the OXN2-gate is so small.
The OXN2-gate is VdW-minimal and but not unique. Here the ancillary bit is necessary such that $\boldsymbol{x}_1 \notin \boldsymbol{x}_2, \boldsymbol{x}_3$. One could imagine another realization with $w =$ XNOR.

9 | Outlook

In this chapter we want to give a brief overview over interesting, open questions and further topics we deem worth studying.

➔ A first natural idea is to apply the developed machinery to further exemplary systems. Most notably is the tessellated *quantum spin-ice on the pyrochlore lattice*[1] which is found in rare-earth ions[15]. Here each unit cell is a regular tetrahedron which $\mathbb{Z}_2$ degrees of freedom on the corners which are shared with its adjacent unit cells. This results in an effectively antiferromagnetic interaction that is frustrated.

➔ In (amalgamated) structures throughout this thesis we observed a '*clumping*' of the ground states and the excited states to be optimal for the quality and the effective gap. However both measures only consider the extremal energies; they are not able to resolve or quantify such clumping. This suggests that a *finer measure* including the *distribution of states* might be useful to consider in future studies. It is possibly interesting to study whether this clumping is a general phenomenon and what determines the number of 'bands' which arise during clumping.

➔ Another interesting ansatz for further studies is to consider *quantum fluctuations on the Rydberg platform in the VdW model* by perturbatively ramping up the RABI frequencies Ω_i of the atoms. This is particularly interesting for highly symmetric structures (cf. subsec. 8.1.2) which promise (due to their symmetry) equal weight-superpositions of the ground states. In that context it is of large interest to find *fully symmetric implementations* of the surface code unit cell.

[1] This is the dual lattice to the diamond lattice.

➔ Lastly in sec. 7.3 we offered an argument for why we believe that one requires in general *exponentially many ancillaries* to implement general BOOLEAN functions. However this is far from a rigorous proof it remains an open question to proof or disprove this statement. This is relevant to continue on the idea of *geometric programming* as an overload of exponentially many ancillaries is neither experimentally nor numerically feasible.

List of Figures

2.1 Minority-model unit cell MINU with diverging robustness. 34

3.1 Three PXP-minimal NOR-realizations implemented in the VdW-model via the rejection sampling algorithm. 42
3.2 Tree of ISs for the cycle graph C_6. 54
3.3 Three PXP-minimal NOR-realizations implemented in the VdW-model via the minimization algorithm. 57

4.1 PXP-minimal logic primitives optimal in ΔE_{eff} and r. 76
4.2 Family of ΔE_{eff}-optimal minimal ICPY- and CPY-gates. 79
4.3 r-optimal realization of the CPY2-gate. 80
4.4 PXP-minimal (inverted) crossing optimal in ΔE_{eff} and r. 81
4.5 Family 1 of PXP-minimal logic elementaries optimal in ΔE_{eff}. 83
4.6 Family 2 of PXP-minimal logic elementaries optimal in ΔE_{eff}. 85
4.7 XOR2b-Gate optimal in ΔE_{eff} and r. 86
4.8 Complete list of VdW-minimal (inverted) crossings optimal in ΔE_{eff} and r. . . . 88
4.9 Family 3 of VdW-minimal logic elementaries optimal in ΔE_{eff}. 91
4.10 XNOR4a-gate optimal in ΔE_{eff} and r. 96
4.11 The non-minimal realizations XNOR-4b – 4d optimal in ΔE_{eff}. 98
4.12 The non-minimal realizations XNOR-4d – 4g optimal in ΔE_{eff}. 99

5.1 Optimized PXP-minimal surface code unit-cell in the VdW model. 105
5.2 Optimized VdW-specific surface code unit-cell. 108
5.3 SCUII-1 unit cell in representation II with one ancillary. 110
5.4 Optimized PXP-elementaries of the FIBONACCI model. 115
5.5 Optimized PXP-minimal elementaries of the FIBONACCI model. 116

5.6 Optimized VdW-minimal elementaries of the FIBONACCI model. . . . 118
5.7 The measure ΔI as a function of the parameters r_{AB} and r_{AD}. . . . 122
5.8 PXP-minimal SCUI-1 unit cells. . . . 124
5.9 Two additional SCUI-2b unit cells. . . . 125
5.10 Ansatz for a SCII unit cell in $d = 2$ dimensions with one ancillary. . . . 126
5.11 Sketch of possible blockade graphs for the FMSI-2 site. . . . 128
5.12 The measure ΔI as a function of the parameters r_{BC} and r_{BE}. . . . 131
5.13 PXP-minimal FMUI-2 unit cell. . . . 133
5.14 VdW-minimal FMUI unit cells. . . . 134

6.1 SCI-1 unit cell on a 1×1 grid with OBCs and PBCs respectively. . . . 137
6.2 SCI-1 2×1 and 2×2 grid with OBCs and PBCs respectively. . . . 138
6.3 Hexagonal FIBONACCI model grid with hexagonal cells 1 and 2. . . . 144
6.4 Sketch of the honeycomb grid with the relevant quantities. . . . 151
6.5 Upper bounds on the local ratio $Q_R = \delta E_R / \Delta E_R$ for the FIBONACCI model in realization FMI-3 as a function of the radius R and the number N_E of LNK1-gates between the sites. . . . 154
6.6 Lower bounds on the local ratio $Q_R = \delta E_R / \Delta E_R$ for the FIBONACCI-model in realization FM3 as a function of the radius R and the number N_E of LNK1-gates between the sites. . . . 155
6.7 Upper and lower bounds on the ratio in FIBONACCI-model realization FMI3. . . . 156
6.8 Asymptotic behavior of the local energy splitting $\delta E_R(N_E)$ and the distance $l_-(R, N_E)$ between loops in state $|-\rangle$ for realization FMI-3. . . . 157
6.9 Asymptotic behavior of the local energy splitting $\delta E_R(N_E)$ and the distance $l_-(R, N_E)$ between loops in state $|-\rangle$ for realization FMI-2. . . . 158
6.10 Sketch of the LNK4-gate with $N = 9$ atoms. . . . 160
6.11 NOTm-Gates and LNKm-Gates for $m = 1$ and $m = 5$ constructed by the algorithm of lemma XII. . . . 164

7.1 Virtual ancillaries appended to the VdW-minimal CRS-2a-gate, the PXP-minimal SCUI-1 unit cell and the VdW-minimal SCUI-2b unit cell. . . . 180
7.2 Sketch of the the construction for a scalar, ternary target function according to the proof. . . . 189

8.1 The XNOR3ii-gate optimal in ΔE_{eff} and r. . . . 195
8.2 Family of ICRS3-multigates optimized for ΔE_{eff} and r. . . . 197
8.3 Two-dimensional, ternary NOORO-gate with four ancillaries. . . . 200
8.4 Family of ternary, scalar, symmetric logic gates with unit effective HAMMING weight $w_H = 1$. . . . 201
8.5 Family of ternary, scalar, symmetric logic gates with effective HAMMING weight $w_H = 3$. . . . 203
8.6 Part 1 of the family of ternary, scalar and symmetric logic gates with effective HAMMING weight $w_H = 2$. . . . 204
8.7 Part 2 of the family of ternary, scalar and symmetric logic gates with effective HAMMING weight $w_H = 2$. . . . 205
8.8 Full Adders based on different Gates. The ternary logic gates MAJ and ODD allow for a simpler implementation. . . . 206
8.9 Non-minimal ternary, scalar and symmetric logic gates with two ancillaries. . . . 208
8.10 TOFFOLI-gate (TOFF) with one ancillary. . . . 210

8.11 ISWITCH-gate with one ancillary defined in eq. (8.4). The *switch* A determines whether the gate outputs $\bar{\mathsf{B}}$ or $\bar{\mathsf{C}}$. The connective and the language are intrinsically asymmetric. . . . 211
8.12 Inverse FREDKIN-gate in two realizations, inspired from the inverted crossing ICRS1. 213
8.13 Double Logic Gates constructed by amalgamating two elementary gates from fig. 4.9 by their input ports. . . . 216
8.14 Triple Logic Gates constructed by amalgamating elementary gates from fig. 4.9. 217
8.15 Quasiplanar SCUI unit cells in two realizations 3a,b. . . . 220
8.16 Quasiplanar SCUII-2ii unit cell with one ancillary. . . . 221
8.17 VdW-minimal (inverted) crossings optimal in ΔE_{eff} and r. . . . 222
8.18 FIBONACCI model site with check function (5.16) in representation IV. . . . 224
8.19 FIBONACCI model site with check function (5.14) in realization FMSII-1. . . . 225
8.20 FIBONACCI model site with check function (5.14) in realization FMSII-2. . . . 226
8.21 FIBONACCI model site with check function (5.15) in representation III. . . . 227
8.22 Additional ternary, scalar, symmetric logic gates with unit effective HAMMING weight $w_H = 1$. . . . 231
8.23 Additional ternary, scalar, symmetric logic gates with effective HAMMING weight $w_H = 3$. . . . 233
8.24 Further double logic Gates which implement vectorial connectives with $q = 2$. . . . 237
8.25 Two-dimensional multi gates which include OR. . . . 238

Bibliography

[1] N. Alon and V. H. Vũ. Anti-hadamard matrices, coin weighing, threshold gates, and indecomposable hypergraphs. *Journal of Combinatorial Theory, Series A*, 79(1):133–160, 1997. ISSN 0097-3165. doi:https://doi.org/10.1006/jcta.1997.2780.

[2] R. Barends, J. Kelly, A. Megrant, A. Veitia, D. Sank, E. Jeffrey, T. C. White, J. Mutus, A. G. Fowler, B. Campbell, et al. Superconducting quantum circuits at the surface code threshold for fault tolerance. *Nature*, 508(7497):500–503, 2014. doi:https://doi.org/10.1038/nature13171.

[3] D. Barredo, S. de Léséleuc, V. Lienhard, T. Lahaye, and A. Browaeys. An atom-by-atom assembler of defect-free arbitrary two-dimensional atomic arrays. *Science*, 354(6315):1021–1023, 2016. doi:10.1126/science.aah3778.

[4] D. Barredo, V. Lienhard, S. De Leseleuc, T. Lahaye, and A. Browaeys. Synthetic three-dimensional atomic structures assembled atom by atom. *Nature*, 561(7721):79–82, 2018. doi:https://doi.org/10.1038/s41586-018-0450-2.

[5] J. Bourgain. On lipschitz embedding of finite metric spaces in hilbert space. *Israel Journal of Mathematics*, 52:46–52, 1985. doi:https://doi.org/10.1007/BF02776078.

[6] S. B. Bravyi and A. Y. Kitaev. Quantum codes on a lattice with boundary. *arXiv preprint quant-ph/9811052*, 1998. doi:https://doi.org/10.48550/arXiv.quant-ph/9811052.

[7] M. Bădoiu, E. D. Demaine, M. T. Hajiaghayi, and P. Indyk. Low-dimensional embedding with extra information. In *Proceedings of the twentieth annual symposium on Computational geometry*, pages 320–329, 2004. doi:https://doi.org/10.1145/997817.997866.

[8] S. Cabello, E. D. Demaine, and G. Rote. *Planar embeddings of graphs with specified edge lengths*. Citeseer, 2005. doi:https://doi.org/10.7155/jgaa.00145.

[9] E. Dennis, A. Kitaev, A. Landahl, and J. Preskill. Topological quantum memory. *Journal of Mathematical Physics*, 43(9):4452–4505, 2002. doi:https://doi.org/10.1063/1.1499754.

[10] I. Dokmanić and R. Gribonval. Beyond moore-penrose part i: generalized inverses that minimize matrix norms. *arXiv preprint arXiv:1706.08349*, 2017. doi:https://doi.org/10.48550/arXiv.1706.08349.

[11] S. Ebadi, T. T. Wang, H. Levine, A. Keesling, G. Semeghini, A. Omran, D. Bluvstein, R. Samajdar, H. Pichler, W. W. Ho, et al. Quantum phases of matter on a 256-atom programmable quantum simulator. *Nature*, 595(7866):227–232, 2021. doi:https://doi.org/10.1038/s41586-021-03582-4.

[12] P. Fendley. Topological order from quantum loops and nets. *Annals of Physics*, 323(12): 3113–3136, 2008. ISSN 0003-4916. doi:https://doi.org/10.1016/j.aop.2008.04.011.

[13] E. Fredkin and T. Toffoli. Conservative logic. *International Journal of theoretical physics*, 21(3):219–253, 1982. doi:https://doi.org/10.1007/BF01857727.

[14] J. Ghosh, A. G. Fowler, and M. R. Geller. Surface code with decoherence: An analysis of three superconducting architectures. *Physical Review A—Atomic, Molecular, and Optical Physics*, 86(6):062318, 2012. doi:https://doi.org/10.1103/PhysRevA.86.062318.

[15] A. W. Glaetzle, M. Dalmonte, R. Nath, I. Rousochatzakis, R. Moessner, and P. Zoller. Quantum spin-ice and dimer models with rydberg atoms. *Physical Review X*, 4(4):041037, 2014. doi:https://doi.org/10.1103/PhysRevX.4.041037.

[16] G. H. Golub and C. F. Van Loan. *Matrix computations*. JHU press, fourth edition, 2013.

[17] W. Ibrahim, V. Beiu, and M. H. Sulieman. On the reliability of majority gates full adders. *IEEE Transactions on Nanotechnology*, 7(1):56–67, 2008. doi:10.1109/TNANO.2007.915203.

[18] W. R. Inc. Mathematica, Version 14.1, 2024. URL `https://www.wolfram.com/mathematica`. Champaign, IL, 2024.

[19] A. Kitaev. Fault-tolerant quantum computation by anyons. *Annals of Physics*, 303(1):2–30, 2003. ISSN 0003-4916. doi:https://doi.org/10.1016/S0003-4916(02)00018-0.

[20] A. Kitaev. Anyons in an exactly solved model and beyond. *Annals of Physics*, 321(1):2–111, 2006. ISSN 0003-4916. doi:https://doi.org/10.1016/j.aop.2005.10.005. January Special Issue.

[21] J. B. Kogut. An introduction to lattice gauge theory and spin systems. *Rev. Mod. Phys.*, 51:659–713, Oct 1979. doi:10.1103/RevModPhys.51.659.

[22] S. Kuhr. Quantum-gas microscopes: a new tool for cold-atom quantum simulators. *National Science Review*, 3(2):170–172, 04 2016. ISSN 2095-5138. doi:10.1093/nsr/nww023.

[23] M. Lanthaler, C. Dlaska, K. Ender, and W. Lechner. Rydberg-blockade-based parity quantum optimization. *Phys. Rev. Lett.*, 130:220601, May 2023. doi:10.1103/PhysRevLett.130.220601.

[24] E. L. Lawler, J. K. Lenstra, and A. Rinnooy Kan. Generating all maximal independent sets: Np-hardness and polynomial-time algorithms. *SIAM Journal on Computing*, 9(3):558–565, 1980. doi:https://doi.org/10.1137/0209042.

[25] I. Lesanovsky. Many-body spin interactions and the ground state of a dense rydberg lattice gas. *Phys. Rev. Lett.*, 106:025301, Jan 2011. doi:10.1103/PhysRevLett.106.025301.

[26] M. A. Levin and X.-G. Wen. String-net condensation: A physical mechanism for topological phases. *Phys. Rev. B*, 71:045110, Jan 2005. doi:10.1103/PhysRevB.71.045110.

[27] J. Matoušek and A. Naor. Open problems on embeddings of finite metric spaces. In *Workshop on discrete metric spaces and their algorithmic applications*, 2002.

[28] C. Morgan. Embedding metric spaces in euclidean space. *Journal of Geometry*, 5:101–107, 1974. doi:https://doi.org/10.1007/BF01954540.

[29] C. Nayak, S. H. Simon, A. Stern, M. Freedman, and S. Das Sarma. Non-abelian anyons and topological quantum computation. *Rev. Mod. Phys.*, 80:1083–1159, Sep 2008. doi:10.1103/RevModPhys.80.1083.

[30] M.-T. Nguyen, J.-G. Liu, J. Wurtz, M. D. Lukin, S.-T. Wang, and H. Pichler. Quantum optimization with arbitrary connectivity using rydberg atom arrays. *PRX Quantum*, 4: 010316, Feb 2023. doi:10.1103/PRXQuantum.4.010316.

[31] D. Ohl de Mello, D. Schäffner, J. Werkmann, T. Preuschoff, L. Kohfahl, M. Schlosser, and G. Birkl. Defect-free assembly of 2d clusters of more than 100 single-atom quantum systems. *Phys. Rev. Lett.*, 122:203601, May 2019. doi:10.1103/PhysRevLett.122.203601.

[32] P. Scholl, M. Schuler, H. J. Williams, A. A. Eberharter, D. Barredo, K.-N. Schymik, V. Lienhard, L.-P. Henry, T. C. Lang, T. Lahaye, et al. Quantum simulation of 2d antiferromagnets with hundreds of rydberg atoms. *Nature*, 595(7866):233–238, 2021. doi:https://doi.org/10.1038/s41586-021-03585-1.

[33] M. D. Schulz, S. Dusuel, K. P. Schmidt, and J. Vidal. Topological phase transitions in the golden string-net model. *Phys. Rev. Lett.*, 110:147203, Apr 2013. doi:10.1103/PhysRevLett.110.147203.

[34] SciPy. Webpage scipy.optimize.dual_annealing, 2024. URL `https://docs.scipy.org/doc/scipy/reference/generated/scipy.optimize.dual_annealing.html`.

[35] G. Semeghini, H. Levine, A. Keesling, S. Ebadi, T. T. Wang, D. Bluvstein, R. Verresen, H. Pichler, M. Kalinowski, R. Samajdar, A. Omran, S. Sachdev, A. Vishwanath, M. Greiner, V. Vuletić, and M. D. Lukin. Probing topological spin liquids on a programmable quantum simulator. *Science*, 374(6572):1242–1247, 2021. doi:10.1126/science.abi8794.

[36] C. E. Shannon. A mathematical theory of communication. *The Bell System Technical Journal*, 27, 1948. doi:10.1002/j.1538-7305.1948.tb01338.x.

[37] S. Stastny. *Functional Rydberg Complexes in the PXP-Model*. PhD thesis, Master's thesis, University of Stuttgart, 2023. URL `https://www.itp3.uni-stuttgart.de/buechler-group/theses/`.

[38] S. Stastny, H. P. Büchler, and N. Lang. Functional completeness of planar rydberg blockade structures. *Phys. Rev. B*, 108:085138, Aug 2023. doi:10.1103/PhysRevB.108.085138.

[39] U. Tietze and C. Schenk. *Halbleiter-schaltungstechnik*. Springer-Verlag, 2013.

[40] T. Toffoli. Reversible computing. In *International colloquium on automata, languages, and programming*, pages 632–644. Springer, 1980. doi:https://doi.org/10.1007/3-540-10003-2_104.

[41] C. Tsallis and D. A. Stariolo. Generalized simulated annealing. *Physica A: Statistical Mechanics and its Applications*, 233(1):395–406, 1996. ISSN 0378-4371. doi:https://doi.org/10.1016/S0378-4371(96)00271-3.

[42] R. Verresen, M. D. Lukin, and A. Vishwanath. Prediction of toric code topological order from rydberg blockade. *Phys. Rev. X*, 11:031005, Jul 2021. doi:10.1103/PhysRevX.11.031005.

[43] R. Verresen, M. D. Lukin, and A. Vishwanath. Prediction of toric code topological order from rydberg blockade. *Phys. Rev. X*, 11:031005, Jul 2021. doi:10.1103/PhysRevX.11.031005.

[44] D. West. *Introduction to Graph Theory*. Featured Titles for Graph Theory. Prentice Hall, 2001. ISBN 9780130144003. URL `https://books.google.de/books?id=TuvuAAAAMAAJ`.

[45] W. Willis. *Bounds for the independence number of a graph*. PhD thesis, Virginia Commonwealth University, 2011.

[46] Y. Xiang and X. G. Gong. Efficiency of generalized simulated annealing. *Phys. Rev. E*, 62: 4473–4476, Sep 2000. doi:10.1103/PhysRevE.62.4473.

[47] Y. Xiang, D. Sun, W. Fan, and X. Gong. Generalized simulated annealing algorithm and its application to the thomson model. *Physics Letters A*, 233(3):216–220, 1997. ISSN 0375-9601. doi:https://doi.org/10.1016/S0375-9601(97)00474-X.

Acknowledgments

Even though this thesis was written by myself only, science is never a solitary effort. Therefore I would like to dedicate this last page to the people who have supported and looked after me throughout the last year.

First of all, I would like to thank Prof. Hans Peter Büchler for the opportunity to do research at his institute.

Special thanks go to Dr. Nicolai Lang, who supervised me throughout the year and guided me through my thesis. He supported me with my questions and with fruitful discussions and contributed many valuable ideas. Nevertheless, he gave me the necessary space to research independently and to develop and pursue my own ideas. His lectures are unique and I am very grateful that I have been able to listen to them over the past few years. I would also like to thank the rest of the institute for a very nice time, many great game nights and volleyball mornings.

I would like to thank Benjamin, Manja and Yanek, who were always with me the last year and who provided distractions besides the Master's thesis. I would also like to thank you for many great coffee breaks and the support on the coffee list.

Finally, my special thanks go to my family and my girlfriend, who have always stood by me during the year and supported me a lot outside of work.